atomic structure and chemical bond

INCLUDING MOLECULAR SPECTROSCOPY

SECOND EDITION

MANAS CHANDA

৳- ১২-০০

১৬২১

ATOMIC STRUCTURE AND CHEMICAL BOND
Including Molecular Spectroscopy

SECOND EDITION

Atomic Structure and Chemical Bond

Including Molecular Spectroscopy

SECOND EDITION

MANAS CHANDA
Indian Institute of Science
Bangalore

Preface

This book is written as an introduction to modern concepts of atomic and molecular structure, the nature of the chemical bond, and molecular spectroscopy. In its present form, the book should be useful for a university course in general chemistry. It should also prove useful to students of physics looking for an introduction to the quantum theory and its applications especially to atomic structure and bonding, and to spectroscopy. Students who, following a course in materials science, have to search for more detailed information on atomic and molecular structure and the nature of binding in materials than what is usually given in materials science texts, should find this book a useful supplement.

In order to be able to interpret chemical and physical phenomena in terms of molecular behaviour the student must learn as much as he can about the nature and behaviour of individual molecules, a satisfactory account of which can be given, however, only in terms of wave mechanics. Powerful notions which have been developed and applied to the problems of atomic structure and chemical bonding in recent years are not easy to grasp in their complex mathematical form. However, when stripped of their formal language, the essential ideas are simple enough to be presented to the undergraduate student. This book represents an endeavour to give practical shape to this view.

The opening chapter of the book presents a historical account of the origin of the quantum theory. The application of the quantum theory to the problem of atomic spectra and atomic structure and the results stemming from it are discussed in Chapter 2. Electronic configuration of atoms on the four-quantum number system, symbols for atomic states, and classification of elements and their distribution in the periodic table form the subject matter of Chapter 3, which, however, uses the classical approach in its treatment. Chapter 4 introduces the reader to the wave-mechanical concept, its physical significance and application to real problems. The next chapter is devoted to wave-mechanical treatment of the single-electron atom—hydrogen—and discussion of the theory of atomic orbitals, the radial and angular wave functions, and charge-cloud representation, with the help of tables and figures to help the reader understand the topic. Valence bond and molecular orbital methods of chemical bonding, hybridization, orbital structures of com-

mon hydrocarbons, and theory of coordination compounds are discussed in Chapter 6. In this revised edition, the treatment on the bonding in coordination compounds has been expanded to include all the important theories in a more systematic manner. Starting with a brief account of the classical concepts of valency, Chapter 7 presents discussion of various topics related to ionic and covalent bonding. Chapters 8 and 9 are concerned with the theories of bonding in metals and the secondary bond forces.

The last chapter of the book is devoted to an account of the more important physical methods used in the determination of the molecular structure. It is essentially a chapter on molecular spectroscopy at an introductory level. In its various branches, spectroscopy is becoming of increasing value as an analytical tool. The qualitative and quantitative analysis of mixtures, the determination of molecular symmetry and molecular parameters form some of the important facets to its application, and almost every scientist at some time or other makes use of the results obtained from it. It is, therefore, desirable that he should know what type of information is available from a spectroscopic method and what its limitations are. Consequently, emphasis has been laid on physical principles and relationships between experimental readings and molecular parameters rather than on experimental and theoretical details. In this revision, besides broadening some of the existing topics, a few new topics have been incorporated; these are electron spin resonance spectroscopy, Mössbauer spectroscopy, and mass spectrometry.

One of my delights since the publication of the first edition of the book has been the receipt of suggestions, comments and criticisms from many individuals. This help from the outside was invaluable in the work of revision. Specific thanks are due to Professor C. N. R. Rao, Head of the Solid State and Structural Chemistry Unit, Indian Institute of Science; Professor R. D. Patel, Vice-Chancellor, Sardar Patel University; Professor Paul A. Vatakencharry, Head of Applied Chemistry, Cochin University; Professor S. Brahmaji Rao, Head of Chemistry, Sri Venkateswara University; and Dr. C. Srinivasan, Reader in Physical Chemistry, Madurai University. I am grateful also to my students Messrs. M. N. Chandrashekara, P. Raghavendrachar, and C. C. Lakshmanan for their assistance in checking final proofs and help in many other ways. Finally, I am deeply indebted to the editorial staff at Tata McGraw-Hill for their proficient and patient editing and processing of the manuscript.

Bangalore   MANAS CHANDA

Contents

ATOMIC STRUCTURE AND CHEMICAL BOND
Including Molecular Spectroscopy

SECOND EDITION

Chapter 1

Beginning of the Quantum Theory

1.1 Introduction

The importance of the quantum theory in the study of chemical problems cannot be overemphasized. The classical theories, although they have rendered great service and continue to be very useful in modern chemistry, are however not always sufficient in the study of chemical problems. For example, the spectra, the structure of the periodic table, the nature of the chemical bonding, the structure of molecules and their properties cannot be properly understood without recourse to quantum theory. However, the quantum theory itself had its origin in the branch of physics dealing with radiation. It was the study of the radiation problem, which had been defying solution on the basis of classical theories, that led Max Planck in 1901 to introduce the concept of quanta, making the foundation of the quantum theory. It is therefore pertinent to start with a discussion of this historic problem.

1.2 Black-body Radiation

In a state of rapid vibration, the particles composing a solid emit radiant energy in the form of waves, which, according to Maxwell's electromagnetic theory, are identical with electromagnetic waves. At low temperatures, the emission is mainly in the infrared region, but as the temperature is raised the spectral range of radiation widens, opening up fresh regions of the spectrum. And if the temperature gets high enough, such as white

heat, a range of waves covering the visible light spectrum are emitted in addition to the radiations of higher wavelengths that have started at a lower temperature.

Thus the total radiation emitted by a hot body is composed of electromagnetic waves of varying range of wavelengths constituting a spectrum. The total intensity of radiation, as well as its distribution among the various wavelengths of the spectrum, is different at different temperatures, and may also be quite different for different objects even at the same temperature. If, however, the radiation emerging through a small hole in the wall of an isothermal hollow body is measured, it is found that the total intensity of radiation and its distribution among wavelengths are independent of the material and of the size and shape of the enclosure. This radiation is called black-body radiation.

A black-body is an idealized radiator. It absorbs all the radiation incident upon it, and is heated by this radiation to a higher temperature than any other body. And conversely, when a black-body is heated, it radiates more intensely than other bodies at the same temperature.

For experimental purposes, a black-body can be very well approximated, as noted above, by a small hole in the wall of an enclosure. Nearly all the radiation entering the hole will be absorbed by successive reflections inside the enclosure, and thus the hole almost exactly fulfils the definition of a black-body. The radiation emerging from the hole will also be very nearly equal to that of a black-body, being dependent only on the temperature of the enclosure and independent of the nature of the interior matter. Such black-body radiation was investigated in the most complete series of experiments conducted by O. Lummer and E. Pringsheim during the period 1897 to 1899. The typical curves from a black-body at different temperatures are as shown in Fig. 1.1. The ordinate is the intensity E_λ, which is defined (Fig. 1.2) so that $E_\lambda d\lambda$ gives the rate of emission of energy per unit area of surface, in the wavelength range λ to $\lambda + d\lambda$; the total intensity E, i.e. the total energy radiated per unit area of surface per unit time, is

$$E = \int_0^\infty E_\lambda d\lambda \qquad\qquad (1.1)$$

The task of theory was then to fit the curves of Fig. 1.1 and to lead to the two fundamental laws of thermal radiation formulated earlier. These laws are detailed in the following:

The Stefan-Boltzmann law. The law, which was discovered experimentally by Stefan in 1879 and derived using the principles of thermodynamics by Boltzmann in 1884, states that *the intensity of total radiation from a black-body* (i.e. the areas of the curves shown in Fig. 1.1) *is proportional to the fourth power of its absolute temperature*, that is,

$$E = \sigma T^4 \qquad\qquad (1.2)$$
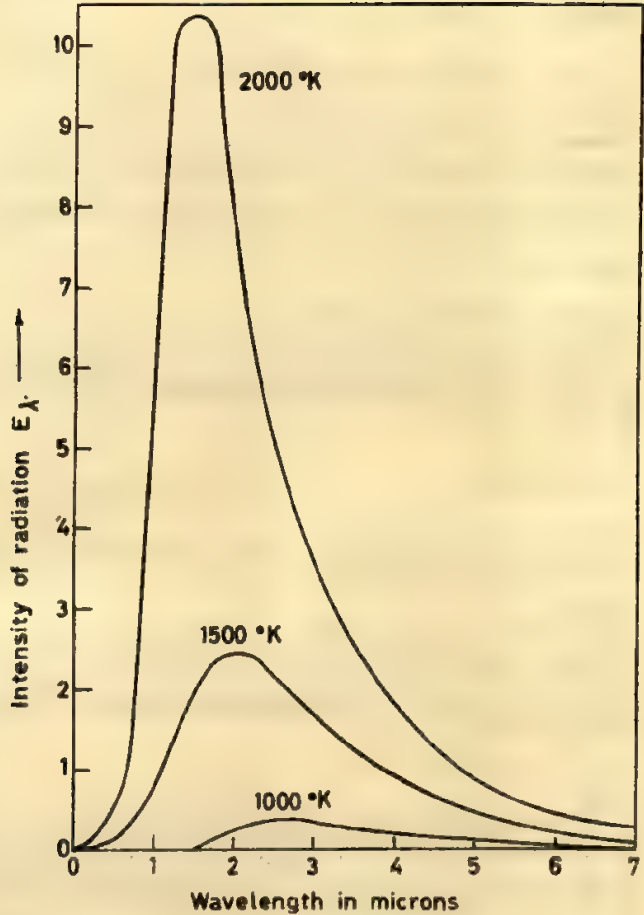
Fig. 1.1 Emission of radiation from a black-body at different temperatures. The area under the curve between two different wavelengths gives the energy in calories emitted by 1 cm² surface of a black-body in the specified range of wavelengths.
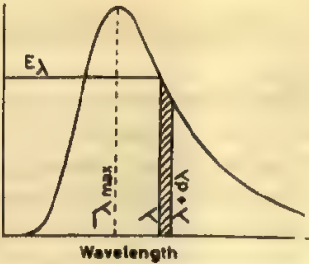
Fig. 1.2 Definition of the intensity of radiation E_λ. The shaded area ($E_\lambda \, d\lambda$) gives the rate of emission of energy in the wavelength range λ to $\lambda + d\lambda$ from unit area of surface.

where σ = Stefan's constant

$= 5 \cdot 669 \times 10^{-5}$ erg sec^{-1} cm^{-2} (K deg)$^{-4}$

$= 5 \cdot 669 \times 10^{-8}$ W m^{-2} (K deg)$^{-4}$

Wien's law. The wavelength of maximum intensity is inversely proportional to the absolute temperature of the black-body. That is to say, the product of the absolute temperature (T) at which a particular curve of Fig. 1.1 is measured and the wavelength (λ_{max}) at which the curve has a maximum, is a constant.

$$\lambda_{max} T = 2 \cdot 8976 \times 10^{-3} \text{ m deg} \tag{1.3}$$

This is indeed a special case of Wien's displacement law formulated in 1894 from theoretical considerations. This law expresses E_λ by the following formula:

$$E_\lambda = \frac{a}{\lambda^5 e^{b/\lambda T}} \tag{1.4}$$

This formula holds true for short wavelengths, if the constants a and b are properly chosen, but is ineffective in the range of longer wavelengths.

The British scientists Rayleigh and Jeans developed a unified law of radiation which is accepted as the correct result of the laws of classical physics. In terms of the Boltzmann constant k, an expression for the Rayleigh-Jeans law is:

$$E_\lambda = 2\pi c k T / \lambda^4 \tag{1.5}$$

This equation is found to agree satisfactorily with experimental results in the case of long wavelengths or low frequencies, but it is clearly not correct since it predicts an impossible situation, namely that at shorter and shorter wavelengths the radiation intensity should increase without bound! This paradox, also known as the 'ultraviolet catastrophe', dealt a terrible blow to the nineteenth century classical physics and catapulted it into an entirely new area, that of the quantum theory.

1.3   Planck's Radiation Law

As has been pointed out above, Wien's law agrees well with experiment, except in the region of long wavelengths while the Rayleigh-Jeans law proves to be approximately correct in the limit of long wavelengths but when applied to short wavelengths leads to the 'ultraviolet catastrophe'. Max Planck, a German theoretical physicist, started his consideration of the radiation problem by finding, empirically, an interpolation formula between Wien's law and Rayleigh-Jeans law and eventually stumbled upon an equation of the form

$$E_\lambda = \frac{2\pi hc^2}{\lambda^5 (e^{hc/\lambda kT} - 1)} \tag{1.6}$$

which proved to agree remarkably well with experiment and had come to be known as Planck's radiation law. In attempting to explain this law, which started out to be an empirical one but worked so well, Planck was led in 1901 to the bold new hypothesis that, contrary to the classical law of interaction between matter and radiation, the radiation cannot be absorbed or emitted in arbitrary amounts but only in quanta of energy $h\nu$, where h is a constant, now called Planck constant, and ν is the frequency of the radiation.

Eq. (1.6) predicts successfully the spectral distribution of radiation from a black-body over the entire experimental range. Again, the integration of this equation over all wavelengths yields

$$E = \int_0^\infty E_\lambda d\lambda = 2\pi hc^2 \int_0^\infty \frac{1}{e^{hc/\lambda kT} - 1} \frac{d\lambda}{\lambda^5} \tag{1.7}$$

The definite integral in Eq. (1.7) can be converted into a standard form. The result is

$$E = \frac{2\pi^5 k^4}{15c^2 h^3} T^4 \tag{1.8}$$

Eq. (1.8) is exactly of the same form as Eq. (1.2) expressing the Stefan-Boltzmann law. So,

$$\sigma = \frac{2\pi^5 k^4}{15c^2 h^3} \tag{1.9}$$

The numerical evaluation of the constant σ from Eq. (1.9) accords with the experimental value of σ.

The Wien displacement law of Eq. (1.3) can be derived from Planck's radiation law by differentiating Eq. (1.6) and equating this derivative to zero.

It can also be shown that Planck's radiation law reduces to Wien's law of Eq. (1.4) for short wavelengths and to Rayleigh-Jeans law of Eq. (1.5) for long wavelengths. Plots corresponding to these three radiation laws are shown in Fig. 1.3.

Thus, despite the fact that Planck's assumption about quantization of energy is arbitrary, his formula does, nevertheless, reproduce correctly the data on black-body radiation. And if h is treated as a constant, evaluated from other phenomena — as for instance, from the photoelectric effect, discussed later — Planck's formula and the deductions stemming from it show quantitative agreement with black-body observations without any adjustable parameter. This revolutionary theory was later to be the origin of Einstein's theory of the photoelectric effect and of Bohr's theory of atomic spectra.
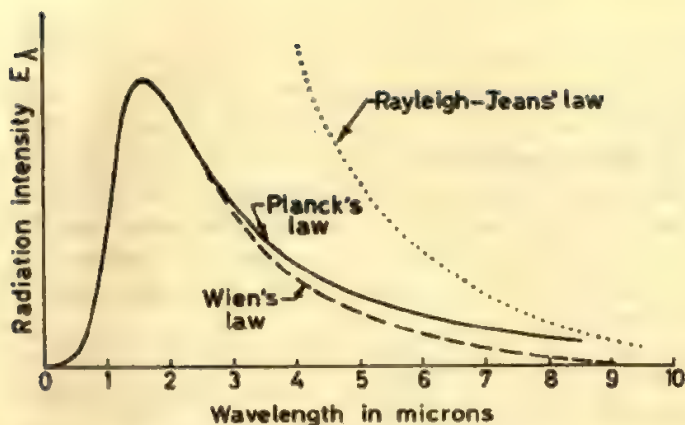
Fig. 1.3 Curves corresponding to the three radiation laws

1.4 *Einstein's Theory of Photoelectricity*

If the quantum theory had remained confined to its original sphere in the realm of radiation, it would never have attained its present importance and prominence. This prominence is largely due to the splendid way in which the theory had helped solve problems with which, at first sight, it is entirely unconnected. The first outstanding application of the theory was in the explanation of the photoelectric effect by Albert Einstein in 1905. It was all the more important because it really put the quantum theory on its feet. It should be noted that though Planck introduced the idea that radiation must be emitted in quanta or bundles of energy, he however believed that, after being so emitted, the radiation spread in waves. Einstein extended Planck's idea further and introduced the important concept that the radiation energy is not only emitted in quanta but the quanta also preserved their identity until they were finally absorbed.

Photoelectric effect is the ejection of electrons from various materials when irradiated by visible or ultraviolet light. This effect is the basis of the photoelectric cell, an extremely sensitive instrument used for detection and measurement of radiation.

An arrangement that can be used for observing the photoelectric effect is shown schematically in Fig. 1.4. When a beam of light falls on a metal surface S in an evacuated tube, electrons are emitted by the surface and are attracted to the positively charged anode A, thus completing the circuit. The current can be measured by the galvanometer G.

Laws of photoelectricity, established from experimental facts, are as follows:

(a) *The total photoelectric current is proportional to the intensity of the light striking the surface.*
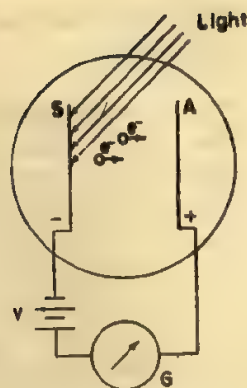
Fig. 1.4 Schematic diagram of apparatus for investigating the photoelectric effect

The surface S in Fig. 1.4 is irradiated by monochromatic light, and sufficiently high voltage V is applied to the anode to collect all the electrons emitted photoelectrically. This is then the *total photoelectric current*. It is found, experimentally, that, in any photoelectric emission, the total photoelectric current is strictly proportional to the intensity of the incident light.

(b)   *For each particular metal used to form the surface, there exists a threshold frequency (or wavelength) such that, at frequencies below the threshold, no electrons are emitted, no matter how great the intensity.*

If the photoelectric current from any given surface is measured for monochromatic light rays of constant intensity, but of various wavelengths, it is found that the current stops entirely at an upper wavelength limit, called the *threshold wavelength* (Fig. 1.5). For any wavelength longer than this, no photoelectric current is produced, regardless of the intensity of the incident monochromatic light. The frequency corresponding to the threshold wavelength is called the *threshold frequency*.
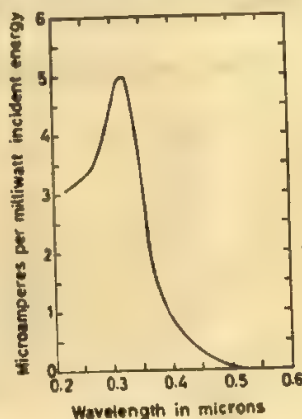
Fig. 1.5 Photoelectric response of sodium surface as a function of incident wavelength

(c)   The maximum energy of the emitted electrons is independent of the incident light intensity.

For measuring the energies of photoelectrically emitted electrons there exist various ways, the best of which, however, involves either deflecting the electrons with a magnetic field or subjecting them to a retarding electric field. By applying a *negative* voltage to the anode A in Fig. 1.4, the speed of the emitted electrons can be retarded. It is, however, found that even when the anode is several volts negative, some photoelectric current flows, which indicates that some electrons are ejected from the cathode surface S with sufficient speed to enable them to overcome a retarding potential of several volts. The negative voltage is gradually increased till it cuts off all the photoelectric current. This limiting potential, V_s in Fig. 1.6, is called the *stopping potential* for that particular surface and irradiation. Since V_s is required, evidently, to stop electrons with maximum speed, i.e. with maximum kinetic energy, it follows from the law of conservation of energy that

$$\tfrac{1}{2} m v^2_{max} = e V_s \tag{1.10}$$

Thus if the stopping potential for a particular tube is 2·57 V, then the most energetic electrons have an energy of 2·57 eV. The stopping potential is thus a measure of the maximum kinetic energy of electrons. Now, if the stopping potential for a given surface, irradiated by monochromatic light of a given frequency, is measured as a function of the incident light intensity, a surprising result is encountered: The stopping potential is found to be independent of the light intensity. This means that an increase in the amount of energy of a monochromatic light of a given frequency striking the surface per unit time does not change the maximum energy of the electrons emitted from the surface. It only increases the total photoelectric current, as noted earlier.

(d)   The maximum energy of the emitted electrons is linearly dependent on the frequency of the incident light.

If the stopping potential is measured for various frequencies of inci-
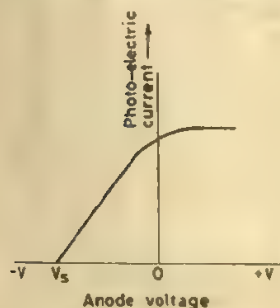
Fig. 1.6   Variation of total photoelectric current as a function of anode voltage for a given surface and irradiation

dent monochromatic light, a linear relationship is observed, as shown in Fig. 1.7. Below a definite frequency, the stopping potential is nil, i.e. no electrons are emitted below this frequency, which, as we have already seen in (b), is called the threshold frequency. Above the threshold, however, the stopping potential and hence the maximum energy of the electrons emitted, is directly proportional to the frequency.

Considered on classical grounds, item (a) is quite expected, item (b) involving a discontinuity is quite surprising, item (c) is totally unexpected, while item (d) is an unexplained phenomenon. Clearly, the photoelectric effect must require an explanation radically differing from classical electromagnetic theory. Einstein's celebrated note of 1905 provided the correct explanation. Going even further than Planck, who limited himself to the introduction of discontinuity in the mechanism of absorption or emission, Einstein postulated that light radiation itself was discontinuous, consisting of a beam of corpuscles, named as photons. A photon is thus a single quantum of electromagnetic radiation and has the energy $h\nu$, where ν is the frequency of the radiation and h is the Planck constant.

According to Einstein's explanation, when a photon strikes a metal surface, a given electron at the surface would receive either *all* of its energy $h\nu$ or *no* energy at all. Thus instead of being spread evenly on the surface, the incident energy would be received by only certain electrons.

Again, as the electron escapes from the metal, it uses up a certain energy, W, in overcoming the surface forces. This energy is called the work function of the surface. Moreover, if the electron originates below the surface, additional amount of energy may be used up in reaching the surface. So, for an electron originating at the surface or one which loses no energy in reaching the surface, the kinetic energy after leaving the surface will be a maximum. Obviously, this maximum kinetic energy will be the difference between the energy $h\nu$ imparted by the incident photon and the energy used up at the surface, W. So,

$$\tfrac{1}{2} m v^2_{max} = h\nu - W \tag{1.11}$$

This is the Einstein photoelectric equation.

Combining this with Eq. (1.10), we have the following equation:

$$eV_s = h\nu - W \tag{1.12}$$

The three experimental laws of photoelectricity, which could not be
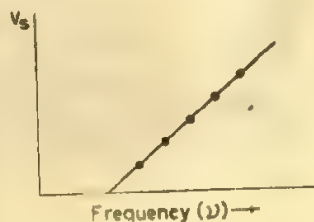
Fig. 1.7 Variation of stopping potential with frequency of incident light

explained on classical grounds can now be accounted for. Thus, from Eq. (1.11), we see that if the energy of the incident photon is less than the energy needed by an electron to escape from the surface, no emission can take place, regardless of the incident light intensity, i.e. the number of photons which strike the surface per second. The threshold frequency below which no electrons are emitted is seen to be W/h from Eq. (1.12):

$$h\nu - W = eV_s = 0, \quad \nu = W/h \tag{1.13}$$

Eqs. (1.11) and (1.12) further show that the maximum kinetic energy as also the stopping potential are independent of intensity but linearly related to frequency of the incident light.

Einstein's photoelectric equation [Eq. (1.12)] was later carefully verified by Millikan. When the maximum kinetic energy of the emitted electrons, i.e. eV_s, is plotted against frequency ν, a straight line (Fig. 1.8) is obtained, the slope of which, according to Eq. (1.12), should be given by

$$\tan\theta = h$$

From a determination of this slope, Millikan found the value of h to be 6.55×10^{-27} erg sec, in accord with the value obtained from black-body measurements. Furthermore, the intercepts on the eV_s-axis and ν-axis are seen to be $-W$ and W/h respectively. The quantity W is called the photoelectric work function of the surface, while W/h, as already explained, is the threshold frequency.

Example 1.1 Assuming that a 25-watt bulb emits monochromatic yellow light of wavelength 0.57μ, calculate the rate of emission of quanta per second.

Solution

Energy of a single quantum of radiation

$$E = h\nu = \frac{(6.62 \times 10^{-27})(3 \times 10^{10})}{0.57 \times 10^{-4}}$$
$$= 3.48 \times 10^{-12} \text{ erg}$$

1 watt = 1 joule/sec = 10^7 erg/sec

Hence, the rate of emission of quanta

$$= \frac{25 \times 10^7}{3.48 \times 10^{-12}} = 7.18 \times 10^{19} \text{ sec}^{-1}$$

Example 1.2 Light of wavelength 4000 Å strikes a certain metal which has a photoelectric work function of 2.13 eV. Find (a) the energy of the photon in eV, (b) the kinetic energy of the
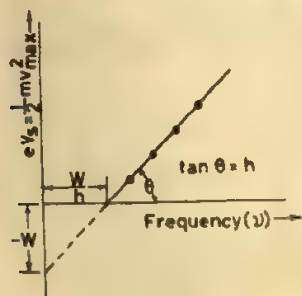
Fig. 1.8 Plot of maximum energy of photoelectrons versus frequency of incident light to verify Einstein's photoelectric equation

most energetic photoelectron in ergs and in eV, (c) the velocity of these electrons, and (d) the stopping potential.

Solution
Frequency of the light of wavelength 4000 Å

$$= \frac{\text{Velocity of light}}{\text{Wavelength}}$$

$$= \frac{3 \times 10^{10} \text{ cm/sec}}{4000 \times 10^{-8} \text{ cm}}$$

$$= 7 \cdot 5 \times 10^{14} \text{ sec}^{-1}$$

(a) Energy of the photon $= h\nu$

$$= 4 \cdot 13 \times 10^{-15} \times 7 \cdot 5 \times 10^{14}$$

$$= 3 \cdot 10 \text{ eV}$$

(b) Photoelectric work function, W

$$= 2 \cdot 13 \text{ eV}$$

$$= 2 \cdot 13 \times 1 \cdot 6 \times 10^{-12} \text{ erg}$$

$$= 3 \cdot 41 \times 10^{-12} \text{ erg}$$

From Eq. (1.11), the kinetic energy of the most energetic electron

$$= \tfrac{1}{2} mv^2{}_{max} = h\nu - W$$

$$= (6 \cdot 62 \times 10^{-27}) \times (7 \cdot 5 \times 10^{14}) - 3 \cdot 41 \times 10^{-12}$$

$$= 1 \cdot 56 \times 10^{-12} \text{ erg}$$

$$= 0 \cdot 97 \text{ eV}$$

(c) The velocity of the most energetic electrons is obtained from

$$\tfrac{1}{2} mv^2{}_{max} = 1 \cdot 56 \times 10^{-12} \text{ erg}$$

Mass of an electron is $9 \cdot 11 \times 10^{-28}$ g.

Hence, $v_{max} = \sqrt{\dfrac{2 \times 1 \cdot 56 \times 10^{-12}}{9 \cdot 11 \times 10^{-28}}}$

$$= 5 \cdot 85 \times 10^{7} \text{ cm/sec}$$

(d) From Eq. (1.10)

$eV_s = \tfrac{1}{2} mv^2{}_{max} = 0 \cdot 97$ eV

Hence the stopping potential $= 0 \cdot 97$ V.

Example 1.3 When a metal surface is irradiated by light of wavelength 300 mμ the stopping potential is found to be 0·5V. Compute the work function and the threshold wavelength. Also calculate the stopping potential required for light of wavelength 200 mμ.

Solution
The frequency ν of the incident light of wavelength

$$300 \text{ m}\mu = c/\lambda$$

$$= \frac{3 \times 10^{10} \text{ (cm/sec)}}{300 \times 10^{-7} \text{ (cm)}}$$

$$= 10^{15} \text{ sec}^{-1}$$

$h = 6 \cdot 62 \times 10^{-27}$ erg sec $= 4 \cdot 13 \times 10^{-15}$ eV sec

Hence, $h\nu = 4 \cdot 13 \times 10^{-15} \times 10^{15} = 4 \cdot 13$ eV

From Eq. (1.10), the maximum kinetic energy is 0·5 eV. Hence from Eq. (1.11), $W = 4 \cdot 13$ − 0·5 = 3·63 eV. According to Eq. (1·13) the threshold frequency is W/h or $3 \cdot 63/(4 \cdot 13 \times 10^{-15})$ or $8 \cdot 78 \times 10^{14}$ sec^{-1}. Hence the threshold wavelength is $3 \times 10^{10}/8 \cdot 78 \times 10^{14}$ cm or 342 mμ.

The quantum energy $h\nu$ of the light of wavelength 200 mμ calculated as above is 6·20 eV. Hence from Eq. (1.12), the stopping potential $= eV_s = 6 \cdot 20 - 3 \cdot 63 = 2 \cdot 57$ eV.

1.5   The Compton Scattering

Planck introduced the idea that radiation must be emitted in quanta
or bundles of energy, but he believed that after being emitted in bund-
les the energy however spreads in waves. In providing his explanation of
the photoelectric effect Einstein extended the quantum idea of Planck
to the absorption of radiation by making the additional assumption that
once a quantum of energy, called photon, was radiated it preserved its
identity until it was finally absorbed. According to the theory of rela-
tivity, mass and energy are equivalent so that mass is energy and energy
can be observed as mass. Since photons have energy, they must have
mass, and if this is true, it should be possible to treat a collision between
a photon and a material particle such as an electron in the same man-
ner as, say, billiard-ball collisions are treated in accordance with the
usual laws of mechanics. Let us then consider a photon striking an elec-
tron which is initially at rest at the origin relative to the coordinate
frame shown in Fig. 1.9. (A correction can be made for the initial ther-
mal motion of the electron, but this motion is negligible compared with
the other velocities in the following analysis.) Let us further assume
that the impact is almost at a grazing angle so that the electron after
receiving the impulse begins to move below the x-axis while the photon
is deflected above the x-axis.

Since the electron is assumed to be at rest, initially, its momentum M_1
is zero and its energy E_1 is only its rest-mass energy which is m_0c^2. The
photon has an energy

$E = h\nu = hc/\lambda$ (1.14)

The photon has no rest mass; so its moving mass, m_p, is equivalent to
its total energy E and is given by
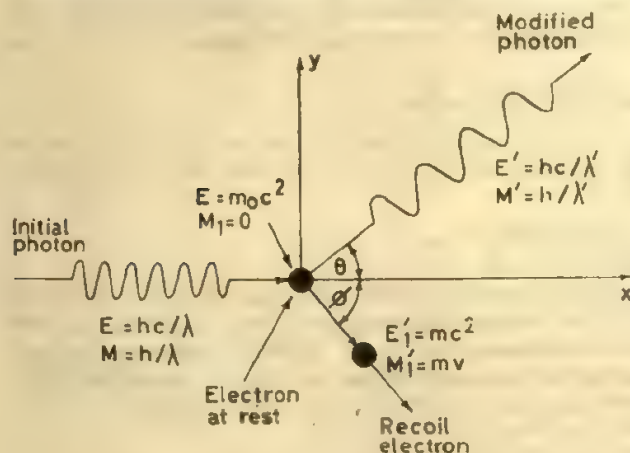
Fig. 1.9   Impact of a photon on a free electron initially at rest

$$m_p = E/c^2 = h/c\lambda \qquad (1.15)$$

The velocity of the photon, as we have seen earlier, is c, and hence its momentum M, which is its mass times its velocity, is

$$M = hc/c\lambda = h/\lambda \qquad (1.16)$$

This is the momentum of the photon moving along the x-axis before the impact. Following the impact its energy is reduced to hc/λ', while its momentum is changed in magnitude and direction to h/λ' at an angle θ to the x-axis.

The electron gains energy from the impact. Let its total energy now be mc^2 and its momentum be mv directed at an angle φ to the x-axis, as shown in Fig. 1.9. It should be noted that the electron mass m in these statements following the impact is the relativistic moving mass.

We will now apply the conservation principles of classical mechanics to the impact situation as stated above and summarized in Fig. 1.9. We will treat this collision just as if it were a collision between two balls, one moving and the other at rest. Thus, applying the law of conservation of energy we obtain

$$\frac{hc}{\lambda} - \frac{hc}{\lambda'} = mc^2 - m_0 c^2 \qquad (1.17)$$

Momentum, unlike energy, is a vector quantity, having magnitude as well as direction, and in the collision involving two bodies momentum must be conserved in each of two mutually perpendicular directions. Applying this principle we may write for the x-component of the momentum,

$$\frac{h}{\lambda} = \frac{h}{\lambda'} \cos\theta + mv \cos\varphi \qquad (1.18)$$

and for the y-component,

$$0 = \frac{h}{\lambda'} \sin\theta - mv \sin\varphi \qquad (1.19)$$

The rest mass, m_0, of the electron is known and so also the wavelength λ of the incident photon. Then experimentally we can measure the wavelength λ' of the scattered photons as a function of the angle of scattering, θ. We however find that, in addition to the variables λ' and θ, the three equations (1.17) to (1.19) contain three other variables, m, v, φ; the last three variables must then be eliminated so as to facilitate an experimental test of the theory we are developing. We first eliminate φ between Eq. (1.18) and (1.19) by separating the terms containing φ, squaring the resulting equations and then adding them, whereupon we obtain:

$$m^2 v^2 = h^2 \left(\frac{1}{\lambda^2} - \frac{2\cos\theta}{\lambda\lambda'} + \frac{1}{\lambda'^2} \right) \qquad (1.20)$$

We now use the relativistic interdependence of m and v given by the equation

$$m = \frac{m_0}{\sqrt{1 - \dfrac{v^2}{c^2}}}$$

which on squaring and rearranging, further yields

$$m^2 v^2 = c^2(m^2 - m_0^2) \tag{1.21}$$

Eliminating v between Eqs. (1.20) and (1.21) we obtain

$$c^2(m^2 - m_0^2) = h^2 \left(\frac{1}{\lambda^2} - \frac{2 \cos\theta}{\lambda\lambda'} + \frac{1}{\lambda'^2} \right) \tag{1.22}$$

In order to eliminate m, we next solve Eq. (1.17) for m, square it and substitute into Eq. (1.22). The resulting equation, on simplification, assumes the form of Eq. (1.23) which gives the change in wavelength between the original photon and a photon scattered at an angle θ:

$$\Delta\lambda = \lambda' - \lambda = \frac{h}{m_0 c} (1 - \cos\theta) \tag{1.23}$$

Thus the scattered wavelength is always greater than the incident wavelength. Eq. (1.23) was derived by Compton in the early 1920's to describe the change in wavelength of X-rays produced by scattering — a phenomenon first observed by him and known as the *Compton effect*. The experiments carried out by Compton verified the predictions of this theoretical equation quite accurately and thus gave additional support to the hypothesis of the quantum nature of radiation.

Example 1.4 A monochromatic X-ray beam whose wavelength is 0·558 Å is scattered through an angle of 46°. What is the wavelength of the scattered beam?

Solution If numerical values of the constants are put into Eq. (1.23), we find that the constant $(h/m_0 c)$ has the value $2 \cdot 426 \times 10^{-10}$ cm. Expressing the wavelength shift in angstroms, Eq. (1.23) then becomes

$$\Delta\lambda = \lambda' - \lambda = 0 \cdot 02426 \ (1 - \cos\theta)$$

Since $\cos 46° = 0 \cdot 6947$,

$$\lambda' = 0 \cdot 558 + 0 \cdot 02426 \ (1 - 0 \cdot 6947)$$
$$= 0 \cdot 565 \ \text{Å}$$

The experimental demonstration of the Compton effect can be made with apparatus which is schematically represented in Fig. 1.10. A beam of monochromatic X-rays of known wavelength is directed at a target of the scattering substance, and the wavelengths of the scattered X-rays are determined, at various angles θ, with the help of an X-ray spectrometer, which can be swung in an arc about the scatterer. The results, presented in Fig. 1.11, give the wavelengths as predicted by Eq. (1.23). The solid vertical lines in Fig. 1.11 are the unmodified lines and correspond to the initial wavelength, λ, while the broken lines M (representing the modified lines) correspond to the modified wavelength, λ', of Eq. (1.23). The fact that at each angle the scattered X-rays also include a substantial proportion having the initial wavelength may appear sur-
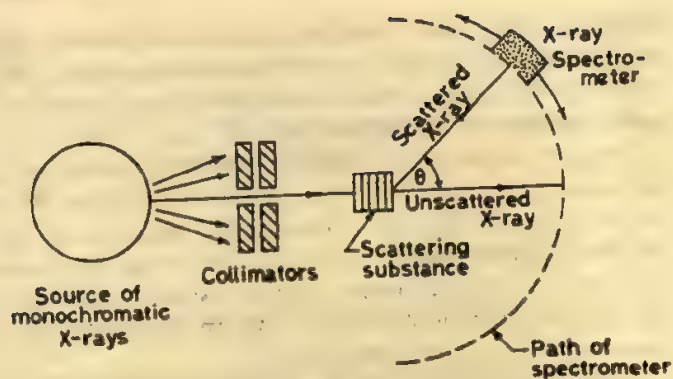
Fig. 1.10 Schematic diagram of the apparatus for measuring Compton scattering

prising at the first look but is not hard to understand. If the photon collides with a tightly-bound electron, the entire atom recoils instead of the single electron. In this event, the value of m_0 in Eq. (1.23) becomes the mass of the entire atom rather than the mass of an electron. Since the mass of the atom is several thousand times greater than that of an electron, the Compton wavelength shift due to collision is accordingly too small to be detectable. This accounts for the presence of the unmodified line in the spectrum of the scattered radiation. There are, however, electrons in matter which are either free or loosely bound. These electrons, when hit, modify the photon wavelength, and the wavelength displacement of the modified line M in the spectrum of the scattered radiation (Fig. 1.11) is then given by Eq. (1.23). [It will be recalled that in deriving Eq. (1.23) we assumed that the electron getting scattered was at rest initially. The broadening of the peaks (see Fig. 1.11) of both
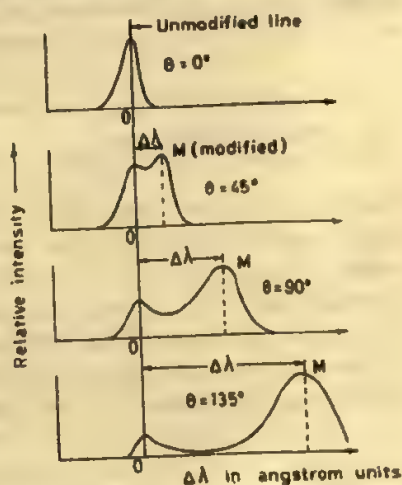
Fig. 1.11 Compton scattering: Wavelength displacement of the modified line (M) of scattered X-rays for different scattering angles.

the unmodified and modified photons is however due to the motion of the target electron. Because of this motion some photons undergo a change of energy which is a little more or less than would be expected for electrons which are initially at rest.]

For very high-energy photons most of the atomic electrons appear free, and consequently, a large fraction of the incident photons suffer a Compton wavelength shift. For low-energy photons, on the other hand, most electrons appear bound. For still lower energy photons, such as visible photons, all the electrons appear bound; consequently, no Compton wavelength shift is observed and, in its place, the photoelectric effect assumes the greatest importance.

We thus see that the likelihood of a Compton wavelength shift depends on the incident photon energy and the scattering material. It should be noted, however, that the amount of wavelength shift is independent of the value of the incident wavelength (and hence energy) and of the nature of the scattering material. This aspect of the Compton scattering, as implied by Eq. (1.23), has also been supported by experiments. The photoelectric effect is stronger than the Compton effect when X-rays of energy less than $0 \cdot 1$ MeV are used. In the process involved in the photoelectric effect, the energy of an X-ray photon is completely given up to an electron of the atomic system. Since it is impossible for a photon to give up all its energy to a free electron, the photoelectric effect can take place only when photons strike bound electrons. At higher X-ray energies (about $0 \cdot 1$ MeV) the Compton scattering becomes more important; an X-ray photon in this case is scattered and not really absorbed, since it does not lose a very large fraction of its energy. At still higher energies, above 1 MeV (wavelengths less than $0 \cdot 012$ Å), the process of *pair formation* plays a part in the absorption of X-rays. This process becomes more important than either photoelectric absorption or Compton scattering as the photon energy increases.

1.6 Pair Formation

Gamma rays are very short electromagnetic waves. We can describe these rays as photons whose energy range overlaps that of X-rays and extends to several MeV. Under suitable conditions a gamma-ray photon converts itself into a pair of material particles — a positive electron and a negative electron. The former is called the *positron*, while the word electron is used only for negative electrons. Since in this process of pair formation, discovered by Anderson in 1932, two particles, each of mass m_0, are being created out of energy, the initial gamma-ray energy must at least be equal to $2m_0c^2$. According to the Einstein mass-energy relation $E = mc^2$, the energy required to create an electron is $0 \cdot 511$ MeV.

Thus, pair formation cannot take place until the energy of the photon is at least 1·022 MeV, which is thus the threshold energy for pair formation. Experimentally, this is found to be true. If the initial photon energy is greater than this threshold value, the excess appears as kinetic energy shared equally by the positron and the electron.

Suggested Reading

RICHTMYER, F. K., E. H. KENNARD, and T. LAURITSEN, *Introduction to Modern Physics*, 5th Ed., McGraw-Hill, New York, 1955.

BLIGH, N. M., *The Evolution and Development of the Quantum Theory*, Longmans Green, New York, 1926.

HUGHES, A. L. and L. A. DUBRIDGE, *Photoelectric Phenomena*, McGraw-Hill, New York, 1932.

COMPTON, A. H., *Phys. Rev.*, 21, 483, (1923).

Problems

1.1 An enclosure having an opening of 1 cm² area is heated to a temperature of 800°K. Calculate the rate of emission of the total energy at this temperature.

1.2 Find the wavelength and frequency of a photon of energy 5×10^{-12} erg.

1.3 Find the frequency of an X-ray photon whose momentum is $1·2 \times 10^{-18}$ g. cm/sec.

1.4 Find the number of visible quanta emitted per second by a 100-W incandescent bulb. Assume that 5% of the energy consumed by the bulb is radiated as visible light, at a wavelength of 5600 Å.

1.5 The threshold wavelength for photoelectric emission from tungsten is 2,300 Å. Calculate the velocity of the fastest electrons emitted as the result of absorption of light of wavelength 1800 Å.

1.6 The threshold frequency for photoelectric emission from lithium is $5·77 \times 10^{14}$ sec⁻¹. Find the energy in ergs and electron volts for the fastest photoelectrons emitted when light of frequency $7·5 \times 10^{14}$ sec⁻¹ is directed on a lithium surface.

1.7 Prove that the maximum value of the Compton wavelength shift is 0·0485.

1.8 A beam of X-rays when scattered by free electrons shows a wavelength change of 0·007. Find the angle of scattering.

1.9 An X-ray photon of initial frequency 2×10^{20} sec⁻¹ collides with an electron. Find the frequency of the photon scattered through an angle of 45°.

Atomic Spectra and the Bohr-Rutherford Atomic Model

2.1 Introduction

The quantum hypothesis, which was introduced by Planck, received brilliant confirmation at the hands of Einstein in his explanation of the laws of photoelectric emission and obtained very strong support from the Compton effect. It was, however, not until Niels Bohr produced his theory of the structure of the hydrogen atom in 1913 that the quantum theory made another decisive stride. Bohr's imaginative use of the quantum theory gave it a new dimension and opened the way for its application in the study of atomic dynamics.

Bohr's advance has to be viewed against the background of the then existing knowledge of the quantum theory, the atomic spectra, and the atomic structure. We have already seen in Chapter 1 the early stages in the development of the quantum theory. We now give an account of what was known about atomic spectra and atomic structure till 1913 before starting out on a discussion of Bohr's theory.

2.2 Atomic Spectra

The experimental knowledge of atomic spectra has accrued from the use of instruments, known as spectroscopes, which are capable of analysing light according to its distribution of frequency or colour. Essentially,

spectroscopes contain an entrance slit and lens, a dispersing device such as a prism (which disperses, i.e. separates light into component colours by refraction) or grating (which disperses light by diffraction), and an optical system either for visual observation or for producing an image of the slit on a detector, commonly a photographic plate. The spectrum produced in this way consists of a series of lines, each being an image of the slit produced by the radiation of a particular wavelength. Consequently, light which has continuous frequency distribution such as the light emitted by a hot solid body, forms a continuous succession of slit images giving the appearance of a wide image. On the other hand, light having discontinuous distribution of frequency gives rise to discrete slit images called spectral lines. Such discontinuous spectral lines are produced by the light from any element in gaseous form. The spectral lines occupy definite positions and thus correspond to definite wavelengths or frequencies. And because of the extreme sharpness of the spectral lines the respective wavelengths can be measured with a large degree of precision.

Two types of spectra can be clearly distinguished, the *line spectra* and the *band spectra*. The line spectra consist of distinct lines and are produced by gaseous atoms; consequently, the line spectra are often referred to as *atomic spectra*. But the spectra produced by gaseous molecules contain distinct bands, which are, in fact, families of closely spaced lines.

Every chemical element emits a characteristic line spectrum when the atoms are excited in a flame, a furnace or an electric arc. Each element can therefore be identified by its spectrum analysis. It may be noted in passing that whereas gases and vapours, containing either atoms or molecules, emit discontinuous spectrum when excited, the light emitted by hot solid bodies, however, represents a mixture of all wavelengths and hence forms a continuous spectrum.

In the emission spectrum of a hot gas the spectral lines appear as bright lines when viewed through a spectroscope. Many of these spectral lines may also appear as dark lines on the continuous background in a spectrum if a continuous radiation such as white light emitted by a hot solid body is passed through the gas and observed spectroscopically. Generally, the dark line (which shows that light of the corresponding wavelength has been absorbed) appears exactly at the same position as the bright line appears in the emission spectrum of the same element in gaseous form. This means that the wavelengths absorbed by a given type of atom (or molecule) are identical with wavelengths emitted by the same atom (or molecule). The best known example of absorption lines is the multitude of thin dark lines which appear in the continuous spectrum of the sunlight. These lines discovered by Fraunhofer in the early part of the nineteenth century are known as Fraunhofer lines. These lines occur because the luminuous part of the sun, which emits continuous radiation almost exactly according to theoretical predictions for

any object at a temperature of 5800°K, is enveloped by cooler gases which absorb light of certain wavelengths. The study of Fraunhofer lines is thus a source of definite information about the chemical composition of the sun. It has been revealed by such study that, save for the large predominance of hydrogen and helium, the chemical composition of the sun is identical with that of our earth.

The simplest spectrum, as might be anticipated, is that of atomic hydrogen. Fig. 2.1 illustrates a part of the hydrogen-atom spectrum in the visible region. It was discovered by Balmer, as early as 1885, that the wavelengths λ of the nine lines, then known in this spectrum, could be accurately expressed by the simple formula,

$$\lambda = K\,\frac{n^2}{n^2 - 4} \tag{2.1}$$

where K is a constant and n an integer.

The different wavelengths corresponding to the lines H_α, H_β, H_γ, H_δ etc., are obtained by putting the integers 3, 4, 5, 6 etc., respectively, in place of n. This set of lines constitutes a spectral series and is known as the Balmer series.

It is seen from Eq. (2.1) that the value of n cannot be less than 2, since λ would then be a negative number, which is meaningless; the value of n cannot be 2 either since λ would then be infinite. As integer n becomes greater than 2, the corresponding wavelength λ becomes smaller. But when the value of n is already large, its further increase, however, causes λ to decrease only very slightly, the latter ultimately reaching the limiting value of K when n approaches infinity. This situation is reflected in the continuous radiation, in Fig. 2.1, at wavelengths less than that corresponding to this limit.

In spectroscopic work, frequencies are commonly expressed in terms of wavenumbers, that is, the number of waves per unit length, denoted by $\bar{\nu}$ (in cm⁻¹) and given by the reciprocal of wavelength. It should be noted, however, that the true frequency is the number of vibrations per second, ν sec⁻¹. Expressing in terms of wavenumber, Eq. (2.1) is rearranged as
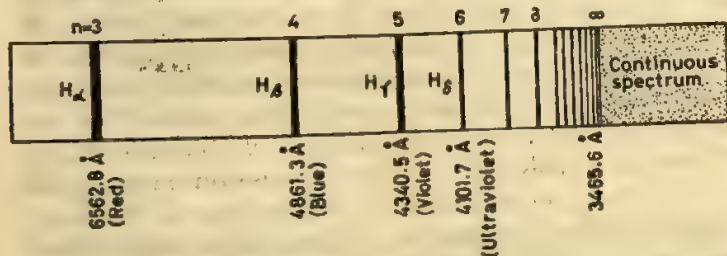
Fig. 2.1 Balmer series of atomic hydrogen excited by an electric discharge. The dark lines correspond to the bright emission lines of the spectrum.

$$\overline{\nu} = \frac{1}{\lambda} = R\left(\frac{1}{2^2} - \frac{1}{n^2}\right) \qquad (2.2)$$

Here R denotes a frequency constant having the value 109,677·8 cm^{-1} and is usually called the *Rydberg constant* in tribute to the Swedish physicist Rydberg who found this frequency to occur in expressions for the spectral lines of a number of elements. Rydberg showed that besides the simple spectrum of hydrogen, the spectra of many other elements contain a series of lines whose frequency (wavenumber) is approximately given by

$$\overline{\nu} = \frac{1}{\lambda} = A - \frac{R}{(n + \alpha)^2} \qquad (2.3)$$

where R is the Rydberg constant and n is a running integer, while A and α are adjustment constants that depend on the element and the spectral series or the part of the spectrum to which the equation is applied.

Ritz, in 1908, introduced his *combination principle*, which, in its simplest form, states that *the wavenumber of any spectral line can be represented as the combination of two terms*. Ritz noted that the term A of the Rydberg equation [Eq. (2.3)] was indeed a particular value of a term just like the second term of the same equation. Using this combination principle Ritz rewrote the Rydberg equation as

$$\overline{\nu} = \frac{R}{(m + \beta)^2} - \frac{R}{(n + \alpha)^2} \qquad (2.4)$$

where α and β are adjustment constants which depend on the element; m takes on different integral values for different spectral *series*. Throughout each spectral series, however, m remains constant, while n takes on different integer values corresponding to the different lines in the same series. Obviously, Balmer formula for hydrogen is a special case of Eq. (2.4), that is, when $\alpha = \beta = 0$ and $m = 2$.

In the same year, 1908, Paschen discovered another spectral series for atomic hydrogen in the infrared region. Eq. (2.4) could be fitted to this series, called Paschen series, by making $\alpha = \beta = 0$, $m = 3$ and $n = 4$, 5, 6, etc. Two more series were later found in the infrared region for the hydrogen-atom spectrum by Brackett (1922) and Pfund (1924) respectively. In the ultraviolet region also, one series had earlier been observed by Lyman (1906, 1916). All these series were found to be in excellent agreement with the requirements of Eq. (2.4), α and β being zero with m and n having integral values, as shown in Table 2.1. Thus all the hydrogen series could be represented by the general equation,

$$\overline{\nu} = \frac{R}{m^2} - \frac{R}{n^2} \qquad (2.5)$$

where R is the Rydberg number, as given before, and m and n are integers, the former being constant and n varying throughout in any given series (Table 2.1).

Table 2.1 The Atomic Spectrum of Hydrogen

Series	Region	m	n
Lyman	Ultraviolet	1	2,3,4,......
Balmer	Visible	2	3,4,5,......
Paschen	Near-infrared	3	4,5,6,......
Brackett	Far-infrared	4	5,6,7,......
Pfund	Far-infrared	5	6,7,........

Though Eq. (2.5) represented with great precision the entire known spectrum of atomic hydrogen, it was however only an empirical formula derived from experiments. The interpretation of this correct but underived formula was first given by the theory of Niels Bohr (1913).

2.3 The Thomson Model of the Atom

The early studies of atomic spectra, as described above, dealt with the identification of various lines and the mathematical formulation of the results, but the fundamental question as to why atoms begin to emit light when heated remained a mystery. The first model of the atom, propounded in 1898 by the English physicist Thomson, that pictured atoms as uniform spheres of positively charged substance ('positive electric fluid') with negative electrons (in quantities sufficient to neutralize the charge) embedded in it, seemed to solve this mystery. The electrons were supposed to assume certain stable positions inside the atomic body as a result of two forces — attraction by the centre of positive charge and repulsion by other electrons. If this distribution were disturbed by some applied energy, the electrons were supposed to vibrate about their equilibrium positions causing emission of light waves of corresponding frequencies. However, attempts to correlate the calculated emission frequencies of electrons in Thomson's atom with those actually observed for different elements met with no success. Moreover, Thomson's model could not explain, in terms of classical electromagnetism, the stability of the atomic charge system. Thus in view of Earnshaw's classical theorem which states that no system of charged particles can remain in static equilibrium under the action of electrostatic forces alone, the matrix of positive charges in Thomson's atoms would indeed be expected to fly apart. Despite the importance of the problem, it was only after 13 years that a definite experimental test of the Thomson model was made. This experiment, performed by Geiger and Marsden in 1911 at the suggestion of Ernest Rutherford, compelled the abandonment of Thomson model, leaving in its place a new concept of atomic structure.

2.4 The Rutherford Nuclear Atom

Rutherford probed matter with alpha particles and developed a model of the nuclear atom. Alpha particles are doubly ionized helium atoms, i.e. helium atoms that have lost two electrons leaving them with two units of positive charge. Alpha particles are spontaneously emitted by certain radioactive elements. Radium, for example, is an excellent source of high-energy alpha particles.

It was realized by Rutherford that very important information about the inner structure of atoms could be gained from the study of collisions between fast-moving alpha particles and the atoms constituting a target. In the classic experiment of Geiger and Marsden, performed at Rutherford's suggestion, a speck of alpha-particle-emitting radioactive material was placed behind a lead screen that had a small hole in it and the resulting narrow beam of alpha particles was directed at a thin gold foil, as in Fig. 2.2. On the other side of the foil was placed a zinc sulphide screen which produced visible flashes, called scintillations, when struck by an alpha particle. Geiger and Marsden found that, while most of the alpha particles went straight through the foil or were deflected only by very small amounts, some were, however, deflected through large angles, and what was more, a few particles were even deflected back to the side from which they came. This behaviour was at variance with what would be anticipated from the Thomson atomic model. Since in this model the charges within an atom were assumed to be uniformly distributed throughout its volume, alpha particles in passing through a thin metallic foil would, if this model were correct, experience only weak electric forces and hence their initial moments should be enough to carry them through with only slight deflections at the most.

The scattering results of Geiger and Marsden were thus incompatible with the Thomson model of the atom. Rutherford further showed that the observed large-angle scattering could not be explained as being the combined effect of a series of successive small deflections caused by the
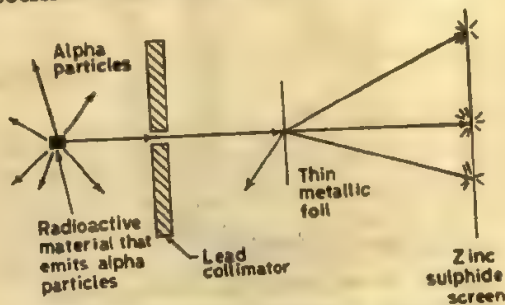
Fig. 2.2 Schematic diagram of apparatus for observing the scattering of alpha particles

atoms of the foil. This led him to the consideration that the large-angle scattering of an alpha particle resulted from a *single* encounter between the particle and a metal atom; and then he showed, on the basis of this consideration, that the large scattering angles through which some of the alpha particles were deflected could be explained by assuming the whole of the positive charge of the atom to be concentrated in a very small region, or nucleus, of the whole atom. He then postulated that surrounding the central nucleus at some distance away from it there were necessary number of electrons — the extra-nuclear electrons — to give a neutral atom. The electrons, being so light, will not appreciably affect the motion of fast-moving alpha particles, the majority of which will therefore pass through the atom without significant scattering; but an occasional alpha particle which happens to move into the strong electric field in the vicinity of the positively charged tiny nucleus, will be violently deflected from its course.

The quantity actually measured in the scattering experiment is the number, $N(\theta)$, of alpha particles per unit area striking the screen at an angle θ. If a total of N_i alpha particles strike the foil during the course of the experiment, the fraction, $f(\theta)$, of the total number of alpha particles scattered over unit area (of the fluorescent screen) at a distance r from the scattering nucleus in a direction making an angle θ with the original direction of incidence (see Fig. 2.3) is given by the Rutherford scattering formula:

$$f(\theta) = \frac{N(\theta)}{N_i} = nt\left(\frac{Ze^2}{mv^2r}\right)^2 \operatorname{cosec}^4 (\theta/2) \tag{2.6}$$

where n is the number of atoms per unit volume of the scattering foil material, and t is its thickness; Z is the number of unit charges on the
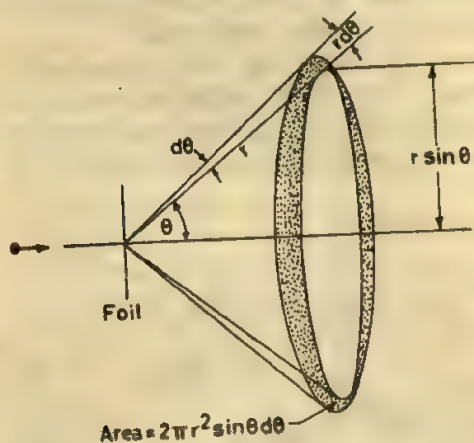
Fig. 2.3 In the Rutherford scattering experiment particles scattered between θ and $\theta + d\theta$ are detected

nucleus and e is the electronic charge; m is the mass and v is the velocity of the alpha particle. The experimental data confirmed the general accuracy of this famous formula and thereby also Rutherford's atom model from which the formula was derived.

Example 2.1 A beam of 5-MeV alpha particles is incident normally on a gold foil of thickness 10^{-4} cm. What fraction of the incident particles that undergo single Rutherford type scattering would be received by a detector per unit area at an angle 60° with respect to the incident direction and at a distance 20 cm from the point of traversal of the foil?

Solution. We begin by finding n, the number of gold atoms per unit volume in the foil, from the relationship

$$n = (\text{atoms/mass}) \times (\text{mass/volume})$$
$$= (N_0/w)\rho$$

where N_0 is Avogadro number, ρ the density of gold and w its atomic weight. Since $N_0 = 6 \cdot 02 \times 10^{23}$ atoms/g mole, $\rho = 19 \cdot 32$ g/cm^3 and $w = 197$, we have

$$n = \frac{6 \cdot 02 \times 10^{23} \times 19 \cdot 32}{197} = 5 \cdot 90 \times 10^{22} \text{ atoms/cm}^3$$

The kinetic energy T of the alpha particle is 5 MeV, which is $5 \cdot 0 \times 10^6$ eV $\times 1 \cdot 60 \times 10^{-12}$ erg/eV $= 8 \cdot 0 \times 10^{-6}$ erg.

$$T = (1/2)mv^2$$

Therefore $mv^2 = 2 \times 8 \cdot 0 \times 10^{-6}$ erg. The atomic number Z of gold is 79, and $\theta = 60°$. From Eq. (2.6) we find that

$$f(\theta) = 5 \cdot 9 \times 10^{22} \times 10^{-4} \times \left[\frac{(79) \times (4 \cdot 8 \times 10^{-10})^2}{(16 \cdot 0 \times 10^{-6}) \times (20)} \right] \times 16$$

$$= 3 \cdot 05 \times 10^{-7}$$

The magnitude of the deflection that an alpha particle experiences when it passes near an atomic nucleus depends on the magnitude of the latter's charge. So by comparing the relative scattering of alpha particles by different target materials the nuclear charge of the atoms involved can be estimated. It was found in this way that all of the atoms of any one element had the same nuclear charge, but from element to element in the periodic table the nuclear charge increased regularly. The nuclear charge was always found to be an integer multiple of $+ e$; this integer, denoting the number of unit positive charges in the nucleus of an element, is called the *atomic number* of the element.

2.5 Dimensions of the Nucleus

As we have seen above, the Rutherford scattering of alpha particles is due to their interaction with the nucleus. The charge on the alpha particle carrying two units of positive charge is $+ 2e$ and that on the nucleus having an integral number Z of positive charges is $+ Ze$, and so, if Coulomb's law applies, the repulsive force at a distance r from the nucleus is (2.7)

$$F = 2eZe/r^2$$

Though the alpha particle and the atomic nucleus of the scattering

metallic foil both experience the force given by Eq. (2.7), the nucleus is so much more massive than the alpha particle that it remains fixed during the interaction. We see, moreover, from Eq. (2.7) that the force on the alpha particle is inversely proportional to the square of its distance from the nucleus. It is shown in advanced mechanics that such a force always results in an orbit. When the force is attractive such as that between the sun and planets of the solar system, the orbits are parabolas, ellipses, as also circles or straight lines as special cases of the latter. When, however, the force is repulsive the orbit is hyperbolic (or its degenerate form, a straight line). So in the present case, the path of the alpha particle is, in general, a hyperbola with the nucleus at the outer focus (Fig. 2.4). If the alpha particle is not perfectly aimed, as it will generally be the case, the particle will begin moving parallel to a line (AO), which is one asymptote of a hyperbolic orbit. Because of the repulsive force which varies with $1/r^2$, as given by Eq. (2.7), the alpha particle moves away from this asymptote of its trajectory and finally straightens out to become parallel to the other asymptote (OC) of the hyperbolic orbit. The alpha particle is thus scattered through an angle θ, which is the angle between these two asymptotes. While moving along a hyperbolic trajectory, as shown in Fig. 2.4, the alpha particle is nearest to the nucleus at the point B. If, however, no force were exerted on the alpha particle, it would move past the nucleus along a straight line, viz. AO in the present case, and the minimum distance to which the alpha particle would approach the nucleus under such a condition is called the *impact parameter* (b in Fig. 2.4). In other words, the *impact parameter* is the minimum distance between the nucleus and the asymptotic direction of approach of the alpha particle. The angle of scattering θ is obviously related to the impact parameter b; mathematically this relation is given by

$$\tan \frac{\theta}{2} = 2Ze^2/mv^2b \tag{2.8}$$

where m is the mass and v is the velocity of the particle; the charge on the nucleus is Ze, corresponding to the atomic number Z, and that on the alpha particle is $2e$.
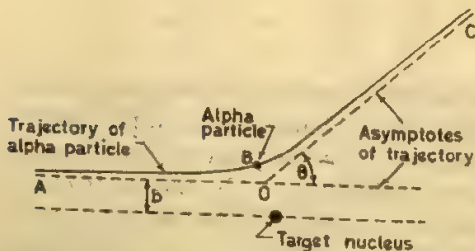
Fig. 2.4 Trajectory of an alpha particle scattered by the Rutherford nuclear atom

Example 2.2 A 5-MeV alpha particle is scattered by 10° when it approaches a gold nucleus ($Z = 79$). Calculate the impact parameter.

Solution. From Eq. (2.8)

Impact parameter $b = \dfrac{2\,Ze^2}{(mv^2)\left(\tan\dfrac{\theta}{2}\right)}$

We have

$Z = 79$

$e = 4{\cdot}8 \times 10^{-10}$ e.s.u. ($g^{1/2}$ cm $^{3/2}$ sec^{-1})

$mv^2 = 2 \times$ kinetic energy

$\quad = 2 \times 5 \times 10^6$ eV $= 2 \times 5 \times 10^6 \times 1{\cdot}6 \times 10^{-12}$ erg

$\tan \theta/2 = \tan 5° = 0{\cdot}0875$

Therefore, $b = 2{\cdot}6 \times 10^{-11}$ cm

Example 2.3 Determine what fraction of a beam of 7·5-MeV alpha particles incident upon a 3×10^{-5} cm thick gold foil is scattered by 90° or more.

Solution. Implicit in Eq. (2.8) is the assumption that both the alpha particle and the nucleus it interacts with are small enough to be considered as point objects. Equation (2.8) further tells us that all alpha particles approaching a target nucleus with an impact parameter b or less will be scattered through an angle of θ or more. We can therefore assume that an alpha particle that is initially projected anywhere within an area πb^2 around the nucleus would be scattered through the angle θ or more. The area πb^2 is thus, the cross-section for scattering through θ or more, per nucleus. If the metallic foil, used as a target, is of thickness t and contains n atoms per unit volume, a target area A of the foil contains ntA nuclei. The aggregate cross-section for scattering through angles of θ or more is this number of target nuclei multiplied by the cross-section for such scattering per nucleus, i.e. $ntA\pi b^2$. The fraction f of incident alpha particles scattered through θ or more is then equal to the ratio between this aggregate cross-section and the total target area A. So,

$\quad f = ntA\pi b^2/A = \pi ntb^2$

Combining this with Eq. (2.8) we get

$\quad f = \pi nt\left(\dfrac{2\,Ze^2}{mv^2}\right)^2 \cot^2\dfrac{\theta}{2}$

$n = 5{\cdot}9 \times 10^{22}$ atoms/cm^3 (from Example 2.1)

$t = 3 \times 10^{-5}$ cm

$Z = 79$

$e = 4{\cdot}8 \times 10^{-10}$ e.s.u.

$mv^2 = 2 \times 7{\cdot}5 \times 10^6 \times 1{\cdot}6 \times 10^{-12}$ erg

$\cot \dfrac{\theta}{2} = \cot 45° = 1$

Therefore, $f = 1{\cdot}28 \times 10^{-5}$

Thus, with a gold foil 3×10^{-5} cm thick approximately four alpha particles in 300,000 are deflected through 90° or more.

At large values of b, θ will be practically zero and consequently the alpha particle will suffer little deflection (Fig. 2.5). This is the case of a wide miss, and this, in fact, is most common. The other extreme is the case of perfect aim, where the alpha particle is aimed perfectly at the nucleus; corresponding to this head-on approach, b is zero and so according to Eq. (2.8), θ is 180°, which means that the alpha particle will be deflected back along the same line by which it approached (Fig. 2.5). Analysing this situation we can derive a simple expression for determin-
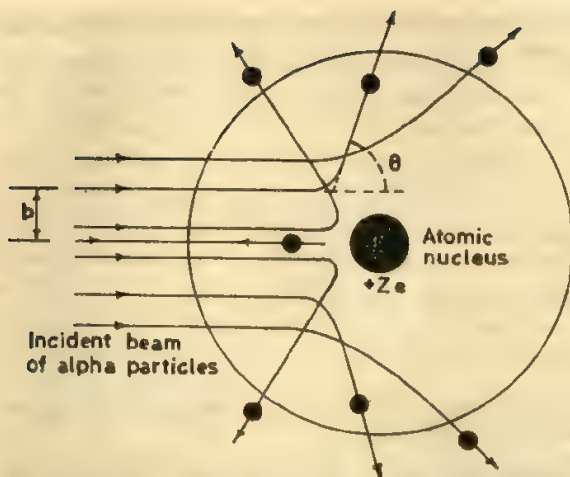
Fig. 2.5 Schematic representation of the scattering of alpha particles by an atom showing that the scattering angle θ decreases with increasing impact parameter, *b*. When *b* is zero, as in the case of perfect aim, the particle is deflected back along the line of approach. The extra-nuclear region of the atom is occupied by atomic electrons, which, being so light, do not appreciably affect the motion of alpha particles.

ing the size of the nucleus. Thus supposing, as a rough approximation, that the alpha particle commences to reverse its direction when its kinetic energy $(mv^2)/2$ is equal to the potential energy [cf. Eq. (2.18)] due to repulsion as given by Eq. (2.7), the distance of closest approach r_0 at which this occurs is given by

$$\frac{1}{2} mv^2 = \frac{2Ze^2}{r_0} \qquad\qquad (2.9)$$

or $\qquad r_0 = 4\,Ze^2/mv^2 \qquad\qquad\qquad\qquad\qquad (2.10)$

This r_0 may be taken as the effective radius of the nucleus. The mass of the alpha particle, which is four times that of the hydrogen atom, is $4 \times 1·67 \times 10^{-24}$ g; the velocity v of an alpha particle is approximately 2×10^9 cm per sec. Taking the electronic charge as $4·8 \times 10^{-10}$ e.s.u. and taking Z as 79, which is the atomic number of gold, a typical foil material, the value of r_0 is found to be $2·72 \times 10^{-12}$ cm. Other similar calculations made of the smallest distance of approach between an atomic nucleus and an alpha particle indicate that all nuclear radii are of the order of 10^{-12} to 10^{-13} cm. This is very much less than the radius of the space the atom occupies, as computed, for instance, from the density of the metal and the Avogadro number or from the kinetic theory of matter. The atomic radius is about 10^{-8} cm. The radius of an atomic nucleus must therefore be well under 1/10,000 the radius of the atom as a whole.

Furthermore, the distance of nearest approach as computed above is only an upper limit to the nuclear dimension at which Coulomb's law still applies. It is thus clear that an atom is mostly 'empty' space, the most massive part of the atom being concentrated in a region of density about 10^{13} g/cm^3.

2.6 Electron Orbits

The Rutherford model of the atom that emerges from the above discussion is a tiny, massive, positively charged nucleus surrounded by electrons at a relatively large distance. The positive charge of the nucleus is equal to the atomic number of the element multiplied by the electronic charge, and the surrounding electrons are also equal in number to the atomic number of the element, so that the atom, as a whole, is electrically neutral. The electrons in the Rutherford atom cannot be stationary, since there is nothing to hold them in place against the electrostatic attractive force exerted by the nucleus. The electrons are therefore postulated to move around the nucleus in dynamically stable orbits, in much the same way as the planets revolve round the sun. The application of Newton's laws of motion and Coulomb's law of electric force to this model then affords a way of calculating the radius of the electron orbit. Thus, for instance, the total energy E_t (which is the binding energy) of the orbital electron in the hydrogen atom is related to its orbit radius by

$$E_t = - e^2/2r \tag{2.11}$$

It is known from experiments that 13.6 eV is required to dissociate the hydrogen atom into a proton and an electron; so its binding energy E_t $= - 13\cdot6$ eV. Taking the electronic charge e as $4\cdot8 \times 10^{-10}$ e.s.u. (g$^{1/2}$ cm$^{3/2}$ sec^{-1}) and the energy E_t in ergs, as $13\cdot6 \times 1\cdot6 \times 10^{-12}$ erg, we can find the radius of the electron orbit in a hydrogen atom from Eq. (2.11) to be:

$$r = - \frac{e^2}{2 E_t} = - \frac{(4\cdot8 \times 10^{-10})^2}{2 \times (- 13\cdot6 \times 1\cdot6 \times 10^{-12})}$$
$$= 0\cdot53 \times 10^{-8} \text{ cm}$$

This order of magnitude of an atomic radius is in satisfactory agreement with estimates made in other ways.

The Rutherford atomic model is therefore consistent with Newton's laws of motion and with Coulomb's law, both pillars of classical physics. But when viewed in terms of electromagnetic theory, another pillar of classical physics, the Rutherford atom appears to be highly unstable. Electromagnetic theory predicts that oscillating or revolving electric charges radiate energy in the form of electromagnetic waves, and the predictions, whenever they have been directly tested, have always accorded with experiment. So the atomic electron, as it moves in an
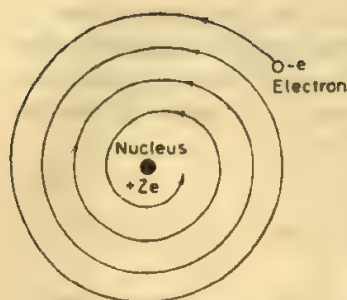
Fig. 2.6 An electron in the Rutherford atom spirals into the nucleus as it radiates energy due to acceleration

orbit, will continuously lose energy in the form of electromagnetic waves, and will consequently move, as can be seen from Eq. (2.11), into orbits of successively smaller radii (Fig. 2.6) radiating more and more energy of higher and higher frequency, until it plunges into the nucleus when all its rotational energy has been spent on the electromagnetic radiation. And all this could happen within an extremely short period of time. For instance, Bohr showed from calculations that the emission of electromagnetic radiation would cause the orbiting electron to lose all its energy and fall into the nucleus within one hundred-millionth of a second! This catastrophe would have to happen to a classical atom, postulated by Rutherford, consisting of a nucleus and electrons. But our experience with atoms actually does not suggest that such a thing happens.

The Rutherford model faces a further difficulty in explaining the experimentally observed fact that atoms produce sharp spectral lines. Since the spectrum of the atom would be related to the energy radiated by the orbiting electron and since this energy would be changing continuously as the electron spiralled towards the nucleus revolving about it more and more rapidly, the spectrum produced would be expected to be continuous, covering all frequencies in a range, instead of consisting of well-defined lines that correspond to only definite frequencies.

In order to overcome these difficulties, Niels Bohr (1913) made the revolutionary suggestion that electrons moved in definite, closed orbits, and that as long as the electron remained in the orbit it did not emit (or absorb) energy. This view was in direct opposition to the concepts enshrined in classical theory.

The Bohr model of the atom is, however, inaccurate and too mechanical for modern physics. Nevertheless, its great merit lies in the fact that it makes the understanding of modern concepts easier. And, on account of its mathematical simplicity, it still continues to find a number of applications. So the Bohr model will be first developed before discussing the more modern wave-mechanical concept of the atom.

2.7 The Bohr Theory

The main concepts of the Bohr theory (1913) proposed to interpret the spectrum of hydrogen and hydrogen-like atoms are as follows:

(*i*) Electrons revolve round the nucleus in definite, closed, stable orbits termed stationary states. As long as the electron moves in a closed orbit it is 'prohibited' from emitting any electromagnetic radiation. This view is in direct opposition to the concepts enshrined in conventional electrodynamics.

(*ii*) More than one stable orbit or stationary state is possible for any electron but the number of these possible stationary states is limited by the quantum condition that the angular momentum of the electron in its path about the nucleus must be an integral multiple of $h/2\pi$, where h is the Planck constant.

(*iii*) Electrons may 'jump' from one orbit to another, in which case radiation of a definite frequency is emitted or absorbed, thus producing a definite spectral line.

Though the above postulates appear incredible from the angle of classical conceptions, the sort of information about the atom and the atomic spectra which was available when Bohr had started thinking about them does, in fact, inevitably lead to these conclusions. We shall show this from the following line of argument.

We observe that atoms emit exceedingly sharp spectral lines; coupling this fact with the knowledge of quantum theory we have gained thus far, it seems plausible that each line of the emission (or absorption) spectrum should be due to the emission (or absorption) of a photon, whose energy $h\nu$ is equal to the difference between the initial and final energies of the extranuclear electron. The presence of discrete spectral lines therefore requires that the electron should lose (or absorb) its energy in finite steps; in other words, the electrons cannot take on any arbitrary energy, but could, instead, assume only a discrete set of energies. We may therefore conclude that the electron must exist in distinctly different stationary states, i.e. states in each of which its energy remains constant.

Each of these stationary states would have a definite energy and when the electron takes a jump, say, from the stationary state of energy E_2 to one of lower energy E_1, the photon emitted in this process will be given, according to the law of conservation of energy, by

$$h\nu = E_2 - E_1$$

Hence, $\bar{\nu} = \nu/c = \dfrac{E_2}{hc} - \dfrac{E_1}{hc}$ \hfill (2.12)

Eq. (2.12) affords a most simple explanation of Ritz's combination

Fig. 2.7 Formation of the various series of emission spectra of atomic hydrogen

principle. According to Eq. (2.12) the frequency (in terms of wavenumber) of an emitted photon, and hence that of the corresponding spectral line, is given by a difference of energies of two stationary states, divided by a constant hc. Ritz's term values are, therefore, simply the appropriate energy levels of the electron, expressed in units of wavenumbers. The formation of the various series (see Table 2.1) in the atomic spectrum of hydrogen could then be ascribed to electron jumps between definite energy levels, as shown in Fig. 2.7.

2.8 The Bohr Atom: Energy Levels and Spectra

We have seen that Eq. (2.5) is an empirical formula but it precisely represents the entire known hydrogen spectrum. So far we have thus a correct but underived formula representing the hydrogen spectrum. We now proceed to see how Bohr could derive this equation and the correct value for the Rydberg constant on the basis of his postulates. For this we have to consider at first the mechanism of the situation.

Bohr started with Rutherford's planetary model of the atom. In the case of hydrogen, Bohr considered the atom to consist of the nucleus (i.e. a proton) with one electron revolving about it. Hydrogen, according to this model, is a tiny one-planet solar system in which the gravitational attractive force of the solar system has been replaced by Coulombic force of attraction between the oppositely charged particles. Both the gravitational and electrostatic forces are inversely proportional to the square of the distance between the bodies. In the solar system, planets have elliptical orbits, which are however nearly circular. Bohr assumed that the planetary electron of the hydrogen atom moves in a circular orbit, as it greatly simplifies the dynamical analysis of the problem from classical principles.

Let v be the tangential velocity (Fig. 2.8) of the electron of mass m and charge $-e$ revolving around the nucleus of charge $+Ze$ in a circu-
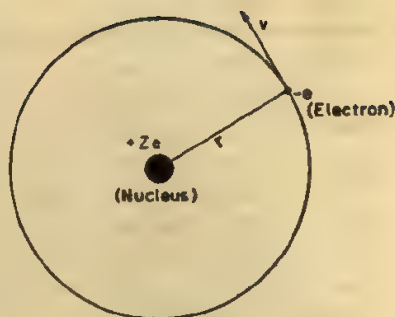
Fig. 2.8 Electron revolving in a circular orbit about a fixed nucleus of charge $+Ze$

lar orbit of radius r. (Z is the atomic number or the effective charge of the nucleus. For hydrogen Z is equal to 1. Here, however, we include Z for generality.) To keep the electron moving along the circular path there must be a centripetal force of magnitude mv^2/r. The gravitational force between the electron and the nucleus is negligible, and so the centripetal force could be safely equated to the Coulombic force. Thus,

$$\frac{mv^2}{r} = \frac{Ze^2}{r^2} \qquad (2.13)$$

From Eq. (2.13) we find that

$$r = Ze^2/mv^2 \qquad (2.14)$$

Eq. (2.14) provides a relationship between the variables v and r. Classical physics imposes no restriction on the number of solutions that Eq. (2.14) can have, that is, it permits any pair of values of v and r which satisfy Eq. (2.14). Bohr, however, assumed that not all the possible orbits that can be computed from Eq. (2.14) are permitted, but only those which satisfy a certain condition, as we shall see below.

The total energy E_t of the atom is given by the sum of the kinetic energy E_k and potential energy E_p of the orbital electron, i.e.

$$E_t = E_k + E_p \qquad (2.15)$$

The kinetic energy is given by

$$E_k = \tfrac{1}{2} mv^2$$

Combining this relation with Eq. (2.13)

$$E_k = \frac{1}{2}\frac{Ze^2}{r} \qquad (2.16)$$

Before deducing the expression for the potential energy E_p, a few words need be said about the energy concepts. Every energy calculation is, fundamentally, the result of the evaluation of either a definite integral (which involves an initial and a final state) or an indefinite integral (which involves an arbitrary constant). We arbitrarily assign, for the sake of convenience, a certain energy to a particular state. Thus when considering kinetic energy we take the body at rest as having no kinetic

energy, and when we say that the potential energy of a mass m at a height x above a reference plane is mgx we necessarily mean that at $x = 0$, the potential energy is zero.

In energy calculations relating to a planetary electron, the usual convention of the field theory is used, namely that the potential energy of the electron is zero when it is at rest infinitely far from the nucleus. When an electron moves closer to the positive nucleus, it does work and consequently loses electric potential energy. But since the potential energy of the electron is zero at infinity, it must become more and more negative as the electron approaches the nucleus.

It follows from the above discussion that, in order to derive an expression for the electric potential energy, E_p, of an electron at a finite distance from the nucleus, we should integrate the differential work done by the electron which is given by the product of the electrostatic force exerted by the nucleus on the electron and a differential displacement along the direction of action of the force. The limits of integration are, evidently, infinity and the radius of the electron orbit r:

$$E_p = \int_{\infty}^{r} F \, dr \qquad (2.17)$$

The electrostatic force F, as stated previously, is equal to Ze^2/r^2. Hence,

$$E_p = \int_{\infty}^{r} \frac{Ze^2}{r^2} \, dr = -\frac{Ze^2}{r} \qquad (2.18)$$

From Eqs. (2.15), (2.16) and (2.18)

$$E_t = \frac{1}{2} \frac{Ze^2}{r} - \frac{Ze^2}{r} = -\frac{Ze^2}{2r} \qquad (2.19)$$

The total energy of an atomic electron is thus negative; this is, however, necessary if the electron is to be bound to the nucleus, for with E_t greater than zero, the electron would have too much energy to remain in a closed orbit round the nucleus.

In the present case where we are concerned with a small particle like an electron revolving in an orbit the expression for angular momentum is quite simple. Just as linear momentum is given by the product of mass and velocity, angular momentum, which is the momentum a body has by virtue of its rotation, is given by the product of the moment of inertia I and the angular speed ω. The angular momentum of any body is thus given by $I\omega$. For a single particle the moment of inertia I is the mass of the particle times the square of its distance from the axis of rotation, i.e. mr^2. We can also express the angular speed of rotation ω as v/r, and hence the angular momentum of the electron is simply mvr. Denoting this angular momentum by p_θ,

$$p_\theta = mvr \qquad (2.20)$$

From Eqs. (2.14) and (2.20) we find

$$r = p_\theta^2/mZe^2 \tag{2.21}$$

Substituting this value of r in Eq. (2.19),

$$E = -\frac{mZ^2e^4}{2p_\theta^2} \tag{2.22}$$

As we have explained previously, Ritz's term values can be looked upon as energies of appropriate stationary levels, and hence it appears from Eq. (2.5) that the energy of a stationary level is inversely proportional to the square of an integer. But according to Eq. (2.22) the energy is inversely proportional to p_θ^2. This suggests that the angular momentum p_θ is proportional to an integer, say, n. Since the Planck constant h has the same dimension as angular momentum, Bohr postulated that

$$p_\theta = n\left(\frac{h}{2\pi}\right) \tag{2.23}$$

[No particular physical significance is attached to the factor 2π in Eq. (2.23), for the Planck constant could as well have been $h/2\pi$ instead of being simply h. Planck took the energy E of a radiation as equal to $h\nu$ and used the frequency ν in cycles per second. If, instead of this, he had used angular frequency f, in radians per second, given by $f = 2\pi\nu$, then his constant would have been $h/2\pi$, since $h\nu = (h/2\pi)(2\pi\nu) = (h/2\pi)f$.]

Through Eq. (2.23) Bohr actually postulated that the angular momenta of the planetary electrons are integral multiples of $h/2\pi$, or, in other words, the angular momentum is quantized in units of $h/2\pi$. There was no justification for this postulate on classical grounds but Bohr showed that by using it one could derive the empirical formula suggested previously for the hydrogen spectrum, as we shall presently see.

Energy levels. Substituting p_θ from Eq. (2.23) into Eq. (2.22) we get the quantized energy E_n as:

$$E_n = -\frac{2\pi^2 Z^2 e^4 m}{h^2 n^2} \tag{2.24}$$

The energy of an electron in the circular orbit characterized by the quantum number n, i.e. having an angular momentum $nh/2\pi$, is thus E_n, as given by Eq. (2.24). We cannot, however, call this E_n precisely the energy of the electron, because in its derivation we have so far assumed that the electron moves about a stationary nucleus; in fact, the nucleus cannot really be at rest, for we know from the laws of dynamics that whenever a particle moves in a circle about another particle of finite mass, the latter also must move in a circle about the common centre of mass (Fig. 2.9). To correct the above expression for E_n, we must therefore, take into account the motion of the nucleus. There is a theorem in mechanics which often simplifies considerably the analysis of the motions of bodies. In a two-body problem, such as the present one, this theorem
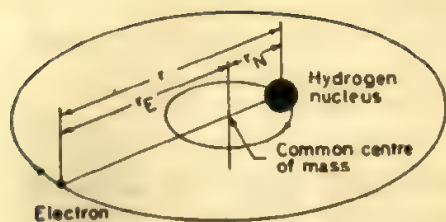
Fig. 2.9 As the electron moves in a circle about the hydrogen nucleus, the latter also moves in a circle about the common centre of mass. The centripetal force on the electron depends upon the radius of its orbit r_E, while the electrostatic force depends upon the distance r between the electron and the nucleus.

states that the motion of one body may be neglected if the mass of the other body is replaced by the reduced mass of the two bodies (vide Appendix 1), which is defined as the product divided by the sum of the two masses, i.e. $mM/(m + M)$ or $m/(1 + m/M)$. Replacing the electron mass m in Eq. (2.24) by the reduced mass we obtain

$$E_n = - \frac{m}{(1 + m/M)} \frac{2\pi^2 Z^2 e^4}{h^2 n^2} \tag{2.25}$$

Eq. (2.25) now correctly describes the energy of the electron. Similarly, in all other equations the electron mass should be replaced by the reduced mass.

Energy levels are most conveniently expressed in electron-volts. Eq. (2.25) gives the energy levels of a one-electron atom. Upon substituting the values of the constants in this equation and putting $Z = 1$, we find that the energy levels of the hydrogen atom are given by

$$E_n = - \frac{13 \cdot 58}{n^2} \text{ (in eV)} \tag{2.26}$$

Fig. (2.10) graphically represents these energy levels, the quantum numbers being shown at the left and the corresponding energies of the hydrogen atom in electron volts at the right. The lowest energy level E_1 is called the *ground state* of the atom, and higher levels E_2, E_3, E_4, ..., are called *excited states*. As the value of n increases, the value of E_n increases, that is, becomes less negative, and corresponding to $n = \infty$, the energy is zero.

Relation of spectral lines to energy levels. A hydrogen atom is usually in the normal state, called the *ground state*, with $n = 1$. An electron in this ground state is stable and moves without radiating energy. However, if the electron absorbs energy in some way it becomes excited and moves to a higher energy level. This 'excitement' can be brought about in a variety of ways. If the hydrogen is heated, the electron may be excited by a collision due to thermal motion. If the hydrogen is illuminated, the electron may absorb energy from a photon of the illuminating light. If the hydrogen is subjected to an electric discharge, a free electron or atomic ion which has been accelerated may collide with it and impart energy. If the electron absorbs, for instance, just 13·58 eV in one of these
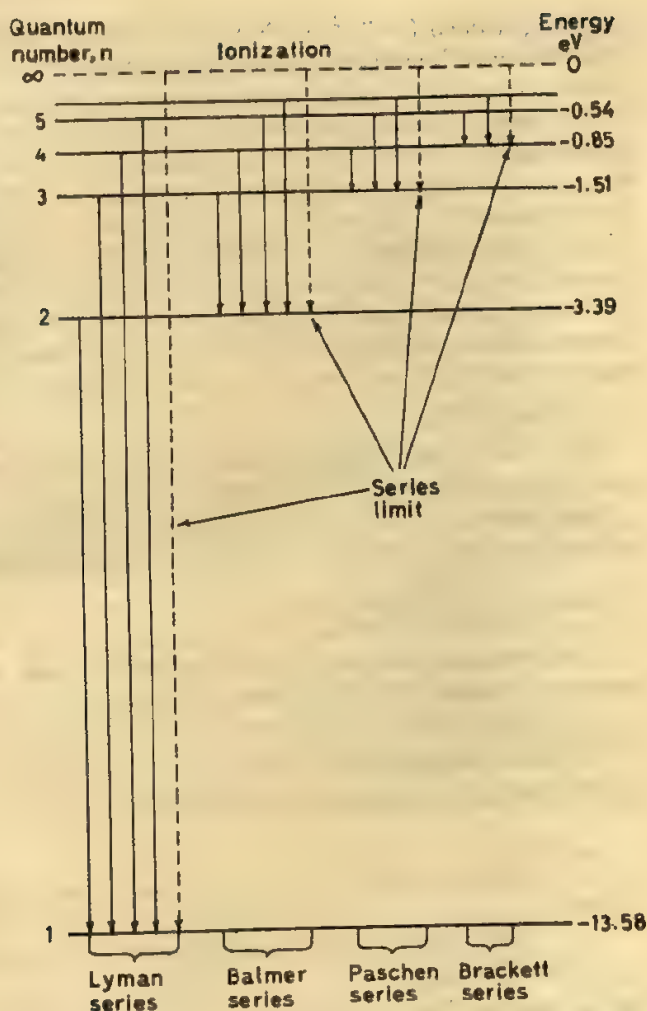
Fig. 2.10 Energy-level diagram of atomic hydrogen. Spectral lines originate in transitions between energy levels

ways, it is lifted to $n = \infty$ with no potential energy left over. The electron in this case being merely freed from the bounds of the nucleus, drifts about with only its thermal kinetic energy. If, however, the electron absorbs more than 13·58 eV energy, the freed electron possesses some additional kinetic energy; for example, if 20 eV of energy is absorbed, the electron made free of its home nucleus carries with it (20 − 13·58) or 6·42 eV of extra kinetic energy. In both these cases the remaining nucleus is an ion, and the atom is said to be ionized. If, however, the energy supplied is less than 13·58 eV, the electron can absorb only the right amount of energy that will raise it to one of the permitted energy levels. It can, for

instance, absorb $(-3\cdot39+13\cdot58)$ or $10\cdot19$ eV of energy which will raise it to the second energy level, or it may absorb $(-1\cdot51+13\cdot58)$ or $12\cdot07$ eV and so on. The atom in this case is excited but not ionized.

The excited electron next makes a return trip to its normal state, either in one step or in a number of successive steps. For instance, if it was excited to $n=4$, it may return to $n=1$ in one step, or it may also follow the sequence $4 \rightarrow 3 \rightarrow 2 \rightarrow 1$, or $4 \rightarrow 3 \rightarrow 1$, or $4 \rightarrow 2 \rightarrow 1$.

Bohr's third postulate, as stated earlier, says that when an electron jumps from one orbit to another the energy difference between these two states of motion is radiated all at once as a single photon of light. Let the quantum number n_2 represent a higher energy state and n_1 a lower energy state $(n_2 > n_1)$, then the above postulate can be written as

$$h\nu = E_{n_2} - E_{n_1} \qquad (2.27)$$

Fig. 2.10, which represents Eq. (2.27), shows schematically how spectral lines are related to the energy levels.

Substituting for the energies from Eq. (2.25) we have for the frequency ν of the corresponding line in the emission spectrum:

$$\nu = \frac{2\pi^2 Z^2 e^4 m}{h^3 (1+m/M)} \left(\frac{1}{n_1^2} - \frac{1}{n_2^2} \right) \qquad (2.28)$$

The frequency, expressed in wavenumber, $\bar{\nu}$ is obtained by dividing ν by the velocity of light c; thus,

$$\bar{\nu} = \frac{2\pi^2 Z^2 e^4 m}{h^3 c(1+m/M)} \left(\frac{1}{n_1^2} - \frac{1}{n_2^2} \right) \qquad (2.29)$$

Eq. (2.29) can be rewriten in the form

$$\bar{\nu} = RZ^2 \left(\frac{1}{n_1^2} - \frac{1}{n_2^2} \right) \qquad (2.30)$$

so that,

$$R = \frac{2\pi^2 e^4 m}{h^3 c (1+m/M)} \qquad (2.31)$$

For hydrogen $Z=1$, hence

$$\bar{\nu} = R \left(\frac{1}{n_1^2} - \frac{1}{n_2^2} \right) \qquad (2.32)$$

The correctness of the Bohr theory is proved by the fact that Eq. (2.32) is identical in form with the empirical but precise formula of Eq. (2.5) embodying the combination principle discovered earlier by Ritz.

The merit of the Bohr theory is that it gives not only the form of the empirical equation (2.5) for the entire spectrum of hydrogen, but also a very good value for the Rydberg constant. For hydrogen, for instance, the mass M of the nucleus (i.e. proton) is $1\cdot673 \times 10^{-24}$ g, while the other quantities involved in Eq. (2.31) are universal constants: $h = 6\cdot624 \times 10^{-27}$ erg sec, $c = 2\cdot9977 \times 10^{10}$ cm/sec, $e = 4\cdot802 \times 10^{-10}$ e.s.u., $m = 9\cdot107 \times 10^{-28}$ g. Substituting these values in Eq. (2.31)

we obtain the Rydberg constant for hydrogen $R_H = 1096 \times 10^2 \text{ cm}^{-1}$, which is in excellent agreement with the experimental value, 109,677·8 cm^{-1}.

Equation (2.30) has been derived for an atomic system in which only one electron moves round the central nucleus. It thus represents the spectra not only of atomic hydrogen but also of hydrogen-like (i.e. one electron) systems, such as singly ionized helium He$^+$, doubly ionized lithium Li^{+2} and trebly ionized beryllium Be^{+3}. The spectrum of He$^+$ is obtained by taking $Z = 2$, the spectrum of Li^{+2} is obtained by taking $Z = 3$, and the spectrum of Be^{+3} is obtained by taking $Z = 4$. Differences in the nuclear mass M for the respective systems referred to will evidently cause slight variation in the value of the Rydberg constant according to Eq. (2.31). For heavier atoms, that is for higher values of M, the Rydberg constant will be somewhat greater. It will however approach a limiting value for atoms of high atomic weight.

Moreover, since R is related to energy levels, the slight variation of R with nuclear mass will be expected to give rise to slight differences in the spectra of various one-electron systems. For instance, the first line of the Balmer series of hydrogen is 1·79Å greater than the corresponding line in the spectrum of heavy hydrogen (deuterium), and this can be explained by the fact that the mass of a deuterium nucleus is twice that of a hydrogen nucleus. It is indeed a triumph of the Bohr atomic model that the differences between the atomic spectra of ordinary hydrogen and of deuterium can be attributed to the influence of the mass of the nucleus. The discovery of deuterium was, in fact, first made spectroscopically by Urey in 1932.

Radius of the hydrogen atom. The radii of hydrogen orbits can be calculated from Bohr's theory by combining Eqs. (2.13) and (2.23). Since Z is unity for hydrogen, we get from Eq. (2.13)

$$v^2 = e^2/mr \qquad (2.33)$$

It is also readily deduced from Eq. (2.23) that

$$v^2 = \frac{n^2h^2}{4\pi^2r^2m^2} \qquad (2.34)$$

By combining Eqs. (2.33) and (2.34) it is found that

$$r = n^2h^2/4\pi^2me^2 \qquad (2.35)$$

Using known values of h, m, and e, the radius of the first Bohr orbit, that is when n is 1, is found to be 0.53×10^{-8} cm. It should then represent the radius of the normal hydrogen atom, that is, when the electron occupies the lowest level. This radius is found to be of the same order as the radius of the hydrogen atom, determined from the spectrum of the hydrogen molecule.

2.9　The Franck-Hertz Experiment

Starting in 1913, shortly after Bohr announced his theory of the hydrogen atom, Franck and Hertz performed a series of experiments which provided direct confirmation of the presence of discrete energy levels within atoms and, furthermore, demonstrated that these levels are the same as those suggested by the study of atomic spectra. The basic ideas of Bohr thus received independent confirmation from the Franck-Hertz electrical experiments. Spectroscopic values of energy levels are, however, usually more accurate than the electrical values, so that the main use of the Franck-Hertz experiments is the confirmation of the existence of energy levels within atoms.

One way of raising atoms to excited states is bombardment by electrons, and this coupled with the fact that the energy of bombarding electrons can be controlled affords an electrical method for measuring the energy levels of atoms. Consider an arrangement as shown in Fig. 2.11. The radio-tube-type tube contains a filament-heated cathode, a plate as anode and is filled by the gas being studied. As the accelerating potential, i.e. the potential difference between the anode and the cathode, is increased, it is found that at a certain potential the current begins to increase more rapidly than before, as shown in Fig. 2.12 for the hydrogen-filled tube. The value of the critical potential in this case is found to be 13.6 V. The marked increase in the plate current at the critical potential is attributed to the ionization of the gas atoms that are present. When the accelerating
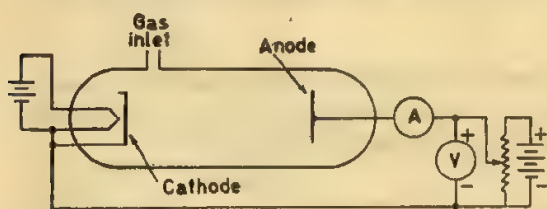
Fig. 2.11 Apparatus for determining ionization potential of a gas
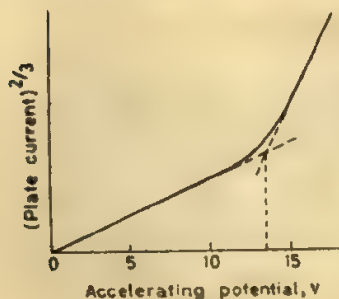
Fig. 2.12 Variation of plate current with accelerating potential in a hydrogen-filled tube

potential reaches the critical value, some of the electrons emitted from the cathode acquire enough energy to knock orbital electrons off the colliding gas atoms. This critical potential is thus the ionization potential. The electrons liberated by ionization add to the plate current, while the positive ions cancel some of the space charge, thus causing further increase in the current. Experimenting with hydrogen gas, the aforesaid ionization potential is found to be 13.6 V, which means that a bombarding electron with 13.6 eV energy can just ionize a hydrogen atom. Thus the ionization energy of atomic hydrogen representing, in terms of the energy level concept of Bohr, the difference between the energy levels at $n = 1$ and $n = \infty$, is 13.6 eV; it is a remarkable fact that this value, derived from electrical measurement, is in excellent agreement with that measured by the very different technique of spectroscopy. It can be seen from Fig. 2.12 that the two straight line portions of the graph do not actually meet at a point, but are joined by a short curved part, which is explained by the fact that the electrons themselves are emitted from the cathode with an initial velocity distribution, and consequently, some of them acquire the necessary energy for producing ionization at lower accelerating potentials than others. This short curved part notwithstanding, the break in the current–voltage curve of Fig. 2.12 is quite abrupt, which indicates that ionization of an atom is produced by collision with a single electron. If the ionization of the hydrogen atom could be produced by the combined efforts of several low energy electrons, the abrupt change of slope would not be observed.

Elastic and inelastic collisions. We know from the aforesaid experiment that there is a minimum potential through which electrons must be accelerated before they can produce ionization by raising the orbital electrons from their lowest energy state, i.e. ground state, to infinity. But even before the bombarding electrons can acquire enough energy to cause ionization of the gas atoms, they may however have enough energy to raise the orbital electron to an excited state. As we have already noted, the orbital electron can absorb only certain definite amounts of energies represented by transitions between energy levels. When an orbital electron, on being hit by a high-energy bombarding electron, absorbs a certain energy by making a transition, the latter is left with that much less energy. Such a collision in which the bombarding electron is left with less energy than it had before the collision is said to be *inelastic*. But if the bombarding electron possesses less energy than the minimum required for an energy transition of the orbital electron, the latter absorbs no energy from the bombarding electron and the collision is said to be perfectly *elastic*.

Resonance potentials. A look at Fig. 2.10 reveals that the least amount of energy that the orbital electron in the ground state can absorb is

13·58 — 3·39 or 10·19 eV. Now, considering the aforesaid ionization experiment, as the potential difference across the tube is increased, the electrons coming from the heated cathode are accelerated to higher and higher velocities. And when, in this process, a bombarding electron acquires an energy of 10·19 eV it can 'resonate' with hydrogen and transfer its energy completely to the latter. After transferring its energy the electron moves more slowly while the hydrogen exhibits its 'excite-ment' by emitting radiation, which is evidently caused by the return of the excited electron from $n = 2$ to $n = 1$. This resonance radiation therefore corresponds to a line of the Lyman series in the ultraviolet region and can accordingly be detected by ultraviolet spectroscopy. Since this resonance produces no ioniziation, the current through the tube is not changed. Consequently, the resonance phenomenon cannot be demonstrated electronically with the simple tube shown in Fig. 2.11, and for this we need a more elaborate tube such as that used by Franck and Hertz, the principal parts of which are shown schematically in Fig. 2.13.

Since the effect of resonance on the bombarding electron is to slow it down, we need, for observing the resonance phenomenon electronically, a device which will measure the energy of the bombarding electron after it has undergone collision. The tube shown in Fig. 2.13 incorporates such a device. The technique involved is very much same as the one we have earlier encountered in our consideration of the photoelectric effect, where the energy of photoelectrons is measured by making them move against the force of an electric field, and the energy of photoelectrons is given by the stopping potential. The anode of the ionization tube of Fig. 2.13 is perforated or made of wire mesh so that some of the bombarding electrons will pass through the anode rather than hit it. In order to measure the energy of these electrons a collector electrode is inserted in the tube beyond the perforated anode and is maintained less positive than the anode. The electrons that pass through the anode are thus slowed by the field between the anode and the collector electrode. Suppose the potential of this field is 0·5 V (Fig. 2.13). Then the electrons which reach the collector electrode must have passed through the perforated anode with an energy of 0·5 eV at the least.
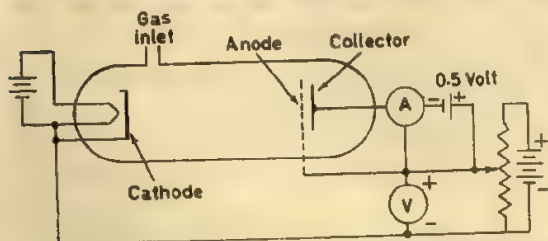
Fig. 2.13 Apparatus for determining resonance potential of a gas

The experimental procedure now suggests itself. The collector current is measured as a function of the accelerating potential V, i.e. the potential difference between the cathode and the anode. Fig. 2.14 shows typical results of such an experiment for hydrogen. As we have applied a retarding potential of 0·5 V there is no collector current from $V = 0$ to $V = 0·5$ V. However, above $V = 0·5$ V the collector current increases because the number of electrons which have at least the minimum energy (0·5 eV) required to surmount the 0·5 V barrier increases. But when V reaches the resonance potential of the gas, 10·2 V in the present case, the collector current drops abruptly. The interpretation of this effect is that some of the bombarding electrons are slowed down by inelastic collisions with orbital electrons in the gas. As V is further stepped up, the current again increases, and this happens because, the field being stronger, bombarding electrons can transfer energy to orbital electrons by inelastic collision at an early stage and then undergo enough acceleration to overcome the 0·5 V barrier. Fig. 2.14 shows a second dip at an accelerating potential of about 20·4 volt. Since this is twice the resonance potential, the second dip is evidently caused by two inelastic collisions of the same kind. The third dip is similarly due to three successive inelastic collisions by the same bombarding electron with three gas atoms. The separation of successive resonance peaks is found to be 10·2 V for hydrogen. These electronic data thus indicate that a minimum electron energy of 10·2 eV is required to bring about the 'excitement' of the hydrogen atom. The aforesaid electronic experiment thus provides an independent confirmation of the spectroscopic observations and further strengthens the energy level concept of Bohr. (It should be mentioned that if the tube shown in Fig. 2.13 is used the second resonance peak will be masked by the effects of ionization of the gas which starts at 13·6 V. However, by using a more complicated tube the resonance and ionization effects can be differentiated. Fig. 2.14 depicts only the resonance effects for hydrogen.)
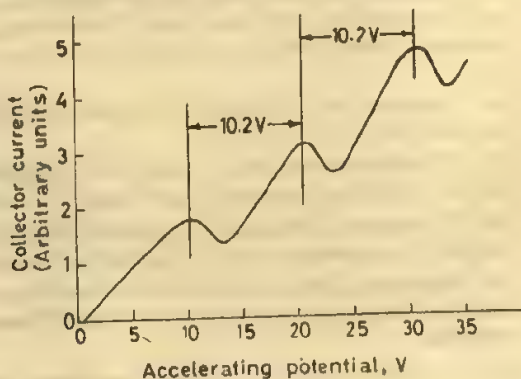
Fig. 2.14 Resonance potential curve for hydrogen

Franck and Hertz also checked the above interpretation of resonance potential by observing the emission spectra of vapours during electron bombardment. In the case of mercury vapour, for example, they found that the resonance potential of 4·9 V excited the 2536 Å spectral line of mercury, while according to Bohr's theory the 2536 Å line is associated with the emission of photon of energy 4·9 eV.

Suggested Reading

BEYER, R. T., *Foundations of Nuclear Physics*, Dover Publications, New York, 1949.

BOHR, N., *The Theory of Spectra and Atomic Constitution*, 2nd Ed., University Press, Cambridge, England, 1924.

WHITE, H. E., *Introduction to Atomic Spectra*, McGraw-Hill, New York, 1934.

HERZBERG, G., *Atomic Spectra and Atomic Structure*, Dover Publications, New York, 1944.

ROBERTSON, J. K., *Introduction to Physical Optics*, 4th Ed., D. Van Nostrand, Princeton, N. J., 1954.

RICHTMEYER, F. K., E. H. KENNARD, and T. LAURITSEN, *Introduction to Modern Physics*, 5th Ed., McGraw-Hill, New York, 1955.

Problems

2.1　An alpha particle having a kinetic energy of 5-MeV is projected directly towards the nucleus of a thorium atom. What is their distance of closest approach? The mass of an alpha particle is four times that of the proton and the atomic number of thorium is 90.

2.2　What fraction of a beam of 8-MeV alpha particles incident upon a gold foil 0·0004 mm thick is scattered by less than $10°$?

2.3　Calculate the binding energy (in Joules and in eV) of the electron in hydrogen in the ground state.

2.4　Evaluate from atomic constants the Rydberg constant for the three isotopes of hydrogen, H^1; deuterium, H^2; and tritium, H^3. (Ans: 109668·7 cm^{-1}, 109698·5 cm^{-1} and 109708·5 cm^{-1})

2.5　The values of the Rydberg constant for hydrogen and singly ionized helium are 109677·76 cm^{-1} and 109722.4 cm^{-1} respectively. The helium nucleus has 3·9726 times the mass of the hydrogen nucleus or proton. Calculate the ratio of the mass of the proton to that of the electron. (Ans: 1839)

2.6　Calculate the wavelengths of the first four spectral line of the Balmer series of hydrogen. Compute also the series limit.

2.7　Calculate the wavelength of the H_β line in the Balmer series for the three isotopes of hydrogen, viz., hydrogen, deuterium and tritium. (Ans: 4863·13 Å, 4861·80 Å and 4861·36 Å)

2.8　If a mixture of ordinary hydrogen and tritium is excited and its spectrum observed, how far apart in wavelength would the H_α lines of the two kinds of hydrogen be?

2.9　How many different possibilities of spectral line emission are there for the hydrogen atom when the electron is excited to the $n = 4$ state? Compute the wavelengths and frequencies of these lines.

2.10　Compute the value of the largest wavelength found in the Paschen series. (Ans: 18750Å)

2.11　Electrons accelerated through 12·85 V strike hydrogen gas. Compute the wavelengths

of all spectral lines which could be observed.

2.12 What excitation potential is needed to bring out the first line of the Balmer series of hydrogen (6562·8 Å) by electron bombardment?

2.13 (a) The spectra of He+ ($Z = 2$), Li+² ($Z = 3$), and Be+³ ($Z = 4$) are very much like that of H° ($Z = 1$). Why?

(b) Calculate the wavelength, in angstroms, of the first spectral lines in the Balmer series for He+², Li+², and Be+³, respectively.

2.14 Given the ionization potential of atomic hydrogen as 13·6 eV, calculate from this the ionization potentials of the following ionic species:

He+, Li+², Be+³, B+⁴, C+⁵

Electronic Configuration of Atoms

3.1 Introduction

The Bohr theory as outlined in Chapter 2 gives the positions of the lines in hydrogen spectrum in terms of a single quantum number n, called the principal quantum number. When observed with spectroscopes of high resolving power, the hydrogen spectral line is found to have a fine structure, i.e. it appears as a set of closely-spaced components. The fine structure of spectral lines of other elements is often observable even with spectroscopes of smaller resolving power. (Thus, for instance, ordinary spectroscopes are often able to separate the yellow line of the sodium atom spectrum into two lines differing in wavelength by about 6 Å.) It turns out, therefore, that energy levels associated with the spectral lines have fine structure. Further subdivision of spectral lines, and hence of energy levels, also occurs if the substance under study is placed in a magnetic field or an electric field. These are known as the *Zeeman effect* and *Stark effect*, respectively. It is thus obvious that one quantum number is inadequate and that additional quantum numbers are needed in order to specify in detail the energy levels of atomic electrons. Actually, four quantum numbers are necessary as we shall see in the following.

3.2 Azimuthal Quantum Number

Planetary motion under the influence of a central force, results in general, in elliptical orbits with the central body (such as the atomic

nucleus, in the present case) situated at a focus. (The circular orbit is also possible, but it is then a special case of an elliptical orbit with the major and minor axes having the same length.) An obvious extension of the Bohr model would thus be to allow for the possibility of elliptical orbits. This extension was made by Sommerfeld in 1915 in the following manner.

In contrast to the case of circular orbits, where only the angular position of the electron from the nucleus changes during a revolution, in the case of elliptical orbits, however, both the distance of the electron from the nucleus and its angular position change simultaneously. Thus, since the motion of a particle in an ellipse has two degrees of freedom, two quantum numbers are needed to represent the electronic motion in place of one employed by Bohr.

The tangential velocity and hence the momentum of a particle moving in an ellipse may be resolved into two components, one along the radius vector and the other at right angles to it. The latter represents the angular momentum and, applying quantizing condition in line with the treatment used by Bohr, this may be supposed to have one of a definite series of values, given by the expression $k(h/2\pi)$. Here k is an integer, and is called the *azimuthal quantum number*. The momentum in the direction of the radius vector is also quantized in the same way, the integer in this case being called the *radial quantum number* and represented by n_γ.

Using a combination of the two momenta, in place of one in Bohr's treatment outlined above, we get the following equation for the energy of the electron in a hydrogen-like atom:

$$E = -\frac{2\pi^2 Z^2 e^4}{h^2 (n_\gamma + k)^2} \frac{m}{(1 + m/M)} \tag{3.1}$$

Eq. (3.1) may be written as

$$E_n = -\frac{2\pi^2 Z^2 e^4}{h^2 n^2} \frac{m}{(1 + m/M)} \tag{3.2}$$

where n representing the sum of n_γ and k, both of which are whole numbers, is evidently an integer. The number n is now called the *principal quantum number*. Since Eq. (3.2) is identical with Eq. (2.25), deduced for circular orbits, it is proved that in terms of the principal quantum number the energy of the elliptical orbits is given by the same formula as for the circular orbits.

It can be proved by the methods of classical dynamics that the ratio of n to k is the same as the ratio of the major to minor axis of an elliptical orbit in which the electron is supposed to revolve; thus,

$$\frac{n}{k} = \frac{\text{length of major axis}}{\text{length of minor axis}}$$

The principal quantum number n, thus, determines the major axis of the elliptical orbit, which is the same as the diameter of the Bohr circular orbit, being equal to twice the radius given by Eq. (2.35). The azimuthal quantum number k, on the other hand, determines the minor axis or the eccentricity of the elliptical orbit. Both n and k being integers, the quantum number k, for a given value of n, may have n values, viz., n, $n-1$, ... 1; k cannot be zero, since in that case the minor axis of the ellipse would be zero, that is, the elliptical orbit would be reduced to a straight line passing through the nucleus of the atom; however, this type of linear motion does not appear possible when the electron is regarded, as in the present model, as a particle moving in a definite path. When k is equal to n, the orbit is circular, whereas for other values there result elliptical orbits with different eccentricities. The smaller the value of k, for any n, the greater is the eccentricity of the elliptical orbit and more deeply does it penetrate into the core of the atom. The Bohr–Sommerfeld orbits for different values of n and k are presented in Fig. 3.1.
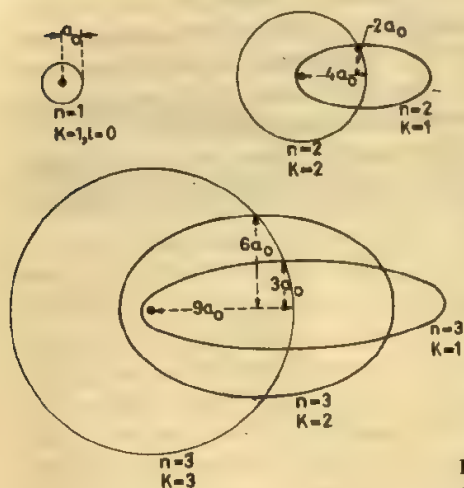
Fig. 3.1 Bohr-Sommerfeld orbits for $n = 1,2,3$
(a_0 is the radius of the first Bohr orbit.)

Since n equals the sum of n_γ and k, it follows that for all orbits having the same principal quantum number n, the energies as derived by Eq. (3.1) are the same, irrespective of the value of k. This would therefore lead to the same result as obtained from the Bohr model. But there is a necessity, as was first pointed out by Sommerfeld, for a correction term to take into account the fact that the actual velocity of an electron, as a consequence of its movement in an elliptical orbit, is not uniform; thus the velocity of the electron in its 'perihelion' position, that is when it is closest to the nucleus, is greater than when it is farthest from the nucleus, that is in the 'aphelion' position.

This velocity variation will cause difference in the effective mass of the electron at different positions of its orbit. According to the theory of

relativity, the effective mass m of a particle moving with a velocity v is given by

$$m = m_0 / \sqrt{1 - v^2/c^2} \qquad (3.3)$$

where m_0 is the so-called rest mass, i.e. the mass of the particle at rest, and c is the velocity of light. It follows from Eq. (3.3) that the effective mass of the electron will vary with its velocity, being greatest at perihelion and least at aphelion. Taking into consideration this relativistic mass change, the energy of the electron in a hydrogen-like, i.e. one-electron, atom is found to be

$$E = - \frac{2\pi^2 Z^2 e^4}{n^2 h^2} \cdot \frac{m}{(1 + m/M)} \left[1 + \frac{\alpha^2 Z^2}{n} \left(\frac{1}{k} - \frac{3}{4n} \right) \right] \qquad (3.4)$$

where α, known as the fine-structure constant, is given by $2\pi e^2 / hc$ and is equal to 1/137.0.

It will be seen from Eq. (3.4) that, for a given principal quantum number n, the energy in any orbit depends, to some extent, on the value of k. Consequently, the frequency of the radiation emitted in electron transition from a level n_2 to a level n_1 would be slightly different depending on the various values of k, and so in the spectra of hydrogen-like atoms a group of closely spaced lines should appear instead of a single line. For large n, since k can assume many values, it would appear that the number of fine structure lines would also be very large. However, this is not so in practice and the actual number of lines is limited—a fact that is explained by the *selection principle*, according to which k always changes by one unit only, or in other words, those transitions only are allowed in which $\triangle k$ is ± 1. A theoretical interpretation of this selection principle has been provided by wave mechanics.

Applied to the Balmer series of hydrogen and to the spectrum of ionized helium, the formula of Eq. (3.4) leads to calculated values of frequency separations in good agreement with those observed for a few fine-structure lines. Moreover, since Eq. (3.4) involves Z^4, the frequency separation should depend on the fourth power of the effective nuclear charge. The frequency separation for singly ionized helium should thus be 2^4 or 16 times as great as for hydrogen. This has been corroborated by experimental observations.

It is now necessary to point out a weakness of the Sommerfeld method of elliptical orbits, as described above. This method of course affords the correct total of possible azimuthal quantum numbers, namely, that for any principal quantum number n there is a total of n different quantum .

numbers; but the actual values assigned to azimuthal quantum numbers are incorrect. Experimental observation as well as the theoretical treatment based on wave mechanics show that the azimuthal quantum number begins with zero, so that, corresponding to a given value of n for the principal quantum number, the values of the azimuthal quantum number are $0, 1, 2, \ldots n - 1$, making a total of n possibilities. The new azimuthal quantum number is given the symbol l in order to avoid the risk of confusion with the earlier one; l is therefore related to k by $l = k - 1$. Henceforth the azimuthal quantum number l will be adopted in all discussions.

It has been noted previously that the azimuthal quantum number specifies the number of units of angular momentum $(h/2\pi)$ associated with an electron in a given orbit. Now, since for $n = 1$, l must equal zero, it follows that the electron in the smallest orbit will have no angular momentum. For a larger orbit, such as one with $n = 3$, there are three values of l, viz., 0, 1 and 2, and hence three possible orbital shapes or eccentricities: (i) a straight line orbit through the nucleus without angular momentum for $l = 0$, (ii) an ellipse with an angular momentum $(h/2\pi)$ for $l = 1$, and (iii) a 'rounder' ellipse with greater angular momentum $2(h/2\pi)$, for $l = 2$. It may seem to be absurd, mechanically, that an electron passes through the nucleus as envisaged by the straight-line orbit for $l = 0$, but in the treatment of wave mechanics it is found to be reasonable.

3.3 *Magnetic Quantum Number*

In a strong magnetic field the lines of the spectrum are split up; this is called *Zeeman effect*. There is also a splitting of lines by an electric field which is known as the *Stark effect*. The presence of more lines in the spectrum of an atom in a magnetic or an electric field indicates that the energy levels are further sub-divided by the field. An additional quantum number, called the *magnetic quantum number*, is therefore needed to specify these energy sublevels, as shown below.

The electron rotating in its orbit is equivalent to a current in a loop of wire. A current circulating in a closed loop is equivalent to a magnetic dipole and has thus a magnetic moment associated with it. Consequently, when the atom is placed in an external magnetic or electric field, each electronic orbit will be subject to a torque.

The angular momentum of a spinning system can be represented by a vector along the spin axis with a magnitude $I\omega$, where I is the moment of inertia and ω the angular velocity. Let us consider a particle rotating with uniform angular velocity ω about an axis x. The angular velocity can be represented by a vector of length ω extending along x in the direction in which a right-handed screw would advance if subjected to the same

rotation as the particle ('right-hand screw rule'). Since I is a scalar, the vector representing the angular momentum, $I\omega$, will be in the same direction as ω . Moreover, we have seen earlier that the angular momentum of an electron in a given orbit is determined by the azimuthal quantum number l , the orbital angular momentum being equal to l $(h/2\pi)$.* The latter quantity can therefore be vectorially represented, as shown in Fig.3.2, by a straight line of length l extending along the axis of rotation in the same direction as ω.

Fig. 3.2 Vector representation of orbital angular momentum.

Since each electronic orbit has a magnetic moment, in a magnetic field the electronic orbit will be subject to a torque which tends to make the l vector parallel to the field. Because of this righting torque exerted by the field on the electronic orbit, the l vector will precess about the field, as shown in Fig. 3.3. A familiar example of precession is provided by a spinning top; its angular momentum vector (along the spin axis) does not line up with the direction of the gravitational field but precesses around this direction. The precession of an electronic orbit in a magnetic field (Fig. 3.3) is called the *Larmor precession*; this precessional motion of the orbit introduces additional energy states into the atomic system. The amount of energy of any of these new energy states depends upon the precessional velocity, which again depends upon the righting torque, and the righting torque, in turn, depends upon θ, the angle between the l vector and the external magnetic field (Fig. 3.3). Hence, the number of

Fig. 3.3 Larmor precession of an electron orbit in a magnetic field.

energy states will be determined by th : number of possible values of θ. If all values of θ could occur, then, obviously, there would be an infinite

---

* It should be noted that according to modern theory based on quantum mechanics, the orbital angular momentum is $= \sqrt{l(l+1)}\ h/2\pi$, instead of $lh/2\pi$.

number of new energy states and, consequently, the emission spectrum of an atom in a magnetic field would be a continuous one. But, since the Zeeman effect shows only a few additional lines, only a few values of θ are therefore 'allowed': these include values for which $l \cos \theta$, that is, the projection of the l vector in the direction of the magnetic field, is an integer. This means that the component of the orbital angular momentum along the magnetic field is limited to integral multiples of $(h/2\pi)$.

The aforesaid condition that $l \cos \theta$ must be a whole number gives rise to a third quantum number called the magnetic quantum number, m_l, which was introduced by Lande in 1921. The allowed values of θ are given by $l \cos \theta = m_l$; and since m_l is limited to whole numbers, it turns out that for any given value of l there may be $(2l+1)$ values for the magnetic quantum number m_l, viz., $0, \pm 1, \pm 2, \ldots \pm l$. This is shown in Fig. 3.4 for $l=3$. Each value of m_l corresponds to a possible value of θ
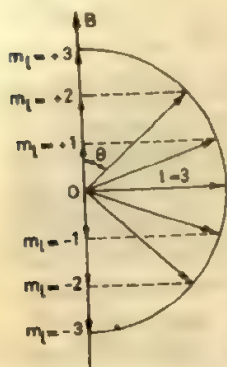
Fig. 3.4 Possible orientations of three units of orbital angular momentum in a magnetic field.

and hence to a possible orientation of the electron orbit in a magnetic field. The possible orientations of an electronic orbit in an applied magnetic field are thus dependent on the azimuthal quantum number l and are restricted to only $(2l+1)$ in number. Because of this restriction on the orientations of the electronic orbits with respect to the direction of the field, the orbits are said to be space quantized. It may be noted that even in the absence of applied magnetic field, such fields are present in a multi-electron atom due to orbital rotations of inner electrons.

3.4 Spin Quantum Number

Even the three quantum numbers, n, l, and m_l were found to be inadequate for explaining the multiplicity and fine structure of some spectral lines that could be observed with a spectroscope of high resolving power. The idea of 'electron spin' was therefore advanced by Uhlenbeck and Goudsmit in 1925 to account for this. An electron, according to this concept, can execute, in addition to its orbital rotation, a spin around its own axis. This spin is analogous to the rotation of the earth as it moves

along its orbit around the sun. Because of its spin the electron has a spin angular momentum of magnitude $s(h/2\pi)^*$, where the spin s is given by $1/2$. The rotating electron also has a magnetic moment and so will orient itself in an external magnetic field. Spectroscopic observations, however, show that the electron may orient in an external magnetic field only in two ways, namely, those in which the vector representing the spin angular momentum is either in the direction of the field or opposed to the field. Hence, the spin quantum number m_s, which is the component of the s vector in the direction of the field, can have only two values $+1/2$ or $-1/2$.

In the absence of an external magnetic field, the positive direction of the l vector is taken as the reference direction for m_s.

3.5 *Four-Quantum-Numbers System*

The state of an electron in an atom is described by the four quantum numbers mentioned above. To summarize, the values and designations given to these four quantum numbers are as follows:

Principal quantum number, $n = 1,2,3,4,5,$ ....$,n-1$
Azimuthal quantum number, $l = 0,1,2,3,4,$ ....$,n-1$
Magnetic quantum number, m_l; for each value of l there are $(2l+1)$ values of m_l, ranging from l to $-l$.
Spin quantum number, m_s; for each set of value of n, l, and m_l there are two values of m_s, viz., $\frac{1}{2}$ and $-\frac{1}{2}$.

The principal electronic shells in an atom are designated as K,L,M,N,O,P, etc., and correspond to the principal quantum number $n = 1,2,3,4,5,6$, etc., respectively. Each of these shells is associated with a group of quantum states or energy states as illustrated in Table 3.1 for the first five shells.

It is apparent from this table that the maximum number of different energy states or the maximum number of electrons for each principal quantum number n can be represented $2n^2$. Each energy state is associated with only one electron. This follows from the Pauli exclusion principle, which states that in any particular atom no two electrons can have the same four values for the four quantum numbers.

3.6 *Symbols for Atomic States*

Descriptions of the atomic states that correspond to the allowed energies are given most simply and directly in terms of the angular momenta of

---

* It is important to note that according to modern quantum theory the spin angular momentum is $\sqrt{s(s+1)}h/2\pi$ instead of $sh/2\pi$.

the atomic states. These are represented by certain symbols (called *Russell-Saunders symbols*) using a *Vector model* of the atom that provides a simple way of describing the stationary states of the atom. In the Russell-Saunders vector model, which describes the most frequent type of coupling, the vectors representing the spin of the individual electrons combine to form a resultant spin vector represented by the quantum number S; this is equal to the algebraic sum of the s values for the separate electrons. (We here use a capital letter for the state of a whole atom and a small letter for the state of an individual electron. The distinction is however trivial for the hydrogen atom which has only one electron.)

For example, the spin angular momentum vectors of two electrons each having spin quantum number $\frac{1}{2}$ ($s_1 = \frac{1}{2}$, $s_2 = \frac{1}{2}$) combine to form a resultant total spin angular momentum vector corresponding to the values 0 and 1 for the total spin quantum number S, as shown in Fig. 3.5.
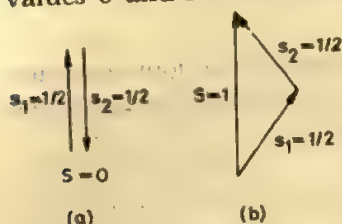
Fig. 3.5 Vector combination of spin angular momenta of two electrons: (a) antiparallel; (b) parallel (see text).

The state $S = 0$ is usually described by saying that the two vectors are *antiparallel* (or *paired or opposed*) and the state $S = 1$ by saying that they are *parallel*. (The figure, however, shows that they are not exactly parallel, but are as close to parallel as could be allowed.)

Similarly the orbital angular momenta of the different electrons couple together to give an orbital angular momentum vector for the atom, represented by the quantum number L; this must be *integral* and equal to the vectorial sum of the l values (Section 3.5) for all the electrons. However, the electrons in closed shells (Table 3.1) do not contribute to L, so that only a few electrons need to be considered even for elements of high atomic weight. For example, if there are two such electrons each having azimuthal quantum number l ($l_1 = 1$, $l_2 = 1$), the orbital angular momentum vectors can combine to form the resultant total angular momentum vector, with values corresponding to 0, 1 and 2 for the total angular momentum quantum number L, as shown in Fig. 3.6.
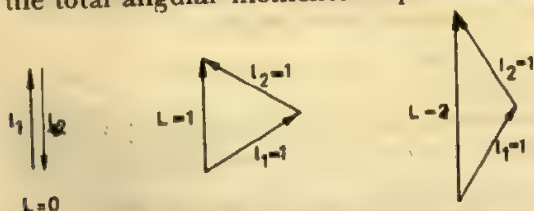
Fig. 3.6 Vector combination of orbital angular momenta for two p electrons ($l_1 = 1$, $l_2 = 1$)

Electronic Configuration of Atoms

Table 3.1 The Number of Quantum States in the First Five Shells of an Atom

Principal quantum number, n	Energy levels (shells)	Azimuthal quantum number, l	Energy sublevels (subshells)	Magnetic quantum number, m_l	Spin quantum number, m_s	No. of energy states	Total No. of electrons
1	K	0	s	0	$\frac{1}{2}, -\frac{1}{2}$	2	2
2	L	0	s	0	$\frac{1}{2}, -\frac{1}{2}$	2	8
		1	p	1,0,−1	$\frac{1}{2}, -\frac{1}{2}$	6	
3	M	0	s	0	$\frac{1}{2}, -\frac{1}{2}$	2	18
		1	p	1,0,−1	$\frac{1}{2}, -\frac{1}{2}$	6	
		2	d	2,1,0,−1,−2	$\frac{1}{2}, -\frac{1}{2}$	10	
4	N	0	s	0	$\frac{1}{2}, -\frac{1}{2}$	2	32
		1	p	1,0,−1	$\frac{1}{2}, -\frac{1}{2}$	6	
		2	d	2,1,0,−1,−2	$\frac{1}{2}, -\frac{1}{2}$	10	
		3	f	3,2,1,0,−1,−2,−3	$\frac{1}{2}, -\frac{1}{2}$	14	
5	O	0	s	0	$\frac{1}{2}, -\frac{1}{2}$	2	50
		1	p	1,0,−1	$\frac{1}{2}, -\frac{1}{2}$	6	
		2	d	2,1,0,−1,−2	$\frac{1}{2}, -\frac{1}{2}$	10	
		3	f	3,2,1,0,−1,−2,−3	$\frac{1}{2}, -\frac{1}{2}$	14	
		4	g	4,3,2,1,0, −1,−2,−3, −4	$\frac{1}{2}, -\frac{1}{2}$	18	

In general, the different vectorial combinations of l_1 and l_2 are

$$L = l_1 + l_2, \; l_1 + l_2 - 1, \; l_1 + l_2 - 2, \ldots l_1 - l_2 \qquad (3.5)$$

Further, the above two resultant vectors, S and L, combine to form a total angular momentum vector for the atom, represented by the quantum number J; this must be *integral* if S is integral and *half-integral* if S is half-integral. Two simple examples, with $S=1$, $L=1$ and with $S=1$ and $L=2$, are shown in Fig. 3.7, where it is seen that three values of J are
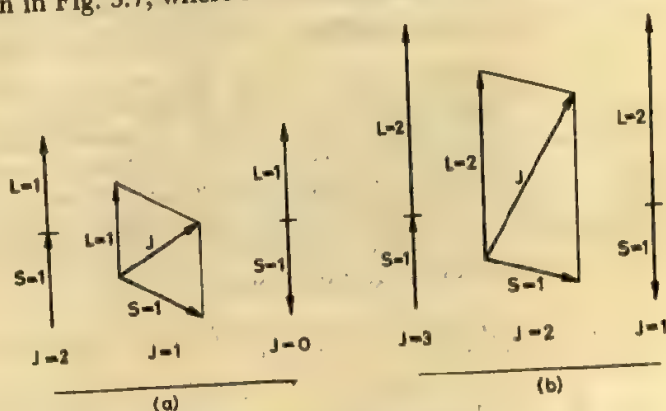
Fig. 3.7 Combination of vectors S and L: (a) $S=1, L=1$; (b) $S=1, L=2$

possible in each case. It can be shown that, in general, the possible values of J are

$$J = L + S, \ L + S - 1, \ L + S - 2, \ .. \ |L - S|$$ (3.6)

The symbol $|L - S|$ is used here to indicate that only positive (or zero) values of J are significant when $S > L$. The above relation shows that there will be a total of $2S + 1$ values of J, for each value of L.

We may now explain the significance of the Russell - Saunders symbols. The scheme introduced by H.N. Russell and F.A. Saunders (1925), for representing more completely the electronic state of an atom, is based on the use of spectral term symbols. The term letters* $S, P, D, F, G, \ldots$ are used according as the value of L in the particular atomic state is $0, 1, 2, 3, 4, \ldots$ The term letter is preceded by a superscript, which is equal to $2S + 1$; it represents the *multiplicity* of the energy level and corresponds to the number of ways in which the quantum number S can be oriented in space. The term letter is further followed by a subscript giving the corresponding value of J [Eq. (3.6)]. Thus the term symbol for a particular atomic state is written as follows:

Term symbol $= {}^{2S+1}$(Term Letter)$_J$.

For example, if the electronic coupling, as described previously, gives $S = 1$ and $L = 2$, the term symbols would be ${}^3D_3$, ${}^3D_2$ and ${}^3D_1$, according as $J = 3$, 2, and 1, each term symbol representing one component of the triplet term or energy level. Further, the term symbol may be preceded by the principal quantum number so as to identify a particular electronic level; for example, the symbol $5\ {}^3D_3$, to be read as 'five-triplet-D-three', represents a particular energy state of the atom as a whole having $n = \ L = 2, \ S = 1$ and $J = 3$. Such descriptions of atomic states are very useful in the discussion of atomic spectra.

When there is only one valence electron, as in an alkali atom, the spin quantum number (S) for the atom has the value $1/2$, which gives the multiplicity $2S + 1 = 2$. Since there will be a total of $2S + 1$ values of J, for each value of L, in accordance with Eq. (3.6), the various possible terms are then

${}^2S_{1/2}$, ${}^2P_{3/2}$, ${}^2P_{1/2}$, ${}^2D_{5/2}$, ${}^2D_{3/2}$, ${}^2F_{7/2}$, ${}^2F_{5/2}$,

which are read 'doublet-S-one-half', 'doublet-P-three-halves' and so forth. Some of the lower energy levels of lithium are sketched in Fig. 3.8. The P, D, and F levels of alkali metals are thus *doublets*. This accounts for the fact that the spectral lines for all the alkali metals are doublets. The spectral lines arise from transitions, as shown in Fig. 3.8. The selective rule, in general, for such transitions is:

$$\Delta S = 0, \ \Delta L = \pm 1, \ \Delta J = 0, \pm 1$$

* Note that the capital letter S is used in two different ways—as a term symbol and as a symbol for the resultant spin quantum number.
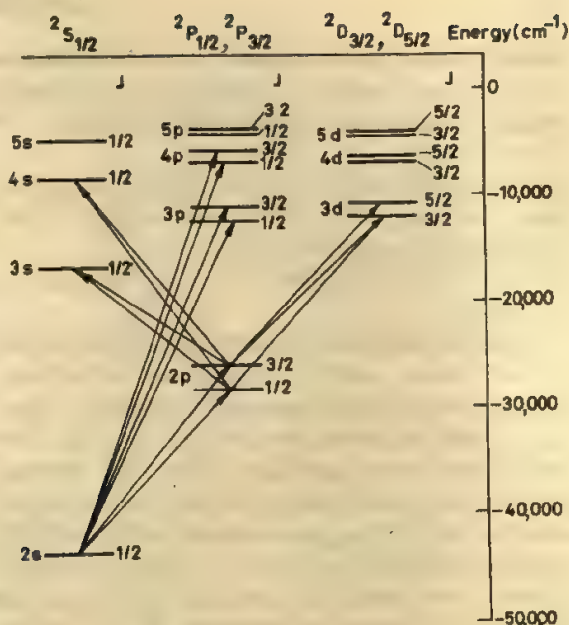
Fig. 3.8 Some of the energy levels of the lithium atom showing the separation of the doublet levels (*j*-splitting is greatly exaggerated). Some allowed transitions are also shown.

(There is also a further rule that a state with $J = 0$ cannot make a transition to another $J = 0$ state.) Theoretically, the S term is also a doublet, since the multiplicity $2S + 1$ is 2. Actually, however, the term $^2S_{\frac{1}{2}}$ is a singlet, since the two J values are indistinguishable as far as the total angular momentum is concerned. It is nevertheless the practice to retain the doublet superscript, viz., $^2S_{\frac{1}{2}}$.

It is easy to see from the above line of argument that for an element with two valence electrons there will be two series of terms, namely, singlets ($S = 0$) and triplets ($S = 1$), with J values equal to L, and to $L + 1$, L and $L - 1$, respectively. The various possible terms are then easily deduced to be $^1S_0$, $^1P_1$, $^1D_2$, and $^1F_3$ for the singlets, and $^3S_1$, $^3P_2$, $^3P_1$, $^3P_0$, $^3D_3$, $^3D_2$, $^3D_1$, $^3F_4$, $^3F_3$, $^3F_2$ for the triplets. Here also, the term $^3S_1$ is actually a singlet, but nevertheless the triplet superscript is retained.

3.7 The Aufbau Principle and the Periodic Table

The electronic configurations of the various atoms are based on the spectral study and on the quantum theory. While optical spectra have furnished evidence for the outer sphere electrons, the X-ray spectra have produced evidence about electronic inner shells. The distribution of

electrons in an atom is based on the following two principles:

(1) The Pauli exclusion principle, stated earlier, which implies that the maximum number of electrons in s,p,d,f,g,. . .subshells are, respectively, 2,6,10,14,18,.......

(2) The electrons in a given atom occupy the lowest possible quantum state, i.e. one with the lowest energy. The energy of the sublevels increases in the following order:

$$1s < 2s < 2p < 3s < 3p < 4s < 3d < 4p < 5s < 4d < 5p < 6s < 4f < 5d < 6p < 7s < 5f < 6d$$

A marked difference between the energies of the subshells is characteristic of lower quantum numbers while this difference continuously decreases with higher quantum numbers (Fig. 3.9). Moreover, it is to be noted that the arrangement given in Fig. 3.9 characterizes elements of low atomic numbers only. With the increase in atomic number the relative energies of many of the levels change somewhat and to various degrees. Such changes are shown schematically in Fig. 3.10 which shows that, for elements of atomic number less than 20, the energy of the 3d sublevel is higher than that of the 4s orbital. Beyond this atomic number, however, this order is reversed. The relative positions of the 4f and 5d sublevels suffer similar change before and after the atomic number 57.

In Appendix 2 are given the electronic configurations of the various elements, built up by the 'aufbau' (building-up) process, which is a purely imaginary process of constructing the atoms of elements by adding a proton (thus increasing the atomic number by one) and an extranuclear

Subshell	s	p	d	f
Capacity	2	6	10	14
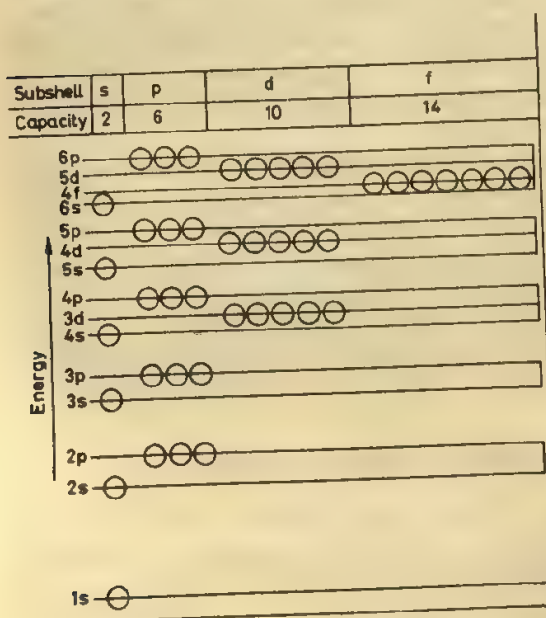
Fig. 3.9 Schematic energy level diagram for lighter atoms. Each circle represents an electron pair of opposite spins.
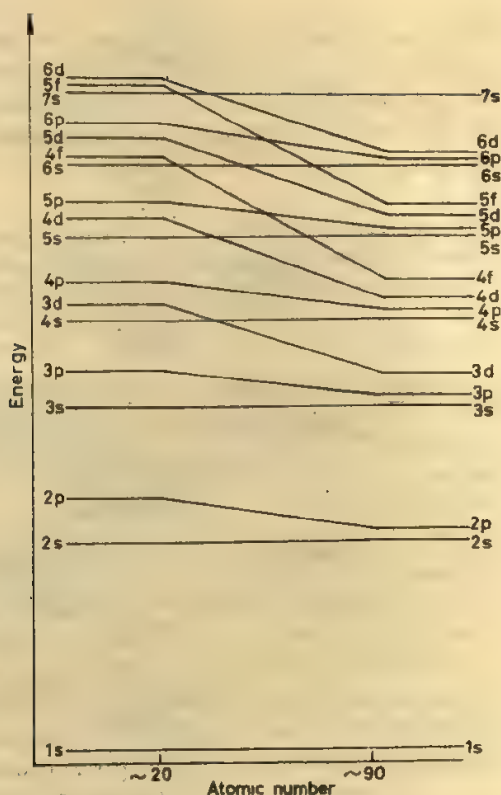
Fig. 3.10 Variation of the relative order of energy levels with atomic number.

electron (to balance the nuclear charge) in successive stages. The added electron obeys the two principles enunciated above in choosing the particular shell and subshell. The 'aufbau' process of deriving the electronic structure of the atoms is schematically represented in Fig. 3.11.

Direct experimental confirmation of these electronic configurations lies in the analysis of atomic spectra. That apart, the correlation between these configurations and the observed chemical properties leaves little doubt as to the validity of the former. The arrangement of the atoms in the periodic table, in accordance with the periodicity of these properties, is a direct result of the electronic configurations.

3.8 Types of Elements

On the basis of similarities and differences in electronic configurations of the atoms as presented in Appendix 2, four different types of atoms can be discerned, and correspondingly, elements characterized by these
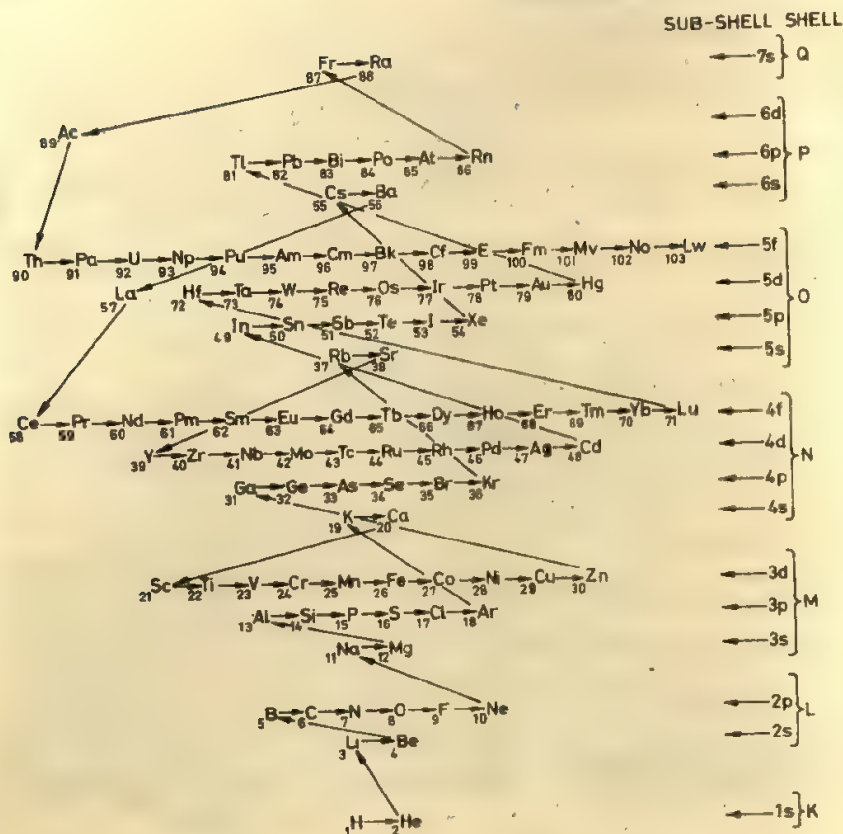
Fig. 3.11 Electron-shell configuration of the 103 atoms of the periodic table according to the 'Aufbau' principle.

atoms, can be classified into four groups— inert gas elements, representative elements, transition elements, and inner transition elements.

Inert gas elements. Helium, neon, argon, krypton, xenon, and radon (including actinon and thoron) are the inert gas elements. They have completed electronic groups. Thus helium has the configuration $1s^2$, while each of the rest has in its level of maximum principal quantum number (n) the arrangement $ns^2\,np^6$ and no incompletely filled inner levels. The chemical inertness of these elements may therefore be ascribed to the presence of completed electronic groups.

Representative elements. All nonmetallic elements and metallic elements from Periodic Group Ia, Ib, IIa, IIb, IIIb and IVb are classed as representative elements. These elements are characterized by atoms in which levels of maximum principal quantum number are incompletely filled, but all occupied inner levels are filled to capacity. Thus, elements with atomic numbers ranging from seven less to two more than

that of a given inert gas element are included in this group, and the electronic configuration embraces anything from ns^1 to $ns^2\,np$ for a given maximum principal quantum number n. The reactivity of the representative elements is due to their tendency to achieve the electronic configuration of the nearest inert gas element by electron loss or gain, as the case may be.

Transition elements. Atoms of elements of this type are characterized by the presence of an inner incompletely filled d-level. In general, the electronic configuration can be represented by $(n-1)d^{1-9}ns^2$; however, the presence of two electrons in the ns level is not a rigid requirement since examples are known of transition elements with the arrangement ns^1 or even ns^0 (see Appendix 2). Four transition series appear among the elements corresponding respectively to n being 4, 5, 6 and 7. All the series begin with Group IIIa elements, namely scandium ($3d^14s^2$), yttrium ($4d^15s^2$), lanthanum ($5d^16s^2$) and actinium ($6d^17s^2$). In terms of the definition given above, the first three transition series end at nickel, palladium, and platinum, respectively. Since, however, the adjacent elements from Periodic Groups Ib (copper family) and IIb (zinc family) are quite analogous to the transition elements in respect of properties, they are often classified with the latter elements. Thus the entire series of atoms corresponding to the filling of $3d$, $4d$ and $5d$ levels, as shown in Fig. 3.7, may be considered to belong to the 1st, 2nd and 3rd transition series, respectively. The membership of the fourth transition series which begins with actinium is limited by the number of known elements.

Appendix 2 shows that in passing from vanadium to chromium in the fourth period there occurs a temporary transfer of one $4s$ electron to the $3d$ state which, therefore, shows a jump from $3d^3$ to $3d^5$. In manganese, however, the new electron again enters the $4s$ state and thereafter the filling process continues normally up to nickel. In passing from nickel to copper again a similar jump, viz $3d^8$ to $3d^{10}$, occurs. This irregularity stems from the increased stability of the $3d^5$ and $3d^{10}$ electronic configurations. Analogous situations can be observed in $4d$ and $5d$ sublevels, as also in the $4f$ and $5f$ sublevels.

The small energy differences between the $3d$ and $4s$ electrons result in variable valency of the transition elements, since even a small increase in energy of the atom caused by ordinary chemical reactions may excite some of the $3d$ electrons, apart from the $4s$ outer electrons. Moreover, the incompleteness of the sublevel allows electronic transitions even at low-energy quanta (e.g those corresponding to the visible light) and thereby gives rise to colour of the ions. Again, the presence of some unpaired electrons in the incomplete sublevel results in the paramagnetic behaviour of the transition elements . . . .

With the increasing quantum number, the stability of the outermost s

sublevel increases considerably. This is reflected in the fact that the $6s$ and $7s$ sublevels do not easily lose electrons and consequently the corresponding elements display considerable chemical inertness. Thus mercury with its stable $6s$ sublevel is the most volatile of metals and resembles inert gases, producing always monatomic vapour.

Inner transition elements. These elements belong to the transition series described above. They are, however, more precisely described as constituting a transition series within transition series, and hence termed as inner transition elements. In addition to incompletely filled d levels, the inner transition elements contain incompletely filled f levels as well

The first inner transition series comprises the rare earth elements. By rigid definition given above and according to the electronic configurations given in Appendix 2, this series should start at cerium (atomic number 58) and end at thulium (atomic number 69). However, in discussing these elements, it has been customary to adopt the idealized general configuration $4f^{1-13}5s^25p^65d^16s^2$ for the series and to assume that there occurs a regular filling of the $4f$ orbitals from cerium ($4f^1$) to lutetium ($4f^{14}$), as shown in Fig. 3.11. Since lanthanum (atomic number 57) has $4f^0$ and lutetium (atomic number 71) has $4f^{14}$, both of them, by rigid definition, would be excluded from this series. Their inclusion, however, appears justified on the grounds that there exist similarities in chemical and physical characteristics between these and other inner transition elements. Thus the whole *lanthanide series* (see periodic table) including both lanthanum and lutetium is commonly regarded as the first inner transition series.

Though the series of fourteen rare-earth elements arises from the gradual filling of the $4f$ sublevel by fourteen electrons, the $4f$ electrons do not participate in the formation of chemical bonds, since they are shielded by electrons in the $5s$, $5p$ and $6s$ sublevels and are, consequently, only slightly perturbed by the electrical fields associated with neighbouring atoms. The $4f$ electrons, however, give rise to colour and strong paramagnetism.

As in the sixth period of the periodic table the rare earths or lanthanides, representing the first transition series, arise from the gradual filling of the inner $4f$ sublevel, so in the seventh period a similar filling of the $5f$ sublevel gives rise to a second inner transition series, also called the *actinide series* (see Fig. 3.11). This series includes the 'transuranium elements' with atomic number greater than 92, namely, neptunium, plutonium, americium, curium, berkelium, californium, einsteinium, fermium, mendelevium, nobelium, and lawrencium. All isotopes of elements of atomic number greater than 92 have relatively short life periods and so could be found only in minor quantities in natural ores. They have been produced artificially in the laboratory.

3.9   *s, p, d, f Block Elements*

Since the various portions of the periodic table correspond to the filling of different levels, it is possible to write down the essential framework of the periodic table showing only the energy levels, as follows:

		$1s$
$2s$		$2p$
$3s$		$3p$
$4s$	$3d$	$4p$
$5s$	$4d$	$5p$
$6s$	$4f$ and $5d$	$6p$
$7s$	$(6d, 5f)$	

It is the sequence in which the various energy levels are filled (see Fig. 3.11) which determine the number of elements contained in each period of the periodic table. The various periods thus contain successively 2, 8, 8, 18, 18, 32, . . . elements. It is apparent from the framework presented above that the periodic table can be divided into four regions depending on whether the elements are filling up *s, p, d* or *f* levels. Generally the chemical properties are broadly determined by the region in which an element is situated. Thus, for instance, each *s*–block element is a strongly electropositive metal, yields colourless ions in solution and exhibits the same oxidation state in almost all its compounds. The *p*–block elements, on the other hand, are mostly non-metals (and such metallic elements as occur in this region are perhaps not truly metallic, e.g. As, Sb); they exist in different oxidation states equal to N and $(N-2)$, N denoting the *number* of the group of the periodic table in which the element occurs.

The *d*–block elements are called the 'transition elements', as they are located between the *s*– and *p*–blocks. The transition elements are metals, producing usually coloured ions, and forming, in most cases, several series of compounds, in which the metal occurs in different oxidation states. In contrast to the *p*–block elements, for which, as mentioned above, the oxidation states differ from each other by two units, the oxidation states of a *d*–block element can differ from each other by as small as one unit. Chromium, for instance, exhibits oxidation states of $+2, +3$ and $+6$.

The *f*–block elements arise from the filling of *f* sublevels. They constitute the inner transition series (see Section 3.7).

Suggested Reading

Brown, G.I., *A Simple Guide to Modern Valency Theory*, Longmans Green, London, 1953.

Day, M.C. and J. Selbin, *Theoretical Inorganic Chemistry*, Reinhold, New York, 1962.

HESLOP, R. B. and P. L. ROBINSON, *Inorganic Chemistry*, Elsevier, Amsterdam, 1960.

MOELLER, T., *Inorganic Chemistry*, John Wiley, New York, 1952.

Problems

3.1 Specify by quantum numbers the various energy states of the electrons in the O-shell.

3.2 Show that the maximum number of electrons that can have the same principal quantum number n is $2n^2$.

3.3 Supposing that atoms could contain electrons with principal quantum numbers up to and including $n = 6$, how many elements should there be?

3.4 What will be the values for the total spin quantum number S for three electrons? In how many ways can the state $S = 1/2$ be realized for three electrons? (*Ans.* 1/2, 3/2; 3).

3.5 What will be the values of J if (a) $L = 2$, $S = 3/2$ and (b) $L = 2$; $S = 1$? [*Ans.* (a) 7/2, 5/2, 3/2, 1/2; (b) 3,2,1].

3.6 Show that the ground state for lithium is $^2S_{\frac{1}{2}}$, while for helium it is $^1S_0$ (Hint: Apply Pauli's principle that two electrons can occupy the same orbital if their spins are opposed.)

3.7 Write down the various term symbols for a beryllium atom with one valence electron in a $2s$ orbital and the other in a $3s$ orbital, in addition to the two electrons in a K-shell.

3.8 Write the electronic configurations for the following species: H^-, Li^+, O^{-2}, F^-, Na^+, S^{-2}, Cd^{+2} and Al^{+3}.

3.9. Discuss the general electronic configurations of inert gas elements, representative elements, transition elements and inner transition elements. Predict certain general properties of these types of elements on the basis of their electronic configurations.

Wave-mechanical Approach

4.1 *Introduction*

Basically, *wave mechanics* is a mathematical treatment of the behaviour of small particles and involves the application of a fundamental concept in physics, namely the concept of a wave — a wave, that is characterized by wavelength and frequency as its measurable attributes and expressed by a mathematical function describing the variation of its amplitude in space and time. The physical concept of a particle characterized by mass and velocity is, however, more familiar to us; and naturally so, because the results of most experiments dealing with particles lend themselves to ready interpretation in terms of mass and velocity by Newton's laws of motion. But this classical approach was evidently not adequate for some experiments, the results of which appeared to contravene Newton's laws; and it was to explain this situation that the concept of wave mechanics was introduced. Its application, first to atomic and then to molecular structure, revolutionized the physical sciences, and gave birth to the new chemistry that we know today.

The mathematics of wave mechanics has been developed in several alternative ways, the most popular of which, however, is the one initiated by Schrödinger in 1926, and subsequently developed by others. The popularity of this approach stems from the fact that its results can usually be presented in terms of a physical picture. Schrödinger's system of mechanics, based on the wave equation bearing his name, has been justified in the best possible way. It is very difficult to find analytical solutions of Schrödinger's equation; so it has been solved exactly only

for a few problems. **These** few solutions have, however, shown excellent agreement with experiment. Moreover, many approximate solutions derived for other cases have also indicated the correctness of the method. The Schrödinger wave equation forms a fundamental law of nature, applying with great generality to quantum mechanics, just in the same way that Newton's laws of motion form the fundamental laws of classical mechanics or Maxwell's equations provide the basic laws for electromagnetism.

It was de Broglie's proposal of waves accompanying particles, which he made in 1924, that led Schrödinger to the formulation of the wave equation, which bears his name. So we next direct our attention to the de Broglie hypothesis.

4.2 The de Broglie Hypothesis

While most of the optical problems, such as refraction, diffraction, etc., may be treated quite successfully by considering light to be electromagnetic waves, some other phenomena such as those of photoelectric effect and atomic spectra convince us that light is absorbed or emitted in energy quanta, i.e. in particles called photons. This dual nature of light possessing both wave and particle properties is clearly illustrated by combining Planck's expression for the energy of a photon $E = h\nu$ with Einstein's mass-energy relation $E = mc^2$ (where c is the velocity of light) to give $h\nu = mc^2$. Introducing $\lambda = c/\nu$, we get

$$\lambda = h/mc = h/p \tag{4.1}$$

Thus photons of mass m and velocity c, or momentum $p = mc$, are accompanied by waves of wavelength λ, as given by Eq. (4.1).

The Compton effect in X-ray scattering (see Section 1.5) provided an early experimental confirmation of this relation and, more than anything else, convinced physicists of the reality of photon particles, and hence of the dual character of light, possessing both wave and particle properties. In contemplating this dual nature of light, de Broglie had the novel idea that nature must be symmetrical and that the dual nature of light should be matched with a dual nature of matter. He proposed in 1924 that Eq. (4.1) is a general equation, which is applicable to photons as well as to material particles. According to this proposition, a material particle of mass m and velocity v has, associated with it, a wavelength given by

$$\lambda = h/mv \tag{4.2}$$

where λ denotes the de Broglie wavelength and h is the Planck constant.

Evidently, the de Broglie wavelength for ordinary objects should be extremely small, since the numerator is the Planck constant, which is extremely small: 6.62×10^{-27} erg sec. For example, a stone of mass

100 g travelling with a velocity of 100 cm/sec would be associated with a de Broglie wavelength of $6·6 \times 10^{-31}$ cm, which is, indeed, too small to be detectable. But it is altogether different in the case of the electron. For instance, an electron accelerated through 100 V, so that its velocity is $5·94 \times 10^8$ cm/sec, would have associated with it a de Broglie wavelength given by

$$\lambda = \frac{6·62 \times 10^{-27}}{9·1 \times 10^{-23} \times 5·94 \times 10^8}$$

$$= 1·23 \times 10^{-8} \text{ cm} = 1·23 \text{ Å}$$

Thus the wavelength to be associated with an electron of moderate energy is in the X-ray region. So it is suggested that electrons, in passing through a crystal, should produce diffraction patterns on a photographic plate as do X-rays. This was eventually verified in 1927 by Davisson and Germer. They reported the diffraction of a beam of electrons by a nickel crystal; and the values of wavelengths calculated from the angles of maximum electron intensity were also in good agreement with the de Broglie relation. In 1928, G. P. Thomson reported the diffraction of fast-moving electrons. In his experiment, a fine beam of electrons (cathode rays), travelling in an evacuated tube with a speed about one-third that of light, was allowed to fall on a photographic plate after passing through a very thin metal foil. The plate showed, on development, not only a dark central spot where it had been hit by the undeflected electron beam but also a series of concentric rings resembling those of an X-ray powder photograph. While this proved that the electrons had been diffracted like X-rays by the array of atoms in the metal lattice, detailed measurements further yielded the effective wavelength, agreeing with that predicted by the de Broglie equation. Direct verification of de Broglie's hypothesis of the wave nature of moving bodies was thus obtained.

Electrons, however, are not the only material bodies whose wave property can be demonstrated. Beams of neutrons and even beams of whole atoms like hydrogen and helium have been found capable of producing diffraction patterns when scattered by suitable crystals. In fact, like X-ray and electron diffraction, neutron diffraction is today a widely-used tool for delving into crystal structures.

The wave behaviour of material bodies having been established, the distinct nature of 'material waves' must now be emphasized. Material waves are different from electromagnetic waves occurring in radiation. Thus, while radiation (in vacuum) always travels with the same velocity, namely, 3×10^{10} cm/sec, material waves do not. So, very similar appearances notwithstanding, X-ray diffraction patterns and electron-diffraction patterns should not be confused. Since material waves are capable of propagating in vacuum, they are also different from mechanical waves like sound waves.

4.3 The Heisenberg Uncertainty Principle

The uncertainty principle can be derived in a variety of ways. Let us here illustrate the principle by a simple informal argument based on the particle nature of waves. If we want to know the position of something we have to touch it physically or illuminate it with light or produce some other interaction with it. Suppose we wish to know the position of an electron. We cannot, obviously, see it with visible light since its wavelength is perhaps a million times as large as the diameter of the electron. So we try by using radiation of shorter wavelength, say, X-rays of wavelength λ. But in any case, the uncertainty in the measurement of the position cannot be less than λ; at best it can only be equal to λ. So, the smaller the wavelength used the more accurate will be the measurement of the position.

The X-ray, however, will not reveal the position of the electron unless first scattered by it. But the X-ray scattering by electron, as we have noted earlier, is accompanied by a Compton effect. An X-ray photon, on colliding with the electron, will change its momentum. Since this momentum change cannot be precisely predicted, the measurement of original momentum of the electron will be quite uncertain. Moreover, since the momentum of a photon is given by h/λ, the smaller the wavelength of the X-rays the greater is the photon momentum and, consequently, the greater the uncertainty in electron momentum. We thus see, the shorter the wavelength we use in order to achieve greater accuracy in locating the position the greater becomes the uncertainty in momentum, and vice versa. It is thus impossible to determine both the original momentum as well as the position; and this uncertainty of either position or momentum is evidently not a matter of physical imperfections in the measuring apparatus, nor is it one that may be overcome by some improved technique. This uncertainty represents a fundamental limit of nature and sets a fundamental limit to our knowledge.

The uncertainty in the measurement of the original momentum p of the electron is, therefore,

$$\Delta p = h/\lambda \qquad (4.3)$$

and it evidently stems from the act of measurement itself. Since Δp is inversely proportional to λ, the longer the wavelength of the radiation used for observing the electron the smaller the consequent uncertainty in its momentum.

A mathematical expression of the uncertainty relation was derived by Heisenberg (1927) from the general laws of quantum mechanics. For the pair of variables, position and momentum, the relation* is

$$\Delta x . \Delta p > h \qquad (4.4)$$

* A more widely used expression is $\Delta x . \Delta p > h/2\pi$.

where Δx is the uncertainty in position and Δp the uncertainty in momentum. The product of these two uncertainties cannot be less than the Planck constant h.

In order to measure the position of a particle with absolute accuracy, Δx must become zero; so

$\Delta p = h/\Delta x = h/0 = \infty$

This means that the momentum of the particle being measured becomes completely indeterminate. In other words, the simultaneous measurement of velocity and position with absolute accuracy is impossible. A compromise is therefore to be made by admitting a certain degree of inaccuracy in the measurement of both position and momentum.

Let us consider a dust particle of diameter 1 micron or 10^{-4} cm and mass $6 \cdot 6 \times 10^{-12}$ g moving under a microscope with a small velocity of 1 micron per second. Expressing Δp as $\Delta v.m$, where Δv is the uncertainty in velocity and m the rest mass, the uncertainty relation becomes

$\Delta x.\Delta v > h/m$ (4.5)

Now let us choose the compromise values of uncertainty as $\Delta x = 10^{-8}$ cm and $\Delta v = 10^{-7}$ cm/sec, so that

$\Delta x.\Delta v = h/m = 10^{-15}$

The ratio of Δv to v in the present case is $10^{-7}/10^{-4} = 10^{-3}$. As an uncertainty in the velocity measurement this is quite satisfactory. As for uncertainty in the position of the dust particle, Δx, its ratio to the dimensions of the particle, namely $10^{-8}/10^{-4}$ or one ten-thousandth, is also negligible. That is why in measuring velocities and positions of dust particles or more massive objects the existence of uncertainty relation is never perceived.

But, for electrons the situation is quite different. Let us assume that the electron has a diameter of 10^{-13} cm (though it is not exactly correct to speak of the dimensions of an electron), a mass of 10^{-27} g and a velocity of 10^7 cm/sec. Then the right-hand side of the uncertainty relation comes out to about $6 \cdot 6$. The quantities Δx and Δv can now be constructed in different ways. If it is desired to measure the electron velocity with the same accuracy as in the case of the aforesaid dust particle, i.e. the ratio of Δv to v to be 10^{-3}, then the uncertainties will be: $\Delta v = 10^4$ cm/sec, and $\Delta x = 6 \cdot 6 \times 10^{-4}$ cm. So the ratio of Δx to electron dimension is $6 \cdot 6 \times 10^9$ which means that the uncertainty in the position of the electron will be thousands of millions of times the size of the electron! It can be shown from other combinations as well that no compromise in the measurement of both position and velocity can be made in the case of an ultrasmall particle, e.g. the electron.

It is the uncertainty of knowing exactly both the position of the electronic orbit and the velocity of electron within it that renders the Bohr concept of these orbits inexact. An example would make it clear. The velocity of an electron (of mass $9 \cdot 1 \times 10^{-28}$ g) moving round the nucleus

in the first Bohr orbit (of diameter 1·058 Å) could be calculated to be 2·2 × 10⁸ cm/sec, and its momentum is therefore 2×10^{-19} g cm/sec. In order to know this small momentum within 1 %, $\Delta v.m$ would have to be less than 2×10^{-21}. Eq. (4.5) then tells that Δx would be not less than $6.6 \times 10^{-27}/2 \times 10^{-21}$ or 330×10^{-8} cm, i.e. 330 Å, which is more than 300 times the diameter of the Bohr orbit. It implies that we could not even say whether the electron was in the atom at all!

The Heisenberg uncertainty principle may also be stated in terms of energy and time, that is,

$$\Delta E.\Delta t > h/2\pi \tag{4.6}$$

where ΔE is the uncertainty in an energy measurement and Δt the uncertainty in the time at which the measurement is made. To illustrate the significance of Eq. (4.6), let us consider the radiation emitted from an 'excited' atom. As we have seen, an excited atom gets rid of its excess energy by emitting one or more photons of definite frequency. The average time gap between the excitation of an atom and the consequent photon emission is 10^{-8} sec, i.e. $\Delta t = 10^{-8}$ sec. The uncertainty ΔE in in the measurement of photon energy is, therefore,

$$\Delta E = h/2\pi\Delta t \approx 10^{-19} \text{ erg}$$

The frequency of the emitted radiation is therefore uncertain by

$$\Delta v = \Delta E/h = 1.5 \times 10^{7} \text{ cycles/sec}$$

which then represents the limit to the accuracy in our determination of the frequency of the radiation emitted by an atom.

Energy can be precisely known, i.e. ΔE can be zero, only if Δt is infinite. Thus a system can be said to have an accurately defined energy only if it remains in that state for an infinite time.

What emerges from the foregoing discussion is that the uncertainty relation comes to the fore in dealing with phenomena on an atomic scale. As we have already shown, the Bohr model of the atom, which assigns precisely defined orbit to an atomic electron with precisely defined momentum, is untenable on uncertainty considerations. Our picture of atom or molecule should be such that it does not contravene the uncertainty principle. For this the wave-mechanical approach is essential. We cannot precisely know the position of an atomic electron, but we can derive by the mathematical technique of wave mechanics the probability of occurrence of the electron at a given point in the space surrounding the nucleus.

4.4 Sinusoidal Wave Motion

If a block of wood floating on a water surface is pushed regularly up and down, a series of waves will be propagated outward from it. This is an

example of an important type of wave motion known as the regular wave train or continuous wave, in which, evidently, a regular succession of pulses is created and transmitted through the medium. The simplest type of regular wave train is a sinusoidal wave motion, described below.

A sinusoidal wave motion can be produced and propagated in a long, stretched string one end of which is attached to a weight supported by a spring, the weight being arranged so that it can move freely in the vertical direction, up and down (Fig. 4.1). When the weight is pulled downward a distance A and released, the weight executes a simple harmonic motion of certain period, say T, in the vertical direction and thus acts as a source of a sinusoidal transverse wave that travels along the string in a manner indicated in Fig. 4.1(b), the curves in which may be looked upon as successive 'snap shots' of the shape of the string during one half-cycle, i.e. $t = 0$ to $T/2$, after the motion has been well established. The wavelength denoted by λ is the distance between two successive crests or troughs. Since the period of oscillation of the weight is T, in time T the wave moves a distance of one wavelength λ, and so the wave velocity v is given by

$$v = \lambda/T \tag{4.7}$$

In terms of frequency $\nu = 1/T$, the velocity becomes

$$v = \nu\lambda \tag{4.8}$$
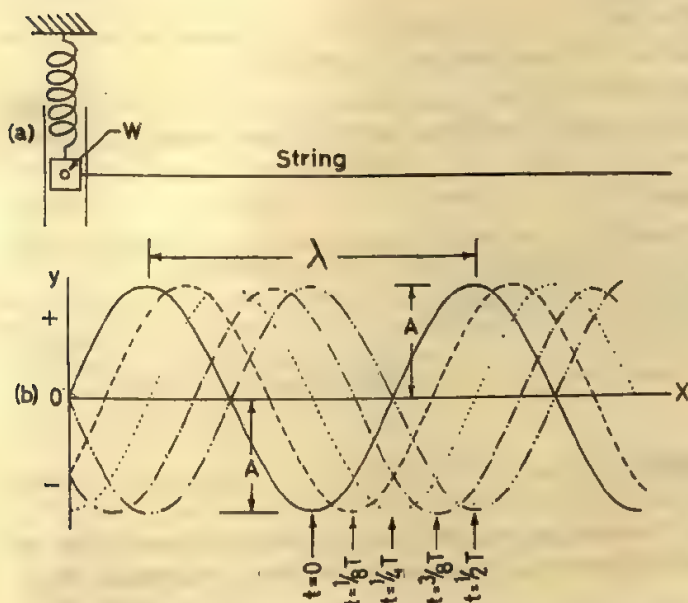
Fig. 4.1 (a) Arrangement for production and propagation of a sinusoidal transverse wave in a long string. (b) Successive waves corresponding to $t = 0$ to $t = T/2$ show the motion of the string during one half-cycle of oscillation of W, from $y = 0$ to $-A$ and back to 0.

A mathematical description of the sinusoidal transverse wave shown in Fig. 4.1, can now be formulated. Sometime after the wave is established, if we take $t = 0$ when the weight is moving downward through the equilibrium position 0, then the shape of the string at $t = 0$ will be as shown by the solid curve in Fig. 4.1(b) and represented by the following equation

$$y = A \sin 2\pi x/\lambda \tag{4.9}$$

where A is the maximum amplitude of the string and y is the amplitude of the string at point x, at $t = 0$. Thus, at $x = 0, \lambda/2, \lambda, 3\lambda/2, 2\lambda, \ldots$, the amplitude is zero, while at $x = \lambda/4, 5\lambda/4, 9\lambda/4, \ldots$ it is maximum in the positive direction, and at $x = 3\lambda/4, 7\lambda/4, 11\lambda/4, \ldots$ it is maximum in the negative direction.

At $t = T/8$, i.e. one-eighth of a cycle $(= 2\pi)$ later, the equation of the string is

$$y = A \sin (2\pi x/\lambda - \pi/4) \tag{4.10}$$

For example, at $x = \lambda/8$, the amplitude is zero, and at $x = 3\lambda/8$, it is maximum, and so on.

Similarly, at later times, as shown in Fig. 4.1(b), namely, at $t = (1/4)T$, $(3/8)T$, and $(1/2)T$, the equations are

$$\begin{align}
y &= A \sin (2\pi x/\lambda - \pi/2) \\
y &= A \sin (2\pi x/\lambda - \tfrac{3}{4}\pi) \\
y &= A \sin (2\pi x/\lambda - \pi)
\end{align} \tag{4.11}$$

In general, all the above equations can be written as

$$y = A \sin (2\pi x/\lambda - 2\pi t/T) \tag{4.12}$$

Substituting $T = 1/\nu$, and $\lambda = v/\nu$ in Eq. (4.12) we obtain the convenient form

$$y = A \sin 2\pi\nu(x/v - t) \tag{4.13}$$

This is the equation for a sinusoidal transverse wave moving in the positive x-direction with amplitude A.

The corresponding cosine expression

$$y = A \cos 2\pi\nu(x/v - t) \tag{4.14}$$

describes the same wave but with a phase shift of $\pi/2$ in the angle.

4.5 Wave Equation

When considering a sinusoidal function it is generally convenient in mathematical physics to write this function in complex exponential form. We know that

$$\exp (iu) = \cos u + i \sin u$$

where $i = \sqrt{-1}$.

So, if we write an expression in such a complex form, the real and

imaginary parts will equal the cosine and sine, respectively. We can then write the sinusoidal wave in the form

$$y = A \exp \left[2\pi \nu i (x/\nu - t) \right] \tag{4.15}$$

recognizing that the real part is to be employed in a physical problem. Eq. (4.15) can also be rewritten as

$$y = A \exp \left(2\pi i x/\lambda \right) . \exp \left(-2\pi i \nu t \right) \tag{4.16}$$

where λ, which equals ν/ν, is the wavelength. In the form of Eq. (4.16), the solution can thus be written as a product of a sinusoidal function of x and a sinusoidal function of time. This will be made use of in the following.

Differentiating y with respect to x, keeping t constant, we get from Eq. (4.16)

$$\frac{\partial^2 y}{\partial x^2} + \frac{4\pi^2}{\lambda^2} y = 0 \tag{4.17}$$

In Eq. (4.17) we are regarding the transverse displacement or amplitude y as merely the part of the function depending on the coordinate x. In other words, Eq. (4.17) determines only the space part, and not the time part, of the amplitude. It is thus a suitable starting point for setting up a wave function to describe wave mechanics.

4.6 The Schrödinger Wave Equation

The Schrödinger wave equation may be formulated, as shown below, by combining two relationships: on the one hand, the purely mathematical property of waves, namely, Eq. (4.17), and on the other hand, the wave property of matter as represented by de Broglie equation [Eq. (4.2)].

Eq. (4.17) represents wave motion in one direction. It may be extended to movement in three directions, represented by the coordinates x, y, z. Replacing y, the amplitude function for one coordinate, by $\psi(x,y,z)$ which is the amplitude function for three coordinates, Eq. (4.17) takes the form

$$\frac{\partial^2 \psi}{\partial x^2} + \frac{\partial^2 \psi}{\partial y^2} + \frac{\partial^2 \psi}{\partial z^2} + \frac{4\pi^2}{\lambda^2} \psi = 0 \tag{4.18}$$

where ψ has been written in place of $\psi(x,y,z)$ for the sake of brevity.

Utilizing the symbol ∇^2 for the differential (Laplacian) operator, Eq. (4.18) can be more concisely written as

$$\nabla^2 \psi + \frac{4\pi^2}{\lambda^2} \psi = 0 \tag{4.19}$$

It is the fundamental postulate of the Schrodinger treatment that an equation of the type of Eq. (4.19) may be applied to all particles including photons, electrons and atoms. As a further postulate, the de Broglie

relationship $\lambda = h/mv$ is introduced in Eq. (4.19) whereupon it becomes

$$\nabla^2\psi + \frac{4\pi^2 m^2 v^2}{h^2}\,\psi = 0 \qquad\qquad (4.20)$$

where m is the mass of the particle moving with a velocity v.

The total energy E of the particle is equal to the sum of the potential energy U and kinetic energy T, which, in turn, is equal to $\frac{1}{2}mv^2$, i.e.

$$E - U = T = \tfrac{1}{2}\,mv^2 \qquad\qquad (4.21)$$

Combining Eq. (4.21) with Eq. (4.20) we get

$$\nabla^2\psi + \frac{8\pi^2 m}{h^2}\,(E - U)\psi = 0 \qquad\qquad (4.22)$$

This is the famous wave equation described by Schrödinger in 1926. This equation describes, in very general terms, the motion of a particle of mass m under a potential U, and has been applied to a number of problems concerning atomic and molecular structures.

Since the Schrödinger equation in the form of Eq. (4.22) has been derived from Eq. (4.17), it does not involve the time part but only the space part of the wave function and so applies only to stationary states. The energy and the probability distribution are frequently the only quantities of experimental and theoretical interest; since these are not dependent on time, the time factor can be ignored, and hence the time-independent Schrödinger equation [Eq (4.22)] is sufficient for the purpose.

The mathematical task in applying the Schrödinger equation to a particular problem is to obtain a suitable expression for ψ showing how the wave amplitude varies with distances along the x-, y-, and z-axes, and then to derive solutions of the differential equation. There will be, in every case, many expressions for ψ satisfying the Schrödinger equation, all of which are, however, not acceptable. Only those wave functions which satisfy certain conditions are acceptable and are called *eigenfunctions* of the system, while the energies E corresponding to these *eigenfunctions* are called *eigenvalues*. The conditions which a wave function ψ must satisfy before it is acceptable can be summarized as follows:

(a) ψ must be finite and single valued for all values of the coordinates.
(b) ψ must be a continuous function of the coordinates.
(c) $\partial\psi/\partial x$, $\partial\psi/\partial y$ and $\partial\psi/\partial z$, must be continuous functions of x, y and z, respectively.
(d) $\int \psi^2 d\tau$ must be finite when the integration is carried out over the whole of space, of which $d\tau$ is a small volume element.

4.7   *Importance of the Schrödinger Equation*

The Schrödinger equation, like Newton's laws of motion, is a funda-

mental relationship, showing logical coherence to a vast amount of experimental observation. However, Newton's laws agree with experimental observations only so long as they are restricted to macroscopic systems and events, for experiments have proved that they are not completely valid when applied to phenomena on the microscopic scale.* In comparison, the Schrödinger equation has been found to hold true in both the cases. Thus, the deductions which have been made about atomic systems from the Schrödinger equation have been confirmed experimentally, and further, when applied to macroscopic bodies, the Schrödinger equation has been found to lead to the same conclusions as are derived from classical theory. In this context, Newton's laws seem to have become superfluous. However, Newton's laws are considerably much easier to apply and appreciate than the Schrödinger equation, and for objects, large enough in comparison to atoms, equally accurate as the latter. Nobody would therefore think of abandoning them. But, when Newton's laws disagree with the Schrödinger equation, as when applied to microscopic systems and events, the Schrödinger equation must be used in spite of its difficulties.

4.8 Physical Interpretation of the Wave Function

The only dependent variable in the Schrödinger equation is the wave amplitude or wave function ψ and it depends on the coordinates of the particle. In some cases it may turn out to be a complex function of the form $\psi = u + iv$, where u and v are real functions of the coordinates and $i = \sqrt{-1}$. The complex conjugate of ψ is $\psi^* = u - iv$. Their product $\psi\psi^* = u^2 + v^2$, and if ψ is real, $\psi\psi^*$ is identical with ψ^2. Neither ψ nor ψ^* has any physical significance, but $\psi\psi^*$ (or ψ^2, when ψ is real) has. In dealing with all forms of wave motion, such as light waves, sound waves, electrical fields, or matter waves, the square of the wave amplitude at any point is interpreted as the intensity of the effect at that point. So the value of ψ^2 (ψ^2 can be used instead of $\psi\psi^*$, since most of the wave functions in atomic or molecular structure problems contain real terms only) at any point around the nucleus gives a measure of the electronic charge density at that point. This interpretation was originally suggested by Schrödinger. According to this view the electron is to be regarded as smeared out forming a cloud of electricity, the density of which varies from point to point around the nucleus.

A statistical interpretation of the electron wave function was proposed

* The microscopic scale is defined as the one of atomic or subatomic phenomena, where the lengths entering into consideration are of the order of several angstroms at the most. The 'macroscopic' scale, on the contrary, is the one relating to phenomena that can be observed with the naked eye or with an ordinary microscope having resolution of the order of one micron ($= 10^{-4}$ cm) at the most.

by Max Born in 1926. This interpretation has been widely adopted since it has many advantages. According to this view, the electron is still considered as a particle, and the value of ψ^2 at any point is taken to represent the probability of finding the electron at that point at a given instant. It should be noted that consideration of the electron as a particle necessitates this statistical interpretation, for although a particle can be only in one position at a given instant, the Heisenberg uncertainty principle tells us that this position can never be precisely known. So what we can do is only to state the probability of the electron being found at a given point in space. Thus, ψ^2 is interpreted as giving a direct measure of this probability. Consequently, the greater the wave amplitude the greater is the probability of finding the electron at that point at a given instant, or, if a time interval is considered, the longer, on average, is the total time the electron spends at that point.

4.9 The Particle-in-a-Box Problem

Wave-mechanical treatment of physical problems is highly involved mathematically. The mathematics entailed in the complete solution of the wave equation even for the simplest of the atomic systems, viz. the hydrogen and hydrogen-like atoms, is extremely complicated. For this reason, the study of wave mechanics is reserved for those who have the required proficiency in mathematics. Nevertheless, even a relatively limited mathematical background is sufficient for one to grasp the basic procedures involved in the wave-mechanical treatment. To show this we consider here a very simple problem, namely, the particle-in-a-box problem, which, though hypothetical, bears some relevance to real molecular problems. Broadly, our objective in considering this problem is threefold: (*a*) To see how Schrödinger's equation is solved satisfying the given conditions; (*b*) to study the characteristic properties of these solutions; and (*c*) to compare the results of wave mechanics with those of Newtonian mechanics. Finally, we will illustrate the application of this model.

Particle in a one-dimensional box. Consider a particle of mass m bouncing back and forth between the walls of a box [Fig. 4.2(*a*)]. Suppose that the particle travels only along the x-axis and is confined between $x = 0$ and $x = a$ by two infinitely hard walls so that the particle has no chance of penetrating them. Suppose that the particle does not lose energy when it collides with such walls, so that its total energy remains constant. This box can then be represented by a potential well or box of width a with potential walls of infinite height [(Fig. 4.2(*b*)] at $x = 0$ and $x = a$, so that the potential energy V of the particle is infinitely high on both sides of the box, while on the inside, throughout the length a,
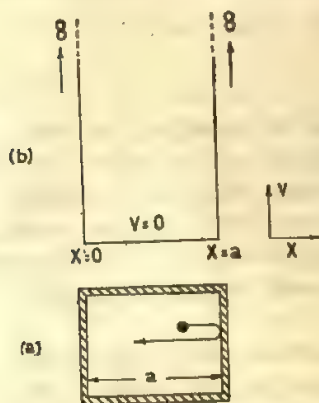
Fig. 4.2 A one-dimensional potential box with walls of infinite height at $x = 0$ and $x = a$

V is uniform. We may conveniently take this V inside the box to be zero.

Since the potential outside the box is infinitely high, the probability of finding the particle outside must be zero, that is to say, ψ^2 and hence ψ must be zero when $0 > x > a$. To avoid a discontinuity at $x = 0$ and $x = a$ the wave function must be zero at these points also and so the boundary conditions to be satisfied in the present problem are $\psi = 0$ at $x = 0$ and $\psi = 0$ at $x = a$. Our task is now to find what ψ is inside the box, in the region $0 < x < a$.

Since $V = 0$ inside the box, the one-dimensional wave equation reduces to

$$\frac{d^2\psi}{dx^2} + \frac{8\pi^2 m}{h^2} E\psi = 0 \tag{4.23}$$

The solution of this equation is

$$\psi = A \sin \left(\frac{8\pi^2 mE}{h^2}\right)^{1/2} x + B \cos \left(\frac{8\pi^2 mE}{h^2}\right)^{1/2} x \tag{4.24}$$

To satisfy the condition, $\psi = 0$ at $x = 0$, the parameter B in Eq. (4.24) must be zero. Consequently, the wave function reduces to

$$\psi = A \sin \left(\frac{8\pi^2 mE}{h^2}\right)^{1/2} x \tag{4.25}$$

Applying the condition $\psi = 0$ at $x = a$,

$$\psi = A \sin \left(\frac{8\pi^2 mE}{h^2}\right)^{1/2} a = 0$$

Since $A \neq 0$, $\sin (8\pi^2 mE/h^2)^{1/2} a = 0$. Therefore,

$$\left(\frac{8\pi^2 mE}{h^2}\right)^{1/2} a = n\pi \tag{4.26}$$

where $n = 0, 1, 2, 3, \ldots\ldots\ldots$

From Eq. (4.26) we get

$$E_n = n^2 h^2/8ma^2 \tag{4.27}$$

and correspondingly,

$$\psi_n = A \sin\left(\frac{n\pi}{a}\right) x \hspace{5cm} (4.28)$$

Therefore, only certain values of E, namely, E_n, are possible, and these are the only ones allowed. The energy values E_n are usually called eigenvalues and ψ_n eigenfunctions; the integer n may be termed a *quantum number*, and it arises here merely as a consequence of the boundary conditions imposed. This quantum number can be equal to $1,2,3,\ldots$ but not zero because then ψ, and hence ψ^2 or probability of finding the particle, would be zero everywhere within the box.

What emerges from the above treatment is that the energy is quantized and so cannot vary continuously. This wave-mechanical result is seemingly in sharp contrast to the prediction of classical mechanics that there is a continuous range of possible energies. However, it should be noted that h^2 is very small, so that for a particle in a box with dimensions of, say centimetres, the energy levels computed from Eq. (4.27) are so close together that we may as well say that the range of possible energies is continuous, in agreement with classical mechanics.

For example, the permitted energies of an electron, confined in a box 1 Å wide, are

$$E_n = \frac{n^2 \times (6{\cdot}63 \times 10^{-27})^2}{8 \times 9{\cdot}1 \times 10^{-28} \times (10^{-8})^2}$$
$$= 6 \times 10^{-11}\ n^2\ \mathrm{erg} \approx 38\ n^2\ \mathrm{eV}$$

The minimum energy that the said electron can have is 38 eV, corresponding to $n = 1$. The other permitted energy levels are $E_2 = 152$ eV, $E_3 = 342$ eV, $E_4 = 608$ eV, and so on. These energy levels are evidently quite far apart to make the quantization of electron energy in such a box conspicuous. If, however, the box is of macroscopic dimensions, say, 1 cm wide, the permitted electron energies are $E_n = 38 \times 10^{-16}\ n^2$ eV. The permissible energy levels are now so close together as to appear continuous.

In the domain of our everyday experience we do not feel the quantum effects, since on macroscopic scale they are imperceptible. Suppose, a ball of mass 10 g is rolling on the smooth floor of a 10 cm wide box with a speed of 3·3 cm/sec. The permitted energies for the ball, according to Eq. (4.27), are $E_n = 5{\cdot}49 \times 10^{-57}\ n^2$ erg. The kinetic energy of the ball is 54·4 ergs, and this corresponds to the energy level of quantum number $n = 10^{29}$! There is no way of determining whether the ball can take only those energies predicted by Eq. (4.27) for $n = 10^{29} + 1$, $10^{29} + 2$ etc., or any energy whatever, so that we may as well say that a continuous range of energies is possible. This illustrates Bohr's *correspondence principle* which states that quantum mechanics must yield identical results with those of classical physics in the limit of large quantum numbers.

The values of energy that the particle in the box can possess are 1, 4, 9, 16,......n^2 times the unit $h^2/8ma^2$. There are no energy values in between these values. It is significant that the electron cannot have zero energy since n cannot be zero, for the reason cited above. Like quantization of energy, this exclusion of $E = 0$ as a possible value for the energy is a quantum-mechanical result, which finds no counterpart in classical mechanics. On the basis of classical mechanics, all energies, including zero, are permissible. The minimum energy in the present case, namely, E_1, is $h^2/8ma^2$. It is the *zero point energy* of the system. Any system involving vibratory motion is associated with a zero point energy.

Fig. (4.3) shows, schematically, the three energy levels corresponding to the quantum number 1, 2 and 3, together with the plots of the respective wave functions and probability distributions for the particle. It is seen from this figure that, for the lowest or ground state, one half-wavelength covers the box and so there is no internal node. In higher energy levels, however, the wave functions have internal nodes — one in the second level, two in the third, and in general, $n - 1$ in the nth. So the greater the number of nodes, and hence the more the curvature in the wave function, the greater is the total energy, which, it may be noted, is equal to the kinetic energy alone, since in this particular problem the potential energy has been assumed to be uniformly zero inside the box.

A question may now be asked: What is the value of A, the maximum amplitude of the wave function? It may be noted that the solutions of the wave equation are independent of the magnitude of A and this permits us to choose a value for A in order to satisfy any condition we want to impose. Customarily, the value of A is adjusted so that ψ^2 becomes actually

WAVE FUNCTION ψ
PROBABILITY FUNCTION ψ^2
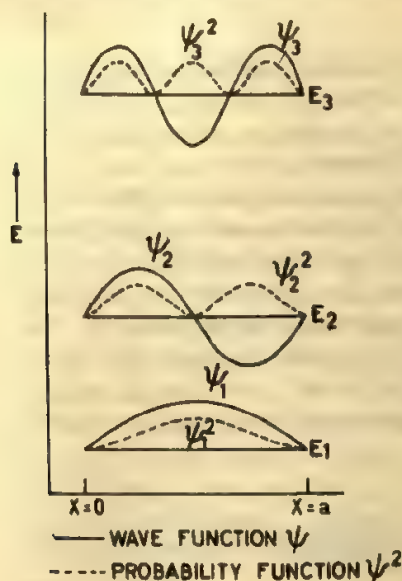
Fig. 4.3 Schematic representation of energy levels and corresponding wave functions and probability distribution functions of a particle in a one-dimensional box with infinite potential walls

equal to the probability (P_x) of finding the particle at a point x, instead of being simply proportional to this probability, as is the case otherwise. This is done by a process known as normalization, which involves setting to unity the integral of the probability between two fixed limits. Thus, since the particle must be somewhere between $x = 0$ and $x = a$, the integral of probability between these two limits must, obviously, be unity, that is,

$$\int_0^a P_x dx = \int_0^a \psi^2_n \, dx = 1$$

Substituting ψ_n from Eq. (4.28)

$$\int_0^a \left[A \sin \left(\frac{n\pi x}{a} \right) \right]^2 dx = 1$$

$$A^2 \int_0^a \frac{1}{2} \left[1 - \cos \left(\frac{2n\pi x}{a} \right) \right] dx = 1$$

or

$$\frac{1}{2} A^2 \left[x - \frac{a}{2n\pi} \sin \left(\frac{2n\pi}{a} x \right) \right]_0^a = 1$$

Hence

$$A = \sqrt{2/a} \qquad\qquad\qquad\qquad\qquad\qquad\qquad\qquad (4.29)$$

Therefore, the normalized wave function is

$$\psi_n = \sqrt{2/a} \, \sin \left(\frac{n\pi}{a} x \right) \qquad\qquad\qquad\qquad (4.30)$$

It is obvious from Eq. (4.30) that the probability of finding the particle at the nodes, i.e. at $x = a/n$, where n is an integer, is zero, and that, in between the nodes, this probability passes through a maximum of $2/a$. Thus, at a particular point in the box between $x = 0$ and $x = a$, the probability of the particle being present may be quite different for different quantum numbers. For instance, in the lowest energy level of $n = 1$, the particle is most likely to be in the middle of the box $(x = a/2)$, while in the next higher state of $n = 2$, the particle is never to be found there! It is interesting to compare this result with what would be expected from the classical point of view. Thus, since the potential is, by assumption, uniformly zero inside the box, classical theory would require that the probability of finding the particle be equal at all values of x. So,

$$\int_0^a P_x dx = P_x \int_0^a dx = P_x a = 1$$

from which $P_x = 1/a$. The probability from classical theory is thus half of the maximum probability from wave theory.

Before leaving our discussion of the wave-mechanical treatment of a particle in a one-dimensional box it is convenient to introduce an important mathematical property of eigenfunctions of the wave equation, namely, that any two eigenfunctions are *orthogonal*. Thus, if we consider the eigenfunctions ψ_n and ψ_m corresponding to two different states of the system, that is $n \neq m$, then it is found that, whatever the values of n and m,

$$\int_0^a \psi_n \psi_m \, dx = 0 \tag{4.31}$$

Functions for which this relation is true are said to be orthogonal to one another.

On examining the wave functions illustrated in Fig. 4.3 we find that, if the quantum number n is odd, $\psi(x) = \psi(a - x)$; for example, if $n = 3$, ψ at $a/6$ is the same as ψ at $5a/6$, and so on. On the other hand, if the quantum number is even, $\psi(x) = -\psi(a - x)$. Consequently, if n is even and m odd (or vice versa), on integrating Eq. (4.31), the region on one side of the centre cancels the region on the other side. (Consider for example, the integral when $n = 2$, $m = 3$ with reference to Fig. 4.3.) We can also show that Eq. (4.31) is true whatever the values of n and m, Thus, supposing $n > m$,

$$\int_0^a \psi_n \psi_m \, dx = \int_0^a \left[\sqrt{2/a} \, \sin\left(n\pi \frac{x}{a}\right) \sqrt{2/a} \, \sin\left(m\pi \frac{x}{a}\right) \right] dx$$

$$= \frac{1}{a} \int_0^a \left[(\cos(n - m)\pi(x/a) - \cos(n + m)\pi(x/a) \right] dx$$

$$= \frac{1}{a} \left[\frac{a}{(n - m)\pi} \sin(n - m)\pi(x/a) \right.$$

$$\left. - \frac{a}{(n + m)\pi} \sin(n + m)\pi(x/a) \right]_0^a$$

Since n and m are integers, $(n - m)$ and $(n + m)$ are also integers; consequently, the sines of all the angles in this expression are zero and the integral is therefore zero. Thus any two eigenfunctions for the particle in a box are orthogonal. In fact, it is a general feature that solutions of the Schrödinger equation corresponding to different energy eigenvalues are always mutually orthogonal.

Particle in a three-dimensional box. In place of a one-dimensional box considered above, we now consider a three-dimensional rectangular box having sides a_x, a_y and a_z, and with potential zero everywhere inside the box but infinite outside. The wave function $\psi(x, y, z)$ in this case depends on three coordinates x, y and z. So in place of Eq. (4.23) we have to write

$$\frac{\partial^2\psi}{\partial x^2} + \frac{\partial^2\psi}{\partial y^2} + \frac{\partial^2\psi}{\partial z^2} + \frac{8\pi^2 m}{h^2} E\psi = 0 \tag{4.32}$$

The particle inside the box must satisfy the differential equation (4.32). To solve this equation we first see whether the same wave function can be factorized into the product of three independent functions $X(x)$, $Y(y)$ and $Z(z)$, each being dependent only on one coordinate, namely, x, y and z respectively. Let us assume that

$$\psi(x,y,z) = X(x)\,Y(y)\,Z(z)$$

or simply, for the sake of convenience,

$$\psi = XYZ$$

Since X is dependent on x only,

$$\frac{\partial\psi}{\partial x} = YZ\frac{\partial X}{\partial x};\ \frac{\partial^2\psi}{\partial x^2} = YZ\frac{\partial^2 X}{\partial x^2}.$$

Similarly

$$\frac{\partial^2\psi}{\partial y^2} = XZ\frac{\partial^2 Y}{\partial y^2},\ \text{and}\ \frac{\partial^2\psi}{\partial z^2} = XY\frac{\partial^2 Z}{\partial z^2}$$

Substituting these relations in Eq. (4.32), dividing throughout by XYZ and rearranging, we obtain

$$-\frac{h^2}{8\pi^2 m}\left(\frac{1}{X}\frac{\partial^2 X}{\partial x^2} + \frac{1}{Y}\frac{\partial^2 Y}{\partial y^2} + \frac{1}{Z}\frac{\partial^2 Z}{\partial z^2}\right) = E \tag{4.33}$$

If the total energy E is written as the sum of three contributions associated with the three coordinates, then Eq. (4.33) can be separated into three equations. For example, for motion parallel to the x-axis (i.e. when x varies, y and z remaining constant), the second and third terms on the left-hand side of Eq. (4.33) will be constant. Now, since E is constant, the first term must also be constant. We call this constant value E_x and write the following equation.

$$-\frac{h^2}{8\pi^2 m}\left(\frac{1}{X}\frac{\partial^2 X}{\partial x^2}\right) = E_x \tag{4.34}$$

From similar arguments, we have

$$-\frac{h^2}{8\pi^2 m}\left(\frac{1}{Y}\frac{\partial^2 Y}{\partial y^2}\right) = E_y \tag{4.35}$$

and

$$-\frac{h^2}{8\pi^2 m}\left(\frac{1}{Z}\frac{\partial^2 Z}{\partial z^2}\right) = E_z \tag{4.36}$$

The total energy E is given by

$$E = E_x + E_y + E_z \tag{4.37}$$

Factorization of the wave function into the product of three independent functions thus leads to three independent equations (4.34)–(4.36), the sum of which represents the original equation [Eq. (4.33)].

Since Eqs. (4.34)–(4.36) are of the same form as Eq. (4.23), the solution for which is given by Eq. (4.30), we can straightaway write the solution of Eq. (4.33) as

$$\psi = XYZ = \left[\sqrt{2/a_x} \, \sin \left(\frac{n_x \pi x}{a_x} \right) \right] \left[\sqrt{2/a_y} \, \sin \left(\frac{n_y \pi y}{a_y} \right) \right]$$
$$\left[\sqrt{2/a_z} \, \sin \left(\frac{(n_z \pi z)}{a_z} \right) \right]$$
$$= \sqrt{8/V} \, \sin \left(\frac{n_x \pi x}{a_x} \right) \sin \left(\frac{n_y \pi y}{a_y} \right) \sin \left(\frac{n_z \pi z}{a_z} \right) \tag{4.38}$$

since the volume of the box $V = a_x.a_y.a_z$.

Comparison of Eqs. (4.27) and (4.37) shows that the expression for the allowed energy levels in the present problem is

$$E = \frac{h^2}{8m} \left(\frac{n_x^2}{a_x^2} + \frac{n_y^2}{a_y^2} + \frac{n_z^2}{a_z^2} \right) \tag{4.39}$$

In this three-dimensional problem, n_x, n_y and n_z are the quantum numbers, respectively in x, y, and z-directions of the Cartesian system.

If the particle be in a cubic box, in which case $a_x = a_y = a_z = a$, Eq. (4.39) reduces to

$$E = \frac{h^2}{8ma^2} \, [n_x^2 + n_y^2 + n_z^2] \tag{4.40}$$

The energy thus depends on the *sum* of the squares of the three quantum numbers and, evidently, it is possible for groups of different states, each specified by a unique set of the three quantum numbers, to possess the same energy. In such a case, the energy level and the corresponding independent states are said to be *degenerate*. Thus, for the level for which the energy is $6h^2/8ma^2$, there are three independent states having quantum numbers (2,1,1), (1,2,1) and (1,1,2) for (n_x,n_y,n_z). This level is therefore three-fold degenerate or triply degenerate. Some other similar combinations are shown in Fig. 4.4. It will be noted that the ground state (1,1,1) as also several other states like (2,2,2) are *non-degenerate*. The number of degenerate states will, however, be less if only two sides of the box are equal and will be nil if the three sides are unequal.

The degeneracy breaks down on applying even a small modification to the system. Consider, for example, the triply degenerate level having $E = 6h^2/8ma^2$, as referred to above. Now suppose that the x-dimension were increased by a small amount ∂a. The corresponding change in energy of the first state (2,1,1), which has $4h^2/8ma^2$ associated with the x-direction, will be different from that for the other two states (1,2,1) and (1,1,2), which have $h^2/8ma^2$ associated with the x-direction. To a first approximation, the energy will decrease by $(8\partial a/a)(h^2/8ma^2)$ for the first state, but for the other two states it will decrease only by $(2\partial a/a)(h^2/8ma^2)$. Breakdown of degeneracy, which thus occurs due to
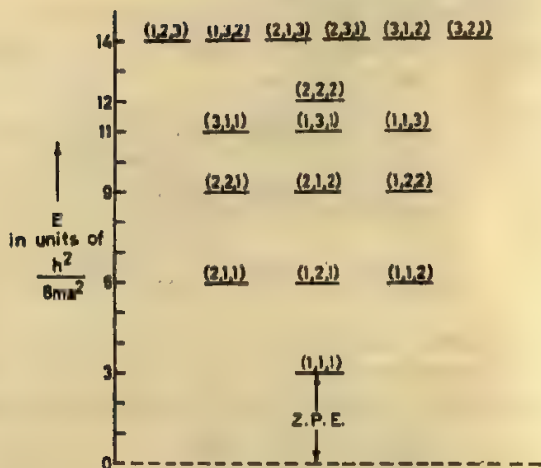
Fig. 4.4 Quantized energy levels of a particle of mass m in a cubic box of side a illustrating degeneracy and zero-point energy (Z.P.E.). Sets of quantum numbers (n_x, n_y, n_z) lying on the same energy level denote degenerate states.

some modification applied to the system, has relevance to what is often observed in practice, such as the splitting of spectral lines in a magnetic or electric field. As a result of the application of a magnetic or electric field the degenerate level breaks up into separate levels, and consequently, spectral lines which were single become multiplets.

4.10 Application of the Particle-in-a-Box Model

The simple problem considered above has, in fact, some counterparts in real molecular problems. As an illustration, let us calculate, on the basis of the particle-in-a-box model, the wavelength of the radiation that will be absorbed in the lowest energy transition of the double-bonding or π electrons (see Section 6.10) of hexatriene. Hexatriene molecule with its conjugated three double bonds has six π-electrons. Due to delocalization, these electrons are relatively free to move throughout the length of the molecule. We can therefore approximately represent the molecule as a one-dimensional region of constant potential bounded on both sides by regions of infinitely large potential. The permissible energies of the π electrons are then given (ignoring electron–electron repulsion) by Eq. (4.27). Evidently, all the electrons cannot be accommodated in a state represented by a single quantum number since that would violate Pauli's exclusion principle, according to which no two electrons of a molecule can have all their quantum numbers the same. Since, however, the orientation of the electron spin can give a spin quantum number of
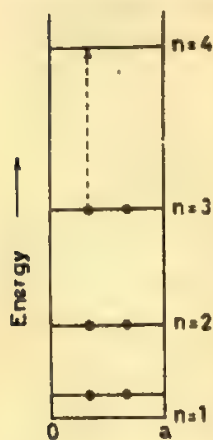
Fig. 4.5 Particle-in-a-box model for π-electrons of hexatriene. The broken arrow shows the lowest energy transition.

+ 1/2 or − 1/2, each state specified by the principal quantum number n can accommodate two electrons at the most. The six π electrons therefore occupy three lowest energy levels corresponding to $n = 1$, 2, and 3, as represented in Fig. 4.5. The lowest energy transition then occurs with the promotion of one electron from $n = 3$ state to the next higher state, as shown by the broken arrow in Fig. 4.5. The quantum radiation energy absorbed in the said transition is given by

$$h\nu = E_4 - E_3 = \frac{h^2}{8ma^2} \, (4^2 - 3^2)$$

Taking $a = 7{\cdot}3$ Å as the length of the molecule, we obtain $h\nu = hc/\lambda$ $= 7{\cdot}93 \times 10^{-12}$ erg or, $\lambda = 2{,}507$ Å. This compares quite well with the observed value, namely, $\lambda = 2{,}580$ Å.

Suggested Reading

HEITLER, W., *Elementary Wave Mechanics*, Clarendon Press, Oxford, 1956.

LINNETT, J. W., *Wave Mechanics and Valency*, Methuen, London, 1960.

CUMPER, C.W.N., *Wave Mechanics for Chemists*, Heinemann, London, 1966.

Problems

4.1 Calculate the wavelength (in angstrom units) and energy (in eV) of a body with a mass of 1 g moving with a velocity of 1 cm/sec.

4.2 Calculate the wavelength of an electron having 1 eV of energy.

4.3 Calculate the energy (in ergs and in eV) of an electron in the first four quantum states of a one-dimensional box of length (a) 2×10^{-8} cm and (b) 1 cm.

4.4 A 10 g marble is rolling back and forth between the sides of a level box 10 cm wide with a speed of 10 cm/sec. Calculate the quantum number of the energy level.

Chapter 5

Wave Mechanics of the Hydrogen Atom

5.1 Introduction

The hydrogen atom and hydrogen-like ions, like He^+, Li^{+2}, Be^{+3}, comprising simply one electron and a nucleus, represent the simplest of atomic systems. The Schrödinger equation has been exactly solved only for these simple atomic species, because the occurrence of more than one electron, as in other atoms, complicates the mathematics so greatly as to permit only approximate solutions. The hydrogen atom has thus secured a unique place in the wave theory of atoms. In the following discussion of the hydrogen atom, however, we will present only a broad outline of the procedure involved in the wave-mechanical treatment, and put more emphasis on the interpretation and significance of the formal mathematical results in terms of familiar concepts.

5.2 Schrödinger Equation for the Hydrogen Atom

The hydrogen atom consists of a nucleus (proton) of electric charge $+ e$ which exerts a Coulombic force e^2/r^2 on a single electron of charge $- e$ at a distance r. The electric potential energy of the electron is zero at infinity and at a finite distance r from the nucleus it is given by

$$U = \int_\infty^r F.dr = \int_\infty^r \frac{e^2}{r^2}\, dr = - \frac{e^2}{r}$$

Using this value of U and taking the nucleus as the centre of our system of coordinates the Schrödinger equation [Eq. (4.22)] now takes the form

$$\frac{\partial^2\psi}{\partial x^2} + \frac{\partial^2\psi}{\partial y^2} + \frac{\partial^2\psi}{\partial z^2} + \frac{8\pi^2 m}{h^2}\left(E + \frac{e^2}{r}\right)\psi = 0 \tag{5.1}$$

For the sake of convenience we shall consider the nucleus to be stationary. However, as in the Bohr theory, the correction for the motion of the nucleus can be obtained by simply replacing the electron mass m by the reduced mass μ. The above physical model for the hydrogen atom can be applied to hydrogen-like ions (He^+, Li^{+2}, Be^{+3}) simply by taking $U = -Ze^2/r$, corresponding to a nuclear charge of $+Ze$, Z being the atomic number. In the more general form, Eq. (5.1) is thus written as

$$\frac{\partial^2\psi}{\partial x^2} + \frac{\partial^2\psi}{\partial y^2} + \frac{\partial^2\psi}{\partial z^2} + \frac{8\pi^2\mu}{h^2}\left(E + \frac{Ze^2}{r}\right)\psi = 0 \tag{5.2}$$

The electron-nuclear distance r which appears in the potential energy term can be expressed in terms of the Cartesian coordinates as $r^2 = x^2 + y^2 + z^2$. However, owing to the symmetry of the physical situation it will be more convenient to express Eq. (5.2) in terms of the spherical polar coordinates r, θ, φ (Fig. 5.1), where r is the length of the radius vector, θ the angle between the axis of the sphere and the radius vector (or, in other words, it corresponds to $\pi/2 -$ 'latitude'), and φ the angle between a fixed meridian plane and the meridian plane in which r is measured (i.e. it corresponds to the 'longitude'); θ is called the zenith angle and φ the azimuthal angle.

The transformation of Eq. (5.2) from the Cartesian to spherical coordinates yields

$$\frac{1}{r^2}\left[\frac{\partial}{\partial r}\left(r^2\frac{\partial\psi}{\partial r}\right) + \frac{1}{\sin\theta}\frac{\partial}{\partial\theta}\left(\sin\theta\frac{\partial\psi}{\partial\theta}\right)\right.$$

$$\left. + \frac{1}{\sin^2\theta}\frac{\partial^2\psi}{\partial\varphi^2}\right] + \frac{8\pi^2\mu}{h^2}\left(E + \frac{Ze^2}{r}\right)\psi = 0 \tag{5.3}$$

This is the partial differential equation for the wave function ψ of
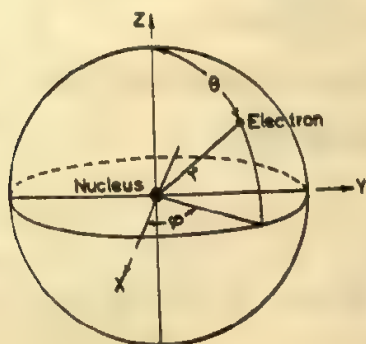
Fig. 5.1 Positions of coordinates of the electron. Clearly, θ varies from 0 to π and φ varies from 0 to 2π.

the electron in a one-electron atom. Coupled with the various conditions ψ must satisfy (see Section 4.6), this equation completely specifies the behaviour of the electron.

5.3 Separation of Variables

The advantage of writing the Schrödinger equation in terms of spherical polar coordinates for the problem of one-electron atom, as we have done above, is that in this form it may be readily separated into three independent equations each involving only one coordinate. Let us assume that $\psi\,(r,\,\theta,\,\varphi)$ can be written as the product of three functions: $R(r)$, which depends upon r alone; $\Theta\,(\theta)$, which depends upon θ alone; and $\Phi(\varphi)$, which depends upon φ alone. Thus,

$$\psi(r,\theta,\varphi) = R(r)\Theta(\theta)\Phi(\varphi) \tag{5.4}$$

The function $R\,(r)$ describes how the wave function ψ of the electron varies with the radial distance from the nucleus, with θ and φ constant. The function $\Theta\,(\theta)$ describes how ψ varies with the zenith angle θ along a meridian on a sphere centred at the nucleus, r and φ being constant. The function $\Phi\,(\varphi)$, on the other hand, describes how ψ varies with the azimuthal angle φ along a circle on a sphere centred at the nucleus with r and θ constant.

We may write Eq. (5.4) in a simpler form as

$$\psi = R\Theta\Phi \tag{5.5}$$

and correspondingly,

$$\begin{aligned}
\partial\psi/\partial r &= \Theta\Phi\,\partial R/\partial r \\
\partial\psi/\partial\theta &= R\Phi\,\partial\Theta/\partial\theta \\
\partial\psi/\partial\varphi &= R\Theta\,\partial\Phi/\partial\varphi
\end{aligned} \tag{5.6}$$

Substituting Eqs. (5.5) and (5.6) into (5.3) we find

$$\frac{1}{r^2}\left[\Theta\Phi\,\frac{\partial}{\partial r}\left(r^2\frac{\partial R}{\partial r}\right) + \frac{R\Phi}{\sin\theta}\frac{\partial}{\partial\theta}\left(\sin\theta\,\frac{\partial\Theta}{\partial\theta}\right) + \frac{R\Theta}{\sin^2\theta}\frac{\partial^2\Phi}{\partial\varphi^2}\right] + \frac{8\pi^2\mu}{h^2}\left(E + \frac{Ze^2}{r}\right)R\Theta\Phi = 0 \tag{5.7}$$

Multiplying each term in Eq. (5.7) by the factor $r^2\sin^2\theta/R\Theta\Phi$, we get

$$\frac{\sin^2\theta}{R}\frac{\partial}{\partial r}\left(r^2\frac{\partial R}{\partial r}\right) + \frac{\sin\theta}{\Theta}\frac{\partial}{\partial\theta}\left(\sin\theta\,\frac{\partial\Theta}{\partial\theta}\right) + \frac{1}{\Phi}\frac{\partial^2\Phi}{\partial\varphi^2} + \frac{8\pi^2\mu}{h^2}\left(E + \frac{Ze^2}{r}\right)r^2\sin^2\theta = 0 \tag{5.8}$$

It is seen that the third term of Eq. (5.8) is a function of φ only, while the other terms are independent of φ. Let us rearrange Eq. (5.8) to read

$$-\frac{1}{\Phi}\frac{\partial^2\Phi}{\partial\varphi^2} = \frac{\sin^2\theta}{R}\frac{\partial}{\partial r}\left(r^2\frac{\partial R}{\partial r}\right) + \frac{\sin\theta}{\Theta}\frac{\partial}{\partial\theta}\left(\sin\theta\frac{\partial\Theta}{\partial\theta}\right) +$$

$$\frac{8\pi^2\mu}{h^2}\left(E + \frac{Ze^2}{r}\right)r^2\sin^2\theta \tag{5.9}$$

Since the two sides of Eq. (5.9) are functions of different variables, this equation can be correct only if each side is equal to the same constant, which we shall call m^2. We then have two equations:

$$-\frac{1}{\Phi}\frac{d^2\Phi}{d\varphi^2} = m^2 \tag{5.10}$$

and $\dfrac{\sin^2\theta}{R}\dfrac{\partial}{\partial r}\left(r^2\dfrac{\partial R}{\partial r}\right) + \dfrac{\sin\theta}{\Theta}\dfrac{\partial}{\partial\theta}\left(\sin\theta\dfrac{\partial\Theta}{\partial\theta}\right) +$

$$\frac{8\pi^2\mu}{h^2}\left(E + \frac{Ze^2}{r}\right)r^2\sin^2\theta = m^2 \tag{5.11}$$

Dividing each term in Eq. (5.11) by $\sin^2\theta$ and rearranging we find that

$$\frac{1}{R}\frac{\partial}{\partial r}\left(r^2\frac{\partial R}{\partial r}\right) + \frac{8\pi^2\mu}{h^2}\left(E + \frac{Ze^2}{r}\right)r^2$$

$$= \frac{m^2}{\sin^2\theta} - \frac{1}{\Theta\sin\theta}\frac{\partial}{\partial\theta}\left(\sin\theta\frac{\partial\Theta}{\partial\theta}\right) \tag{5.12}$$

Here also we have an equation the two sides of which involve two variables and must therefore be equal to the same constant, which we shall call L. We then have the following two separate equations:

$$\frac{1}{\sin\theta}\frac{d}{d\theta}\left(\sin\theta\frac{d\Theta}{d\theta}\right) + \left(L - \frac{m^2}{\sin^2\theta}\right)\Theta = 0 \tag{5.13}$$

and $\quad\dfrac{1}{r^2}\dfrac{d}{dr}\left(r^2\dfrac{dR}{dr}\right) + \dfrac{8\pi^2\mu}{h^2}\left(E + \dfrac{Ze^2}{r}\right)R - \left(\dfrac{L}{r^2}\right)R = 0 \tag{5.14}$

We have thus separated the variables in the partial differential equation (5.3), in place of which we now have three ordinary differential equations to solve — Eqs. (5.10), (5.13) and (5.14).

5.4 Quantum Numbers

The procedure for solving the above set of differential equations is as follows:

(i) We first solve Eq. (5.10) for $\Phi(\varphi)$ and find the values of m which yield well-behaved solutions.

(ii) The values of m so obtained are used in Eq. (5.13) and the values of L which yield well-behaved solutions, $\Theta(\theta)$, are found.

(iii) These values of L are used in Eq. (5.14) and the values of E which

yield well-behaved solutions, $R(r)$, are found. These values of E are the allowed values of the electron energy of the atomic system we are studying.

Equation (5.10) is readily solved, with the result

$$\Phi(\varphi) = Ae^{im\varphi} \tag{5.15}$$

where A is the constant of integration.

One of the conditions (see Section 4.6) that the wave function ψ, and hence $\Phi(\varphi)$ which is a component of ψ, must satisfy is that it should have a single value at a given point in space. Since φ and $\varphi + 2\pi$ refer to the same meridian plane (see Fig. 5.1), it must be true that $\Phi(\varphi) = \Phi(\varphi + 2\pi)$, or

$$Ae^{im\varphi} = Ae^{im(\varphi + 2\pi)}$$

This can happen only when m is zero, or a positive or negative integer, that is, when $m = 0, \pm 1, \pm 2, \ldots \ldots$ Therefore, m is a quantum number. It is usually called the *magnetic quantum number*, because the energy of a hydrogen atom in a magnetic field depends on the value of this quantum number; it is analogous to m_l in the old-quantum-theory treatment (Section 3.3).

The acceptable values of m found are now substituted into Eq. (5.13) and the allowed values of L, which yield well-behaved solutions, $\Theta(\theta)$, are investigated. This problem being beyond the scope of this book, we shall only state the results. It is found that for $\Theta(\theta)$ to be well-behaved, L must be of the form

$$L = l(l + 1) \tag{5.16}$$

where l is an integer equal to or greater than $|m|$, the absolute value of m. In other words,

$$l = |m|, |m| + 1, |m| + 2, \ldots \tag{5.17}$$

The integer l is known as the angular momentum (or azimuthal) quantum number, because it determines the angular momentum. The angular momentum associated with a particular value of l is given by $\sqrt{l(l + 1)}$ $(h/2\pi)$. The relation between the permissible values of m and l given by Eq. (5.17) can be expressed in the form $m = 0, \pm 1, \pm 2, \ldots \ldots, \pm l$.

The value of L from Eq. (5.16) is then substituted into Eq. (5.14) and the allowed values of E are investigated. The mathematics of the problem being too complicated to be worked out here, only the results will be stated. It is found that all positive values of E are associated with well-behaved functions, $R(r)$. This result is, of course, quite expected, since, as we have already seen in Section 2.8, positive values of the energy correspond to ionization, so that the electron is free from the bounds of the nucleus and therefore can take up a continuous range of energies. However, here we are interested in the negative values of E, since E being negative signifies that the electron is bound to the atom. But it is found

that only certain, and not all, negative values of E yield well-behaved $R(r)$. These allowed values are specified by

$$E_n = \frac{-2\,\pi^2\,\mu\,Z^2\,e^4}{n^2 h^2} \tag{5.18}$$

where $n = l + 1,\ l + 2,\ l + 3, \ldots$ \hfill (5.19)

We recognize that Eq. (5.18), which is the result of the wave-mechanical treatment, is precisely the same as Eq. (2.25), found by the Bohr theory. We thus see that the concept of energy quantization in atoms, which was first introduced by Bohr merely as a hypothesis, now appears inevitably in the wave-mechanical treatment as a result of demanding only well-behaved solutions. The constant n is known as the principal or total quantum number, and its relation to l, as given by Eq. (5.19), can be expressed in the form $l = 0, 1, 2, \ldots\ldots, (n-1)$.

We have thus, obtained three quantum numbers which we may list together with their permissible values as follows:

$n = 1, 2, 3, \ldots\ldots$

$l = 0, 1, 2, \ldots\ldots, (n-1)$

$m = 0, \pm 1, \pm 2, \ldots\ldots, \pm l$

To sum up, all the quantum numbers are integers and their relative values are specified by the inequality:

$$n > l \geq |m| \tag{5.20}$$

Indicating by subscripts the quantum numbers upon which each function depends, we can now rewrite Eq (5.4) as

$$\psi_{nlm}(r,\theta,\varphi) = R_{nl}(r)\Theta_{lm}(\theta)\Phi_m(\varphi) \tag{5.21}$$

A quantum state is characterized by a set (triplet) of three quantum numbers (n, l, and m), whose relative values satisfy (5.20), but the energy of the one-electron system, as given by Eq. (5.18), is specified only by the total quantum number n. So more than one set of quantum numbers, with the same principal quantum number n, may correspond to the same energy — a situation which we have already encountered in the particle-in-a-box problem in the previous chapter. For $n > 1$, the energy states of the one-electron system are thus *degenerate*.

The degeneracy, however, is removed when the atom is subjected to an external electromagnetic field. Under this condition a state of total quantum number n breaks up into several substates, the energies of which are slightly more or slightly less than the energy of the original state in the absence of the field. This phenomenon is manifested in the splitting up of individual spectral lines into separate lines when atoms radiate in an external magnetic field (*Zeeman effect*), or in an external electric field (*Stark effect*).

In addition to the three quantum numbers, discussed above, which arise in the solution of the Schrödinger equation, there is the fourth

quantum number, m_s, called spin quantum number which can take on only the values $+ 1/2$ or $- 1/2$. The notion of electron spin with its associated magnetic moment and quantum number was first introduced by Goudsmit and Uhlenbeck in order to obtain empirical agreement between theory and experiment. It should be noted, however, that the classical picture of electrons as spinning charged spheres, which Goudsmit and Uhlenbeck had in mind, hardly accords with quantum mechanics. But in 1928 Dirac devised a relativistic form of the quantum mechanical treatment on the basis of which it was shown that a particle having the charge and mass of the electron must behave exactly as if it had the intrinsic angular momentum and accompanying spin magnetic moment postulated earlier by Uhlenbeck and Goudsmit.

What emerges from the above discussion is that the value of the principal quantum number, n, is the most important determining factor for the energy of the electron, but in the presence of an electromagnetic field, the energy depends on all four quantum numbers, so that a given electronic energy is specified by the quartet of quantum numbers (n, l, m, and m_s). However, even in the absence of applied electric or magnetic fields, such fields are present in a multi-electron atom because of the movement of inner electrons.

5.5   Hydrogen-like Wave Functions

The complete wave function of a one-electron or hydrogen-like atom is equal to the product of the radial wave function and the spherical wave functions, as given by Eq. (5.21). The interpretation of the wave function has been considered in Chapter 4 (see Section 4.8). Here we may only state that the probability of finding an electron, which is in the quantum state (n, l, m), in a certain elemental volume $dv = r^2 dr \sin\theta \, d\theta \, d\varphi$, in the neighbourhood of the point (r, θ, φ) is given by $\{\psi_{nlm}(r,\theta,\varphi)\}^2 \, dv$. (It is understood that here, as well as in all subsequent cases, the square of any wave function is to be replaced by the product of it and its complex conjugate, if the function is a complex quantity.) So, ψ^2_{nlm} may be called the *probability density* for the electron. From Eq. (5.21) we can write

$$\psi^2_{nlm} = R^2_{nl}\Theta^2_{lm}\Phi^2_m \tag{5.22}$$

Expressed in this way, Φ^2_m gives the probability density ψ^2_{nlm} as a function of the angle φ alone; Θ^2_{lm} gives the probability density as a function of the angle θ alone, and R^2_{nl} gives the probability density as a function of r alone.

The probability of the electron being found in the atom is unity since the electron must exist somewhere. Therefore, the integral of the probability density over the entire volume of the atom must equal unity, that is,

$$\int_0^\infty \int_0^\pi \int_0^{2\pi} \psi_{nlm}\ (r,\theta,\varphi)\ \psi^*_{nlm}\ (r,\theta,\varphi)\ r^2\ \sin\theta\ d\theta\ d\varphi\ dr = 1 \qquad (5.23)$$

Eq. (5.23) gives the condition for normalization of the total wave function. Similarly, the conditions for normalization of the spherical and radial wave functions are:

$$\int_0^{2\pi} \Phi_m\ (\varphi)\ \Phi^*_m\ (\varphi)\ d\varphi = 1 \qquad (5.24)$$

$$\int_0^\pi \{\Theta_{lm}\ (\theta)\}^2\ \sin\theta\ d\theta = 1 \qquad (5.25)$$

$$\int_0^\infty \{R_{nl}\ (r)\}^2\ r^2\ dr = 1 \qquad (5.26)$$

It is easy to show that the probability density does not depend on the azimuthal angle φ at all. Earlier in this chapter, we found that

$$\Phi_m\ (\varphi) = Ae^{im\varphi}$$

The complex conjugate of $\Phi(\varphi)$ is

$$\Phi^*_m\ (\varphi) = Ae^{-im\varphi}$$

and so

$$\Phi_m(\varphi)\Phi^*_m(\varphi) = A^2 e^{(im\varphi - im\varphi)} = A^2$$

This result means that for all values of m the probability density is symmetrical about the z-axis, so that the probability of the electron being found in a small element of angle $d\varphi$ is the same in all directions, i.e. φ from 0 to 2π. This situation may be graphically represented by a circle, as shown in Fig. 5.2.

To evaluate A we make use of the normalization condition given by Eq. (5.24). We thus obtain $2\pi A^2 = 1$ and $A = 1/\sqrt{2\pi}$. The normalized function $\Phi_m(\varphi)$ is therefore

$$\Phi_m(\varphi) = \frac{1}{\sqrt{2\pi}}\ e^{im\varphi} \qquad (5.27)$$

Analytical expressions for the normalized functions $\Theta_{lm}(\theta)$ are given in Table 5.1

The azimuthal quantum number $l = 0, 1, 2, 3, \ldots\ldots$, as we have noted earlier, correspondes to the states $s, p, d, f, \ldots$, respectively. So
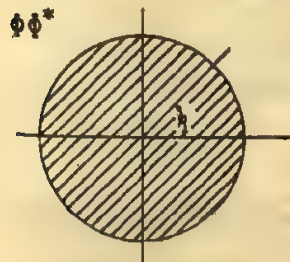
Fig. 5.2 $\Phi\Phi^*$, i.e. the probability density distribution $\psi\psi^*$ as a function of φ

the wave function $\Theta_{0,0}(\theta)$, as mentioned in Table 5.1, describes the s electrons; $\Theta_{1,0}(\theta)$ and $\Theta_{1,\pm1}(\theta)$ describe the p electrons; and so on.

Table 5.1   The Normalized Functions, $\Theta_{lm}(\theta)$, for a Hydrogen-like Atom

$l = 0$ $m = 0$	$\Theta_{0,0}(\theta) = \dfrac{1}{\sqrt{2}}$		s electrons
$l = 1$ $m = 0$	$\Theta_{1,0}(\theta) = \dfrac{\sqrt{6}}{2} \cos\theta$	$\Big\}$	p electrons
$l = 1$ $m = \pm1$	$\Theta_{1,\pm1}(\theta) = \dfrac{\sqrt{3}}{2} \sin\theta$		
$l = 2$ $m = 0$	$\Theta_{2,0}(\theta) = \dfrac{\sqrt{10}}{4}(3\cos^2\theta - 1)$		
$l = 2$ $m = \pm1$	$\Theta_{2,\pm1}(\theta) = \dfrac{\sqrt{15}}{2} \sin\theta.\cos\theta$	$\Big\}$	d electrons
$l = 2$ $m = \pm2$	$\Theta_{2,\pm2}(\theta) = \dfrac{\sqrt{15}}{4} \sin^2\theta$		

By plotting $[\Theta_{lm}(\theta)]^2$ as a function of the angle θ on the xz-plane we obtain the polar representation of probability density distribution as a function of the zenith angle. Such polar curves are shown in Fig. 5.3 for s, p and d electrons. The significance of these plots is that a measure of the electron's probability of being located in any direction is given by the magnitude of a straight line extending from the centre up to the curve boundary in the same direction.

For an s electron, $l = 0$, $m = 0$ and $[\Theta_{0,0}(\theta)]^2 = 1/2$, a constant independent of the angle θ. This means there is equal probability in all
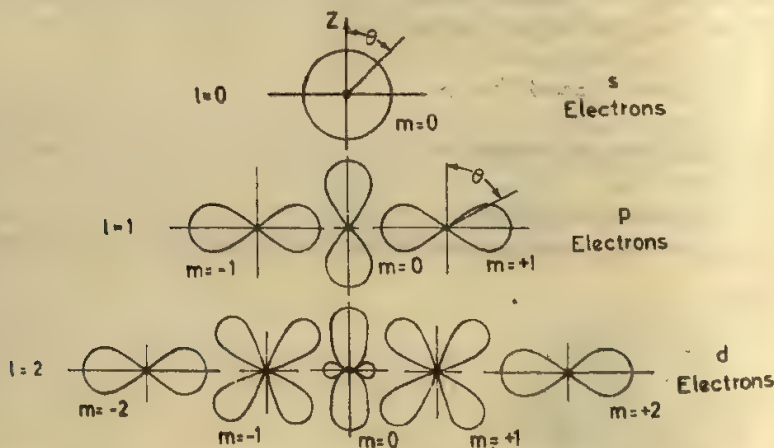
Fig. 5.3 Polar representation of probability density distribution as a function of the zenith angle θ for s,p,d electrons of hydrogen

directions about the nucleus with θ value being between 0 and π, so that graphically this situation can be represented by a half circle on the *xz*-plane. Since, as mentioned before, the electron's probability density on the *xy*-plane is symmetrical about the *z*-axis, i.e. independent of φ, regardless of the quantum state it is in, by taking θ and φ together the said half circle results in a full circle on the *xz*-plane, as shown at the top of Fig. 5.3, while in three dimensions the result will evidently be a sphere. For an *s* electron, therefore, the probability density function is said to be *spherically symmetrical* about the nucleus.

For *p* electrons, $l = 1$ and *m* may take three values + 1, 0, − 1. In the second line of Fig. 5.3 are presented the probability density distributions as a function of θ, corresponding to these three states.

For *d* electrons, $l = 2$, and *m* may take five values 2, 1, 0, − 1, − 2. The last row of Fig. 5.3 shows the distributions for each of these five states.

It is seen from the polar graphs of Fig. 5.3 that (*i*) for all $m = 0$, with the exception of *s* electrons, the electron's probability density is greatest in polar directions, i.e. in the directions of $\theta = 0$ and $\theta = \pi$; (*ii*) with $m = + l$ or $- l$, the probability density is greatest in the direction of the equatorial plane, i.e. in the directions of $\varphi = 0$ and $\varphi = \pi$; and (*iii*) with $m = (l - 1)$ or $- (l - 1)$, the probability density is greatest in the directions lying exactly between the polar and equatorial planes.

Angular wave function. The product of the two functions $\Phi_m(\varphi)$ and $\Theta_{lm}(\theta)$ describes the *angular* part of the complete wave function ψ and is determined by the quantum numbers *l* and *m*. We shall refer to it as *angular wave function* $\psi_{lm}(\theta, \varphi)$:

$$\psi_{lm}(\theta, \varphi) = \Theta_{lm}(\theta) \Phi_m(\varphi) \qquad (5.28)$$

While we no longer consider the electron to be moving in a fixed orbit as proposed by Bohr, the wave function ψ for an electron does, in a sense, describe the motion of the electron (in a field of only one atom) and so ψ is generally referred to as an *atomic orbital*. Since $l = 0$ designates *s* electrons, the corresponding wave function is called an *s* orbital. Similarly, the wave functions corresponding to $l = 1$ are called *p* orbitals, while *d* orbitals are those for which $l = 2$.

Analytical expressions for the normalized angular wave functions, for *s*, *p* and *d* orbitals, are obtained by multiplying the appropriate $\Theta_{lm}(\theta)$ from Table 5.1 by $\Phi_m(\varphi) = (1/\sqrt{2\pi}) \, e^{im\varphi}$.

Thus for the *s* orbital, $l = 0$, $m = 0$, and so the normalized angular wave function, which we shall denote by $\psi(s)$, is

$$\psi(s) = \frac{1}{2\sqrt{\pi}}$$

For $l = 1$, there are three values of *m*, namely 1, 0, − 1 and so there are three *p* orbitals. The corresponding angular wave functions may be designated as $\psi(p_{+1})$, $\psi(p_0)$ and $\psi(p_{-1})$. Using Eq. (5.28) and appro-

priate functions given in Table 5.1, they are expressed in the form

$$\psi(p_{+1}) = \left(\frac{3}{8\pi}\right)^{1/2} \sin\theta.e^{i\varphi}$$
$$\psi(p_0) \ \ = \left(\frac{3}{4\pi}\right)^{1/2} \cos\theta \qquad\qquad\qquad (5.29)$$
$$\psi(p_{-1}) = \left(\frac{3}{8\pi}\right)^{1/2} \sin\theta.e^{-i\varphi}$$

For $m \neq 0$ the orbitals are imaginary functions. It is usually more convenient, however, to deal with an equivalent set of real functions obtained by linear combination of these functions. For the p orbitals, we take the following linear combinations:

$$\psi(p_x) \ = \frac{\psi(p_{+1}) + \psi(p_{-1})}{\sqrt{2}}$$
$$\psi(p_z) = \psi(p_0) \qquad\qquad\qquad (5.30)$$
$$\psi(p_y) \ = -\ i\ \frac{\psi(p_{+1}) - \psi(p_{-1})}{\sqrt{2}}$$

Introducing expressions for $\psi(p_{+1})$ and $\psi(p_{-1})$, the expression for $\psi(p_x)$ becomes

$$\psi(p_x) = \left(\frac{3}{4\pi}\right)^{1/2} \sin\theta \cos\varphi$$

Clearly, this angular wave function has its maximum value in the *x*-direction. Hence the designation p_x. The expression for $\psi(p_y)$ can be obtained in the same way.

For $l = 2$, there are five values of m and hence there are five d states, which we may designate as $\psi(d_{+2})$, $\psi(d_{+1})$, $\psi(d_0)$, $\psi(d_{-1})$, $\psi(d_{-2})$. The following linear combinations are taken to derive five real d functions:

$$\psi(d_{z^2}) \ \ = \psi(d_0)$$
$$\psi(d_{xz}) \ \ = \frac{\psi(d_{+1}) + \psi(d_{-1})}{\sqrt{2}}$$
$$\psi(d_{yz}) \ \ \ = -\ i\frac{\psi(d_{+1}) - \psi(d_{-1})}{\sqrt{2}}$$
$$\psi(d_{x^2-y^2}) = \frac{\psi(d_{+2}) + \psi(d_{-2})}{\sqrt{2}} \qquad\qquad (5.31)$$
$$\psi(d_{xy}) \ \ \ = -\ i\frac{\psi(d_{+2}) - \psi(d_{-2})}{\sqrt{2}}$$

Analytical expressions for the real d functions along with those for *s*- and *p*-functions are given in Table 5.2.

Polar representations of the angular wave functions are shown in Fig. 5.4. The significance of these plots, which give surfaces in three dimensions, is that the value of the angular wave function in any direc-

Table 5.2 Normalized Angular Wave Functions, $\psi_{lm}(\theta,\varphi)$, for a Hydrogen-like Atom

$l = 0$	$m = 0$	$\psi(s) = \dfrac{1}{2\sqrt{\pi}}$
$l = 1$	$m = 0$	$\psi(p_z) = (3/4\pi)^{1/2} \cos\theta$
$l = 1$	$m = +1$	$\psi(p_x) = (3/4\pi)^{1/2} \sin\theta\,\cos\varphi$
$l = 1$	$m = -1$	$\psi(p_y) = (3/4\pi)^{1/2} \sin\theta\,\sin\varphi$
$l = 2$	$m = 0$	$\psi(d_{z^2}) = (5/16\pi)^{1/2}\,(3\cos^2\theta - 1)$
$l = 2$	$m = +1$	$\psi(d_{xz}) = (15/4\pi)^{1/2} \sin\theta\cos\theta\,\cos\varphi$
$l = 2$	$m = -1$	$\psi(d_{yz}) = (15/4\pi)^{1/2} \sin\theta\cos\theta\,\sin\varphi$
$l = 2$	$m = +2$	$\psi(d_{x^2-y^2}) = (15/16\pi)^{1/2} \sin^2\theta\,\cos2\varphi$
$l = 2$	$m = -2$	$\psi(d_{xy}) = (15/16\pi)^{1/2} \sin^2\theta\,\sin2\varphi$

NOTE: The purpose of putting bracket is to indicate, for instance, that the p_x and p_y orbitals are not identical with $\psi_{1,1}$ and $\psi_{1,-1}$, respectively. The latter functions are actually complex but appropriately normalized sums and differences of them give the real functions $\psi(p_x)$ and $\psi(p_y)$. The same applies to bracketed d orbitals.

tion, specified by the angles θ and φ, is proportional to the length of a straight line extending from the origin up to the surface in the same direction. The shape and orientation of an atomic orbital are largely determined by the angular wave function $\psi_{lm}(\theta,\varphi)$, and since the latter is independent of n we can expect orbitals of the same l but different n to be similar in shape. The directional properties of atomic orbitals, which we are discussing here, are of particular importance in view of
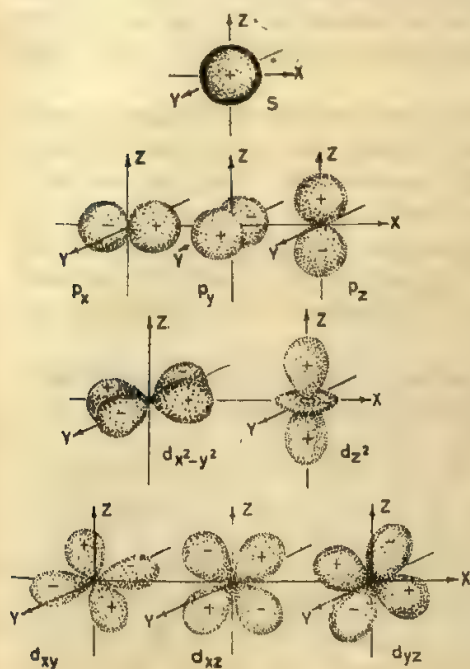

Fig. 5.4 Polar representation of the angular wave functions for s, p and d orbitals. The squares of these are the probability distribution functions.

the part atomic orbitals play in molecular geometry, as we shall see in later chapters.

The following important generalizations can be made about the various orbitals represented in Fig. 5.4.

(1)   All s orbitals ($l = 0$) are spherically symmetrical and there is no dependence of the wave function on angle. All other orbitals have characteristic directional properties.

(2)   Each p orbital ($l = 1$) is made of two lobes touching at the origin and aligned along one of the three axes — p_x orbital along x-axis, p_y along y-axis and p_z along z-axis. The two lobes of the p_x orbitals are separated by the yz-plane in which the wave function has zero value; this is called a *nodal plane*, and all p orbitals have one such plane. The sign of the angular wave function changes as the nodal plane is crossed; the two lobes of p orbitals are thus of opposite sign.

The three p orbitals, it is seen, are mutually equivalent — having similar size and shape, and being oriented similarly, namely, along one axial direction.

Under normal conditions, i.e. in the absence of an external electric or magnetic field, orbitals of the same l-value have the same energy, the energy depending on the total quantum number, n; the three p orbitals are therefore *degenerate*, and an electron, say, in the $n = 2$, $l = 1$ level may occupy any of three $2p$ orbitals of equal energy. This degeneracy is, however, removed in the presence of an external magnetic field, because then the orbitals are oriented differently with respect to the external field, and consequently, the energies of the p_x, p_y and p_z orbitals differ slightly, even for the same value of n, depending on the values of m.

(3)   The d orbitals, it is seen, are more complicated in shape than the p-orbitals; all of them, except the d_{z^2} orbital, have four lobes alternating in sign, i.e. opposing pairs being of the same sign. Thus, in contrast to the p-orbitals, which, as mentioned before, have one nodal plane, the d-orbitals are characterized by the fact that they have two nodal planes. In general, the energy of an orbital increases as the number of nodal planes increases; thus, for a given value of n, the energy of the orbitals increases in the order $s < p < d$.

The five d orbitals, for the same reason as given above, are degenerate. The d orbitals are, however, not mutually equivalent in contrast to the p orbitals which, as mentioned before, are equivalent. Three of the five d orbitals have lobes lying symmetrically between the axial directions, namely, between x- and y-axes (d_{xy} orbital), y- and z-axes (d_{yz} orbital), and x- and z-axes (d_{xz} orbital). In contrast to this, the lobes of the $d_{x^2-y^2}$ orbital lie along the x- and y-axes, while those of the d_{z^2} orbital lie on the z-axis. The d-orbitals can thus be divided into two sets; one set comprises the $d_{x^2-y^2}$ and the d_{z^2} orbitals, i.e., those which point along the axial directions, and the other set comprises the d_{xy}, d_{yz}, and d_{xz} orbitals,

i.e. those which point along 45° to the axial directions. Because of this difference in orientation, the energies of the two sets of orbitals are differently affected by electrostatic fields such as those of ligands; this is discussed more fully in a later section.

Squaring the angular wave function we get the angular probability density function. The angular probability density distributions for s, p and d electrons are therefore given by the squares of the polar representations of the respective angular wave functions shown in Fig. 5.4.

Radial wave function. The radial part of the wave function ψ, i.e. the radial wave function $R_{nl}(r)$, determines the spatial extent of the orbital. The radial wave function, in contrast to the angular wave function not only varies with r but does so in a different way for each set of quantum numbers n and l. Analytical expressions for the radial wave functions for one-electron or hydrogen-like atoms are listed in Table 5.3.

Table 5.3 Normalized Radial Wave Functions, $R_{nl}(r)$

$$\left[\rho = \frac{Z}{a_0} r; \ a_0 = \frac{h^2}{4\pi^2\mu e^2} = 0.529 \ \overset{\circ}{A} \ \text{(Radius of the first Bohr orbit)} \right]$$

$n = 1$	$l = 0$	$1s$	$R_{1,0}(r) = 2\left(\dfrac{Z}{a_0}\right)^{3/2} e^{-\rho}$
$n = 2$	$l = 0$	$2s$	$R_{2,0}(r) = \dfrac{1}{2\sqrt{2}}\left(\dfrac{Z}{a_0}\right)^{3/2}(2-\rho)\,e^{-\rho/2}$
$n = 2$	$l = 1$	$2p$	$R_{2,1}(r) = \dfrac{1}{2\sqrt{6}}\left(\dfrac{Z}{a_0}\right)^{3/2}\rho e^{-\rho/2}$
$n = 3$	$l = 0$	$3s$	$R_{3,0}(r) = \dfrac{2}{81\sqrt{3}}\left(\dfrac{Z}{a_0}\right)^{3/2}(27-18\rho+2\rho^2)\,e^{-\rho/3}$
$n = 3$	$l = 1$	$3p$	$R_{3,1}(r) = \dfrac{4}{81\sqrt{6}}\left(\dfrac{Z}{a_0}\right)^{3/2}(6\rho-\rho^2)\,e^{-\rho/3}$
$n = 3$	$l = 2$	$3d$	$R_{3,2}(r) = \dfrac{4}{81\sqrt{30}}\left(\dfrac{Z}{a_0}\right)^{3/2}\rho^2 e^{-\rho/3}$

Fig. 5.5 contains graphs of the radial wave function, $R_{nl}(r)$, versus r for $1s$, $2s$, $2p$, $3s$, $3p$ and $3d$ electrons. The radial function always contains the factor e^{-Zr/na_0}, where n is the principal quantum number and $a_0 = h^2/4\pi^2\mu e^2$ is the Bohr radius (0·529Å). As the effective nuclear charge (Z) increases, the radial wave function falls off more rapidly with increasing r. The abscissa of Fig. 5.5 is given in terms of Bohr radii. It is seen that R_{nl} is maximum at $r = 0$, i.e. at the nucleus itself, for all s states, while for other states it is zero at $r = 0$.

We are more interested, however, in the probability density for the electrons than in the wave function. The *probability density* as a function of r is given by the square of the radial wave function, i.e. $[R_{nl}(r)]^2$. We may conveniently draw a parallel between this probability density and mass density; water, for instance, has a mass density of 1 g/cm³ but in
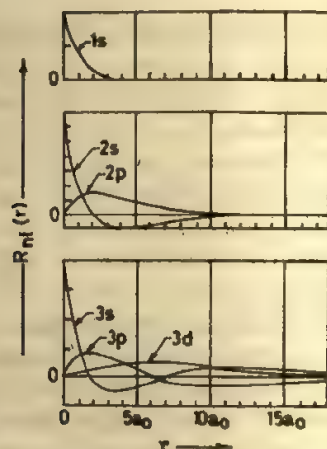
Fig. 5.5 Variation of the radial part of the electron wave function with distance from the nucleus in hydrogen for various quantum states

order to know its actual mass we must multiply this density with the volume of water in question. Similarly while $[R_{nl}(r)]^2$ gives the probability density of the electron at a distance r from the nucleus, the actual probability P of finding it there is given by $[R_{nl}(r)]^2 \, dv$, where dv is an infinitesimal volume element between r and $r + dr$, or in other words, dv is the volume of a spherical shell whose inner radius is r and outer radius is $r + dr$. The volume of such a spherical shell is $4\pi r^2 \, dr$. So the actual probability of finding the electron at a distance between r and $r + dr$ from the nucleus in a one-electron atom is

$$P = D.dr = 4\pi r^2 \, [R_{nl}(r)]^2 dr \qquad (5.32)$$

The plot of the distribution function, D, i.e. $4\pi r^2 \, [R_{nl}(r)]^2$ versus r gives the radial distribution curve. The radial distribution curve for $1s$ electron is presented in Fig. 5.6(b); for comparison, Fig. 5.6(a) displays the probability density distribution as a function of r for $1s$ electron. It is seen that even though the electron density is maximum at the centre, i.e. at $r = 0$, the probability of finding the electron exactly there is zero, which is because mathematically the centre is a point of zero volume. On moving outwards, however, the area of the sphere, $4\pi r^2$, increases and this combining with the falling value of $[R_{nl}(r)]^2$ results in a curve with a maximum; the value of r at which this maximum occurs — that means the most probable distance of the electron from the nucleus — is seen from Fig. 5.6(b) to be $a_0 = 0.529$ Å, which, significantly, is just the radius of the normal Bohr orbit for hydrogen. There is, however, a fundamental difference between the wave-mechanical atom and the Bohr atom. In the latter, the electron always rotates in an orbit at a fixed distance around the nucleus, whilst according to wave mechanics the electron is most likely to be located at this distance, but may also be found elsewhere.

Fig. 5.7 contains all the radial distribution curves corresponding to

Fig. 5.6 (a) Probability density distribution as a function of r for 1s electron. (b) Plot of radial distribution function (D) for 1s electron.

Fig. 5.7 Radial distribution curves for different electronic states of the hydrogen atom

the radial wave functions which have been listed in Table 5.3 and graphically presented in Fig. 5.5. It is seen that there is a principal maxi-

mum in each of the plots (there are also subsidiary maxima in some of
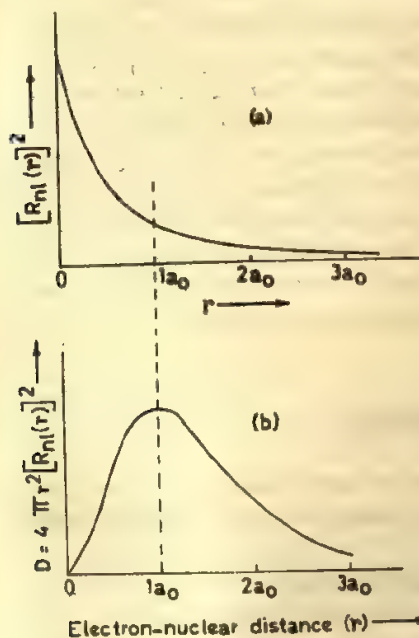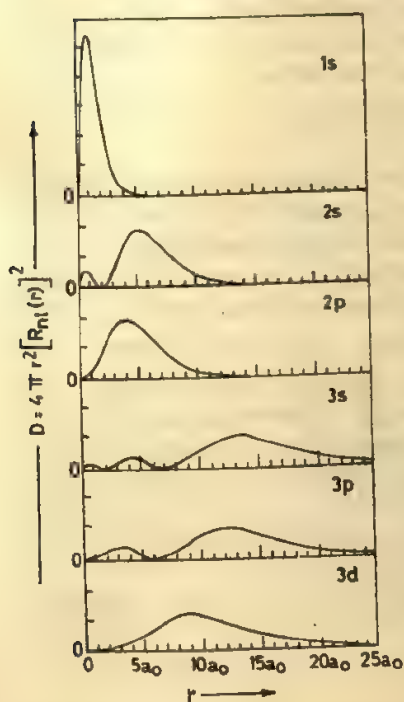the plots because of the nature of the radial wave functions) and that, as
n increases, the radius of the principal maximum increases. Comparing
1s and 2s, for instance, the principal maximum occurs at about a_0 and
$5a_0$, respectively; this means that the 1s electron is most likely to occur
at a distance of 0·529 Å, but the 2s electron at a distance of 5×0.529 Å,
from the nucleus. Of particular interest also are the distances at which
the probability of electron occurrence is zero; while for both the 1s and
2s states the probability is zero at $r = 0$ and $r = \infty$, for the 2s state the
probability is zero also at $2a_0$, i.e. 1·06 Å from the nucleus.

5.6 Sectional Representation of Orbitals

We can now draw sections through some of the orbitals we have dis-
cussed earlier. For this we write the expression for the complete wave
function:

$$\psi_{nlm}(r,\theta,\varphi) = R_{nl}(r)\Theta_{lm}(\theta)\,\Phi_m(\varphi) = R_{nl}(r)\,\psi_{lm}(\theta,\varphi) \tag{5.33}$$

Let us consider the 3s orbital. Eq. (5.33) then becomes

$$\psi_{3,0,0}(r,\theta,\varphi) = R_{3,0}(r)\,\psi_{0,0}(\theta,\varphi) = R_{3,0}(r)\,\psi(s)$$

Substituting the expressions for the normalized radial and norma-
lized angular wave functions from Tables 5.3 and 5.2 respectively, the
normalized complete wave function takes the form

$$\psi_{3,0,0}(r,\theta,\varphi) = \frac{1}{81\sqrt{3\pi}}\left(\frac{Z}{a_0}\right)^{3/2}(27 - 18\rho + 2\rho^2)e^{-\rho/3}$$

We can now obtain a section through the 3s orbital by tracing contour
lines of constant values of the total wave function. Fig. 5.8 shows such
a section. Its pattern follows quite obviously from the spherical sym-
metry of s orbitals (see Fig. 5.4) coupled with the characteristic spatial
variation of the radial wave function $R_{nl}(r)$ for the 3s state (see Fig. 5.5).
The broken lines in Fig. 5.8 represent nodes ($\psi_{nlm} = 0$). These nodal
lines occur at about 1Å and 4Å, i.e. the distances at which $R_{nl}(r)$ for
the 3s state passes through zero value. The sign of the total wave function
in different regions of the 3s section is determined by the sign of the 3s
radial wave function at corresponding radial distances from the nucleus
(see Fig. 5.5). Thus, the region from the nucleus up to the inner nodal
line and that beyond the outer nodal line are positive, whereas in bet-
ween the two nodal lines the region is negative.

For the 2p$_x$ orbital, the normalized complete wave function is given by

$$\left.\begin{array}{l}\psi_{2,1,1}(r,\theta,\varphi)\\\psi_{2,1,-1}(r,\theta,\varphi)\end{array}\right\} = R_{2,1}(r)\,\psi(p_x)$$

$$= \frac{1}{4\sqrt{2\pi}}\left(\frac{Z}{a_0}\right)^{3/2}\rho e^{-\rho/2}\sin\theta\,\cos\varphi \tag{5.34}$$
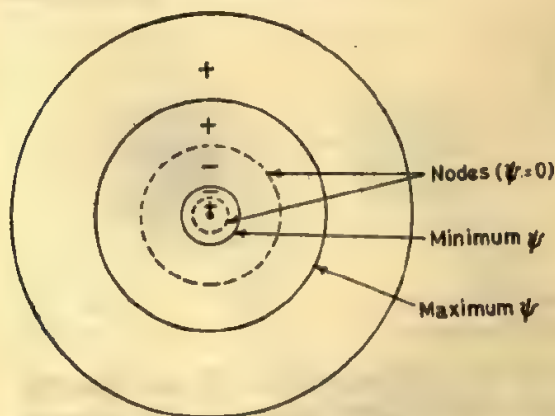
Fig. 5.8 Section through 3*s* orbital showing positive and negative regions

While drawing contour line on the *xz*-plane, φ is constant, being 0° in the + ve *x*-direction and 180° in the opposite direction, so that the wave function is only a function of *r* and θ. Fig. 5.9(*a*) represents the section through the $2p_x$ orbital showing the positive and negative regions enclosed by contour lines on the *xz*-plane. The section through the $3p_x$ orbital on the same plane is represented in Fig. 5.9(*b*).

5.7 Charge-cloud Representation of Orbitals

If we could imagine ourselves being able to photograph the 1*s* electron (i.e. electron in 1*s* quantum state) in a hydrogen atom, a snap shot would locate it in a certain position; but if we should take a long-time exposure of this 1*s* electron jumping around, so that the pictures of the electron pile up on top of each other, the developed plate would look something
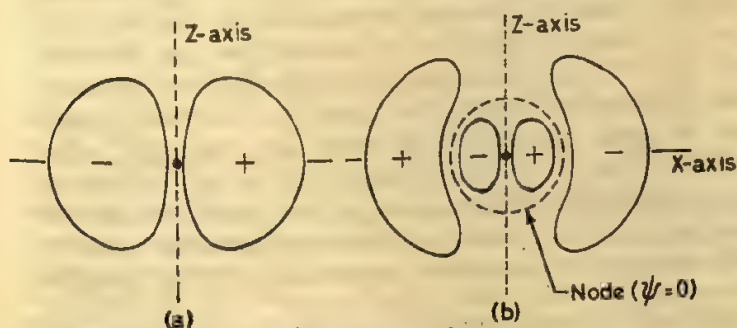
Fig. 5.9 Sections through (*a*) $2p_x$ orbital and (*b*) $3p_x$ orbital, showing positive and negative regions (Not drawn to scale)
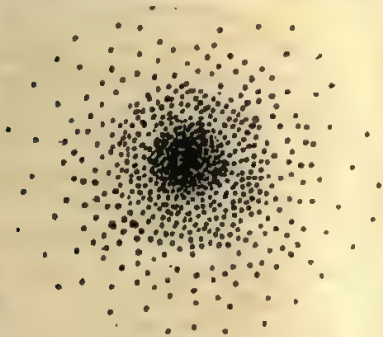
Fig. 5.10 Charge-cloud representation of $1s$ electron with cloud density proportional to probability density

like a cloud picture as shown in Fig. 5.10 (except for the fact that Fig. 5.10 shows the cross-section while our imaginary camera would, however, see the whole depth). This gives the 'charge-cloud' representation of the $1s$ electron. The maximum blackening of the cloud in the immediate vicinity of the nucleus indicates that the $1s$ electron spends most of its time in this region, or, we can say, the electron probability density is maximum in the region just surrounding the nucleus. The so-called charge-cloud is thus really a probability cloud, and the density of this charge-cloud corresponds to the probability density which, as we noted earlier, is given by the square of the complete wave function, ψ^2, or the product of the square of the radial wave function and the square of the angular wave function.

We can, therefore, visualize the qualitative shape of the charge-clouds associated with different orbitals. Since the angular wave function for the s state, and hence its square, is spherically symmetrical, and since the spatial variation of the square of the radial wave function for the $1s$ state has the form as shown in Fig. 5.6(a), the $1s$ electron may be considered to form over a period of time a ball-shaped charge-cloud with maximum density just about the nucleus. Similarly, the electron in the $2s$ state may be considered to form around the nucleus a ball and an outer shell, in the $3s$ state to form a ball and two concentric shells, and so on. Fig. 5.11 depicts these charge-cloud representations and also those for the $2p$, $3p$ and $3d$ states. It might be mentioned that the electronic charge-clouds of Fig. 5.11 are the modern substitutes for the electron orbits of the Bohr-Sommerfeld theory. The clouds or their solid figures showing surfaces of equal probability densities are, therefore, often referred to as orbitals. Thus an orbital, in contrast to an orbit of the old theory, denotes a rather more diffuse region in which the electron can be said to exist. Figs. 5.12 and 5.13 show the probability distribution on the xz-plane of the electron in some of the eigenstates with the principal quantum number $n = 3$.

While Fig. 5.11 shows $1s$ to $3d$ orbitals, there are also orbitals corresponding to the states $4s$, $4p$, $4d$, $4f$, $5s$, and so on *ad infinitum*. It should
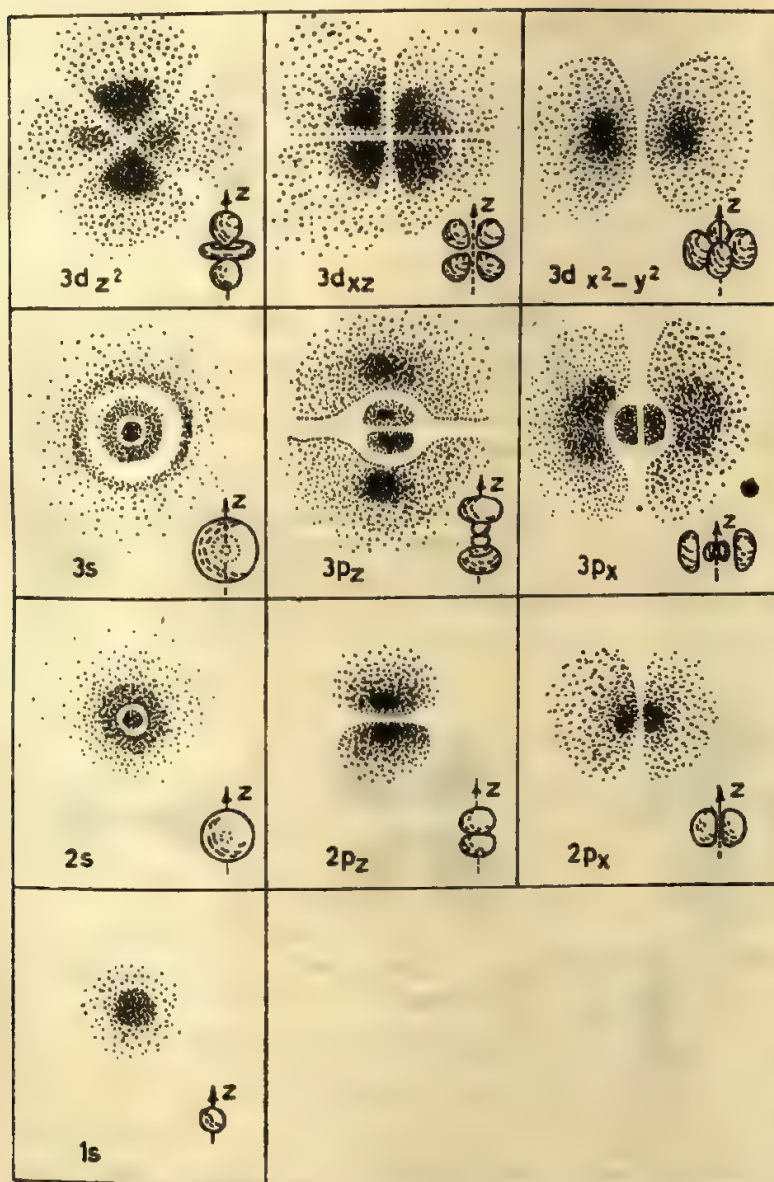
Fig. 5.11 Some orbitals of a one-electron atom. Electron-cloud pictures are cross-sections through centre of atom, while solid pictures are perspective views of atom. Interpretation of cloud pictures is that the electron spends more time at darker places. Solid pictures, however, merely enclose the regions in space where the electron spends most time, but do not display the gradual fade-out and cloud-like nature of the electronic distribution. (After W. F. KIEFFER, and R. K. FITZGEREL, 'Supplementary Readings of Chemical Bond Approach,' *Journal of Chemical Education*, 1960.)
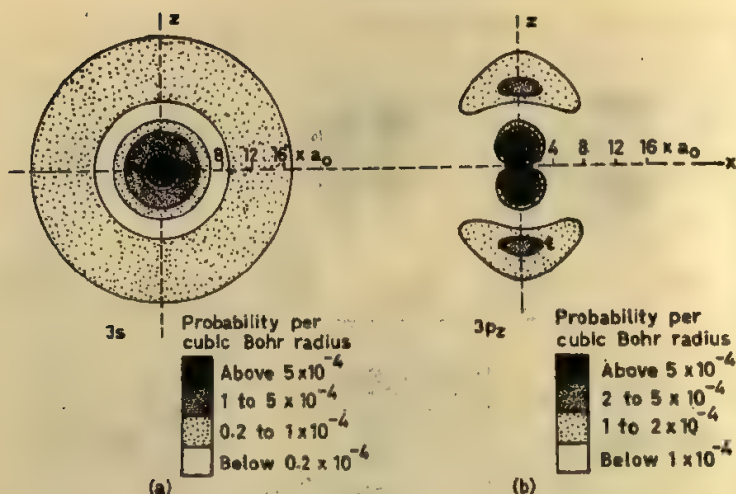
Fig. 5.12 Electron probability density distribution on the xz-plane: (a) $3s$ orbital and (b) $3p_z$ orbital. Contour lines represent levels of equal probability density. (After U. FANO, and L. FANO, *Basic Physics of Atoms and Molecules*, John Wiley, New York, 1959.)
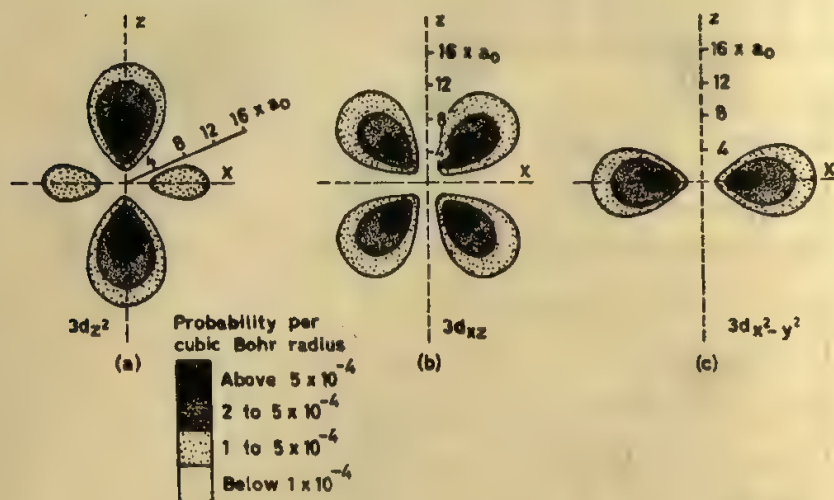
Fig. 5.13 Electron probability density distribution on the xz-plane: (a) $3d_{z^2}$ orbital, (b) $3d_{xz}$ orbital, and (c) $3d_{x^2-y^2}$ orbital. Contour lines represent levels of equal probability density. (After U. FANO, and L. FANO, *Basic Physics of Atoms and Molecules*, John Wiley, New York, 1959.)

be noted that the pictures in Fig. 5.11 show the different possible orbitals of the single-electron atom. The shapes of these orbitals, when the atom has more than one electron would be somewhat altered; the general picture would, nevertheless, remain the same.

5.8 Wave-mechanical Model for Many-Electron Atoms

When we try to apply the methods, laid out in Section 5.2 for one-electron atoms, to atoms with a population of more than one electron, complications arise at once because in these atoms, any particular electron, apart from being attracted to the oppositely charged nucleus, is also repelled by the rest of the electrons, and consequently, terms containing inter-electronic distances appear in the expression for the potential energy of the said electron. The presence of such terms in the wave equation makes an exact solution impossible. Approximate methods have, therefore, to be used, and one widely used method involves solving the Schrödinger equation individually for each electron, moving in the combined potential field of the nucleus and of all the remaining electrons. This is, in essence, the Hartree self-consistent field (SCF) method for treating many-electron atoms.

Hartree's SCF method is based on a series of successive approximations and requires a vast amount of laborious computation, as will be indicated by a brief outline given here. Since consideration of instantaneous interactions of a single electron with all of the remaining electrons renders the problem insoluble, a simplifying assumption is made, namely, that the single electron is acted upon by the average charge distribution of the other electrons. In the first place, plausible wave functions, ψ, are guessed; the summation of the individual charge distributions $(\Sigma\psi^2)$ then gives a potential which is itself very nearly symmetrical spherically. In the approximation of the SCF method, moreover, the potential is made completely spherical by the fact that a spherical average is taken. The Schrödinger wave equation formulated with this potential can be solved to obtain a 'first improved' wave function for the electron concerned. The wave function so obtained may then be used along with the other trial wave functions to obtain, in the same way, a first improved wave function for a second electron. Repetition of the process for the other electrons, taken singly, yields a complete set of first improved wave functions. A second cycle of calculation is then carried out, all over again, to obtain a more improved set of wave functions in place of the first. The process is repeated over a number of cycles till, to a good approximation, the wave functions exhibit no further change. The set of wave functions is then said to be self-consistent.

Radial distribution curves of a large number of ions and neutral atoms derived in this way reveal a characteristic arrangement of electrons in concentric shells, the inner electrons generally being close to the nucleus. Fig. 5.14 shows the radial distribution curves for the neutral alkali atoms. These indicate the probability of finding the electron at any given distance from the centre. In each of the curves the distribution due to inner electrons is shown by a shaded area and that due to the valence electron by
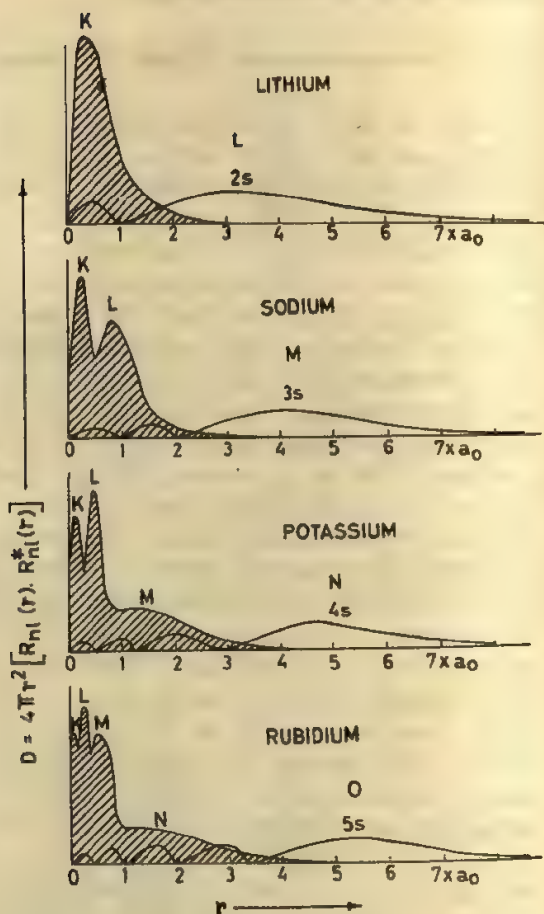
Fig. 5.14 Radial distribution curves for different quantum states of neutral alkali atoms

another curve which extends to the extreme right. Radial distance has been reckoned as multiples of the Bohr radius (a_0), which is the radius of the first Bohr circular orbit of hydrogen. It is seen that the major shells in each atom lie well inside the radius $r = a_0$. The valence electron, moreover, lies well inside the corresponding hydrogen state; thus for example, the radial distribution for a 5s electron in the hydrogen atom is quite large as far out as $50a_0$; whereas in rubiduim the curve (for the 5s electron) seems to be pulled in to about one-tenth of this, which is evidently due to higher nuclear charge in the latter. Fig. 5.14 further highlights the penetration of the 'valence' s-type electron into the inner K, L, M, etc., shells as against the concept of non-penetrating orbits belonging to the earlier point of view. The radial distribution curves for the various subshells of the rubidium atom are shown in Fig. 5.15, the thick curve in which represents the sum of all the curves corresponding to the total of 36 core
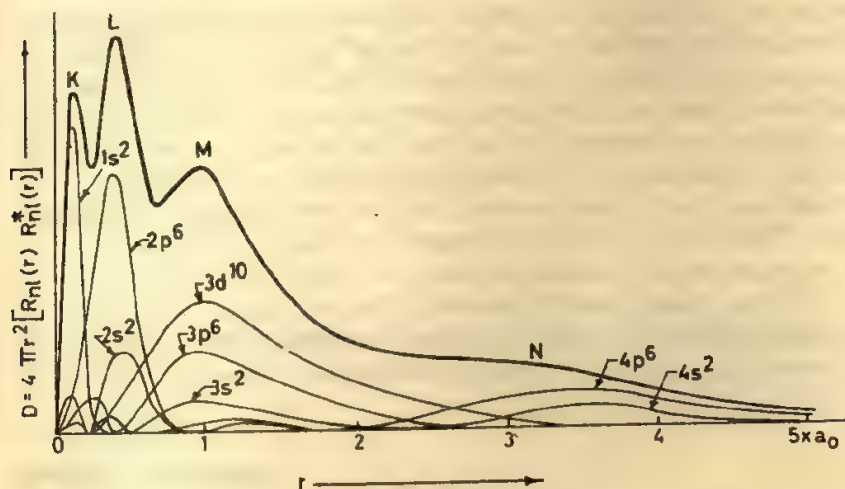
Fig. 5.15 Radial distribution curves for the different quantum states of the rubidium atom core of 36 electrons. The thick line represents the sum of all the inner curves.

electrons. The figure reveals interpenetrating nature of the subshells, which implies that every electron contributes something to each shell, even though the humps in the 'sum' curve have been taken to represent the principal shells K,L,M, and N.

5.9 Summary

That part of the Rutherford theory which describes the atom as consisting of a small, heavy, positively charged nucleus with light, negatively charged electrons surrounding it, has stood firm ever since it was proposed. However, the idea of fixed electronic orbits proposed by Bohr, though useful, has had to be abandoned, one reason for which is the impossibility of perceiving the electron in any fixed orbit with the use of any tools we have available, and the other reason is the discovery of wave nature of electrons —the reasons which are embodied in the Heisenberg uncertainty principle. In place of a fixed orbit, we now have its wave-mechanical equivalent, denoted by the term orbital. The orbital represents a diffuse region around the nucleus in which the electron can be said to exist and the probability of finding the electron per unit volume at any given point in this region is proportional to the square of the wave function, ψ^2 (or $\psi\psi^*$), at that point. For convenience, orbitals are also represented by pictures of electron clouds with cloud density proportional to ψ^2 (or $\psi\psi^*$), or by solid figures (Fig. 5.11) with probability density contour surfaces, i.e. surfaces at all points on which the probability of finding the electron per unit volume is the same.

Since no two orbitals in one atom will have the same shape and size as well as the same location in space, the overall picture of a multi-electron atom would be more blurred than those in Fig. 5.11, and would also be more spherical in shape. Sometimes, however, we would see one or more orbitals sticking out further than the rest, as could be guessed from Fig. 5.14. If such a projecting orbital should have only one electron in it, the atom could use it as a 'hook' to bind itself to other atoms in forming a molecule. This will be discussed in more detail in a later chapter.

The appearance of a multi-electron atom can thus be visualized as follows. It has a small, heavy, positively charged nucleus at the centre, which is surrounded by an electron cloud which is made up of orbitals having various shapes and sizes and containing one or two electrons each.

Suggested Reading

PAULING, L. and E.B. WILSON, *Introduction to Quantum Mechanics*, McGraw-Hill, New York, 1935.

EYRING, H., J. WALTER and G.E. KIMBALL, *Quantum Chemistry*, John Wiley, New York, 1944.

TAYLOR, H.S. and S. GLASSTONE, *A Treatise on Physical Chemistry,: Vol.* I, *Atomistics and Thermodynamics*, D. Van Nostrand, New York, 1942.

Problems

5.1   A good indication of the relative size of any particular orbital is the radius at which the distribution function $4\pi r^2 \, [R_{nl}(r)]^2$ has its maximum. Compare on this basis the sizes of the $1s$, $2s$ and $3s$ orbitals and of $2p$ and $3p$ orbitals.

5.2   Draw for the ground state of the hydrogen atom a contour map of electron density (ψ^2) in a planar section showing contours of constant ψ^2. Find the radius of the boundary line (surface) enclosing most of the charge (say 90%).

5.3   What would be the shapes of the charge clouds of an electron in the one-electron atom in the following states: (a) $n = 3$, $l = 2$, $m = 0$; (b) $n = 3$, $l = 2$, $m = \pm 1$ and (c) $n = 3$, $l = 2$, $m = \pm 2$.

Wave-mechanical Picture of Chemical Bonding

6.1 Introduction

While the basic mechanism underlying electrovalency — namely the bonding of oppositely charged atoms, i.e. ions, through the electrostatic attraction — was easy to understand, the origin of covalent bonding, however, was obscure before the advent of wave mechanics. On the basis of classical physics, it is quite impossible to understand why two neutral atoms, such as two H atoms, form a molecule, The covalent bond, more-over, has the striking feature of showing saturation, which is described by the chemist in terms of valence, i.e. an atom joins with only a limited number of other atoms. Thus a H atom can bind only one other H atom, a carbon atom can bind not more than four H atoms, and so on. This feature of saturation is entirely foreign to classical physics. For, even if sufficiently strong attractive forces between neutral molecules were explicable by classical physics, it would be quite impossible to understand why two atoms already bound should not attract a third atom as well.

A clue to the mystery of homopolar or covalent bond has been provided by wave mechanics. Therein lies one of the greatest merits of the new mechanics. Not only does wave mechanics explain the attraction between neutral atoms but also afford, as we shall see later, a full understanding of the saturation properties.

The first application of wave mechanics to valency problems in 1927 led to the origin of the valence bond method when Heitler and London

Fig. 6.1 Model of two identical pendulums tied to a spring-held thread fixed to two poles
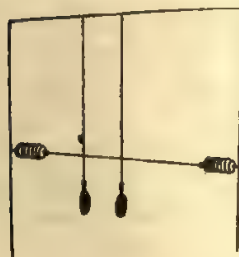
demonstrated how the stability of the covalently-bonded hydrogen molecule could be explained. In this valence-bond (VB) theory, complete atoms are brought together and allowed to interact.

6.2 Interaction of Coupled Identical Systems

When two atoms are coupled together a certain interaction always exists due to electric and magnetic fields, because the atomic systems consist of charged elementary particles in motion. Now the problem is to find what happens when two identical atoms with equal total energy are coupled together, i.e. when their interaction is taken into account.

In order to get an idea of the effect of the coupling of two identical atomic systems as involved in the formation of the homopolar or covalent bond, we consider a macromechanical model of two coupled identical pendulums. As shown in Fig. 6.1, the two identical pendulums suspended from the top bar are coupled by tying them to a spring-held thread fixed to the two poles. It is observed that if any one pendulum is set to oscillate, its oscillation will gradually die down and stop, while the other pendulum begins to oscillate and ultimately reaches (neglecting the frictional dissipation of energy) the amplitude of oscillation initially given to the first, and that this process of transfer of vibrational energy from one pendulum to the other repeats itself over and over. The mode of oscillation of each of the two pendulums in this coupled state is as shown in Fig. 6.2. (It might be
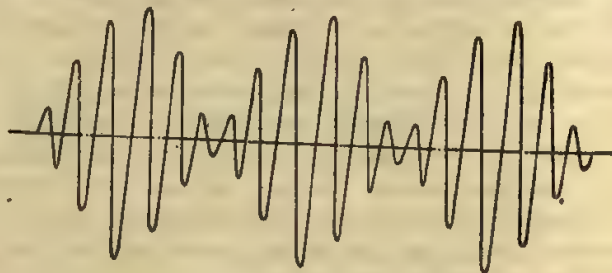
Fig. 6.2 Beat vibration as a result of coupling of two identical pendulums

mentioned, however, that in the uncoupled state each pendulum oscillates with a purely sinusoidal motion of constant amplitude.) We thus see that as a result of the coupling of the two pendulums of identical frequency, beat oscillations appear. Such beat oscillations, however, usually occur only when two frequencies, which are slightly dissimilar, are superimposed — as for example, when two slightly different tuning forks are simultaneously excited. The beat oscillation of each of the coupled pendulums, as shown in Fig. 6.2, is therefore the result of a superimposition of two different frequencies; and these two new frequencies are evidently produced by the splitting of the original frequency as a consequence of the coupling. The difference of the two new frequencies into which the frequency of the uncoupled pendulum splits because of the coupling is the exchange frequency of the vibrational amplitude between the pendulums.

The splitting of the original frequency, as a result of coupling, into two new frequencies, one higher and one lower than the original one, follows very clearly from the pendulum model described above. The lower and higher frequencies correspond, respectively, to symmetric and antisymmetric modes of vibration (Fig. 6.3). In the symmetric mode both the pendulums vibrate towards the same side; they therefore help each other to swing outwards; the restoring couple is thus decreased, and consequently, the resulting frequency must be less than the original frequency of the uncoupled pendulum. In the antisymmetric mode the coupled pendulums vibrate to opposite sides; the pendulums, in this case, pull one another back, so to speak, augmenting thereby the restoring couple. The frequency must therefore be greater than the original one. It might be noted that the actual motion of the pendulums, that can be observed, is the result of a superimposition of the symmetric and antisymmetric modes of vibration.

From the above discussion we thus find that by coupling two mechanical systems which in the uncoupled state have the same frequency, there result two new frequencies — one higher (corresponding to the antisymmetric mode) and one lower (corresponding to the symmetric mode) than the original one. Since the kinetic energy E, changes proportional to the frequency, we see, by transferring the above result to atomic systems, that the two equal-energy states of two identical uncoupled atomic systems split, on coupling, into a lower and a higher energy state due to interaction. The lower energy state corresponds to the symmetric mode of interaction. Thus if we consider two contiguous hydrogen atoms, the antisymmetric mode of interaction corresponds to a higher energy and hence

SYMMETRIC   ANTISYMMETRIC
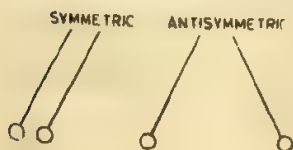
Fig. 6.3   Two modes of vibration of two interacting pendulums

no stable molecule can result. On the other hand, the symmetric mode leads to a lower energy and hence to stable hydrogen molecule.

We also get a simple intuitive physical picture of the homopolar or covalent bond from the pendulum model. The result of coupling two identical pendulums, as we have noted, is the exchange of vibrational amplitude between the pendulums. Transferring this result to the case of two coupled atoms, we expect an exchange of the amplitude ψ of the vibration, and since the square of ψ corresponds to the electron probability density, this means an electron exchange among the coupled atoms. In the exchange process the electrons spend, on the average, more time in the internuclear region than on the outside; the resulting concentration of negative charge between the two positive nuclei holds them together.

6.3 Valence-bond Theory

We shall now consider the above problem of homopolar bond from the point of view of valence-bond (VB) theory. In the VB theory, it is assumed that atoms, complete with electrons, come together to form the molecule. The theory uses the following two principles:

(i) If ψ_A and ψ_B are wave functions for two independent systems A and B, then we can write the total wave function (ψ) for the separated systems as a simple product

$$\psi = \psi_A \psi_B \qquad (6.1)$$

and the total energy E as $E = E_A + E_B$.

(ii) If ψ_1, ψ_2, ψ_3 etc., are the acceptable wave functions for the same system, then the true wave function ψ can be obtained by taking a linear combination of all these wave functions, i.e.

$$\psi = c_1\psi_1 + c_2\psi_2 + c_3\psi_3 + \cdots \qquad (6.2)$$

where c_i, c_2 etc., are coefficients which are adjusted to give a state of lowest energy. We can interpret the squares of the coefficients as a qualitative measure of the relative contribution of each wave function to the true wave function.

This theory was first applied by Heitler and London in 1927 to the hydrogen molecule. We shall begin with two hydrogen atoms far enough apart so that no appreciable interaction can occur. Although the two hydrogen atoms are identical, for convenience of treatment we may label the electrons as 1 and 2 and the nuclei as A and B; the orbital wave functions for the separate atoms $H_A(e_1)$ and $H_B(e_2)$ would then be given by $\psi_A(1)$ and $\psi_B(2)$, respectively. By using Eq. (6.1) the total orbital wave function for the separated atoms can be written as

$$\psi = \psi_A(1)\psi_B(2) \qquad (6.3)$$
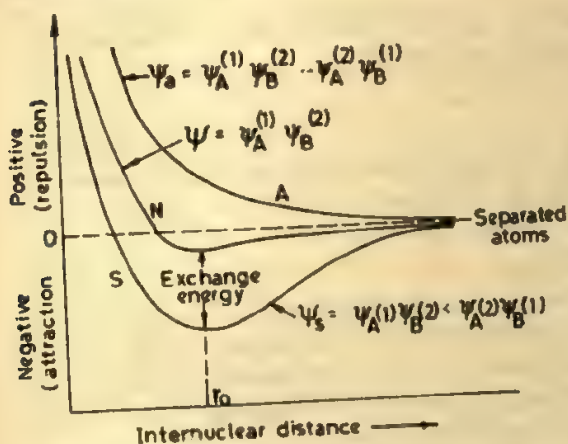
Fig. 6.4 Curves showing VB potential energy for the H_2 molecule

Using the wave function of Eq. (6.3) the energy of the system compris-
ing two identical hydrogen atoms can be calculated as a function of the
internuclear distance r_{AB}. This is shown graphically by the curve N in
Fig. 6.4. It may be noted that in Fig. 6.4 the total energy of two isolated
hydrogen atoms at infinite separation has been taken as zero so that the
energy curve on this plot shows how much the energy of the system of two
hydrogen atoms is above or below that of two isolated atoms. Consequently,
the energy value at the point of minimum on an energy curve represents
the bonding energy at the equilibrium internuclear distance for the mole-
cule described by the corresponding wave function. It is seen that the
energy curve N exhibits a minimum, thus indicating that a molecule is
formed; the bonding energy, however, is far too small — only about 6
kcal/mole, which is only a small fraction of the observed value, namely,
109 kcal/mole.

Evidently, the wave function of Eq. (6.3) cannot be correct. To reveal
this error we must recall that in forming the wave function of Eq. (6.3)
we supposed that the two electrons were distinguishable, so that the elec-
trons, labelled 1 and 2, could be associated with the nuclei A and B,
respectively. We know, however, that when the two atoms are very close
together, so that the atomic orbitals overlap, we can no longer be sure
that the electron 1 will always be near the nucleus A and the electron 2
near the nucleus B. We can, in fact, no longer distinguish one electron
from the other and hence the system of two H atoms may be represented
by two different states I and II as

$$H_A(e_1)H_B(e_2) \qquad H_A(e_2)H_B(e_1)$$
$$\text{I} \qquad\qquad \text{II}$$
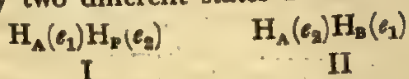
In I, we have the nucleus A with the electron 1 and the nucleus B with
the electron 2, while in state II, the electrons have been exchanged. Let

ψ_I and ψ_{II} be the wave functions for the states I and II, respectively. Following Eq. (6.1) they can be written as

$$\psi_I = \psi_A(1)\psi_B(2)$$
$$\psi_{II} = \psi_A(2)\psi_B(1) \tag{6.4}$$

The true wave function, ψ, is likely to be some combination of these two wave functions. Following Eq. (6.2) we can write

$$\psi = c_1\psi_I + c_2\psi_{II}$$
$$= c_1\psi_A(1)\psi_B(2) + c_2\psi_A(2)\psi_B(1) \tag{6.5}$$

In the case of hydrogen molecule, because of symmetry, the two component wave functions ψ_I and ψ_{II} must contribute with equal weight. As the weight is proportional to the square of the coefficients, we can write $c_1^2 = c_2^2$ or $c_1 = \pm c_2$. Moreover, since the coefficients are relative quantities we can put $c_1 = 1$, and hence $c_2 = \pm 1$.

There are thus two possible wave functions:

$$\psi_s = \psi_A(1)\psi_B(2) + \psi_A(2)\psi_B(1) \tag{6.6}$$
$$\psi_a = \psi_A(1)\psi_B(2) - \psi_A(2)\psi_B(1) \tag{6.7}$$

Eq. (6.6) represents symmetric combination since ψ_s remains unchanged by exchange of electrons 1 and 2, whereas Eq. (6.7) represents the antisymmetric combination since ψ_a changes sign by exchange of electrons. The energy of the system (as a function of internuclear distance) calculated by using the wave function ψ_s is shown as curve S in Fig. 6.4, while that calculated by using ψ_a is shown as curve A. It is thus evident from these energy curves that ψ_a represents a repulsive or nonbonding state, but ψ_s represents a bonding state. We thus find that *the antisymmetric combination of the two possible wave functions of the system of two contiguous H atoms will always lead to repulsion between the two atoms, so that the stable H_2 molecule cannot be formed, while the symmetric combination will lead to attraction of the two hydrogen atoms with the formation of a stable H_2 molecule, the equilibrium value for the internuclear distance being given by r_0, at which the energy is minimum.* The value of r_0 found to be 0·80 Å is in rough agreement with the experimental value 0·74 Å. The bonding energy corresponding to this separation is found to be about 72 kcal/mole, which is in much better agreement with the experimental value (109 kcal/mole) than the energy calculated from Eq. (6.3). Evidently this improvement in result has stemmed from the introduction of the concept of electron exchange between the two constituent atoms. The additional bonding energy which has resulted from this, viz. (72 − 6) or 66 kcal/mole, is consequently known as the *exchange energy*.

It turns out from the above discussion that ψ_s and not ψ_a is the orbital wave function of the normal hydrogen molecule. It is also referred to as a covalent wave function because one electron is considered to be on one nucleus and another on the other.

It may be recalled that the calculated bonding energy (≈ 72 kcal/mole),

obtained by using the orbital wave function ψ_s, though considerable in magnitude, is still far short of the experimental value of about 109 kcal/mole. The orbital wave function for the hydrogen molecule may, however, be further improved — so that a still higher bonding energy for the hydrogen molecule is obtained — by modifying the wave functions of atomic orbitals of the electrons slightly to allow for the screening of nucleus A from nucleus B by the increased probability of the electrons being found directly between the nuclei, and also to allow for the fact that the atomic orbitals will no longer be spherically symmetrical when the atoms are close together. An additional improvement is also obtained by allowing for the possibility that both electrons may be simultaneously near one of the nuclei giving rise to the following two equally likely ionic configurations:

$$\underbrace{\overset{(e_2)}{H_A(e_1)} H_B}_{III} \quad \text{and} \quad \underbrace{H_A \overset{(e_2)}{H_B(e_1)}}_{IV}$$
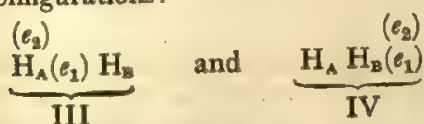
The wave function for the ionic form of a hydrogen molecule may therefore be represented equally well by $\psi_A(1)\psi_A(2)$ or $\psi_B(1)\psi_B(2)$. Inclusion of all these modifications leads to a bonding energy of about 95 kcal/mole. Further refinements can be effected by taking into account explicitly the inter-electron distance, and these lead to a bonding energy which is only 0·5 kcal/mole less than the experimental value. This demonstrates strikingly the validity of the VB approach.

Taking into consideration the possibility of ionic configurations, the combined wave function for the H_2 molecule can be written as

$$\psi_s = [\psi_A(1)\psi_B(2) + \psi_A(2)\psi_B(1)] + \lambda[\psi_A(1)\psi_A(2) + \psi_B(1)\psi_B(2)]$$

or more conveniently as

$$\psi_s = \psi_{cov} + \lambda\psi_{ion} \qquad (6.8)$$

When atoms are brought together so that atomic orbitals, each containing one electron, overlap, a combined wave function of the form of Eq. (6.8) is obtained. This, indeed, is the essential principle of the VB theory, and the result is the *pairing of electrons* which is equivalent to the formation of a single bond. It might be mentioned that in more complicated molecules multiple bonds may arise from the pairing of four or six electrons; in such cases the principle of maximum overlapping is used to decide the way in which the electrons are paired. It should be noted that, since bonding involves pairing of electrons, atomic orbitals containing two electrons will not take part in bond formation since the electrons are already paired.

The coefficient λ in Eq. (6.8) is a measure of the degree to which the ionic forms contribute to the bonding. Since λ can be adjusted so as to give the best value of bonding energy, it affords a means of judging the extent of the ionic character of the bond. For instance, for H_2, λ is 0·17

and the ionic contribution to the total bonding energy amounts to only 5·5 kcal/mole.

The physical interpretation of Eq. (6.8) is that the molecule is represented adequately neither by the pure covalent structure H—H nor by the ionic structures $H_A^+H_B^-$ and $H_A^-H_B^+$ but that the true state of affairs lies somewhere between these two extremes. In such a case it is said that there is 'resonance' between the various possible structures. As a result of resonance the total energy of the system will seek a minimum value lying below that for any of the resonating structures. This gives rise to extra stability of the actual molecule, measured in terms of the so-called *resonance energy*, which is taken to be equal to the difference in energy between the actual molecule and the most stable of the resonating structures. This concept of resonance is of fundamental importance in VB treatment.

To consider a more complicated case, the structure of the carbon dioxide molecule is described. The total of 16 valence electrons can be arranged as in structures I, II, and III below, in which all three atoms still have completed octets, though the oxygen atoms in II and III bear formal charges.

$$:\ddot{O}::C::\ddot{O}: \qquad ^-:\ddot{O}:\ddot{C}:::O:^+ \qquad ^+:O:::C:\ddot{O}:^-$$

$$\text{I} \qquad\qquad\qquad \text{II} \qquad\qquad\qquad \text{III}$$
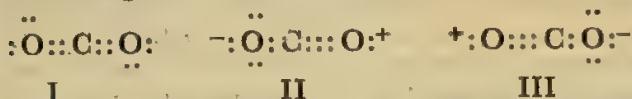
Each of the above three structures makes approximately the same contribution and so a suitable combination of all the three is a better approximation to the true state than any single formula. The CO_2 molecule is, therefore, said to be a resonance hybrid between forms I, II and III. The individual covalent bonds in the molecule owe their stability to an effect just like that in the H—H bond and the molecule moreover achieves extra stability due to multiplicity of formula and resultant resonance.

Formally, *resonance amounts to an effective rearrangement of electrons among two or more structures*. It should be noted, however, that none of the individual resonance structures has any physical existence as such and the importance of resonance lies in its contribution to the structure as a whole.

The total wave function is the product of the orbital wave function and spin wave function. So far we have only dealt with orbital wave functions. Now we have to take into consideration the spins of the electrons. As already mentioned, only two types of spins are possible; let the corresponding spin wave functions be denoted by α and β. Now, for the spin wave functions various possibilities arise. Thus, if both the electrons under consideration have the same spin α or β, the combined spin wave function may be written as $\alpha(1)\alpha(2)$ or $\beta(1)\beta(2)$. If, however, the spins are different, both $\alpha(1)\beta(2)$ and $\alpha(2)\beta(1)$ are equally acceptable wave functions,

since the electrons are indistinguishable, and the allowed linear combinations are then given by

$$\alpha(1)\beta(2) + \alpha(2)\beta(1) \tag{6.9}$$
$$\alpha(1)\beta(2) - \alpha(2)\beta(1) \tag{6.10}$$

The spin wave functions may now be combined with the orbital wave functions to obtain total wave functions. But some combinations are forbidden by the Pauli exclusion principle, which, in a more general form, implies that in any atomic or molecular system the total wave function must be *antisymmetric* with respect to exchange of electrons. Therefore, if the orbital wave function is symmetric, the spin wave function must be antisymmetric, and vice versa. We have already noted that the symmetric and antisymmetric forms of the orbital wave function are given by Eqs. (6.6) and (6.7); it may now be noted that of the four possible spin wave functions, given above, all except that given by Eq. (6.10) are symmetrical with respect to exchange of electrons. The allowed combinations of orbital and spin wave functions are therefore restricted to the following:

$$\psi_s[\alpha(1)\beta(2) - \alpha(2)\beta(1)] \tag{6.11}$$

$$\left.\begin{array}{l}\psi_a[\alpha(1)\alpha(2)] \\ \psi_a[\beta(1)\beta(2)] \\ \psi_a[\alpha(1)\beta(2)+\alpha(2)\beta(1)]\end{array}\right\} \tag{6.12}$$

The wave function ψ_a, defined by Eq. (6.7), as already mentioned, leads to a higher energy than that associated with ψ_s of Eq. (6.6); so ψ_s describes the ground state (the state of lowest energy) and ψ_a the excited state of the molecule. Now we see, considering Eqs. (6.11) and (6.12), that the ground state wave function can have only one spin wave function, whereas the excited state wave function has three spin wave functions. Since, the multiplicity of a state is, in general, equal to the number of spin wave functions associated with the state, we can thus say that the ground state of the molecule is *singlet* and the excited state is a *triplet*.

Moreover, it is apparent from Eq. (6.11), which represents the total wave function for the molecule in the ground state, that two hydrogen atoms can combine to form a molecule only when the two electrons have antiparallel, i.e. oppositely directed, spins.

Finally, we may now summarize the important results of the VB theory and discuss their significance. The VB theory considers the involvement of electrons in terms of atomic orbitals. The covalent bond is formed by pairing and resultant neutralization of opposite electron spins, as has been discussed above for the H—H bond. For an atom to form covalent bonds it must possess one or more electrons which can pair with those of another atom by cancelling their spins. The number of unpaired electrons possessed by the atom thus determines the valency. Electrons already paired, cannot obviously participate in bond formation as such. They can, however, do so if they can be unpaired with only small expenditure

of energy. And, in a general way, this is possible if the unpairing of the paired electrons involves no change in the principal quantum number (n). Nitrogen, for example, with an outer electronic configuration of $2s^2 2p^1_x 2p^1_y 2p^1_z$ shares its three unpaired $2p$ electrons with fluorine to form nitrogen fluoride (NF_3) but is unable to form a pentafluoride, since $n = 2$ level does not contain any other orbital to accommodate one of the unpaired $2s$ electrons. In contrast to this, phosphorus having the configuration $3s^2 3p^1_x 3p^1_y 3p^1_z$ can form a pentafluoride because $3d$ orbitals are available.

The VB theory, however, is inadequate in many cases. It assumes that the two electrons of the shared pair constituting the internuclear bond must come from two different atoms. The formation of coordinate valency, therefore, remains unexplained on this basis. Moreover, according to this theory the atoms in the oxygen molecule should have close electronic shells resembling that of neon, which would make the molecule diamagnetic. Normally, however, oxygen exhibits strong paramagnetic moment indicating the presence of unpaired electrons.

6.4 Molecular Orbital Theory

The molecular orbital (MO) approach is quite different from the VB approach. In the VB approach, as discussed above, complete atoms are brought together and allowed to interact so that the resulting molecule consists of atoms which, although interacting, retain a large measure of their individual character. In the MO approach, on the other hand, orbitals are devised for the molecule as a *whole*, i.e. involving the nuclei of all the constituent atoms separated by fixed equilibrium distances (the molecular orbitals are thus polycentric), and then it is imagined that electrons are fed into these molecular orbitals one at a time such that each entering electron secures the lowest possible quantum state and also obeys the Pauli exclusion principle (i.e. each orbital may contain no more than two electrons, the spins of which must be opposed or antiparallel). So in the same fashion as series of closed electronic groups are built up in the extranuclear structures of isolated atoms by the 'aufbau' process, closed electronic groups are built up surrounding the nuclei of the composite molecule by electron-filling of the molecular orbitals. The basic principles of the MO treatment are thus largely the same as those relevant to atoms; and this accounts for the relative simplicity of the MO theory.

Let us now treat a diatomic molecule by the MO method. The first problem is to fashion a plausible molecular orbital for the two electrons. When an electron is closer to one nucleus (say A) than to the other (say B) the forces acting on this electron will be much the same as those in the isolated atom A; so we may reason that the molecular orbital in the region of nucleus A must resemble the atomic orbital (AO) of the isolated atom

Fig. 6.5 Relative energy levels of atomic and molecular orbitals in a homonuclear diatomic molecule (atoms A and B identical)

A. Similar considerations will also apply to the nucleus B. So, we are justified in assuming that a reasonable approximation to a molecular orbital will be a *linear combination of the two atomic orbitals* (LCAO). Thus the wave function for the single electron moving in the field of the two nuclei A and B can be written as

$$\psi = c_A\psi_A + c_B\psi_B \qquad (6.13)$$

where ψ_A and ψ_B are atomic orbitals, and c_A and c_B are coefficients chosen to give lowest energy value for the molecular orbital. Eq. (6.13) is applicable to diatomic molecules generally and it illustrates the common technique of obtaining MOs, namely, that of LCAO.

In the case of homonuclear diatomic molecule (i.e. atoms A and B identical), equal weights must be given to ψ_A and ψ_B on symmetry grounds so that $c_A{}^2 = c_B{}^2$ or $c_A = \pm c_B$. Moreover, since, the coefficients are relative quantities we can also put $c_A = 1$, and hence $c_B = \pm 1$. We can thus have two molecular orbitals from the atomic orbitals. We write them as

$$\psi_b = \psi_A + \psi_B \qquad (6.14)$$
$$\psi_a = \psi_A - \psi_B \qquad (6.15)$$

One of these molecular orbitals ψ_b has a lower energy (Fig. 6.5) than that of the atomic orbitals from which it is formed; it thus leads to the formation of a stable molecule and is therefore termed a *bonding* MO. The other MO, namely ψ_a, has an energy higher than that of the atomic orbitals and is therefore referred to as *antibonding* MO.

Considering first the case of the hydrogen molecule, there is little doubt that for the ground state of the hydrogen molecule the appropriate atomic orbitals to be employed for formulating MOs are the $1s$ ones. The bonding and antibonding MO's are then

$$\psi_b = H_A(1s) + H_B(1s) \qquad (6.16)$$
$$\psi_a = H_A(1s) - H_B(1s) \qquad (6.17)$$

Pictorial representations of these MOs are shown in the first two rows of Fig. 6.6. Evidently, the positive sign in Eq. (6.16) leads to a build-up of electron density in the region between the nuclei, whereas the negative sign of Eq. (6.17) leads to a depletion of electron density in this region. This fact is more clearly evident from Fig. 6.7 depicting contours of constant electron probability density for the bonding and antibonding states of H_2. A build-up of electronic charge between the nuclei is thus characteristic of the bonding or attractive state, and a depletion of charge between the nuclei, as a result of which there is no shielding between the

WAVE FUNCTION	ATOMIC ORBITALS	MOLECULAR ORBITALS	SYMBOL OF THE MOLECULAR ORBITAL
$\psi_g = \psi_A(s) + \psi_B(s)$			$1s\sigma_g\ (=1s\,\sigma)$
$\psi_u = \psi_A(s) - \psi_B(s)$			$1s\sigma_u\ (1s\sigma^*)$
$\psi_g = \psi_A(p_x) + \psi_B(p_x)$			$2p\sigma_g\ (=2p\sigma)$
$\psi_u = \psi_A(p_x) - \psi_B(p_x)$			$2p\sigma_u\ (=2p\ \sigma^*)$
$\psi_u = \psi_A(p_y) + \psi_B(p_y)$			$2p\pi_u\ (=2p\pi)$
$\psi_g = \psi_A(p_y) - \psi_B(p_y)$			$2p\pi_g\ (=2p\pi^*)$

Fig. 6.6 Schematic illustration of the formation of molecular orbitals by combination of atomic orbitals. The positive and negative signs in the diagram give the sign of the wave function and the broken lines show the nodal planes. If the regions of the orbitals marked + overlap, the corresponding atomic orbitals are added; if the region + of one orbital overlaps with a region — of the other, the orbitals are subtracted from one another. The subscripts g and u are used to indicate respectively the symmetry and antisymmetry of the molecular orbital, while * denotes that the orbital is of the antibonding type.
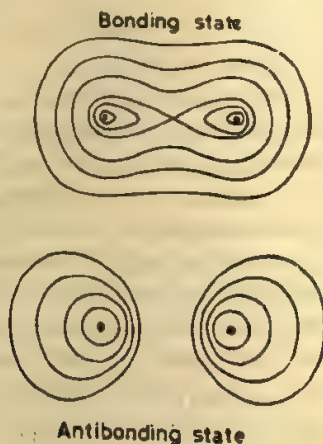
Bonding state

Fig. 6.7 Contours of constant electron probability density for the bonding (ψ^2_g) and anti bonding (ψ^2_u) states of H_2

Antibonding state

positively charged nuclei, is characteristic of antibonding or repulsive state. The same observations also apply to the formation of MOs from other more complicated atomic orbitals as shown in Fig. 6.6.

The subscripts *g* and *u* refer to the symmetry of molecular orbitals. The subscript *g* means that the orbital does not change sign on inversion through the centre of symmetry at the midpoint between the two nuclei, whereas the subscript *u* means that it does change sign under such operation.

While in the foregoing we have classified molecular orbitals in terms of

bonding and antibonding orbitals it is now ne~essary to classify them in terms of their symmetry about the internuclear axis. It is seen from Fig. 6.6 that the two molecular orbitals resulting from the combination of two atomic s orbitals are symmetrical about the internuclear axis; so also are the two molecular orbitals arising from the combination of two atomic p_x orbitals. All of them are called *sigma* orbitals, or σ orbitals using the greek letter σ for short. On the other hand, the two molecular orbitals arising from the combination of the two atomic p_y orbitals as also the two molecular orbitals arising from the combination of two atomic p_z orbitals are all unsymmetrical about the internuclear axis, and are called *pi* orbitals, designated as π orbitals.

Wave functions which describe more than one orbital are called 'degenerate'; thus $p\pi$ orbitals are doubly degenerate, since two orbitals of *equal energy* exist $(p_y\pi = p_z\pi)$; the antibonding $p\pi^*$ orbitals are also doubly degenerate $(p_y\pi^* = p_z\pi^*)$.

Before going to discuss electron arrangements in molecules, we must arrange the molecular orbitals in the order of their energies. These energies have been determined from spectroscopic measurements and show the following sequence when placed in increasing order of magnitude:

$$1s\sigma < 1s\sigma^* < 2s\sigma < 2s\sigma^* < 2p_x\sigma < 2p_y\pi = 2p_z\pi < 2p_y\pi^* = 2p_z\pi^* < 2p_x\sigma^*$$

A similar arrangement possibly exists for the $3s\sigma$ to $3p\sigma^*$ molecular orbitals.

An alternative form of terminology has been suggested by Mulliken for the orbitals $2s\sigma$ to $2p\sigma^*$, as follows:

$$z\sigma < y\sigma < x\sigma < w\pi < v\pi < u\sigma$$

One should be familiar with both the notations. As is obvious, $z\sigma$ corresponds to $2s\sigma$, and similarly $y\sigma = 2s\sigma^*$, $x\sigma = 2p_x\sigma$, $w\pi = 2p_y\pi = 2p_z\pi$, $v\pi = 2p_y\pi^* = 2p_z\pi^*$, $u\sigma = 2p_x\sigma^* \ldots$

The above notation of Mulliken can also be used for 1-quantum (K shell) and 3-quantum (M shell) molecular orbitals by writing, for K shell, $(K)z\sigma$ and $(K)y\sigma$, and for M shell, $(M)z\sigma$, $(M)y\sigma$, $(M)x\sigma$, ... etc.

Summary of the fundamental ideas of the molecular orbital theory. (1) All the atomic orbitals in the valence shells of the interacting atoms are combined in pairs.

(2) Each pair consists of one atomic orbital from each of the interacting atoms. The atomic orbitals may be originally occupied by electrons or not.

(3) For the combination of each pair of atomic orbitals to occur the following conditions must be satisfied:

(*a*) The combining orbitals must be associated with approximately same energy.

(*b*) The combining orbitals must be capable of overlapping.

(*c*) The combining orbitals must have the same symmetry.

(4)   The number of molecular orbitals produced is equal to the number of combining atomic orbitals. Half of the molecular orbitals so produced are bonding, and half antibonding.

(5)   The molecular orbitals are arranged in ascending order of energy and all the electrons originally occupying the valence shells are redistributed into these orbitals on the 'aufbau' (i.e. building-up) principle and obeying Pauli's exclusion principle, which limits the maximum number of electrons in each orbital to two.

(6)   If the number of electrons in the system is less than the number required to completely fill the molecular orbitals, the bonding orbitals outnumber the antibonding orbitals, producing the overall effect of bonding.

6.5   Comparison of VB and MO Methods

The VB and MO methods described above are the two basic approaches to the quantum theory of molecules. Let us now see how they compare with each other.

As we saw earlier, the VB method starts with individual atoms and considers the interaction between them. Consider two atoms A and B with two electrons 1 and 2. The orbital wave functions for the separate atoms are $\psi_A(1)$ and $\psi_B(2)$ respectively, and the total orbital wave function, following Eq. (6.1), is $\psi_1 = \psi_A(1)\,\psi_B(2)$. But since the electrons are indistinguishable, the wave function $\psi_2 = \psi_A(2)\psi_B(1)$ is also equally possible. Then the VB wave function is

$$\psi_{VB} = c_1\,[\psi_A(1)\psi_B(2) + \psi_A(2)\psi_B(1)]$$

The MO treatment of the molecule starts with the nuclei of the constituent atoms. For a diatomic molecule with the nuclei A and B, the wave function for a single electron moving in the field of two nuclei can be written as an LCAO, $\psi_1 = c_A\psi_A(1) + c_B\psi_B(1)$. Similarly, for the second electron, $\psi_2 = c_A\psi_A(2) + c_B\psi_B(2)$. The combined wave function is the product of these two, or

$$\psi_{MO} = c_A{}^2\psi_A(1)\psi_A(2) + c_B{}^2\psi_B(1)\psi_B(2) +$$
$$c_A c_B[\psi_A(1)\psi_B(2) + \psi_A(2)\psi_B(1)]$$

The terms $\psi_A(1)\psi_B(2)$ and $\psi_A(2)\psi_B(1)$, like those in the expression for ψ_{VB}, correspond to structures in which one electron is near one nucleus and and other is near the other. However, the two additional terms $\psi_A(1)\psi_A(2)$ and $\psi_B(1)\psi_B(2)$ correspond to structures in which both electrons 1 and 2 are near the same nucleus; that is, in the molecule AB they correspond to the ionic structures A^+B^- and A^-B^+. We see, by comparing the expressions for ψ_{VB} and ψ_{MO}, that the wave function given by the simple valence bond theory differs from that given by the simple molecular orbital theory by lack of ionic terms. Actually, for most molecules,

the simple MO theory considerably overestimates the ionic term, whereas the simple VB theory considerably underestimates these terms by neglecting them altogether. It is thus necessary to add further terms to the expressions for the wave functions to improve them. For instance, ionic terms can be added to the VB function as in Eq. (6.8).

6.6 *Electronic Configurations of Molecules in Terms of the MO Concept*

The homonuclear diatomic molecules contain two identical nuclei, as in H_2, Li_2, N_2 or O_2. The MO aufbau process used to derive electronic configurations of molecules is quite analogous to the aufbau process used for atoms. It is, however, necessary to first ascertain, according to the principles stated above, which AOs may be combined to form MOs.

(*a*) H_2

$$H(1s) + H(1s) \longrightarrow H_2[(1s\sigma)^2]$$
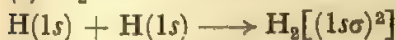
The hydrogen molecule thus contains two bonding electrons in the bonding molecular orbital of lowest energy, viz. $1s\sigma$.

(*b*) He_2

$$He(1s^2) + He(1s^2) \longrightarrow He_2[(1s\sigma)^2(1s\sigma^*)^2]$$
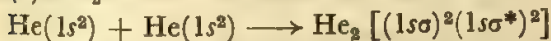
Here the bonding power of $(1s\sigma)^2$ would be more than cancelled out by the antibonding $(1s\sigma^*)^2$, and so the molecule does not exist.

(*c*) Li_2

$$2Li(1s^22s) \longrightarrow Li_2[KK(2s\sigma)^2]$$

Here, as well as in the subsequent examples, the Ks which appear inside the brackets mean merely that the K shells are present, but they are essentially atomic in character and take virtually no part in the bonding. The bonding between the two lithium atoms stems from the pairing of the $2s$ electrons in the bonding $2s\sigma$ orbital.

The diatomic molecules of other alkali metals also have similar type of configurations, e.g.

$$2Na(1s^22s^22p^63s^1) \longrightarrow Na_2[KKLL(3s\sigma)^2]$$

Such diatomic molecules have been detected in the vapour state.

(*d*) N_2

$$2N(1s^22s^22p^3) \longrightarrow N_2[KK(2s\sigma)^2(2s\sigma^*)^2(2p_x\sigma)^2(2p_y\pi = 2p_z\pi)^4]$$
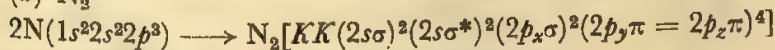
or alternatively, $N_2[KK(z\sigma)^2(y\sigma)^2(x\sigma)^2(w\pi)^4]$

The bonding power of $(z\sigma)^2$ is effectively cancelled out by the antibonding $(y\sigma)^2$. The remaining orbitals, viz. $(x\sigma)^2$ and $(w\pi)^4$, both being of bonding type, provide molecular bonding. These six electrons produce a $N\equiv N$ triple bond — one bond being of σ and the other two of π type.

(*e*) O_2

$$2O(1s^22s^22p^4) \longrightarrow O_2[KK(z\sigma)^2(y\sigma)^2(x\sigma)^2(w\pi)^4(v\pi)^2]$$
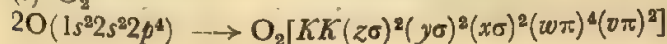
It is seen that the oxygen molecule contains two electrons more than the nitrogen molecule. These additional electrons now enter the anti-bonding $v\pi$ orbitals. Consequently, the triple bond due to $(x\sigma)^2$ and $(w\pi)^4$ is reduced to a double bond. It may be mentioned here that the molecular orbital concept affords an explanation of the well known paramagnetism of the O_2 molecule, as follows: According to Hund's rule when a set of orbitals is being filled with electrons, the electrons distribute themselves so as to retain parallel spins as far as possible. (Thus, for example, the $2p$ electrons in carbon will be arranged as $2p_x^1 2p_y^1$ since $2p_x^2$ with both electrons having parallel spins would mean violation of Pauli's principle.) Now, since there are two $v\pi$ antibonding molecular orbitals, by the aforesaid rule one electron will enter each of these, giving a paramagnetic molecule with two unpaired electrons. Fig. 6.8 assists in visualizing how the molecular orbitals are derived from the atomic orbitals of the individual oxygen atoms.

(f) F_2

$$2F(1s^2 2s^2 2p^5) \longrightarrow F_2[KK(z\sigma)^2(y\sigma)^2(x\sigma)^2(w\pi)^4\ (v\pi)^4]$$
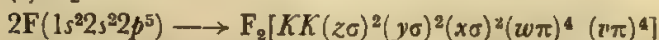
The bonding and antibonding, $(z\sigma)^2$ and $(y\sigma)^2$ cancel out one another, and the same applies to $(w\pi)^4$ and $(v\pi)^4$. Consequently, effective bonding is provided by $(x\sigma)^2$ alone, and these two electrons produce a single F—F bond.

Structures similar to the above are possessed by Cl_2 and Br_2, with Cl_2
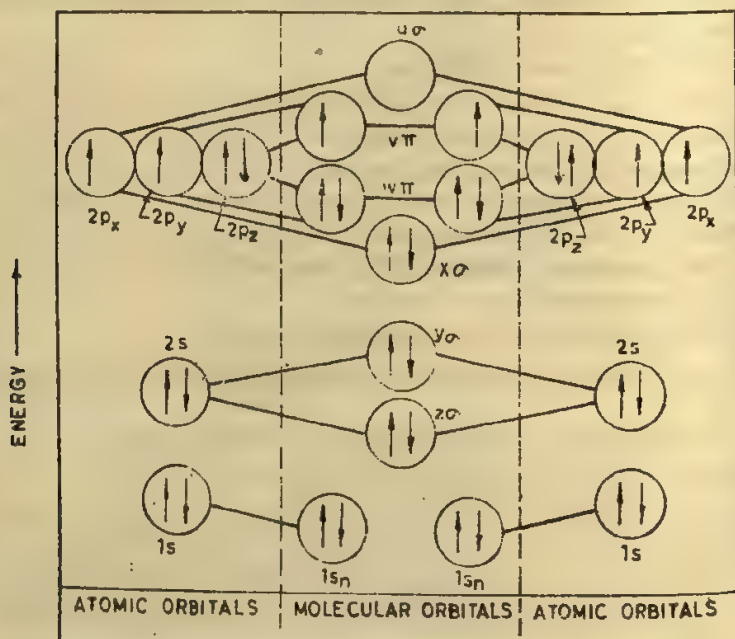
Fig. 6.8 The formation of the molecular orbitals for O_2

having its inner K and L shells and Br_2 its inner K, L and M shells full.

(g) Ne_2

$$2Ne(1s^2 2s^2 2p^6) \longrightarrow Ne_2[KK(z\sigma)^2(y\sigma)^2(x\sigma)^2(w\pi)^4(v\pi)^4(u\sigma)^2]$$
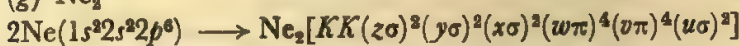
It is seen that the number of bonding electrons and that of antibonding electrons are equal. Ne_2 molecule, therefore, does not exist.

Heteronuclear diatomic molecules. In describing electronic configurations of simple heteronuclear diatomic molecules—that is, molecules in which the two constituent atoms are not identical—the same general principles that underline the above treatment of homonuclear molecules may be used. However, whereas in the homonuclear case the atomic orbitals combining together are of the same type (i.e. 1s with 1s, 2s with 2s etc.), care must be taken in dealing with hetero-atoms to select atomic orbitals that can combine effectively. Guidelines in this regard emerging from the quantum theory are that for effective combination, the atomic orbitals must have (*i*) similar energies, (*ii*) the same symmetry properties with respect to the internuclear axis, and (*iii*) sufficiently over-lapping charge clouds.

(a) HF

$$H(1s) + F(1s^2 2s^2 2p^5) \longrightarrow HF[K(2s)^2(x\sigma)^2(2p_y)^2(2p_z)^2]$$

It is known from spectroscopic observations that the energies of the $1s^2$ and $2s^2$ electrons in fluorine are too low to combine with 1s electron of hydrogen. They therefore remain essentially in atomic orbitals.

The $2p$ electrons are the only ones of suitable energy for combination with 1s of H. Moreover, if we take H—F axis as the x-axis it can be shown that the $2p_x$ orbital permits a much greater overlap with the hydrogen 1s orbital for a given internuclear distance than does the $2p_y$ orbital, as shown in Figs. 6.9(a) and 6.9(b) respectively. Furthermore, whereas in Fig. 6.9 (a) the overlapping orbitals are of the same sign and hence give bonding molecular orbital, in Fig. 6.9(b) the H(1s) orbital is overlapped by oppositely charged lobes of the p orbital, so that the bonding and antibonding effects cancel out one another. Thus, it is practically the H(1s) and $F(2p_x)$ electrons alone that contribute to the formation of the

(a)   (b)

Fig. 6.9 (a) Combination of the hydrogen 1s orbital with the fluorine $2p_x$ orbital. (b) Combination of the hydrogen 1s orbital with fluorine $2p_y$ orbital.

bonding orbital (namely, $x\sigma$), whereas the rest of the fluorine electrons remain essentially unaffected. HF has thus a single bond.

The remaining hydrogen halides have similar single-bonded structures; the atomic orbitals of chlorine, bromine and iodine, involved in bonding orbital formation are, respectively, $3p_x$, $4p_x$ and $5p_x$.
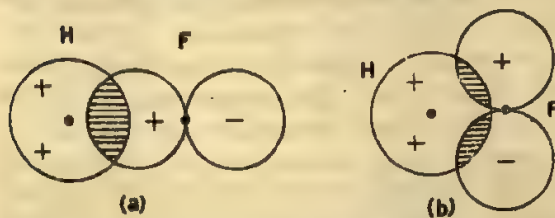
(b) CO

$$C(1s^2 2s^2 2p^2) + O(1s^2 2s^2 2p^4) \longrightarrow CO[KK(z\sigma)^2(y\sigma)^2(x\sigma)^4(w\pi)^4]$$

It is seen that this configuration is the same as that of the nitrogen molecule discussed earlier, and consequently, a triple bond between carbon and oxygen atoms is implied.

(c) NO

$$N(1s^2 2s^2 2p^3) + O(1s^2 2s^2 2p^4) \longrightarrow NO[KK(z\sigma)^2(y\sigma)^2(x\sigma)^2(w\pi)^4(v\pi)]$$
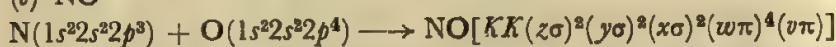
The nitric oxide molecule has one electron more than the nitrogen molecule. This single electron gives rise to paramagnetism in NO. Moreover, since the electron enters the antibonding $v\pi$ orbital. the bonding in NO is weaker than in the nitrogen molecule.

6.7 Directed Bonds

As has been mentioned earlier, the strength or energy of a covalent bond stems from the energy of resonance or exchange of electrons between two atoms. It has been shown by Pauling that the magnitude of the resonance and hence the strength of a covalent bond is approximately proportional to the amount of overlap of the wave functions or atomic orbitals of the two electrons constituting the bond. The strongest covalent bonds will, therefore, result where the maximum overlapping of the atomic orbitals occurs, that is, where there is maximum inter-penetration of charge densities of the electrons involved in bond formation. Accordingly, the bond formed by a given orbital will tend to lie in the direction in which that orbital has its maximum value. Furthermore, bonds will be stable when formed with the use of stable atomic orbitals corresponding to the normal or ground state of the atom.

We have seen that the distributions of charge densities of electrons are geometrical in character. Thus, s orbitals are spherically symmetrical, whereas the three p orbitals lie on three mutually perpendicular axes, with the nucleus at the centre. Being spherically symmetrical, s orbitals overlap to the same extent in all directions, whereas in the case of a p orbital the electron density is greatest along an axis, and so it overlaps to the maximum extent if the bond is formed in this direction. It follows, therefore, that p orbitals should overlap more effectively for a given internuclear distance than should s orbitals belonging to the same principal quantum number. If the radius of a spherical contour surface representing the maximum value of the s orbital is r, then the length of a p orbital from

nucleus to the boundary along the axis can be calculated, from Table 5.2, to be $\sqrt{3}r$. The relative magnitudes or strength of the p and s orbitals should be approximately in the ratio of $\sqrt{3} : 1$. If, starting from the condition of maximum overlapping, we take the bond strength as being proportional to the product of the magnitudes of the bond orbitals of the two atoms forming the bond, then the strength of an s-p bond (i.e. bond formed by the overlap of s and p orbitals) should be $\sqrt{3}$ times that of an s-s bond. Similarly a p-p bond should be $\sqrt{3}$ times stronger than an s-p bond and 3 times stronger than an s-s bond.

The aforesaid ideas enable us to deduce the structure and bond angles for many molecules. The oxygen atom, for instance, has the electronic configuration $1s^2 2s^2 2p^2_x 2p^1_y 2p^1_z$, which shows that there are two unpaired electrons in orbitals which are at right angles to one another. When combination with hydrogen occurs these unpaired electrons in p_y and p_z orbitals pair up with $1s$ electrons of hydrogen atoms, and since p_y and p_z are at right angles to each other, the resulting structure (Fig. 6.10) should have two O—H bonds at 90° to each other. In practice, we find that the H—O—H angle is not the predicted 90° but 105°. This increase has been attributed to mutual repulsion between the H atoms since the bonds are not ideally covalent but possess a partial ionic character, making the hydrogen atoms somewhat positive. The related molecules H_2S and H_2Se, however, are found to have bond angles much closer to the predicted 90°, namely, 93° and 91° respectively. This may be attributed to the decrease in the mutual repulsion of the H atoms on account of greater bond lengths and reduced ionic character of the H atoms.

With the nitrogen atom ($1s^2 2s^2 2p^1_x 2p^1_y 2p^1_z$), there are three unpaired $2p$ electrons so that by analogy we would expect three mutually perpendicular bonds in NH_3 [Fig. 6.10(b)]. The related molecules, PH_3, AsH_3
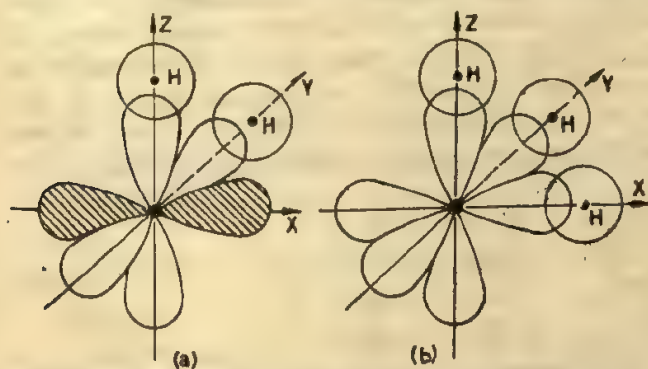

(a)   (b)

Fig. 6.10 (a) The formation of water molecule. The lone pair $2p_x$ orbital is shown shaded. The singly-occupied $2p_y$ and $2p_z$ orbitals overlap with the hydrogen $1s$ orbitals. (b) The formation of ammonia molecule. The singly-occupied $2p_x$, $2p_y$ and $2p_z$ orbitals overlap with the hydrogen $1s$ orbitals.

and SbH_3, should also have similar structure. The observed values of bond angles are 108° for NH_3, 93° for PH_3, 92° for AsH_3, and 91° for SbH_3. Here again, as the repulsions between the hydrogen atoms diminish, the bond angle approaches 90°.

6.8 Hybrid Orbitals

Carbon in its normal state $(1s^2 2s^2 2p^1_x 2p^1_y)$ has two unpaired $2p$ electrons and hence might be expected to form only two bonds at right angles to each other. But we know the carbon atom to be usually quadrivalent; to achieve which one of the electrons from the $2s$ orbital must be promoted to the p level, thus giving the configuration $1s^2 2s^1 2p^1_x 2p^1_y 2p^1_z$. According to the preceding discussion on directional bond formation, this configuration would then be expected to form three bonds at right angles to one another and a fourth weaker bond with its s orbital in any direction (since s orbital is spherically symmetrical). But such spatial form is at sharp variance with the observed fact that the four bonds of carbon are equivalent and directed to the four corners of a regular tetrahedron in saturated compounds. It follows, therefore, that the valence state of the carbon atom is one in which its four valence electrons are in four equivalent orbitals whose lobes are directed towards the corners of a regular tetrahedron. These four equivalent directed orbitals constitute a set of hybrid orbitals and are commonly referred to as sp^3 hybrids to indicate that they are formed by the combination or *mixing* of one s and three p orbitals. The general phenomenon of such combination or mixing of pure orbitals is termed *hybridization* and the resulting mixed orbitals are called *hybrid orbitals* or simply *hybrids*.

Supposing that the quadrivalent carbon is represented by the electronic state $1s^2 2s^1 2p^1_x 2p^1_y 2p^1_z$, we can write the four valence orbitals of carbon as $\psi(2s)$, $\psi(2p_x)$, $\psi(2p_y)$, $\psi(2p_z)$. These are to be combined in suitable proportions to produce a set of four new orbitals ψ_1, ψ_2, ψ_3, ψ_4, which will be *equivalent* and directed towards the corners of a tetrahedron. A set of such *tetrahedrally oriented orbitals*, called sp^3 hybrids, is the following:

$$\begin{aligned}
\psi_1 &= \tfrac{1}{2}\left[\psi(2s) + \psi(2p_x) + \psi(2p_y) + \psi(2p_z)\right] \\
\psi_2 &= \tfrac{1}{2}\left[\psi(2s) + \psi(2p_x) - \psi(2p_y) - \psi(2p_z)\right] \\
\psi_3 &= \tfrac{1}{2}\left[\psi(2s) - \psi(2p_x) + \psi(2p_y) - \psi(2p_z)\right] \\
\psi_4 &= \tfrac{1}{2}\left[\psi(2s) - \psi(2p_x) - \psi(2p_y) + \psi(2p_z)\right]
\end{aligned} \qquad (6.18)$$

The factor of $1/2$ is determined from the normalization condition and the condition that the bonding power of the hybrid orbitals should be a maximum (see Appendix 3). It can be shown by substituting (from Table 5.2) the expressions for the angular parts of the s and p wave functions into the above set of equations, that the four hybrid wave

functions $\psi_1, \psi_2, \psi_3, \psi_4$ all have the same spatial form, and that the angles between the directions of the maximum magnitude of these wave functions are each 109°28′, which is just the tetrahedral angle, i.e. the angle formed by lines from the centre of a regular tetrahedron to any two of its vertices.

sp Hybrids.

We now proceed to a systematic consideration of hybridization, beginning with the simplest common type, namely, the *sp* hybridization.

It has been deduced from wave-mechanical treatment that a linear combination of *s* and *p* wave functions (or orbitals) in suitable proportions results in strong hybrid *sp* wave function or bond orbital, which is considerably stronger than both *s* and *p* orbitals.

Consider, for example, the formation of hybrid wave functions from *s* and p_z wave functions. The two new hybrid wave functions are, in general,

$$\psi_1 = a_1 \, \psi(s) + b_1 \, \psi(p_z) \tag{6.19}$$

$$\psi_2 = a_2 \, \psi(s) + b_2 \, \psi(p_z) \tag{6.20}$$

where a_1, b_1, a_2, and b_2 are coefficients determined by (*i*) the normalization condition for the wave functions ψ_1 and ψ_2, i.e. $\int \psi_1^2 \, dv = 1$ and $\int \psi_2^2 dv = 1$, (*ii*) the orthogonality condition $\int \psi_1 \psi_2 \, dv = 0$, and (*iii*) the equivalence condition for the wave functions ψ_1 and ψ_2.

From the sphericity of the *s* wave function and the equivalence condition it follows that $\psi(s)$ contributes with equal weight to the new wave functions. The weight is proportional to the square of the coefficients. Therefore,

$$a_1^2 = a_2^2 = 1/2 \quad \text{and} \quad a_1 = a_2 = 1/\sqrt{2} \tag{6.21}$$

From Eq. (6.19) we get,

$$\int \psi_1^2 \, dv = a_1^2 \int \psi^2(s) dv + 2a_1 b_1 \int \psi(s) \, \psi(p_z) dv + b_1^2 \int \psi^2(p_z) dv \tag{6.22}$$

Applying the normalization condition to ψ_1 and the normalization and orthogonality conditions to $\psi(s)$ and $\psi(p_z)$ we get from Eq. (6.22),

$$a_1^2 + b_1^2 = 1, \text{ so } b_1 = \frac{1}{\sqrt{2}} \tag{6.23}$$

Again applying the orthogonality condition to the hybrid wave functions ψ_1 and ψ_2 we have from Eqs. (6.19) and (6.20),

$$\int \psi_1 \psi_2 \, dv = a_1 a_2 + b_1 b_2 = \frac{1}{2} + \frac{b_2}{\sqrt{2}} = 0 \tag{6.24}$$

So, $b_2 = -1/\sqrt{2}$

Substituting into Eqs. (6.19) and (6.20) the values of the coefficients from Eqs. (6.21), (6.23) and (6.24) we obtain the following equations for ψ_1 and ψ_2:

$$\psi_1 = \frac{1}{\sqrt{2}} \, [\psi(s) + \psi(p_z)] \tag{6.25}$$

$$\psi_2 = \frac{1}{\sqrt{2}} \, [\psi(s) - \psi(p_z)] \qquad\qquad (6.26)$$

To learn more about these hybrid orbitals, let us introduce into their equations approximate expressions for the wave functions $\psi(s)$ and $\psi(p_z)$. The radial parts of the s and p wave functions do not greatly differ from each other. Following Pauling, we therefore neglect the difference between the radial parts and pay attention to the angular parts as given in Table 5.2, because they determine the shape of the orbitals. Writing in place of $\psi(s)$ and $\psi(p_z)$ the expressions from Table 5.2, we obtain the following expressions for the sp hybrid wave functions:

$$\psi_1 = \frac{1}{2\sqrt{2\pi}} \, (1 + \sqrt{3} \, \cos\theta) \qquad\qquad (6.27)$$

$$\psi_2 = \frac{1}{2\sqrt{2\pi}} \, (1 - \sqrt{3} \, \cos\theta) \qquad\qquad (6.28)$$

In Fig. 6.11 are depicted the sp functions ψ_1 and ψ_2 which are seen to be equivalent but pointing in the opposite direction: one in the direction of the positive z-axis, the other in the direction of the negative z-axis, the valence angle being thus $180°$.

We can state here the general rules pertaining to hybridization: (i) the number of hybrid orbitals is the same as the number of atomic orbitals used in their construction, and (ii) hybrid orbitals of one kind are equiva-

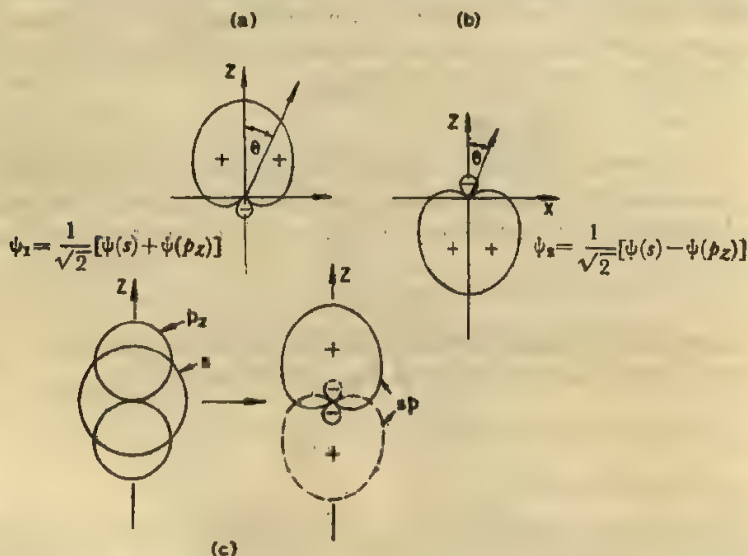**Fig. 6.11** Polar representation of sp hybrid orbitals. The two hybrid orbitals are pointing in positive (a) and negative (b) directions of z-axis. (c) Geometrical representation of the formation of sp hybrid orbitals from s and p orbitals.

lent, differing from one another, by and large, only in their direction in space.

The sp hybrid orbital is stronger than pure s and p atomic orbitals from which it originates. Thus taking the strength of the s bond as unity, the bond strength connected with the sp hybrid orbital will be 1.932:

$$\frac{(\psi_1)_{max}}{(\psi_s)_{max}} = \frac{(\psi_2)_{max}}{(\psi_s)_{max}} = \frac{1 + \sqrt{3}}{\sqrt{2}} = 1.932$$

sp^2 hybrids. Suppose the initial functions involved in sp^2 hybridization are one s, one p_x and one p_y. The three new wave functions formed by their combination are, in general:

$$\psi_1 = a_1\psi(s) + b_1\psi(p_x) + c_1\psi(p_y) \tag{6.29}$$
$$\psi_2 = a_2\psi(s) + b_2\psi(p_x) + c_2\psi(p_y) \tag{6.30}$$
$$\psi_3 = a_3\psi(s) + b_3\psi(p_x) + c_3\psi(p_y) \tag{6.31}$$

Since $\psi(s)$ has spherical symmetry and the three new functions are equivalent it follows that $a_1^2 = 1/3$, $a_1 = a_2 = a_3 = a = 1/\sqrt{3}$.

Out of the three new functions let ψ_1 have a maximum in the direction of the x-axis; then the function $\psi(p_y)$ will play hardly any part in it, so that we can put $c_1^2 = 0$ or $c_1 = 0$.

So Eq. (6.29) becomes

$$\psi_1 = a_1\psi(s) + b_1\psi(p_x) \tag{6.32}$$

Applying normalization and orthogonality conditions we get from Eq. (6.32), $a_1^2 + b_1^2 = 1$ or $b_1 = \sqrt{2/3}$.

Similarly from Eqs. (6.29) and (6.30) we obtain $a_1a_2 + b_1b_2 + c_1c_2 = 0$ and $\frac{1}{3} + b_2\sqrt{2/3} + 0 = 0$. So, $b_2 = -1/\sqrt{6}$.

The normalization condition applied to ψ_2 gives $a_2^2 + b_2^2 + c_2^2 = 1$. So, $c_2 = 1/\sqrt{2}$.

From the orthogonality condition $\int \psi_1\psi_3 dv = 0$ we obtain

$a_1a_3 + b_1b_3 + c_1c_3 = 0$. So, $b_3 = -1/\sqrt{6}$.

Similarly, $\int \psi_2\psi_3 dv = a_2a_3 + b_2b_3 + c_2c_3 = 0$. So, $c_3 = -1/\sqrt{2}$.

Introducing the values found for the coefficients into Eqs. (6.29)-(6.31) we obtain the equations for the three equivalent sp^2 orbitals as:

$$\left. \begin{array}{l} \psi_1 = \dfrac{1}{\sqrt{3}}\,\psi(s) + \sqrt{\dfrac{2}{3}}\,\psi(p_x) \\[3mm] \psi_2 = \dfrac{1}{\sqrt{3}}\,\psi(s) - \dfrac{1}{\sqrt{6}}\,\psi(p_x) + \dfrac{1}{\sqrt{2}}\,\psi(p_y) \\[3mm] \psi_3 = \dfrac{1}{\sqrt{3}}\,\psi(s) - \dfrac{1}{\sqrt{6}}\,\psi(p_x) - \dfrac{1}{\sqrt{2}}\,\psi(p_y) \end{array} \right\} \tag{6.33}$$

We can now substitute for the s-, p- wave functions in Eq. (6.33) the corresponding expressions for the angular part from Table 5.2. If,
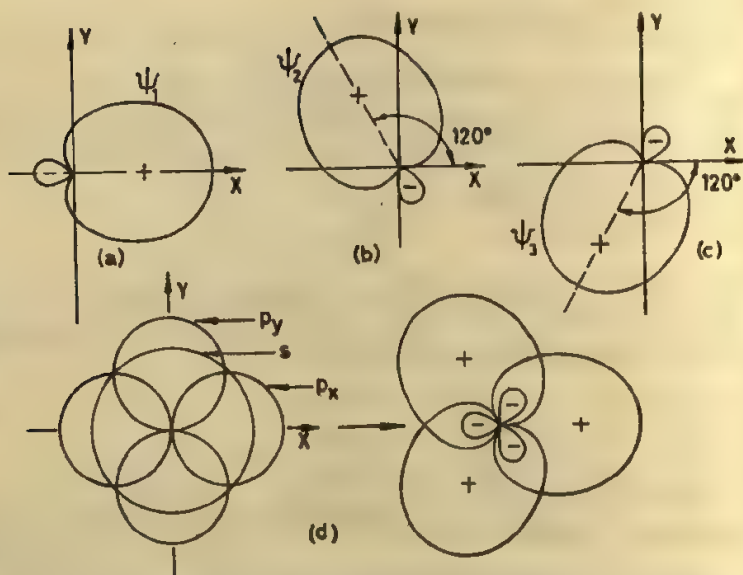
Fig. 6.12 Polar representation of sp^2 hybrid orbitals: (a) ψ_1, (b) ψ_2, and (c) ψ_3. (d) Geometrical representation of the formation of sp^2 hybrid orbitals from one s and two p orbitals.

however, we want to draw polar diagrams of the hybrid orbitals on xy-plane for which $\theta = 90°$, the expressions for the three sp^2 hybrid orbitals are:

$$
\left.
\begin{aligned}
\psi_1 &= \frac{1}{2\sqrt{\pi}}\left[\frac{1}{\sqrt{3}} + \sqrt{2}\cos\varphi\right] \\
\psi_2 &= \frac{1}{2\sqrt{\pi}}\left[\frac{1}{\sqrt{3}} - \frac{1}{\sqrt{2}}\cos\varphi + \sqrt{\frac{3}{2}}\sin\varphi\right] \\
\psi_3 &= \frac{1}{2\sqrt{\pi}}\left[\frac{1}{\sqrt{3}} - \frac{1}{\sqrt{2}}\cos\varphi - \sqrt{\frac{3}{2}}\sin\varphi\right]
\end{aligned}
\right\} \tag{6.34}
$$

The polar representation of the sp^2 hybrid functions ψ_1, ψ_2 and ψ_3 on the xy-plane, is shown in Fig. 6.12. The maximum value of ψ_1 lies on the x-axis, while ψ_2 has its maximum value in the direction for which $\varphi = 120°$. The three sp^2 hybrid orbitals thus, lie in the plane of the p orbitals and are oriented at 120° with respect to each other.

The bond strength connected with the sp^2 hybrid orbitals, taking the strength of the s-bond as unity, is

$$
(\psi_1)_{max} = (\psi_2)_{max} = (\psi_3)_{max} = \frac{1}{\sqrt{3}} + \sqrt{2} = 1{\cdot}991
$$

So the strength of the sp^2 hybrid orbitals exceeds not only the strength of the pure s- and p- orbitals but also that of the sp hybrid orbitals.

sp^3 Hybrids. One s and three p orbitals will lead to a set of four sp^3

hybrid orbitals. The four hybrid functions will be of the type

$$\psi_i = a_i \psi(s) + b_i \psi(p_x) + c_i \psi(p_y) + d_i \psi(p_z) \quad \text{(where } i = 1,2,3,4) \quad (6.35)$$

From the sphericity of the s-state and the equivalence condition $a_i^2 = 1/4$. So, $a_1 = a_2 = a_3 = a_4 = a = 1/2$.

From normalization conditions we get four relations of the type

$$a_i^2 + b_i^2 + c_i^2 + d_i^2 = 1 \qquad (6.36)$$

or $b_i^2 + c_i^2 + d_i^2 = 3/4$

The orthogonality conditions give six relations of the type

$$(6.37)$$

$$\tfrac{1}{4} + b_i b_k + c_i c_k + d_i d_k = 0$$

where $i = 1,2,3,4$; $k = 1,2,3,4$; and $i \neq k$.

Let the function ψ_1 have a maximum in the direction of the z-axis. Consequently, the functions p_x and p_y hardly participate in the formation of this function. Therefore, $b_1 = c_1 = 0$. Putting $i = 1$, we get from Eq. (6.36) $d_1 = \sqrt{3}/2$. When $i = 1$ and $k = 2$, Eq. (6.37) yields $d_2 = -\ 1/2\sqrt{3}$. Putting $i = 2$, we get from Eq. (6.36)

$$(6.38)$$

$$b_2^2 + c_2^2 = 2/3$$

Assuming that the direction of the maximum value of ψ_2 lies in the xz-plane, so that the function p_y hardly participates in it, $c_2 = 0$, and, consequently, from Eq. (6.38)

$$b_2 = \sqrt{2/3}$$

Proceeding in this way we can evaluate the other coefficients.

Introducing the values found for the coefficients into Eqs. (6.35), we obtain the following expressions for the four sp^3 functions:

$$\left.\begin{aligned}
\psi_1 &= \frac{1}{2}\,\psi(s) + \frac{\sqrt{3}}{2}\,\psi(p_z) \\[4pt]
\psi_2 &= \frac{1}{2}\,\psi(s) + \frac{\sqrt{2}}{\sqrt{3}}\,\psi(p_x) - \frac{1}{2\sqrt{3}}\,\psi(p_z) \\[4pt]
\psi_3 &= \frac{1}{2}\,\psi(s) - \frac{1}{\sqrt{6}}\,\psi(p_x) + \frac{1}{\sqrt{2}}\,\psi(p_y) - \frac{1}{2\sqrt{3}}\,\psi(p_z) \\[4pt]
\psi_4 &= \frac{1}{2}\,\psi(s) - \frac{1}{\sqrt{6}}\,\psi(p_x) - \frac{1}{\sqrt{2}}\,\psi(p_y) - \frac{1}{2\sqrt{3}}\,\psi(p_z)
\end{aligned}\right\} \quad (6.39)$$

This set of equations is mathematically equivalent to the set in Eq. (6.18). Both sets represent four equivalent sp^3 hybrid orbitals. The only difference is that the two sets are oriented differently with respect to the chosen set of coordinate axes (see Appendix 3). Since the orientation of our set of coordinate axes in space is arbitrary, it follows that there will be an infinitely large number of different but mathematically equivalent ways in which the hybrid wave functions can be expressed.

Writing in place of wave functions, $\psi(p_x)$ and $\psi(p_z)$, in Eqs. (6.39) the expressions for the corresponding angular wave functions from Table 5.2,

we can anlyse the positions of the maxima, and hence, the spatial directions of the hybrid functions.

The first hybrid function ψ_1 is of course oriented, according to our assumption, in the z-direction. We also assumed that the axis of ψ_2 lies in the xz-plane. In this plane $\varphi = 0°$, and thus $\psi(p_x) = (\sqrt{3}/2\sqrt{\pi}) \sin\theta$. Substituting in the equation for ψ_2 this expression for $\psi(p_x)$ and the expressions for $\psi(s)$ and $\psi(p_z)$ from Table 5.2, we obtain the following equation for ψ_2 as a function of the angle θ:

$$\psi_2 = \frac{1}{4\sqrt{\pi}} + \frac{1}{\sqrt{2\pi}} \sin\theta - \frac{1}{4\sqrt{\pi}} \cos\theta$$

To find the value of θ for which ψ_2 has the maximum magnitude, we differentiate ψ_2 with respect to θ and equate the derivative to zero. Thus,

$$\frac{d\psi_2}{d\theta} = \frac{1}{\sqrt{2\pi}} \cos\theta + \frac{1}{4\sqrt{\pi}} \sin\theta = 0$$

The solution of the equation is $\theta = 109°28'$ which is just the tetrahedral angle mentioned before. When we use similar procedure to find the orientation of ψ_3 and ψ_4, it turns out that the angle between the spatial directions of any two of the sp^3 hybrid orbitals is the tetrahedral angle (109°28').

The equation for ψ_1, on introducing the expressions for $\psi(s)$ and $\psi(p_z)$ from Table 5.2, becomes

$$\psi_1 = \frac{1}{4\sqrt{\pi}} + \frac{3}{4\sqrt{\pi}} \cos\theta$$

Since the axis of ψ_1, according to our assumption, is the x-axis for which $\theta = 0°$, the magnitude of ψ_1 is $1/\sqrt{\pi}$. This is twice the magnitude of $\psi(s)$. The relative magnitude of ψ_1, with the magnitude of the s orbital as unity, is thus 2. It can be similarly shown that ψ_2, ψ_3 and ψ_4 also have a relative magnitude of 2 in their respective axial directions. Compared to this the relative magnitudes of the sp and sp^2 hybrid orbitals, derived before, are 1.932 and 1.99. We thus see that among the equivalent hybrid orbitals that can be formed from s and p orbitals, sp^3 hybrid orbitals are the strongest.

Other hybrids. In addition to the three types of hybrid orbitals discussed so far, there are a number of others, representing different mixtures of atomic orbitals, that are used in describing directed covalent bonding. In general, the important distinction between atomic orbitals and hybrid orbitals resides in the fact that the latter are much more concentrated into one direction in space than the former and have a different geometrical relation to one another. Table 6.1 lists various hybrid orbitals, their spatial arrangements and the bond strengths associated with them. The numbers listed under bond strength provide a measure of the relative

Table 6.1 Hybrid Orbitals

Orbital	No. of orbitals	Spatial arrangement	Bond strength*
sp	2	Linear	1·93
sp^2	3	Planar, 120°	1·99
sp^3	4	Tetrahedral	2·00
dsp^2	4	Square planar	2·69
dsp^3	5	Trigonal bipyramidal	2·80
d^2sp^3	6	Octahedral	2·92

* Relative to the bond strength of pure s orbital taken as 1

sp
(linear 180°)

sp²
(trigonal planar, 120°)

dsp²
(square planar 90°)

sp³ or d³s
(tetrahedral 109°)

dsp³ or d³sp
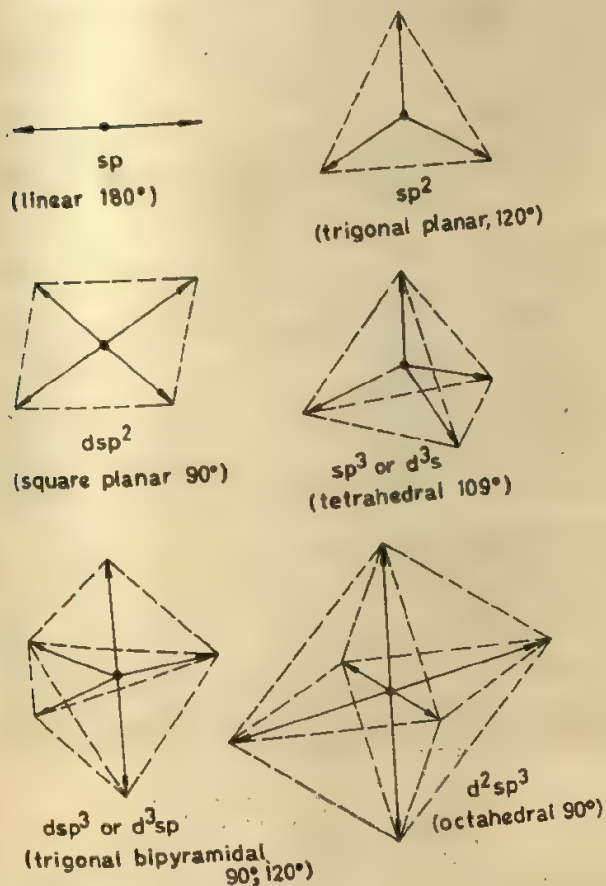(trigonal bipyramidal,
90°; 120°)

d²sp³
(octahedral 90°)

Fig. 6.13 Directional characteristics of various types of hybrid bonds

concentration, or the relative degree of protrusion, in one direction. The geometrical arrangements of bonds obtainable by hybridization of various orbitals are illustrated in Fig. 6.13.

The valence state. Before proceeding to a further discussion of hybridization, we may introduce here the term *valence state*. When electrons of an atom are placed in hybridized orbitals the atom is said to be in the valence state. Since there are many types of hybrids, there are also many different valence states. It must be emphasized that the valence state is not identical with any observable stationary state of the atom. The valence state would not be assumed by an isolated atom because of the difference in energies of the orbitals used to form the hybrid orbitals. We may sometimes describe the valence state as the state assumed by the atom during the process of bonding. This description also is not completely correct, because at the point of bonding it is really the MOs and not AOs with which we are concerned. Energy is required for hybridization, so the energy of an atom in the imaginary valence state will be always somewhat higher than that of the atom with the ground-state configuration. However, this energy of 'promotion to the valence state' is more than compensated for by a greater gain in binding energy through the formation of stronger bonds from hybrid orbitals.

Examples of hybridization. Let us now consider, by way of illustration, the types of hybridization in some common molecules and ions.

Beryllium atom ($1s^2 2s^2$), with $2s$ electrons, has completed shell in the ground state and as such would be inactive. If, however, the beryllium atom receives sufficient energy, one of the $2s$ electrons will be promoted into a $2p$ orbital forming the excited state $1s^2 2s^1 2p^1_x$. Now from $2s$ and $2p$ orbitals two sp hybrid orbitals are formed; these are collinear and point in opposite directions (Fig. 6.14). This explains the linear form of the molecule $BeCl_2$.

The boron atom has the configuration $1s^2 2s^2 2p^1_x$, and the promotion of one $2s$ electron produces the excited state $1s^2 s^1 2p^1_x 2p^1_y$. The three unpaired electrons in this structure give rise to three bonds in simple molecules such as BCl_3. That the three bonds are equivalent and coplanar with 120° orientation to other, as observed experimentally, is accounted for by the formation of three equivalent or hybridized sp^2 orbitals from the s orbital and the two p orbitals containing unpaired electron (Fig. 6.15).
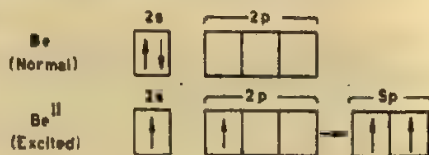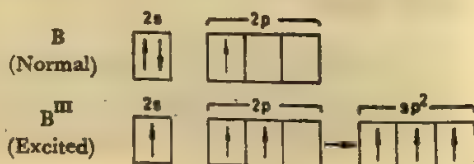

Fig. 6.14 The formation of sp hybrid orbitals of beryllium

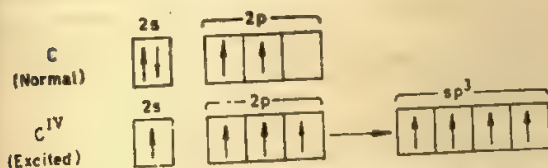Fig. 6.15 The formation of sp^2 hybrid orbitals of boron

Fig. 6.16 The formation of sp^3 hybrid orbitals of carbon

The formation of sp^3 hybrid orbitals in carbon becomes evident from the representation in Fig. 6.16. The four sp^3 hybrid orbitals formed from one s- and three p-orbitals containing unpaired electrons are directed towards the four corners of a tetrahedron forming tetrahedral bond angles (109°28') to each other.

Four strong, equivalent tetrahedral hybrid orbitals are formed by the linear combination of three d orbitals of the penultimate valence shell and one s orbital of the valence shell (Fig. 6.17). These hybrid orbitals are responsible for the configuration of complex ions of the oxyacids of the transitional elements, e.g. $(CrO_4)^{-2}$, $(MnO_4)^{-}$, $(MoO_4)^{-2}$. They have a strength of 2.95, as against 1 of an s orbital.

Hybridization of d, s and p orbitals gives stronger covalent bonds than those involving s and p orbitals alone. In d^2sp^3 hybridization six strong equivalent hybrid orbitals with strength 2.92 (as against 1 of s orbital) directed to the corners of a regular octahedron are formed by the combination of two d orbitals of the penultimate valence shell with one s- and three p-orbitals of the valence shell. Owing to the availability of d orbitals among transition metal ions d^2sp^3 is common to many of them, which explains the preponderance of 6-coordinate octahedral complexes derived from such ions. Fig. 6.18 presents some such examples.

Consider, for example, the ferrocyanide ion $[Fe(CN)_6]^{-4}$. In order to make two of the five $3d$ orbitals available for bond formation three electrons in the $3d$ orbitals of the ferrous ion become paired. The vacant d^2sp^3 hybridized orbitals can then accept the lone pairs of electrons from the cyanide ions.

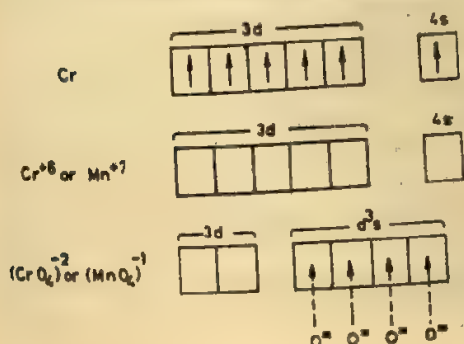We have seen in Section 6.7 how the structures of simple compounds

Fig. 6.17 The formation of d^3s hybrid orbitals in complex ions. Each dashed arrow denotes an electron pair supplied by an oxygen ion.
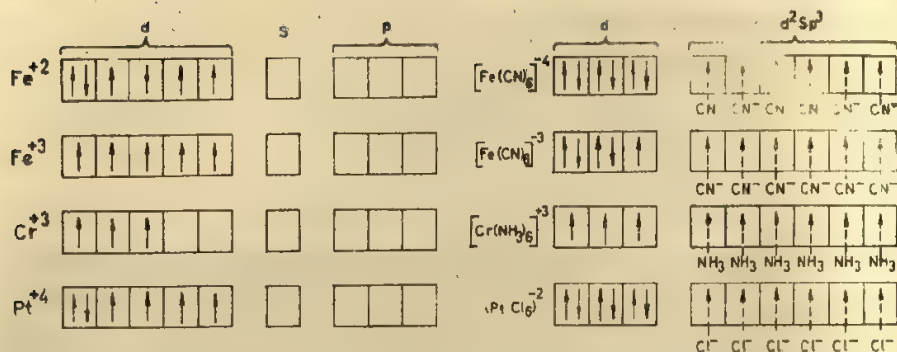
Fig. 6.18 The formation of d^2sp^3 hybrid orbitals. On the left are the electronic configurations of the free metal ions. The electronic configurations of the complexes, shown on the right, include the twelve electrons of the ions or coordinating groups. Each broken arrow denotes a pair of such electrons.

of nitrogen and of oxygen, such as ammonia and water, could be deduced from the directional properties of pure atomic orbitals, using the criterion of maximum overlap. It might be noted that such structures can also be considered in terms of hybrid orbitals; this treatment has certain advantages over that involving pure atomic orbitals. Consider, for example, the formation of the ammonia molecule. The five outer electrons of nitrogen $(2s^2 2p^3)$ can use the four tetrahedral hybrid orbitals formed by sp^3 hybridization, three being singly-occupied and one containing a lone pair of electrons (i.e. two electrons with opposite spins). The ammonia molecule formed by the pairing of the electrons of the singly-occupied sp^3 hybrid orbitals with $1s$ electrons of hydrogen should therefore have approximately tetrahedral (i.e. 109°28′) bond angle. This is much closer to the observed angle of 107°18′ than the 90° expected when pure p orbitals are used.

Similarly, the six outer electrons of the oxygen atom $(2s^2 2p^4)$ can occupy four tetrahedral hybrid orbitals, two being occupied by lone pair electrons and the other two by single electrons. The electrons in the latter orbitals can then pair up with hydrogen $1s$ electrons forming the water molecule. Accordingly, the HÔH angle in water should be 109°28′. This is seen to be much closer to the experimentally observed value of 104°27′ than the 90° predicted earlier from the consideration of pure orbitals. Furthermore, the remaining 5° difference also can be closed up if we do not restrict ourselves to pure sp^3 hybridization but *mix* varying degrees of s- and p-orbitals to produce hybrid orbitals with the desired angular relationship. The hybrid orbitals formulated in this way are however, no longer equivalent.

Table 6.2 gives some more examples of hybridization.

Table 6.2 Hybridization in some Common Molecules and Ions*

sp	$\underline{C}O$, $\underline{C}O_2$, $\underline{C}_2H_2$, $(\underline{C}N)^-$, $\underline{N}_2$
sp^2	$\underline{B}Cl_3$, $\underline{C}_2H_4$, $\underline{C}_6H_6$, $(\underline{C}O_3)^{-2}$, $(\underline{N}O_3)^-$, $\underline{S}O_2$, $\underline{S}O_3$
sp^3	$\underline{C}H_4$, $\underline{C}_2H_6$, $\underline{N}H_3$, $(\underline{N}H_4)^+$, $(\underline{S}O_4)^{-2}$, $(\underline{C}lO_3)^-$, $(\underline{C}lO_4)^-$
dsp^2	$[\underline{N}i(CN)_4]^{-2}$, $(\underline{P}dCl_4)^{-2}$
dsp^3	$\underline{P}F_5$, $\underline{P}Cl_5$
d^2sp^3	$(\underline{A}lF_6)^{-3}$, $(\underline{P}F_6)^-$, $\underline{S}F_6$, $[\underline{F}e(CN)_6]^{-3}$, $[\underline{F}e(CN)_6]^{-4}$, $(\underline{P}tCl_6)^{-2}$

* For the underlined atom

6.9 Localized Bonding and Overlap Criterion

A striking feature of the chemical bond, as revealed by much of the evidence relating to its properties such as the length and binding energy, is that it is in most cases very localized and concerns primarily the two atoms which are being joined; adjacent atoms, even if attached to one of the bonded atoms, have only secondary effect on the bond. There are, of course, exceptions to this general rule, but in almost all cases such exceptions can be associated with some special feature of the molecule itself.

The general molecular orbital theory centres on the idea that when two or more atoms combine to form a molecule there are formed molecular orbitals which embrace all the nuclei in the molecule. These are referred to as delocalized molecular orbitals. Quite often, however, in dealing with polyatomic molecules it is more advantageous to modify the general theory and discuss molecular orbitals enclosing only the two nuclei directly involved in bonding rather than all the nuclei in the molecule. Such molecular orbitals are then referred to as localized molecular orbitals. Conceptually, localized MOs are more closely allied than delocalized MOs to our empirical ideas of chemical bonding and are therefore easier to visualize and handle.

Moreover, in view of the structural properties of covalent compounds, we have to accept that the covalent bond, in addition to being localized, is also very directional in character. Since hybrid orbitals have strong directional properties, it is advantageous to use hybrid atomic orbitals for describing localized molecular orbitals in covalent bonding. It might be mentioned, moreover, that the concepts of localized bonds and directed valence are very closely linked. The application of the criterion of maximum overlap to localized molecular orbitals forms the basis of the explanation for directed valence.

In terms of the VB concept, however, the localized bond means that the pairing of electrons from two different atoms in the formation of a bond is independent of any other pairing that may occur in the rest of the molecule. The explanation for directed valence, however, is provided,

as in the MO theory, by the criterion of maximum overlap. Thus the approach to localized bonding in polyatomic molecules is much the same, at least from a qualitative point of view, in both VB and MO theories.

6.10 Orbital Structures of Some Hydrocarbons

In view of the unique bonding properties of carbon and the considerable theoretical study that these properties have received, it will be appropriate here to present a discussion on the structural features of some common hydrocarbon molecules. As we shall see in the following, the introduction of hybrid orbitals provides considerable insight into the structural details.

Methane (CH_4). Methane has four equivalent tetrahedrally directed carbon–hydrogen bonds. We may therefore picture the carbon atom in CH_4 as tetrahedrally hybridized and describe the molecule as being formed by the end-on overlap of the s orbitals of the hydrogen atoms with the sp^3 hybrid orbitals of the carbon atom. These overlaps are very effective, since, as has been pointed out earlier, the charge clouds of hybrid orbitals are characterized by extended axial concentration. The bonds in methane are therefore particularly strong.

The localized MO formed by the end-on overlap of an s orbital and an sp^3 hybrid orbital, as referred to above, is known as a σ orbital or, more loosely, when occupied by the two permitted electrons, a σ bond. In the σ bond, therefore, the charge distribution is symmetrical about the internuclear axis. Fig. 6.19 shows the localized MO configuration of methane.
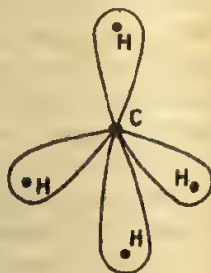
Fig. 6.19 Tetrahedral configuration of CH_4. The four lobes are localized MOs.

The VB description of the methane molecule in terms of electron pairing also pictures the carbon atom as hybridized tetrahedrally so that four C—H bonds of σ type are formed by pairing these sp^3 electrons of carbon with the $1s$ electrons of hydrogen.

Ethane (C_2H_6). It can be described in much the same way as methane. Each carbon atom uses four sp^3 hybrid orbitals—three for overlapping with the s orbitals of three hydrogen atoms and the fourth one for
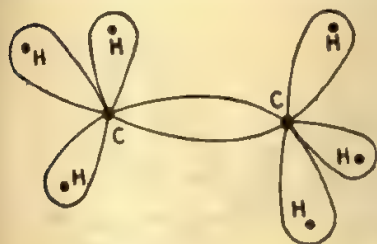
Fig. 6.20 Localized MOs (bonds) in ethane

overlapping with its counterpart of the second carbon atom. This leads to four localized σ MOs as shown in Fig. 6.20. Since rotation about the axis of a single σ MO does not affect the overlap of the orbitals concerned, free rotation about the central bond in ethane would appear to be possible. Actually, however, the rotation in ethane is not completely free, since it is hindered somewhat by the repulsion of the electrons in the σ MOs. In fact, because of this repulsion the staggered configuration of Fig. 6.20 is preferred.

In VB terms, the ethane molecule can be described as follows. The carbon atom is hybridized tetrahedrally and two of the sp^3 electrons, one from each carbon atom, are paired to form a single bond between the carbons. The remaining six sp^3 electrons of the carbon atoms pair with the $1s$ electrons of hydrogen atoms to form σ-type carbon–hydrogen bonds, as in methane. This gives the H-C-H bond angles in accord with the observed value of 109.3°.

Cyclopropane (C_3H_6). In the cyclopropane molecule the carbon interbond angles are 60°. For maximum overlap in the carbon–carbon bond formation in cyclopropane, two orbitals of each carbon atom should be directed towards the other two carbon atoms, necessitating that one of the angles between orbitals for each carbon be 60°. Quantum mechanics, however, stipulates that, when a carbon atom forms four single bonds, interbond angles approaching 109° are favoured. Even if the angle between the orbitals is 109°, substantial overlap may still occur, but it has been calculated that an inter-orbital angle of 104° represents the best compromise from energy considerations. In any case, since bonds to attached atoms are generally assumed to correspond to the lines of maximum electron density or maximum overlap, it follows that the bonds between carbons in cyclopropane are 'bent', somewhat like bananas, so that three regions of maximum charge density lie outside the triangle of carbon nuclei (Fig. 6.21). The carbon–carbon distance (i.e. the conventional bond length) in cyclopropane should therefore be less than that for, say, ethane. The measured values for the two cases are 1.51 Å and 1.54 Å, respectively.

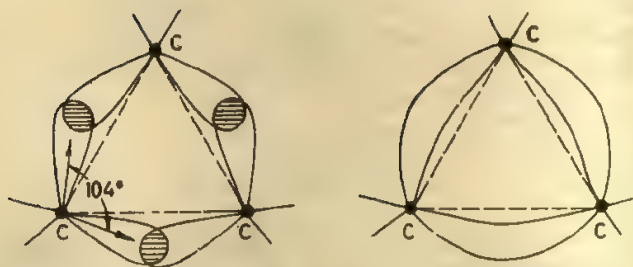*Ethylene* (C_2H_4). In the ethylene molecule, the H-C-H bond angles

Fig. 6.21 The formation of 'banana' bonds in cyclopropane

angles are close to 120°. So the MOs are evidently formed by using sp^2 hybrid orbitals. The s orbital and two p orbitals of each carbon atom in ethylene hybridize to form three coplanar sp^2 hybrid orbitals, two of which form localized (i.e. bicentric) MOs of σ type by overlapping with $1s$ orbital of hydrogen, while the third overlaps with its counterpart of the second carbon atom to form another localized σ MO. These MOs, each being occupied by two electrons of opposite spin, are also loosely called σ bonds. All the σ bonds in ethylene obviously lie in a plane [see Fig. 6.22(a)] and the molecule is thus coplanar. Each carbon atom is now left with a singly-occupied p orbital having its axis perpendicular to the plane of the atoms. The lateral overlap of these two p orbitals gives rise to a localized MO (bond) between the two carbon atoms [see Fig. 6.22(b)]. The π bond, occupied by two electrons, makes the second component of the carbon—carbon double bond. Since the π bond is formed by the lateral overlap of the p orbitals, it is weaker than the σ bond formed by end-on overlap of sp^2 hybrid orbitals. The configuration of ethylene in terms of σ and π MOs, called the σ-π configuration, is shown in Fig. 6.22(c). The σ electrons, i.e. the electrons occupying the σ bond, dominate the interior situation while the π electrons of the π bond do the exterior. The π electrons are therefore not held so firmly by the positive fields of the carbon nuclei as the electrons of the σ bond. Consequently, the π electrons are more mobile, more easily detached, and more easily brought into chemical reaction.

The description given above of carbon–carbon double bond also accounts for the absence of free rotation about this bond as follows. Since the π bond is formed by lateral overlap of p orbitals it is appreciably strong when the axes of the p orbitals are parallel, the strength being clearly related to the extent of parallelism. Such parallelism, however, would be destroyed if the molecule were twisted about the carbon–carbon axis. In other words, such twisting requires breaking the π bond and, therefore, cannot take place easily.

A further consequence of the formation of a π bond by lateral overlap of the p orbitals is the shortening of carbon–carbon internuclear distance. Thus it is 1.34 Å in ethylene in contrast to 1.54 Å in ethane.

Fig. 6.22 Molecular orbital formation in ethylene. (a) Localized σ MOs (bonds) in *xy*-plane. (b) Localized π MO (bond) in *xz*-plane; σ bonds (in *xy*-plane) are shown as lines. (c) σ-π configuration; there is a hydrogen nucleus (proton) embedded in each of the four σ orbitals protruding from the carbon nuclei.

VB description. According to the VB description of ethylene in terms of electron pairing, the carbon atoms are hybridized trigonally and two of the sp^2 electrons (one from each carbon) are paired to form a single bond between the carbons, while the remaining four sp^2 electrons (two from each carbon) pair with H(1s) electrons to form four C—H bonds. Each carbon is now left with a p_z electron. The pairing of these p_z electrons gives rise to the second component of the carbon–carbon double bond.

Acetylene. In line with the above theory of the double bond in ethylene, the formation of triple bond in acetylene requires that the *s* orbital and one *p* orbital of each carbon atom will hybridize to form two linear hybrid orbitals, one of which forms a σ bond with a hydrogen atom by overlapping with its 1s orbital, while the other overlaps with its counterpart of the other carbon atom forming a carbon–carbon σ bond [see Fig. 6.23(a)]. All the atoms are, therefore, along a straight line. Each carbon atom is now left with two unchanged *p* orbitals whose axes are perpendicular to each other and to the internuclear line. Two π bonds are formed by the lateral overlap of these *p* orbitals [Fig. 6.23(b)]. So the
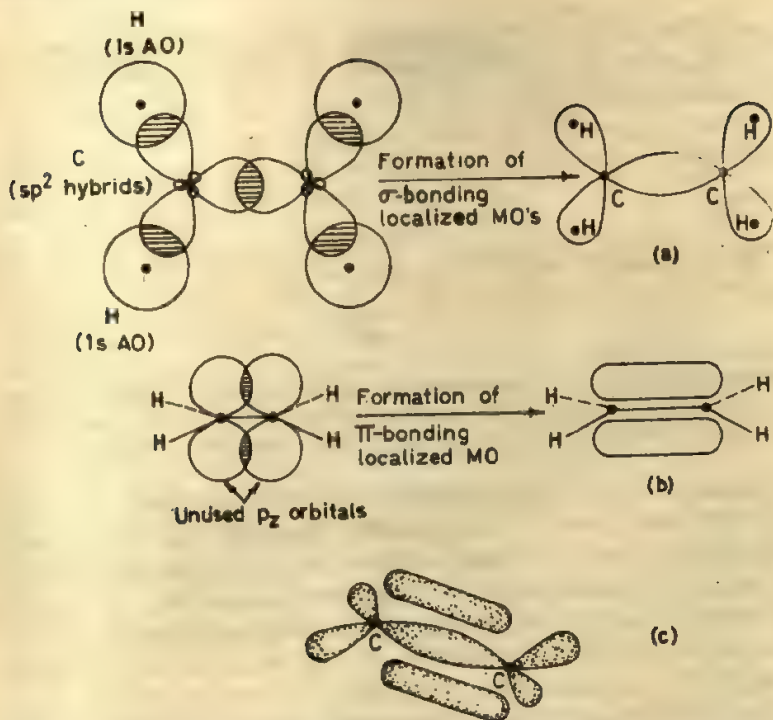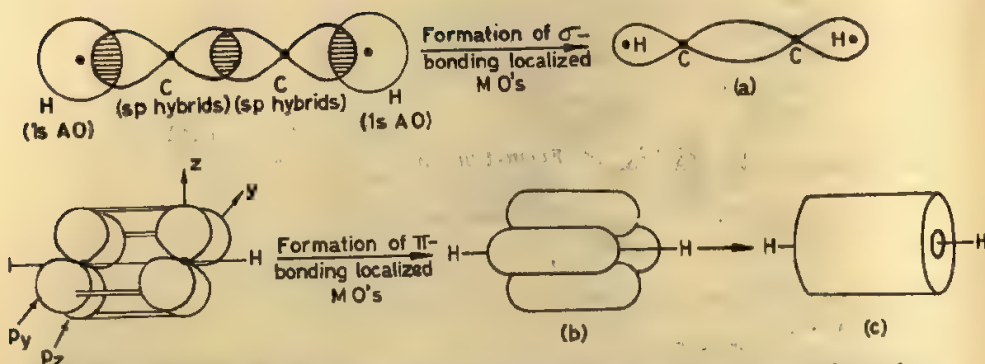
Fig. 6.23 Molecular orbital formation in acetylene. (a) Localized σ MOs (bonds) in xy-plane. (b) Localized π MOs (bonds) formed by the overlap (indicated by horizontal double lines) of p_y and p_z orbitals. (c) Charge cloud of two π bonds (σ C-H bonds shown as lines).

triple bond is made of one σ bond and two π bonds, each being occupied by two electrons with paired (i.e. oppositely directed) spin. Moreover, since two equally occupied π orbitals produce a total electron distribution which is circularly symmetrical about the internuclear line, it follows that the electronic charge cloud of the π bonds in acetylene is of the form of cylindrical sheath about the C—C axis with the axial interior relatively empty of π electrons [Fig. 6.23(c)].

As with the double bond it is the externally located electrons of the triple bond that are relatively more easily removed or disturbed and brought into chemical reaction. However, in contrast to the double bond, the π component of which might be uncoupled by torsion, the cylindrical π sheath of a triple bond is not disrupted by torsion. This situation is amply reflected in the great thermal stability of some triple-bonded compounds.

The presence of two π bonds in the carbon–carbon triple bond, in contrast to one in the double bond, leads to further shortening of the internuclear distance. Thus it is 1.20 Å in comparison to 1.34 Å in ethylene.

One interesting trend, observed along the series methane, ethylene and acetylene, is the increasing polarity of C—H bonds — the hydrogen becoming positive — which is climaxed by the ability of acetylene to form metallic compounds. This behaviour has been related to the increase in the proportions (1/4, 1/3, and 1/2) of the s component in the hybrid orbitals of carbon along the above series. Being lower on the energy scale, an s orbital keeps the electrons closer to the nucleus than does the corresponding p orbital; similar contrast is also displayed by s- and p-components of a hybrid orbital, the former showing greater tendency to keep the electrons closer to the carbon nucleus.

VB description. As in the MO treatment, so also in the VB description, we picture the carbon atoms as diagonally hybridized in C_2H_2. Two sp

electrons (one from each carbon atom) are paired to form a single bond between the carbon atoms and the remaining two sp electrons pair with H(1s) electrons to form two C—H bonds. Each carbon is now left with one p_y electron and one p_z electron. The pairing of the two p_y electrons and that of the two p_z electrons form the second and third components of the carbon–carbon triple bond.

Butadiene (C_4H_6). The most widely known conjugated diene is butadiene-1, 3, often referred to simply as butadiene. In calssical valency terms it can be written as $CH_2 = CH—CH = CH_2$.

MO description. The butadiene molecule is coplanar and the C-Ĉ-C bond angles are close to 120°. We can therefore assume that each carbon atom uses three sp^2 hybrid orbitals as in ethylene. The four carbon atoms are bonded to each other by the overlap of these hybrid orbitals and to the hydrogen atoms by overlap with their 1s orbitals. This gives the completely coplanar skeletal arrangement of four carbon and six hydrogen nuclei, as shown in Fig. 6.24. Each carbon atom is now left with a singly-occupied p orbital which is perpendicular to the plane of the nuclei. The remaining carbon–carbon bonds are to be formed by the overlapping of these unhybridized p orbitals. A point of particular interest which now arises is that the p orbital of, for example, the second carbon atom can overlap with that of the first carbon atom or with that of the third carbon atom. In other words, p orbital overlap is possible over all four carbon nuclei of the conjugated system. Conjugation of double bonds thus, turns out to be the formation of polycentric or delocalized MO. In butadiene, the four p orbitals overlap to form a delocalized π MO. extending over all four carbon nuclei of the system. It is in two segments,
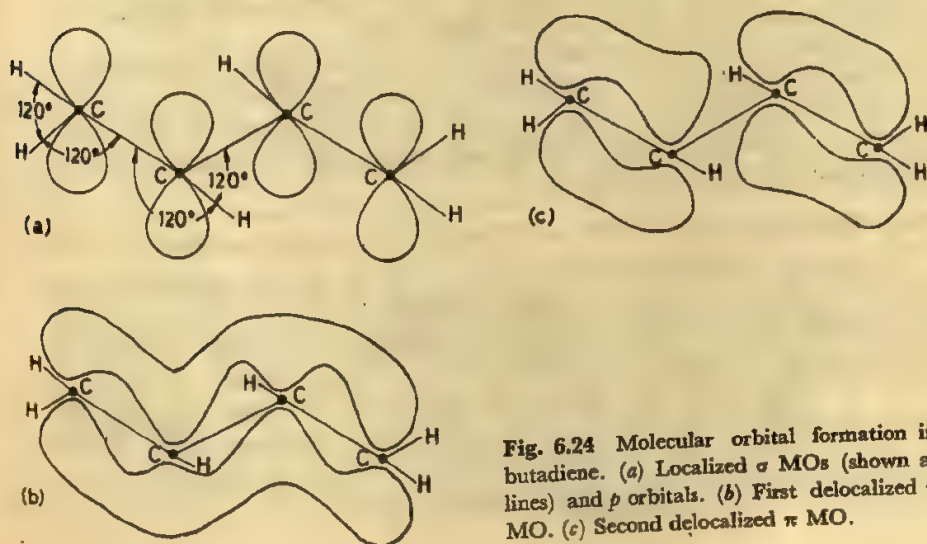

Fig. 6.24 Molecular orbital formation in butadiene. (*a*) Localized σ MOs (shown as lines) and p orbitals. (*b*) First delocalized π MO. (*c*) Second delocalized π MO.

one above and one below the plane of molecule [Fig. 6.24(*b*)]. This π MO has a single nodal plane (coinciding with the plane of the molecule) and is of lowest energy. Now since any one MO can accommodate up to two electrons whereas the diene system has four p electrons in the overlapped orbital, a further π orbital is required to take the remaining two electrons. This second π MO is also formed from overlapping of the p orbitals and is delocalized, encompassing all four carbon nuclei. It has two nodal planes, one perpendicular to the plane of the molecule and another coinciding with the plane of the molecule. There are thus four segments, two above and two below the plane of the molecule [Fig. 6.24(*c*)]. The energy of this MO is slightly higher than that of the first. However, the total energy of the electrons in these two delocalized orbitals is less than the total energy that would be if they were located in the localized (bicentric) MOs of two isolated double bonds. The difference in energy is the delocalization energy, often called the resonance energy, and is a measure of the additional stabilization of the molecule caused by electron delocalization. In the case of butadiene this amounts to about 7 kcal/mole.

We thus see that the source of resonance energy is the same as that of any other type of bonding energy. As the energy of a single or double bond arises from the ability of an electron to encompass two positive nuclei in a molecule in place of one in an atom, so also resonance stabilization is merely a manifestation of the ability of an electron to encompass more than two nuclei instead of two.

Since the four π electrons, in terms of the MO picture given above, are not localized in particular bonds, but are free to move in the region encompassing all four carbon nuclei of the conjugated system, we can draw the inference that the central single bond has some share of the π electrons, and hence has some double bond character. For example, its length is shorter than that of a pure single bond.

VB description.   In terms of the VB theory the structure of the butadiene molecule is regarded as a combination of contributions from three different primary or canonical structures each of which is a structural formula, written in classical valency terms and expressing a possible electron distribution for the molecule as:

$$CH_2{=}CH{-}CH{=}CH_2 \longleftrightarrow \bar{C}H_2{-}CH{=}CH{-}\overset{+}{C}H_2 \longleftrightarrow \overset{+}{C}H_2{-}CH{=}CH{-}\bar{C}H_2$$
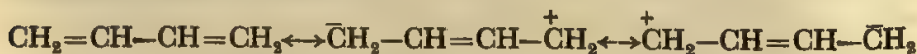
The use of a double-headed arrow ($\longleftrightarrow$) as the link symbol implies that each structural form contributes to the true structure of the molecule. All however do not make equal contributions. Uncharged forms, in general, make a greater contribution than charged forms. It must be borne in mind that the canonical structures are only hypothetical structures and the true structure lies somewhere between them. Colloquially, we may say that there is resonance between the canonical structures and the true structure is a resonance hybrid.

The inclusion of the second and third canonical structures leads to the same general conclusion concerning the central bond, i.e. it is not a pure single bond, but has some double-bond character. These structures also show clearly that polarization affects positions 1 and 4, which explains the observation that addition reactions occur at positions 1 and 4 to the system as a whole.

Benzene (C_6H_6). It is found by experiment that the six carbon atoms in benzene are coplanar and arranged as a regular hexagon. Also, all six carbon-carbon bonds in the ring are equivalent, having the same length 1.39 Å. The carbon-carbon bond in benzene is thus intermediate in length between a carbon–carbon single bond (1.54 Å) and a carbon–carbon double bond (1.34 Å).

MO description. In view of the general shape of the benzene molecule stated above, the MOs are evidently formed from hybrid carbon atomic orbitals of the sp^2 type. The overlap of two sp^2 hybrid orbitals of each carbon atom leads to a regular hexagon of six carbon nuclei held in a plane by localized σ MOs (bonds). Each of the remaining six sp^2 hybrid orbitals then overlaps with a hydrogen $1s$ orbital forming a localized σ MO. We thus get a planar system of carbon and hydrogen nuclei as shown in Fig. 6.25(*a*).

Each carbon is now left with a singly-occupied p orbital oriented at right angles to the plane of the ring as illustrated in Fig. 6.25(*b*). Since any p orbital can overlap both p orbitals on either side of it equally well, all six orbitals overlap right round the ring to form delocalized π MOs. And since six atomic orbitals are involved in the process, six MOs of this type are possible, each of which is capable of holding two electrons. The energies of the orbitals may be calculated and the complete set of MO energy levels constructed, as shown schematically in Fig. 6.26. In the ground state of the molecule the six electrons will occupy the three π MOs of lowest energy. These are the bonding orbitals and the remaining three of higher energy are the antibonding orbitals. The shapes of the bonding orbitals are illustrated in the three parts of Fig. 6.25. They all encompass all six nuclei. The first π MO, it can be seen, has only one nodal plane and it coincides with the plane of the molecule. This is the most stable orbital having the lowest energy, because it has no nodal plane perpendicular to the plane of the molecule — a condition that gives the longest possible electron wavelength and hence the lowest electronic energy. The two next most stable molecular orbitals, namely, the second and the third MOs are degenerate, having equal energies, and each has a nodal plane perpendicular to the plane of the ring in addition to that coinciding with the molecular plane.

Referring to the pattern of the delocalized π MO energy levels, as shown in Fig. 6.26, it is easy to understand, why a sextet of electrons as in benzene is so stable. The set of six π electrons, called the aromatic
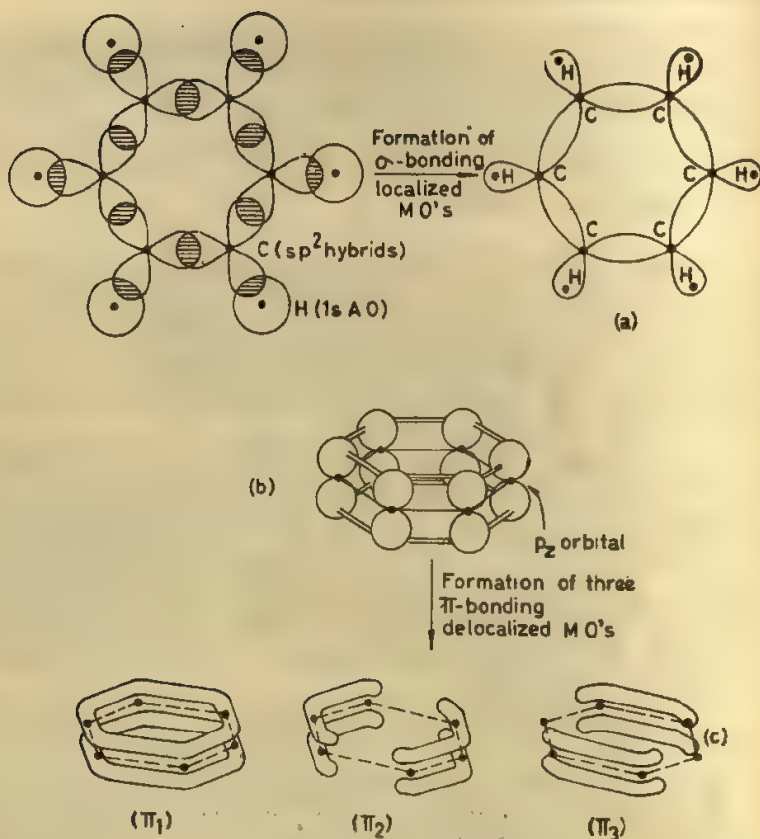
Fig. 6.25 Molecular orbital formation in benzene. (a) Localized σ MOs (bonds) in xy-plane. (b) All six p_z orbitals overlap each other (indicated by horizontal double lines) to form delocalized π MOs. (c) First, second and third bonding delocalized π MOs
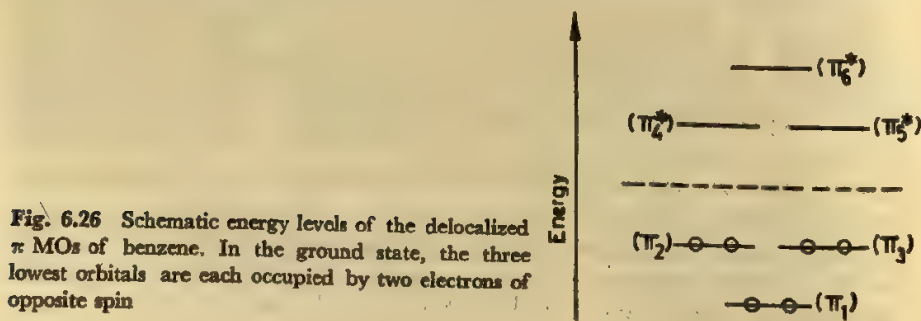
Fig. 6.26 Schematic energy levels of the delocalized π MOs of benzene. In the ground state, the three lowest orbitals are each occupied by two electrons of opposite spin

sextet, completely fills the three lowest MOs and this gives the benzene ring high stability and high resistance to disruption by chemical attack. If the MOs were occupied by five π electrons instead of six, there would

be an electron vacancy that would give the molecule an electron-attracting power and thus make it chemically reactive. If, on the other hand, the molecule had seven π electrons, one would have to occupy a higher energy orbital and so would be prone to be lost, again rendering the molecule chemically reactive.

We may now consider some of the important consequences of π electron delocalization in benzene. Since the six π-electrons are free to move anywhere in the π MOs encompassing all six carbon nuclei, which means that all π electrons are active in the binding of each carbon–carbon pair, we can draw the conclusion that all six bonds must be mutually equivalent, and furthermore, they must be shorter than a pure single bond. These conclusions are in accord with experiment. Sharing out the π electrons over the whole system, moreover, decreases the likelihood of the system undergoing addition reactions. In other words, the stability is increased by delocalization.

The heat of combustion for benzene may be calculated assuming that it is a cyclic triolefin of six carbon atoms held together by alternating double and single bonds. Such a calculated value, however, exceeds the measured heat of combustion by 36 kcal/mole showing that benzene is more stable by this quantity than would be expected if its bonds were pure single and pure double bonds. This lowering of energy, i.e. increased stability, is the result of the greater freedom allowed to the electrons in delocalized MOs relative to simple localized MOs between alternate pairs, and is termed *delocalization energy* or *resonance energy*. Representative values of the delocalization energy for benzene and some other benzenoid aromatics are shown in Table 6.3. It is seen that in these

Table 6.3   Resonance Energies of Benzenoid
           Aromatics (kcal/mole)

Molecule	*Resonance energy*	*Resonance energy per electron*
Benzene	36	6·0
Naphthalene	61	6·1
Anthracene	86	6·1
Phenanthrene	99	7·1
Diphenyl	74	6·2
Dibenzyl	70	5·8

simple aromatic hydrocarbons each π electron contributes about 6 kcal per mole to the resonance energy.

The resonance stabilization may be taken as a physical criterion of aromatic character. Besides benzenoid molecules, there are also non-benzenoid molecules which give indications of resonance stabilization. For example, azulene and diphenylene (Fig. 6.27) are not aromatic compounds in the proper sense, but in view of their significant resonance
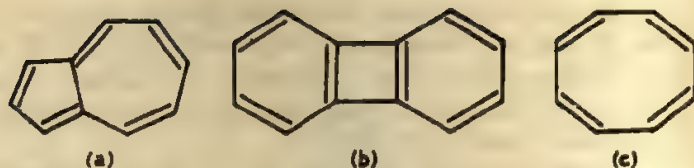
Fig. 6.27 Structures of (a) azulene, (b) diphenylene, and (c) cyclo-octatetraene

energies, namely, 31 kcal/mole and 20 kcal/mole respectively, they can be said to have aromatic character according to this physical criterion. By the same token, cyclo-octatetraene (Fig. 6.27) with a resonance energy of only 4 kcal/mole, has no aromatic type stabilization.

Since the π electrons are free to move anywhere in the delocalized MO, the benzene ring is like a little loop of wire containing mobile electrons. Applying a magnetic field normal to the planes of the rings in solid benzene these electrons can be induced to circulate about it and they then make a disproportionately large contribution to the diamagnetism of the system; moreover, this contribution is confined to the direction perpendicular to the plane of circulation, i.e. the molecular plane. The mean diamagnetism and its anisotropy, both of which are measurable quantities, can therefore be used to assess the aromatic character.

The π-electron circulation induced by a magnetic field has another consequence that can be exploited in determining the aromatic character. If an external magnetic field is applied normal to the plane of the molecule in solid benzene, the induced circulation of the π electrons produces a magnetic field (Fig. 6.28), which, measured at points within the hexagon, is opposed to the external field, but at the positions of the hydrogen atoms outside the hexagon it contributes to the field, making the total field greater than the applied field alone. An increment to the field of this kind can be detected by measuring the proton magnetic resonance which is a sensitive measure of the total field. Consequently,

Fig. 6.28 Schematic diagram of the aromatic ring current contribution to the magnetic field at the positions of the hydrogen atoms (P) of benzene. H is the external magnetic field and the curved lines are the lines of force of the magnetic field due to the induced circulation of π electrons.

proton magnetic resonance measurements have proved to be useful in identifying molecules with aromatic ring current.

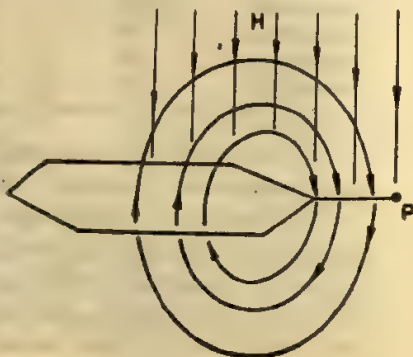We thus see that the origin of certain characteristic physical properties of aromatic molecules is in the delocalization of the aromatic π electrons. This consideration has been one of the main factors in the generalization of the term 'aromatic character' and extending it to molecules even beyond those of strictly aromatic class. Thus molecules like azulene, diphenylene, pyridine, borazole, etc., which are not aromatic in the strict sense, can, however, be said to have aromatic character in so far as they possess the physical properties of delocalized electrons.

VB description. In view of the regular hexagonal configuration of benzene, it is assumed that all six carbon atoms are trigonally hybridized and twelve sp^2 electrons (two from each carbon) are paired to form six single bonds giving a regular hexagonal skeleton of six carbon atoms in a plane. The remaining six sp^2 electrons (one from each carbon) pair with H(1s) electrons to form six C—H bonds in the plane of the hexagon. The problem now is in describing the participation of the six carbon p_z electrons in the bonding. For example, we may couple the alternate pairs of the p_z electrons to fashion either of the Kekule structures I and II, as shown in Fig. 6.29, equally well so that the resulting structure must be a superposition of the two. We might therefore say that the actual structure of benzene is formed by *resonance* between the two hypothetical Kekule structures. The Kekule structures are, however, the principal but not the only contributors to the actual benzene structure; smaller contributions are also made by the three Dewar structures, shown as III, IV and V in Fig. 6.29. These five are the more important canonical structures of benzene.

In VB terms, benzene can be said to be a resonance hybrid of the hypothetical canonical structures and the true wave function describing the molecular structure can be obtained by a linear combination of the wave functions for the various canonical structures (cf. Eq. 6.2). As before, the problem is to determine the values of the coefficients in such a way as to make the energy of the system a minimum. The relative contributions of the different structures to the true structure of the molecule are then given by the relative magnitudes of the squares of the coefficients of the corresponding wave functions. Such calculations show that each Kekule structure contributes just under 40 per cent and each Dewar structure about seven per cent to the true structure. It must be
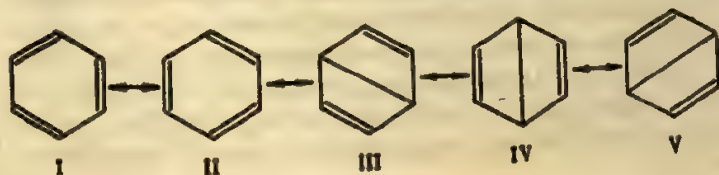

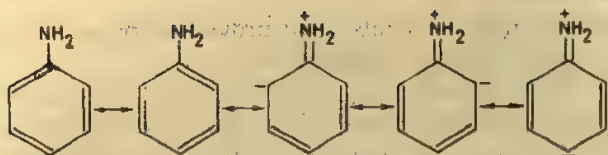Fig. 6.29 Canonical structures of benzene

Fig. 6.30 Canonical structures of aniline.

clearly understood that the aforesaid resonance description does not mean that some molecules have one structure and some another or that the benzene molecule remains, for example, in the Kekule structure I for about 40 per cent of the time, but that the true structure lies somewhere between the resonance structures and can only be described as a sort of weighted average of them. The inference from this resonance picture is that all the carbon—carbon bonds are equivalent and somewhere between single bond and double bond in character.

In substituted benzene compounds, contributions from ionic structures must be included. In the case of aniline, for example, the more important canonical structures are as shown in Fig. 6.30. The inclusion of the ionic structures results in an additional energy of 7 kcal, compared to benzene, and moreover leads to a prediction of a net negative charge at the *ortho* and *para* positions of the molecule. This accounts for the fact that the NH_2 group in aniline directs electrophilic (i.e. electron-seeking) approaching substituents (e.g. NO_2^+, Br^+) to these positions.

6.11 Bonding in Coordination Compounds

Coordination compounds of transition metal ions constitute the largest class of compounds in which *d* orbitals are involved. Such compounds consist of a central transition metal ion surrounded by electron-rich coordinating groups. Coordinating groups in complexes are referred to as *ligands*. Ligands are usually negatively charged atoms or groups of atoms, such as, halogen ions, OH^-, CN^-, NO_2^-, etc. Sometimes ligands may even be neutral molecules, e.g. NH_3 and H_2O; these are however, polar and the negative end of the dipole is directed towards the metal ion.

Three different methods of treating the bonding in coordination compounds have been developed, marking three stages in the development of a description of such compounds. The earliest of these, the *valence-bond* approach developed by Pauling (1931), considers bond formation in various ways by overlapping of atomic orbitals, particularly hybridized orbitals, making use of resonance structures when appropriate. The valence-bond approach has an intuitive appeal and in some respects it is the most satisfying method. Its principal drawback, however, is that the theory is qualitative. In order to obtain quantitative results it is sometimes necessary to consider participation of a very large number of resonance structures.

Crystal-field theory (Bethe, 1929, and Van Vleck, 1932) was originally developed to describe the effect, on a metal ion in a crystal, of the electric field due to the presence and arrangement of neighbouring ions in the crystal. Essentially the same theory has been applied to coordination compounds with surprising success. Despite the fact that covalent bonding is completely neglected in this approach, the theory provides a reasonably good interpretation of the stereo-chemical, magnetic and optical absorption properties of complexes.

A third approach treats the bonding in coordination compounds from the molecular orbital point of view adopting the method used previously for covalent bonding (Section 6.4). In practice, however, the MO approach alone has not been completely successful and developments in the field have led to a blend of the crystal field and MO theories, known as *ligand field theory*.

Valence-bond theory In the valence-bond approach as applied to coordination compounds we determine how the d-orbitals of a transition metal atom can be hybridized with other orbitals (Section 6.8) of the same atom to provide new orbitals according to the symmetry of the compound under consideration. These new orbitals are then considered to overlap those of ligand orbitals, each occupied by a pair of electrons.

When a transition-metal atom is surrounded octahedrally by six ligands, their directions of approach coincide precisely with the directions along which the d_z and $d_{x^2-y^2}$ orbitals are concentrated (cf. Figs. 5.4 and 6.13), while the other three, d_{xy}, d_{xz} and d_{yz} lie in the regions between the ligands. The d_{z^2} and $d_{x^2-y^2}$ are therefore suitable for formation of hybrid AO's. In applying the valence-bond theory, it is assumed that the $(n-1)d$ AO's (where n is the principal quantum number of the valence electrons of the metal atom) and ns and np AO's are sufficiently close in energy to be hybridized. Thus if the six orbitals ns, $np_x, np_y, np_z, (n-1)d_z^2$ and $(n-1)d_{x^2-y^2}$ are hybridized, six new $d^2.sp^3$ hybrid orbitals (see p. 137) are formed, pointing towards the six corners of an octahedron (Fig. 6.13). These hybrid orbitals are used in bonding with ligands, each of which contributes a pair of electrons shared with the metal atom in coordinate bonds. The disposition of the d electrons of the metal atom depend on the particular compound. Figure 6.18, for example, shows the valence-bond diagrams for complexes of Fe^{+2}, Fe^{+3} and Cr^{+3}, having six, five and three d electrons, respectively. The electron configurations on the left are for the free ions, while those on the right include twelve electrons from six ligands or coordinating groups. Hund's rule applies to the nonbonding electrons; hence they occupy separate orbitals with their spins parallel. These unpaired electrons contribute to the magnetic moment of a complex ion. We shall consider this topic in Section 6.12.

Some of the transition metals adopt a lower coordination number of four in their complexes, for which two configurations, tetrahedral and square planar, are found. While the tetrahedral structure can be considered to arise from bonding with four sp^3 hybrid orbitals formed by combination of ns, np_x np_y and np_z AO's, the square planar structure can be accounted for with four dsp^2 hybrid orbitals using the set $(n-1)dx^2-y^2$, ns, np_x and np_y (see Fig. 6.31)
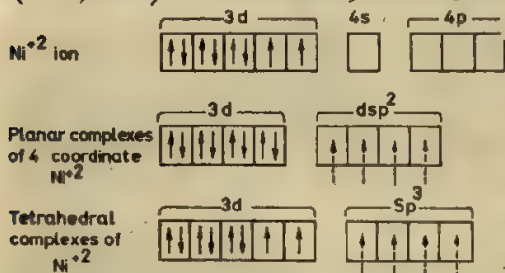
Fig. 6.31 The formation of planar and tetrahedral complexes of 4-coordinate Ni^{+2}. (Each dashed arrow denotes an electron pair supplied by a ligand.)

Crystal-field theory. The crystal-field theory deals with the origins and consequences of the splitting of the inner orbitals, especially of the d orbitals, of ions by their surroundings in chemical compounds. The theory considers that the transition metal atom, constituting the central atom in a molecule or ion, is a positive ion and it is surrounded by a number of ions or molecules referred to as ligands. The bonding between the central atom and the surrounding ligands is assumed to be completely electrostatic even if it happens to be appreciably covalent. The theory considers the effect of ligand fields (i.e. electrostatic fields due to ligands) on the d orbitals of the central metal atom.

In order to discuss this effect, it is necessary to recall the directional feature of the latter. It is seen from Fig. 5.4 that in the $d_{x^2-y^2}$ orbital, the lobes lie along x- and y-axes, and in dz^2 orbital they lie on the z-axis, whereas in the other three d orbitals (d_{xy}, d_{xz}, d_{yz}) the lobes lie between the axial directions. Hence the orbitals can be divided into two sets: the first set comprises the $d_{x^2-y^2}$ and d_{z^2} orbitals (both referred to as the $d\gamma$ orbitals) whose angular probability distributions are concentrated along the axial directions, whereas the second set comprises the d_{xy}, d_{xz} and d_{yz} orbitals (collectively referred to as the $d\varepsilon$ orbitals) whose angular probability distributions are at maximum at 45° to the axial directions and are zero along the three axial directions.

When negatively charged ligands approach the central atom, the electrons of the central atom are subjected to repulsive forces, which are obviously strongest in the approach directions of the ligands; that is to say, the energy of the orbitals which point in these directions is consequently increased. So the d electrons will tend to occupy those

orbitals which are farthest away from the approach directions of the ligands. Since the most common approach directions, or rather the arrangement of ligands around a central atom, are octahedral and tetrahedral, only the effects of ligands of these symmetries will be discussed here.

Octahedral ligand field. When a transition metal ion is surrounded octahedrally by six ligands, their directions of approach coincide with the x-, y- and z- axes (Fig. 6.32) which are also precisely the directions
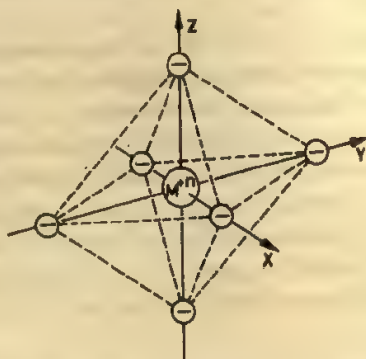
Fig. 6.32 Arrangement of ligand ions ⊖ around the central metal ion M^{+n} in an octahedral complex.

along which the $d\gamma$ orbitals, referred to above, are concentrated (Fig.6.33).
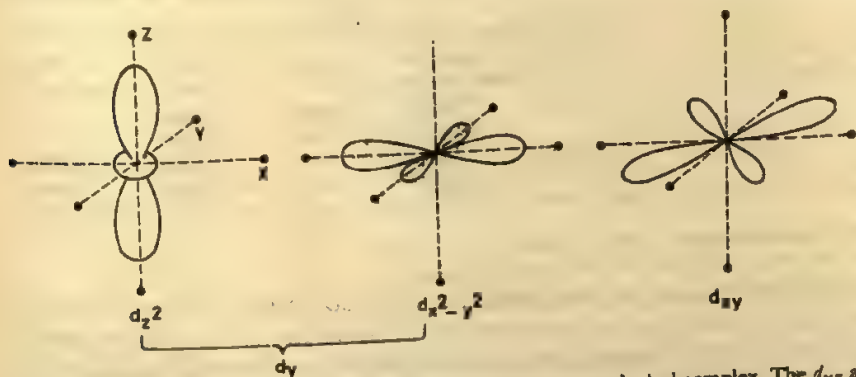
Fig. 6.33 Angular probability distributions of d orbitals in an octahedral complex. The d_{xz} and d_{yz} orbitals are similar to d_{xy} but lie in the planes xz and yz respectively.

Since the $d\gamma$ orbitals point in the direction of the ligands, these orbitals are raised in energy owing to the repulsion between the negative charge density in the d orbitals and that in the ligands. On the other hand, the d_ε orbitals which point away from the ligands are lowered in energy. Thus the five d orbitals which have the same energy and are, therefore, degenerate in a free metal ion, are split in an octahedral ligand field into two sets, namely, a higher energy, doubly degenerate set of orbitals d_{z^2} and $d_{x^2-y^2}$ (designated as $d\gamma$ or e_g orbitals), and a lower energy, triply degenerate set, d_{xy}, d_{xz} and d_{yz} (designated as d_ε or t_{2g} orbitals), as
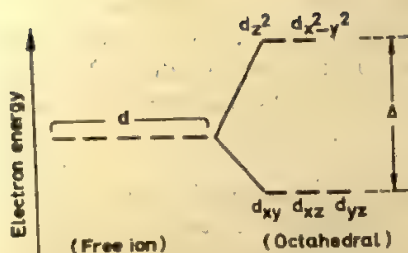
Fig. 6.34 Splitting of d orbitals in an octahedral ligand field.

shown in Fig. 6.34. So, in an octahedral ligand field the d_γ orbitals are destabilized with respect to the d_ε orbitals.

The energy difference, Δ, between the e_g or d_γ and t_{2g} or d_ε orbitals is the *crystal-field splitting*. Its magnitude depends on the particular ligands as well as on the central metal ion.

Usually, the crystal-field splitting, Δ, can be measured directly from the absorption spectrum of a complex and so is commonly quoted in units of frequency, cm^{-1}. The crystal-field splittings, Δ in cm^{-1}, observed for some metal complexes are as shown in Table 6.4.

Table 6.4 Crystal-field Splitting, Δ (in cm^{-1}) of some Metal Complexes

Metal ion	Ligand				
	Cl^-	H_2O	NH_3	en*	CN^-
Ni (II)	7,300	8,500	10,800	11,600	—
Cu(II)	—	12,600	15,100	16,400	—
Cr(III)	13,600	17,400	21,600	21,900	26,300
Co(III)	—	18,600	23,000	23,300	34,000

*en = ethylene diamine.

From such spectroscopic measurements of crystal-field splitting, various ligands can be arranged in a spectrochemical series, in the order given below, in which Δ increases, for any given metal ion, from left to right:
$I^- < Br^- < Cl^- < F^- < OH^- < C_2O_4^{-2} < H_2O < py$
$\approx NH_3 < en < dipy < phen < NO_2^- < CN^-$
The ligands which are near the beginning of the series, e.g. the halide ions, have weak electrostatic field associated with them, and the crystal-field splitting is therefore small. On the other hand, ligands such as NO_2^- and CN^-, which give rise to a strong field, and hence cause a large splitting, are in the latter part of the spectrochemical series. For different metal ions, the change from a weak field to a strong field does not occur at the same point in the spectro-chemical series of ligands. This is because, as reference to Table 6.4 will show, even the same ligand gives rise to different splittings for different metal ions.
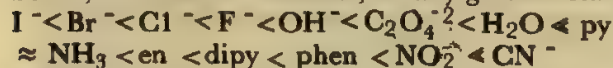
Chemical Bonding

It is customary to consider the effects of weak and strong field separately. A weak ligand field has no appreciable effect on the relative energies of the d_γ and d_ε orbitals, so that the d electrons fill the d orbitals in the normal way following Hund's rule; that means, no d orbital can receive two electrons until all the others have received one electron each. However, Hund's rule breaks down when there is a strong ligand field. Thus in the presence of an octahedral strong ligand field, the electrons in d_γ -orbitals are forced to occupy the lower-energy d_ε orbitals, and consequently, the d_ε orbitals may receive an electron pair even before d_γ orbitals have received one electron each. An example is cited below to illustrate the different effects of strong and weak ligand fields.

The electronic configuration of a neutral iron atom is represented by $4s^2 3d^6$ (omitting the inner electrons), and since the s electrons of a transition metal atom are ionized before any d electron, the configuration of a ferric ion is $4s^0 3d^5$ (see Fig.6.35), in which the five d electrons occupy
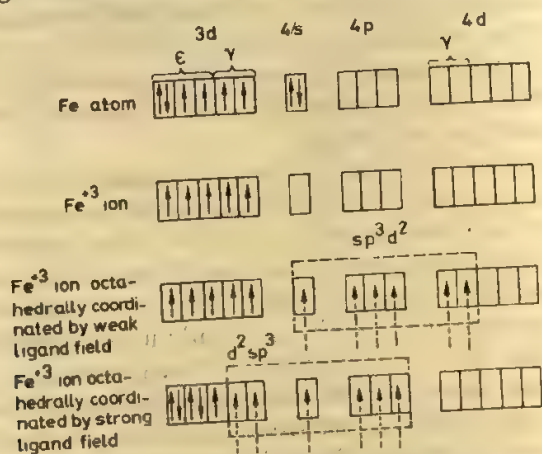
Fig. 6.35 Octahedral coordination of Fe$+3$ ion by weak and strong ligand fields. (Each dashed arrow denotes an electron pair supplied by a ligand.)

the five d orbitals singly, in accordance with Hund's rule. We can now consider the effect on these d electrons when six ligands approach the ferric ion octahedrally. If the approaching ligands exert a weak field, the relative energies of d_γ -and d_ε -orbitals are not appreciably altered, so that the free electrons remain in the same orbitals. If, however, the ligands exert a strong field, the d_γ -orbitals are destabilized with respect to the d_ε -orbitals, for reasons stated before, and so all the five electrons now occupy the d_ε -orbitals. In this case, only one electron remains unpaired. This may be compared with the number of unpaired electrons, namely five, when the ligand field is weak. The configuration in the weak field case is therefore referred to as *spin-free* and that in the case of strong field as *spin-paired*. The complexes

$[FeF_6]^{-3}$ and $[Fe(H_2O)_6]^{+3}$ represent the weak field case, while the complexes $[Fe(phen)_3]^{+3}$ and $[Fe(CN)_6]^{-3}$ represent the strong-field case.

Since in the case under consideration the arrangement of ligands is octahedral, sp^3d^2 hybrid orbitals would be expected to be used, and because of their directional properties, d_γ-orbitals would more probably be included rather than d_ε-orbitals. These are indicated in Fig. 6.35. Since in the weak-field case the $3d_\gamma$-orbitals are already occupied by electrons of the iron atom, the $4d$ orbitals are used for bond formation, and the hybridization is therefore referred to as sp^3d^2 or 'outer' hybrids. In the strong-field case, however, the $3d$-orbitals can be used for bond formation, because the $3d_\gamma$ orbitals are not occupied by electrons of the iron atom; the hybridization in this case is referred to as d^2sp^3 or 'inner' hybrids.

The octahedral arrangement of ligands around the central element is sometimes distorted; in order to understand the distortion, it becomes necessary to consider the electronic configuration of the central element. The arrangement of ligands is found to be regular if the electric field due to non-bonding d electrons is symmetrical. On the other hand, if this field is not symmetrical, the octahedral arrangement of the ligands is likely to be distorted.

The field due to the non-bonding electrons is perfectly symmetrical only if both the d_γ and d_ε sets are symmetrical. The condition for either of the two sets of d orbitals being symmetrical is that it should be completely unoccupied, completely full, or half full (i.e. each component orbital occupied singly). So the electronic configurations which are symmetrical are $d^0{}_\gamma$, $d^2{}_\gamma$ (only in the weak-field case), $d^4{}_\gamma$, and $d^0{}_\varepsilon$, $d^3{}_\varepsilon$ and $d^6{}_\varepsilon$. It should be noted that in the strong-field case $d^2{}_\gamma$ is unsymmetrical because of spin-pairing in the d_γ orbital.

In Table 6.5 are listed the different possible electronic configurations for the ion of a d block element when it is octahedrally surrounded by six ligands. The configurations differ depending on whether the ligands are associated with strong or weak field, because, as has been mentioned earlier, the former causes spin-pairing whereas the latter does not. It is evident from Table 6.5 that the d_ε orbitals of the metal atom are occupied before the d_γ orbitals (which is because d_ε orbitals are farther removed from the negatively charged ligands producing the repulsive force) both when the ligand field is weak and when it is strong. Hund's rule is obeyed in the weak field case so that the d orbitals (i.e. d_ε orbitals followed by d_γ orbitals) are at first singly-occupied by the filling electrons, after which the double filling occurs, first of the d_ε orbitals and then of the d_γ orbitals due to the same aforesaid reason. In the strong field case, however, Hund's rule is not obeyed, as is borne out by the fact that the d_ε orbitals are completely filled up (thus involving double filling) before the filling of d_γ orbitals can start; this is because the d_γ orbitals, lying as they do along the directions of approach of ligands, are subjected to strong repulsion forces due to the ligands.

Since the directions of the d_γ orbitals of the central atom correspond with the directions of the ligands disposed octahedrally around the atom, the octahedral arrangement of the ligands is likely to be more severely distorted by the dissymmetry of the d_γ orbitals than by that of the d_ε orbitals. Table 6.5 discloses that such a distortion originating from the dissymmetry of the d_γ orbitals is likely when the configurations are d^9-, d^7—spin-paired (i.e. $d^6_\varepsilon d^1_\gamma$) and d^4— spin-free (i.e. $d^3_\varepsilon d^1_\gamma$); and this expectation has been amply proved by a large number of observed cases.

Table 6.5 The Sequence of Filling of the d-orbitals of an Atom when at the Centre of an Octahedral Ligand Field

No. of d electrons	Weak ligand field (spin-free)		Strong ligand field (spin-paired)	
	Electronic config.	Type of dissymmetry	Electronic config.	Type of dissymmetry
1	$d^1_\varepsilon d^0_\gamma$	X	$d^1_\varepsilon d^0_\gamma$	X
2	$d^2_\varepsilon d^0_\gamma$	X	$d^2_\varepsilon d^0_\gamma$	X
3	$d^3_\varepsilon d^0_\gamma$	—	$d^3_\varepsilon d^0_\gamma$	—
4	$d^3_\varepsilon d^1_\gamma$	XX	$d^4_\varepsilon d^0_\gamma$	X
5	$d^3_\varepsilon d^2_\gamma$	—	$d^5_\varepsilon d^0_\gamma$	X
6	$d^4_\varepsilon d^2_\gamma$	X	$d^6_\varepsilon d^0_\gamma$	—
7	$d^5_\varepsilon d^2_\gamma$	X	$d^6_\varepsilon d^1_\gamma$	XX
8	$d^6_\varepsilon d^2_\gamma$	—	$d^6_\varepsilon d^2_\gamma$	XX
9	$d^6_\varepsilon d^3_\gamma$	XX	$d^6_\varepsilon d^3_\gamma$	XX
10	$d^6_\varepsilon d^4_\gamma$	—	$d^6_\varepsilon d^4_\gamma$	—

NOTE: Those electronic configurations which cause unsymmetrical force fields are indicated by X and XX: X when dissymmetry is due to the d_ε orbitals and XX when it is due to the d_γ orbitals.

Distortion of the octahedral arrangement of ligands is caused by a metal ion of electronic configuration d^4 when the ligands are associated with a weak field, e.g. halogen ions; but for d^7—configuration the distortion mentioned is produced when the ligands exert a strong electrostatic field, e.g. cyanids ions. However, irrespective of whether the ligands exert a strong or weak electrostatic field, the octahedral arrangement of ligands is always distorted by a metal ion having the configuration d^9.

Distortion arises mainly from the repulsion of ligands by electrons occupying d_γ orbitals. Considering, for example, the configuration $d^3_\varepsilon d^1_\gamma$, the single electron in the set of d_γ orbitals occupies the d_{z^2} orbital, and so when the ligands approach the central metal ion octahedrally

they can do so more closely along the directions of x-and y-axes (since there are no electrons in $d_{x^2-y^2}$ orbital) than along the z-axis; thus the ligands approaching along the direction of z-axis remain at a greater distance from the central metal ion than do the remaining four, and this amouts to a distortion of the regular octahedral arrangements of ligands poised at equal distances from the central metal ion. The distortion produced by d^7- and d^9-configurations can also be visualized in a similar way.

In both the weak and strong field cases, the configuration d^8 is given by $d^6_\varepsilon d^2\gamma$. Whereas in the former case there is no dissymmetry, in the latter case, however, on account of spin-pairing within the d_γ orbitals, both electrons occupy the d_{z^2} orbital, the $d_{x^2-y^2}$ orbital remaining unoccupied; consequently the repulsion of the ligands by the d_{z^2} orbital becomes great enough to render even a distorted octahedral arrangement impossible, or to express differently, the two ligands lying on the z –axis are repelled by the electrons in the d_{z^2} orbital to 'infinity' with the result that, in effect, a square planar arrangement with four ligands results. Experimental evidence for the square planar arrangement for the d^8 electronic configuration has been obtained for several compounds of Ni (II). It should be noted, however, that if the ligand field is weak the d^8 configuration can afford a regular octahedral arrangement.

Tetrahedral ligand field.   When four ligands approach the central metal ion tetrahedrally, the directions of their approach coincide exactly neither with the d_γ nor the d_ε set of orbitals. Nevertheless, these approach directions correspond more closely with the d_ε than with the d_γ set. This is evident from Fig. 6.36. The central metal ion is at the centre of the cube; the d_γ orbitals are concentrated along three directions which are perpendicular to each other and pass through the face-centres of the cube, while the d_ε orbitals are directed from the centre of the cube towards the midpoints of the cube edges [Fig. 6.36 (b) however, shows only the d_{xy} orbital]. A line drawn through a position (i.e. an alternate cube corner) of a ligand to the cube centre (occupied by the central metal ion) makes angles of $54°44$ and $35°16$ with the directions of a d_γ orbital and those of a d_ε orbital respectively. This makes the situation with tetrahedral ligands an inverse of that with octahedral ligands. Thus the tetrahedral ligand field causes splitting of the d orbitals of the central metal ion into an upper triplet of d_ε orbitals and a lower doublet of d_γ orbitals, as shown in Fig. 6.37, but the effect is much smaller than for the octahedral case. The effect of orbital splitting in the tetrahedral field is clearly reflected in the sequence of filling of the d orbitals, as listed in
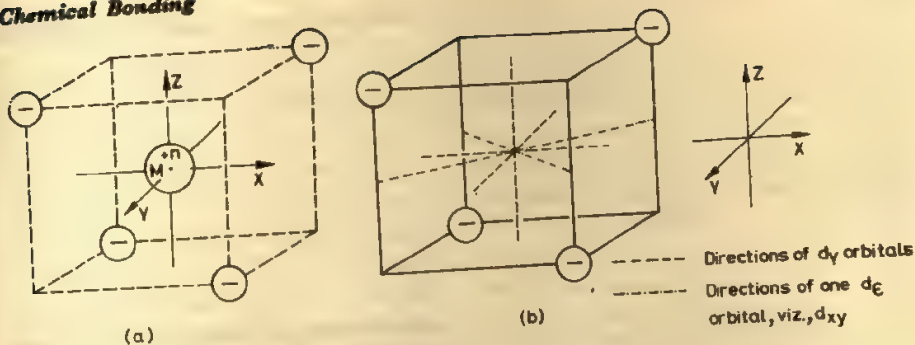
Fig. 6.36 (a) Arrangement of ligand ions $\ominus$ around the central metal ion M^{+n} in a tetrahedral complex. (b) The directions of d orbitals in a tetrahedral complex in relation to the arrangement of ligands.
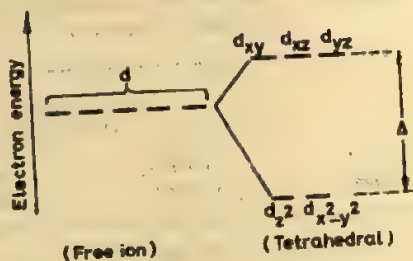
Fig. 6.37 Splitting of d orbitals in a tetrahedral ligand field.

Table 6.6. It follows, therefore, that the distortion of a regular tetrahedral arrangement is more likely to be produced by the d_ε orbitals rather than by the d_γ orbitals. Since, however, the tetrahedral coordination is apparently less stable or energetically less favourable than the octahedral configuration, not only the configurations marked XX (i.e. unsymmetrically occupied d_ε orbitals) but also those marked X (i.e. unsymmetrically occupied d_γ orbitals) generally fail to appear in tetrahedral coordination. Tetrahedral coordination is found for the compounds in which the central ion has one of the following configurations: d^0, d^1, d^2, d^5, d^7, or d^{10}. Of these, only the configuration of d^1 might be expected to produce distortion of the tetrahedral arrangement or it might even fail to exist, since it is associated with dissymmetry due to d_γ orbital.

Square planar ligand field. The splitting of the d orbitals in a square planar ligand field is shown schematically in Fig. 6.38. Since the $d_{x^2-y^2}$

Electron energy

d

$d_{x^2-y^2}$

d_{xy}

d_{z^2}

d_{xz} d_{yz}

(Free ion)   (Square planar)

Fig. 6.38 Splitting of d orbitals in a square planar ligand field.

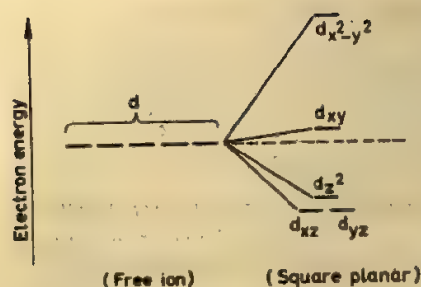orbital is concentrated just in the ligand directions, it is considerably increased in energy with strong field ligands. Considering, for instance,

Table 6.6   The Sequence of Filling of the d orbitals of an Atom when at the Centre of a Tetrahedral Ligand Field.

No. of d electrons	Weak ligand field (spin-free)		Strong ligand field (spin-paired)	
	Electronic config.	Type of dissymmetry	Electronic config.	Type of dissymmetry
1	$d^1 \gamma d^0{}_\varepsilon$	X	$d^1 \gamma d^0{}_\varepsilon$	X
2	$d^2 \gamma d{}_\varepsilon$	—	$d^2 \gamma d^0{}_\varepsilon$	—
3	$d^2 \gamma d^1{}_\varepsilon$	XX	$d^3 \gamma d^0{}_\varepsilon$	X
4	$d^2 \gamma d^2{}_\varepsilon$	XX	$d^4 \gamma d^0{}_\varepsilon$	—
5	$d^2 \gamma d^3{}_\varepsilon$	—	$d^4 \gamma d^1{}_\varepsilon$	XX
6	$d^3 \gamma d^3{}_\varepsilon$	X	$d^4 \gamma d^2{}_\varepsilon$	XX
7	$d^4 \gamma d^3{}_\varepsilon$	—	$d^4 \gamma d^3{}_\varepsilon$	—
8	$d^4 \gamma d^4{}_\varepsilon$	XX	$d^4 \gamma d^4{}_\varepsilon$	XX
9	$d^4 \gamma d^5{}_\varepsilon$	XX	$d^4 \gamma d^5{}_\varepsilon$	XX
10	$d^4 \gamma d^6{}_\varepsilon$	—	$d^4 \gamma d^6{}_\varepsilon$	—

NOTE: The configurations marked X and XX have dissymmetry due to unsymmetrical occupancy of the d_γ-and d_ε-orbitals respectively.

the complex ion $[Ni\,(CN_4)]^{-2}$ in which the central metal ion has the configuration d^8 and is surrounded by four strong field ligands, CN^-, in a square planar arrangement, the $d_{x^2-y^2}$ orbital remains unoccupied and all the eight d electrons are paired in the lowest four orbitals. It might be mentioned that earlier we visualized the square planar ligand arrangement as stemming from excessive distortion of the octahedral arrangement.

Ligand Field Theory In applying ligand-field theory we need to formulate delocalized MO's with a symmetry appropriate to the complex being treated. The choice of metal AO's suitable for use in achieving the desired symmetry is limited to $(n-1)$ d AO's (n is the principal quantum number of valence electrons) and the ns and np AO's Table 6.7 lists the appropriate metal orbitals to be used for a given symmetry and the type of ligand AO involved in bonding. The idea of covalency in complexes is arrived at by the fact that the MO's are always mixtures of both metal and ligand orbitals. Considering first an octahedral metal complex containing six ligands, let us assume that each ligand has available an AO of σ-symmetry which can be used in forming delocalized MO's. These σ AO's might be, for example, the p orbitals of halogens or the lone pair sp^3 hybrid of an ammonia molecule. Figure 6.39 shows schematical-
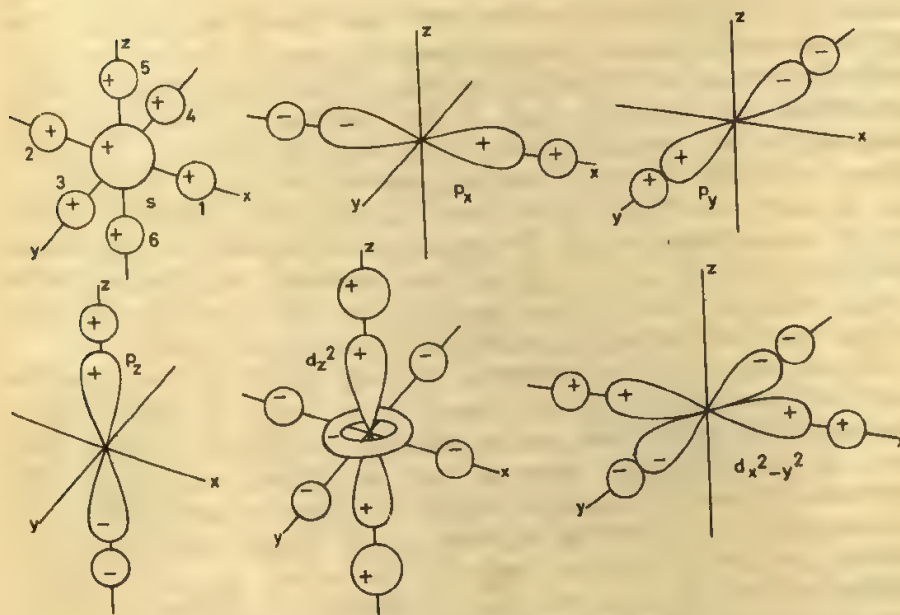

Fig. 6.39 Symmetry combinations of ligand σ orbitals and metal AO's used in forming MO's for an octahedral complex.

ly the symmetry combinations of the ligand σ AO's and the appropriate metal AO's used in forming MO's for an octahedral complex.

Table 6.7 Metal orbitals used in LCAO-MO Treatment of Complexes

Structure of Complex	With ligand σ orbitals	With ligand π orbitals
Square planar	$d_{x^2-y^2}, s, p_x, p_y$	p_x
	$d_{x^2-y^2}, d_{z^2}, p_x, p_y$	d_{xz}, d_{yz}
Tetrahedral	s, p_x, p_y, p_z	p_x, p_y, p_z
	$s, d\,xy, d\,xz, d\,yz$	All d orbitals
Octahedral	$s, p_x, p_y, p_z, d_{x^2-y^2},$	$p_x, p_y, p_z,$
	d_{z^2}	d_{xy}, d_{xz}, d_{yz}

Following the LCAO – MO method (Section 6.4) proper linear combinations of symmetry-adapted AO's are formed to yield MO's of the general form:

$$\psi_{MO} = C_M \psi_M + C_L \psi_L \tag{6.40}$$

where ψ_M and ψ_L are the proper metal and ligand AO's entering the MO under consideration. The coefficients C_M and C_L are subject to the normalization and orthogonality conditions. The energy of each molecular orbital wave function ψ_{MO} is then calculated. The energy level diagram for the metal and ligand AO's and the resulting σ AO's is shown in Fig.6.40. It is seen from this diagram that the t_{2g} orbitals (d_{xy}, d_{xz}, d_{yz}) are not affected by the bonding, while the e_g orbitals (d_{z^2} and $d_{x^2-y^2}$), on combination with the ligand orbitals produce two degenerate bonding MO's (ψ_{z^2}, $\psi_{x^2-y^2}$) and two degenerate antibonding MO's ($\psi^*_{z^2}$, $\psi^*_{x^2-y^2}$). The electrons must now be distributed among these orbitals in accordance with Hund's rule for degenerate orbitals.

The six ligands in an octahedral complex contribute two electrons each and these 12 electrons are paired in the lowest six MO's. The d electrons of the metal atom occupy the next lowest lying orbitals. This result is essentially the same as that we found earlier from the crystal-field theory (cf. Fig. 6.34), namely that there are available for the d electrons in an octahedral complex a lower triply degenerate set of orbitals (t_{2g}), the d_{xy}, d_{yz} and d_{yz} AO's, and an upper doubly degenerate set, the $\psi^*_{z^2}$ and $\psi^*_{x^2-y^2}$ orbitals. A difference now is that the upper doubly degenerate sets represent antibonding MO's rather than AO's. Thus the splitting of the d orbitals which in the crystal-field theory, discussed earlier, arose due to electrostatic interaction with the ligands now comes about through combination with ligand orbitals. Treatment of tetrahedral and square planar complexes similarly produces results which are in essential agreement with those of the electrostatic approach.

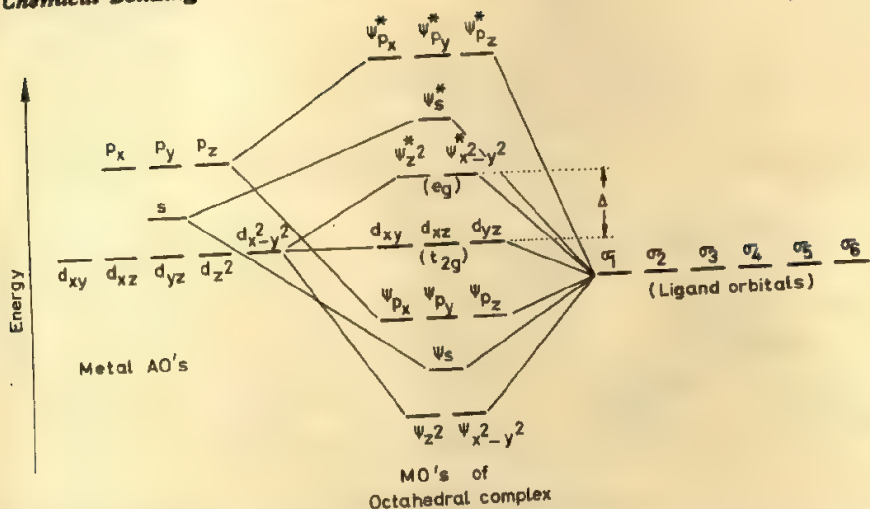It is easy to see that octahedral complexes with the configuration d^9

Chemical Bonding

Fig. 6.40 Energy diagram of MO's (bonding σ and antibonding σ^*) involved in the formation of an octahedral complex.

d^7 spin-paired (low spin) and d^4 spin-free (high spin) will have an odd number of electrons in the antibonding MO's, ψ^*_z2 and $\psi^*_{x^2-y^2}$. This results in a distortion of the complex and splitting of these orbitals thereby removing the degeneracy (Jahn-Teller effect†). For example, a d^9 complex has three electrons in these antibonding MO's, so that either of the configurations $(\psi^*_z2)^2 (\psi^*_{x^2-y^2})^1$ or $(\psi^*_z2)^1(\psi^*_{x^2-y^2})^2$ is possible. The first configuration implies that there is more antibonding in the z-direction than in the x- and y-directions, while the second implies the opposite. Since more antibonding character of a bond implies a weaker and hence longer bond, the two configurations would lead to distortions of the octahedral shape in different directions, as indicated in Fig. 6.41. Energetically this means that the degeneracy of the antibonding MO's, ψ^*_z2 and $\psi^*_{x^2-y^2}$, will be removed. According to the concepts of the ligand-field theory not only can the e_g metal orbitals ($d_{z^2}, d_{x^2-y^2}$) form σ MO's with ligand orbitals, but there is also the possibility of π-bonding with the t_{2g} metal orbitals (d_{xy}, d_{xz}, d_{yz}) which have the correct symmetry (see Table 6.7). Figure 6.42 illustrates the way in which a d_{xy} metal orbital can combine with p_x and p_y-ligand orbitals, provided the metal and ligand AO's do not differ too much in energy. This gives rise to π-type delocalized MO's.

---

† The Jahn-Teller theorem states that a non-linear molecule with an orbitally degenerate ground state is not stable and should distort itself so as to remove the orbital degeneracy of the ground state.
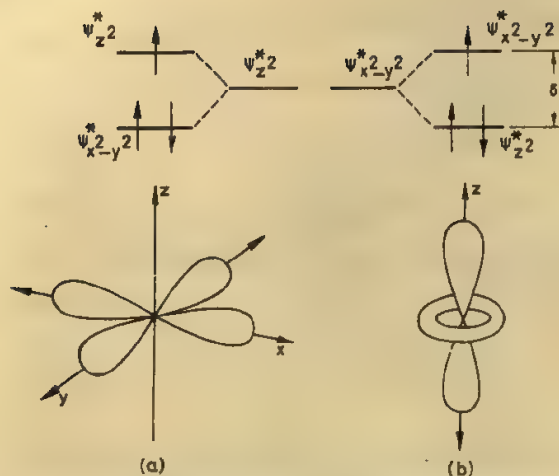
Fig. 6.41 Splitting of e_g antibonding MO's in distorted octahe-
dral field (Jahn-Teller effect): (a) Extension in $x-$ and y–direc-
tions; (b) extension in z-direction.

The effect of π - interaction on ligand-field splitting is illustrated in
Fig.6.43. On the left is shown the situation when the ligand π orbitals

Fig. 6.42 Combination of d_{xy} AO with ligand π
orbitals.

are fully occupied; the t_{2g} orbitals are now raised in energy thereby
decreasing the value of ligand-field splitting, Δ, over that without
π -bonding. On the right is shown the situation when the ligand π
orbitals are empty, which results in a stabilization of the molecular

Fig. 6.43 Energy levels for π-bonding with donor and acceptor ligands.

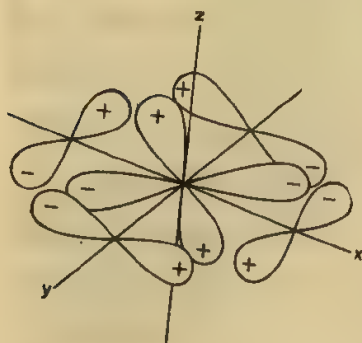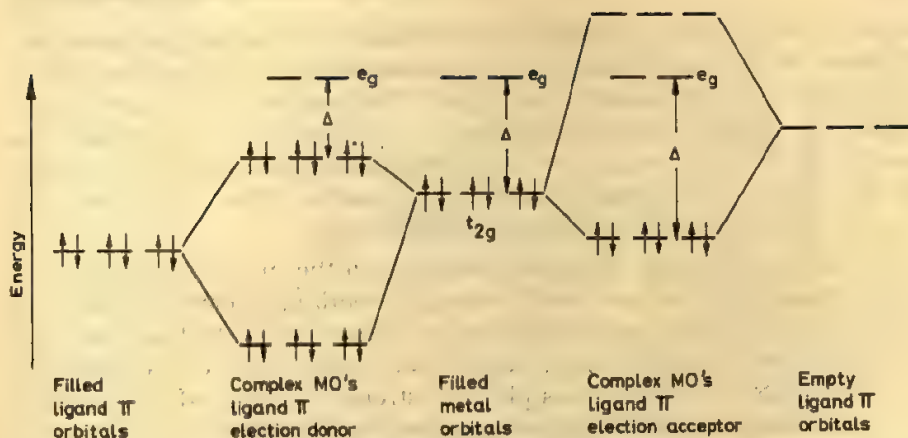orbital mainly based on the metal; the d electrons occupy the bonding t_{2g} orbitals which are lower in energy than the original t_{2g} orbitals, thus increasing the ligand-field splitting Δ. This describes a situation in which ligand π orbitals can act as electron acceptors, and accounts for the large ligand field splittings observed with some ligands, e.g cyanide ion and orthophenanthroline. Such an interaction is called π - *back- bonding* (or π-*back- donation*) and the appropriate ligands are referred to as *acceptor ligands*.

The cyanide ion is a unique ligand in that it usually produces a larger Δ than any other ligand. The cyanide ion, although it has no empty π orbitals of low energy, does have antibonding π^* orbitals of only slightly higher energy (Fig.6.44). The π^* orbitals have just the right symmetry to
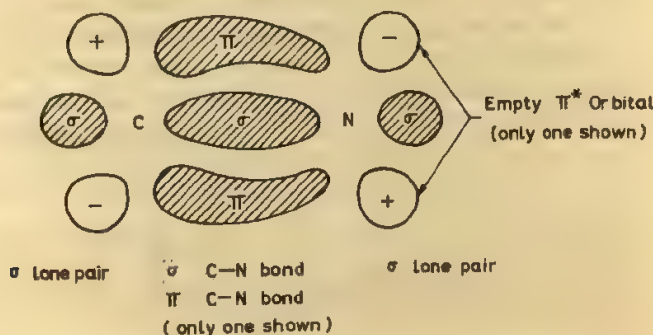

Fig. 6.44 Mo's in CN$^-$ ion [KK $(z\sigma)^2(y\sigma)^2(x\sigma)(w\pi)^4$].

combine with the t_{2g} orbitals of the metal in an octahedral complex; electrons in the t_{2g} orbitals which are released towards them are said to undergo π-back-donation to the ligand. The resultant fall in the energy of the t_{2g} orbitals increases the gap (Δ) between this energy and the energy of the e_g orbitals (see Fig. 6.43). Thus, according to the MO theory, it is the strong electron accepting property of the cyanide ion that places it at the head of the spectrochemical series.

The acceptor ligand offers the possibility to the metal atom to get rid of its excess charge accumulated through σ-bonding. Clearly, the effect of π-back-donation is to increase the covalent character of the bond between the metal and the coordinating atom of the ligand, thereby strengthening the bond. In the above example, the strength of the $M-C$ bond is increased; however, at the same time, the $C-N$ bond is also weakened a little because of the partial filling of its antibonding orbitals. The strength of the $C-N$ bond should therefore be different in cyanocomplexes of different metals; this can be demonstrated by infrared spectroscopy (Section 10.7)

Metal carbonyls, which are neutral molecules having carbon monoxide ligands, fall in the above category. The formation of stable carbonyls can thus be explained by appreciable double bond formation involving the π-antibonding orbitals of the ligand (see Section 6.6). Being a neutral molecule, carbon monoxide would indeed be a better electron acceptor than the cyanide ion and so would be able to stabilize the metal atom as well as or even better than cyanide.

Metal atoms also form complexes with unsaturated hydrocarbon molecules involving a rather different type of bonding. Structural information gathered about these compounds shows that the double-or triple-bond axis of the ligand is perpendicular to the metal-ligand axis. Figure 6.45, for example, shows the structures of two compounds obtained from ethylene and a chloroplatinate. While the bond arrangement around the platinum atoms is approximately square, the bonding from the metal atom to the ethylene molecule is perpendicular to the carbon-carbon bond. The highest energy electrons lie in the π MO; the unfilled antibonding $\pi *$ MO's [Fig. 6.46 (a)] are however only of slightly higher energy. Bonding with the metal can be described as due to overlap of a metal d orbital with the filled π orbital of the carbon-carbon bond and back-donation from a metal d orbital of correct symmetry to the unfilled $\pi *$ orbital [Fig. 6.46 (b)]. Transition-metal organometallic compounds containing similar π bonds have been prepared from a variety of olefinic hydrocarbons, usually by their direct contact on a metal halide or a complex such as a carbonyl.
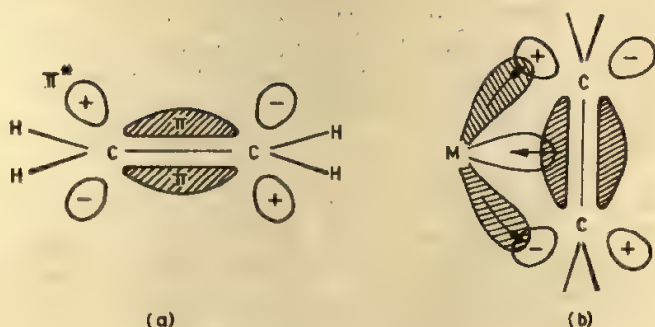
Fig. 6.46 (a) Ethylene molecule, with filled π orbitals and unfilled π^* orbitals. (b) Bonding of ethylene to a transition metal by overlap of the filled π orbital with metal d orbital, the system being stabilized by back donation from the metal to the unfilled π^* orbital.

Another class of metal-olefin compounds is that in which cyclic olefinic or aromatic compounds act as ligands. Some of these compounds, for example, bicyclopentadienyl iron, $Fe(C_5H_5)_2$, commonly known as *ferrocene*, are exceptionally stable. Ferrocene forms stable crystals which vaporize without decomposition. Cyclopentadiene derivatives of more than fifty metals have been made. In the majority of these compounds the metal is bound to the ring by π-bonding. Metal-olefin coordination compounds, especially those with two-ring systems, have been given the descriptive name *sandwich compounds,* which follows from their structure. The structure of ferrocene [Fig. 6.47 (a)], for example, consists of two
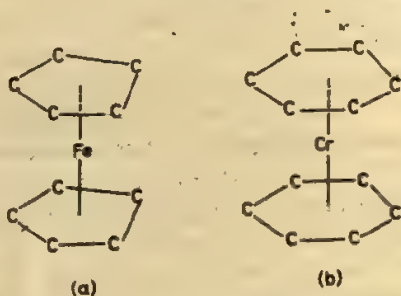

Fig. 6.47 Structures of sandwich compounds: (a) ferrocene and (b) dibenzene-chromium.

planar C_5H_5 rings with an iron atom sandwiched in between; in corresponding benzene compounds, such as dibenzene chromium, $Cr(C_6H_6)_2$, the metal atom is sandwiched between two planar benzene rings [Fig. 6.47 (b)].

6.12 Magnetic Moment and Electronic Arrangement in Complex Ions

Much information has been obtained about the arrangement of electrons in ions from magnetic moment measurements. The magnetic moment of a substance can be measured with the magnetic balance by comparing the weight of the substance, when suspended so that part of it is in a strong magnetic field, to the weight when it is free of the magnetic field.

Substances having a negative magnetic susceptibility are said to be *diamagnetic*. When suspended in a magnetic field, a diamagnetic substance tends to orient itself at right angles to the field. In a nonuniform magnetic field it tends to move towards the weaker part of the field. Substances with a positive magnetic susceptibility are said to be *paramagnetic*. Paramagnetic substances tend to be oriented parallel to a magnetic field. In an inhomogeneous magnetic field they tend to move into the region of higher field strength. Substances whose magnetic susceptibility is very large and positive, and whose magnetic moment does not fall to zero when the applied magnetic field is removed, are said to be *ferromagnetic*.

The evidence regarding the electronic arrangement in ions is based on the theoretical principle that those substances in which all electrons are paired are diamagnetic, while those with unpaired electrons are paramagnetic. Moreover, the magnetic moment μ of a paramagnetic ion containing n unpaired electrons is given by $\mu_0 \sqrt{n(n+2)}$, where μ_0 represents one Bohr magneton (BM)*, which is the unit of magnetic moment. So ions containing 0,1,2,3,4 and 5 unpaired electrons will be expected to have magnetic moments of 0, 1.73, 2.83, 3.87, 4.90 and 5.90 Bohr magnetons, respectively. A direct experimental measurement of the magnetic moment of an ion can therefore give information as to the number of unpaired electrons in it.

Compare, for instance, the electronic configuration of a free Fe^{+2} ion with that of the Fe^{+2} surrounded by strong-field ligands, such as the ferrocyanide ion $[Fe(CN)_6]^{-4}$. The electronic configuration of the Fe^{+2} ion is shown in Fig. 6.18, omitting the inner electrons, which are however all paired. It is seen that there are four unpaired electrons in Fe^{+2} ion and so the expected magnetic moment of compounds containing this ion would be 4.90 BM; the measured magnetic moment of hydrated ferrous sulphate is, in fact, 5.25 BM. However, in the Fe^{+2} ion octahedrally coordinated by strong ligand field, the electrons rearrange and are all paired, as shown in Fig.6.18. It would therefore be expected that the ferrocyanide ion would be diamagnetic; this is found to be so experimentally.

---

*An electron revolving in an orbit is like an electric current in a loop of wire and as such behaves as a magnet. The moment of such a magnet is $eh/4\pi mc = 9.27 \times 10^{-21}$ erg gauss^{-1}.

Here e represents the electronic charge, h is the Planck constant, m is the mass of an electron, and c is the velocity of light. This is a natural unit of magnetic moment and is referred to as a Bohr magneton.

Consider again the electronic configurations of the free Fe^{+3} ion and of the Fe^{+3} ion octahedrally surrounded by ligands, as shown in Fig. 6.35. There are five unpaired electrons in the free Fe^{+3} ion and the calculated magnetic moment of 5.92 BM corresponds with the measured values for ferric compounds, e.g. 5.86 BM for ferric sulphate. In an octahedral complex involving weak field ligands, e.g. in $(FeF_6)^{-3}$, the Fe^{+3} ion still has five unpaired electrons which should lead to a magnetic moment of 5.92 BM; the measured moment of $(FeF_6)^{-3}$ is, in fact, 5.98 BM. On the other hand, in an octahedral complex involving strong field ligands, e.g. in $[Fe(CN)_6]^{-3}$, Fe^{+3} has only one of the $3d$ electrons unpaired. This should lead to a magnetic moment of 1.73 BM; the observed value for $[Fe(CN)_6]^{-3}$ is 2.40 BM. We thus see that the weak-field case and strong-field case can be conveniently differentiated by magnetic moment measurements.

Magnetic moment measurements can also lead to the elucidation of configuration of metallic complexes. Classic examples are provided by planar and tetrahedral complexes of nickel. Thus, whereas Ni^{+2} forming four tetrahedral sp^3 bonds has two unpaired $3d$ electrons, and so will be paramagnetic, Ni^{+2} forming four square coplanar dsp^2 bonds has none (Fig.6.39) and so will be diamagnetic. It was on these considerations that Pauling first pointed out that diamagnetic complexes of 4-coordiante Ni^{+2} should be planar; this was, in fact, confirmed later by structural studies.

Suggested Reading

CARTMELL, E. and G.W.A. FOWLES, *Valency and Molecular Structure*, Butterworths, London, 1961.

COULSON, C.A., *Valence*, Oxford, New York, 1961.

HEITLER, W., *Elementary Wave Mechanics*, Oxford, New York, 1956.

MULLIKEN, R.S., 'Bonding Power of Electrons anc Theory of Valence', *Chem. Rev.* 9, 347 (1931).

PAULING, L., *The Nature of the Chemical Bond*, Cornell, Ithaca, New York, 1960.

RAY, P., *The Theory of Valency and the Structure of Chemical Bonds*, Calcutta, 1946.

RYCHEKEWITSCH, G.E., *Chemical Bonding and the Structure of Molecules*, Reinhold, New York, 1963.

KETELAAR, J.A.A., *Chemical Constitution*, Elsevier, Amsterdam, 1958.

HESLOP, R.B. and P.L. ROBINSON, *Inorganic Chemistry*, Elsevier, Amsterdam, 1960. 960.

ADDISON W. E., *Structural Principles in Inorganic Compounds*, Longmans, Green and Co. Ltd., London, 1961.

COTTON F.A., 'Ligand Field Theory', *J. Chem. Educ.* 41 (9), 466 (1964).

COTTON, F.A. and G. WILKISON, *Advanced Inorganic Chemistry*, Wiley Eastern, New Delhi, 1969.

Problems

6.1 Write the electronic configurations in MO terms for the following diatomic molecules:

(a) LiH, (b) HI, (c) ClF, and (d) SO.

6.2 State which of N_2 and NO you would expect to have the higher bond energy, and give your reasons.

6.3 The binding energy of N_2^+ is less than that of N_2, whereas the binding energy of O_2^+ is greater than that of O_2. How would you explain this in terms of the MO concept?

6.4 Show that the four equivalent $sp3$ hybrids are oriented in space tetrahedrally, the angle between each pair being $109°28$.

6.5 The methyl radical is planar. Discuss its orbital structure and the location of the unpaired electron.

6.6 How does the hybridization of the ring carbon atoms change when benzene is hydrogenated to cyclohexane?

6.7 The molecule of cyclo-octatetraene adopts a non-planar boat structure and has a polyolefinic electronic character with alternate double and single bonds. Discuss the nature of the bonding in this molecule.

6.8 Sketch a molecular orbital picture of allene ($CH_2 = C = CH_2$).

6.9 Describe the nature of the hybrid orbitals of the metal atom used in the following:
$(CrO_4)^{-2}$, (MnO_4) $[Ni(H_2O)_6]^{+2}$, $[Ni(CN)_4]^{-2}$, and VF_5.

6.10 Show the valence bond diagram and disposition of d electrons for the following complexes:
$[Ti(H_2O)_6]^{+3}$, $[V(H_2O)_6]^{+3}$, $[Cr(CN)_6]^{-3}$ and $[Mn(CN)_6]^{-3}$

6.11 Show the disposition of electrons of octahedral complexes with one to ten d electrons. Distinguish between low spin (or spin paired) and high spin (or spin free) cases. Indicate in each case the number of unpaired electrons. Repeat the same for tetrahedral complexes.

6.12 Account for the fact that cyanide ligands cause a large ligand-field splitting in complexes.

6.13 Explain the bonding in $[Ni(CN)_4]^{-2}$ and $[Ni(CO)_4]$. Compare the bonding characteristics of CN^- and CO ligands.

6.14 Discuss the nature of bonding in metal-olefin complexes.

6.15 The complex ions $[Mn(CN)_6]^{-4}$, $[Mn(CN)_6]^{-3}$, $[CO(NH_3)_6]^{+2}$ and $[CO(CN)_6]^{-4}$ have octahedral structures. Predict their magnetic moments.

Valency, Ionic Bonds and Covalent Bonds

7.1 *Introduction*

Valency, in its broadest sense, is a term used to describe the power or ability of elements to combine with one another. Frankland's suggestion, in 1852, that an atom of an element possessed a certain 'combining power' that determined the number of atoms of another element with which it would combine led to the idea of the valency of an element being expressed as a number that gave a quantitative measure of the 'combining power' of the element. Hydrogen being chosen as the unit of 'combining power', the valency of an element was defined as the number of atoms of hydrogen with which one atom of the element could combine (or which it could replace in a formula). However, oxygen (with a valency of 2) was also adopted as an alternative reference element, since oxides of many elements could be more easily studied than hydrides. The terms 'oxidation number' and 'oxidation state' which originated in this way are often used to this day, especially for metals, even though these terms may have no logical connection with oxygen as such. Seemingly, had fluorine chemistry developed at an earlier date, fluorine with its valency of one and power of combining with all elements except inert gases (?) would have been the obvious choice as reference element.

The idea of valency as a number is a useful one; by assigning the correct valency number (or numbers) to each atom or radical it is possible to build up the correct formulae for many chemical compounds. It might

be noted, however, that on the ideas of modern valency theory it is not possible always to express the valency of an element as a number. Formulae in terms of valence number convey no information as to the nature of the valency bonds present in the compounds or as to the mechanism of the formation of such bonds. Modern valency theory, however, accounts for the mechanism of formation and provides much information regarding the nature of the bonds.

The development of modern views on valency and bond formation which was necessarily linked to the development of the theory of atomic structure may be said to have started with the discovery of the electron. J. J. Thomson himself was of the view that valency must be associated with electrons. He put forward the suggestion, by about 1904, that valency bonds or links between atoms might be formed by electrostatic attractions resulting from the transfer of electrons from one atom to another. Earlier, Mendeleev had indicated, in developing his periodic table, a relation between valence number and the group in which the element was placed. It is a significant feature of the periodic table that the valence number of an element is often equal to its group number or to eight minus the group number. For example, nitrogen occurring in group five has valencies of $+5$ and -3, as in N_2O_5 and NH_3 respectively. The suggestion that if an element has two valencies then their sum (sign not considered) will be equal to eight was put forward in 1904 by Abegg as the so-called 'rule-of-eight'. He ascribed to each element positive and negative valence numbers (both maximum) such that the sum of their absolute values is eight and the positive valence is equal to the group number. The significance of Abegg's rule-of-eight was pointed out by Drude (1904) who put it into essentially modern terminology by suggesting that 'Abegg's positive valence number v signifies the number of loosely held negative electrons in the atom; his negative valence number v' means that the atom has the power of removing v' negative electrons from other atoms, or at least attaching them more firmly to itself'.

Further progress in the development of valency theory was possible only after Mosley had established the concept of atomic number in 1913, for then the number of electrons in an atom became known. The special stability of a complete outer octet of electrons was at once evident, since all the inert gases (with the exception of helium) have the electronic structure of ns^2np^6 in the outermost shell. It followed from this that atoms of other elements with atomic numbers close to those of the inert gas elements would, in order to become more stable, tend to achieve these structures through the involvement of their outermost electrons. Two important papers published independently by Kossel and Lewis in 1916, to which all modern views may be traced, were essentially the outcome of these considerations.

Kossel pointed out that those elements just following the inert gas elements in atomic numbers could attain an inert gas structure by losing

electrons and forming positively charged ions. These elements would thus show tendencies to possess positive valence numbers. Likewise, those elements just preceding the inert gas elements in atomic numbers could achieve an inert gas structure by gaining electrons and hence forming negatively charged ions. These elements would therefore be expected to have tendencies to possess negative valence numbers. On this basis, Kossel proposed that when atoms of such elements enter into chemical combination they lose or gain sufficient electrons to achieve the electronic structures of inert gas atoms and that the compounds so formed are ionic in character, consisting of ions held together by electrostatic attraction. The valence number is then equal to the ionic charge or the number of electrons lost or gained. Though many simple compounds can be formulated on Kossel's idea of ionic bond formation, there are also many compounds which cannot be fitted into this concept, either because they are non-electrolytes, e.g. carbon tetrachloride, or because the atoms constituting the molecule are the same (e.g. in diatomic chlorine) so that neither of the atoms would be expected to transfer an electron to the other.

However, this difficulty was overcome, in a large measure, by the concept advanced by Lewis that atoms might attain inert gas structures by sharing electrons, the shared electrons between any two atoms being considered as belonging to both atoms and contributing to inert gas structures for both. Each shared pair of electrons constitutes what is known as a covalent bond. The term 'covalence' was suggested by Langmuir to describe the sharing of electrons as opposed to electrovalence to describe complete transference of electrons. The compounds described in terms of covalence are non-ionic in character, the essential opposites of ionic (electrovalent) compounds treated by Kossel.

The Kossel and Lewis concepts were the foundations of the electronic theory of valency. Subsequent developments in valency theory centred largely in extensions and modifications of these two concepts and their incorporation into quantum mechanical theory. The electrovalent and covalent bonds as envisaged in the Kossel and Lewis concepts are, however, not the only types of chemical bonds. The concept of the chemical bond as a force, holding groups together at once makes it apparent that there may exist a variety of such forces, and consequently, bonds of various types. These may be conveniently classified as:

(A)   Electrostatic type
    (i)   Ionic or electrovalent bonds
    (ii)   Dipole attractions
    (iii) Hydrogen and hydroxyl bonds
(B)   Non-electrostatic type
    (i)   Non-ionic or covalent bonds
    (ii)   Coordinate or dative covalent bonds
    (iii) Van der Waals and long-range bonds
(C)   Metallic bonds.

7.2 Ionic or Electrovalent Bonds

The bonding force constituting the ionic bond arises from the electrostatic attraction between the oppositely charged ions. It is, therefore, necessary to consider the conditions which promote the formation of ions of the various elements.

(a) Inert gas structure. One important consideration, as we have already noted, is the possibility of attaining an inert gas electronic structure. Considering, for instance, the electronic structures of chlorine, argon and potassium,
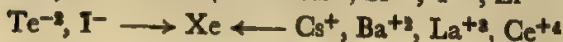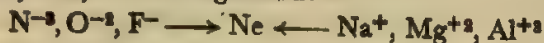
Cl $1s^2 2s^2 2p^6 3s^2 3p^5$ or 2.8.7

Ar 2.8.8

K 2.8.8.1

it is apparent that if the 4s electron is transferred from a potassium atom to a chlorine atom then both will acquire the electronic structure of argon, viz. 2.8.8. The donor potassium atom, by losing an electron, will gain a positive charge and thus form a cation while the chlorine atom, on acquiring this electron, will form a negatively charged anion; and the two ions will be held together by electrostatic attraction. A compound, potassium chloride, is thus obtained, in which both ions have acquired inert gas type of electronic structure with its consequent stability.

In many cases more than one electron requires to be transferred in order to achieve the inert gas structure. Thus, aluminium, having the electronic structure 2.8.3, loses three electrons to assume the structure 2.8, which is that of neon; oxygen, on the other hand, having the structure 2.6 gains two electrons to become 2.8. In the formation of the compound aluminium oxide from Al^{+3} and O^{-2} ions, consideration of electrical neutrality, moreover, requires that they combine in the ratio of 2:3.

In brief, the following ions which attain inert gas structures in this way may be distinguished:

$$N^{-3}, O^{-2}, F^- \longrightarrow Ne \longleftarrow Na^+, Mg^{+2}, Al^{+3}$$

$$S^{-2}, Cl^- \longrightarrow Ar \longleftarrow K^+, Ca^{+2}, Sc^{+3}$$

$$Se^{-2}, Br^- \longrightarrow Kr \longleftarrow Rb^+, Sr^{+2}, Y^{+3}, Zr^{+4}$$

$$Te^{-2}, I^- \longrightarrow Xe \longleftarrow Cs^+, Ba^{+2}, La^{+3}, Ce^{+4}$$

$$At^- \longrightarrow Rn \longleftarrow Fr^+, Ra^{+2}, Ac^{+3}, Th^{+4}$$

The two-electron helium structure is attained by H^-, Li^+, and Be^{+2}.

(b) 18-Electron group structure. So far as negatively charged ions (anions) are concerend, the only ions known are those with an inert gas structure. But among cations there are many which do not have inert gas structures. To account for the formation of such cations it then becomes

necessary to attribute stability to some electronic structures which are not those of inert gases. Since many of the elements in the B sub-groups of the periodic table form ions having 18 electrons in the outermost shell, this electronic arrangement must have a certain degree of stability. Zinc, for example, having the electronic configuration 2.8.18.2 loses two electrons to form a zinc ion Zn^{+2} with the configuration 2.8.18, and copper (2.8.18.1) forms the cuprous ion Cu^+ with the same configuration 2.8.18; the configurations of Cd^{+2} and Hg^{+2} are 2.8.18.18 and 2.8.18.32.18, respectively. It might be noted, however, that an ion with an 18-electron group structure is less stable than an ion with an inert gas structure. Thus, for instance, the Ca^{+2} ion, which has the inert gas structure 2.8.8, is formed with greater ease than the Zn^{+2} ion with the structure 2.8.18.

The elements copper, silver and gold exhibit variable valency, as shown below:

Cu 2.8.18.1	Ag 2.8.18.18.1	Au 2.8.18.32.18.1
Cu^+ 2.8.18	Ag^+ 2.8.18.18	Au^+ 2.8.18.32.18
Cu^{+2} 2.8.17	Ag^{+2} 2.8.18.17	Au^{+3} 2.8.18.32.16

The Ag^+ ion is more stable than the Ag^{+2} ion, but Cu^{+2} is more stable than Cu^+; and of the ions Au^+ and Au^{+3}, the latter is more stable. This means that the arrangement of 18 electrons in the outermost shell does not necessarily connote stability. This is possibly due to the nuclear charge not being high enough to hold firmly the group of 18 electrons in the outermost shell. That trivalent ions of zinc, cadmium and mercury are not known (which means that none of the 18-electron group in the respective divalent ions ionizes) may then be attributed to stronger nuclear attractions firmly holding the 18 electrons in the outermost shell.

Some of the B sub-group elements which would be expected to form only ions with an 18-electron group do, in fact, form other ions too with 18-plus-2-electrons outer arrangements. These ions retain two of the valence electrons, i.e. two valence electrons do not play their full part in ion formation. Such electrons are known as an *inert pair*; they amount to a pair of *s* electrons in the outermost shell for which sufficient energy to cause unpairing has not been supplied.

Generally speaking, however, the inert pair effect is observed in the heavier B sub-group elements, namely, those in the lower half of the table given below:

Be	B	C	N	O	F
Mg	Al	Si	P	S	Cl
Zn	Ga	Ge	As	Se	Br
Cd	In	Sn	Sb	Te	I
Hg	Tl	Pb	Bi		

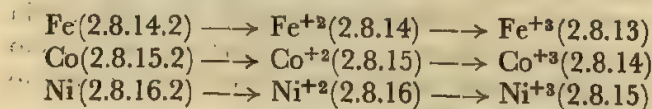Like the inert gases, mercury vapour is monatomic, which points to

mercury behaving as Hg (2.8.18.32.18.2). This may be attributed to the outer s-electron pair being inert.

In any one vertical series in the above table, the effect shows itself more markedly as one passes down the series. This will be illustrated with the following examples: Thallium (Tl) with the electronic structure 2.8.18. 32.18.3 forms both the expected trivalent ion Tl^{+3} (2.8.18.32.18) and a monovalent ion Tl^+ (2.8.18.32.18.2); likewise indium (In) in the same group forms both In^{+1} and In^{+3} ions. But, whereas Tl^+ is more stable than Tl^{+3}, as is evident from the fact that thallic salts are oxidizing agents, in the case of indium, however, stability is achieved by the conversion of In^+ to In^{+3} and the metal in the presence of water. Gallium (Ga), on the other hand, forms no monovalent compounds.

Both tin (2.8.18.18.4) and lead (2.8.18.32.18.4) form the expected tetravalent ions Sn^{+4} and Pb^{+4}, and also divalent ions Sn^{+2} (2.8.18.18.2) and Pb^{+2} (2.8.18.32.18.2). The effect of the inert pair is however more marked in the heavier element, i.e. lead. Thus, Pb^{+2} is more stable than Pb^{+4}, whereas Sn^{+4} is more stable than Sn^{+2}. This explains why plumbic oxide PbO_2 and lead tetrachloride are oxidizing agents whereas stannous oxide and stannous chloride are reducing agents.

Again, antimony (2.8.18.18.5) and bismuth (2.8.18.32.18.5) both form trivalent ions Sb^{+3} (2.8.18.18.2) and Bi^{+3} (2.8.18.32.18.2), and give definite trivalent salts. But the effect of the inert pair is more pronounced in the heavier element bismuth. Thus, for instance, bismuth does not form a pentachloride, whereas antimony does.

(c) Transitional ion structure. A feature of transition elements is their variable valency. The formation of two or more ions by these elements is due to the small difference in stability of two or more alternative ionic structures. Considering, for example, the series iron. cobalt and nickel, the ions formed are:

Fe(2.8.14.2) $\longrightarrow$ Fe^{+2}(2.8.14) $\longrightarrow$ Fe^{+3}(2.8.13)

Co(2.8.15.2) $\longrightarrow$ Co^{+2}(2.8.15) $\longrightarrow$ Co^{+3}(2.8.14)

Ni(2.8.16.2) $\longrightarrow$ Ni^{+2}(2.8.16) $\longrightarrow$ Ni^{+3}(2.8.15)

The formation of Ni^{+3} is, however, doubtful. In fact, in this series of iron, cobalt and nickel, the divalent ion becomes more stable as one passes from iron to nickel. It is reasonable to assume that this is due to the increase in the nuclear charge in this order so that the outer d electrons are held more firmly.

The more stable an ionic structure is, the more easily is that ion formed. Of the possible ionic structures (a), (b) and (c), discussed above, the stability decreases from (a) to (c). The tendency of simple ions to form complex ions, however, increases in the order (a), (b) and (c). This trend is of course expected, since through the formation of a complex ion a

simple ion attemps to increase its stability; consequently, the more stable a simple ion is, the less tendency will it have to form complex ions.

However, for the formation of an ionic compound the consideration which is more important than the one of attaining a stable electronic structure is that the compound in question should be energetically favourable. If the compound is exothermic and possesses high energy of formation it is likely to be stable. The energy of formation of ionic compounds can be computed by means of the so-called *Born-Haber cycle*, which is based on the assumption that the formation of an ionic crystal may occur either by the direct combination of the constituent elements or by an alternative process in which the reactants are vaporized, the gaseous atoms are converted into ions and the gaseous ions are then combined to give the product. The process is illustrated below by considering the energetics of sodium chloride formation.

The experimental value of the thermochemical heat of formation (Q) of sodium chloride is 98.2 kcal/g mole, that is, when one g. mole of solid sodium chloride is formed from solid sodium and gaseous chlorine 98.2 kcal of heat is liberated. It is also possible to proceed from the same starting materials and derive the same product through a series of steps as follows:

(i) *First step.* Formation of gaseous sodium atoms from solid sodium. Energy supplied is the energy of sublimation (S); and for each g. atom of sodium formed it is 26.0 kcal.

(ii) *Second step.* Removal of outermost valence electron from each gaseous sodium atom resulting in the formation of gaseous sodium ions. Energy is to be supplied for this process and it is equal to the ionization potential (I), namely, 119.1 kcal.

(iii) *Third step.* Dissociation of chlorine molecules producing gaseous chlorine atoms. The energy to be supplied for this process is the dissociation energy D. Since, however, the formation of 1 g. mole of sodium chloride (involving only 1 g. atom of chlorine) is being considered, the value to be used is that of $D/2$, namely, 29.0 kcal.

(iv) *Fourth step.* Addition of an electron to each gaseous chlorine atom to form a chlorine ion. In contrast to the ionization of the second step, this process is, however, accompanied by liberation of energy and is known as the electron affinity (E). The energy liberated per g. atom of chlorine is 91.0 kcal.

(v) *Final step.* Formation of solid compound from gaseous ions. Energy is given out in this process and is known as the lattice energy (U_0). For sodium chloride U_0 is 181.3 kcal.

Diagrammatically the process can be shown as in Fig. 7.1.

Considering the magnitude of the terms in the cycle, depicted in Fig. 7.1, the most important ones are seen to be the ionization potential, the electron affinity and the lattice energy. If the ionization potential of one element is relatively low but the electron affinity of the other element and
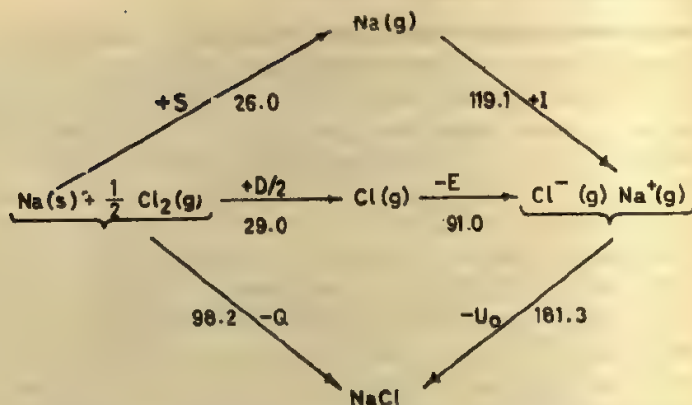
Fig. 7.1 Energetics of the formation of sodium chloride. Note that a positive sign associated with an energy quantity indicates absorption of energy and a negative sign indicates evolution of energy.

the lattice energy of the compound are both high, then the energy of formation will be large; and this condition would favour the formation of an ionic compound. In the following is presented a brief discussion of these three important properties.

Ionization potential. This is defined as the energy required to remove an electron completely from a gaseous atom. As more and more energy is supplied to an electron, it ascends to successively higher energy levels till finally it moves out of the attractive force of the nucleus completely. The energy required up to this final stage is the ionization potential. Experimentally, it can be measured by spectroscopic methods. Usually, ionization potentials are expressed in electron volts [one electron volt (eV) is the energy acquired by an electron falling through a potential difference of one volt; $1 \text{ eV} = 1.6 \times 10^{-12}$ erg]. The ionization potential values tabulated for the various elements in Appendix 4 are expressed in eV.

Some of the factors influencing the magnitude of the ionization potential of an electron are:

(*i*) *Distance of the electron from the nucleus.* The greater is this distance the smaller is the ionization potential, since the attractive force exerted by the positively charged nucleus becomes smaller the farther the electron is removed from it. This is evident from the fact that if an atom is raised to an excited state by promoting an electron to a higher energy level, i.e. to a greater distance from the nucleus, then that electron is more easily ionized than from the same atom in the ground state.

(*ii*) *Nuclear charge.* The greater the charge on the nucleus the more difficult it is to remove an electron from its influence and hence the higher is the value of the ionization potential.

In a vertical group of elements in the periodic table, the nuclear charge, i.e. the number of protons in the nucleus, increases with increasing atomic

number; its effect of augmenting the ionization potential is, however, more than balanced by the opposing effect of the increase in the distance of the valency electrons (i.e. outer electrons) that accompanies the increase in the atomic number. So the net effect is the decrease of ionization potential with increase in atomic number within a vertical group. This is illustrated by the values of ionization potential (in eV) of the first electron for the alkali metals: Li 5.4, Na 5.1, K 4.3, Rb 4.2, and Cs 3.9. This trend is, however, less marked (and there are also exceptions to it) in the *d*-block elements.

Considering again a horizontal group of elements in the periodic table, the increase in atomic number is accompanied by diminution of atomic size and increase of the nuclear charge, both of which lead to an increase in the ionization potential of the outermost electron. This is illustrated by the values for the first ionization potentials (in eV) of the elements belonging to the first short period: Li 5.4, Be 9.3, B 8.3, C 11.3, N 14.5, O 13.6, F 17.4, and Ne 21.6. This trend is apparently broken at Be and N, both of which show values slightly higher than what would be expected. These higher values are possibly due to the stability of a full *s*-level and a half-filled *p*-level respectively.

(iii) *The shielding effect of other electrons of the atom.* The attractive force exerted by the nucleus on the most loosely held outer electrons is partially counterbalanced by the repulsive forces exerted by the inner electrons. The electron to be removed is thus shielded by the inner electrons resulting in some decrease in ionization potential. The more numerous the inner electrons the more effective is the shielding, and consequently, the less is the ionization potential. So when successive ionization potentials of the same element are considered, the values will show large increase, since successive ionization reduces the number of electrons screening the nucleus. This is illustrated by the values quoted in Table 7.1.

Table 7.1 Ionization Potentials of some Elements

Element	Electronic config.	Ionization potential, eV						
		1st	2nd	3rd	4th	5th	6th	7th
Li	$1s^2 2s^1$	5.4	75.6	122.4				
Be	$1s^2 2s^2$	9.3	18.2	153.9	217.7			
B	$1s^2 2s^2 2p^1$	8.3	25.1	37.9	259.3	340.1		
C	$1s^2 2s^2 2p^2$	11.3	24.4	47.9	64.5	392.0	489.8	
N	$1s^2 2s^2 2p^3$	14.5	29.6	47.4	77.4	97.9	551.9	666.8

Apart from the diminution of the screening effect, another effect of successive ionization by removal of the outermost electrons is to pull the remaining electrons nearer to the nucleus. This also must be a factor contributing to the large increase of ionization potential referred to above.

The disproportionately large values of the 2nd, 3rd, 4th, 5th and 6th

ionization potentials of Li, Be, B, C and N respectively, are attributed to these elements attaining the configuration of the inert gas helium $(1s^2)$ at the respective stages. Similarly, the 3rd ionization potential of magnesium is greater than would be expected by comparison with the values for the 1st and the 2nd, as is evident from the following:

	Ionization potential, eV		
	1st	2nd	3rd
Mg	7.6	15.0	80.1

Here also this is attributed to the stability of the inert gas configuration; the removal of the two valence electrons from a magnesium atom produces a magnesium ion having the neon configuration, and hence the energy required to remove a third electron abruptly becomes greater.

Summarizing, it can be said that the ionization potentials decrease from top to bottom in a group of the periodic table and also from right to left across a period. Furthermore, the smaller the number of electrons to be ionized the lower will be the ionization potential. And since low ionization potential favours ionic bond formation, as has been pointed out earlier, consideration of the aforesaid trends reveals which elements are likely to become cations in ionic compounds. In such a consideration, however, the stability of the configuration ns^2np^6 should also be taken into account.

Electron affinity. The energy released when an electron is added to a neutral gaseous atom to from an ion is termed the *electron affinity.* Adding a second electron to an ion which already carries one negative charge always requires an input of energy, rather than its release, because of the repulsive force of like charges.

Only halogens release energy when they are converted into anions. The electron affinity in these cases is, therefore, *exoergic* (i.e. energy given out) and hence favourable for formation of ionic bonds. The electron affinity for all the other elements (involving addition of more than one electron to form anions) is, however, *endoergic* (i.e. energy absorbed).

Only the electron affinities of most electronegative elments have been evaluated. This has been done with the help of the Born-Haber cycle, described above, by using thermodynamic data for ionic compounds. Values so obtained are summarized in Table 7.2, which also contains, for comparison, the directly determined values for halogens.

The electron affinity of an element is essentially the ionization energy of the negative ion with sign reversed and so the foregoing discussion on factors influencing the ionization potential may be extended to electron affinity also. It leads to the conclusion that the greater the nuclear charge and smaller the size of the atom the more highly exoergic (and hence more favourable for ionic bond formation) the electron affinity will be.

Table 7.2 Electron Affinities of some Elements

Element	Electron affinity (kcal/mole) at 25°C	
	By Born-Haber cycle	By direct method
F	82.7	83.5
Cl	91.0	87.3
Br	81.8	82.0
I	73.4	75.7
O	−168.0*	—
S	− 79.4*	—
Se	− 97.0*	—

*For two electrons

Lattice energy. At least three forces are operative in an ionic crystal on the balancing of which the stability of the latter depends. These are: (i) The electrostatic attractive forces between the ions, inversely proportional to the square of the distance; (ii) van der Waals forces of attraction, inversely proportional to the seventh power of the distance, and (iii) interatomic repulsive forces, inversely proportional to an approximately tenth power of the distance. Thus the repulsive forces become significant at much shorter range than the attractive forces. The attractive and repulsive forces are shown in Fig. 7.2 together with their resultant (or sum). The distance r_0, corresponding to the minimum potential energy, represents the equilibrium value of the interionic distance in the stable crystal lattice. (At all temperatures, however, there occurs some thermal oscillation about the so-called equilibrium position and, again, when the thermal energy exceeds the potential energy of the lattice, free rotation can also set in.)

Assuming that the potential energy of the ions, that are separated by an infinite distance, is zero (as shown in Fig. 7.2 by the extension of the curve to the right), the minimum potential energy (at r_0) becomes numerically equal to the lattice energy of the crystal. The lattice energy of an ionic crystal may, therefore, be defined as the decrease in energy that accompanies the process of bringing the ions from an infinite distance to their equilibrium positions in the stable lattice. Alternatively, the lattice energy of an ionic crystal may be defined as the energy released when a large number of positive and negative gaseous ions (representing a mole of the compound) are brought together from infinity into a solid lattice to form one mole of the compound. Hence the lattice energy is the same in magnitude but opposite in sign to the energy of dissociation of the crystal. It follows from this that the greater the lattice energy, numerically, the greater is the energy required to decompose the crystal into the constituent ions. A theoretical value of the lattice energy can be obtained from the relation
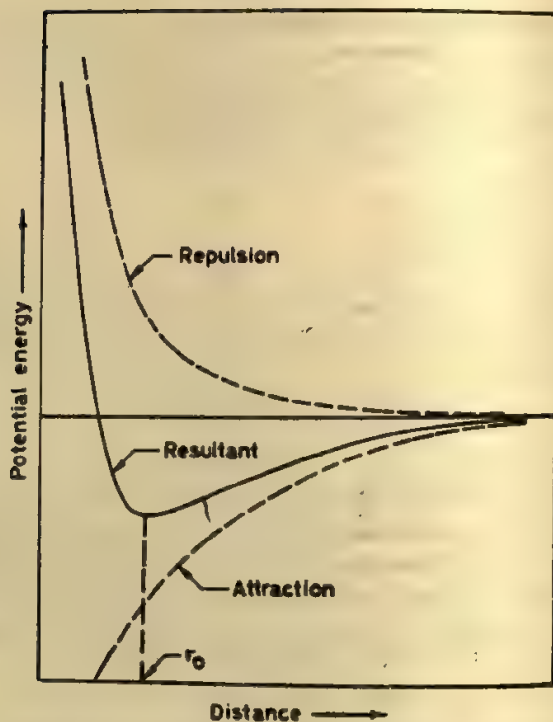
Fig. 7.2 Potential energy of a crystal lattice

$$U_0 = \frac{e^2 z^2 NA}{r_0} (1 - 1/n) \qquad\qquad (7.1)$$

where U_0 is the lattice energy, e the charge of an electron, z the highest common factor of the valences of the two ions, N the Avogadro number, r_0 the interionic distance, n a constant called the *Born exponent* and A a constant, called the *Madelung constant*. The Born exponent n can be evaluated from the results of experimental measurements of the compressibility of the crystal. For all crystals the value of n is found to lie in the neighbourhood of 9. The Madelung constant is the geometrical correction factor whose magnitude is dependent on the geometry of the crystal lattice and can be evaluated by straightforward mathematical methods.

It follows from Eq. (7.1) that if both ions are polyvalent the lattice energy will be large, because of the term z^2. Since high value of lattice energy contributes to the increase of the heat of formation, the large charges on both ions would seem to be conducive to greater stability of ionic compounds. However, this is true in some compounds, but not in all, since the removal of successive electrons from cations is associated with increasing ionization potential (I) and the addition of successive electrons to anions involves endoergic electron affinity (E), both of which would compensate for the increase in lattice energy (U_0) with corresponding

effect on the heat of formation, as can be seen from Hess's law applied to the cycle in Fig. 7.1, that is,

$$-Q = S + I + D/2 - E - U_0 \qquad (7.2)$$

Moreover, if the cation is small, a closer approach of the two oppositely charged ions can occur, and since this results in a larger value of lattice energy, the formation of an ionic lattice would seem to be favoured by the small size of cations. But a small metal atom (which will give a small cation) can also make the term I unfavourable for the formation of a stable ionic bond. So a very careful balancing of different factors is necessary in order to predict whether a given compound will be ionic or not.

Values of S, I, D and E are usually readily available, so that the thermochemical heat of formation (Q) of a given compound can be calculated from Eq. (7.2), provided the lattice energy (U_0) is known. For computing the value of U_0 from Eq. (7.1) a probable structure for the compound must be guessed in order to derive the Madelung constant and also a reasonable value of interionic distance must be assumed. An ionic lattice should be expected if the heat of formation, so obtained, is found to be highly exothermic. Otherwise, the compound is likely to become exothermic by forming a covalent lattice, to which, however, the aforesaid procedure is inapplicable, since the lattice is not constituted of ions in this case.

Summarizing, the formation of an ionic bond between the atoms will, in general, be favoured:

(a) if the metal atom forms a cation bearing small positive charge and the ionization potential, i.e. the energy required to remove the valence electron(s), is small;

(b) if the metal atom is large, because this gives rise to a low value for the ionization potential;

(c) if the metal attains inert gas type of configuration on ionization, since in such a case the nuclear charge is most effectively screened by electrons, which in turn leads to a low ionization potential;

(d) if the non-metallic atom is small and produces an anion of small charge, since both these conditions enhance the possibility that the process of adding electron(s) to form the anion would be an exoergic, or weakly endoergic, process.

7.3 Electronegativity

In discussing bonds between unlike atoms, it is convenient to associate with every atom a quantity (termed *electronegativity*), say, x, which represents its electron-attracting power in a bond, so that the ionic character

of a bond A—B is given by $x_A - x_B$. Mulliken suggested that $\frac{1}{2}(I+E)$, that is, the average of the first ionization potential (I) and the electron affinity (E) should be taken as a measure of the electronegativity of an atom. This seems reasonable from the following considerations. The first ionization potential is a measure of the energy of the process $A \longrightarrow A^+ + e$, and the electron affinity is that of the reaction $A + e \longrightarrow A^-$. So the ionization potential is regarded as the average of the electron attraction of a positive ion and a neutral atom, and the electron affinity as the average of the electron attraction of an atom and its negative ion; hence, the arithmetic mean can be regarded as the electron attraction of a neutral atom. Despite the apparent simplicity of Mulliken's formula, it is however difficult to apply it to most elements.

It is possible to determine by thermochemical and spectroscopic methods the quantities described as bond energies. The energy of a bond is equal to the contribution of that bond to the heat of formation of the molecule containing it. For diatomic molecules containing a single bond (e.g. Cl_2) the bond energy is equal to the dissociation energy of the gaseous molecule to gaseous atoms. In general, it is found that the experimentally determined energy of a bond between unlike atoms is greater than the energy expected for 'normal covalent bond' or truly covalent bond (formed by equal sharing of electrons) between these atoms. This additional bond energy, which amounts to additional stability of the bond, is caused by *resonance* between truly covalent state and ionic state of the bond, and is therefore, called the 'additional ionic resonance energy', or simply, *ionic resonance energy*.

Thus selecting any bond A—B between unlike atoms A and B, the ionic resonance energy could be obtained by subtracting from the experimentally found energy of the actual bond A—B the energy of the truly covalent state of the same bond. But the latter quantity cannot be measured since a *truly covalent bond is in most cases hypothetical*. Pauling has however postulated that the bond energy of a truly covalent bond A—B must be intermediate between the bond energies of the bonds A—A and B—B, because the latter are between like atoms and are therefore essentially completely covalent.

Pauling has assumed in the first place that the bond energy D_{A-B} of the truly covalent bond A—B is the arithmetic mean of the energies D_{A-A} and D_{B-B} of the bonds A—A and B—B, respectively, i.e.

$$D_{A-B} = (D_{A-A} + D_{B-B})/2$$

However, in more accurate but less simple considerations, Pauling has taken the geometric mean instead of the arithmetic mean, i.e.

$$D_{A-B} = \sqrt{D_{A-A} \times D_{B-B}}$$

The difference between the value of D_{A-B} (calculated in either way) and the measured value of the energy of the actual A—B bond is the ionic resonance energy. The ionic resonance energy determined in this way

found to increase as the two atoms A and B become more and more unlike with respect to the property termed *electronegativity*, i.e. the power of an atom in a molecule to attract an electron to itself. Thus, for instance, as can be seen from the results summarized in Table 7.3, the ionic

Table 7.3 Ionic Resonance Energies of Hydrogen-Halogen Bonds
(Values are given in kcal/g mole)

	H—F	H—Cl	H—Br	H—I
Calculated bond energy, D_{A-B} (arithmetic mean of D_{A-A} and D_{B-B})	70.4	81.1	75.2	70.2
Actual bond energy of bond A-B	134.6	103.2	87.5	71.4
Difference (Δ) =Ionic resonance energy	64.2	22.1	12.3	1.2

resonance energy (Δ) increases rapidly in the sequence HI, HBr, HCl and HF, in which, while the hydrogen component is constant, the halogen changes from iodine (an element regarded by virtue of its general chemical properties to be only a little more electronegative than hydrogen) to fluorine, which is the most electronegative of all elements.

Though Δ values increase with the increase in electronegativity differences between the bonded atoms, these values do not satisfy a relationship amounting to a difference between numerical properties of the atoms concerned. Pauling has found, however, that the square roots of the values do satisfy approximately a relation of this sort. The results summarized in Table 7.4 for the triad, silicon-oxygen-flourine, illustrate this.

Table 7.4 Ionic Resonance Energies: Silicon-Oxygen
-Fluorine

	Si—O	O—F	Si—F
Calculated bond energy, D_{A-B} (arithmetic mean of D_{A-A} and D_{B-B}), kcal/g mole	37.7	34.9	39.4
Actual bond energy of bond A-B kcal/g mole	88.2	44.2	129.3
Ionic resonance energy (Δ_{A-B}), kcal/g mole	50.5	9.3	89.9
$(\Delta)^{1/2}$	7.1	3.0	9.5

We see that the values of Δ are not additive, i.e. $\Delta_{Si-O} + \Delta_{O-F} \neq \Delta_{Si-F}$, but $(\Delta)^{1/2}$ values are much more nearly so. Thus, square roots of ionic resonance energies (Δ) may be taken as electronegativity differences of the respective pairs of atoms. It is moreover found that if the ionic resonance energies (Δ) are expressed in electron-volts (1 eV = 23 kcal),

then their square roots, representing electronegativity differences, lie in the convenient range between 3.3 and 0. For the triad silicon-oxygen-fluorine the electronegativity differences are then:

$$\left.\begin{array}{l} x_O - x_{si} = 1.5 \\ x_F - x_O = 0.6 \\ x_F - x_{si} = 2.0 \end{array}\right\} \tag{7.3}$$

where x_O is the electronegativity of oxygen and so on.

In this way, differences between pairs of electronegativities are derived, and to obtain numerical magnitudes of electronegativity, it is obviously necessary to assign an arbitrary value to one element. Pauling has fixed the electronegativity of the most negative element fluorine as 4.0, and correspondingly, assigned values to other elements on the basis of electronegativity differences. A typical set of these values is given in Table 7.5.

Table 7.5 Electronegativity Values for some Elements (after Pauling)

H 2.1			
C 2.5	N 3.0	O 3.5	F 4.0
Si 1.8	F 2.1	S 2.5	Cl 3.0
Ge 1.8	As 2.0	Se 2.4	Br 2.8
			I 2.5

On this scale, fluorine is by far the most electronegative of atoms, followed by oxygen occupying the second place, while nitrogen and chlorine come third. Furthermore, carbon, sulphur and iodine have equal electronegativities, as do nitrogen and chlorine. The C—S, C—I and N—Cl bonds should therefore be almost completely covalent, since, as already explained, the difference in the electronegativity values between the bonded atoms gives a measure of the ionic character of the bond.

It should be noted that the above treatment is only approximate. For instance, in Eq. (7.3) the sum of $(x_O - x_{si})$ and $(x_F - x_O)$ approaches the value of $(x_F - x_{si})$ but is not exactly equal to it. Similar comparisons for other groups of three elements for which ionic resonance energies have been determined generally give even poorer agreement. However, the values in Table 7.5 have been so adjusted as to give the best approach to additivity in the largest number of cases.

We have seen that the actual bond energy can be expressed as a sum of purely covalent bond energy and ionic resonance energy (Δ). Applying the method of arithmetic mean for computing the energy of covalent bonds we can, therefore, write

Actual bond energy of bond $A-B = \frac{1}{2}[D_{A-A} + D_{B-B}] + \Delta$

$$= \frac{1}{2}[D_{A-A} + D_{B-B}] + 23(x_B - x_A)^2 \qquad (7.4)$$

where x_A and x_B are the electronegativities of the elements A and B, respectively; the factor 23 serves to convert eV to kcal. It follows from Eq. (7.4) that the contribution of bond $A-B$ to the heat of formation of a substance containing it is equal to $23(x_B - x_A)^2$ in kcal. The heat of formation is therefore obtained by summing this expression over all the bonds in the molecule. However, corrections are called for if the substance contains single-bonded nitrogen and oxygen atoms, for reasons discussed below.

The standard states $N_2(g)$ and $O_2(g)$ are far more stable than they would be if the molecules involved three single N—N and two single O—O bonds, respectively. Energy of an N—N bond is 38.4 kcal/mole while the dissociation energy of N_2 molecule is 226 kcal/mole $[N_2(g) + 226$ kcal $\rightarrow 2N]$; hence the standard state $N_2(g)$ for nitrogen is far more stable than it would be if the molecule merely had three single N—N bonds, the extra stability amounting to 110.8 kcal/mole for N_2 or 55.4 kcal/mole per nitrogen atom. Similar arguments apply to oxygen also. Since the energy of the bond O—O is 33.2 kcal/mole, whereas the oxygen dissociation energy is 118.3 kcal/mole, there is an extra stability of 52.0 kcal/mole for O_2 in its standard state, or 26.0 kcal/mole per oxygen atom. Hence if the substance concerned contains single-bonded nitrogen and oxygen atoms, the heat of formation (ΔH^0_f) of that substance in its standard state can be calculated approximately by use of the expression

$$- \Delta H^0_f = 23 \; \Sigma(x_B - x_A)^2 - 55.4 \; n_N - 26.0 \; n_O \qquad (7.5)$$

Here n_N and n_O are, respectively, the number of nitrogen and oxygen atoms in the molecule, while the summation embraces all the bonds in the molecule. The correction terms for nitrogen and oxygen are due to the fact that, as mentioned above, a triple bond in N_2 is much more stable than three single N—N bonds and the bond in O_2 is more stable than two single O—O bonds.

The above equation for the heat of formation does not apply to substances containing double or triple bonds.

It follows from Eq. (7.5) that the heat of formation of a molecule containing an atom of nitrogen held by single bonds to other atoms having the same electronegativity, such as chlorine, should be about 55.4 kcal/mole, and consequently, the compound would be very unstable in relation to the elements. An example is provided by nitrogen trichloride whose measured heat of formation in solution in carbon tetrachloride is 54.7 kcal/mole; apparently the instability of NCl_3 molecule is not due to the weakness of the N—Cl bonds but rather the extraordinary strength of the triple bond in N_2. The ionic character of N—F bonds in nitrogen trifluoride is sufficient to outweigh the nitrogen correction term in Eq. (7.5) to give the molecule a negative heat of formation. For OF_2 and Cl_2O

the ionic resonance energy of the bonds (with $x_B - x_A = 0.5$) is not enough to overcome the term -26.0 kcal/mole for the oxygen; these substances, therefore, have positive heats of formation. Other normal oxides, however, have negative heats of formation.

Basing on the assumption that the heat of formation of a compound in its standard state from its elements in their standard states is given by Eq. (7.5), the difference in electronegativity of the two elements can be calculated from the heats of formation of the compounds formed by them. Electronegativity values can then be calculated from the so derived electronegativity difference. For example, the heat of formation (ΔH^0_f) of BCl_3 being -95.7 kcal/mole, the ionic resonance energy per bond, from Eq. (7.5), is $95.7/3 = 31.9$ kcal/mole, which leads to $x_{Cl} - x_B = 1 \cdot 18$ and hence to 1.82 for the electronegativity of boron. The value 2.0 has been accepted for the element. The values recorded in Table 7.6, except

Table 7.6 Electronegativity Scale of Elements (after Pauling)

Li	Be											B	C	N	O	F
1.0	1.5						H					2.0	2.5	3.0	3.5	4.0
							2.1									
Na	Mg											Al	Si	P	S	Cl
0.9	1.2											1.5	1.8	2.1	2.5	3.0
K	Ca	Sc	Ti	V	Cr	Mn	Fe	Co	Ni	Cu	Zn	Ga	Ge	As	Se	Br
0.8	1.0	1.3	1.5	1.6	1.6	1.5	1.8	1.8	1.8	1.9	1.6	1.6	1.8	2.0	2.4	2.8
Rb	Sr	Y	Zr	Nb	Mo	Tc	Ru	Rh	Pd	Ag	Cd	In	Sn	Sb	Te	I
0.8	1.0	1.2	1.4	1.6	1.8	1.9	2.2	2.2	2.2	1.9	1.7	1.7	1.8	1.9	2.1	2.5
Cs	Ba	La	Hf	Ta	W	Re	Os	Ir	Pt	Au	Hg	Tl	Pb	Bi	Po	At
0.7	0.9	1.1	1.3	1.5	1.7	1.9	2.2	2.2	2.2	2.4	1.9	1.8	1.8	1.9	2.0	2.2
Fr	Ra	Ac														
0.7	0.9	1.1														

The lanthanide elements: Ce—Lu
1.1—1.2

The actinide elements: Th   Pa   U   Np-No
1.3   1.5   1.7   1.3

those which have already appeared in Table 7.5, were derived in this way. It is seen from Table 7.6 that in the first short period, Li to F, the electronegativity values differ by a constant amount, namely, 0.5; in the subsequent periods the differences are smaller for the metals than for the non-metals. As one passes down the halogen column, the atoms become less electronegative because of the increasingly effective screening of the charge on the nucleus by inner electrons. The alkali metal atoms have low electronegativities because they have a great tendency to lose their outer electrons. Here also, the electronegativity decreases as one passes down the column because of the increasingly effective screening of the charge on the nucleus by inner electrons. Furthermore, for a given column in the periodic table the values are seen to change less in the metallic region than in the non-metallic region.

According to Mulliken's definition, as already mentioned, the electronegativity value is given by one-half of the sum of the first ionization potential and the electron affinity of an element. This definition is more precise than Pauling's since it is directly based on observable quantities. In practice, however, one is greatly handicapped by the lack of accurate electron affinity data. Pauling's method is consequently more useful than Mulliken's. There is, however, an empirical relationship between the electronegativity values of Pauling and Mulliken. If the first ionization potential (I) and the electron affinity (E) are expressed in kcal/mole, then, as can be seen in Table 7.7, the Pauling electronegativity value

Table 7.7 Comparison of Mulliken and Pauling
Electronegativity Scales

Element	Ionization potential (I)	Electron affinity (E)	$\dfrac{I+E}{125}$	x
F	402.7	83.5	3.89	4.0
Cl	301.2	87.3	3.11	3.0
Br	273.5	82.0	2.84	2.8
I	241.2	75.7	2.53	2.5
H	315.0	17.8	2.66	2.1
Li	126.1	0	1.01	1.0
Na	119.1	0	0.95	0.9
K	100.7	0	0.81	0.8
Rb	98.3	0	0.79	0.8
Cs	91.4	0	0.73	0.7

(x) for univalent atoms (assuming that the electron affinity of the alkali metals is zero) is $x \simeq (I + E)/125$.

The electronegativity of an element in different compounds is not necessarily a constant. It may vary to either side of the stated value (Table 7.7), depending on several factors, such as multiple bonds, change in coordination number, formal charges, and the character of adjacent atoms. For instance, the C—H bonds in acetylene have more ionic character than those in ethane, as revealed by the fact that acetylene can react to lose proton, whereas ethane reacts in this way only with extreme difficulty. This might be interpreted as signifying an increase in the electronegativity of carbon due to the presence of a triple bond.

The presence of a formal charge affects the electron-attracting power, and hence the electronegativity, of a bound atom. (To find the formal charge of an atom in a molecule, note the group number of the atom in the periodic table, then subtract from it the number of unshared electrons about the atom and one-half of the number of electrons shared by the atom.) A positive formal charge on a bound atom tends to pull electrons closer to it and thus effectively increases its electronegativity. For instance, the N—H bond in ammonium ion is more ionic in character than

the N—H bond in ammonia, because of the +1 formal charge on the nitrogen atom.

To illustrate the effect of adjacent atoms on the electronegativity of a bound atom we shall compare the compounds methanol (CH_3OH) and hypochlorous acid (ClOH), both containing an oxygen-hydrogen bond. Since hypochlorous acid donates a proton more readily than does methanol, the O—H bond is evidently more ionic in the former than in the latter. This can be explained as follows: since the electronegativity of chlorine is greater than that of the methyl carbon, substitution of a Cl atom for the CH_3 group in methanol results in a shift of electron density away from oxygen, and oxygen, in turn, tends to pull the electrons of the O—H bond closer to itself (*inductive effect*). Thus substitution of Cl for CH_3 increases, in effect, the electronegativity of the adjacent oxygen.

The electronegativity concept is useful in determining the bond character. The electronegativity values are also useful in approximating bond energies and heats of formation of compounds.

7.4 Ionic Radii

From the crystal structure data of many compounds the distance of closest approach, or internuclear distances, between various ionic species can be deduced. The regularities observed in these internuclear distances lend credence to the views of Barlow and Pope, expressed as early as 1906-07, that a crystal may be regarded as an essentially geometrical entity composed of a set of spherical atoms (or ions), each of characteristic size, packed together in contact. This is illustrated from the internuclear distances in the alkali halides deduced from the observed cell dimensions. Table 7.8 lists in concise form both the internuclear distances of the

Table 7.8   Internuclear Distances (in Å) in Alkali Halides

	Li	Δ	Na	Δ	K	Δ	Rb	Δ	Cs
F	2.01	0.30	2.31	0.36	2.67	0.15	2.82	0.19	3.01
Δ′	0.56	—	0.50	—	0.47	—	0.47	—	0.55
Cl	2.57	0.24	2.81	0.33	3.14	0.15	3.29	0.27	3.56
Δ′	0.18	—	0.16	—	0.15	—	0.15	—	0.16
Br	2.75	0.22	2.97	0.32	3.29	0.15	3.44	0.28	3.72
Δ′	0.25	—	0.26	—	0.24	—	0.22	—	0.24
I	3.00	0.23	3.23	0.30	3.53	0.13	3.66	0.30	3.96

various alkali halides and the two types of differences between them, Δ and Δ′, which reveal the change in internuclear distances accompanying a progressive substituion involving, respectively, alkali cations and halide ions.

It is seen that Δ for the halides of any consecutive pair of alkali metals

$r_A =$ Ionic radius of A
$r_B =$ Ionic radius of B
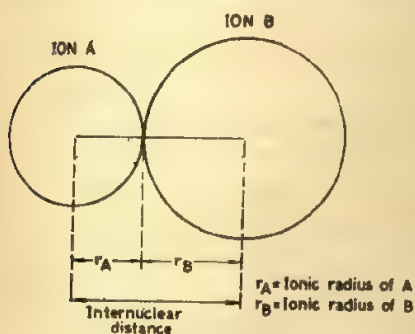
Fig. 7.3 Internuclear distance and ionic radii

and any one halogen is nearly independent of the particular halogen in combination; and conversely, Δ' for the halides involving any consecutive pair of halogens and any one alkali metal is very nearly the same which-ever alkali metal is considered. It is at once evident, in view of these regularities, that to each ion can be assigned a characteristic size of ionic radius. The observed internuclear distances then represent only the sum of two ionic radii (Fig. 7.3); but if any one radius is known, other radii may consequently be deduced one after another. Based on this principle, the values of ionic radii in Table 7.9 are derived from the various internuclear distances (deduced from crystal structure data) and the radii of certain ions estimated separately by independent methods.

It should be borne in mind, however, that the assumption that an ion may be regarded as a sphere, on the basis of which the ionic radii given in Table 7.9 are derived, is not really accurate, since, on the one hand, the arrangement of extranuclear electrons is rather diffuse which makes it difficult to sharply define the boundary of an ion, and on the other, the interaction of adjacent ions causes deformation. In any event, the ionic radius is an empirical concept and since the additivity principle also is just an approximation, the values of ionic radii, given in Table 7.9, are essentially empirical in nature. They do have, nevertheless, practical usefulness in the field of structural chemistry.

A study of the numerical values given in Table 7.9 leads to the follow-ing generalizations:

(i) In a group of comparable ions, the increase in atomic number (Z) is associated with an increase in the number of extranuclear electrons, and hence with an increase in ionic radii, as is illustrated in the case of alkali metal ions:

Ion	Li^+	Na^+	K^+	Rb^+	Cs^+
Atomic No. (Z)	3	11	19	37	55
Radius (Å)	0.60	0.95	1.33	1.48	1.69

It is seen, however, that the increase in ionic radius is by no means proportional to the increase in Z. This is obviously due to the fact that along with Z there also occurs an increase in nuclear charge that casts

Table 7.9 Values of Ionic Radii (in Å) Corresponding to 6-Coordination

	1	2	3	4	5	6	7	8
1							H^- 1.54	
2	Li^+ 0.60	Be^{+2} 0.31				O^{-2} 1.40	F^- 1.36	
3	Na^+ 0.95	Mg^{+2} 0.65	Al^{+3} 0.50	Si^{+4} 0.41		S^{-2} 1.84	Cl^- 1.81	
4	K^+ 1.33; Cu^+ 0.96	Ca^{+2} 0.99; Zn^{+2} 0.74	Sc^{+3} 0.81; Ga^{+3} 0.62	Ti^{+3} 0.76, Ti^{+4} 0.68; Ge^{+4} 0.53	V^{+2} 0.88, V^{+3} 0.74, V^{+4} 0.60	Cr^{+2} 0.84, Cr^{+3} 0.63, Cr^{+4} 0.56; Se^{-2} 1.98	Mn^{+2} 0.80, Mn^{+3} 0.66, Mn^{+4} 0.54; Br^- 1.95	Fe^{+2} 0.80, Fe^{+3} 0.64; Co^{+2} 0.72, Co^{+3} 0.63; Ni^{+2} 0.69, Ni^{+3} 0.62
5	Rb^+ 1.48; Ag^+ 1.26	Sr^{+2} 1.13; Cd^{+2} 0.97	Y^{+3} 0.93; In^{+3} 0.81	Zr^{+4} 0.80; Sn^{+4} 0.71		Te^{-2} 2.21	I^- 2.16	Ru^{+4} 0.63; Rh^{+3} 0.68; Pd^{+2} 0.80, Pd^{+4} 0.65
6	Cs^+ 1.69; Au^+ 1.37	Ba^{+2} 1.35; Hg^{+2} 1.10	La^{+3} 1.15; Tl^+ 1.44, Tl^{+3} 0.95	Hf^{+4} 0.78; Pb^{+2} 1.21, Pb^{+4} 0.84		W^{+4} 0.66	Re^{+4} 0.72	Os^{+4} 0.65; Ir^{+4} 0.64; Pt^{+4} 0.65
7	Fr^+ 1.76	Ra^{+2} 1.43	Ac^{+3} 1.11					
Lanthanide elements			Ce^{+3} 1.02, Tb^{+3} 1.00	Pr^{+4} 1.00, Dy^{+3} 0.99	Nd^{+3} 0.99, Ho^{+3} 0.97	Pm^{+3} 0.98, Er^{+3} 0.96	Sm^{+3} 0.97, Tm^{+3} 0.95	Eu^{+3} 0.97, Yb^{+3} 0.94; Gd^{+3} 0.97, Lu^{+3} 0.93
Actinide elements			Th^{+3} 1.08, Th^{+4} 0.95	Pa^{+3} 1.06, Pa^{+4} 0.91	U^{+3} 1.04, U^{+4} 0.89	Np^{+3} 1.02, Np^{+4} 0.88	Pu^{+3} 1.01, Pu^{+4} 0.86	Am^{+3} 1.00, Am^{+4} 0.85

increasingly greater attractive influence on the extranuclear electronic population.

(*ii*)   In a series of positive ions with constant number of extranuclear electrons, the radius decreases rapidly with increasing positive charge, as illustrated by the two series quoted below:

Ion:	Na+	Mg+²	Al+³	Si+⁴	Au+	Hg+²	Tl+³	Pb+⁴
No. of extra-nuclear electrons	10	10	10	10	78	78	78	78
Units of nuclear charge	11	12	13	14	79	80	81	82
Radius (Å)	0.95	0.65	0.50	0.41	1.37	1.10	0.95	0.84

We can discern two factors in each series: (*a*) Increasing nuclear charge which means greater attractive influence of the nucleus on the extranuclear electrons causing shrinkage of ionic radius, and (*b*) increasing charge of the cation which means stronger attractive force between the cation and its coordinating anions resulting in reduction of interionic distance and hence of the ionic radius. Both these effects contribute to a rapid decrease in radius.

(*iii*)   On the other hand, in the case of negative ions having dissimilar charges but the same number of extranuclear electrons, the radius increases with increasing negative charge, as illustrated below for a few pairs of negative ions:

Ion:	F⁻	O⁻²	Cl⁻	S⁻²	Br⁻	Se⁻²
No. of extranuclear electrons	10	10	18	18	36	36
Units of nuclear charge	9	8	17	16	35	34
Radius (Å)	1.36	1.40	1.81	1.84	1.95	1.98

The increase in ionic radius in any pair is obviously owing to the influence of the smaller nuclear charge. The increase is, however, seen to be very small; this may be attributed to the compensating effect of the ionic charge increase, namely, that the force of attraction between anion and its coordinating cations increases with the consequent decrease of interionic distance and hence of the effective radius.

(*iv*)   In the lanthanide series, it may be recalled (vide Appendix 2), the successive increase of 14 units in nuclear charge is accompanied by the successive filling of the $4f$ quantum level and the outer arrangement of $5s^2 5p^6 5d^{0\ or\ 1} 6s^2$ remains unaltered. The differentiating electrons being thus deeply buried in the extranuclear structure and all the elements possessing nearly the same configuration in the outermost shell, there occurs no compensation for increasing nuclear charge with increasing

atomic number, which is therefore associated with a decrease in the atomic size—a phenomenon, known as the *lanthanide contraction*. As can be seen from Table 7.9, the lanthanide contraction is also reflected in the ionic radii of the lanthanide elements. Moreover, as a consequence of this lanthanide contraction, these ions which occur immediately after the rare earth elements in the periodic table have radii little or no larger than those of the ions belonging to the same group in the preceding period.

An exactly similar contraction (*actinide contraction*) is also found among the actinide elements and is also amply reflected in the values of ionic radii for the limited number of ions of the actinide series recorded in Table 7.9.

(*v*)   The magnitudes of the ionic radii depend on the number of electrons lost or gained in ion formation. If several oxidation states are distinguishable for a given element, then the higher the positive oxidation number the smaller the ion; several instances of this effect can be seen from Table 7.9. Metallic iron atom, for instance, has a radius of 1.24 Å, while ferrous ion (Fe^{+2}) has a smaller radius, namely, 0.80 Å; this decrease in size occurs because with the removal of the two outer valence electrons in the formation of Fe^{+2} ion (Fig. 7.4) the remaining 24 electrons are drawn in closer to the nucleus (which retains its positive charge of 26). Removal of another electron to produce the ferric ion (Fe^{+3}) causes, owing to the same reason, a further reduction in size. The radius of Fe^{+3} ion (Fig. 7.4) is thus only 0.64 Å, which is nearly one-half of the radius of metallic iron.

(*vi*)   A survey of Table 7.9 reveals that the majority of cations are considerably smaller than 1 Å, whereas many common anions, including O^{-2} and Cl^-, are much larger than 1 Å. It is obvious, therefore, that in simple ionic crystals comprising cations and anions in association, the greater bulk of the volume is occupied by anions, and consequently, it is the arrangement of the latter that has the major say in the structure to be adopted by the crystal.

Limitations. In the above discussion the ionic radii have been treated as constant and characteristic of the ions concerned. It should, however,

(a) 1.24 Å   (b) 0.80 Å   (c) 0.64 Å
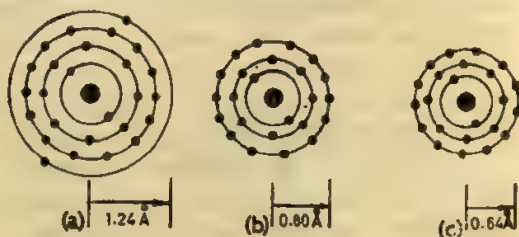
Fig. 7.4 Sizes of (*a*) iron atom and of (*b*) ferrous and (*c*) ferric ions

be conceded at this stage that such a concept is subject to certain qualifications.

(*i*) *Influence of coordination number.* The radius of a given ion is influenced by the coordination in which it occurs. Thus, for instance, the radius of the Cl^- ion in sodium chloride with 6-fold coordination is somewhat less than that in caesium chloride, characterized by 8-fold coordination. This effect may be attributed to the interaction between neighbouring ions; the more the number of neighbours the less is the attraction to any one of them, and consequently, the greater are the internuclear distances or effective ionic radii. In the three common structures of *AB*-type compounds (viz. sodium chloride structure, caesium chloride structure and zinc blende structure), decreasing coordination number is found to be associated with a *significant* (*though small* in its absolute magnitude) decrease in the effective radius of a given ion. Thus taking the radii corresponding to the sodium chloride structure as standard, those in the caesium chloride structure with 8-fold coordination are generally found to be three per cent higher while those in the zinc blende having 4-fold coordination are about five per cent less. Numerically, these facts can be represented as follows:

Coordination No.	4	6	8
Radius (relative)	0.95	1.00	1.03

It is necessary, in view of the aforesaid effect of coordination, to express ionic radii in a form appropriate to a certain coordination number. Conventionally, the coordination of the sodium chloride structure is chosen as standard. The crystal radii recorded in Table 7.9 are thus those for 6-fold coordination. For use in structures having a different coordination, the values are to be accordingly modified. As shown above, for coordination from 6 to 4 the conversion factor is 0.95, and from 6 to 8 it is 1.03. It is seen that the changes are not very large.

(*ii*) *Influence of radius ratio.* Besides the coordination number, another factor influencing the ionic radii is the value of the radius ratio r^+/r^-. As this radius ratio decreases toward the limiting value for anion-anion contact the repulsion between anions will progressively increase, thereby tending to distend the structure and thus to increase the apparent radii of the component ions. This effect is illustrated by the following data for alkali halides, all of which have 6-coordinated structures.

Halide	r^+/r^-	*Sum of radii* (Å) (*from Table* 7.9)	*Observed internuclear distance* (Å)
RbBr	0.76	3.43	3.43
KBr	0.68	3.28	3.29
NaBr	0.49	2.90	2.98

As is seen from these data, the discrepancy between the radius sum

and the observed internuclear distance is practically nil when the radius ratio is in the neighbourhood of 0.7, but assumes considerable magnitude as the ratio falls. Thus, in addition to the condition that the structure be a 6-coordinated one, the other condition to be satisfied before the ionic radii data of Table 7.9 can be applied is that the ratio r^+/r^- should be approximately 0.7. When applied to NaCl-type structures having r^+/r^- appreciably less than 0.7, Table 7.9 will, therefore, prove erroneous.

7.5 Non-ionic or Covalent Bonds

As has been already mentioned in Section 7.1, the idea of the *electron-pair bond* or *covalent bond* was introduced in 1916 by G. N. Lewis. His proposal was that one or more electron pairs 'shared' by two atoms could bond them together and that an inert gas structure could be attained in chemical combination by such sharing of electron pairs. For example, the formation of the methane molecule can be represented, according to this idea, as

$$4H^{\cdot} \quad + \quad \cdot\overset{\displaystyle\cdot}{\underset{\displaystyle\cdot}{C}}\cdot \longrightarrow \quad H\overset{\displaystyle H}{\underset{\displaystyle H}{:\overset{\cdot\cdot}{\underset{\cdot\cdot}{C}}:}}H, \quad \text{i.e.} \quad H - \overset{\displaystyle H}{\underset{\displaystyle H}{\overset{|}{\underset{|}{C}}}} - H$$
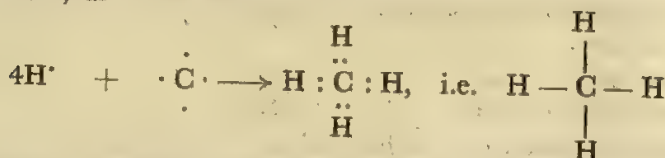
The four hydrogen atoms contribute one electron each and the carbon atom contributes four electrons towards the formation of four shared pairs. *Each shared pair constitutes a single covalent bond*, and for convenience may be denoted by a single line; in methane there are four such bonds. Now since each shared pair is regarded as belonging to both the contributor atoms, the carbon atom in methane can be said to have acquired an outermost layer of eight electrons corresponding to the electronic structure of neon, and the hydrogen atoms two electrons each as in helium.

In the above idea of covalent bonding there are two essential points to notice. The first is that sharing of electrons occurs in pairs, each pair being equivalent to a single chemical bond. Lewis was led to this suggestion of the electron-pair bond by the remarkable fact that *barring a few exceptions* (e.g. nitric oxide, nitrogen dioxide, chlorine dioxide and free radicals) *all known compounds contain an even number of electrons*. The second point is that in covalent union each atom tends to acquire an outer arrangement of eight electrons corresponding to the electronic configurations of inert gases. Hydrogen is, of course, an exception since its tendency is to acquire the two-electron structure of helium.

On the idea of the electron-pair bond coupled with the so-called rule-of-eight, the majority of compounds of non-metals in the first two (eight-membered) periods can be formulated (though, however, not without

some serious objections). We can also picture the arrangement of atoms in some polyatomic ions (for example, NH_4^+, SO_4^{-2}, AlH_4^-, and BF_4^-) using the Lewis rules.

Lewis represented multiple (double and triple) bonds as quartets or sextets of electrons. For example, the double bond and triple bond between carbons, as exemplified by ethylene and acetylene, are represented by
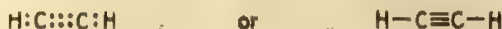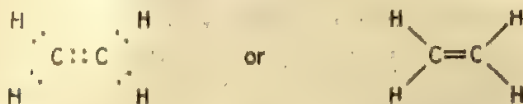
It will appear from such pictures that the two bonds comprising a double bond are equivalent and so also are the three bonds comprising a triple bond. There is, however, considerable evidence that this is not so.

Though the Lewis picture of the chemical bond is useful in formulating many compounds and ions, it, however, shows a lack of universal applicability. For example, stable compound (e.g. NO, NO_2 and ClO_2) are known which have an odd number of electrons. There are, moreover, compounds in which octets are not achieved or in which octets are exceeded. Two cases may be cited to illustrate this point. Boron has the electronic configuration $1s^2 2s^2 2p^1$, and since in the compound boron trifluoride, BF_3, it forms only three covalent bonds, gaining thereby three shared electrons, the number of electrons in the outermost shell becomes six, which is still short of the neon configuration $1s^2 2s^2 2p^6$. Again sulphur has the configuration $1s^2 2s^2 2p^6 3s^2 3p^4$, and in the compound sulphur hexafluoride, SF_6, it forms six covalent bonds thereby gaining six shared electrons, so that the total number of outer electrons is now twelve, i.e. four more than the number required to reach the argon configuration $1s^2 2s^2 2p^6 3s^2 3p^6$. However, it should be noted that, as in the ionic compounds, the covalently-bonded atoms too have an even number of s- and p-electrons. This is almost invariably true (the most important exceptions being some of the oxides of nitrogen and chlorine), and is perhaps more important than gaining octets. The concept of octet, though useful, is limited in its applications, but the concept that electrons seek to pair with each other is nearly universal in its application. The *rule of two* is more fundamental than the *rule of eight*.

Wave-mechanical picture of the covalent bond.

While it is understandable that the ions forming an ionic bond are held together by electrostatic forces, it is not immediately clear as to what holds two atoms together in a covalent bond. Indeed it was not until the development of the wave mechanics that any reasonable hypothesis as to the stabilities of atomic combinations from the sharing of electrons could be offered.

The VB theory and the MO theory provide two alternative approaches to this problem. They have been dealt with in Sections 6.3 and 6.4. In brief, mutual interaction of the pair of electrons is considered to be responsible for the stability of a covalent bond.

It must be pointed out that the Lewis theory of covalent bond as involving a pair of electrons for each bond was advanced before the development of the wave-mechanical concept, which later brought out, in effect, a reinterpretation of the Lewis picture of the chemical bond in terms of the detailed description of the electronic structure of atoms. Thus in VB terms, the covalent bond in the H_2 molecule, for instance, is considered to be formed by pairing of two electrons, or more precisely, by an overlapping of their orbitals, but pairing is now possible only between electrons having opposite spins. On the other hand, the MO treatment of the H_2 molecule predicts a cloud of two electrons (spin-paired), relatively thick between two nuclei. Such a description also conforms to the Lewis single bond between the two atoms in H_2. Considering again a much more complicated system, say the F_2 molecule, the MO treatment ultimately leads to a picture qualitatively similar to that of H_2, for it predicts that only two of the fourteen valence electrons of F_2 have appreciable probability densities in the internuclear region. It thus conforms to the Lewis picture of F_2 as two fluorine atoms held together by an electron-pair bond.

A very important point which emerges from the wave-mechanical concept (see page 115) is that resonance imparts additional stability to a covalent bond by virtue of the fact that energetically a resonance structure is more favourable than any of the individual configurations which contribute to it. In fact, the very existence of the covalent bond is largely a consequence of the phenomenon of resonance, as can be illustrated by considering the simplest possible example, namely, the hydrogen molecule; as we have seen, the energy of the covalent bond in a hydrogen molecule is largely due to the resonance energy between two possible structures (see page 112).

7.6 Covalent/Ionic Resonance

An important consequence of the resonance theory is that, contrary to the older idea, ionic and covalent bonds are not distinct types, but that there is possible a continuous transition from one to the other, and consequently bonds of transitional types, i.e. bonds which are partially covalent and partially ionic, may also occur. In fact, it is known that in the majority of cases transitional types of bonds do occur, and a *true covalent or homopolar bond probably does not exist.*

Consider, for example, the simplest molecule involving like atoms, namely, the hydrogen molecule. As we have already shown, there are,

apart from the two principal structures (I) and (II), (see page 112), which conform to the interchange of two electrons between the two component atoms, two other possible structures, shown below as III and IV, in which the binding is ionic between a proton H^+ and a H^- ion.

$$H_A^+ \; \ddot{H}_B^- \quad \text{and} \quad :H_A^- \; H_B^+$$
$$\text{(III)} \qquad\qquad \text{(IV)}$$
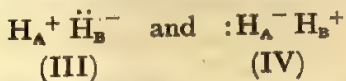
The subscripts A and B have been used only to distinguish the two hydrogen atoms. Since the ionization potential of hydrogen is high (315 kcal/mole) and the electron affinity is low (17.8 kcal/mole), the ionic structures (III) and (IV) are relatively unstable as compared with the first two. Nevertheless, they do make some contributions, though small, to the total structure of the molecule, as a result of which the so-called covalent bond in hydrogen has about 2% of ionic character. This, however, does not signify any dipole moment for hydrogen, because the two possible ionic configurations contribute equally to resonance.

Similar consideration applied to a molecule like hydrogen fluoride (HF) will, however, show it to be polar. Here three configurations are possible — one covalent (I) and two ionic, viz. (II) and (III), — as shown below:

$$H \; :\ddot{F}: \qquad H^+ \; :\ddot{F}:^- \qquad :H^- \; \ddot{F}:^+$$
$$\text{(I)} \qquad\quad \text{(II)} \qquad\quad \text{(III)}$$
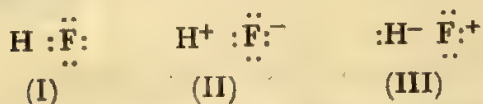
Now the two ionic configurations (II) and (III) cannot be expected to contribute equally, since, fluorine being considerably more electronegative than hydrogen, configuration (II) is far more stable than (III). It turns out, therefore, that the HF molecule is a resonance hybrid to which configurations (I) and (II) make the chief contributions and hence the hybrid is polar, while the magnitude of the dipole moment depends on the relative contributions of these two configurations. A similar picture applies to other hydrogen halides as well; however, the relative contribution of the structure of type (II) — and hence the magnitude of the dipole moment — would be expected to be less, as fluorine is replaced by successively less electronegative elements: chlorine, bromine and iodine.

7.7 *Partial Ionic Character in Covalent Bonds*

As has been noted previously, ionic bonds are favoured in combinations involving elements markedly differing from each other in electronegativity; and as such differences become less pronounced, the bonds become increasingly covalent in character, reaching the highest degree when the atoms concerned are of the same electronegativity. However, as

mentioned earlier, even in combinations between identical atoms, equal sharing of electrons may not occur, as for instance, the bond in hydrogen molecule has about two per cent of ionic character which arises from the small contributions of the ionic resonance structures (see page 192) to the total structure. Similar situation obtains in other comparable cases. It is, therefore, possible to describe any covalent bond in terms of its degree of ionic character.

By referring to covalent linkages possessing appreciable ionic character as *polar linkages* and to those possessing only slightly ionic character as *non-polar linkages*, it can be said, in a general way, that the sharing of electrons approaches equality in a non-polar bond but deviates to a greater or lesser extent from equality in a polar linkage; and the degree of this deviation, or rather the degree of polarity, is often reflected in the magnitude of the dipole moment. Consequently, zero dipole moment ($\mu = 0$) is indicative of non-polar linkage, i.e. equality of electron distribution, in a simple diatomic molecule. (It should be noted, however, that a molecule containing a number of bonds, each of which possesses dipole moment, can also have zero dipole moment when there is complete symmetry of bond distribution, e.g. in CCl_4). This is clearly borne out by the dipole moment value (μ expressed in Debye units; $1D = 1 \times 10^{-8}$ esu) of the compounds of hydrogen with the halogens and with the oxygen group of elements, cited below; these are seen to qualitatively reflect the trend of polarity of the molecules, which in turn parallels the variation of electronegativity on the part of the element combined with hydrogen:

	HF	HCl	HBr	HI	
μ	1·98	1·03	0·79	0·38	Debye

	H_2O	H_2S	H_2Se	H_2Te	
μ	1·85	1·10		0	Debye

The percentage ionic character of the bond can, in some cases, be determined from dipole moments and bond lengths. Thus, since the dipole moment of a completely ionized hydrogen halide would be *e.r*, where *e* is the electronic charge and *r* the bond length, $100\mu/e.r$ represents the percentage ionic character of the bond whose dipole moment is μ. Values obtained in this way are 45 per cent for HF, 17 per cent for HCl, 12 per cent for HBr, and 5 per cent for HI.

Pauling derived at first the following empirical equation to relate the amount of ionic character in a bond to the electronegativities of the bonded atoms:

$$\% \text{ Ionic character} = 100 \left[1 - \exp \left\{ -\tfrac{1}{4} (x_A - x_B)^2 \right\} \right] \tag{7.6}$$

where x_A and x_B are respectively the electronegativities of the atoms *A* and *B* bonded together.

At the time Eq. (7.6) was formulated, the value of the dipole moment of HF was not known. For HF, having an electronegativity difference of

1.9, this equation leads to an estimate of 60 per cent ionic character. However, as shown above, the dipole moment of HF corresponds to only 45 per cent ionic character. For more exact calculations Eq. (7.6) has consequently been revised by Hannay and Smyth to the following form:

$$\% \text{ Ionic character} = 16(x_A - x_B) + 3{\cdot}5\ (x_A - x_B)^2 \tag{7.7}$$

However, in molecules containing a number of bonds the picture is more complex. For water, for example, the electronegativity difference between O and H is 1.4, which corresponds, according to Pauling's equation, to 39 per cent ionic character in the O—H bond. The water molecule can accordingly be described as resonating among four electronic structures as follows:

H   H⁺   H   H⁺

:O:H   :Ö: ⁻ H   :Ö: ⁻ H⁺   :Ö: ⁼ H⁺

   I   II   III   IV
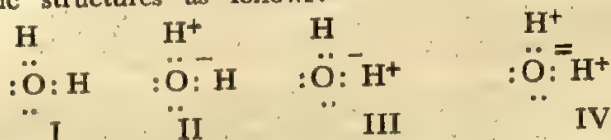
The structure (I) is completely covalent; each of the structures (II) and (III) has one ionic and one covalent bond to hydrogen, while (IV) has both bonds ionic. If the bonds were independent, the structures (I) to (IV) would make contributions of 37, 24, 24 and 15 per cent respectively, (note that $0 \times 37 + 1/2 \times 24 + 1/2 \times 24 + 1 \times 15 = 39$). However, the structure (IV) is probably of minor importance because of the strong attraction likely to be exerted for protons by the O^{-2} ions; hence its contribution would be diminished and consequently that of others would increase. Pauling's conclusion is that the first three structures contribute, respectively, 44, 28 and 28 per cent to the total structure. These values are obtained on the assumption that the doubly-ionic structure makes no contribution and that the ratio of the other three remains the same, namely, 1.54:1:1.

In dealing with other molecules containing more than one bond of intermediate type, a resonance concept of the above sort is to be applied. For the ammonium ion $(NH_4)^+$, for instance, it is necessary to consider sixteen structures, namely, one completely covalent structure, four structures with one bond ionic, six structures with two bonds ionic, four structures with three bonds ionic and one completely ionic structure. Thus though the structural formula of the ammonium ion is completely written as,

$$\left[\begin{array}{c} H \\ | \\ H-N-H \\ | \\ H \end{array} \right]^+$$
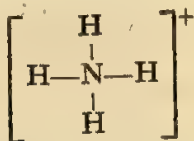
it actually stands for the 16 structures mentioned above, and the contributions of these 16 structures are such as to give each N—H bond the required amount of ionic character. This is how the amounts of ionic character of bonds in molecules, in general, are interpreted.

According to the Hannay-Smyth equation [Eq. (7.7)], an electronegativity difference of about 2.1 corresponds to 50 per cent ionic character of the bond. Bonds with a larger electronegativity difference are essentially ionic, having more than 50 per cent ionic character, while those with a smaller difference are essentially covalent. Below are summarized the partial ionic characteristics (based on the Hannay-Smyth equation and the electronegativity data presented in Table 7.6) of the single bonds formed by the elements:

(a)   *Alkali metals.* Bonds of the alkali metals with fluorine, oxygen and other strongly electronegative non-metallic elements are essentially ionic.

(b)   *Alkaline earth metals.* Bonds of magnesium, calcium, strontium and barium with fluorine, oxygen and other strongly electronegative non-metallic elements are essentially ionic. The bond of beryllium with fluorine is essentially ionic. All other beryllium bonds are essentially covalent.

(c)   *Third group elements.* Boron forms almost purely covalent bonds with hydrogen. Its bonds with other elements have varying degrees of ionic character, but in all cases the covalent character predominates. Bonds of aluminium with elements other than fluorine are essentially covalent. The Al—F bond, however, is more than 50 per cent ionic.

(d)   *Fourth group elements.* Bonds of carbon with all other elements are primarily covalent. The most ionic of these is, however, the C—F bond. Except, perhaps, the Si—F bond, bonds between silicon and all other elements are essentially covalent.

Ion deformation or polarization.   A useful, though somewhat less quantitative, approach to the problem of transition between ionic and covalent bonds is based upon the concept of ion deformation or polarization. When two ions approach each other closely, the cation attracts the electron atmosphere of the anion and simultaneously repels the anion nucleus; this causes a deformation, distortion or polarization of the anion, which can be crudely represented as in Fig. 7.5.
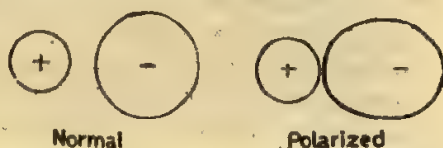
Fig. 7.5 Schematic representation of the polarization of ions

Normal   Polarized

Similarly, the cation would also be polarized by the anion but the effect would be less pronounced because of the smaller size of the cation. The net result of the ion polarization is the increase in the degree of electron sharing, or, in other words, in the degree of covalent character.

Ion deformation or polarization is favoured by a number of factors, which are summarized in a series of generalizations known as *Fajan's* rules. Thus a compound will tend to have appreciable covalent character, if

> (*i*)   the cation is small,
> (*ii*)   the anion is large,
> (*iii*) either the anion or the cation is highly charged, and
> (*iv*)   the cation does not have an inert gas type of electronic configuration.

The cation is small/the anion is large. A small cation has a stronger polarizing effect on the anion than a larger cation since the former can approach more closely; similarly a large anion is more easily polarizable than a small anion since the outermost electrons of the former are farther from the positive charge on the nucleus.

Either the anion or the cation is highly charged. A cation which has a charge greater than $+1$ will attract the electrons of the anion more strongly than a unipositive cation; in other words, the polarizing power of the cations increases with their charge. Similarly, a highly charged anion will tend to repel its outermost electrons more strongly than a uninegative anion; in other words, anions increase in polarizability with increase in their charge.

The cation does not have an inert gas type of electronic configuration. The compounds of copper (I) and silver (I), in contrast to those of alkali metals, show properties associated with appreciable covalent character. This cannot be attributed to ionic size, since there is no marked difference in that regard. (The silver ion is intermediate in size between the sodium and potassium ions and the cuprous ion is only slightly smaller than the sodium ion.) There is, however, greater difference in the patterns of electronic configurations. Thus, whereas the electronic configuration of the sodium and potassium ions is ns^2np^6, that of copper (I) and silver (I) is ns^2np^6 $(n-1)d^{10}$. The d electrons are considered to be less effective than s and p electrons in screening the nuclear charge from the outermost electrons and consequently the ions containing them behave as if they had a greater charge and hence exhibit polarizing properties. This behaviour is true of the transition metals as a whole when their ions do not possess inert gas configurations.

It is manifestly impossible to estrange one factor from all others in every case. The aforesaid rules are nevertheless very helpful in making qualitative comparisons. A generalization underlying these rules is evidently that increasing covalence is to be expected with increasing atomic number in families containing non-metals and with decreasing atomic number in families containing metals.

Since polarization of an anion is augmented by increasing cation charge and decreasing cation size, the two factors can be combined into one term, such as *ionic potential* (φ), first defined by Cartledge as,

$$\varphi = \frac{\text{cation charges}}{\text{cation radius}}$$

It follows, therefore, that large ionic potentials are associated with

strong polarizing effects or increased covalence. Thus it has been found that anhydrous halides, for which φ is less than 2.2, are ionic and conduct electricity in the fused state, whereas those with φ greater than 2.2 are non-ionic and non-conductors.

7.8 Covalent Radii

The internuclear distance between two atoms joined (as ions) by an ionic bond is not the same as that between the same two atoms joined by a covalent bond. We have already seen how, on the basis of internuclear distances determined by X-ray analysis of ionic crystals, it is possible to assign to each ion a characteristic radius such that internuclear distances are given with reasonable precision by the sum of the appropriate radii. It is, therefore, natural to enquire whether characteristic radii can be similarly assigned to atoms such that their sum will give covalent bond lengths. As shown below, such radii can, in fact, be assigned and are of great value in predicting covalent bond lengths with reasonable accuracy.

Bond lengths or *internuclear distances* (hereafter we shall employ the terms interchangeably) between atoms linked by the covalent bond can be determined from the study of crystals with covalent lattices by X-rays, and of gas molecules by electron diffraction and spectroscopic methods. It is found from such measurements that the length of the bond between a given pair of atoms is often the same, or very nearly the same, in many different molecules. The C—C bond, for instance, is 1·54 Å whether the bond occurs in diamond, ethane, propane, isopropyl alcohol or many other carbon compounds. Similarly, the C—Cl bond length is approximately the same (1·76–1·77 Å) in methyl chloride, methylene chloride, chloroform and carbon tetrachloride.

It is found, moreover, that the *A—B* bond length is equal to the arithmetic mean of the lengths of the bonds *A—A* and *B—B*. Thus, for example, the Cl—Cl bond length in the chlorine molecule is 1·988 Å and the C—C bond length in diamond, as mentioned above, is 1·542 Å, while the arithmetic mean of these, 1·765 Å, is seen to be in exact agreement with the C—Cl bond length 1·766 ± 0·003 Å, observed in CCl$_4$.

We can therefore assign a covalent radius of 0·99 Å (i.e. half of Cl—Cl distance, 1·99 Å) to chlorine, and a covalent radius of 0·77 Å (i.e. half of C—C distance 1·54 Å) to carbon, so that the C—Cl bond length is then given by their sum which is 1·76 Å, or conversely, by subtracting the covalent radius of, say, chlorine from the C—Cl bond length we can get the covalent radius of carbon.

It must be pointed out that the covalent radius of an atom (unlike the ionic radius) does not imply that the atom is a sphere of that size. Consider, for example, the case of chlorine. The Cl—Cl bond length, 1·99 Å,
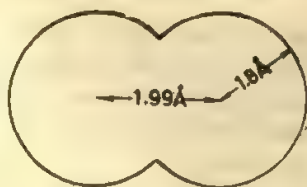
Fig. 7.6 The dimensions of the chlorine molecule

represents the centre-to-centre distance of two chlorine atoms constituting a molecule. The covalent radius of chlorine 0·99 Å representing half of this distance is seen to be considerably smaller than the van der Waals radius 1·8 Å derived by halving the internuclear distance 3·6 Å between contiguous chlorine atoms of different molecules, which are bound together only by van der Waals forces as in the crystal of solid chlorine. The chlorine molecule must, therefore, be considered as having the form shown in Fig. 7.6. Obviously, the covalent radii are applicable only to the calculation of internuclear distances between atoms linked by covalent bonds, and do not tell us anything about internuclear distances between adjacent molecules.

Single-bond normal covalent radii. It is possible to carry the aforesaid derivation process further to obtain a complete set of covalent radii such that their sums represent average internuclear distances for bonded atoms in molecules and crystals. Such a set of single-bond covalent radii for the non-metallic elements is given in Table 7.10. The values were

Table 7.10 Single-bond Normal Covalent Radii (Values in Å) for Non-metallic Elements

H	B	C	N	O	F
0.30	0.88	0.77	0.70	0.66	0.64
		Si	P	S	Cl
		1.17	1.10	1.04	0.99
		Ge	As	Se	Br
		1.22	1.21	1.17	1.14
		Sn	Sb	Te	I
		1.40	1.41	1.37	1.33

obtained largely from X-ray diffraction studies of crystals. It must be emphasized that the values given are applicable only when the elements exhibit their normal covalences, i.e. when they form the number of covalent bonds appropriate to the their position in the periodic table, e.g. one bond for fluorine, two bonds for oxygen, and so on. The values in Table 7.10 are, therefore, referred to as single-bond normal covalent radii.

It is seen from Table 7.10 that for elements in any horizontal period those with higher atomic numbers have the smaller radii. This is because, though elements in any one period have their outer electrons in the same

orbit, the electrons are more strongly attracted by the increasing posi-
tive charges on the nuclei as one passes from lower to higher atomic
number. On the other hand, in any one group of the periodic table,
elements with higher atomic numbers have their outer electrons in larger
orbits and are consequently associated with larger radii.

It should be mentioned that the values of the covalent radii for F, O
and N, as given in Table 7.10, were formulated before the experimental
values for F—F, O—O and N—N single bonds were available. Subsequent
measurements of these bond lengths showed large deviations from the
values expected from the old radii. Thus, whereas the old radius of
fluorine would require the F—F distance to be 1·28 Å, the value given by
the electron diffraction study of F_2 is, however, 1·45 Å. The O—O bond
length calculated from old radius is 1·32 Å, but in H_2O_2, the O—O bond
length is found to be 1·47 Å. The N—N bond length in N_2H_4 is found to be
1·47 Å, whereas the value from old radius is 1·40 Å. It should be pointed
out, however, that these discrepancies notwithstanding, the distances for
many bonds of F, O and N with other atoms are rather well given by the
old radii.

The covalent radius value of 0·30 Å assigned to hydrogen in Table
7·10 represents the approximate average of the values of the H-radius
derived from the experimental M—H distances (M = element other than
H) in a number of compounds of hydrogen. It might be mentioned,
however, that the experimental value of the H—H length in the H_2
molecule is 0·74 Å, from which the covalent radius for hydrogen would
be 0·37 Å.

Multiple-bond normal covalent radii. A double and triple bond
between two atoms is characterized by a fairly constant length in many
different molecules, and the arithmetic mean relationship also holds, as
for single bonds. It is therefore possible to assign double-bond or triple-
bond covalent radii to the elements in the same way as the single-bond
radii. Table 7.11 lists some numerical values of double and triple bond

Table 7.11   Multiple-bond Normal Covalent Radii
(Values in Å)

	B	C	N	O
Double bond	0·76	0·67	0·60	0·57
Triple bond	0·68	0·60	0·55	—
	Si	**P**	**S**	
Double bond	1·07	1·00	0·94	
Triple bond	1·00	0·93	—	
	Ge	**As**	**Se**	
Double bond	1·12	1·11	1·07	
	Sn	**Sb**	**Te**	
Double bond	1·30	1·31	1·27	

normal covalent radii. By comparing with single-bond radii it will be seen that the double-bond radii are about 7 to 14 per cent and the triple-bond radii about 15 to 23 per cent less than the corresponding single-bond radii.

Tetrahedral radii. So far as internuclear distances in crystals are concerned, the distance depends on the crystal type, and therefore the covalent radii for use in solid crystals are not necessarily the same as the normal covalent radii that are applicable only when the elements exhibit their normal covalency. This has led to the formation of different sets of covalent radii (Table 7.12) corresponding to different crystal arrangements.

Table 7.12 Tetrahedral Covalent Radii (sp^3 Hybrids) (Values in Å)

	Be	B	C	N	O	F
	1·06	0·88	0·77	0·70	0·66	0·64
	Mg	Al	Si	P	S	Cl
	1·40	1·26	1·17	1·10	1·04	0·99
Cu	Zn	Ga	Ge	As	Se	Br
1·35	1·31	1·26	1·22	1·18	1·14	1·11
Ag	Cd	In	Sn	Sb	Te	I
1·52	1·48	1·44	1·40	1·36	1·32	1·28
Au	Hg	Tl	Pb	Bi		
1·50	1·48	1·47	1·46	1·46		

The set of values of tetrahedral covalent radii (Table 7.12) was derived from the observed internuclear distances in crystals of the tetrahedral types in which the atom of interest forms four covalent bonds with four neighbouring atoms surrounding it tetrahedrally. These values are therefore meant for use in crystals of tetrahedral types. For example, the sulphur-sulphur distance would be, according to the value from Table 7.12, 2·08 Å in tetrahedral arrangement. This agrees well with the sulphur-sulphur distance 2·09 Å observed in the cubic crystal pyrite, FeS_2, in which each sulphur atom is linked by covalent bonds to three iron atoms and one sulphur atom disposed tetrahedrally around it.

It may be noted that the tetrahedral covalent radii for Group IV elements are exactly the same as the normal single-bond covalent radii for these elements given in Table 7.10. This is because these elements, as has been discussed previously, can be quadrivalent only in the sp^3 tetrahedral hybrid state. Identity of normal and tetrahedral radii in numerical magnitudes is also seen for first-row and second-row elements. For the heavier elements there are, however, small differences.

Octahedral radii. In the cubic crystal pyrite, FeS_2, referred to

earlier, whereas each sulphur atom is surrounded tetrahedrally by one sulphur atom and three iron atoms, each iron atom is surrounded octahedrally by six sulphur atoms corresponding to the formation by iron of six octahedral bonds using d^2sp^3 hybrid orbitals. So by subtracting the tetrahedral radius of sulphur (1.04 Å) from the iron–sulphur distance in pyrite (2.27 Å) one gets the value (1.23 Å) for the d^2sp^3 octahedral covalent radius of bivalent iron. (FeS_2 is a derivative of hydrogen disulphide, H_2S_2).

From similar data for other crystals with the pyrite structure or a closely related structure, values of octahedral radii for other transition-group elements can be obtained. These octahedral radii correspond to bond formation with d^2sp^3 hybrid orbitals, and are listed in Table 7.13.

Table 7.13 Octahedral Covalent Radii (Values in Å)

d^2sp^3 hybrids					
Fe^{II}	Co^{II}	Ni^{II}	Ru^{II}	Os^{II}	
1·23	1·32	1·39	1·33	1·33	
	Co^{III}	Ni^{III}	Rh^{III}	Ir^{III}	
	1·22	1·30	1·32	1·32	
Fe^{IV}		Ni^{IV}	Pd^{IV}	Pt^{IV}	Au^{IV}
1·20		1·21	1·31	1·31	1·40
sp^3d^2 hybrids					
Ti^{IV}	Zr^{IV}	Sn^{IV}	Pb^{IV}	Se^{IV}	Te^{IV}
1·36	1·48	1·45	1·50	1·40	1·52

Also given in Table 7.13 are a few more octahedral radii which, however, correspond to bond formation with sp^3d^2 hybrid orbitals. These values are obtained from internuclear distances in complex ions such as $(SnCl_6)^{-2}$, $(PbBr_6)^{-2}$ and $(SeBr_6)^{-2}$ and from crystals, such as TiS_2, having the cadmium iodide structure. It may be noted that for Sn^{IV} and Pb^{IV} these octahedral radii are greater than those corresponding to tetrahedral radii (Table 7.12) by about 3 per cent.

Other covalent radii. Nickel, palladium and platinum in their bipositive state and gold in its tripositive state form four coplanar bonds using dsp^2 hybrid orbitals, directed to the corners of a square. For these elements Pauling suggested that the same radii should be used as for octahedral d^2sp^3 radii.

In molybdenite (MoS_2) and tungstenite (WS_2), the metal atom is surrounded by six sulphur atoms disposed at the corners of a right-trigonal prism. From the observed internuclear distances in these crystals the following trigonal-prism covalent radii were derived: Mo^{IV} 1·37 Å and W^{IV} 1·44 Å.

In crystalline Cu_2O and Ag_2O, each oxygen atom is surrounded by

four metal atoms disposed at the corners of a tetrahedron, while each metal atom is midway between two oxygen atoms, with which it forms two covalent bonds using the collinear sp hybrid orbitals. Here the metal–oxygen distance minus the tetrahedral radius of oxygen is thus equivalent to the linear (sp) covalent radius of the metal atom. The radius values obtained in this way are 1·18 Å for Cu^I and 1·39 Å for Ag^I. These are seen to be less than the corresponding tetrahedral radii by 0·17 Å and 0·13 Å respectively. The C—Hg and Hg—Cl distances in the linear molecule H_3C—Hg—Cl determined by microwave spectroscopy, are 2·061 Å and 2·282 Å respectively. Similarly the C—Hg and Hg—Br distances in H_3C—Hg—Br are found to be 2·074 Å and 2·406 Å respectively. Substraction of the normal covalent radius of C from the two C—Hg distances and of Cl and Br, respectively, from Hg—Cl and Hg—Br distances, gives the values 1·29, 1·30, 1·29 and 1·27 Å respectively. The average of these four values namely, 1·29 Å, is taken for the linear covalent radius of Hg^{II}. This value is seen to be 0·19 Å less than the tetrahedral radius of Hg.

7.9 Bond Order and Bond Length

The three types of bonds considered so far, — single, double, and triple bonds — are referred to as having bond numbers of 1, 2 and 3, respectively, so that the sum of the bond numbers of the bonds formed by an atom remains equal to the valence of the atom. A bond, however, will not necessarily have an integral bond number. The bond number may be fractional if the bond involves resonance. For instance, in benzene each carbon–carbon bond is a resonance hybrid to which single and double bonds contribute equally; the carbon–carbon bond, therefore, has a bond number 1.5. It might be expected that the length of a bond with bond number 1.5 could be obtained by interpolation between the lengths corresponding to bond numbers 1 and 2. This is, however, not true as shown in Fig. 7.7, where the point(*) representing the carbon–carbon distance 1·39 Å in benzene is seen to be appreciably below the smooth curve
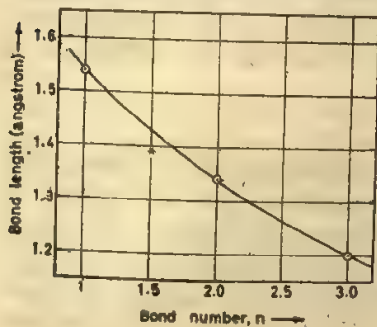
Fig. 7.7 The lengths of the single, double and triple carbon–carbon bonds plotted against bond number (After L. PAULING *The Nature of the Chemical Bond*, Cornell University Press, 1960)

which passes through the points • representing the lengths 1·54, 1·34 and 1·20 Å of pure single, double and triple carbon–carbon bonds respectively. The explanation is that resonance has stabilized the benzene structure and imparted additional strength to the carbon–carbon bond, thus reducing its length. To emphasize this change in bond length caused by resonance between two equivalent structures, Pauling represents the smooth curve in Fig. 7.7 by an equation of the form:

$$D(n') = D_1 - K \log n' \tag{7.8}$$

where D_1 is the bond length of the single bond in angstrom units, n' is the 'bond order', $D(n')$ is the corresponding bond length in angstrom units, and K is a constant. In this equation, the bond order n' is, however, equal to the bond number n for $n' = 1$, 2 and 3. If the observed carbon–carbon bond length in benzene is inserted in place of $D(n')$, Eq. (7.8) leads to $n' = 1·66$. Thus the bond order for carbon–carbon bonds in benzene is somewhat larger than the bond number, reflecting the extra resonance energy of the molecule.

In general, it can be said that when two bonds of different order contribute equally to the resonance hybrid, the resultant bond is shorter than that deduced by direct interpolation, i.e. the resultant bond is closer to the bond with higher order.

7.10 Bond Length Correction for Electronegativity Difference

While predicting the bond length from the covalent radii given in Tables 7.10–7.13, consideration has to be given to the resonance not only between covalent bonds, as in the example of benzene given above, but also between covalent and ionic bonds. The latter requirement arises because many covalent bonds are associated with considerable ionic character (see Section 7.8). The effect of this covalent–ionic resonance may be quite significant, causing a reduction of the resulting bond length by as much as 0·1 Å or more.

Schomaker and Stevenson (1941) suggested that, in general, the interatomic distance for a bond $A{-}B$ be taken equal to the sum of the covalent radii for the atoms A and B, coupled with a correction term $-0·09(x_A - x_B)$, where $(x_A - x_B)$ represents the absolute value of the difference in electronegativity of A and B, that is,

$$D(A - B) = r_A + r_B - 0·09 (x_A - x_B)$$

For some bonds (e.g. for Si—C bond) the application of the Schomaker-Stevenson correction term serves to reduce appreciably the discrepancy between predicted and observed bond lengths, while, however, for others (e.g. for the C—Cl bond) it only increases the discrepancy. According to Pauling, the length of a single bond between two atoms A and B can in most cases be assumed to be reasonably well calculated from covalent

radii r_A and r_B, as given in **Table** 7.10, by the use of the equation

$$D(A - B) = r_A + r_B - c(x_A - x_B) \qquad (7.9)$$

where $(x_A - x_B)$ represents, as stated above, the absolute value of the difference in electronegativity of A and B; and c, the Schomaker-Stevenson coefficient, has different values, depending on the atoms A and B, as given below:

All bonds involving one first row atom (i.e. B,C,N,O,F) or two such atoms $c = 0.08$ Å

Bonds of Si, P and S with a more electronegative atom but not one of
the first row $c = 0.06$ Å

Bonds of Ge, As and Se with a more electronegative atom but not one of
the first row $c = 0.04$ Å

Bonds of Sn, Sb and Te with a more electronegative atom but not one of
the first row $c = 0.02$ Å

For bonds between carbon and 5th, 6th and 7th group elements (beyond the first row), the electronegativity correction is not required. In this case, possibly a still more important effect is produced by the double-bond character.

7.11 Partial Double Bond Character

It is generally observed that a carbon atom which is adjacent to a double bond, has its remaining bonds (single or double) shorter in length than the corresponding pure bonds. For example, the C—H distance in ethylene, benzene and other molecules in which the carbon forms a double bond is about 1.085 Å, whereas in methane, ethane and other saturated hydrocarbons this distance is about 1.100 Å; the decrease in bond length due to the adjacent-double-bond effect is thus about 0.015 Å. Again, in allene, $H_2C = C = CH_2$, the carbon-carbon double bond (1.310 Å) is shorter than pure double bond (1.334 Å), the decrease being 0.024 Å. The average of these and similar other observed decreases is 0.020 Å. Thus, due to the presence of a double bond adjacent to a carbon atom, the effective radius of the latter in the formation of another double bond or two single bonds is about 0.020 Å less than the normal radius.

Similarly, bond lengths also show shortening when adjacent to a triple bond. In acetylene (H—C≡C—H) and hydrogen cyanide (H—C≡N), for example, the C—H bond is about 0.04 Å shorter than that in methane. The correction to the effective radius of carbon forming a triple bond is therefore taken to be −0.04 Å. The contraction is seen to be twice as great as for the double-bond effect.

In a conjugated system of single and double bonds, as in 1, 3-butadiene

($H_2C = CH - CH = CH_2$), the carbon-carbon single bond, being adjacent to two double bonds, would be expected to show a shortening in length by 2×0.02 Å to the value 1·504 Å. The central carbon-carbon distance in butadiene is, however, found to be still shorter, about 1·46 Å. This further decrease may be attributed to single bond-double bond resonance in butadiene molecule, due to which the central bond in the molecule has some double-bond character.

The amount of double-bond character of a bond is given by its bond number. Since bond numbers for pure single and double bonds are taken as 1 and 2, bond numbers in the range 1 to 2 represent amounts of double-bond character ranging from 0 to 100 per cent. For example, each of the six bonds in benzene has 50 per cent single-bond character and 50 per cent double-bond character, and its bond number is accordingly 1·5.

A smooth curve can be drawn by plotting carbon–carbon bond lengths against percentage of double-bond character or bond number. Bond number 1.5 and the corresponding carbon–carbon distance 1·393 Å, as observed in benzene, constitute one point on this curve. Another point is obtained from a consideration of the graphite structure. The length of each carbon–carbon bond in graphite is 1·42 Å and the bond number, as shown in the following discussion, is 1·33.

The graphite crystal is built up of layers of carbon atoms forming a hexagonal network; the layers are superimposed on each other and separated by a distance 3·40 Å [see Fig. 7.8(a)]. The distance is so large that there can be no covalent bonds between atoms of adjacent layers. It is therefore reasonable to suppose that the four valences of each carbon atom are utilized in forming bonds with its three neighbours in the same layer. The valence-bond structure of each layer molecule is thus regarded as an array of fused benzene rings, as shown in Fig. 7.8(b). However, there can be many such valence-bond structures for the layer molecule.
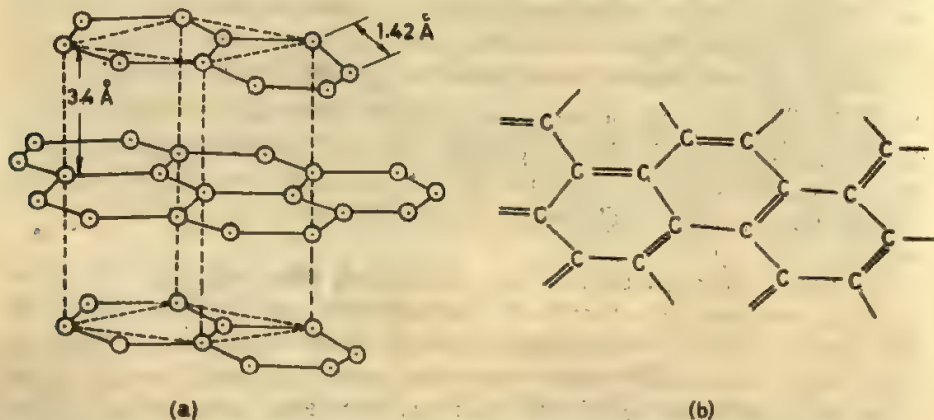
Fig. 7.8 (a) The hexagonal structure of graphite, the unit cell being shown by broken lines, (b) The structure of a graphite layer on the basis of the valence-bond treatment

Resonance among these structures makes all carbon–carbon bonds equivalent and each bond accordingly achieves one-third double-bond character (and hence bond number 1.33).

The pure double-bond distance 1·334 Å provides one end point of the curve at bond number 2. The other end point corresponds to bond number 1 and represents the pure single-bond distance. However, since the curve is for application to conjugated and aromatic systems of single bonds and double bonds, the value for the pure single-bond distance is taken to be 1·504 Å (as corrected for two adjacent double bonds). The curve through these four points is shown in Fig. 7.9. This curve could be used for obtaining information as to the type of a carbon–carbon bond from the observed value of its bond length. For example, it is found by graphical interpolation that the bond length 1·46 Å, as observed for the central carbon–carbon bond in the butadiene molecule, corresponds to about 15 per cent double-bond character.

Pauling showed that this curve can be represented by the equation,

$$D_n = D_1 - (D_1 - D_2)\frac{1·84(n-1)}{0·84n + 0·16} \tag{7.10}$$

in which D_1 and D_2 are the lengths of pure single and double bonds, and D_n is the length of a bond of intermediate type having bond number n. This equation has been used by Pauling to calculate bond lengths in hydrocarbon molecules involving resonance between carbon–carbon single and double bonds.
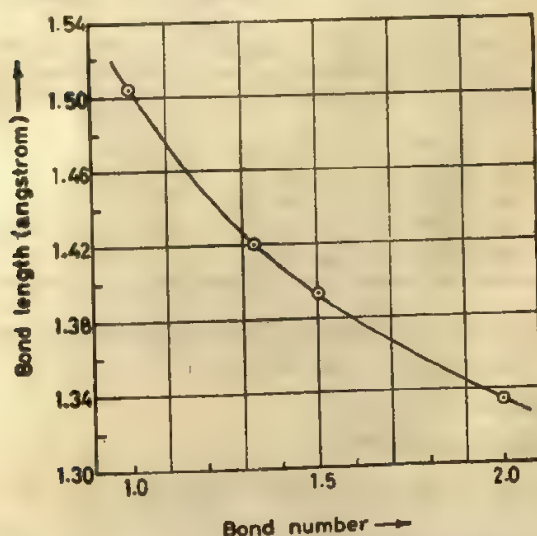
Fig. 7.9 An empirical curve relating carbon-carbon bond length with the amount of double bond character for molecules involving resonance between single and double bonds. (After L. PAULING *The Nature of the Chemical Bond*, Cornell University Press, 1960)

7.12 Bond Energies

There are evidences that the heats of formation associated with particular bonds are to a large extent additive. In many homologous series of organic compounds, for instance, the increase in heats of combustion and hence of formation per CH_2 group, is almost constant at about 160 kcal. It is then possible to assign to any linkage a definite quantity known as the *bond energy*. The bond energy, sometimes also called the heat of formation of a bond, is equal to the energy of dissociation into atoms in the case of a diatomic molecule. In the case of a polyatomic molecule in which all bonds are alike, the bond-energy value, however, represents the average of the energies required to break all the bonds and not the amount required to break just one bond in the molecule. Indeed, the latter quantity is referred to as the *bond strength;* it is obviously not the same as the bond energy. While, in general, the 'strength' of a particular bond will be dependent on its position or type in a given molecule, the bond energy is assumed to be constant. For instance, more energy is required to remove the first hydrogen atom than the other successive atoms from methane, but the bond energy refers to all the four bonds and represents an average of the four bond strengths.

The procedure for computing bond energies involves a knowledge of the heats of formation of *monatomic gases* of elements relative to their standard states (Table 7.14) and the heats of formation of molecules.

Table 7.14 Heat of Formation (kcal/mole) of Monatomic Gases of Elements from their Standard States (after Pauling)

H	52·09								
Li	37·07	C	171·70	N	113·0	O	59·16	F	18·30
Na	25·98	Si	88·04	P	75·18	S	53·25	Cl	29·01
K	21·51	Ge	78·44	As	60·64	Se	48·37	Br	26·71
Rb	20·51	Sn	72·00	Sb	60·80	Te	47·60	I	25·48
Cs	18·83	Pb	46·34	Bi	49·70				

Consider the bond H—O. Since the heats of dissociation of hydrogen and oxygen are 104·18 and 118·32 kcal/mole respectively, i.e.

$H_2 (g) \longrightarrow 2H (g)$; $\Delta H = 104·18$ kcal

$O_2 (g) \longrightarrow 2O (g)$; $\Delta H = 118·32$ kcal

and since the heat of formation of gaseous water from the *elements* is 57·80 kcal/mole, i.e.

$H_2 (g) + \frac{1}{2} O_2 (g) \longrightarrow H_2O (g)$; $\Delta H = - 57·80$ kcal
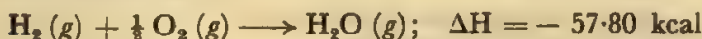
the heat of formation of gaseous water from gaseous hydrogen and oxygen *atoms* is calculated to be 221·14 kcal/mole, as shown below:

$$2H\ (g) \longrightarrow H_2\ (g)\ ; \qquad\qquad \Delta H = -\ 104 \cdot 18\ kcal$$
$$O\ (g) \longrightarrow \tfrac{1}{2}O_2\ (g)\ ; \qquad\qquad \Delta H = -\ 59 \cdot 16\ kcal$$
$$H_2\ (g) + \tfrac{1}{2}O_2\ (g) \longrightarrow H_2O\ (g)\varsigma \quad \Delta H = -\ 57 \cdot 80\ kcal$$
$$\overline{2\ H\ (g) + O\ (g) \longrightarrow H_2O\ (g)\ ; \quad \Delta H = -\ 221 \cdot 14\ kcal.}$$
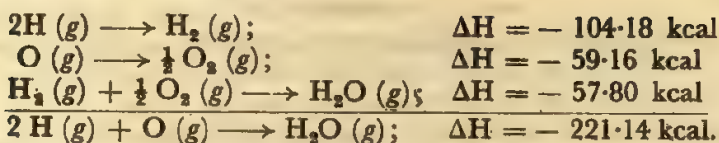
As the water molecule comprises two O—H bonds, their average, 221·14/2 or 110·57 kcal/mole, is taken as the energy of the O—H bond in the water molecule.

Values for single-bond energies representing the average of all bond strengths, as per the definition given above, can be derived for many bonds by this process, e.g. for the S—S bond from the S_8 molecule and for N—H, P—H, S—H, etc., respectively from NH_3, PH_3, H_2S, etc., molecules. These values are recorded in Table 7.15. On the other hand, the tabu-

Table 7.15 Energy Values for Single Bonds (in kcal/mole) (after Pauling)

Bond	Bond energy	Bond	Bond energy	Bond	Bond energy
H—H	104·2	C—Br	65·9	As—Cl	68·9
H—C	98·8	C—I	57·4	As—Br	56·5
H—Si	70·4	Si—Si	42·2	As—I	41·6
H—N	93·4	Si—O	88·2	Sb—Sb	30·2
H—P	76·4	Si—S	54·2	Bi—Bi	25·0
H—As	58·6	Si—F	129·3	O—O	33·2
H—O	110·6	Si—Cl	85·7	O—F	44·2
H—S	81·1	Si—Br	69·1	O—Cl	48·5
H—Se	66·1	Si—I	50·9	S—S	50·9
H—Te	57·5	Ge—Ge	37·6	S—Cl	59·7
H—F	134·6	Ge—Cl	97·5	S—Br	50·7
H—Cl	103·2	Sn—Sn	34·2	Se—Se	44·0
H—Br	87·5	N—N	38·4	Te—Te	33·0
H—I	71·4	N—F	64·5	F—F	36·6
C—C	83·1	N—Cl	47·7	Cl—F	60·6
C—Si	69·3	P—P	51·3	Cl—Cl	58·0
C—N	69·7	P—Cl	79·1	Br—Cl	52·3
C—O	84·0	P—Br	65·4	Br—Br	46·1
C—S	62·0	P—I	51·4	I—Cl	50·3
C—F	105·4	As—As	32·1	I—Br	42·5
C—Cl	78·5	As—F	111·3	I—I	36·1

lated bond-energy values for such bonds as H—H, F—F, Cl—Cl, Br—Br, I—I, H—F, H—Cl, H—Br, H—I, Cl—F, Br—Cl, I—Cl, and I—Br represent the heats of dissociation of respective diatomic molecules determined thermochemically or spectroscopically; the energy values for the bonds Si—Si and Ge—Ge, are taken as half the heats of sublimation (per g atom) of the respective crystals. This is because these crystals have the diamond structure in which each atom is tetrahedrally linked to four other similar atoms around it, so that, on the average, removal of each atom involves

breakage of $4 \times 1/2$ or 2 bonds. The molecules of P_4 and As_4 in vapour consist of regular tetrahedra, each corner of which is occupied by one atom linked to three atoms at the other three corners by covalent bonds. There are thus, six bonds in each molecule, and the energy values for P -P and As—As bonds are therefore one-sixth of the heats of formation of the molecules P_4 (g) and As_4 (g) from separated atoms. Bond energies of S—S and Se—Se bonds are one-eighth of the heats of formation of $S_8(g)$ and Se_8 (g) molecules (eight-membered rings containing eight bonds) from gaseous atoms. The energy value of the O—O bond is derived from the heat of formation of H_2O_2 (g) with the use of the O—H bond energy in H_2O. That for the N—N bond is obtained from the heat of formation of N_2H_4 (g) with the use of the N—H bond energy in NH_3.

The use of the bond-energy values of Table 7.15 rests on the fundamental assumption that the energy of a molecule, which can be represented by a single valence-bond structure, can be closely approximated by the sum of constant energy quantities corresponding to the bonds. Indeed, to a considerable extent, this assumption meets with empirical justification in the fact that for nearly all molecules the experimental heats of formation tally with the summation values of bond energies within a limit of only a few kcal/mole.

Example Calculate the heat of formation of propane from bond energies and compare with the experimental result $\Delta H_f°$ $(C_3H_8,\ g) = -24.82$ kcal/mole.
Solution The heat of dissociation of gaseous propane into gaseous atoms should be equal to
$$2D(C-C) + 8D(C-H) = 2 \times 83.1 + 8 \times 98.8$$
$$= 956.6 \text{ kcal/mole}$$

The heat of formation of gaseous propane from gaseous hydrogen and carbon atoms is therefore $\Delta H = -956.6$ kcal/mole.

The experimental value of the heat of formation of $C_3H_8(g)$ from elements in their standard states is -24.82 kcal/mole. This on addition of suitable terms from Table 7.14 leads to a value of -954.21 kcal/mole as the heat of formation from monatomic gaseous elements. The difference between calculated and experimental values is thus less than 3 kcal/mole.

Bond energies for multiple bonds can also be derived by combining single-bond energies, obtained as above, with the thermochemical data for the molecules to each of which a single valence-bond structure can be assigned unambiguously. In Table 7.16 are recorded the values of bond energies for multiple bonds derived in this way. These bond-

Table 7.16 Values of Bond Energies (kcal/mole) for Multiple Bonds (after Pauling)

Bond	Bond energy	Bond	Bond energy
C = C	147	C = O	164-174
C ≡ C	194	C = S	114
C = N	147	N ≡ N	226
C ≡ N	207-213	O = O	96

energy values can be used in the same manner as the single-bond energies considered above.

Example Calculate the heat of formation of acetylene from gaseous carbon and hydrogen atoms.

Solution The heat of dissociation of acetylene into gaseous atoms would be equal to the sum of the bond energies:

$2D(C—H) + D(C\equiv C) = 2 \times 98 \cdot 8 + 194 = 391 \cdot 6$ kcal/mole

The heat of formation is therefore $-391 \cdot 6$ kcal/mole. This result may now be compared with the experimentally determined value. The heat of formation of acetylene from elements in their standard states is $+53 \cdot 90$ kcal/mole. This on addition of suitable terms from Table $7 \cdot 14$ leads to $-393 \cdot 7$ kcal/mole as the heat of formation from gaseous atoms. The error in the above computed result is thus only 2 kcal/mole.

The bond energy values given in Tables 7.15 and 7.16 are applicable only for molecules containing atoms that show their normal valences, e.g. 4 for carbon, 3 for nitrogen and phosphorus, 2 for oxygen, and so on. Thus, for instance, one should not use the N—H bond energy for an ammonium salt, the N—O bond energy for trimethyl amine oxide, or the P—Cl bond energy for phosphorus pentachloride. Another limitation of the values in Tables 7.15 and 7.16 is that they are meant for use only in the case of bonds between atoms with zero formal charges. For instance, the values are not valid for a molecule such as $^{-}N = N - O^{+}$

7.13 The Coordinate or Dative Covalent Bond

In a normal covalent bond involving a shared electron-pair, each member atom supplies one electron; but sometimes one atom is capable of providing both electrons and then the bond is frequently called *dative* or *coordinate*, the atoms united by this bond being distinguished as donor and accepter. Though often indicated by placing an arrow directed from the donor atom to the acceptor atom, dative bonds are essentially similar to normal covalent bonds, since in both, the two electrons are most likely to be found between the nuclei.

Since in the formation of a dative or coordinate bond both the electrons come from one atom, the symmetrical sharing of these two electrons would then amount to the donor atom acquiring a formal positive charge and the acceptor atom a formal negative charge. For this reason this type of bond was sometimes described as a *semipolar* bond. It is commonly found, however, that the atom which supplies the two electrons, and as a result acquires a formal positive charge, is a strongly electronegative atom, such as oxygen or nitrogen, and consequently, the electrons are, on the average, closer to it than to other less electronegative atom. This results in a considerable reduction of the charge separation and hence in a lessening of the ionic character.

7.14   Covalent Bonds with Odd Number of Electrons

All of the molecules we have treated so far have required only electron-pair bonds. There are also examples of materials containing 1-electron and 3-electron bonds. Such examples are, however, limited in number, which testifies to the importance of electron pairing in bond formation. An important example of 1-electron bond is provided by the hydrogen molecular ion H_2^+. Although this species is observed only spectroscopically, it is associated with a bond energy of 61 kcal/mole. In terms of the VB approach the hydrogen molecular ion may be described as involving resonance between two structures in which the single electron is associated with one nucleus or the other:

H·   H$^+$ and   H$^+$ ·H
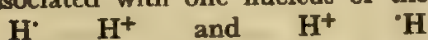
The stability of the 1-electron bond in H_2^+ relative to H plus H$^+$ stems from this resonance. Clearly, such 1-electron bonds can form only between like atoms or those of nearly equal electronegativities, since only then two resonance structures of essentially equal energies can result.

Applying similar considerations to He_2^+, we can write two structures:

He: ·He$^+$ and   He·$^+$:He
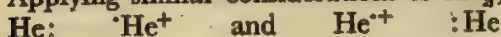
Resonance between these structures results in a lowering of the energy relative to He plus He$^+$, and thus leads to the stabilization of the bond in He_2^+, which in effect involves three electrons, i.e. He · · · He. It should be noted that here we have a pairing of electrons on one or the other nucleus but there cannot be any pairing between the nuclei because of the exclusion principle. Only one electron really plays part in the resonance phenomenon. It is, therefore, not surprising that the 1- and 3- electron bonds have approximately the same energy. The binding energies of the bonds in H_2^+ and He_2^+ are approximately 61 kcal and 58 kcal/mole respectively. Compared to this the strength of the electron-pair bond in H_2 is 109 kcal/mole. Empirically, we may say that 1- and 3-electron bonds are about half as strong as an electron-pair bond.

In view of the observed paramagnetism of oxygen, the linkage in the oxygen molecule is considered to involve a normal (electron-pair) bond and two 3-electron bonds to give the structure

:O$\vdots\vdots$O:

Such a structure would give rise to paramagnetism due to two unpaired electrons in the molecule. The binding energy of this structure would be much the same as that of the structure

:Ö = Ö:
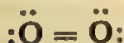
with a double bond. The double-bonded structure, however, as it contains no unpaired electrons, would be diamagnetic. A few other examples of 3-electron bonds are:

NO $:N \overset{\cdots}{=} O:$

NO_2 $:\overset{..}{O} \overset{\cdots}{=} N = \overset{..}{O}:$

OF $:\overset{..}{O} \overset{\cdots}{=} \overset{..}{F}:$

ClO_2 $:\overset{..}{O} - \overset{..}{Cl} \overset{\cdots}{=} \overset{..}{O}:$
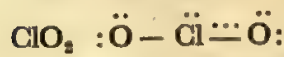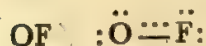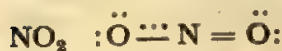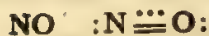
Since the 3-electron bonds arise from resonance stabilization, they can occur only between two like atoms or those differing by not much more than 0·5 in electronegativity, because only then resonance structures of nearly equal stabilities can result.

7.15 *Electron-deficient Covalent Compounds*

There are instances of compounds in which the number of valence electrons present is insufficient to account for electron-pair bonds among all the constituent atoms. A general feature of these compounds, called *electron-deficient*, is that they contain some electron-deficient atoms, having more number of stable bond orbitals than electrons in the valence shell. Boron, for example, has four orbitals in its valence shell but only three valence electrons. Other typical examples are aluminium and platinum.

Electron deficient compounds are more characteristic of the elements of the Group IIIB than those of any other group, because the Group IIIB atoms have the tendency to be 4–covalent but possess only three valence electrons. This, however, does not lead to electron deficiency in all types of compounds. For example, the trivalent halides (see later) are not electron-deficient. However, the hydrides and certain of their derivatives do require electron-deficient bonding. Thus a simple hydride of the composition BH_3 cannot be prepared, and attempts to prepare it lead only to its dimer, B_2H_6, called diborane. Similarly, the simplest hydride of gallium is Ga_2H_6 and that of aluminium is a polymer $(AlH_3)_x$. Let us consider here, for detailed examination, the case of diborane. At first sight it appears to be analogous to ethane. But if we accordingly assign the structure $H_3B—BH_3$, we run into an immediate difficulty, for it shows seven covalent bonds requiring 14 valence electrons, while there are actually 12 electrons in the molecule. Complete electron-pair bonding in the usual sense is thus impossible. The difficulty was resolved by resorting to the unusual concept of hydrogen-bridged structure shown in Fig. 7.10. The structure can be visualized as consisting of two *irregular* BH_4 tetrahedra having one edge in common. The two boron atoms and the four outer hydrogen atoms thus lie in one plane, while the *bridging* hydrogen atoms lie above and below this plane. The length
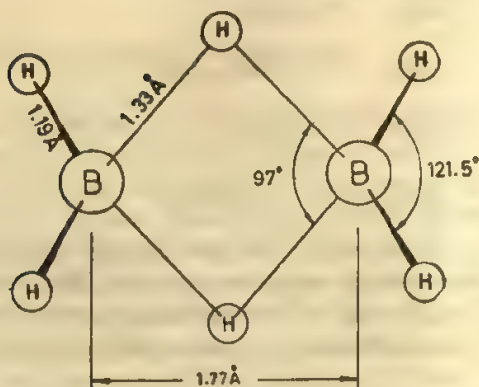
Fig. 7.10   Structure of diborane, B_2H_6

of the outer B—H bonds is 1·19 Å which is about that expected for a single
bond given by the sum of the single-bond normal covalent radii of boron
and hydrogen (Table 7.10). On the other hand, the distance between a
boron atom and a bridging hydrogen atom is considerably larger than the
expected single bond length, indicating the presence of fractional bond.

Several interpretations of the hydrogen bridge have been made. Out
of them, the more likely is perhaps the one involving resonance among
various possible structures (shown below) such as I, II (both covalent),
III and IV (both ionic):
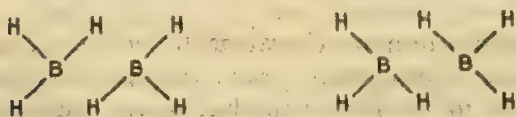
The fact that similar bridge structures are not observed among the
hydrides of the Groups VB, VIB and VIIB elements may be ascribed,
in the light of the above picture, to the presence of unshared electron
pairs that would cause repulsion between the two parts of the molecule.
However, even in the absence of unshared electron pairs it seems unlikely
that two parts of a molecule can be held together solely by resonance
stabilization involving the above four structures. Pauling has given reso-
nance formulations involving, besides these four structures, sixteen other
structures having B--B bond.

In terms of the MO viewpoint, the hydrogen bridge may be visualized as a 3-centre bond, being a special case of multicentre bonds, which may be four-, five-, six- and, in general, n-centred. Here the molecular orbitals are considered to be formed by linear combinations of the atomic orbitals of all the atoms involved in the bond. As many MOs are formed as there are combining atomic orbitals. We have already seen that the MO picture of the electron-pair covalent bond between *two* atoms requires the combination of two atomic orbitals, one on each atom, giving rise to a bonding orbital, ψ_b, and an antibonding orbital ψ_a (see Section 6.4). Now if there are three atoms each with an available orbital, the three orbitals can be combined to form three molecular orbitals, shown schematically in Fig. 7.11 (cf. Fig. 6.6). The first of these, ψ_b, which is formed from the three atomic orbitals of the same sign is the bonding MO. It leads to a continuous electron density encompassing all the three nuclei, which are thus held together. The second MO, ψ_a, which is formed from the combination of the three atomic orbitals of opposite sign, leads to a depletion of electron density in the internuclear region, and is, therefore, antibonding. The third MO, ψ_n, formed only from the orbitals of the two outer atoms which can have only negligible overlap, is very slightly antibonding and so considered to be practically non-bonding. Fig. 7.12 shows the energies of these three 3-centre MOs relative to the energies of the combining atomic orbitals. Now let us consider the filling of the MOs. The first two electrons will fill the lowest-energy bonding orbital and thus give rise to maximum bonding energy. If there were a second pair of electrons, they would occupy the non-bonding orbital and thus have little effect on bonding. In fact, two conventional electron-pair bonds between the three
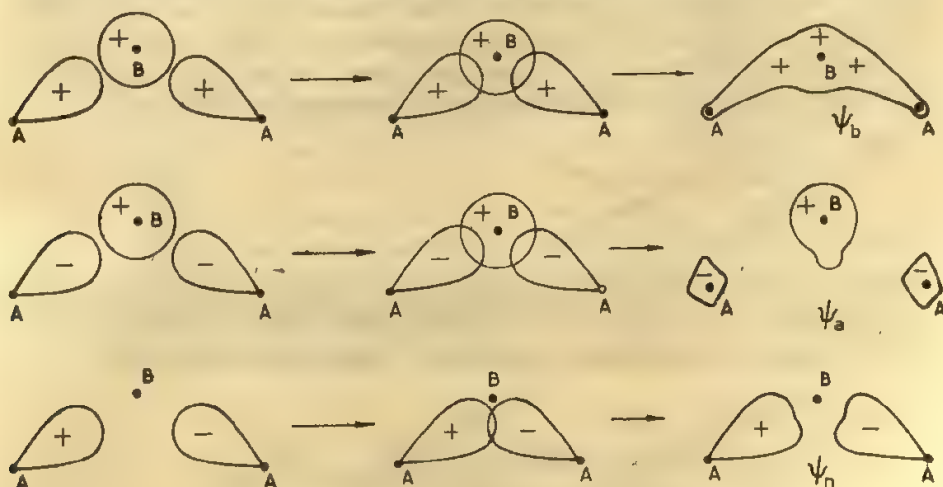
Fig. 7.11 Schematic representation of the formation of 3-centre MOs by combination of atomic orbitals
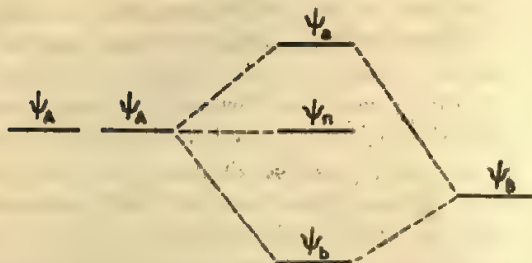
Fig. 7.12 Energy level diagram for 3-centre MOs

atoms would probably be more stable than the system involving 3-centre MOs and four electrons. Clearly, the 3-centre bonding concept is advantageous where there are three atoms but only two electrons for bonding. Let us now examine the situation in B_2H_6 in the light of this. The two boron atoms have six valence electrons and the six hydrogen atoms have six valence electrons, making a total of twelve electrons. Eight of them are used in the formation of four outer B—H bonds. Four electrons are now left: one with each boron atom and one with each of the two inner hydrogen atoms. We thus see that only two electrons are available for each of the two 3-centre (B—H—B) MO systems. As we have already seen, this situation is specially suited for 3-centre bonding. The hydrogen atom uses its $1s$ orbital, while the boron atom uses some sort of hybrid orbitals made up of s- and p-orbitals.

At this stage it is important to point out that bridged structures are not necessarily electron-deficient. A typical example is aluminium chloride, which is a dimer, Al_2Cl_6, having a bridge-type structure with tetrahedral coordination of aluminium. Electron deficiency does not exist here, since each bridging chlorine atom donates an electron pair to form a coordinate linkage with an aluminium atom thus making it 4-covalent. In view of this the structural formula is sometimes written as
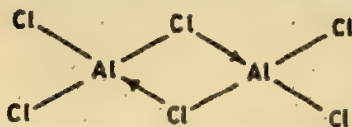
However, this representation should not be taken to indicate that the bridging bonds are not identical. The bridging bonds are, in fact, identical and this may be considered to be due to resonance of the type

The dialkyl compound, $[Al(CH_3)_2Cl]_2$, also has a halogen-bridged structure like Al_2Cl_6 with the outer halogens replaced by alkyl groups.
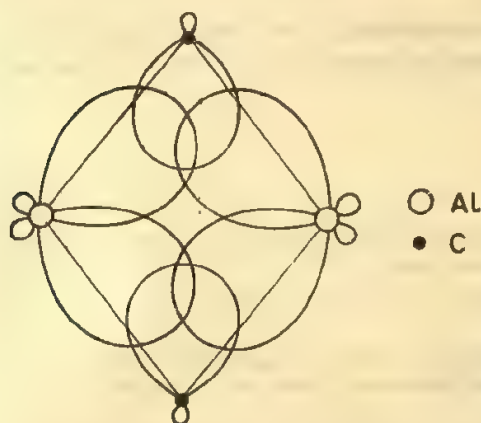
Fig. 7.13 Orbital overlaps in Al–C–Al bridging

On the other hand, the bridging in the trimethyl aluminium dimer, $[Al(CH_3)_3]_2$, is clearly of a different type. The compound is electron-deficient and the bridge-bonding must be explained in terms of delocalized 3-centre MOs as in the case of B_2H_6 and other boron hydrides. To explain the formation of the 3-centre (Al—C—Al) bonding, we assume that each aluminium atom is hybridized to give four hybrid orbitals (resembling, but not exactly, the tetrahedral sp^3 hybrids). Each aluminium atom uses two of these hybrid orbitals and two of its three electrons to form two electron-pair bonds with the outer methyl groups. The aluminium atoms are then left with two hybrid orbitals and one electron each for further bonding. The bridging methyl groups are normal methyl groups and so can be assumed to have one empty sp^3 orbital and one electron each. The situation is thus suited for 3-centre bonding. Three-centre (Al—C—Al) MOs are formed in much the same way as the (B—H—B) MOs (see Fig. 7.11). Fig. 7.13 shows a schematic representation of the overlap of the aforesaid orbitals which lead to the formation of two 3-centre (Al—C—Al) bonding orbitals each occupied by two electrons. The bridging bond angle (Al—C—Al), as found by X-ray diffraction, is 70°. Such a small value implies that, to some extent, the metal orbitals do overlap one another (Fig. 7.13), producing some direct metal–metal bonding. However, such direct bonding is probably not the dominant factor in the bridge-bonding. The structure of $[Be(CH_3)_2]_n$ also involves methyl bridges like those in $[Al(CH_3)_3]_2$. In the former, however, all methyl groups are bridging.

Suggested Reading

PAULING, L., *The Nature of the Chemical Bond*, Cornell University Press, 1960.

BROWN, G.I., *A Simple Guide to Modern Valency Theory*, Longmans Green, London, 1953.

ADDISON, W. E., *Structural Principles in Inorganic Compounds*, Longmans Green, London, 1961.

EVANS, R. C., *An Introduction to Crystal Chemistry*, Cambridge University Press, London, 1964.

DURRANT, P. J. and B. DURRANT, *Introduction to Advanced Inorganic Chemistry*, Longmans, Green, London, 1962.

Problems

7.1 Explain why the covalent bond is directional and the ionic bond is non-directional. How does this affect the arrangement of atoms in the solid?

7.2 Discuss, giving examples, which factors promote the formation of ions and of ionic compounds.

7.3 On the basis of the electronic configurations of the inert gas elements, deduce various possible electronic configurations which on ionization could attain inert gas structures. Identify the elements and the corresponding ions.

7.4 Write the electronic configurations of some ions to illustrate the inert-pair effect.

7.5 Account for the variable valency of the transition elements. What properties can be attributed to this feature?

7.6 Account for the fact that transition elements show greater tendency to form complex ions than representative elements.

7.7 Why does the ionization potential decrease from top to bottom in a Group in the periodic table and from right to left across a period.

7.8 Explain for the fact that the 2nd, 3rd, 4th, 5th and 6th ionization potentials of Li, Be, B, C and N, respectively, are disproportionately large compared to the preceding ionization potential.

7.9 The electron affinity of chlorine is exoergic while that of oxygen is endoergic. Explain.

7.10 Employ the Born-Haber cycle and use the data of Appendix 4 and Tables 7.2 and 7.14 to calculate the lattice energy of KI crystal. Given: The standard heat of formation of solid KI is —78·31 kcal/mole.

7.11 Calculate the standard heat of formation of CH_4, CCl_4 and NH_3 by the use of electronegativity values of Table 7.6.

7.12 Calculate the limiting value of the ionic radius ratio for anion-anion contact in sodium chloride-type lattice.

7.13 Listed below are the lattice constants, i.e. the lengths (in Å) of the sides of the unit cells of alkali halide crystals:

	Li+	Na+	K+
Cl⁻	5·14	5·62	6·28
Br⁻	5·50	5·96	6·58
I⁻	6·04	6·46	7·06

Given the fact that all the aforesaid halides form face-centred cubic crystals, derive a set of ionic radii for the alkali and halide ions involved. Assume that anion-anion contact occurs in lithium iodide.

7.14 Magnesium oxide has the same structure as sodium chloride. Given that the ionic radii of Mg^{+2} and O^{-2}, in angstrom units, are 0·65 and 1·40, respectively, calculate (a) the lattice constant and (b) the ionic packing factor of magnesium oxide.

7.15 Given that $\Delta H_f°$ (C_2H_5OH, g) = —56·63 kcal/mole, calculate the heat of formation of ethanol from monatomic gaseous elements using the data of Table 7·14.

7.16 Calculate the standard heat of formation of gaseous ethanol using the data of Table 7.14 and Table 7.15. Compare your answer with the value given in Problem 7.15.

7.17 Calculate the heats of combustion of gaseous CH_4, CF_4, BF_3 and B_2H_6, using data given in Tables 7.14 and 7.15. Which of these gases would you choose as fuels?

Bonding in Metals

8.1 *Introduction*

A number of characteristic physical properties, of which the high thermal and electrical conductivities and the optical opacity are obviously prominent, sharply distinguish metals from other types of solids. It is logical to infer from these properties the presence of free electrons in metallic solids. In fact, such thinking has had a profound influence in the development of electron theories of metals which started in the early years of the present century and was associated with the work of Drude, Lorentz, Sommerfeld, Fermi and Bloch. As initially proposed, the electron theory was a model for the metallic state, but with the development of the theory it turned out to be a model for the solid state in general and provided a unifying approach to broad aspects of all types of solids. These theories—classical free-electron theory, wave theory and zone theory—form a connected sequence in this development.

8.2 *Classical Free-Electron Theory*

This theory, first proposed by Drude and Lorentz, was based on the idea that high electrical and thermal conductivities of metals are due to the presence of free electrons. They postulated that, since some or all of the valence electrons (i.e. the outermost electrons of an atom) may be removed relatively easily, while the rest of the electronic population is held firmly to the nucleus, the solid metal consists, in effect, of a lattice of rigid spheres

Fig. 8.1 A schematic representation of electron 'cloud' and positive 'cores' in copper, as an example; the attraction between the positive 'cores' and the free electrons constitutes the metallic bond
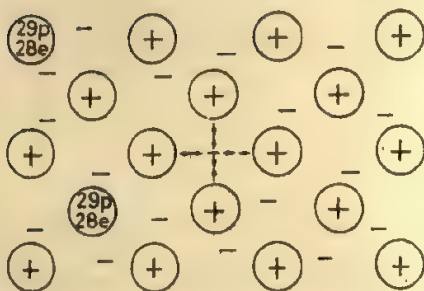
permeated by a gas of the valence electrons (Fig. 8.1). They further postulated that these electrons are free to move throughout the volume of the metal without any restriction; that is, within the metal the valence electrons move in a perfectly uniform electrostatic field. However, the fact that the electrons under normal circumstances do not escape from the metal, indicates that a potential gradient exists at the surface to keep them inside the metal.

Though the Drude-Lorentz theory gives a greatly simplified picture, it does, nevertheless, afford a useful explanation for many of the properties of metals, as briefly enumerated below.

(*i*)   The coherency of the metal structure may be regarded as stemming from the attraction between the positive ions and the electron gas. That a metallic object displays resistance to complete fracture or disruption, despite suffering deformation relatively easily, may be accounted for by the existence of these attractive forces.

(*ii*).   This picture of the coherence of a metal, furthermore, confers on the metallic bond a freedom from spatial or numerical limitations, thus sharply distinguishing it from both covalent and ionic bonds. While in a covalent structure the bonds associated with one atom are severely limited by the number of bonding electrons and by definite directional characteristics, in an ionic crystal, on the other hand, the limitations on the types of structure are imposed by the demands of electrical neutrality. In metallic systems, however, none of these limiting factors arises; here the bonds from any one atom are to be regarded as spherically distributed and consequently as being capable of holding as many neighbours as can be packed around the atom concerned. The structure of a metal would, therefore, be expected to be dictated by geometrical considerations alone. And this seems to be generally the case, since many metallic elements are known to possess one or other of two close-packed structures, which are, indeed, the representatives of the geometrically most compact arrangement of spheres in space. The comparatively high densities of metal are thus immediately accounted for by this picture of the metallic bond. The non-directional characteristics of the metallic bond, moreover, may be held to be responsible for the remarkable mechanical properties of metals,

such as ductility, malleability and flow upon application of stress.

(*iii*)   Since free electrons are free to move in an electrical field and can transfer thermal energy from a high to a low temperature level, they give the metal its characteristically high electrical and thermal conductivities.

8.3   *Wave Theory and Zone Theory of Metals*

The development of quantum mechanics and the enunciation of the Pauli exclusion principle led to the modification of the Drude-Lorentz theory by Sommerfeld. He retained the concept of free electrons moving in a uniform potential within the metal as in the Drude-Lorentz theory, but treated the electrons as obeying the laws of quantum theory instead of those of classical mechanics. A further modification was later introduced by postulating that the potential field inside the metal is not uniform but, instead, the field experienced by a moving free electron varies periodically with the repeated pattern of positive ions in a crystal. These modifications led to this picture of the metallic state: Valence electrons of the atoms within a certain piece of metal constitute a single system of electrons common to the entire piece. They occupy a large number of discrete energy states each of which can hold no more than two electrons. These energy states are very closely spaced so that the resulting band (also called *Brillouin zone*) can, in effect, be regarded as a continuous spread of allowable energies. The electrons in the upper energy levels in these bands or zones may be transferred from one energy state to another without expenditure of large amounts of energy. It is because of this that some (but not all) electrons within the metal are comparatively mobile.

8.4   *Molecular Orbital Approach*

The band theory or zone theory, as we have noted above, is based on the wave-mechanical treatment of the motion of electrons in a periodic field. However, an alternative way of developing the concept of energy bands is by using the molecular orbital (MO) approach. This will now be presented.

We have already seen (in Chapter 3) that isolated atoms in their normal state have a certain complement of electrons, each of which is character-ized by a set of four quantum numbers. These are: principal quantum number, $n = 1, 2, 3, 4, \ldots\ldots$; azimuthal quantum number, $l = 0, 1, 2, 3, \ldots\ldots (n-1)$, corresponding to the designations $s, p, d, f, \ldots\ldots$, etc.; magnetic quantum number, $m_l = l, (l-1), \ldots 0 \ldots, (-l+1), -l$; and spin quantum number, m_s, which can have two values, viz. $1/2$ and $-1/2$ for each different set of three quantum numbers n, l and m_l. According to the Pauli exclusion principle, no two electrons in any

particular atom can have the same set of four quantum numbers, and so an energy state defined by a set of three quantum numbers (n, l and m_l) can be occupied by only two electrons which however differ in the fourth quantum number, ($+$) or ($-$) spin. In an isolated atom these electronic energy states are discrete. The situation however changes if we bring a pair of atoms near one another so that their outermost electron orbitals overlap.

Consider, for example, two isolated hydrogen atoms; each atom has a single electron in the $1s$ energy state. When the two atoms are brought together there are formed, according to the molecular orbital theory, a more stable σ_s molecular orbital and a less stable σ_s^* molecular orbital. The important point is that when two atoms are brought together, for each energy state of the isolated atom there are formed a more stable (lower energy) state and a less stable (higher energy) state. Thus when N atoms are brought together, N new energy states are formed for each energy state in an isolated atom. Moreover, it is an essential feature of the molecular orbital theory that the electrons concerned in inter-atomic bonding are not to be associated with individual atoms, but that they exist in molecular orbitals embracing all the atoms involved. In the case of benzene, for example, we have seen (Section 6.10) that some of the electrons occupy delocalized π molecular orbitals that extend over the whole molecule. Extending the above concepts to a crystalline solid (whether metal or not), which consists of myriad atoms brought together into the solid state, we may regard that the valence electrons of the atoms constitute a single system of electrons common to the entire crystal and that in place of each precisely defined energy level of an individual atom the entire crystal now possesses a *band of energy* made of a very large number of separate levels. The energy levels in a band are therefore very close together, so that the band can in effect be regarded as a continuous spread of allowable energies. The energy bands are therefore the zones discussed earlier.

Consider solid aluminium as a particular example to illustrate the above viewpoint. The electronic configuration of an isolated aluminium atom is $1s^2 2s^2 2p^6 3s^2 3p^1$, and accordingly, the energy level pattern for a single atom can be represented schematically as in Fig. 8.2. The $3s$ electrons of
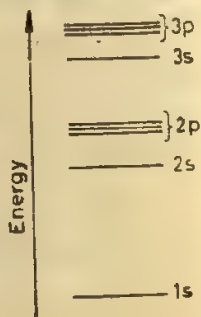
Fig. 8.2 Schematic energy level pattern for an isolated atom. Each energy state can accommodate only two electrons. For aluminium all the states up to the $3s$ level are full, while there is only one electron in the $3p$ level

all the individual atoms have the same energy, and so do the 3*p* electrons. But as an assembly of atoms is (imagined to be) brought closer and closer together, interaction of the 3*s* electrons takes place and new energy states (as many as there are atoms) are established which are distributed over a quasi-continuous range of energies or an *energy band*. Since on account of the Pauli exclusion principle at most only two electrons (of opposite sign) can occupy the same energy state, the 3*s* electrons are now spread over a range of energies in the energy band. The closer the approach of the atoms the broader the band becomes, as indicated schematically in Fig. 8.3. The 3*p* levels in an isolated atom are only slightly higher than the 3*s* level. On bringing the atoms closer, the 3*p* levels, like the 3*s* level, spread out forming a band. However, the core electron levels never actually form bands, since the core electrons (i.e. the non-valence electrons), being too closely associated with their nuclei, do not interact significantly at any realizable internuclear distance.

A band may be symmetrically above and below the value for the corresponding energy level of the isolated atom; or it may have levels which are predominantly above the isolated level or below that level.
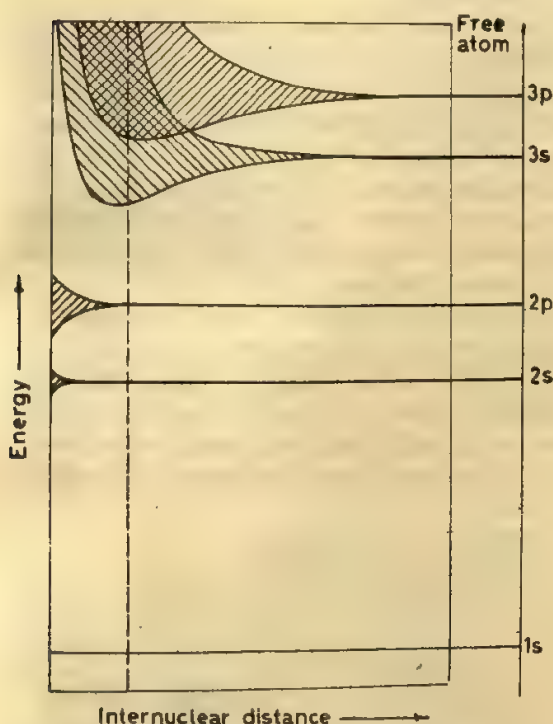
Fig. 8.3 Schematic representation of the spreading of the energy levels of isolated aluminium atoms as the atoms condense to form a crystal. The broken line represents the actual internuclear distance in the solid

The raised levels of a band are said to be promoted and the lowered levels to be depressed. The average energies in the $3p$ and $3s$ bands at first drop below the $3p$ and $3s$ atomic levels, respectively, implying attractive forces. The equilibrium internuclear distance in the solid (as indicated by the dashed line in Fig. 8.3) corresponds to a situation of minimum average energy. If the internuclear distance is continuously decreased, however, all levels will eventually be promoted because of the repulsion forces setting in.

The energy bands may overlap as shown in Fig. 8.3, so that electrons may be exchanged between two or more bands within the overlap region. In such a case, it is impossible to identify the electrons, for example, in solid aluminium as $3s$ or $3p$, and the true state of affairs is better represented as a 'hybrid'. This is another way of describing the phenomenon of hybridization. This emphasizes that when atoms are closely associated as in the solid state, the configurations of the outermost electrons may be quite different from those given in Appendix 2 which are applicable only to isolated atoms in their ground states. This situation is particularly true of the transition metals, in which electron exchange between several bands frequently occurs in the solid state.

The energy bands in a solid, as we have seen, correspond to the energy levels in an isolated atom. An electron in a solid can thus have only those energies that fall within an energy band. Some energy bands in a solid may overlap, as in Fig. 8.3, and in such a case there is then a continuous distribution of allowable energies for its electrons. In other solids, the bands may not overlap, and the gaps between the bands then represent energies which their electrons cannot possess. Such gaps are therefore called *forbidden bands*, and correspond to ranges of forbidden energies that sometimes occur separating successive Brillouin zones.

The energy-band structure as revealed by the E versus interatomic distance graph can be conveniently represented by a bar graph. Fig. 8.4, for example, shows the valence energy band which is characteristic of alkali metals. As has been already shown, a band contains as many energy states as there are atoms in the solid, and each state in the band, like each state in the atom, is able to contain two electrons. Since alkali
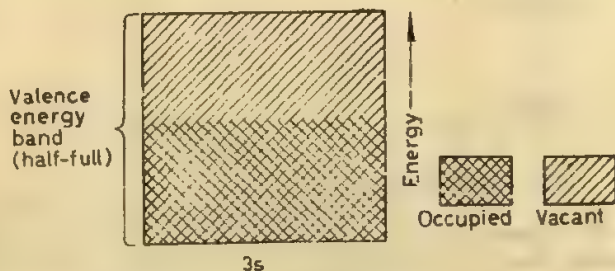
Fig. 8.4 The band structure for sodium

metals have' only one valence electron per atom, their energy bands are only half-full. Applying these arguments to alkaline earth metals, it would appear, since there are now two valence electrons per atom, that the first valence band (e.g. the 3s band in magnesium) would be just filled. However, in these metals it happens that the second valence band (e.g. the 3p band in magnesium) overlaps the first valence band, and in consequence, some electrons overflow into levels in the second band with the result that neither of the bands is completely full. This is shown in Fig. 8.5. (The bands are displaced laterally for clarity.) Fig. 8.6 shows the energy-band structure for aluminium. Here also the first band (i.e. the 3s band) partly overlaps with the second band (i.e. the 3p band), but there being three valence electrons per atom, the first band is completely filled, while there are many vacant levels in the second band. The group IV elements (C, Si, Ge, Sn), with four valence electrons per atom, have no vacant levels in the first two bands, and here the adjacent bands do not overlap,
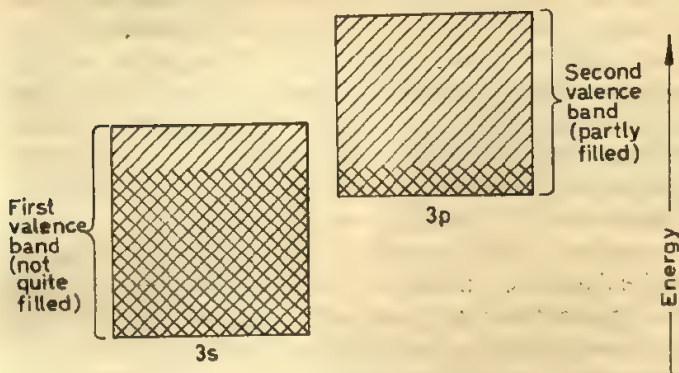
Fig. 8.5 The band structure for magnesium. (The bands are shown displaced laterally for clarity.)
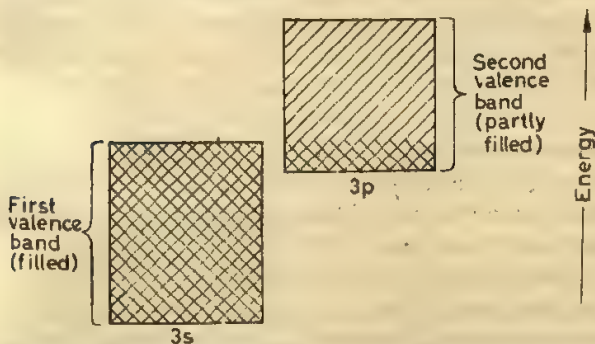
Fig. 8.6 The band structure for aluminium. (The bands are displaced laterally for clarity.)

Empty band

Energy gap (6eV)

Filled band
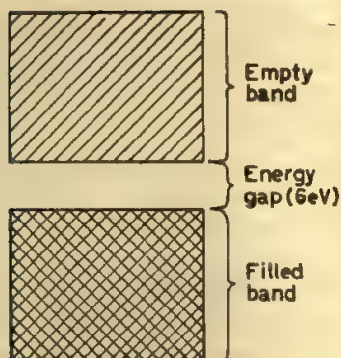
Fig. 8.7 The band structure for diamond

so that energy gaps are present (Fig. 8.7). The size of the energy gap varies from material to material, and so also the property of electrical conduction.

An essential condition for high electrical conductivity is that there should be filled levels and vacant levels within the same energy band or zone, so that the outer electrons can be energized by small electrical fields. This condition is obviously satisfied in the case of common metals whose band structures have been discussed above. Because of the presence of filled bands and energy gaps, the Group IV elements have lower conductivities (and thus high resistivities). The resistivity decreases in the order: carbon (diamond), silicon, germanium and grey tin, and the difference in resistivity is directly associated with the size of the energy gap which also decreases in the above order. If the energy gap is only a few kT (1 kT = 0·025 eV at 25°C), sufficient number of electrons can be raised by thermal energy to the empty levels in a higher energy band across the energy gap to provide semiconduction. Pure materials with this characteristic are called intrinsic semiconductors. In impurity semiconductors, known as extrinsic semiconductors, the impurities provide intermediate energy levels (electron *donor* levels or electron *acceptor* levels) in which electrons can reside, so that even though the energy gap as such may be quite great, the energy needed to activate electrons (from the donor levels to the next higher band or from the filled valence band to the acceptor levels lying closely above it) for conduction is not much.

Band structure of transition metals. The transition metals exhibit relatively large electronic specific heat and low electrical and thermal conductivities as compared to other metals. This behaviour can be traced to the respective band structures. As shown in Fig. 3.6 for isolated atoms, the *d* levels in transition metals actually lie close to or below the *s* levels. As the isolated atoms are (imagined to be) brought together to form the solid state, both the *s*- and *d*- levels spread out to form bands, the former, however, more markedly than the latter [Fig. 8.8(*a*)]. Moreover, there are only two electrons per atom possible in the *s* band, whereas the *d* band can
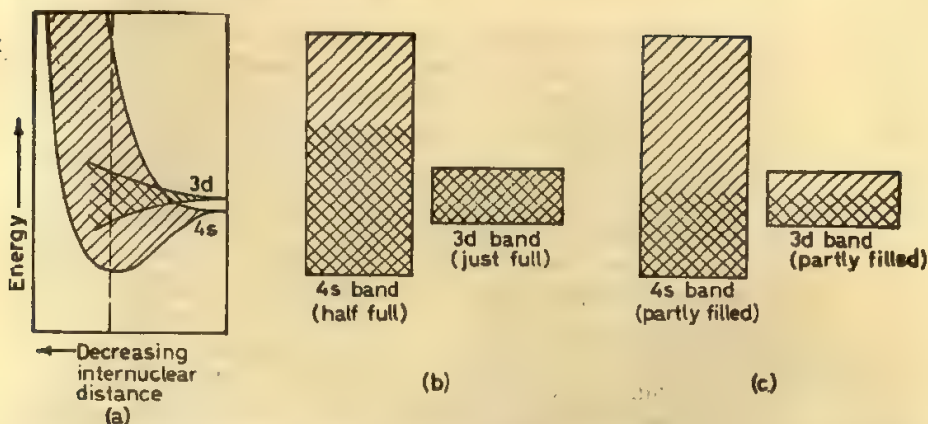
Fig. 8.8 (a) Broadening of 4s and 3d bands in transition metals of the iron group. (b) The band structure for copper. (c) The band structure for iron.

contain ten electrons per atom. The density of energy states is, in consequence, higher in the d band than in the s band. Since the s- and d-bands overlap, there occurs hybridization between the s- and d-orbitals and so both s- and d-electrons are valence electrons. In the case of copper, as shown schematically in Fig. 8.8(b), the 3d band is completely filled, but the 4s band is half-filled, since there is only one s electron per atom. Similarly in silver and gold the 4d and 5d bands are completely filled, and the 5s and 6s bands are half-filled. The elements copper, silver and gold are, therefore, good conductors. The transition elements preceding these have less than the full complement of ten electrons in the d state. For example, the electronic configurations (omitting the inner electrons) of the most important metals, Fe, Co and Ni, preceding Cu are $3d^6 4s^2$, $3d^7 4s^2$, and $3d^8 4s^2$ respectively. Since in the solid state, the s- and d-bands are spread out into overlapping bands, the available s- and d-electrons divide themselves between the two bands in a way that depends on the details of the band structure. Thus, in contrast to the electronic structures for the isolated atoms given above, those for solid iron, solid cobalt, and solid nickel are $3d^{7 \cdot 8} 4s^{0 \cdot 2}$, $3d^{8 \cdot 3} 4s^{0 \cdot 7}$, $3d^{9 \cdot 4} 4s^{0 \cdot 6}$ respectively. There are therefore vacancies or 'holes' in the d band, e.g. 2.2 'holes' in the d band of solid iron [Fig. 8.8(c)]. Vacancies also exist in the s band, and these vacancies plus those in the d band permit increased possibilities for energy transformations among the s- and d-electrons. Because of the d–s electronic energy transitions, the transition elements are characterized by relatively high electronic specific heat and low electrical and thermal conductivity as compared to the non-transition elements.

Paramagnetism is associated with unoccupied levels in the d band, and the amount of such unoccupied levels is taken as being equal to the saturation intensity of magnetization in Bohr magnetons. Since the 3d band in copper is completely filled, copper is expected to be diamagnetic,

as found. The saturation magnetization of nickel corresponds to 0.6 Bohr magneton per atom. The number of electron vacancies in the $3d$ band is accordingly 0.6 per atom. There are, therefore, $(10-0.6)$ or 9.4 d-electrons and $2-(9.4-8)$ or 0.6 s-electrons, so that the electronic structure of solid nickel is $3d^{9.4} 4s^{0.6}$. Similarly, in cobalt and iron the number of electron vacancies in the $3d$ band are 1.7 and 2.2 respectively. The number of s-electrons in cobalt is hence 0.7, and in iron 0.2. Alloying studies furnish an experimental check of the validity of this concept. In copper-nickel alloys, for instance, the components form a complete series of solid solutions. The progressive substitution of nickel (At. No. 28) by copper (At. No. 29) therefore essentially consists in addition of valence electrons to the crystal lattice. These electrons, for energetic reasons, go mostly to the d band so long as it has 'holes' or electron vacancies to be filled up. In accordance with this, the saturation magnetic moment of the ferromagnetic alloys of nickel and copper does fall linearly with increasing copper content in the alloy, and may be extrapolated to zero at about 60 atomic per cent of copper. With this composition, the valency electrons from the copper have filled the 0.6 electron vacancies per atom of nickel in the $3d$ band, so that the alloy is non-magnetic. Similar studies of other alloys of nickel show, for example, that the saturation moment is decreased by 2, 3 and 4 Bohr magnetons per atom for each atom addition of Zn, Al and Sn, respectively to nickel. Alloying with cobalt or iron, however, increases the number of holes in the d band, and the saturation moment thus increases.

8.5 Valence Bond Approach

An alternative view of the metallic bond, on the basis of the valence bond theory, was developed principally by Pauling. It treats metallic bonding as being essentially covalent in origin and pictures the metallic structure as involving resonance of electron-pair bonds between each atom and its nearest neighbours.

It is known that, in the gas phase, certain monovalent metals (lithium, for example) form diatomic molecules which presumably consist of two atoms held together by a covalent electron-pair bond. In terms of the VB theory, such bonds are also assumed to operate between atoms in the solid state, and since the number of valence electrons available (lithium, for example, has only one valence electron per atom) is inadequate for formation of electron-pair bonds between each atom and all its neighbours (eight in lithium), resonance is assumed to take place throughout the solid. Considering lithium as an example, if each atom retains its single valence electron, the resonance of pairs of bonds must be assumed to be synchronized throughout the solid, which, in two dimensions, may be represented as:

$$\text{Li} \overline{\quad\quad} \text{Li} \quad\quad \text{Li} \quad\quad \text{Li}$$
$$\longleftrightarrow \quad | \quad\quad |$$
$$\text{Li} \overline{\quad\quad} \text{Li} \quad\quad \text{Li} \quad\quad \text{Li}$$
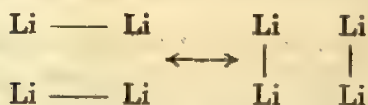
However, the stabilization through this type of resonance would be relatively small. If we assume unsynchronized resonance between arrangements in which ions are also involved, such as

$$\text{Li} \overline{\quad\quad} \text{Li} \quad\quad \text{Li} \overline{\quad\quad} \text{Li}^-$$
$$\longleftrightarrow \quad\quad |$$
$$\text{Li} \overline{\quad\quad} \text{Li} \quad\quad \text{Li}^+ \quad\quad \text{Li}$$
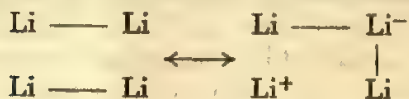
a much greater stability will result because far more numerous structures will be possible through such resonance. This process, however, requires the presence of a low-energy vacant orbital on the lithium atom to receive an extra electron to form the Li^- ion. We find that this condition is satisfied, for in the lithium atom there are three vacant $2p$ orbitals which are energetically only slightly above the $2s$ orbital, so that an electron from the $2s$ orbital of one atom can be easily transferred to a vacant $2p$ orbital of another atom to form Li^- ion with the structure $1s^2 2s^1 2p^1$.

Metallic conductivity. An important and characteristic property of metals is their high conductivity. As in the molecular orbital theory, so also in the valence-bond theory, the essential requirement for metallic conduction is the presence of vacant orbitals, of energy very close to that of the occupied orbitals, to accept conductivity electrons. These orbitals are termed 'metallic' orbitals. Therefore, the requirement, in terms of the VB theory of metals, for the existence of a conducting metallic structure is that there shall be a sufficiency of orbitals, energetically not very different from the outermost occupied orbitals, to permit formation of resonating covalent bonds, and in addition, one or more vacant orbitals to receive conductivity electrons. Let us examine whether these conditions are satisfied in the example of lithium given above. The three vacant $2p$ orbitals in lithium are of energy very close to the $2s$ orbital occupied by the valency electron. While the $2s$ orbital and one of the $2p$ orbitals (in the Li^- ion) are available for the formation of two covalent bonds, the remaining two $2p$ orbitals which are vacant can act as metallic orbitals and contribute to metallic conduction.

Cohesion energy. Metals are characterized by high cohesion energy, much higher than in molecular crystals. This is easily explained by the VB theory. Since in any finite crystal of metal there is an extremely large number of resonance structures, the resonance energy and hence the cohesion energy would be expected to be large.

Cohesion energies of metals are found to be a periodic function of the atomic number. Considering, for instance, the 18-membered periods, it is observed that the cohesion energy increases to a maximum in the

region of the vanadium or chromium groups, drops to a minimum with the zinc group and then again increases. This trend is in agreement with the VB treatment of the 18-membered periods. Thus since the alkaline earths, with two valence electrons per atoms, can form two bonds per atom in any resonance structure, they have a larger cohesion energy than the alkali metals having only one valence electron per atom. This trend continues as the number of valence electrons increases, until sufficient number of electrons become available to doubly fill the *d* orbitals, thereby preventing their use in bond formation — a situation which is reflected in decreasing cohesion energy. The cohesion energy increases again when the *p* orbitals are occupied by unpaired electrons.

Metallic radii. The VB theory of metals has been successfully applied in interpreting atomic radii in metallic systems in relation to those observed in covalent systems. That there should be a close relationship between the two is understandable in terms of the VB theory, since it considers the metallic bond as being essentially covalent in origin.

Distribution of metallic properties. The VB theory of metals gives us a clear picture of the distribution of metallic and non-metallic properties among the elements of the periodic table. Considering first the second and third periods, namely lithium to neon and sodium to argon, we find that only four orbitals (one *s* and three *p*) are available for bond formation, and consequently, if four or more valence electrons are present it will be possible for all the orbitals to be occupied by pairs of electrons through bond formation, as in diamond and silicon crystals, or in molecules of nitrogen, oxygen, fluorine, etc. It is therefore understandable that the metallic properties observed in these two periods are confined to the elements of the first three groups.

Next, as we move to the long periods, the number of orbitals available for bond formation increases to nine, because there are now five *d* orbitals in the penultimate shell differing little in energy from the one *s*- and three *p*-orbitals of the outermost shell. It is, however, the distribution of the available electrons among these nine orbitals that determines the properties of any particular element. Consider, for instance, the element zinc in the first long period. The 12 electrons in the outer group of orbitals, namely, 3*d*, 4*s* and 4*p*, may be distributed differently to give three configurations, say Zn_A, Zn_B and Zn_C, as shown in Fig. 8.9. (Each arrow in the diagram represents an electron.) It is seen that while Zn_A has no wholly vacant 'metallic' orbitals and its configuration corresponds to a purely covalent non-metallic structure of covalency 6, both Zn_B and Zn_C, however, possess vacant metallic orbitals to permit unsynchronized resonance. Assuming that each of these three configurations contributes to the actual structure of zinc, we get an explanation for the fact that zinc does not have all the characteristics of a truly metallic element; its structure, for instance, is not a truly close-packed one.

Fig. 8.9 Three possible electronic configurations for zinc

Fig. 8.10 Two possible electronic configurations for tin

Let us now consider the case of tin, a *B* sub-group element in the second long period. Two possible configurations shown in Fig. 8.10 may be written for this atom. Sn_A with no vacant metallic orbitals corresponds to a purely covalent non-metallic structure of covalency 4, and by analogy with the configuration of carbon it would be expected to adopt the diamond structure. The fact that grey tin (an allotropic modification of tin, stable below 18°C) is an insulator having the same structure as diamond suggests that its configuration corresponds to Sn_A. The alternative configuration, Sn_B, has two orbitals available for covalent bond formation and there is also one vacant metallic orbital to confer metallic properties. White tin, which is the common form of tin, stable above 18°C, has metallic properties but does not have the close-packed structure of metals. This suggests that both Sn_A and Sn_B contribute to the actual structure of white tin.

Before we consider the application of the VB treatment to transition metal structures, we must introduce the idea that all singly-occupied orbitals need not be bonding orbitals. Thus in the *d* shell there may occur some unpaired electrons which do not take part in bonding. These non-bonding unpaired electrons are important as they contribute magnetic dipole moment, and thus confer paramagnetic properties on the structure. On the other hand, a structure in which all the electrons are paired does not have permanent magnetic dipole moment and is therefore diamagnetic. Let us consider the transition metal nickel as an example. We can formulate two configurations for it, shown as Ni_A and Ni_B in Fig. 8.11, where a dotted arrow represents an unpaired electron in a non-bonding orbital. Having no metallic orbital, Ni_A corresponds to a purely covalent non-metallic structure of covalency 6; but the presence of two singly-occupied non-bonding orbitals renders it paramagnetic. Ni_B, on the other hand, possesses a vacant metallic orbital and is therefore metallic, but the absence

	3d	4s	4p	Covalency	No of metallic orbitals
Ni$_A$	⇅ ↿ ⇅ ↿ ⇅	↿	↿ ↿ ↿	6	0
Ni$_B$	⇅ ⇅ ↿ ↿ ↿	↿	↿ ↿	6	1

Fig. 8.11 Two possible electronic configurations for nickel

of singly-occupied non-bonding orbitals makes it diamagnetic. That nickel is a paramagnetic metal indicates that the actual structure is a combination of both the configurations, while the magnitude of the observed paramagnetism is a measure of their relative contributions.

It is apparent from the above theories on the binding in metals that the metallic bond partakes of the characteristics of both ionic and covalent bonds but is at the same time distinct from each. Like covalent and ionic bonds, the metallic bond also constitutes a type of primary bond, but is also perhaps the least understood of all the primary bond types. There are many bonds which do not strictly belong to any of the three types but are intermediate between truly ionic and truly covalent bonds, ionic and metallic bonds, or between covalent and metallic bonds.

Suggested Reading

RAYNOR, G. V., *An Introduction to the Electronic Theory of Metals*, Institute of Metals, London, 1949.

HUME-ROTHERY, W., *Atomic Theory for Students of Metallurgy*, Institute of Metals, London, 1952.

COTTRELL, A. H., *Theoretical Structural Metallurgy*, St. Martin's Press, New York, 1955.

SEITZ, F., *The Modern Theory of Solids*, McGrawHill, New York, 1943.

PAULING, L., *The Nature of the Chemical Bond*, Cornell University Press, N.Y., 1960.

MOTT, N. F. and H. Jones, *The Theory of the Properties of Metals and Alloys*, Clarendon Press, Oxford, 1936.

Problems

8.1 How does the metallic bond differ from truly covalent and ionic bonds?

8.2 Explain why the metallic bond is non-directional. How does this affect the structural arrangement of atoms?

8.3 Account for the ductility of metals in contrast to brittleness of glass.

8.4 Assuming that the valence electrons are free and they obey kinetic laws, as on the classical free-electron theory, calculate the electronic contribution to heat capacity of metals.

8.5 Calculate the total number of energy states needed to accommodate the valence electrons in a cc of silver.

8.6 How do you explain from the zone theory that the free electrons in a metal make very little contribution to its heat capacity?

8.7 Account for the fact that resistivity of metals increases with temperature whereas that for semiconductors and insulators decreases with temperature.

8.8 How do you account for low electrical and thermal conductivity of the transition metals as compared to other metals?

8.9 How can the metallic and non-metallic behaviour of white tin and grey tin be explained?

8.10 The saturation magnetization of iron corresponds to 2.2 Bohr magnetons. Deduce the electronic configuration of solid iron and compare with that of solid copper which is diamagnetic. Which of the two metals will have a higher electrical and thermal conductivity?

Chapter 9

Secondary Bond Forces

9.1 Introduction

While the atoms in a molecule are held together by primary bonds, there are still other forces which act between molecules. These intermolecular forces are generally known as secondary bond forces. Though not of great importance in the formation of stable chemical compounds, these forces are responsible for the aggregation of molecules into solid and liquid phases. The first quantitative statements about intermolecular forces were made by van der Waals in his studies of equation of state for real gases. Intermolecular forces are, therefore, frequently called *van der Waals forces*.

9.2 Chemical Dipoles

Many combinations are known which result from electrostatic attractions but are not related to electron transfer or sharing. These, however, invariably involve chemical dipoles.

A chemical dipole arises when there exists an unequal charge distribution between two atoms of a molecule, the inequality being caused by the differences in the electronegativities of the constituent atoms. A dipole may be a diatomic molecule or an angular polyatomic molecule; in either case, it is, in effect, a non-ionic entity, one end of which bears a positive or a negative charge with respect to the other. The term *dipole moment* (μ) then refers to the product of this charge and the distance

between the charge centres. Having magnitudes of the order of 10^{-18} esu (1 debye or $1D = 1 \times 10^{-18}$ esu), dipole moments are expressed in debye units.

The relation between the numerical magnitude of dipole moments of simple molecules such as those of the hydrogen halides and electronegativity of the halogens has been emphasized earlier in Section 7.7. A polyatomic molecule, however, can have a zero dipole moment even when its individual bonds possess dipole moments The example of carbon tetrachloride has already been cited. Another example is carbon dioxide which has zero dipole moment, notwithstanding that carbon and oxygen differ markedly in electronegativity. Each C—O bond possesses a dipole moment because of the substantial difference in electronegativity. But since the CO_2 molecule is linear (O—C—O), the individual C—O dipoles oppose and neutralize each other with the result that the net dipole moment of the molecule is zero. On the other hand, since the molecule H_2O is angular in arrangement, the individual O—H dipoles cannot neutralize each other and the molecule thus has a net dipole moment. It is of the order of 1.71–1.97×10^{-18} esu.

9.3 Dipole Attractions

The existence of dipoles enables apparently neutral molecules to attract other such molecules or various ions, leading to combinations which are often apparently stoichiometric. Some such attractions are described below.

Between dipole and dipole. Bearing opposite charges at the ends, dipoles will obviously attract each other. Though not large, these attractions are, however, of sufficient magnitude to cause alignment of molecular particles as in many associated liquids of the polar type and are manifested in profound alteration of physical properties. The hydrogen bond is a familiar example of this type of attraction. It is described in greater detail in Section 9.4.

Between ion and dipole. This kind of attraction is responsible for the solvation of ions by polar solvents and the dissolution of ionic substances in such solvents. It also probably plays a part in the formation of many coordination compounds.

Between ion and induced dipole. Dipoles may also arise due to induction by ions. Thus, when a strongly positive or strongly negative ion is brought in the vicinity of a molecule in which the outer electrons are far from the positive nucleus, the electronic structure of the molecule is distorted with the result that an induced dipole is formed, which is then

attracted to the ion. Certain complex ions are possibly formed in this way. For instance, the formation of the tri-iodide ion by the reaction

$$I^- + I_2 \rightleftharpoons I_3^-$$
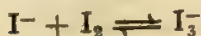
is apparently due to polarization of the iodine molecule by the iodide ion.

Between dipole and induced dipole. Just as ions induce dipoles in molecules having easily deformable electronic structure, so do strong dipoles. The attractive forces arising in the latter cases would, however, be weaker than those associated with ion-induced dipoles. The formation of hydrates of inert gas elements may be attributed to this type of attraction.

Between mutually induced dipoles. Such attractions, though extremely weak, do exist between certain neutral atoms or molecules, as is apparently manifested in the liquefaction of symmetric molecules and inert gas elements at sufficiently low temperatures. These attractions are discussed in Section 9.5.

9.4. The Hydrogen Bond

Under certain conditions an atom of hydrogen is attracted simultaneously to two (more electronegative) atoms, instead of one, so that it may be considered to be acting as a bridge or bond between them. This type of bond in which a hydrogen atom is associated with two other atoms is called the *hydrogen bond.*

Since the hydrogen atom, with its single $1s$ orbital cannot form more than one pure covalent bond, the attraction of two atoms must be due largely to electrostatic or ionic forces. It is easy to see from this conception of the ionic nature of the hydrogen bond that the coordination number of hydrogen is restricted to the value 2. Having no electron shell around it, the hydrogen ion or proton is a vanishingly-small cation. It would attract one anion to the equilibrium internuclear distance which is obviously equal to the anion radius and then attract in the same way another anion to form a stable complex. As shown in Fig. 9.1, a third anion would be stopped by anion–anion contacts, so the hydrogen ion has only two nearest anion neighbours.
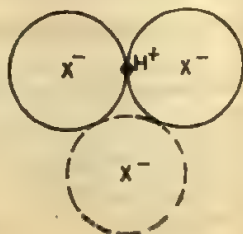
Fig. 9.1

Since the hydrogen bond is ionic in nature, only the most electronegative atoms should form hydrogen bonds, and the strength of such bonds should increase with increase in the electronegativity of the bonded atoms. Consequently, with reference to the electronegativity scale (Section 7.3), fluorine, oxygen, nitrogen and chlorine would be expected to possess hydrogen-bonding ability to an extent decreasing in this order. In fact, empirical observations indicate that fluorine forms very strong hydrogen bonds, while oxygen forms weaker ones and nitrogen still weaker ones. However, a given electronegativity alone cannot account for the hydrogen-bonding tendencies; thus, for instance, though nitrogen and chlorine have the same electronegativity, nitrogen has considerably greater hydrogen-bonding power. This may be due to the small size of nitrogen (relative to chlorine) as a result of which its electrostatic interactions are stronger than those of chlorine.

From the electronegativity difference of O and H, the amount of partial ionic character of the O—H bond is calculated to be 39 per cent. This means the hydrogen atom is liberated from covalent bond with the adjacent oxygen atom to the extent of 39 per cent and hence can form fractional covalent bond (i.e. a bond with bond-number less than 1, and so having bond length greater than that for a single bond) with the oxygen atom of another molecule. Thus the hydrogen atom is close to one of the two adjacent atoms in the hydrogen-bonded group O—H $\cdots$ O. For instance, in ice the two oxygen–hydrogen distances, as determined by neutron diffraction, are 1.00 Å and 1.76 Å.

As is expected, hydrogen bonds are formed primarily between highly electronegative atoms such as F, O, N and Cl. There are, however, evidences that carbon which is substituted with negative groups, e.g. in $CHCl_3$, HCN, etc., also enters into hydrogen bonding.

The hydrogen bond is comparatively weak, its bond energy (that is, the energy of the reaction $A—H + B \rightarrow A—H \cdots B$) is in most cases in the range of 2 to 10 kcal/mole (Table 9.1) as compared to approximately

Table 9.1 Typical Hydrogen Bond Lengths and Energies

Bond	Bond length*, Å	Dissociation energy (kcal/mole)
C–H $\cdots$ N		3
O–H $\cdots$ N	2·8	4·7
O–H $\cdots$ O	2·6–2·8	3–6
O–H $\cdots$ Cl	3·1	
N–H $\cdots$ N	3·1	3–5
N–H $\cdots$ O	2·9–3·0	4
N–H $\cdots$ Cl	3·2	
N–H $\cdots$ F	2·8	5
F–H $\cdots$ F	2·4	7

* Bond length denotes A to B distance in A–H $\cdots$ B.

100 kcal for ionic or covalent bonds. A consequence of the small bond energy and activation energy is that the hydrogen bond is formed as well as ruptured with great ease, and is, therefore, specially suited to play a part in reactions taking place at ordinary temperatures. The hydrogen bond is held by many to be essential to life processes; it is considered to play an important part in the structure of proteins and nucleic acids.

Examples of hydrogen bonding are numerous especially among organic compounds. In the following, some of the important effects of the hydrogen bond on the physical properties of substances, are discussed.

Association among simple hydrides. The melting points and boiling points show decreasing courses (Fig. 9.2) for the sequence of related substance H_2Te, H_2Se and H_2S, which are, of course, expected in view of the decrease, in this order, of molecular weights and van der Waals forces. (The van der Waals forces decrease with decrease in atomic number for atoms of similar structure.) From the continuation of this sequence, in the way indicated by the melting point and boiling point values for the noble gases Xe, Kr, Ar, Ne (Fig. 9.2), the melting point and boiling point of water would be expected to be about $-100°C$ and $-80°C$ respectively. That the actual values are very much higher is the result of the formation of hydrogen bonds.
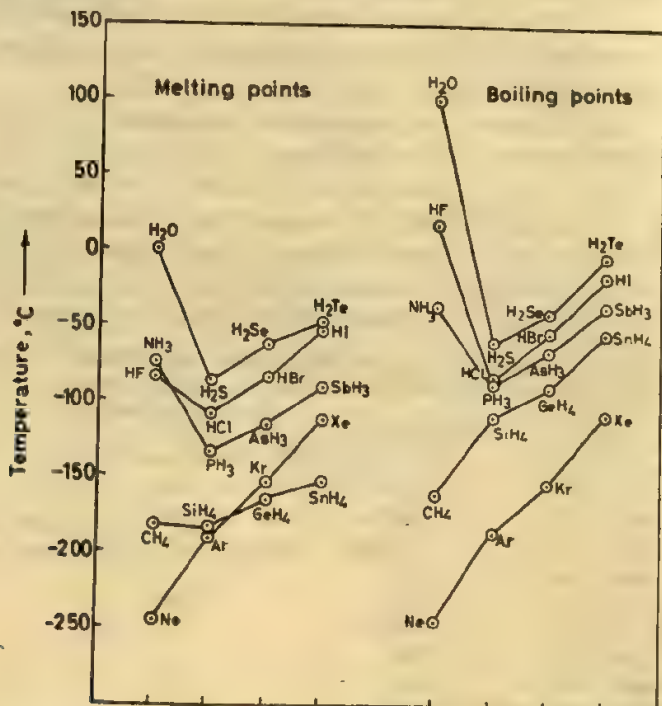
Fig. 9.2 Melting and boiling points of the simple hydrides (Values for inert gas elements are included to afford comparison)

Similarly, the melting points and boiling points of hydrogen fluoride and ammonia are also considerably higher than the values expected from the sequences of analogous compounds (Fig. 9.2). Both the effects are, however, somewhat smaller than for water. The decrease for hydrogen fluoride is due to its ability to form only one-half as many hydrogen bonds as water, in consequence of which the resultant effects of hydrogen bonds are smaller for hydrogen fluoride than for water, even though F—H · · · F bonds are stronger than O—H · · · O bonds. For ammonia, however, the decrease is partly due to the smaller electronegativity of nitrogen compared to oxygen and partly due to the fact that the nitrogen with only one unshared electron pair forms three hydrogen bonds with the N—H groups of other molecules.

The existence of the boiling point effect, apart from the melting point effect, leads to the deduction that all hydrogen bonds are not destroyed on fusion. More than half of the total number of hydrogen bonds existing in crystals of hydrogen fluoride, water and ammonia are retained on fusion. The hydrogen bonds exist even at the boiling point and are ruptured on vaporization. But the F—H · · · F bonds are so strong that they tend to hold the molecules together in vapour, in the form of aggregates $(HF)_n$.

Having no power to form hydrogen bonds, the simple carbon family
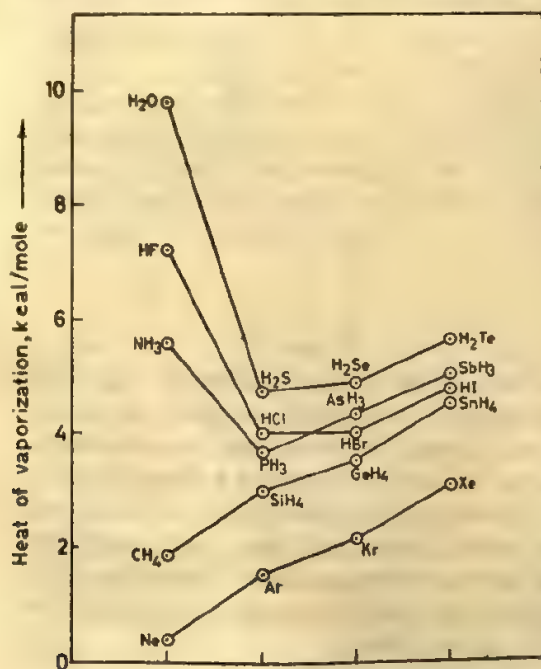
Fig. 9.3 Heats of vaporization of the simple hydrides. (Values for inert gas elements are included to afford comparison.)

hydrides exhibit (Fig. 9.2) rather regular increase in boiling point and melting point with molecular weight.

Properties which are related to melting point and boiling point also exhibit the effect of hydrogen-bond formation, as illustrated for the heat of vaporization in Fig. 9.3.

Association among other hydrogen compounds. Situations similar to those discussed above are also found with liquid hydrogen peroxide, certain alcohols, carboxylic acid, etc.

Liquid hydrogen peroxide is more highly associated than water. Consequently its boiling point is considerably higher; the normal (at 760 mm Hg) boiling point is 151.4°C.

Since H–C $\equiv$ N resonates with the structure H–C$^+$::$\ddot{\text{N}}$:$^-$ involving a positive formal charge on the carbon atom, the electronegativity of this atom is increased sufficiently to permit to form C—H $\cdots$ N hydrogen bonds. These bonds are strong enough to have effect on the melting point and boiling point. Thus the observed values are $-12°$ and $25°$C, which are much higher than those for acetylene, $-81°$ (at 891 mm Hg) and $-84°$C (at 760 mm Hg), respectively, even though the molecular weights are very close.

In crystalline alcohols, molecules are bound to each other through hydrogen bonds giving rise to polymers of the type:
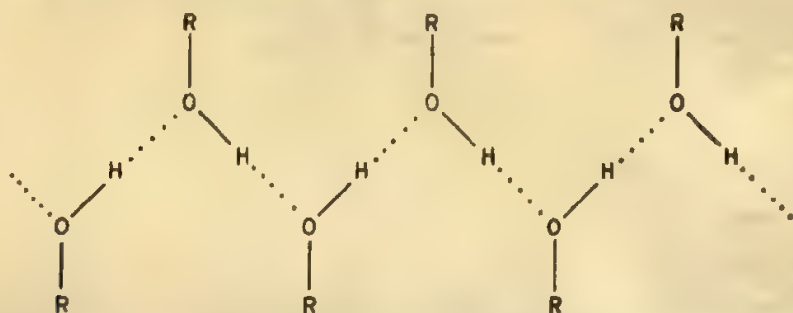
In the liquid state also, alcohols consist of long chains or ring polymers; so it is not necessary that many of the hydrogen bonds be broken for the alcohol crystal to melt to a liquid. However, the transformation into vapour state requires the breaking of the remaining hydrogen bonds. That is why while the heats of fusion and the melting points of alcohols are only slightly abnormal, the boiling points and heats of vaporization exhibit pronounced effects due to the hydrogen bond formation. This is illustrated by the values of some physical constants of ethyl alcohol and its isomer, dimethyl ether, given below:

	C_2H_5OH	$(CH_3)_2O$	Difference
Melting point	$-115°$C	$-141°$C	26°C
Boiling point	78°C	$-25°$C	103°C

The molal heat of sublimation of ethyl alcohol is 11.3 kcal/mole, while that of dimethyl ether is only 6.3 kcal/mole. The difference, 5.0 kcal/mole, may be taken as an approximate value of the hydrogen bond energy in crystalline ethyl alcohol. The oxygen atoms of carboxyl groups can form stronger hydrogen bonds than those of water. Consequently, in contrast to water, which does not show appreciable concentration of polymerized molecules in the vapour phase, formic acid and acetic acid form stable dimeric molecules. As determined by the electron diffraction method, formic acid dimer has the following structure:
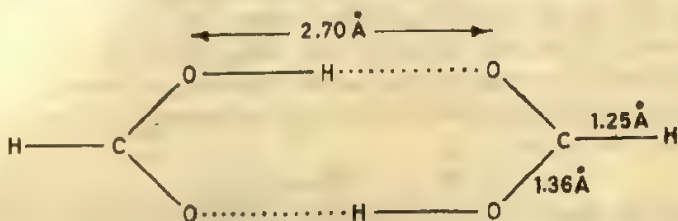
Since the heat of dimerization is 14.12 kcal/mole, the hydrogen bond energy in formic acid is 7.06 kcal/mole. In the same way, the hydrogen bond energy in acetic acid is found to be 7.6 kcal/mole. These values are greater than those for ice by about 50 per cent.

Anion solvation. Certain oxygenated anions form hydrates both in solution and in crystal lattices. In such cases, the anion-solvated water is apparently held by the $O—H \cdots O$ bonds. In $CuSO_4.5H_2O$, for example, four molecules of water are associated with the copper (II) ion as coordinated water, but the remaining one is held to the sulphate ion and to two of the coordinated water molecules by hydrogen bonds to give an overall structure as shown below:
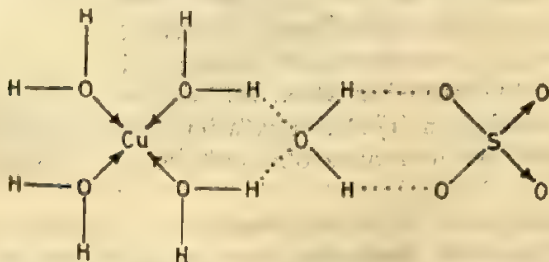
The tendency of the fluoride ion to form FHF hydrogen bond is sufficiently strong so that metal fluorides are often solvated by hydrogen fluoride giving rise to acid fluoride ions of the types HF_2^-, $H_2F_3^-$, and $H_3F_4^-$.

Abnormal solubility relations. It is generally found that compounds containing functional oxygen or nitrogen groups are more soluble in

materials such as $CHCl_3$ or $CHCl_2F$ than in closely related compounds such as CCl_4 or CCl_3F. This phenomenon may be attributed to the ability of the former solvents to form hydrogen bonds with the solute molecules.

Abnormal dielectric constant values. That the dielectric constant values observed for certain liquid substances, like water, hydrogen fluoride, and hydrogen cyanide are abnormally high is attributed to continued polymerization through hydrogen-bond formation. High values of dielectric constant are also exhibited by alcohols, ammonia and methyl amine in the liquid state, and all of these can form hydrogen bonds. As has been mentioned already, the very effect of hydrogen bonding on the dielectric constant is due to the resulting polymerization. For instance, the polymerization of HCN due to hydrogen bonding leads to *linear* molecules, such as

$$H - C \equiv N \ldots \ldots H - C \equiv N \ldots \ldots H - C \equiv N$$
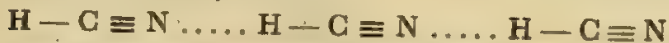
Since the dipole moment of the simple molecule HCN is 3.00×10^{-18} e.s.u., that for the polymer $(HCN)_n$ is equal to about $n \ (3.00 \times 10^{-18})$ e.s.u. The observed value of the dielectric constant of liquid hydrogen cyanide is 116, which is about 3 times the value that would be expected for the monomeric substance. And since the dielectric constant, in terms of its simple theory, varies directly with the first power of the number of molecules in unit volume and with the square of the dipole moment, this threefold increase in dielectric constant would accordingly be attributed to an average degree of polymerization of three.

The dielectric constants of hydrogen fluoride, water, hydrogen peroxide and the alcohols are smaller than that of hydrogen cyanide, even though the degree of polymerization of all the former substances is undoubtedly much greater than that of the latter because of much stronger hydrogen bonds in them. This is because, unlike in HCN, the polymerization in these substances is not accompanied by a linear increase in the magnitude of the dipole moment of the molecule. For instance in hydrogen fluoride the hydrogen bonds are formed at about $140°$ and so a molecule $(HF)_n$ having a structure as shown in (I) may have a very small net dipole moment. There may also be ring molecules, obviously, with zero dipole moment.

Apart from those discussed above, there are various other properties of substances in which hydrogen-bond formation plays an important role. The solubility of organic liquids in water, heat of mixing, viscosity of liquids, structure, cleavage and hardness of crystals, infrared absorption spectra, proton magnetic resonance—all these may be cited as examples.

9.5 *Van der Waals and Long-range Bonds*

When two atoms or molecules approach, there is a weak attraction be-

F———H·······F
                     H
                        F
                    H
                        F
                  H
·······H———F   (I)

tween them long before their electron clouds can overlap appreciably. This is the van der Waals attraction, and it can be considered as a manifestation of various effects, such as, the electrostatic interaction between the charge distributions of the two atoms, the mutual polarization whereby each charge could induce slight change in the other, and the dispersion forces, which are the result of a random fluctuating polarization occurring due to the random movement of the electrons (Fig. 9.4). All these forces are relatively weak and are masked by strong covalent or repulsive forces at internuclear distances existing in compounds. But in a gas they give rise to the van der Waals attraction. The van der Waals binding forces also exist between well-separated units in a crystal; in graphite, for instance, the adjacent layer planes, which are separated by C—C distance of about 3.4 Å instead of the normal C—C bond length of 1.42 Å, are considered to be held together by the van der Waals forces.

Van der Waals radii for the atoms of inert gases can be derived from measurements of the cell dimensions of their crystals. Similarly, the van der Waals radii for other atoms may be deduced from molecular structures by determining the closest distance of approach between adjacent molecules. Table 9.2 present values of some radii derived in this way. A general feature of these values is that they are much larger than the corres-

Electron
distribution

(a)

(b)

Centers of charge
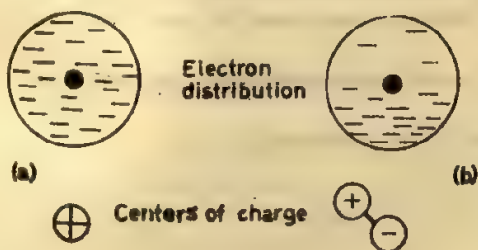
Fig. 9.4 (a) Uniform electron distribution in an atom. (b) Momentary polarized distribution of electrons causing momentary establishment of an electrical dipole.

Table 9.2 Van der Waals Radii (in A) for some Atoms

				H	1.2		
N	1.5	O	1.4	F	1.35	Ne	1.6
P	1.9	S	1.85	Cl	1.8	Ar	1.9
As	2.0	Se	2.0	Br	1.95	Kr	2.0
Sb	2.2	Te	2.2	I	2.15	Xe	2.2

ponding covalent radii (Table 7.10), and it means that the effective radius of an atom within a molecule is significantly different from its radius towards other molecules in a molecular structure (see Fig. 7.6).

Van der Waals radii find application in structural problems involving molecular crystals and in problems of steric hindrance in large molecules.

Suggested Reading

PAULING, L., *The Nature of the Chemical Bond*, Cornell University Press, Ithaca, N.Y., 1960.

PIMENTEL, G. C. and McCLELLAN, A. I.., *The Hydrogen Bond*, W. H. Freeman, San Francisco, 1959.

WELLS, A. F., *Structural Inorganic Chemistry*, Oxford University Press ,New York, 1961.

Problems

9.1 Indicate giving reasons which of the following molecules have appreciable dipole moments: CH_4, CH_3Cl, CCl_4, and H_2O.

9.2 Explain why diethyl ether, $C_2H_5OC_2H_5$, is polar. Given that the C–O–C bond angle in ether and the H–O–H bond angle in water are approximately equal, which of the two substances will have greater dipole moment?

9.3 Account for the fact that HF has much higher boiling point (19.4°C) than HCl (−85°C), although the molecular weight of HF is lower than that of HCl.

9.4 How would you explain that H_2O is liquid but H_2S is a gas at ordinary temperature, although H_2S has higher molecular weight than H_2O?

9.5 Explain why the heat of vaporization of water is much larger than the heat of fusion of ice.

9.6 Explain why, despite the stronger hydrogen bond, HF has a smaller heat of vaporization than H_2O.

9.7 Suggest an explanation for the fact that the density of ice is less than that of water.

9.8 What factors determine the magnitude of intermolecular forces? Give examples.

9.9 In which way do the van der Waals bonds resemble the metallic bond?

9.10 Account for the fact that the crystals of the inert gases possess the same close-packed structure as the true metals.

9.11 Diamond is very hard but graphite is soft though both are essentially carbon. How would you account for it?

9.12 Why are the van der Waals radii larger than the covalent radii?

Determination of Molecular Structure

10.1 Introduction

In earlier chapters we had occasions to mention quantities like molecular shape, interatomic distances (or bond lengths) and bond angles. Collectively, these quantities describe the structure of a molecule. In this chapter we shall take up the principal physical methods used for their quantitative determination. They involve the use of electric and magnetic fields, electromagnetic radiation, and electron and neutron beams.

The shape of a molecule (or for that matter, of any object) can be most conveniently described in terms of its symmetry. It affords a concise description of the molecular structure and leads to considerable simplification of theoretical methods. It is, therefore, pertinent to preface our treatment of molecular structure with an introduction to the subject of molecular symmetry.

10.2 Molecular Symmetry

Symmetry may be defined as regular arrangement. When we say that a molecule has symmetry, we mean that there are some regularities in its dimensions. In the language of structural chemistry, these regularities are most elegantly described in terms of the *symmetry elements* possessed by the molecule and the corresponding *symmetry operations*. Before defining

these terms it is important to point out the distinction between *point symmetry* and *space symmetry*. In the case of an isolated molecule, its symmetry or regular arrangement actually involves repetition of identical parts in that molecule. While considering the symmetry of an isolated molecule we are thus interested in the symmetry about a point, i.e. in the so-called *point symmetry*. On the other hand, the symmetry of a cluster of molecules, as in a crystal, may involve the repetition of a number of identical molecules, and consequently, the symmetry elements may involve translation. One then has to deal with the so-called *space symmetry*. In this section, however, we are solely concerned with the symmetry of an isolated molecule.

In order to define what is a symmetry operation let us consider a simple structure, that of water molecule [Fig. 10.1(a)]. For our convenience we mark the two hydrogen atoms with subscripts A and B. Now let us imagine that the H_2O molecule is rotated through an angle of 180° about an axis passing through O and equidistant from H_A and H_B. This gives the orientation (c) from (b). If the hydrogen atoms were not marked and thus were identical, there would be no way to tell, by observing the orientations (b) and (c), whether the molecule had been rotated or not. In other words, our aforesaid operation has produced an orientation that is indistinguishable from the original. Such an operation whereby an orientation is changed into an indistinguishable one is called a *symmetry operation*.

The rotation of the H_2O molecule through an angle of 180°, described above, is an example of a symmetry operation. A repetition of this operation brings the molecule back to original orientation (b). Because two identical rotations are required to return to the initial orientation, the symmetry operation is called a 2-fold rotation. More generally, the operation of rotation through an angle of $2\pi/n$ radians or 360°/n, where n is an integer, is called an n-fold rotation and symbolized by C_n (C comes from 'Cyclisch'); the rotation axis associated with it is called an *n-fold* axis.

The operation of rotation described above for the H_2O molecule is
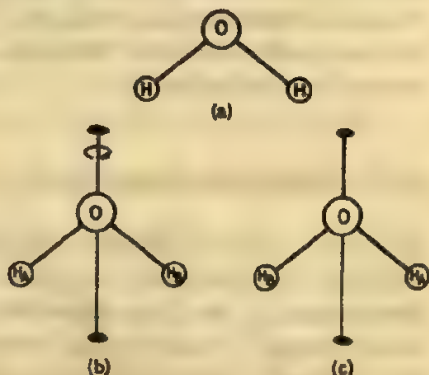
Fig. 10.1 (a) Schematic representation of the structure of H_2O. (b) The 2-fold symmetry axis in H_2O. (c) Orientation produced from (b) by rotation of 180° about the 2-fold axis.
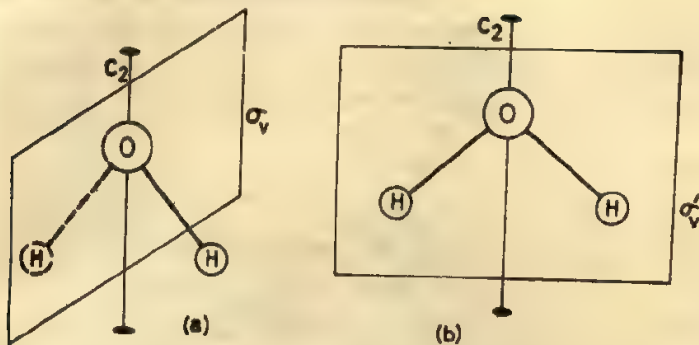
Fig. 10.2 Mirror planes of the H_2O molecule: (a) σ_v and (b) σ_v

not the only type of symmetry operation. Let us imagine that we have passed a plane mirror perpendicular to the plane of the H_2O molecule and containing the 2-fold axis [Fig. 10.2(a)]. When viewed from either side, half of the molecule is reflected in the mirror and the orientation appears to be unchanged. Thus this reflection is a symmetry operation of the H_2O molecule. The operation is called *reflection* and is symbolized σ or C_s.

A mirror plane that contains the principal rotation axis is called a *vertical plane* and the reflection in this plane is represented by σ_v. The reflection for the H_2O molecule, described above, is of the type σ_v.

The H_2O molecule also possesses a mirror plane lying in the plane of the triangle which also contains the principal rotation axis [Fig. 10.2(b)]. Since the top of the molecule is the same as the bottom, reflection in this plane produces a final configuration indistinguishable from the initial one. Reflection in this plane is therefore a symmetry operation and is represented by σ_v'.

The symmetry operations mentioned so far include: (i) a 2-fold rotation C_2, (ii) a reflection σ_v through a mirror plane containing the axis of rotation and perpendicular to the plane of the triangle, and (iii) a reflection σ_v' through a mirror plane lying in the plane of the triangle. This set of symmetry operations completely specifies the symmetry of the H_2O molecule.

So far we have only encountered vertical planes, i.e. mirror planes containing the principal axis. A molecule may also possess a mirror plane perpendicular to the principal rotation axis. Such a plane is said to be a *horizontal plane* and the associated symmetry operation, that is, reflection in this plane, is represented by σ_h.

In order to describe the symmetry of any molecule two additional kinds of symmetry operations are needed. These are *inversion* and *rotation-reflection*.

The operation of inversion is essentially reflection of all atoms through a point in the molecule, referred to as centre of symmetry or inversion
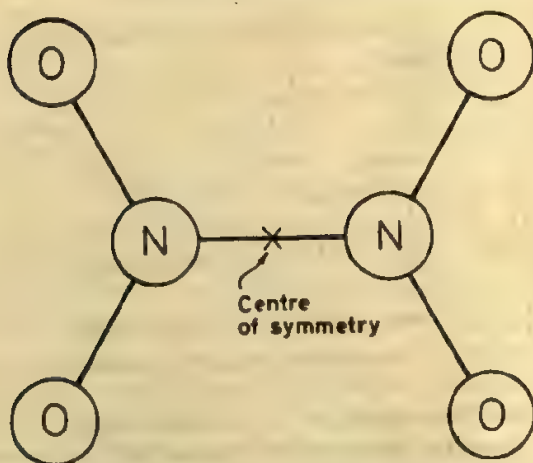
Fig. 10.3   Inversion centre or centre of symmetry in planar N_2O_4

centre. The symmetry operation, therefore, requires that lines joining symmetrically equivalent atoms are bisected by the inversion centre. Dinitrogen tetroxide (N_2O_4), with a planar structure as shown in Fig. 10.3, is an example of a molecule which possesses a centre of symmetry. Other examples of molecules which have centres of symmetry are XeF_4, which has square planar configuration, and benzene, which is a regular hexagon (see later). In the case of XeF_4, there is an atom at the centre of symmetry, while in the case of both N_2O_4 and benzene there is no atom at the centre of symmetry. It should be noted that a molecule cannot have a centre of symmetry unless it has even numbers of all atoms, except one that may be at the centre. The operation of inversion is represented by i or C_i.

A rotation-reflection consists in the combination, in either order, of an n-fold rotation (that is, rotation of the molecule about an axis passing through it by $2\pi/n$) and reflection through a plane perpendicular to axis of rotation. The operation, also called *improper rotation*, is represented by S_n (S comes from 'Spiegelung'). Fig. 10.4 illustrates the rotation-
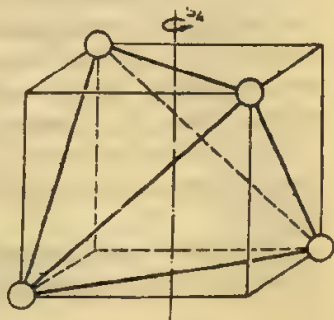
Fig. 10.4   Example of rotation-reflection operation

reflection operation for a molecule, which has the symmetry of a regular tetrahedron. Clearly, a rotation of $2\pi/4$ or 90° about the axis shown in Fig. 10.4 followed by reflection in a plane perpendicular to this axis will produce a configuration indistinguishable from the original one. So for this molecule the operation S_4 exists. It is easy to see that none of the component operations of S_4 (namely, C_4 and σ_h) is a symmetry operation. There are, however, molecules for which the component operations themselves are symmetry operations. The planar molecule of BF_3 will serve to illustrate this. For it a symmetry operation C_3 can be performed about an axis perpendicular to the molecular plane. It is also possible to perform the rotation C_3 followed by reflection in the molecular plane (or vice versa) so that there is an S_3 operation.

Having now defined the symmetry operations, we next turn to another concept, that of *symmetry elements*. We can define a symmetry element as an axis, plane or point, about which or through which a symmetry operation can be performed. Thus, the axis about which an operation C can be performed is a symmetry element, referred to as *n*-fold rotation axis. The symbol C_n is used to represent this axis. Similarly, the axis about which the rotation for an operation S_n is performed is called *n*-fold rotation-reflection axis and represented by the symbol S_n. Obviously, it is possible for one axis to be simultaneously a C_n axis and an S_n axis.

The plane through which a reflection operation, σ, is carried out is a symmetry element, called *mirror plane* and represented by the same symbol σ. Subscripts are often appended to σ in order to indicate the orientation of the plane with respect to the principal rotation axis. The significance of the subscripts v and h has been previously explained. It is, however, necessary to first identify the principal rotation axis. If a molecule has one symmetry axis C_n of uniquely high *order* (n is known as the order of the rotation axis), then this axis is the principal rotation axis. It is customary to regard this axis as being *vertical*. A mirror plane that contains this axis is called a *vertical plane*, σ_v; if there is a mirror plane perpendicular to this axis it is called the *horizontal plane* and represented by σ_h.

The point through which the inversion operation is carried out is called the *centre of symmetry* or *inversion centre*. This symmetry element is represented by the symbol i or C_i.

We can describe the symmetry of a molecule either in terms of the set of symmetry operations which can be performed or in terms of the set of symmetry elements which the molecule possesses. The symmetry operations and the corresponding symmetry elements, described above, are listed in Table 10.1.

In many cases, all the symmetry elements that can be observed for a molecule are not actually required to describe its symmetry, that is, some of the symmetry elements are superfluous or redundant. For instance, in the case of H_2O discussed above, the presence of mirror planes σ_v and $\sigma_v{}'$

Table 10.1 Point Symmetry Operations and Elements

Symmetry operation	Symmetry element	Symbol
n-fold rotation	n-fold rotation axis	C_n
Reflection	Mirror plane	σ or C_s
Inversion	Centre of symmetry or inversion centre	i or C_i
n-fold rotation-reflection	n-fold rotation-reflection axis	S_n

as symmetry elements means that this molecule must also have a 2-fold rotation axis (C_2) along the line of intersection. In fact, in highly symmetrical molecules, redundancy of symmetry elements is a common occurrence, and it is possible to formulate general rules regarding such redundancies.

In the following we shall discuss the symmetries of some common molecules. Consider first diatomic and linear molecules such as HCl, Cl_2, CO_2 molecules (Fig. 10.5). These are more or less trivial cases. All of them have an *infinite rotation axis*, C_∞, i.e. a rotation axis of order ∞, coincident with the internuclear axis. Heteronuclear (that is, containing different atoms) diatomic molecules, such as HCl [Fig. 10.5 (a)], have only this symmetry element. However, homonuclear (that is, containing only one type of atom) diatomic molecules, such as Cl_2 [Fig. 10.5(b)] and linear molecules such as CO_2 [Fig. 10.5(c)] also possess a mirror plane σ_h, a centre of symmetry i and an infinite number of 2-fold axes, C_2, perpendicular to the axis of the molecule. This provides yet another example of redundancy of symmetry elements, since the combination of the plane σ_h and the axis C_∞ implies the presence of a centre of symmetry i and an infinite number of C_2 axes.

The symmetry elements of BF_3 and NH_3 are shown in Fig. 10.6. The BF_3 molecule [Fig. 10.6(a)] possesses (i) a 3-fold axis of symmetry (C_3), because a rotation through $2\pi/3$ produces an orientation indistinguishable
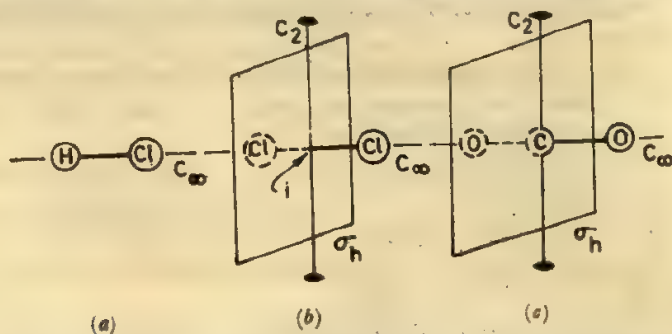
Fig. 10.5 Symmetry elements of linear molecules. (a) Heteronuclear diatomic molecule, HCl. (b) Homonuclear diatomic molecule, Cl_2. (c) Linear triatomic molecule, CO_2.
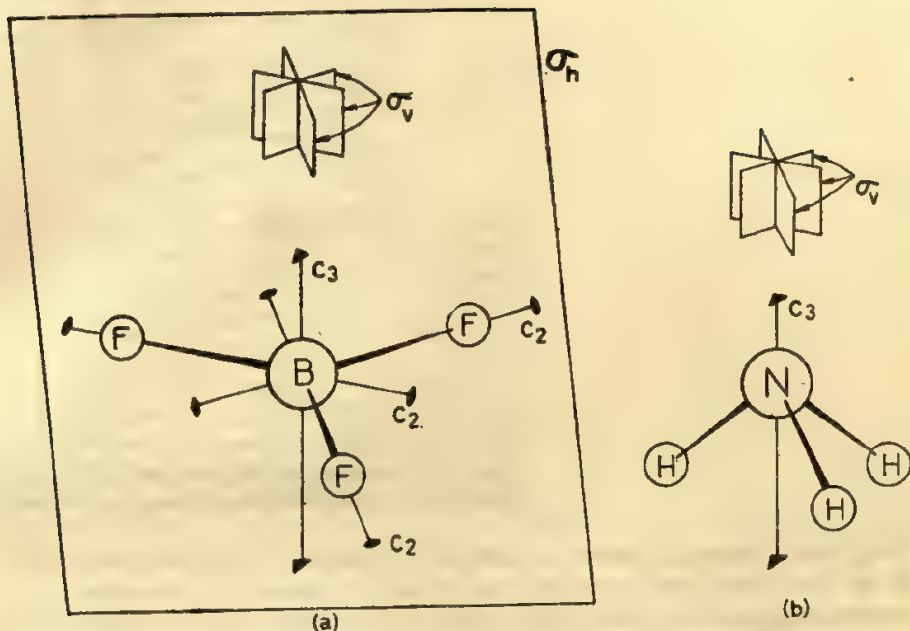
Fig. 10.6 The symmetry elements of (a) BF_3 and (b) NH_3 molecules

from the initial one, (*ii*) three subsidiary 2-fold symmetry axes, (C_2) perpendicular to the principal axis, (*iii*) three mirror planes (σ_v) containing the principal axis, and (*iv*) a mirror plane (σ_h) perpendicular to the principal axis. On the other hand, the NH_3 molecule possesses, as shown in Fig. 10.6(*b*), (*i*) a 3-fold axis of symmetry and (*ii*) three σ_v planes. In terms of symmetry elements, we can distinguish between BF_3 and NH_3 by stating that BF_3 possesses a σ_h plane, while NH_3 does not. Note also that the C_2 axes are not present in the NH_3 molecule.

As an example of molecules with still higher symmetry axes, let us consider the case of the benzene molecule. As shown in Fig. 10.7, the molecule has a hexagonal planar structure with the following symmetry elements: (*i*) a 6-fold rotation axis (C_6) perpendicular to the molecular plane, (*ii*) six 2-fold rotation axes (C_2), (*iii*) six mirror planes (σ_v) containing the principal axis, (*iv*) a mirror plane (σ_h) perpendicular to the principal axis, (*v*) a centre of symmetry (i), and (*vi*) an S_6 axis collinear with the C_6 axis. It should be noted, however, that not all of these symmetry elements are needed for an unambiguous specification of the symmetry of the benzene molecule. In fact, the symmetry of the molecule is completely specified by only saying that it possesses a C_6 axis, six C_2 axes and a σ_h plane, since the rest of the symmetry elements, mentioned above, are simply necessary consequences of the presence of these elements.

A set of point symmetry elements which is just sufficient to specify the symmetry of an object or a molecule is known as a *point symmetry group*.
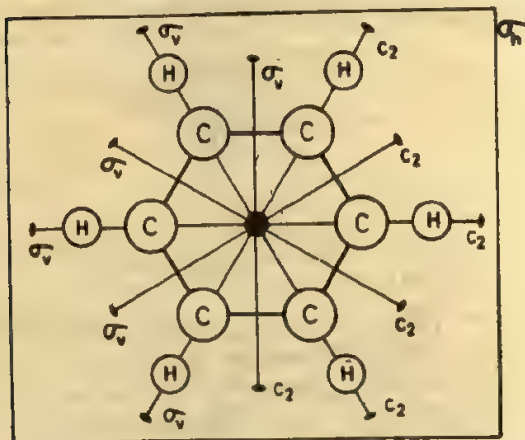
Fig. 10.7 Symmetry in C_6H_6, hexagonal planar. The symbol of the centre represents 6-fold axis of rotation.

Each point group is given a discriptive symbol. The *Schoenflies symbol* is the one most often used for molecules by chemists, physicists and spectroscopists. The main rules by which the symmetry of a molecule is expressed using this symbol are described below:

(1)   When a molecule possesses, besides a principal axis C_n, a set of n vertical planes, σ_v, it belongs to the point group C_{nv}. (A molecule possessing a principal axis C_h and a horizontal plane σ_h belongs to the group C_{nh}.)

(2)   When a molecule possesses a principal axis C_n, a set of n C_2 axes perpendicular to C_n and a horizontal plane σ_h, it belongs to the point group D_{nh} (D comes from 'Dieder').

(3)   All linear molecules belong to one of the two point groups, $C_{\infty v}$ and $D_{\infty h}$. Unsymmetrical molecules such as CO, HCl, HCN, N_2O, OCS, etc., belong to the group $C_{\infty v}$, while symmetrical ones such as Cl_2, N_2, CO_2, C_2H_2, $HgCl_2$, etc., belong to the group $D_{\infty h}$.

(4)   Molecules having the symmetry of a regular tetrahedron belong to the point group T_d. The characteristic symmetry elements for T_d are a set of four C_3 axes, a set of three S_4 axes and a set of six dihedral planes, σ_d (Fig. 10.8).

(5)   Molecules having the symmetry of a regular octahedron belong to the point group O_h.

Some common point symmetry groups with their symbols, symmetry elements and examples are listed in Table 10.2. It should be noted that some of the symmetry elements given in this table are superfluous, as they are simply consequences of the presence of other symmetry elements.
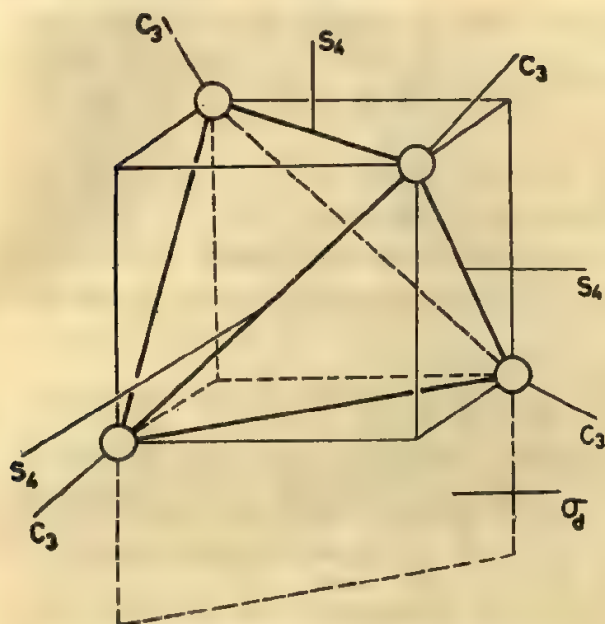
Fig. 10.8 Sketch illustrating the characteristic symmetry elements of a tetrahedron. Only one of the six dihedral planes σ_d is shown.

Table 10.2 Some Common Point Symmetry Groups

Group symbol	Symmetry elements	Examples
C_{2v}	C_2, σ_v, σ'_v	H_2O, SO_2, $BClF_2$
C_{3v}	$C_3,\ 3\sigma_v$	NH_3, PF_3, PCl_3, $CHCl_3$
D_{2h}	$3C_2,\ 3\sigma_v,\ i$	C_2H_4
D_{3h}	$C_3,\ 3C_2,\ 3\sigma_v, \sigma_h$	BF_3, PCl_5
D_{6h}	$C_6, 6C_2, 6\sigma_v, \sigma_h, i$	C_6H_6
T_d	$4C_3,\ 3C_2,\ 6\sigma_d$	CH_4, NH_4^+
O_h	$3C_4,\ 4C_3, 6C_2, 9\sigma, i$	SF_6
$C_{\infty v}$	C_∞	CO, HCl, N_2O, HCN
$D_{\infty h}$	$C_\infty, \infty C_2, \sigma_h, i$	N_2, Cl_2, C_2H_2, CO_2

10.3 Methods of Structure Determination

Since a molecule consists of an assemblage of atoms, the determination of molecular structure essentially consists in the determination of the relative dispositions of these atoms. This problem has two aspects; the shape (or symmetry) of the molecule and the actual dimensions of bond lengths and bond angles, collectively referred to as *molecular parameters*. Molecular

symmetry provides information about the equality of two or more bond lengths and the equality of two or more bond angles, and thus reduces the number of molecular parameters needed to specify the structure of a molecule. For example, in the H_2O molecule of C_{2v} symmetry, the two O—H bond lengths must be equal and the molecule must be bent, so that the only parameters needed to specify the configuration of the molecule are one O—H distance and the $H\hat{O}H$ angle. Molecular symmetry may also give the actual magnitudes of some bond angles. For example, if the BF_3 molecule belongs to the point symmetry group D_{3h}, all the $F\hat{B}F$ angles are 120° and since all the bond lengths are equal, we need to specify only one parameter, the B—F distance.

Of the various experimental methods used for the determination of molecular structure, some methods provide information about both molecular symmetry and molecular parameters, while some others reveal only molecular symmetry. By far the largest part of the information available on molecular structure has come from the application of spectroscopic or diffraction methods. Besides these, there are also a variety of other techniques, some of them quite recent, which often provide crucial bits of information in the determination of molecular structure. We shall discuss the various methods under the headings of spectroscopic methods, diffraction methods, methods based on magnetic effects, and dipole moments.

An attempt to describe even the principal methods of structural study in one chapter of this text is rather pretentious and necessarily demands that we restrict ourselves to bare essentials. In the context of our objective, the essentials will consist mainly of a concise description of the physical basis of each method and an objective evaluation of the type and quality of information each method provides.

10.4 Spectroscopic Methods

The total energy of an individual gas-phase molecule is made up of four different types. Thus, the molecule will have energy due to its translational motion. It will also have energies due to its rotational motion and due to the vibrational motion of its constituent atoms. In addition to these, the molecule will have electronic energy, which is due to the energy of its electrons. All these energies, except the translational energy, will be expected to have quantum restrictions on them. Qualitatively this can be shown as follows.

We saw in Section 4.9 that a significant result of the wave-mechanical treatment of a particle confined to movement in a very small region is that it can have only certain energies, i.e. its energy is quantized. It was also seen that the smaller the space to which the particle movement is

confined, the more accentuated are the restrictions, that is, the fewer and more widely spaced are the allowed energies in a given range. For a gas kept in an ordinary-sized container, the space available for the translational movement of each molecule is very large compared to the molecular dimensions. We can therefore expect the quantum restrictions on translational energies to be insignificant. A rotating molecule, however, is confined to a volume not much larger than the volume of the molecule itself. We can therefore expect significant quantum restrictions on the rotational energy. Again, in vibrational motion, the atoms of a molecule can undergo only as much displacement as the flexibility of the bonds will allow, so that the vibrational energy also will be expected to have quantum restrictions on it. Similarly, the electronic energy of a molecule will also be subject to significant quantum restrictions, since the electrons of a molecule are confined to a part of the molecule or at the most to the whole of its volume. Of the four types of molecular energies, rotational, vibrational and electronic energies will thus be expected to be quantized.

By the *Born-Oppenheimer approximation*, the three types of quantized molecular energies can be treated separately, and the total energy E_t can be considered to be made up of three parts.

$$E_t = E_e + E_v + E_r \qquad (10.1)$$

where E_e, E_v and E_r are the electronic, vibrational and rotational energies per mole, respectively. The quantized levels of these energies are shown schematically in Fig. 10.9. It is seen that the spacing of the electronic energy levels is larger than that of the vibrational energy levels, and the latter, in turn, is larger than the spacing of the rotational energy levels. Thus, whereas the difference between the electronic energy levels is usually some tens of kcal/mole, that between vibrational energy levels is a few kcal/mole, and that between rotational energy levels is only of the order of tens of cal/mole.

It was seen in Section 3.6 that atoms have different electronic energy levels and these are determined by certain quantum numbers. It was also seen that electronic line spectra of atoms are a direct result of this quantization of electronic energies of atoms. A spectral line is exhibited when an atom absorbs a quantum of energy (i.e. photon of frequency equal to $\Delta E/h$) such that an electron is promoted to an excited state, or when an electron in a higher excited state emits quantum of energy and drops to a lower excited state or to the ground state, (see Fig. 2.10).

Molecules also have energy levels as detailed above, and they can absorb or emit radiation energy quanta as a result of transitions between different energy levels. The energies of the quanta that are absorbed or emitted by a molecule can be measured by spectroscopic means, and consequently, the allowed energies of the molecule can be deduced. The allowed energies so obtained can then be used to determine the structure and properties of the molecule.
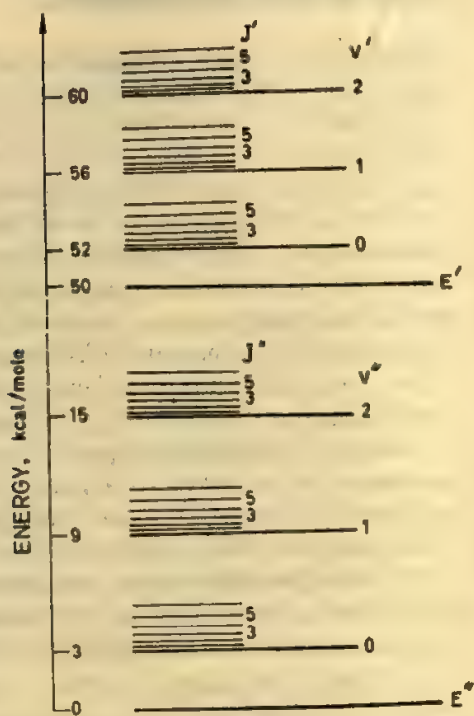
Fig. 10.9 Electronic, vibrational and rotational energy levels of a diatomic molecule. (Note that only the electronic and vibrational levels correspond to the energy scale of the diagram. The spacings of the rotational levels are greatly exaggerated for clarity.)

Since, as we have seen above, the spacings of the different types of molecular energies are different, the various energy transitions correspond to different regions of the electromagnetic spectrum. The electromagnetic spectrum is shown in Fig. 10.10. Knowing the wavelength of a radiation we can calculate the energy associated with it.

Example 10.1 Calculate the energy in cal/mole associated with the infrared region of the electromagnetic spectrum. Assume the wavelength to be 6×10^4 Å.

Solution Since all electromagnetic radiation travels at the same velocity, c, equal to 3×10^{10} cm/sec, and since the velocity is related to the wavelength λ and frequency ν by $c = \lambda\nu$, (where λ and ν are expressed in cm and sec^{-1} respectively), the frequency for the infrared radiation of wavelength 6×10^4 Å or 6×10^{-4} cm is

$$\nu = \frac{3 \times 10^{10}}{6 \times 10^{-4}} = 5 \times 10^{13} \text{ sec}^{-1}$$

The energy, in ergs, of a quantum of radiation of frequency ν sec^{-1} is given by $E = h\nu$, where h is the Planck constant. If every molecule in a gas absorbs one quantum of radiation, the total energy absorbed by one mole of gas will be $N.h.\nu$, where N is the Avogadro number. Therefore the energy per mole associated with infrared radiation is

$$\begin{aligned}
N.h.\nu &= (6.02 \times 10^{23})(6.62 \times 10^{-27})(5 \times 10^{13}) \\
&= 1.99 \times 10^{11} \text{ ergs} \\
&= (1.99 \times 10^{11})/(4.18 \times 10^7) \text{ or } 4.76 \times 10^3 \text{ cal/mole}
\end{aligned}$$

Energies calculated in this way for different regions of the electromagnetic spectrum are shown in Table 10.3.
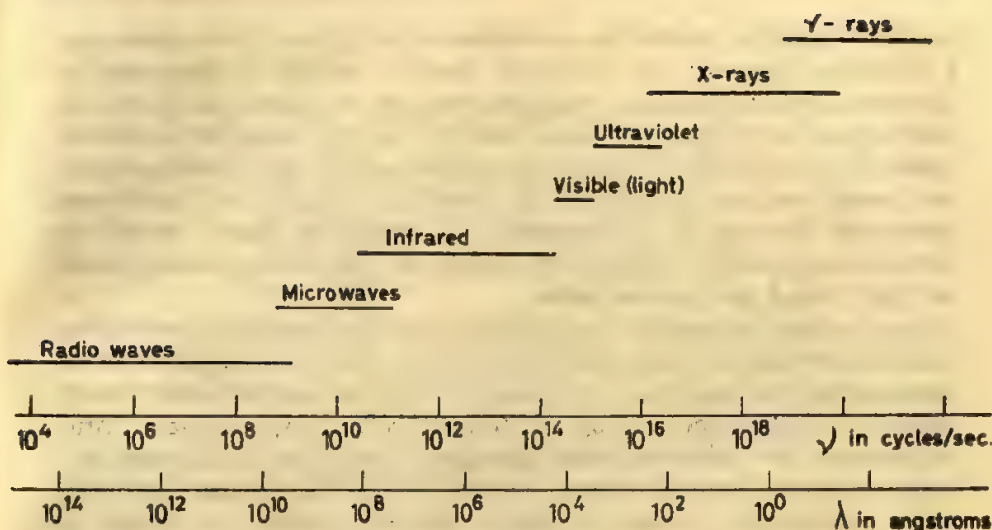
Fig. 10.10 Regions of the electromagnetic spectrum

A comparison of molecular energy levels shown in Fig. 10.9 with the representative energy values given in Table 10.3 enables us to assign different regions of the electromagnetic spectrum to different types of molecular energy transitions. Thus, since the separation of electronic energy levels is usually of the order of tens of kcal/mole, electronic

Table 10.3 Energies Associated with Different Regions of the Electromagnetic Spectrum

Region of spectrum	Wavelength (Å)	Frequency (sec^{-1})	Energy (cal/mole)
X-ray	1	3×10^{18}	$2 \cdot 86 \times 10^{8}$
Ultraviolet	3×10^{3}	1×10^{15}	$9 \cdot 53 \times 10^{4}$
Visible (yellow)	6×10^{3}	5×10^{14}	$4 \cdot 76 \times 10^{4}$
Infrared	6×10^{4}	5×10^{13}	$4 \cdot 76 \times 10^{3}$
Microwave	3×10^{8}	1×10^{10}	$9 \cdot 53$
Radiowave	3×10^{12}	1×10^{6}	$9 \cdot 53 \times 10^{-5}$

energy transitions will give rise to spectra in the visible or ultraviolet region of the electromagnetic spectrum. These spectra are therefore referred to as *electronic spectra*. By the same reasoning, transitions between vibrational levels within the same electronic level will give rise to *vibrational spectra* in the infrared region, whereas transitions between different rotational levels within the same vibrational level will give rise to *rotational spectra* in the far infrared or microwave region.

It should be noted, however, that a transition between two vibrational levels is almost always accompanied by transitions between rotational levels, so that vibrational spectra are really simultaneous vibrational and

rotational spectra, referred to as *vibration-rotation spectra*. In the same way, a transition between two electronic levels is usually accompanied by changes in vibrational and rotational energies; so electronic spectra are really electronic-vibration-rotation spectra, referred to simply as *electronic spectra*. However, if the electronic and vibrational energies remain constant, very small energies are required for transitions between rotational levels alone and this can be accomplished, as mentioned above, in the far infrared or microwave region of the spectrum. The corresponding spectra are then called *pure rotation spectra*.

Spectra may be studied both in absorption and emission (see Section 2.2). To obtain an absorption spectrum, continuous radiation of an appropriate frequency range is passed through the sample under investigation and is then focussed on the entrance slit of a spectrometer. After collimation, the radiation passes through a dispersing device, such as a prism or grating (which disperses, or spreads out, the radiation according to its wavelength), before reaching a detector, which is a device for measuring the amount of radiation of various wavelengths that emerges from the dispersing unit. The prism used for ultraviolet radiation is a quartz prism or grating; for visible radiation it is made from glass, and for infrared radiation it is made from fluorspar or rocksalt. The detector for visible or ultraviolet radiation is a photomultiplier tube or a photographic plate, while for infrared radiation it is a thermocouple. In microwave spectroscopy, however, no specific dispersing is needed, and the detector consists of a quartz crystal which is tuned to vibrate in response to the microwave radiation.

To obtain emission spectra, energy must be supplied to the molecules. Flames and electrical discharge tubes are the usual sources of such spectra. However, these spectra are usually observed only for diatomic and triatomic molecules, because larger molecules readily decompose under these conditions.

10.5 Boltzmann Distribution

We have seen above that electronic, vibrational and rotational energies of molecules are quantized, giving rise to discrete energy levels of the type shown in Fig. 10.9. It is important to know how the molecules are distributed among the various levels corresponding to each type of energy, i.e. what fraction of the molecules, say in a gas sample, have energies corresponding to each of the allowed energies. If the molecules are in thermal equilibrium, such an information can be obtained from the Boltzmann distribution law. Denoting the number of molecules occupying some energy level, say the ith level, by n_i and that occupying the lowest energy level by n , the Boltzmann distribution can be written as

$$\frac{n_i}{n_0} = \frac{g_i}{g_0} e^{-(E_i-E_0)/RT} \tag{10.2}$$

where $(E_i - E_0)$ is the energy difference between the two levels in cal. mole^{-1}, $R = 1.99$ cal deg^{-1} mole^{-1}, and T is the absolute temperature, g_i and g_0 are the degeneracies of the two energy levels. Eq. (10.2) reveals the importance of RT in determining the population of energy levels. If $(E_i - E_0)$ is much greater than RT, the ratio n_i/n_0 is very small. For example, at room temperature RT is approximately 600 cal/mole, whereas both $(E_e)_1 - (E_e)_0$ and $(E_v)_1 - (E_v)_0$ are usually much in excess of this value; consequently, molecules in general will be in their lowest electronic and vibrational energy levels at room temperature. However, because of the small difference between rotational energy levels, molecules will be spread over a number of rotational levels. This distribution is discussed in Section 10.6.5.

10.6 Pure Rotation Spectra

The study of pure rotational spectra provides the most direct approach to the evaluation of molecular parameters for simple molecules that may be obtained in gas phase. In the following, we shall first describe the classification of molecules into the principal rotational classes before discussing the details of the rotational spectra.

The rotation of any three-dimensional rigid body is conveniently described in terms of rotations about three principal axes of inertia which are mutually at right angles and pass through the centre of gravity of the body. Thus the body has three principal *moments of inertia*, one about each axis, conventionally designated I_a, I_b and I_c, in order of increasing magnitude $(I_a < I_b < I_c)$. On the basis of the relationships between the moments of inertia, molecules may be classified into four groups. As we shall presently see, this is equivalent to classifying molecules according to their shapes.

(*i*) *Linear molecules.* These are molecules such as CO_2, HCN, C_2H_2, HCl, OCS, in which all the atoms lie in a straight line. Considering, for instance, the OCS molecule, illustrated in Fig. 10.11, the principal axes of rotation may be taken as (1) the molecular axis a, (2) the axis b in the plane of the paper and perpendicular to the axis a, and (3) the axis c perpendicular to both the axes a and b, all the axes passing through the centre of gravity of the molecule. Since the nuclei on axis a have practically all of the mass of the molecule, the moment of inertia about this axis is zero, i.e. $I_a = 0$. It is also self-evident that the moments of end-over-end rotation about the axes b and c are the same, so that $I_b = I_c$. For linear molecules, we thus have $I_a = 0$; $I_b = I_c$.
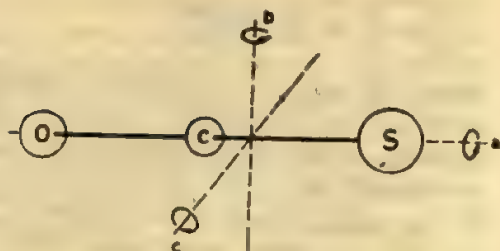
Fig. 10.11 The axes for the principal moments of inertia of the OCS molecule

(ii) *Symmetric tops.* A symmetric top molecule has three non-zero moments of inertia, two of which are equal. Consider, for example, a molecule such as methyl chloride, which is umbrella-shaped with the three hydrogen atoms bonded tetrahedrally to the carbon, as shown in Fig. 10.12. The principal axes of inertia are the C—Cl bond axis a, on which the centre of gravity lies, and two mutually perpendicular axes b and c in a plane perpendicular to the axis a. As in the case of linear molecules, considered above, the end-over-end rotations about the axes b and c are still identical and we have $I_b = I_c$. The moment of inertia of the molecule about the axis a is, however, unique. Such a molecule spinning about this axis resembles a spinning top, and hence the name of 'symmetric top' for the group.

There are two subdivisions of this group: If $I_a < I_b = I_c$, as in the above example of CH_3Cl, the molecule is called a *prolate* symmetric top, and if $I_a = I_b < I_c$, the molecule is referred to as an *oblate* symmetric top. An example of the latter type is BCl_3. This molecule is planar and symmetrical, and in this case $I_c = 2I_a = 2I_b$.
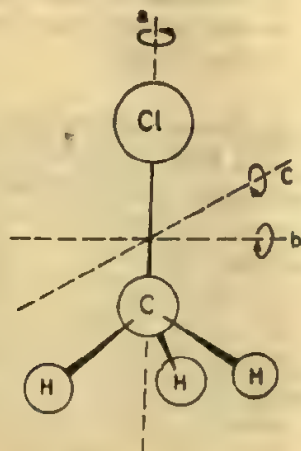
Fig. 10.12 The axes for the principal moments of inertia of the CH_3Cl molecule

(*iii*) **Spherical tops.** When a molecule has all three principal moments of inertia identical, it is called a spherical top. Examples include the tetrahedral molecule CH_4 and the octahedral molecule SF_6.

(*iv*) **Asymmetric tops.** When all the three principal moments of inertia are different (i.e. $I_a \neq I_b \neq I_c$) the molecule is an asymmetric top. The majority of substances belong to this group. Some examples are water H_2O, vinyl chloride ($CH_2=CHCl$), and methyl alcohol (CH_3OH).

We shall now consider the above rotational classes in turn, paying the maximum attention, however, to linear molecules, especially diatomic molecules, because much of their treatment can be directly extended to other classes of molecules.

10.6.1 Rigid Rotor Model

As a suitable model for diatomic molecule we may consider a dumbbell (Fig. 10.13), which consists of two balls of masses m_1 and m_2, representing the atoms, connected by a rigid rod of length r that represents the chemical bond between the atoms. This is known as the *rigid rotor model*. We consider the rotation of this rigid rotor about an axis perpendicular to its own axis and passing through the centre of gravity, as shown in Fig. 10.13.

The moment of inertia (I) for a system consisting of many particles is defined as

$$I = \Sigma m_i r^2_i \qquad (10.3)$$

where m_i is the mass of the ith particle at a distance r_i from the axis of rotation. For the present model, the moment of inertia is therefore

$$I = m_1 r^2_1 + m_2 r^2_2 \qquad (10.4)$$

It is more convenient to express the moment of inertia in terms of the single distance r, rather than two distances r_1 and r_2. If we take moments about the centre of gravity we get $m_1 r_1 = m_2 r_2$. It follows that

$$r = r_1 + r_2 = r_1 + \frac{m_1}{m_2} r_1 = \frac{m_1 + m_2}{m_2} r_1$$

and $\quad r_1 = \dfrac{m_2}{m_1 + m_2} r$
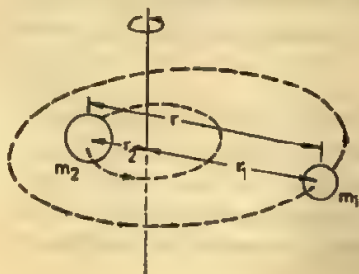
Fig. 10.13 A rotating dumbbell

Similarly

$$r_2 = \frac{m_1}{m_1 + m_2} \, r$$

On substituting these expressions for r_1 and r_2 in Eq. (10.4) and simplifying we obtain

$$I = \frac{m_1 m_2}{m_1 + m_2} \, r^2 = \mu r^2 \qquad (10.5)$$

The symbol μ denotes the reduced mass of the system (Appendix 1).

If v_1 and v_2 are the linear velocities of the balls of masses m_1 and m_2, the kinetic energy of the rotating system can be written in the form

$$\text{KE} = \tfrac{1}{2} m_1 v_1^2 + \tfrac{1}{2} m_2 v_2^2 \qquad (10.6)$$

The velocities v_1 and v_2 are related to the angular velocity ω by $v_1 = r_1 \omega$ and $v_2 = r_2 \omega$.

When we substitute these expressions for v_1 and v_2 in the above expression for KE, we get

$$\text{KE} = \tfrac{1}{2} \omega^2 (m_1 r_1^2 + m_2 r_2^2)$$

Substituting from Eq. (10.4) we get a simpler expression

$$\text{KE} = \tfrac{1}{2} I \omega^2 \qquad (10.7)$$

By analogy with linear momentum which is defined as the product of the linear velocity and mass, the angular momentum is defined as the product of the angular velocity and the moment of inertia. Denoting the angular momentum by p_θ we can therefore write $p_\theta = I \omega$ and so the expression for KE becomes

$$\text{KE} = p_\theta^2 / 2I \qquad (10.8)$$

10.6.2 Rotational Energies of Diatomic Molecules

Eq. (10.8) is the classical expression for the rotational kinetic energy of the rigid rotor model. While this expression is applicable for ordinary-sized systems, quantum restrictions are to be imposed on it before it can be used for molecular systems. This we can do as follows.

Generally, the allowed amounts of angular momentum are multiples of the quantity $h/2\pi$, where h is the Planck constant. Thus from the wave-mechanical treatment of the rigid rotor model for diatomic molecules, the following equation for the angular momentum is obtained:

$$p_\theta = \sqrt{J(J+1)} \; h/2\pi \qquad (10.9)$$

in which J is a rotational quantum number, having only integral values $0, 1, 2 \ldots$. The allowed angular momenta are therefore 0, $\sqrt{2}(h/2\pi)$, $\sqrt{6}(h/2\pi)$, $\sqrt{12}(h/2\pi), \ldots$, and this means that the molecule cannot rotate at speeds that would give it any other angular momenta.

The expression for allowed rotational energies for a diatomic molecule

J		ϵ_r
6	————————————	42hB
5	————————————	30hB
4	————————————	20hB
3	————————————	12hB
2	————————————	6hB
1	————————————	2hB
0	————————————	0
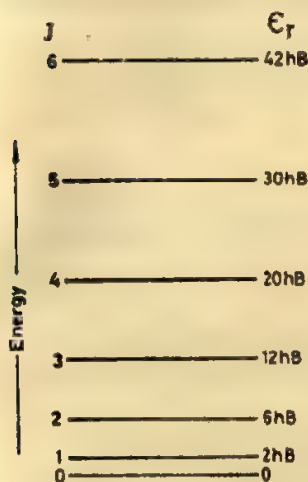
Fig. 10.14 The allowed rotational energies of a diatomic molecule as given by Eq. (10.10)

is then obtained by substituting Eq. (10.9) into Eq. (10.8). Denoting the rotational energy* *for a molecule* by ε_r the expression becomes,

$$\varepsilon_r = \frac{h^2}{8\pi^2 I} J(J+1)$$

$$= B.h.J(J+1) \text{ ergs} \qquad\qquad (10.10)$$

where $B = h/8\pi^2 I \ sec^{-1}$ $\qquad\qquad\qquad\qquad$ (10.11)

B is called the rotational constant. Eq. (10.10) shows how the rotational energies depend on I, which is a molecular property, and on quantum numbers, denoted by J. If $J = 0$, $\varepsilon_r = 0$ and there is thus no zero-point energy of rotational motion. A schematic representation of rotational energy level diagram is shown in Fig. 10.14.

If J' and J'' are the rotational quantum numbers of upper and lower rotational levels respectively, the energy difference between the two levels is

$$\Delta\varepsilon_r = \varepsilon'_r - \varepsilon''_r = B.h \ [J'(J'+1) - J''(J''+1)] \text{ ergs} \qquad (10.12)$$

and the expected frequency of the spectral line associated with this transition is given by

$$h\nu = \Delta\varepsilon_r \text{ or } \nu = \Delta\varepsilon_r/h \ sec^{-1} \qquad\qquad\qquad (10.13)$$

There is, however, a restriction on the energy transition. All transitions between energy levels are not permissible. It can be derived from quantum-mechanical treatment of spectroscopic transitions that for pure rotation spectra of a diatomic molecule J can change only by ± 1, i.e. $\Delta J = \pm 1$.

This condition is called a *selection rule*. The plus sign applies where

---

* It should be noted that in spectroscopic work energy is often given in cm^{-1} instead of ergs. Energy, given in cm^{-1}, is converted to ergs by multiplication by hc, where $c = 3 \times 10^{10}$ cm/sec is the velocity of all electromagnetic radiation.

radiation is absorbed and minus sign where radiation is emitted. Thus, if a molecule is in the rotational level for which $J = 2$, it may reach the $J = 3$ level by absorption or the $J = 1$ level by emission of radiation, but all other transitions are forbidden.

We can now apply the aforesaid selection rule in order to identify the absorption lines in a pure rotation spectrum. Each absorption line in the spectrum can be identified with an energy jump or transition from one rotational energy level to the next higher level. The energy change associated with this transition is equal to the energy of the absorbed radiation quanta. Thus, for the transition of the molecule from $J = 0$ to $J = 1$, which gives rise to the first absorption line in the spectrum, we can write from Eqs. (10.12) and (10.13):

Quantum energy absorbed for
the first absorption line $\quad = h\nu_1 = (\varepsilon_r)_{J=1} - (\varepsilon_r)_{J=0} = 2Bh \quad$ (10.14)

Molecules that are initially rotating with an energy corresponding to $J = 1$ absorb radiation quanta of such frequency that the energy is raised to that corresponding to $J = 2$. This gives rise to the second absorption line. Hence

Quantum energy absorbed for
the second absorption line $\quad = h\nu_2 = (\varepsilon_r)_{J=2} - (\varepsilon_r)_{J=1} = 4Bh \quad$ (10.15)

Identification of other absorption lines can be similarly done. The energy transitions that give rise to the absorption lines in the pure rotation spectrum are indicated in Fig. 10.15 by the solid vertical arrows. The *difference* in quantum energies between the first and second absorption lines obtained from Eqs. (10.14) and (10.15), is

$$h(\nu_2 - \nu_1) = (4 - 2)Bh = 2Bh \qquad (10.16)$$

It is easy to see that this result is true for each pair of adjacent absorption lines. Thus in Fig. 10.15, each arrow is longer than the preceding arrow by an amount equivalent to $2Bh$.

The frequency separation between the first and second absorption lines is obtained from Eq. (10.16) as

$$\Delta\nu = \nu_2 - \nu_1 = 2B \text{ sec}^{-1} \qquad (10.17)$$

The frequency separation for any other pair of adjacent absorption lines is also $2B$. The pure rotation spectrum of a diatomic molecule will therefore consist of a series of equally spaced lines with a frequency separation of $2B$ sec^{-1}. Schematically, this is represented at the bottom of Fig. 10.15.

10.6.3 *Interaction of Radiation with Rotating Molecules*
Pure rotational spectra are caused by rotational energy transitions of molecules due to interaction with radiation. Making use of its wave-nature picture, we can consider the radiation as a fluctuating electric field. A rotating dipole also generates a fluctuating electric field and, therefore,
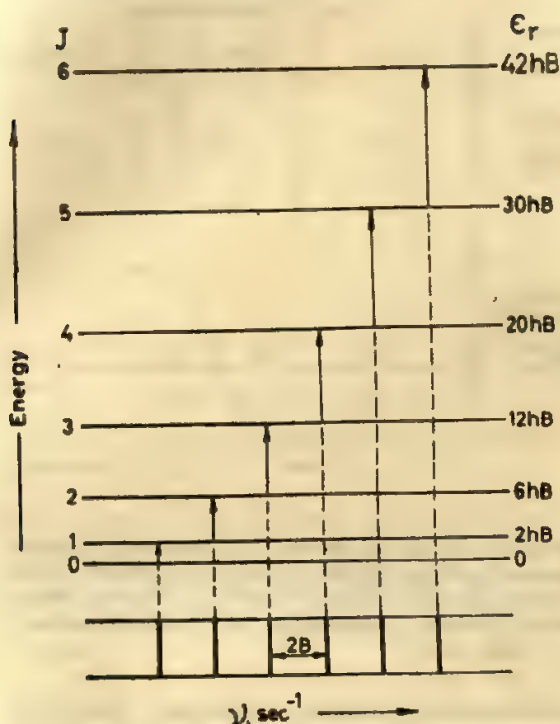
Fig. 10.15 Allowed transitions between the rotational energy levels of a rigid diatomic molecule and the spectrum which arises from them. Note that each arrow is longer than the preceding one by an amount equivalent to $2Bh$. The spectral lines thus show a constant spacing of $2B$.

interacts with the radiation. Suppose a molecule has a dipole, i.e. it has one end more positively charged and one end more negatively charged. When this molecule rotates, the positive and negative ends change places periodically and, as a result, the component dipole moment in a given direction, such as the vertical component in the plane of the paper, fluctuates regularly. This fluctuation, as shown in Fig. 10.16, is exactly similar in form to the fluctuating electric field of radiation, and so interaction can occur, leading to energy transitions, which we observe in the form of rotational spectra. A molecule which does not have a dipole is virtually incapable of this interaction. Thus homonuclear diatomic molecules such as H_2, N_2 and O_2, which have necessarily identical ends and so no dipole moment, do not give pure rotational spectra.

On the other hand, heteronuclear diatomic molecules, such as HCl, CO, NO, etc., have dipoles and so can interact with the microwave radiation. Some heteronuclear molecules like CO_2 and CS_2, however, show absence of radiation absorption in the microwave region. The
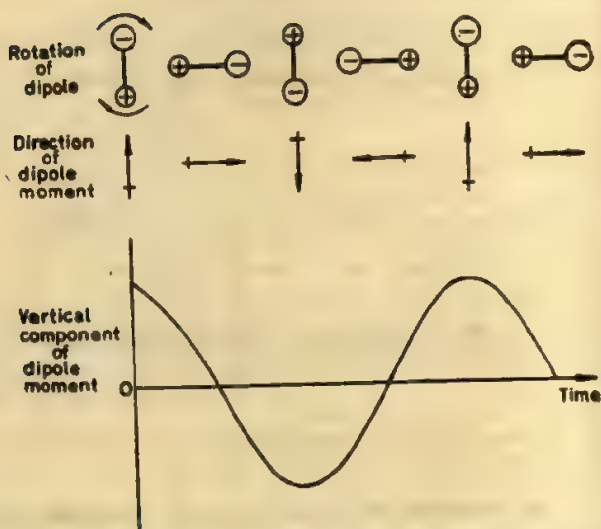
Fig. 10.16 Dipole fluctuation (in a particular direction) associated with the rotation of a diatomic molecule having a permanent dipole moment (After C. N. BANWELL *Fundamentals of Molecular Spectroscopy*, McGraw-Hill Book Co. Inc., New York, 1966)

explanation lies in the fact that these are symmetric molecules, $O=C=O$ and $S=C=S$, whose dipole moments are necessarily zero. For the same reason, spherical top molecules also do not produce pure rotational spectra. All molecules having permanent dipole moment are therefore said to be 'microwave active' and those having no permanent moment are said to be 'microwave inactive'.

10·6·4 *Determination of Moment of Inertia and Bond length from Rotational Spectra*

We have shown above that, for a diatomic molecule which is approximated to a rigid rotor (which signifies that the bond is rigid), the spacing of the lines in the pure rotation spectrum would be constant. However, careful examination of the lines shows that, in fact, the spacing between the lines decreases at higher values of J. This is because the molecule is not truly rigid, so that when in the higher rotational levels the molecule rotates faster, the bond is stretched slightly by the centrifugal force. The increase in bond length increases the moment of inertia, and consequently, the spacing is decreased. However, the correction for this becomes appreciable only for high values of J; for low values of J, the frequency separation can be taken to be constant, and so Eq. (10.17) may be used to obtain the moment of inertia I (and hence the bond length) of the molecule. We can, of course, find the value of I directly from equations such as (10.14) and (10.15), after we have matched the individual absorp-
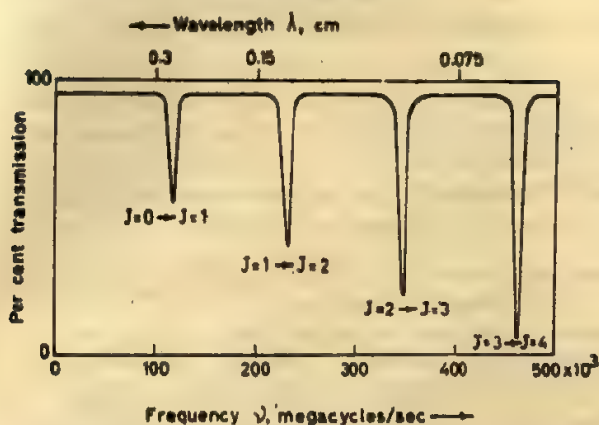
Fig. 10.17 A schematic representation of the rotational spectrum of CO

tion lines in the spectrum with particular transitions between allowed rotational levels of the molecule. That the assignment of the absorption lines to particular transitions has been correctly done is verified when calculations yield essentially same value of I from each of the absorption lines.

As an illustration of the application of the above method we may consider the microwave absorption of CO. A schematic representation of the rotation spectrum is shown in Fig. 10.17. The first line ($J = 0 \rightarrow 1$) in this spectrum occurs at the frequency of 1.153×10^{11} c/s. Hence from Eq. (10.14) $\nu_1 = 1.153 \times 10^{11}$ sec^{-1} = $2B$ or $B = 5.765 \times 10^{10}$ sec^{-1} Now, from Eq. (10.11) we have

$$I_{CO} = \frac{h}{8\pi^2 B} = \frac{6.624 \times 10^{-27}}{8\pi^2 \times 5.765 \times 10^{10}} = 1.45 \times 10^{-39} \text{ g cm}^2$$

We can now find the value of the internuclear distance using the relation of Eq. (10.5), which, in the present case, can be written as $I_{co} = \mu_{co} \cdot r^2_{co}$ where μ_{co}, the reduced mass of the CO molecule, is given by

$$\mu_{c,o} = \frac{m_c m_o}{m_c + m_o} = \frac{(12/6.023 \times 10^{23})(16/6.023 \times 10^{23})}{(12 + 16)/(6.023 \times 10^{23})}$$
$$= 1.14 \times 10^{-23} \text{ g/molecule}$$

The internuclear distance or bond length r_{co} is then calculated as

$$r_{co} = \sqrt{I_{co}/\mu_{co}} = \sqrt{(1.45 \times 10^{-39})/(1.14 \times 10^{-23})}$$
$$= 1.13 \times 10^{-8} = 1.13 \text{ Å}$$

In spectroscopic work, frequency is commonly expressed in terms of wavenumber*, $\bar{\nu}$, which is defined as the reciprocal of wavelength and

---

* In this Chapter we shall always differentiate the wavenumber frequency (cm^{-1}) from the true frequency (c/s) by placing a bar on the frequency symbol (ν).

has the dimension of cm^{-1}. It is related to the true frequency ν in c/s by

$$\nu = c/\lambda = c\bar{\nu} \qquad\qquad (10.18)$$

So when the frequency separation is given as $\Delta\bar{\nu}$, we can calculate the true frequency separation from $\Delta\nu = c.\Delta\bar{\nu}$ and then the moment of inertia I from Eqs. (10.17) and (10.11).

A selection of bond lengths obtained from studies of rotational energy level spacings of diatomic molecules is given in Table 10.4.

Table 10.4   Values of some Bond Lengths Determined by Microwave Spectroscopy

Molecule	Bond length (Å)	Molecule	Bond length (Å)
CO	1·128	HCl	1·275
NO	1·151	HBr	1·414
HF	0·917	HI	1.604

10.6.5 *Relative Intensities of Spectral Lines*

The intensities of the absorption lines in the rotational spectrum are not equal, (see, for example, Fig. 10.17). While Eq. (10.13) gives the positions of the spectral lines, we want now to consider the relative intensities of these spectral lines. We have seen that each absorption line in the rotational spectrum arises from transitions of molecules from one rotational level to the next higher rotational level, i.e. from J to $J + 1$. The relative intensities of the spectral lines would therefore be expected to depend on two factors: (i) the relative probabilities of transition between the various energy levels; as for instance, does a molecule have more, or less, chance of making the transition $J = 0 \rightarrow 1$ than the transition $J = 1 \rightarrow 2$? and (ii) the relative population of the various rotational levels; as for instance, is there more, or less, number of molecules in the $J = 0$ level than in the $J = 1$ level? As for the factor (i), quantum-mechanical calculations show that the probability of all transitions with $\Delta J = \pm 1$ is the same. Thus the intrinsic probability that, say, a single molecule in the $J = 0$ state will move to $J = 1$ is the same as that of a single molecule in the $J = 1$ state moving to $J = 2$. It turns out that, since the intrinsic probabilities are identical, the intensities of the spectral lines will be directly proportional to the population of each rotational level, i.e. the numbers of molecules intially present in each level.

The population of each rotational level is calculated by using Eq. (10.2), which we now rewrite as

$$\frac{n_J}{n_0} = \frac{g_J}{g_0} e^{-(\varepsilon_r)_J/kT} \qquad\qquad (10.19)$$

where n_J is the number of molecules in the Jth level of energy $(\varepsilon_r)_J$; n_0 is the number of molecules in the lowest rotational level for which $J = 0$ and so from Eq. (10.10) the rotational energy is also zero. In Eq. (10.19)

g_J and g_0 represent degeneracies of the Jth level and the lowest level, respectively; k is the Boltzmann constant. Degeneracy is the existence of two or more energy states having exactly the *same* energy. We saw in Chapter 3 that the number of degenerate p orbitals in an atom is $2l+1=3$, since $l = 1$ for a p orbital. Similarly, in the case of d orbitals, for which $l = 2$, the degeneracy is $2l + 1 = 5$. It can be shown that, for similar reasons, the degeneracy of a given rotational energy level is $2J+1$, where J is the rotational quantum number.

For the lowest rotational energy level, $J = 0$, so that $g_0 = 1$ and Eq. (10.19) becomes

$$\frac{n_J}{n_0} = (2J + 1)\ e^{-(\epsilon_r)_J / kT} \tag{10.20}$$

Whereas the term $(2J + 1)$ increases steadily as J increases, the exponential term decreases slowly and then much more rapidly as J increases. Thus, at smaller values of J, the term $(2J + 1)$ predominates, and at higher values of J it is the exponential term which predominates. As a result, the population of rotational levels rises to a maximum and then diminishes, as shown in Fig. 10.18 for the case of CO at 25°C. Differentiation of Eq. (10.20) shows that the population is a maximum at the nearest integral J-value to the value given by
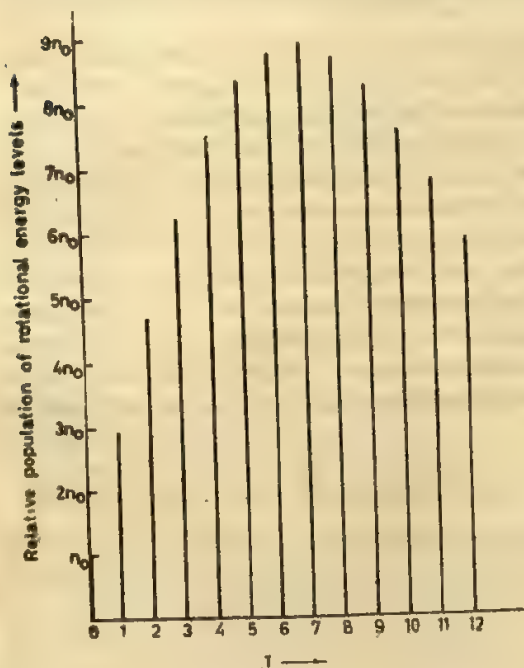
Fig. 10.18 Populations of some of the rotational energy levels of CO at 25°C in terms of n_0, the population of the $J = 0$ level

$$J = \sqrt{\frac{KT}{2hB}} - \frac{1}{2} \qquad\qquad (10.20a)$$

Since line intensities are directly proportional to the populations of the rotational levels, it is obvious that spectral lines arising from transitions between levels with very low or very high J values will have small intensities, and the intensity will be maximum at or near the J value given by Eq. (10.20a).

It is necessary here to briefly mention the following considerations regarding the population of rotational levels of linear molecules possessing a centre of symmetry (e.g. H_2, O_2, CO_2). If the molecule has a centre of symmetry, then nuclear spin (see Section 10.10) affects the population of its rotational levels. Thus for O_2 and CO_2 (since the spin of the oxygen nucleus with even charge and mass is zero) every alternate rotational level is completely unoccupied. In the case of H_2 and other molecules containing nuclei with non-zero spin (e.g. $H-C \equiv C-H$), alternate levels have populations differing by a certain factor; this effect, due to nuclear spin, is superposed on the normal thermal distribution and degeneracy, and this results in an alternation of populations.

10.6.6 Rotation Spectra of Polyatomic Molecules

Linear molecules. The spectral pattern for linear polyatomic molecules is found to be essentially similar to that for diatomic molecules. This stems from the fact that diatomic and linear polyatomic molecules are analogous, both being counterparts of a thin rod and as such the rotational energy expression of Eq. (10.10) is applicable in both cases. By a procedure analogous to that for diatomic molecules, the quantity B and thus the moment of inertia I for the linear polyatomic molecule can be evaluated. But difficulty arises when we wish to derive next the bond lengths. In general, a noncyclic polyatomic molecule containing n atoms has altogether $n-1$ bond lengths to be determined. Thus, in a linear triatomic molecule there are two bond lengths, whereas there is only one moment of inertia for the end-over-end rotation of the molecule, which is given by

$$I = \frac{m_1 m_2 r^2_{12}}{M} + \frac{m_2 m_3 r^2_{23}}{M} + \frac{m_1 m_3}{M}\ (r_{12} + r_{23})^2 \qquad (10.21)$$

where $M = m_1 + m_2 + m_3$ is the total mass of the molecule, and r_{12} and r_{23} are the bond lengths. It is obviously impossible to derive the two bond lengths from the one moment of inertia. The difficulty can be overcome, however, by working with two isotopic species of the same molecule and assuming that the bond lengths in a molecule are independent of isotopic species present. We may thus have two moments of inertia and solve for two bond lengths.

As an illustration, let us consider the rotation of the linear molecule

OCS, called carbonyl sulphide. We may consider two isotopic species of OCS, such as $^{16}O = ^{12}C = ^{32}S$ and $^{16}O = ^{12}C = ^{34}S$. At low values of J the rotational absorption lines for $^{16}O = ^{12}C = ^{32}S$ are found to have a constant frequency spacing, $\Delta\bar{\nu} = 0.4054$ cm^{-1}. The true frequency spacing is, therefore,

$$\Delta\nu = c.\Delta\bar{\nu} = (3.0 \times 10^{10})(0.4054)$$
$$= 1.216 \times 10^{10} \text{ sec}^{-1}$$

From Eq. (10.17) we have

$$B = \Delta\nu/2 = 6.08 \times 10^{9} \text{ sec}^{-1}$$

Then from Eq. (10.11) we obtain

$$I = \frac{h}{8\pi^2 B} = \frac{6.624 \times 10^{-27}}{8\pi^2 \times 6.08 \times 10^{9}} = 137.9 \times 10^{-40} \text{ g. cm}^2$$

Following Eq. (10.21) the moment of inertia of the $^{16}O = ^{12}C = ^{32}S$ molecule is given by

$$I = \frac{m_O m_C r^2_{CO}}{M} + \frac{m_C m_S r^2_{CS}}{M} + \frac{m_O m_S (r_{CO} + r_{CS})^2}{M} \qquad (10.22a)$$

where m_i is the mass of atom i, and r_{CO} and r_{CS} are the bond lengths of the molecule. Considering now the other isotopic molecule, $^{16}O = ^{12}C = ^{34}S$, we may write m'_s for m_s throughout Eq. (10.22a) to obtain

$$I' = \frac{m_O m_C r^2_{CO}}{M} + \frac{m_C m'_s r^2_{CS}}{M} + \frac{m_O m'_s (r_{CO} + r_{CS})^2}{M} \qquad (10.22b)$$

The value of I' derived from the rotational spectrum of the molecule $^{16}O = ^{12}C = ^{34}S$ is 141.4×10^{-40}. The two measured moments of inertia can now be used to solve Eqs. (10.22a) and (10.22b) for r_{CO} and r_{CS}. This gives $r_{CO} = 1.165$ Å and $r_{CS} = 1.558$ Å. Note that we do not need to write r'_{CS} in Eq. (10.22b), since we have assumed that the bond length is not changed if the mass of a nucleus in the molecule is changed. This assumption may be checked by studying the $^{18}O = ^{12}C = ^{32}S$ and $^{18}O = ^{12}C = ^{34}S$ molecules, since we would then have four moments of inertia. The bond lengths are found quite consistent, and this justifies the assumption. However, more accurate results are obtained if all the moments of inertia are found and the two bond lengths are then chosen to give the best agreement with them.

Some molecular data obtained by this procedure are given in Table 10.5.

Table 10.5 Some Molecular Data of Linear Polyatomic Molecules Determined by Microwave Spectroscopy

Molecule	Bond lengths (Å)		Molecule	Bond lengths (Å)	
N_2O	NN 1.126	NO 1.191	BrCN	CBr 1.790	CN 1.159
HCN	CH 1.064	CN 1.156	HC≡C–CN	CH 1.057	C–C 1.382
ClCN	CCl 1.629	CN 1.163		CN 1.157	C≡C 1.203

Symmetric top molecules. Because of the occurrence of more than one principal moments of inertia for non-linear molecules, the energy level patterns, and hence the rotation spectra, of these molecules are more complicated than those of linear molecules. However, because of the symmetry of symmetric top molecules, their rotation spectra are still relatively simple. Considering CH_3Cl (Fig. 10.12), for example, we recall that $I_b = I_c \neq I_a$ and $I_a \neq 0$. So, there are two types of rotation in which the molecule can absorb or emit energy, namely, the rotation about the top axis (i.e. the C—Cl axis, in this case) and that perpendicular to this axis.

We thus need two quantum numbers, J and K, to represent the rotational energy levels of a symmetric top. The quantum number K refers to rotation about the top axis, and J refers to an end-over-end rotation of the molecule. Both the quantum numbers must be integral or zero. The quantum number J, as in the case of linear molecules, may have, integral values from zero upwards, while now the new quantum number K may have values $0, \pm 1, \pm 2 \ldots \ldots \pm J$. Note that K can be negative. We can imagine that the positive and negative values of K correspond to clockwise and anticlockwise rotation about the top axis.

For a *rigid* symmetric top (i.e. a molecule in which the bonds are supposed not to stretch under a centrifugal force), the Schrödinger equation may be solved to give the allowed rotational energy levels as

$$\varepsilon_r = \frac{h^2}{8\pi^2 I_b} \cdot J(J+1) + \left(\frac{h^2}{8\pi^2 I_a} - \frac{h^2}{8\pi^2 I_b} \right) K^2$$

$$= hBJ(J+1) + hK^2(A - B) \text{ ergs} \tag{10.23}$$

where B and A, called rotational constants, are, as before, $B = h/8\pi^2 I_b$ and $A = h/8\pi^2 I_a$.

Since the energy depends on K^2, it is immaterial whether the top rotates clockwise or anticlockwise. Therefore, for all $K > 0$, the rotational levels are doubly degenerate.

The selection rules for rotational energy transitions of symmetric tops are $\Delta J = \pm 1$, as in the case of linear molecules, and $\Delta K = 0$. The physical interpretation of the second selection rule may be given as follows. Because of the symmetry of the molecule, its dipole is directed along the top axis. A rotation of the molecule about this axis, therefore, causes no dipole change, and consequently, the energy associated with this type of rotation cannot be changed by interaction with the electric field of the radiation.

Applying the above selection rules to Eq. (10.23), the energy difference between successive rotational levels is obtained as

$$(\Delta \varepsilon_r)_{J \to J+1} = (\varepsilon_r)_{J+1,K} - (\varepsilon_r)_{J,K}$$
$$= [hB(J+1)(J+2) + hK^2(A-B)] - [hBJ(J+1) + hK^2(A-B)]$$
$$= 2Bh(J+1) \text{ ergs} \tag{10.24}$$

This formula is identical with Eq. (10.12), as can be seen by putting $J'' = J$ and $J' = J + 1$. Consequently, the rotational spectrum of a symmetric top is just the same as for a linear molecule, and the frequency separation of the spectral lines is $2B$ sec^{-1}. Since only one moment of inertia — that for end-over-end rotation — can be obtained, it is necessary, as in the case of linear molecules, to determine the moments of inertia of several isotopic species in order to derive the molecular parameters. Considering our above example of CH_3Cl, the structure is defined by the C—H and C—Cl bond lengths, and the HĈH bond angle. To evaluate these three unknowns, moments of inertia of at least three isotopic species are required. However, four isotopic species of this molecule H_3C—^{35}Cl, H_3C—^{37}Cl, D_3C—^{35}Cl and D_3C—^{37}Cl are readily available, so that cross-checking can be done to ensure accuracy.

The molecular parameters of some symmetric tops obtained by microwave spectroscopy are listed in Table 10.6.

Table 10.6 Molecular Parameters of some Symmetric Top Molecules Determined by Microwave Spectroscopy

Molecule	Bond angle		Bond Length (Å)
CH_3Cl	HCH	110°30′	CH 1.103, CCl 1.782
CH_3F	HCH	110°0′	CH 1.109, CF 1.385
CH_3CN	HCH	109°8′	CH 1.092, CC 1.460, CN 1.158
$CHCl_3$	ClCCl	110°24′	CH 1.073, CCl 1.767
NH_3	HNH	107°18′	NH 1.106

Spherical top molecules. Spherical top molecules have no permanent dipole moment and so cannot produce a pure rotation spectrum. Moreover, since the polarizability of a spherical top molecule does not change during rotation, rotational Raman spectrum (see Section 10.9) is also not observed. Information about the molecular parameters of such a molecule must therefore be obtained from its vibration-rotation spectrum (Section 10.8).

Asymmetric top molecules. The energy levels of asymmetric top molecules cannot be expressed in terms of a single equation like those of linear and symmetric top molecules, and the selection rules are only approximate. Effects of centrifugal distortions are, moreover, rather large. Consequently, the rotational spectra, even for simple asymmetric tops, are extremely complicated and the determination of molecular parameters requires much tedious computation. However, very precise structural data of asymmetric top molecules have been determined by microwave methods; some are listed in Table 10.7.

As a conclusion to this section, it can be said that in microwave spectroscopy we have a method for determining the structural parameters

Table 10.7 Molecular Parameters of some Asymmetric Top Molecules Determined by Microwave Spectroscopy

Molecule	Bond angle	Bond length (Å)
H_2O	HOH 104°30′	OH 0.958
O_3	OOO 116°49′	OO 1.278
CH_3OH	COH 110°15′	OH 0.958
CH_2Cl_2	HCH 112°0′	CH 1.068
	ClCCl 111°47′	CCl 1.772
HNCO	HNC 128°5′	HN 0.987
		CO 1.171
		NC 1.207

of those molecules which possess a permanent electric dipole moment and which can be studied in the gas phase. Values obtained from the analysis of pure rotational spectra are among the most accurate of all structural data.

10.7 Vibrational Spectra

In the rigid rotor model for the diatomic molecule dealt with in the previous section, we assumed that the bond is inflexible. We now consider the fact that atoms in a molecule actually do not remain in fixed relative positions but vibrate about some mean position. We have already noted (Section 10.4) that the absorption of infrared radiation by a molecule increases its vibrational energy. From the measurement of infrared absorption spectrum we can therefore derive information about the spacings of the allowed vibrational energies. Since the spacing of the vibrational energy levels of a molecule, as we shall see later, is related to the stiffness or flexibility of molecules, we can obtain information on this property of the molecule from the infrared spectrum.

It must be borne in mind, however, that when the infrared radiation is passed through a *gaseous* sample, not only does the vibrational energy of a gas-phase molecule change as a result of the absorption of the radiation quanta, but the rotational energy of the molecule may also change. This combination of vibrational and rotational effects results in additional complexity of the spectrum. It can be avoided by using the sample in the pure liquid state, or in a solution. Each molecule, in this case, is surrounded by closely neighbouring molecules which prevent it from rotating like a free molecule of the gas phase, but do not, however, affect the vibrations of the molecule. In this section, we shall concern ourselves with the study of the pure vibrational effects, i.e. the way in which a non-rotating molecule can vibrate, and see how we can use the vibrational spectra to learn about the rigidity of the molecule.
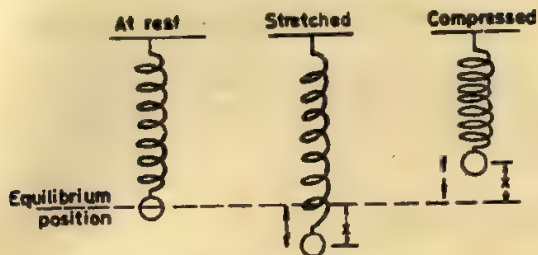
Fig. 10.19 Vibration of a ball-and-spring system

10.7.1 Vibrational Motion of Systems that Behave Classically

The way in which a diatomic molecule vibrates can be approached by considering its ordinary-sized counterpart, consisting of two balls connected by a spring. We shall, however, start with a discussion of the vibrational motion of a simpler system, that of a ball and spring, as shown in Fig. 10.19, and then extend it to the two-ball arrangement. Figure 10.19 shows the direction of the restoring force f of the spring that acts on the ball when the latter is displaced by an amount, say x from the equilibrium position. We assume that our model is a harmonic oscillator, i.e. it obeys Hooke's law, which says that the restoring force is proportional to the amount of displacement of the mass from the equilibrium position; consequently,

$$f = - kx \qquad (10.25)$$

where k is the proportionality constant, called the *force constant* of the spring. The minus sign has been introduced to show explicitly that the direction of f is opposite to that in which x increases. As can be seen, k is the value of the restoring force for a unit displacement, and so it is a measure of the stiffness of the spring. A strong, inflexible spring will have a large value of k whereas a weak spring, which is easily extended or compressed, will have a small value of k.

As the spring moves up and down periodically, the ball attached to the spring also undergoes a periodic motion which can be described by either the sine or the cosine function of time. For the variation of the displacement x with the time t, we can therefore write

$$x = A \sin 2\pi v_0 t \quad \text{or} \quad x = A \cos 2\pi v_0 t \qquad (10.26)$$

Though either function can be used to describe the vibrational motion, we shall, however, use only the cosine function in the following discussion.

The term A is the amplitude of the vibration and $2\pi v_0$ is the constant coefficient of t. Every time t increases by $1/v_0$, the argument $2\pi v_0 t$ increases by 2π and the cosine function completes a cycle. The time interval $1/v_0$ is thus the number of seconds required for the ball to complete one vibration or one cycle. It follows therefore that v_0 is the number of cycles per second, i.e. the frequency of the vibration.

We shall now try to relate this vibrational frequency to the properties

of the spring system, namely, the mass m of the ball and the force constant k of the spring.

Writing d^2x/dt^2 for the acceleration a in the well known Newton's equation $f = ma$ and then combining it with Eq. (10.25), we have

$$- kx = m \frac{d^2x}{dt^2} \tag{10.27}$$

Substituting for x and its second derivative in Eq. (10.27) from Eq. (10.26), we then get

$$- k \, (A \cos 2\pi v_0 t) = m \, (- 4\pi^2 v_0{}^2 \, A \cos 2\pi v_0 t)$$

$$\text{or} \quad v_0 = \frac{1}{2\pi} \sqrt{\frac{k}{m}} \tag{10.28}$$

Eq. (10.28) is our desired relation. We thus see that the system has a characteristic or fundamental frequency of vibration; this frequency is related to the force constant and the mass of the system, and is independent of the amplitude.

We now extend the above treatment to the vibration of a system of two particles connected by a spring, as shown in Fig. 10.20. The displacement coordinates x_1 and x_2 and the directions of the restoring force on the particles, both when the spring is extended and when it is compressed, are indicated in Fig. 10.20. The extension of the spring, according to this representation, is given by $(x_2 - x_1)$; so, Eq. (10.25) now becomes

$$f = - k(x_2 - x_1) \tag{10.29}$$

Considering the system during extension and taking care of the positive and negative directions of displacement, as shown in Fig. 10.20, we can express the accelerations of the first and second particles as $- d^2x_1/dt^2$ and d^2x_2/dt^2, respectively. Corresponding to Eq. (10.27) we now have

$$- k \, (x_2 - x_1) = - m_1 \frac{d^2x_1}{dt^2} \tag{10.30}$$

$$\text{and} - k \, (x_2 - x_1) = m_2 \frac{d^2x_2}{dt^2} \tag{10.31}$$
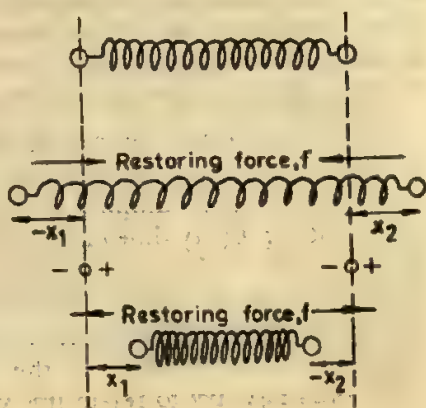
Fig. 10.20 Vibration of a system of two balls and a spring (After G. M. Barrow *The Structures of Molecules*, Benjamin, New York 1963)

The same two equations are also obtained for the system undergoing compression.

Describing the oscillating motion, as before, by the cosine function of time, we can express the vibrational displacements of the two particles as $x_1 = A_1 \cos 2\pi\nu_0 t$, and $x_2 = A_2 \cos 2\pi\nu_0 t$.

Substituting these expressions for x_1 and x_2 and their second derivatives into Eqs. (10.30) and (10.31) and then rearranging, we obtain

$$kA_2 + (4\pi^2\nu_0^2 m_1 - k)\, A_1 = 0$$

and $(4\pi^2\nu_0^2 m_2 - k)\, A_2 + kA_1 = 0$

Eliminating the amplitudes A_1 and A_2 between these two equations, we obtain

$$\frac{4\pi^2\nu_0^2}{k} = \frac{m_1 + m_2}{m_1 m_2} = \frac{1}{\mu}$$

$$\text{or} \quad \nu_0 = \frac{1}{2\pi}\sqrt{\frac{k}{\mu}} \tag{10.32}$$

where μ is the reduced mass of the two-particle system; ν_0 is the fundamental frequency of the system, treated as a classical harmonic oscillator. It can be seen that Eq. (10.32) is of the same general form as Eq. (10.28) for a one-particle system and can be derived from the latter simply by substituting μ for m.

The potential energy of the above model is derived easily. If the spring is to be stretched, a force must be exerted in opposition to the restoring force of the spring, as given by Eq. (10.25). The work done in this process increases the potential energy of the system. If the potential energy for the equilibrium length of the spring is taken to be zero, one obtains the potential energy for other lengths by simply integrating the force kx over the differential distance dx to obtain

$$U = \int_0^x kx\,dx = \tfrac{1}{2}kx^2 \tag{10.33}$$

where x is the distortion from the equilibrium length.

Solving Eq. (10.32) for k and substituting the result into Eq. (10.33), we find that

$$U = 2\pi^2\nu_0^2\mu x^2 \tag{10.34}$$

It is easy to recognize that as a particle approaches the limit of its displacement, its kinetic energy decreases and its potential energy increases, while at the limit, i.e. at $x =$ amplitude A, there is no kinetic energy and all its energy must then be potential energy; consequently,

$$\text{vibrational energy} = 2\pi^2\nu_0^2\mu A^2 \tag{10.35}$$

10.7.2 *Vibrational Energies of Diatomic Molecules*

We have given above an introduction to the vibrational motion of systems that behave classically. Eq. (10.35), which is a classical mechanical

result, means that, since there is no restriction on the value of the amplitude A, the vibrational energy of a classical harmonic oscillator can have any value. In contrast to this, however, the vibrational energy of molecular systems, as we have earlier pointed out, is quantized, so that only certain values are allowed. We must therefore use the quantum-mechanical expression for the vibrational energies of our molecular model. The Schrödinger equation for the harmonic oscillator is

$$\frac{d^2\psi}{dx^2} + \frac{8\pi^2\mu}{h^2}\left(E - \frac{kx^2}{2}\right)\psi = 0 \qquad (10.36)$$

This equation can be solved and the allowed energy values are found to be given by

$$\varepsilon_v = \frac{h}{2\pi}\sqrt{\frac{k}{\mu}}\left(v + \frac{1}{2}\right) \qquad v = 0, 1, 2, \ldots \qquad (10.37)$$

where v, which can have only integer values, is called the *vibrational quantum number*. Combining Eqs. (10.32) and (10.37) we can also write

$$\varepsilon_v = h\nu_0\,(v + \tfrac{1}{2}) \qquad (10.38)$$

in which ν_0 is the *frequency of a classical harmonic oscillator* with force constant k and mass μ.

The allowed vibrational energies for a diatomic molecule, as given by Eq. (10.37), are shown schematically in Fig. 10.21. The energy levels are seen to be equally spaced, with a spacing of $(h/2\pi)\sqrt{k/\mu}$, or more simply, $h\nu_0$. Since the selection rule for the vibrational quantum number, obtained from quantum mechanics, is $\Delta v = \pm 1$, the energy difference between two vibrational levels involved in a transition will always be equal to this spacing, and we would accordingly expect all lines in the spectrum to fall in the same place (see diagram at the foot of Fig. 10.21). To obtain the frequency of the spectral line we equate the spacing of the vibrational energy to the quantum energy of the radiation: $h\nu = h\nu_0$, or $\nu = \nu_0$.
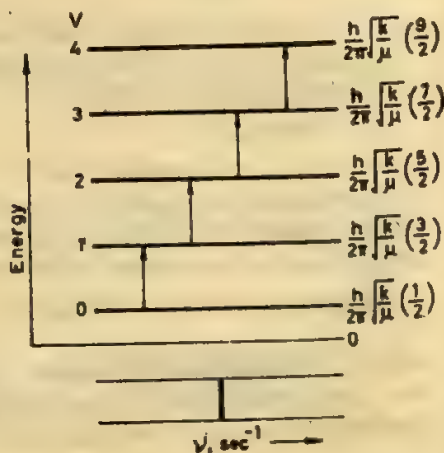
Fig. 10.21 Allowed transitions between the vibrational energy levels and the resulting spectrum for a diatomic molecule that behaves as a simple harmonic oscillator

Thus, for the ideal harmonic oscillator, the spectral absorption occurs *exactly* at the classical vibration frequency.

Since the vibrational energy spacing is usually large compared to kT, it follows from the Boltzmann distribution that at ordinary temperatures most molecules will be in the $v = 0$ vibrational level. Also note that, unlike the rotational energy, the vibrational energy is not zero even at the lowest vibrational level, since when $v = 0$, $\varepsilon_v = \frac{1}{2}h\nu_0$. This half quantum of vibrational energy is known as *zero-point energy*. This means that a molecule must always vibrate and can never be at rest. This is a significant wave-mechanical result which has been amply borne out by experiment.

10.7.3 *Interactions of Radiation with Vibrating Molecules*

When infrared radiation whose quanta are comparable in energy to the spacing of vibrational levels is allowed to fall on a sample of heteronuclear diatomic molecules, the vibrating molecules can grab energy from the radiation beam and thereby increase their vibrational energy. These molecules are therefore 'infrared active'. The mechanism of this transfer of energy between the radiation and the vibrating molecule is similar to that discussed in connection with rotational spectra. We saw that for a molecule to be microwave active its rotational motion must produce fluctuation in the dipole moment. Similarly, for a molecule to be infrared active its vibrational motion must give rise to a fluctuating dipole moment. This explains why heteronuclear molecules like HCl, CO and NO give vibrational spectra, whereas homonuclear diatomic molecules like H_2 and N_2 do not. The former are polar molecules and their dipole moments can generally be expected to be a function of the internuclear distance, whereas the latter have no dipole moment no matter what the internuclear distance is.

It should be noted that whereas a molecule which does not possess permanent dipole moment cannot be microwave active, it may nevertheless be infrared active if its vibration produces oscillating dipole moment. We may consider the carbon dioxide molecule as an example. The molecule has a small positive charge on the carbon atom and small negative charges on outer oxygen atoms; but since the three atoms are arranged linearly, the net dipole moment is zero. The molecule is therefore microwave inactive. We may now consider three modes of vibration for the CO_2 molecule. In the mode of vibration known as the *symmetric stretch*, where the molecule is alternately stretched and compressed with both C—O bonds changing simultaneously (see Fig. 10.22), the dipole moment evidently remains zero throughout the vibrational motion. This mode of vibration is therefore infrared inactive.

In the *asymmetric stretching mode* of vibration, on the other hand, when one bond is stretched, the other bond is compressed (Fig. 10.23). This
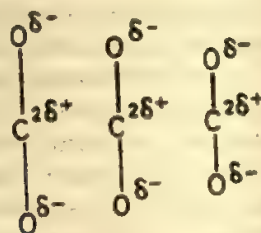
Fig. 10.22 The symmetric stretching vibration of CO_2 Stretched   Normal   Compressed
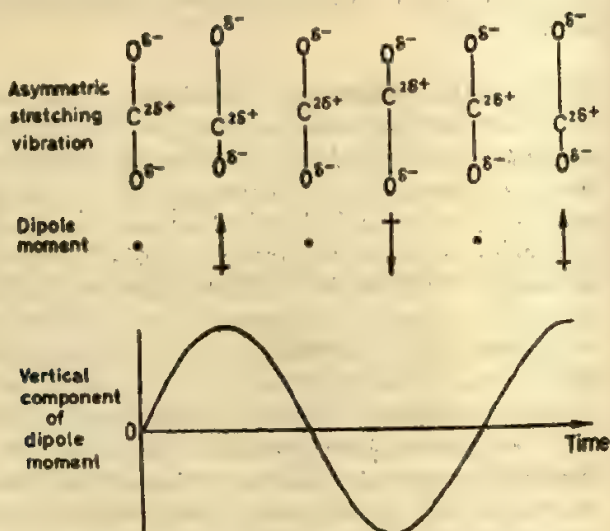
Fig. 10.23 The fluctuation in the dipole moment due to the asymmetric stretching vibration of the carbon dioxide molecule (After C. N. BANWELL *Fundamentals of Molecular Spectroscopy*, McGraw-Hill Book Co. Inc., New York, 1966)

results in a fluctuating dipole moment, as shown in the lower part of Fig. 10.23. This particular vibration is thus infrared active.

The other mode of vibration, known as the *bending mode*, is also associated with a dipole fluctuation (see Fig. 10.24) and is therefore infrared active.

10.7.4 Deduction of Molecular Properties from Vibrational Spectra of Diatomic Molecules

It is convenient to discuss this topic taking a specific example. A solution of carbon monoxide in the inert solvent carbon tetrachloride absorbs the infrared radiation at $\lambda = 4.68 \times 10^4$ Å. (In terms of frequency* units

---

* It should be noted that the wavenumber $(\bar{\nu})$ of a spectral line is often referred to as the 'frequency' of the line. Confusion should not arise, however, if the units of any expression are kept in mind, since $\bar{\nu}$ is in reciprocal cm (cm^{-1}) while the true frequency ν is in cycles/sec.

Bending
vibration

Dipole
moment

Vertical
component
of dipole
moment
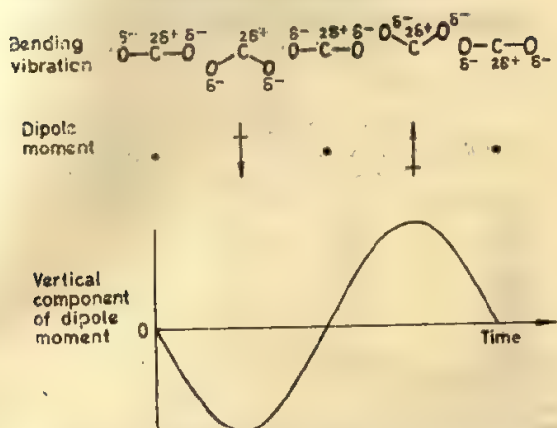
Fig. 10.24 Dipole fluctuation associated with the bend-ing motion of the carbon dioxide molecule (After C. N. BANWELL *Fundamentals of Molecular Spectroscopy* McGraw-Hill Book Co. Inc., New York, 1966)

of cm^{-1}, usually used in the infrared region, this corresponds to $\bar{\nu} = 2140$ cm^{-1}.) The vibrational spectrum of CO thus has an absorption band at this wavelength. It should be mentioned that the solvent does not absorb radiation of this wavelength.

The simple selection rule for the harmonic oscillator undergoing vibra-tional changes is $\Delta v = \pm 1$. Now since molecules, as already mentioned, are mostly in the $v = 0$ vibrational level, we may assume that it is the transition from $v = 0$ to $v = 1$ that leads to the aforesaid absorption by CO. The energy spacing of these two vibrational levels, which is $(h/2\pi)\sqrt{k/\mu}$ from Eq. (10.37), is therefore equal to the quantum energy of radiation of frequency $\bar{\nu} = 2140$ cm^{-1} or $\nu = 6 \cdot 40 \times 10^{13}$ sec^{-1}. Thus,

$$\frac{h}{2\pi}\sqrt{\frac{k}{\mu}} = h\nu = 4 \cdot 24 \times 10^{-13} \text{ erg} \qquad (10.39)$$

The value of μ for CO, which we calculated in the previous section, is $1 \cdot 14 \times 10^{-23}$ g. Eq. (10.39) is then solved to give $k = 18 \cdot 5 \times 10^{5}$ dyne/cm. This is the force constant of the bond in CO.

The above example illustrates a procedure that can be used to obtain bond force constants for other molecules. Some representative data are presented in Table 10.8.

Just as the force constant of a spring is a measure of the force required to stretch or compress the spring so also is the force constant of a chemical bond. In the light of this interpretation the results of Table 10.8 are readily appreciated. It is seen, for instance, that the bond in HF is considerably more rigid than that in HI, and similarly, multiple-bonded molecules like NO and CO have greater rigidiy than single-bonded molecules.

Table 10.8   Bond Force Constants of some Diatomic Molecules deduced from Vibrational Spectra

Molecule	Position of the absorption band ($\bar{v}$, cm^{-1})	Reduced mass ($\times 10^{-24}$ g)	Force constant ($\times 10^5$ dyne/cm)
HF	4138	1.59	9.7
HCl	2886	1.63	4.8
HBr	2650	1.65	4.2
HI	2309	1.66	3.1
CO	2140	11.4	18.5
NO	1876	12.4	15.5

We can also calculate approximately the vibrational amplitude of a diatomic molecule in a simple manner by adopting, in part, the classical picture of a vibrating system. The potential energy of a harmonic oscillator, expressed as a function of extension x from the equilibrium length, is given by Eq. (10.33). Since at the maximum extension, x_{max}, all of the energy of the oscillator is in the form of potential energy, we can write

vibrational energy $= \frac{1}{2}k\, x^2_{max}$

The vibrational energy of the $v = 0$ state is obtained by putting $v = 0$ in Eq. (10.37), and its substitution in the above expression gives

$$\frac{1}{2}\left(\frac{h}{2\pi}\right)\sqrt{\frac{k}{\mu}} = \frac{1}{2}\,kx^2_{max} \tag{10.40}$$

Knowing the values of the bond force constant k and reduced mass μ, we can find x_{max}, i.e. the amplitude of vibration.

For HF, for example, we have from Table 10.8, $k = 9 \cdot 7 \times 10^5$ dyne/cm, and $\mu = 1 \cdot 59 \times 10^{-24}$ g, so that from Eq. (10.40) we obtain

amplitude of vibration $= x_{max}$

$$= 0 \cdot 092 \times 10^{-8}\,cm = 0 \cdot 092\ \text{Å}$$

The equilibrium bond length of HF, determined by the methods of rotational spectroscopy, is $0 \cdot 917$ Å. We thus find that in HF the vibrational amplitude is about 10 per cent of the bond length even in the lowest vibrational state. This highlights the fact that molecules are not rigid structures, and we could rather look upon them as flexible spring systems.

10.7.5   Overtone Transitions of Diatomic Molecules

We shall recall that as a model of the diatomic molecule we took a system consisting of two particles connected by a spring, which behaves as a harmonic oscillator. The potential energy function for this system is given by Eq. (10.33), while Eq. (10.37) represents the quantum-mechanical
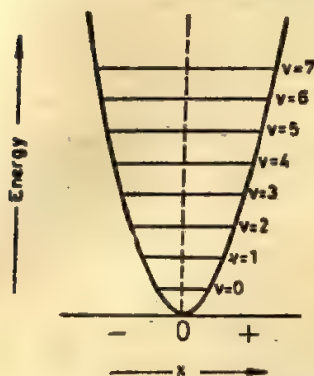
Fig. 10.25 The potential energy curve and the allowed vibrational energy levels for a diatomic molecule undergoing simple harmonic motion

expression for its allowed vibrational energies. The potential energy curve rises parabolically from a minimum, that is zero, at the equilibrium position, as shown in Fig. 10.25, which also shows the allowed vibrational energies forming a pattern of equispaced levels.

While the representation of Fig. 10.25 is true for a simple harmonic oscillator, real molecules, however, do not obey exactly the laws of simple harmonic motion. Thus, although for small compressions and extensions, real bonds may be taken as perfectly elastic obeying Hooke's law, at larger distortions, say more than 10 % of the bond length, they deviate from Hooke's law behaviour. Moreover, when greatly stretched, say 2 times the normal length, the bond is largely destroyed and further extension becomes relatively easy. It thus turns out that at large extensions of the bond, the restoring force will no longer increase in proportion to the extension, but, in fact, will decrease and, at infinite extension, becomes zero. Thus, for small extensions of the bond, where Hooke's law is obeyed, the potential energy will rise parabolically; however, for larger extensions, it will rise more and more slowly until, at very great extensions, it will cease to increase with further extension. On the other hand, if the bond is greatly compressed and the atoms are brought very close together, the repulsive forces will become dominant due to the proximity of the nuclei and that of extranuclear electrons. The compressed bond will, as a consequence, strongly resist further bond shortening, which means that with bond compression the potential curve will rise very steeply. It follows from these qualitative arguments, and also from more quantitative ones that can be given, that the potential energy curve for real molecules, which undergo *anharmonic* extensions and compressions, will have the shape indicated in Fig. 10.26. The ideal potential energy curve (broken line), corresponding to Hooke's law behaviour, is also shown in the same diagram for comparison,

A purely empirical equation, which represents, to a good approximation, the actual potential energy curve for many molecules, was derived by Morse and is called the *Morse function*:
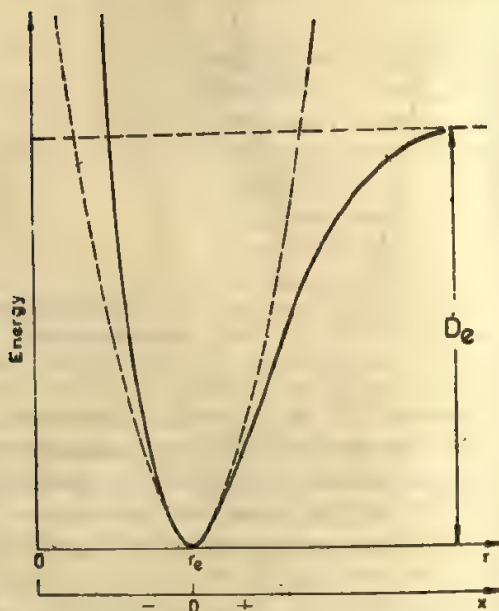
Fig. 10.26 Comparison of the potential energy curve for a diatomic molecule undergoing anharmonic oscillations with that (broken) deduced on the basis of simple harmonic motion

$$U = D_e \, (1 - e^{-\beta x})^2 \tag{10.41}$$

in which U is the potential energy for an internuclear distance r, reckoned as zero at the lowest point of the curve, where it corresponds to the equilibrium distance r_e; x is equal to $(r - r_e)$; β is a constant for the given molecule and D_e is the dissociation energy reckoned from the lowest point of the curve. [It may be noted that as r approaches zero, U, according to Eq. (10.41), remains finite, though actually it should increase to infinity. This weakness of the Morse function is, however, not of much consequence, since the situation where $r = 0$ has little practical significance.]

When Eq. (10.41) is used instead of Eq. (10.33) in the Schrödinger equation, the allowed vibrational energies are found to be

$$\varepsilon_v = h\nu_e \, (v + \tfrac{1}{2}) \, [1 - a(v + \tfrac{1}{2})] \text{ ergs} \tag{10.42}$$

where v is the vibrational quantum number, as before; ν_e is the oscillation frequency, defined below, and a is the corresponding *anharmonicity constant*.

If we compare Eq. (10.42) with Eq. (10.38), we can write

$$\nu_0 = \nu_e \, [1 - a(v + \tfrac{1}{2})] \tag{10.43}$$

where ν_0 is the oscillation frequency of a harmonic oscillator having the same vibrational energy as the anharmonic one.

We thus see that the anharmonic oscillator behaves like the harmonic oscillator, but with an oscillation frequency (and hence a force constant) that decreases with increasing v. We further note that at the equilibrium point with zero vibrational energy, which corresponds to the hypothetical energy state of $v = -\frac{1}{2}$, ν_e equals ν_0. We may therefore regard ν_e as the (hypothetical) *equilibrium oscillation frequency* of the anharmonic oscillator, that is, the oscillation frequency for an infinitely small amplitude of vibration about the equilibrium point.

In the lowest vibrational state, i.e. $v = 0$, the vibrational energy, from Eq. (10.42), is

$$\varepsilon_v = \tfrac{1}{2}h\nu_e(1 - \tfrac{1}{2}a) \text{ ergs} \tag{10.44}$$

The zero-point energy for the anharmonic oscillator thus differs slightly from that for the harmonic oscillator.

For bond stretching vibrations, the anharmonicity constant a is always positive and small, of the order of 10^{-2}. Eq. (10.42) then reveals that, in the lower energy range, the allowed vibrational energies of the anharmonic system are nearly equally spaced, but in the higher energy range they crowd more closely together with increasing v, (see Fig. 10.27). This deviation from constant spacing is revealed by the *overtone* transitions, i.e. transitions of the type $v = 0$ to $v = 2$, $v = 0$ to $v = 3$, and so forth. The selection rule predicted by theory for the anharmonic oscillator is $\Delta v = \pm 1, \pm 2, \pm 3, \ldots\ldots$ However, since at room temperature, as we have already noted, nearly all the molecules in a sample exist in the
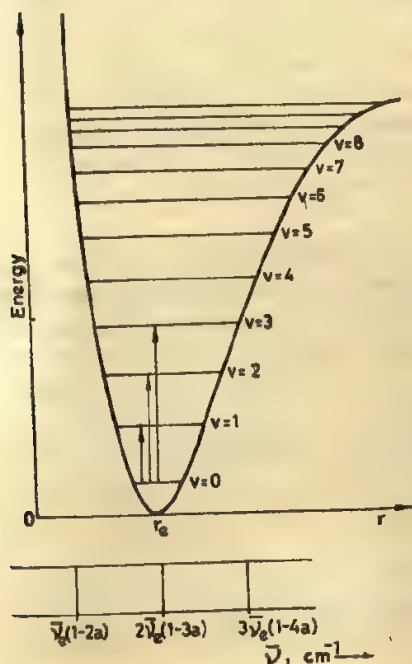
Fig. 10.27 The allowed vibrational energy levels and some transitions between them for a diatomic molecule undergoing anharmonic vibrations

$v = 0$ state, because $\Delta \, \varepsilon_v \gg kT$, we need consider only transitions from the $v = 0$ state, such as $v = 0 \longrightarrow v = 1$, $v = 0 \longrightarrow v = 2$, $v = 0 \longrightarrow v = 3$, etc., which are described respectively as *fundamental*, *first overtone*, *second overtone*, and so on. Further, it is observed that the spectral line intensity falls sharply at higher overtone transitions, so that in practice we can restrict ourselves to the following three possible transitions:

(i) $v = 0 \longrightarrow v = 1$ giving the *fundamental absorption* line of considerable intensity. The energy difference from Eq. (10.42) is

$\Delta \varepsilon_v = h \nu_e (1 - 2a)$ ergs

So the frequency (in wavenumber, cm^{-1}) of the fundamental absorption line is

$$(\bar{\nu})_{v=0 \to v=1} = \frac{h \nu_e (1 - 2a)}{hc} = \bar{\nu}_e (1 - 2a) \text{ cm}^{-1} \qquad (10.45a)$$

where $\bar{\nu}_e = \nu_e / c$ cm^{-1}.

(ii) $v = 0 \longrightarrow v = 2$, which gives the *first overtone* of small intensity at

$$(\bar{\nu})_{v=0 \to v=2} = 2\bar{\nu}_e (1 - 3a) \text{ cm}^{-1} \qquad (10.45b)$$

(iii) $v = 0 \longrightarrow v = 3$, which gives the *second overtone* of normally negligible intensity at

$$(\bar{\nu})_{v=0 \to v=3} = 3\bar{\nu}_e (1 - 4a) \text{ cm}^{-1} \qquad (10.45c)$$

These three transitions are shown in Fig. 10.27, and the corresponding spectrum at the bottom of this figure. Since $a \approx 0 \cdot 01$, the first overtone occurs at frequency approximately twice that of the fundamental absorption, and the second overtone occurs at frequency approximately thrice that of the fundamental absorption. The infrared spectrum of HCl, for instance, shows a very strong absorption (fundamental) at 2,886 cm^{-1}, and a very weak one (second overtone) at 8347 cm^{-1}. We can use these data to obtain from Eq. (10.45) the values of the anharmonicity constant and the equilibrium oscillation frequency for the HCl molecule. We find that $a = 0 \cdot 0174$ and $\bar{\nu}_e = 2 \cdot 99 \times 10^3$ cm^{-1} (hence $\nu_e = 8 \cdot 97 \times 10^{13}$ sec^{-1}).

So far we have considered only the transitions from the $v = 0$ state, because, as we saw earlier, most of the molecules initially exist in this state at ordinary temperatures. However, if the temperature is high, say above 200°C, or the molecule is highly anharmonic, a small fraction of the molecular population may be in the $v = 1$ state to give rise to absorptions characterized by transitions from the $v = 1$ state to higher states. Such absorptions are usually very weak and are referred to as *hot bands* since a high temperature is one necessary condition for their appearance. A true hot band should increase in intensity as the temperature of the sample is increased.

10.7.6 The Vibrations of Polyatomic Molecules

Let us now investigate the vibrational spectra of polyatomic molecules.

Diatomic molecules, as we saw earlier, give only one fundamental absorption band. This is because diatomic molecules have only one fundamental vibration or degree of freedom. In dealing with vibrational absorptions of a polyatomic molecule, we shall therefore first need to consider the number of fundamental vibrations associated with it.

Consider a molecule containing N atoms. First, let us suppose that all the bonds in the molecule are weak so that each atom is free to move independently of the rest. Each atom would then be free to move in three perpendicular or orthogonal directions (e.g. x, y and z Cartesian axes) and would thus have three degrees of freedom. So the collection of N atoms constituting the molecule would have a total of $3N$ *degrees of freedom*. Now let us imagine the bonds to be gradually strengthened till they become normal bonds of the molecule. When we consider this molecule as a whole, we do not ascribe three translational degrees of freedom to the motion of each atoms, but rather we ascribe three degrees of freedom to the translational motion of the whole molecule as a unit. We also have to consider the rotational motion of the molecule. As we saw earlier, a nonlinear molecule can rotate about three mutually perpendicular axes that pass through the centre of gravity of the molecule and thus has three degrees of freedom for its rotational motion. Thus, of the total of $3N$ degrees of freedom for a group of N atoms, the molecular entity uses $3 + 3 = 6$ degrees of freedom. The remaining $3N-6$ degrees of freedom must then be accounted for by other motions of the atoms constituting the internal vibration of the molecule. We thus see that a nonlinear molecule with N atoms has $3N-6$ vibrational degrees of freedom. The number of vibrational degrees of freedom corresponds to the number of basic ways in which the molecule can vibrate. We have thus shown that a non-linear molecule of N atoms can have $3N-6$ fundamental vibrations.

For linear molecules, however, as we saw in Section 10.5, only rotations about the two axes perpendicular to the bond axes constitute rotations of the system; hence only two degrees of rotational freedom are required. The number of vibrational degrees of freedom is therefore $3N-5$. A linear molecule of N atoms can thus have $3N-5$ fundamental vibrations. For diatomic molecules (necessarily linear) such as we have already considered in this section, $N = 2$, and $3N-5 = 1$, so that there can be only one fundamental vibration.

Let us next consider H_2O. The triatomic non-linear molecule has $3N-6 =$ three fundamental vibrations. Each of these fundamental vibrations can be treated as the single vibration of a diatomic molecule leading to a single absorption band. The spectrum for H_2O molecule will therefore be expected to show three dominant absorptions. This is corroborated by the observed spectrum for water dissolved in an inert solvent, schematically shown in Fig. 10.28. Corresponding to each of the three absorption bands in the spectrum, we can draw a vibrational energy level diagram,
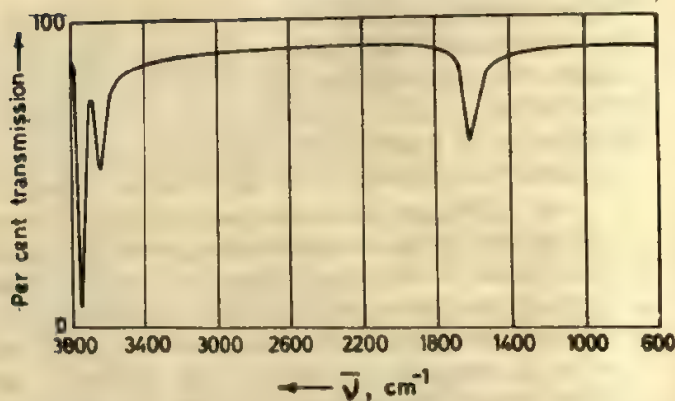
Fig. 10.28 Infrared spectrum (schematic) of H_2O in an inert solvent showing three dominant absorptions

as in Fig. 10.29(a), the energy spacing being given by the quantum energy of the corresponding frequency.

Our next endeavour would be to associate each band with a particular vibrational mode. This can be done relatively easily for small molecules which have a small number of atoms and hence small number of vibrational modes. But the task becomes increasingly difficult for large molecules since the number of vibrations becomes correspondingly large. We can, however, follow an approximate procedure which is nevertheless very useful. The procedure is to associate a bond-stretching vibration, like that of diatomic molecules, with each bond and an angle-bending vibration with each inter-bond angle. In our H_2O example, we may therefore identify the two higher-frequency absorption bands with stretching vibrations of the two O—H bonds and the third one, which occurs at a lower frequency, with the angle-bending vibration. Since, however, the two O—H bonds of H_2O are identical, separately their stretching vibrations cannot give rise to absorptions at different frequencies. Each absorption is therefore not to be attributed to a separate vibration of each bond. Rather the vibrations of the two bonds are coupled to give two different vibrations, namely, a *symmetric stretching vibration* and an *antisymmetirc stretching vibration*. The ways in which the atoms would have to be moved, so that when released these three types of vibrations would occur, are shown in Fig. 10.29(b). It is easily seen that if the vibrating molecule is rotated by 180° about the symmetry axis (C_2), the vibration is unchanged in the symmetric stretching mode, whereas in the antisymmetric mode, the same operation produces a vibration which is in antiphase with the original. Note that we have labelled the three vibrations in Fig. 10.29 as v_3, v_1 and v_2. By convention, vibrations are usually labelled in decreasing frequency within their symmetry type. The label v_1 is thus attached to the symmetric stretching vibration as it
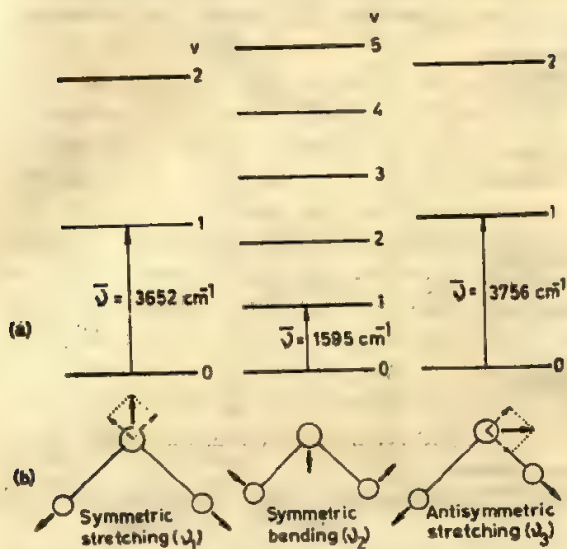
Fig. 10.29 (a) The three vibrational energy levels and the transitions corresponding to the three absorptions in the spectrum of Fig. 10.28. (b) Three fundamental vibrations of the water molecule. The solid arrows show the way in which the atoms would have to be moved so that when released simultaneously the corresponding vibration would occur.

gives the highest symmetric frequency (3652 cm⁻¹) and the label ν_2 to the symmetric bending vibration, having the next highest symmetric frequency (1595 cm⁻¹); the remaining antisymmetric vibration (3756 cm⁻¹) is then labelled as ν_3.

The three vibrational motions in Fig. 10.29(b) are also referred to as the *normal modes of vibration*, or *normal vibrations*, of the molecule. In general, a normal vibration is one in which all the atoms in a molecule vibrate at the same frequency and in phase with each other.

A condition that a vibration is infrared active, as we have already seen, is that there must be a periodic change of the electric dipole moment during the vibration. The dipole moment change may occur either along or across the line of the symmetry axis, and accordingly, the label parallel (∥) or perpendicular (⊥) is attached to it. The nature of the change in the dipole moment for the three vibrations of the H_2O molecule is depicted in Fig. 10.30.

We take the linear triatomic molecule CO_2 as our final example. The fundamental vibrations for this molecule are shown in Fig. 10.31. The symmetric stretching vibration, we have already seen, does not produce any change in dipole moment (which remains zero all through this motion) and is, therefore, infrared inactive. The corresponding vibration frequency
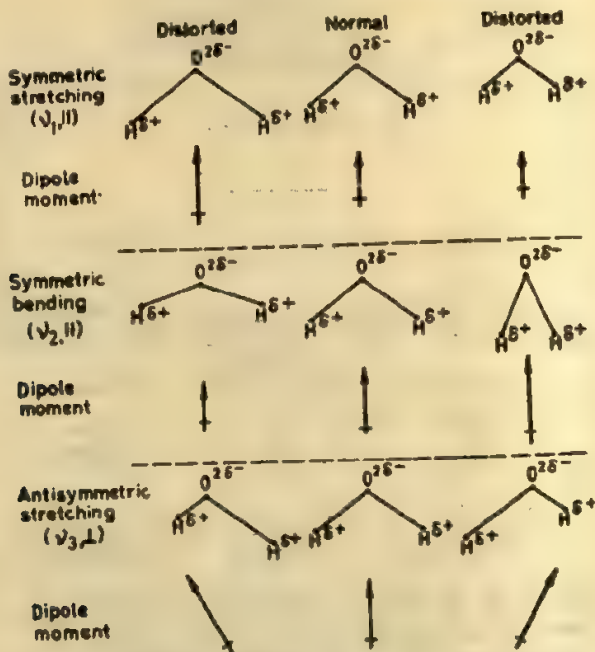
Fig. 10.30 The three vibrations of the water molecule and their associated dipole fluctuations. The amplitudes are exaggerated for clarity. (After C. N. BANWELL. *Fundamentals of Molecular Spetroscopy* McGraw-Hill Book Co. Inc., New York, 1966)

Symmetric stretching (ν_1)

$\bar{\nu} = 1330$ cm^{-1}

Bending $(\nu_2, \perp)$

$\bar{\nu} = 667$ cm^{-1}

Antisymmetric stretching $(\nu_3, \parallel)$

$\bar{\nu} = 2349$ cm^{-1}
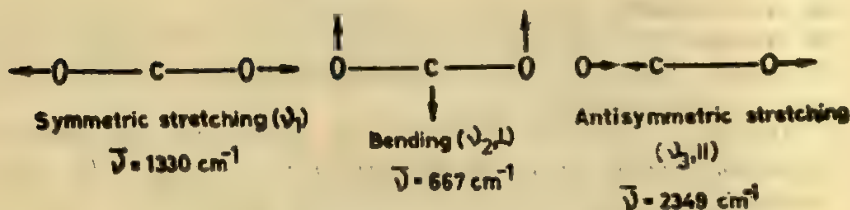
Fig. 10.31 Fundamental vibrations of the carbon dioxide molecule

may, however, be obtained by other methods, which we shall discuss in a later section. The vibrations ν_3 and ν_2 produce dipole moment change (Figs. 10.23 and 10.24) and are therefore infrared active. According to the $3N-5$ rule, we would expect four $(3 \times 3 - 5)$ modes of vibrations for CO_2, instead of the three shown in Fig. 10.31. However, it should be noted that while by ν_2 we have represented a bending vibration in the plane of the paper, an exactly similar type of bending motion can occur in which the oxygen atoms move simultaneously into and out of the plane. Because the only difference between these two bending modes is one of direction, they have the same frequency, and so are said to be *degenerate*; they must, nevertheless, be considered as separate motions.

In summary, there are four normal modes of vibration for CO_2, but there are only three different frequencies because of the degeneracy of two of the normal modes.

As the presence of symmetry in a molecule may make some of the vibrational frequencies the same or may cause absence of some vibrational frequencies, study of vibrational spectra can provide valuable clues to the symmetry of the molecule in question.

It can be seen from the two examples (H_2O and CO_2) given above that the stretching vibration frequencies are much greater than the bending vibration frequency. In view of the dependence of the vibration frequency on the force constant [see, for example, Eq. (10.32)], we can say — and it is indeed a general rule — that bond-stretching force constants are considerably greater than angle-bending force constants. A general conclusion that flows from this is that bond-angles are much more easily deformed than the bonds.

10.7.7 *Overtone and Combination Frequencies for Polyatomic Molecules*

We would expect, in view of our above discussion, that the infrared spectrum of a polyatomic molecule consists essentially of an absorption band at each of the $3N—6$ (or $3N—5$ for linear) fundamental frequencies. Plainly, this is based on the assumption that each vibration is simple harmonic. If, however, this restriction is lifted, as we have seen earlier in the case of diatomic molecules (Section 10.7.5), we have the possibility of overtone transitions. Corresponding to each of the fundamental modes ν_1, ν_2, ν_3, etc., there is now the possibility of first, second, etc., overtones, of diminishing intensities, occurring approximately at twice the fundamental frequency, thrice the fundamental frequency, etc. In addition to this, there may also be bands arising from two or more fundamental frequencies or overtones. Thus bands may occur at such combinations as $\nu_1 + \nu_2$, $2\nu_1 + \nu_2$, $\nu_1 + \nu_2 + \nu_3$, etc. frequencies, and are known as *combination bands*. Similarly, *difference bands* may occur at frequencies such as $\nu_1 - \nu_2$, $2\nu_1 - \nu_2$, $\nu_1 + \nu_2 - \nu_3$, etc. These band are normally weak but often occur in a complex spectrum.

Further, it may happen that in a particular molecule two different modes of vibration, more commonly a fundamental and some overtone or combination, have frequencies very close to each other. Then just as two pendulums of similar frequencies resonate and exchange energy (see Section 6.2), the two close molecular vibrational frequencies may also resonate, resulting in two new frequencies, one higher and one lower than the original frequencies. Such a resonance phenomenon, when it occurs between a fundamental and an overtone, is known as *Fermi resonance*. A simple example of such resonance is found in CO_2 where ν_1 (1330 cm^{-1}) is very close to $2\nu_2$ (1334 cm^{-1}); the two bands observed at frequencies 1285 cm^{-1} and 1385 cm^{-1} (whose mean is seen to be at about 1330 cm^{-1})

are therefore attributed to a resonance between ν_1 and $2\nu_2$. (It may be noted that these bands are not observable in the infrared, but may be observed in the Raman spectrum, discussed in a later section).

10.7.8 Information on Molecular Constitution from Infrared Spectra

With an increase in the number of atoms in a molecule, the number of normal modes increases rather rapidly and a detailed analysis of the vibrational spectrum becomes impossible. One is therefore content to assign the strongest bands and to identify some of the weaker ones as overtones or combinations. For practical purposes, however, a number of very useful generalizations can be made.

A particularly important spectral region is 1430–910 cm^{-1}. This region contains many absorptions caused by bending vibrations and also the absorptions caused by several stretching vibrations (see Table 10.9). Since in a molecule, bending vibrations are in general more numerous

Table 10.9 Characteristic Stretching Frequencies of certain Groups of Atoms

Group	Intensity of absorption peak*	Group frequency range (cm^{-1})
—O—H	(v, sh)	3500–3700
>N—H	(m)	3300–3500
≡C—H	(s)	3300–3400
=C—H	(m)	3000–3100
C—H(aromatic)	(v)	3050–3100
C—H(aliphatic)	(m-s)	2800–3000
—CH$_3$	(s)	2970 (asym. stretch)
	(m)	2870 (sym. stretch)
	(m)	1460 (asym. deform.)
	(s)	1375 (sym. deform.)
—CH$_2$—	(s)	2930 (asym. stretch)
	(m)	2860 (sym. stretch)
	(m)	1470 (deformation)
—S—H	(w)	2550–2650
—C≡N	(m)	2200–2300
—C≡C—	(v, m, w)	2170–2270
>C=O	(s)	1700–1850
>C=C<	(m)	1550–1650
>C—N<	(w)	1000–1200
>C—O—	(s)	1000–1200
>C=S	(s)	1200
>C—F	(s)	1050–1300
>C—Cl	(s)	700–800
>C—Br	(s)	550–650
>C—I	(s)	400–550

*v=variable, sh=sharp, s=strong, m=medium, w=weak

than stretching vibrations, this region of the spectrum is particularly rich in absorption bands. It is seldom possible to assign these bands to particular modes of vibration but the complex of bands as a whole is highly typical of the given molecular structure. Consequently, this frequency region, frequently called *fingerprint region*, is extremely useful in establishing conclusively the identity of two samples. Similar molecules, for instance, may show very similar spectra at frequencies higher than 1430 cm^{-1}, but in the fingerprint region there will usually be discernible differences.

Many commonly occurring functional groups such as $-CH_3$, $>C=O$, $-NH_2$, etc. give rise to one or more characteristic absorption bands when they are present in a molecule. These bands are, to a considerable extent, independent of the structure of the molecule as a whole and can be used for analysis. For example, all compounds containing a $-CH_3$ group possess absorption bands in the region of 3000 cm^{-1} and 1400 cm^{-1}. Similarly, all compounds with a $>C=O$ group have a strong band in the region of 1700 cm^{-1}. With a few exceptions, these characteristic group frequencies fall in the regions well above or well below the fingerprint region. Table 10.9 contains some of the more important group frequencies along with a qualitative indication of their intensities.

A close look at Table 10.9 reveals some logical trends in group frequencies. We see, for instance, that the stretching vibration frequency decreases in the series C—H, C—F, C—Cl, C—Br and C—I. In accordance with Eq. (10.32), this trend is attributed to increasing mass of the atom within the group (and hence increasing μ) in the same sequence. This also accounts for the fact that the stretching frequency of $C=S$ is less than that of $C=O$. On the other hand, an increase in the strength of the bond, and hence an increase in the force constant k, should increase the vibration freqeuncy. This trend is observed in the series C—X, $C=X$, $C\equiv X$, where X is C or N, and also in C—O and $C=O$.

Much more extensive correlations of atomic groups and characteristic absorption frequencies than that given in Table 10.9 are available, and such information is of considerable assistance in the identification and characterization of both organic and inorganic compounds. As an example of the application of the group frequency data, we shall analyse the infrared spectrum of thioacetic acid shown in Fig. 10.32. The bands clearly reveal the presence of $-CH_3$, $-C=O$ and $-SH$ groups. This shows that the molecule is $CH_3CO.SH$, and not $CH_3CS.OH$. One may also make use of a negative evidence: if the spectrum does not contain the absorption bands characteristic of a certain group, the molecule does not contain that group. In the above spectrum, it is seen that, apart from the general background of fingerprint bands, there is no absorption at about 1200 cm^{-1}, thus indicating that the molecule does not contain a $>C=S$ group.

Slight variations in absorption frequencies are found to occur depending
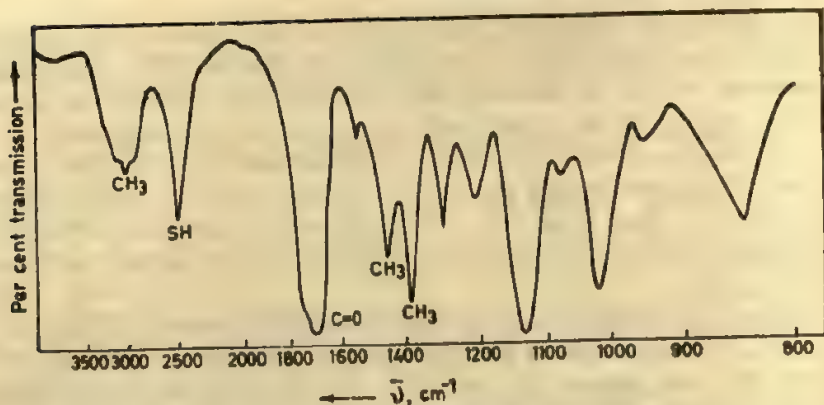
Fig. 10.32 The infrared spectrum of thioacetic acid

on the way in which the groups are joined together in the molecule, i.e. on the structure of the molecule as a whole. Information on structural details may therefore be obtained by measuring the *exact* positions of the absorption bands. For instance, one of the absorptions due to the C—H bond in benzene occurs at 670 cm^{-1}, but moves to about 730 cm^{-1} in a monosubstituted benzene compound, while for a disubstituted benzene compound the absorption moves near to 750, 780, and 820 cm^{-1} for *ortho-*, *para-*, and *meta-*substitutions respectively. One may therefore infer the presence or absence of different isomers, such as in a mixture of xylenes or cresols, simply from an examination of the infrared spectrum.

Resonance and intermolecular effects cause shifts in group frequency position. However, the shifts in themselves are highly characteristic and so are useful for diagnostic purposes. For example, $>C = O$ and $>C=C<$, occurring as isolated groups in a molecule, give the expected group frequencies of 1715 cm^{-1} and 1650 cm^{-1} respectively, but when they occur together in a molecule as $>C = C - \overset{|}{\underset{|}{C}} = O$, their respective frequencies are shifted to 1675 cm^{-1} and to about 1600 cm^{-1}. The intensity of the $>C = C<$ absorption, moreover, increases due to this coupling.

A free O—H bond gives rise to stretching absorption at about 3600 cm^{-1}, but the presence of hydrogen-bonding lengthens and weakens the O—H bond and so lowers its vibrational frequency. If the hydrogen bond is formed, for instance, between the O—H group and a $>C = O$ group, the linkage in the latter is also weakened by the hydrogen-bonding and its absorption frequency is lowered, though to a smaller extent than in the O—H.

Since, as we saw earlier, an infrared spectrum occurs only when the vibration produces a change in the electric dipole moment, an increase in the polarity of a bond will be expected to cause an increase in the intensity of its absorption band. This is generally borne out in practice,

as for instance, the intensities of the C—H, N—H and O—H bands increase in that order and so do the intensities of the C—C, C = N and C = O bands.

10.8 *Vibration - Rotation Spectra*

When a gas-phase molecule absorbs infrared radiation, in addition to the vibrational energy change of the molecule its rotational energy may also change. When this happens, each absorption band, which is due to a particular vibrational energy change, is found to consist of a number of relatively closely spaced absorption lines. These are the rotational components of the band and can be related to the rotational energy changes that occur simultaneously with the vibrational energy change. Studies of such vibration-rotation bands furnish both force-constant and moment-of-inertia data without recourse to microwave spectroscopy. In the following we shall be primarily concerned with the behaviour of diatomic gas phase molecules.

10.8.1 *Diatomic Vibrating Rotator*
Since the energies of rotational and vibrational motions are, in general, largely different (see Section 10.4), it is a good approximation to consider that a diatomic molecule can execute rotations and vibrations quite independently. This is tantamount to assuming that the combined vibrational-rotational energy is simply the sum of the separate vibrational and rotational energies. For the allowed vibrational-rotational energies of a diatomic molecule, considered as a rotating harmonic oscillator, we can therefore write by adding Eqs. (10.38) and (10.10),

$$\varepsilon_{vr} = h\nu_0 \left(v + \tfrac{1}{2}\right) + hBJ(J + 1) \text{ ergs}$$
$$\left. \begin{array}{l} v = 0, 1, 2, \ldots, \\ J = 0, 1, 2, \ldots \end{array} \right\} \qquad (10.46)$$

On inserting the appropriate value of v and J in Eq. (10.46), we obtain the values of vibrational-rotational energies that are allowed to a diatomic molecule. Eq. (10.46) thus allows us to show diagrammatically the allowed energy level pattern for a rotating-vibrating diatomic molecule. This is done in Fig. 10.33, in which, however, only the first two vibrational levels and the first five rotational levels associated with each vibrational level are shown.

It may be shown that the selection rules for vibration-rotational transitions are the same as those for each separately, i.e. $\Delta v = \pm 1$ and $\Delta J = \pm 1$. Strictly speaking, Δv may also be zero, but then this is the case of pure rotational transition, which we have already dealt with in Section 10.5. It may be noted, however, that the transition with $\Delta J = 0$, except under very special circumstances, does not occur; this means that
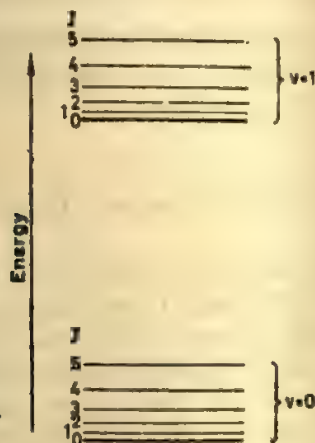
Fig. 10.33 The allowed energy level pattern for a rotating-vibrating diatomic molecule

a vibrational energy change must be accompanied by simultaneous rotational energy change.

Considering a transition from a lower state defined by v'' and J'' to a higher state defined by v' and J' (it is conventional in spectroscopy to use a single prime for the upper state and a double prime for the lower), we have, in general, for the increase in energy of the molecule

$$\Delta\varepsilon_{vr} = h\nu_0 \, (v' - v'') + hB[J'(J' + 1) - J''(J'' + 1)] \text{ ergs} \qquad (10.47)$$

When a gaseous sample is exposed to infrared radiation, molecules of the sample, initially distributed throughout many of the rotational levels in the $v = 0$ state, absorb energy from the infrared radiation and go to certain of the rotational levels in the $v = 1$ state. Since we have assumed that rotational and vibrational energy changes occur independently, we can take B to be identical in the $v = 0$ and $v = 1$ states. So we can have

(*i*) $\Delta J = + 1$, i.e. $J' - J'' = 1$; hence

$$\left.\begin{array}{c} \Delta\varepsilon_{vr} = h\nu_0 + 2hB(J'' + 1) \text{ ergs,} \\ J'' = 0, 1, 2,\ldots. \end{array}\right\} \qquad (10.48)$$

(*ii*) $\Delta J = - 1$, i.e. $J' - J'' = - 1$

$$\left.\begin{array}{c} \Delta\varepsilon_{vr} = h\nu_0 - 2hBJ'' \text{ ergs} \\ J'' = 1, 2, 3,\ldots. \end{array}\right\} \qquad (10.49)$$

Note that in Eq. (10.49), J'' cannot be zero, since this would imply J' having a value of -1. The above two equations may be conveniently combined into the expression

$$\left.\begin{array}{c} \Delta\varepsilon_{vr} = h\nu_0 + m.2hB \\ m = \pm 1, \pm 2, \ldots\ldots \end{array}\right\} \qquad (10.50)$$

where m, replacing $J'' + 1$ in Eq. (10.48) and J'' in Eq. (10.49), has positive values for $\Delta J = + 1$ and negative values for $\Delta J = - 1$; but m cannot be zero since this would require J' or J'' to be -1.

Eq. (10.50) then represents the allowed vibration-rotational energy

changes. The frequencies (in wave-numbers) of the corresponding spectral lines are given by

$$\bar{\nu} = \frac{\Delta \varepsilon_{vr}}{hc} = (\nu_0 + m.2B)/c = \bar{\nu}_0 + m.2\bar{B} \text{ cm}^{-1} \tag{10.51}$$

where $\bar{B} = B/c$.

The vibration-rotation spectrum will consist of equally spaced lines (spacing $\Delta \bar{\nu} = 2\bar{B}$) forming two branches; lines corresponding to negative values of m (i.e. $\Delta J = -1$) are referred to as the *P branch* and those corresponding to positive m (i.e. $\Delta J = +1$) are called the *R branch**. As m cannot be zero, the line corresponding to $m = 0$ will be missing from the spectrum and the position which this line would occupy, i.e.

$$\bar{\nu} = \bar{\nu}_0$$

is known as the *band origin* or *band centre*.

Some of the allowed transitions as given by Eq. (10.50) are shown in Fig. 10.34 and the absorption spectrum that these transitions would produce is shown at the bottom of the figure. The spectral lines in the P and R branches have been labelled according to their J'' values. This is the conventional notation for such spectra.

The pattern for the vibration-rotation absorption band predicted above is nicely corroborated by the illustration in Fig. 10.35 showing the absorption band of gaseous HBr. We know from our above analysis that the spacing of the rotational components within the band is $2\bar{B}$ and the band centre corresponds to $\bar{\nu}_0$. The first quantity thus allows calculation of the moment of inertia and the equilibrium bond length, while the second quantity allows calculation of the bond force constant. Thus from the study of the infrared absorption bands for gas-phase diatomic molecules we can derive information on the structure as well as the rigidity of molecules without recourse to the less convenient microwave spectroscopy. As indicated in the case of vibrational spectra, homonuclear diatomic molecules, as they do not have permanent dipole moment, do not give a vibration-rotation spectrum also.

As can be seen from Fig. 10.35, there is a variation in the intensity of the rotational components of the absorption band. This intensity distribution naturally arises from the initial distribution of the molecules among the various rotational levels, as discussed in Section 10.6.5, (see, for instance, Fig. 10.18).

10.8.2 *Asymmetry of Rotation-Vibration Absorption Band*

If one looks carefully at the finer details of the actual absorption band of Fig. 10.35, one will notice a significant fact that the spacing between the rotational components, in contrast to what would be expected from

---

*The terms P and R belong to the sequence O, P, Q, R and S; these labels are attached to the line series corresponding to $\Delta J = -2, -1, 0, +1$, and $+2$, respectively. The ΔJ values of 0 and ± 2, though not permissible here, do, however, occur in other contexts.
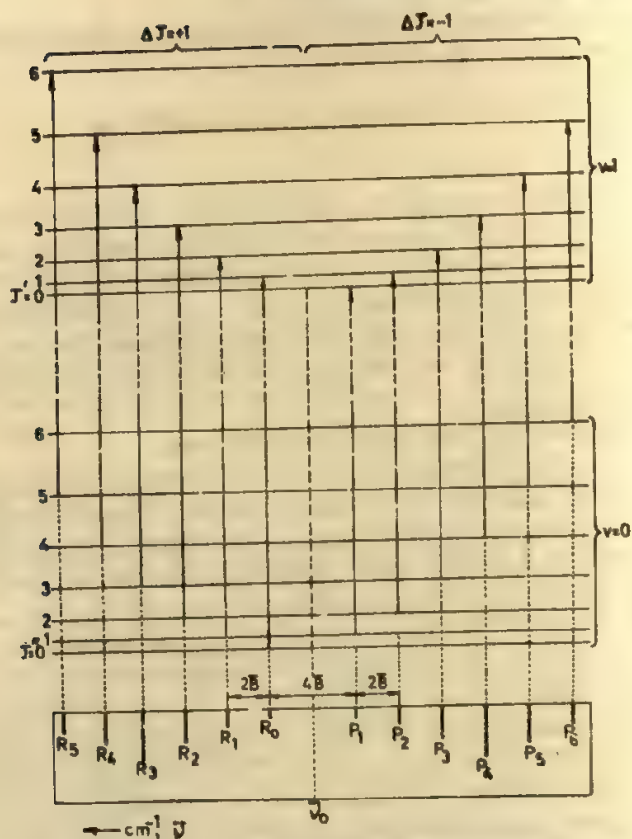
Fig. 10.34 Some transitions between the rotational-vibrational levels of a diatomic molecule. The absorption spectrum that these transitions would produce is shown in the lower part of the diagram.
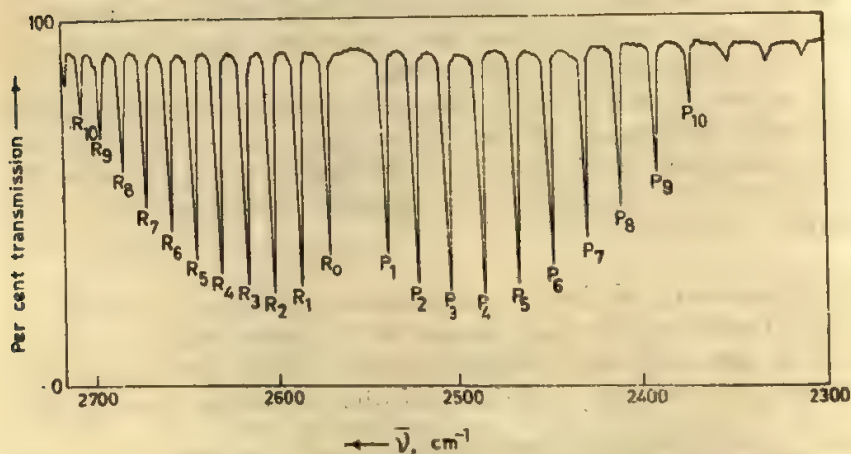
Fig. 10.35 The rotation-vibration absorption band of gaseous HBr in the infrared spectral region. The P and R branch lines are labelled according to their J'' values.

the simple theoretical deduction given above, is not exactly constant throughout the band. The weakness of the above treatment that has led to this failure to account for the actually observed variation is that we have so far assumed vibration and rotation to proceed independently without any interaction, so that the rotational energy does not depend on the vibrational energy. However, this assumption is not strictly correct. Thus, in view of the asymmetric shape of the potential energy curve (for anharmonic vibrations) of Fig. 10.26, showing a tendency to spread out to larger internuclear distances at higher energies, the average bond length, and hence the moment of inertia I, will be expected to increase as the molecule is raised to higher vibrational states. As the rotational constant B, is inversely proportional to I, it is clear that B is *smaller* in the upper vibrational state than in the lower; in other words, B decreases as the vibrational quantum number v increases. To a high degree of approximation, the variation can be represented by an equation of the form

$$B_v = B_e - \alpha(v + \tfrac{1}{2}) \tag{10.52}$$

where B_v is the rotational constant in the vibrational level v, and B_e is that based on the equilibrium bond length; and α is a small positive constant for a given molecule.

Now, considering a diatomic molecule as a rotating *anharmonic* oscillator, we can take its vibrational-rotational energy to be the sum of the vibrational energy ε_v, given by Eq. (10.42), and the rotational energy ε_r, given by Eq. (10.10), in which B, of course, will now be replaced by B_v; thus,

$$\left. \begin{array}{l} \varepsilon_{vr} = h\nu_e(v + \tfrac{1}{2})\,[1 - a(v + \tfrac{1}{2})] + hB_vJ\,(J + 1) \text{ ergs} \\ \qquad\qquad v = 0,\ 1,\ 2, \ldots\ldots, \\ \qquad\qquad J = 0,\ 1,\ 2, \ldots\ldots \end{array} \right\} \tag{10.53}$$

Therefore, for the transition $v = 0 \to v = 1$, we have

$$\varepsilon_{vr} = h\nu_e(1 - 2a) + hB_1J'(J' + 1) - hB_0J''(J'' + 1) \text{ ergs}$$

where B_0 and B_1 are the B values corresponding to $v = 0$ and $v = 1$, respectively. Evidently, $B_0 > B_1$.

As before, we have two cases:

(i) $\Delta J = +1$, i.e. $J' - J'' = 1$,

$$\left. \begin{array}{l} \Delta\varepsilon_{vr} = h\nu_e(1 - 2a) + h(B_1 + B_0)(J'' + 1) \\ \qquad\qquad + h(B_1 - B_0)(J'' + 1)^2 \text{ ergs} \\ \qquad\qquad J'' = 0,\ 1,\ 2, \ldots, \end{array} \right\} \tag{10.54}$$

and

(ii) $\Delta J = -1$, i.e. $J' - J'' = -1$,

$$\left. \begin{array}{l} \Delta\varepsilon_{vr} = h\nu_e(1 - 2a) - h(B_1 + B_0)\,J'' + (B_1 - B_0)\,(J'')^2 \text{ ergs} \\ \qquad\qquad J'' = 1,\ 2,\ 3, \ldots \end{array} \right\} \tag{10.55}$$

These two equations can be combined into the expression

$$\Delta \varepsilon_{vr} = h\nu_e(1 - 2a) + mh(B_1 + B_0) + m^2h(B_1 - B_0) \text{ ergs}$$
$$m = \pm 1, \pm 2, \ldots$$

The frequencies (in wavenumbers) of the corresponding spectral lines are

$$\bar{\nu} = \frac{1}{c}[\nu_e(1 - 2a) + m(B_1 + B_0) + m^2(B_1 - B_0)]$$

$$= \bar{\nu}_e(1 - 2a) + m(\bar{B}_1 + \bar{B}_0) + m^2(\bar{B}_1 - \bar{B}_0) \text{ cm}^{-1} \qquad (10.56)$$

where positive m values refer to the R branch and negative m values to the P branch. If we ignore anharmonicity, so that $a = 0$ [and hence, from Eq. (10.43), $\nu_e = \nu_0$] and $B_1 = B_0$, Eq. (10.56) at once simplifies to Eq. (10.51). For the anharmonic case, however, $B_1 < B_0$ and the last term of Eq. (10.56) is therefore always negative, irrespective of the sign of m. Its effect on the vibration-rotation band is to crowd the rotational lines of the R branch more closely together, with increasing m, while those of the P branch become more widely spaced as the value of (negative) m increases. This is exactly the situation shown in the spectrum of Fig. 10.35. Usually, the difference between B_0 and B_1 is very small, and the effect thus becomes significant only at high values of m.

From the observed frequencies of the P and R rotational lines of the fundamental vibrational band, one can evaluate B_0 and B_1, using Eq. (10.56) and then B_e and α from Eq. (10.52). The equilibrium bond length and the 'average' bond lengths in the $v = 0$ and $v = 1$ vibrational states can then be calculated from B_e, B_0 and B_1 respectively. For CO, these bond lengths are found to be 1.130 Å, 1.133 Å and 1.136 Å respectively.

The infrared absorption spectra of gas-phase polyatomic molecules also exhibit in each of the vibrational absorption bands rotational structure similar to that in the diatomic case considered above, but they are, naturally, more complicated. Thus since an asymmetric top molecule has three principal moments of inertia of different magnitudes, the pattern of allowed rotational energies in both the $v = 0$ and $v = 1$ states are very complicated and so the rotational transitions accompanying the fundamental vibrational transitions will give rise to correspondingly complicated bands. To characterize such spectra and then to deduce from them molecular properties is indeed a difficult job, and, in fact, only in a few cases has it been possible to do it completely.

10.9 Raman Spectra

When a beam of light falls on a substance, it may be transmitted, absorbed, or scattered. If the substance is transparent and does not absorb in the visible region of the electromagnetic spectrum, nearly all of this light is transmitted. A small fraction of the incident light, however, emerges in all directions as a result of scattering. If the light is monochromatic,
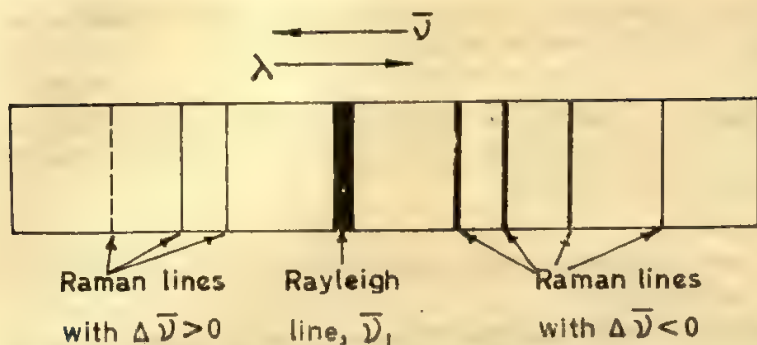
Fig. 10.36 Schematic representation of a Raman spectrum. The Raman lines on the high-frequency side of the Rayleigh line are very weak.

nearly all of the scattered light is observed to be of the same frequency as the incident light (the so-called Rayleigh scattering), but longer exposures show that light of discrete frequencies above and below the incident frequency is also scattered; it is this latter phenomenon which is referred to as *Raman scattering*, after its discoverer C. V. Raman. A schematic representation of a Raman spectrum is shown in Fig. 10.36. The line at the incident (or "exciting") frequency v_I is called the Rayleigh line, while the pattern of weak lines of modified frequency is called the *Raman spectrum* of the scattering substance. The frequency (or wavenumber) difference between the Rayleigh line and a Raman line is independent of the frequency of the incident line, but is characteristic of the scattering substance, being related to its vibrational or rotational transition. The difference, often referred to as the *Raman shift*, can be represented in the following ways:

$$\Delta v = | v_I - v_R | = v_{mol} \quad \sec^{-1}$$

$$\Delta \bar{v} = \left| \frac{1}{\lambda_I} - \frac{1}{\lambda_R} \right| = \bar{v}_{mol} \quad cm^{-1}$$

where the subscripts *I*, *R* and mol refer to the incident light, the Raman line, and the molecule, respectively. The vertical lines indicate the absolute value of the corresponding difference.

10.9.1 Classical Theory of Raman Effect

Some understanding of the Raman scattering may be obtained by considering the process from a classical viewpoint. A concept that is basic to this process is the polarizability of a molecule (see Section 10.13). When a molecule is placed in a static electric field it undergoes some deformation, the electronic cloud being attracted to the positive pole of the field and the positively charged nuclei to the negative pole. This separation of charge gives rise to an *induced dipole moment*, μ_i, and the molecule is said to be *polarized*. The magnitude of μ_i depends on the

intensity of the electric field, E, and on the ease of deformability or polarizability, α, of the molecule. We may write

$$\mu_i = \alpha E \qquad (10.57)$$

When a sample of molecules is subjected to a beam of radiation of frequency ν_i, each molecule in it experiences an electric field which varies according to the equation

$$E = E_0 \sin 2\pi\nu_i t$$

A time-dependent dipole moment is therefore induced in the molecule:

$$\mu_i = \alpha E = \alpha E_0 \sin 2\pi\nu_i t \qquad (10.58)$$

According to the electromagnetic theory, an oscillating dipole emits radiation whose frequency is the same as its oscillation frequency. In Eq. (10.58) we thus have the classical explanation of Rayleigh scattering.

If, moreover, the molecule itself undergoes some motion like vibration or rotation, which changes the polarizability periodically, then the dipole (oscillating with the frequency of the applied field) will have, superimposed on it, the vibrational or rotational oscillation. Consider, for example, a vibration of frequency ν_v, which changes the polarizability. For small displacements from the equilibrium distance, we can express the polarizability in the following way

$$\alpha = \alpha_0 + \beta \sin 2\pi\nu_v t \qquad (10.59)$$

in which α_0 is the polarizability in the equilibrium position and β represents the change in polarizability during the vibration. Consequently, the induced dipole moment is given by

$$\mu_i = \alpha.E = (\alpha_0 + \beta \sin 2\pi\nu_v t)\, E_0 \sin 2\pi\nu_i t$$

Making use of the trigonometric relation

$$2 \sin A \sin B = \cos (A - B) - \cos (A + B)$$

we find

$$\mu_i = \underbrace{\alpha_0 E_0 \sin 2\pi\nu_i t}_{\text{I}} + \underbrace{\tfrac{1}{2}\beta E_0 \cos 2\pi(\nu_i - \nu_v)t}_{\text{II}}$$

$$- \underbrace{\tfrac{1}{2}\beta E_0 \cos 2\pi(\nu_i + \nu_v)t}_{\text{III}} \qquad (10.60)$$

We thus see that the induced dipole moment has three components. The component I changes with the same frequency, as the incident light wave ν_i (called the exciting frequency), while the components II and III change with frequencies which are, respectively, the difference and the sum of the exciting frequency ν_i and the vibrational frequency ν_v of the molecule. We would therefore expect to find three frequencies in the scattered light: ν_i and $\nu_i \pm \nu_v$. The spectral line at the exciting frequency ν_i represents the *Rayleigh line*, while those at frequencies $\nu_i \pm \nu_v$ represent the *Raman lines*. Evidently, the Raman lines will be on both sides of the Rayleigh line. The line which occurs on the low-frequency side of the

Rayleigh line, i.e. at $\nu_i - \nu_v$, is known as a *Stokes line*, while the line on the high-frequency side ($\nu_i + \nu_v$) is called an *anti-Stokes line*.

We see from Eq. (10.60) that the existence of Raman lines depends on β, the change in polarizability with the vibration. The corresponding spectrum is called *vibrational Raman spectrum*. Similarly, the change in polarizability during the molecular rotation also leads to a *rotational Raman spectrum*, in which the shifts from the Rayleigh line are related to rotational frequencies. We thus see that in order to be Raman active a molecular vibration or rotation must cause a change in the polarizability of the molecule. In contrast to this, the condition for infrared and microwave activity, as we have seen previously, is that the molecular motion must produce a change in the electric dipole moment of the molecule.

While the conclusions drawn from Eq. (10.60) are, to a considerable extent, consistent with experimental observations of Raman spectra, there is, however, a marked disagreement. Thus, Eq. (10.60) predicts that the pair of Raman lines with the same absolute value of the frequency shift would appear in the spectrum with equal intensity, while, however, it is found that the lines on the high-frequency side of the Rayleigh line are very weak compared to those on the low-frequency side. We must therefore go beyond the classical interpretation given above.

10.9.2 Quantum Theory of Raman Effect

From a quantum point of view, we can picture the incident light of frequency ν as a stream of particles (called photons) each having energy $h\nu$, where h is Planck constant. These photons are imagined to undergo collisions with molecules. If the collisions are perfectly elastic, there will be no exchange of energy between the molecule and the striking photons, and the latter will be simply deflected unchanged. A detector placed at right angles to the incident beam will thus record photons of energy $h\nu$, i.e. radiation of frequency ν. However, some collisions may also result in exchange of energy between molecule and photon, and they are then called inelastic.

Schematically, these processes can be illustrated as in Fig. 10.37. We may imagine that for the extremely short period that a photon is near a molecule during collision, the two form a sort of "complex" having an energy different from that of any molecular energy level. After the photon has moved away, it is most likely that the molecule will return to the level where it was before colliding with the photon [Fig. 10.37(a)]. In such a case the photon energy is not changed by collision, and Rayleigh scattering occurs. There is also a small probability that, if the molecule was initially in the lowest vibrational level ($v = 0$), after interaction with a photon it will be in the next higher vibrational level ($v = 1$), as shown in Fig. 10.37(b). The scattered photon in this case will have lost some energy, equal to the energy gained by the molecule, and will consequently be of lower frequency. There is again a very small probability that a
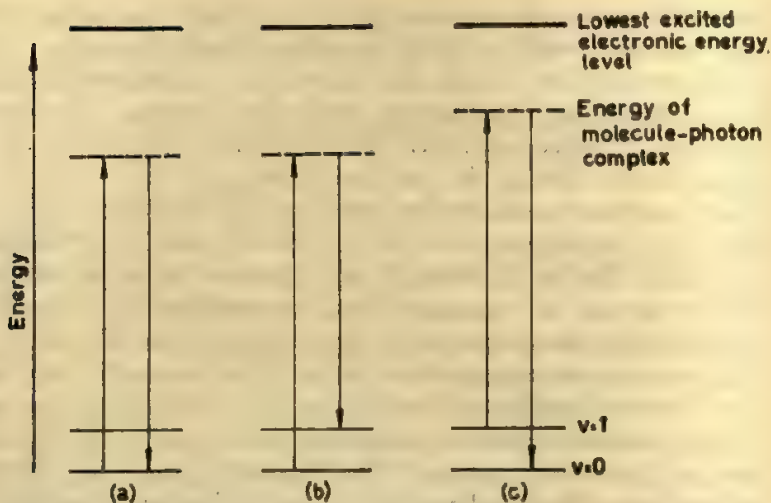
Fig. 10.37 Diagram for (*a*) Rayleigh scattering with $\Delta \bar{v} = 0$. (*b*) Raman scattering with $\Delta \bar{v} < 0$. (*c*) Raman scattering with $\Delta \bar{v} > 0$.

molecule, which is intially in the $v = 1$ level, will, after interaction with a photon, move to the $v = 0$ level [Fig. 10.37(*c*)]. The energy lost by the molecule is gained by the scattered photon, which therefore has a higher frequency. The last two situations pertain to Raman scattering. As we saw earlier, at ordinary temperatures, only a small number of molecules can be in the $v = 1$ level, while the majority of them exist in the $v = 0$ level. It is therefore easy to predict that for a pair of Raman lines having the same value of the frequency shift, the line with frequency higher than the incident frequency will be weaker than the one with the reduced frequency.

10.9.3 Pure Rotational Raman Spectra

For a complete treatment of the Raman scattering, quantum mechanical perturbation theory must be applied. The rotational selection rule which is derived from this theory is $\Delta J = \pm 2$, in contrast to the corresponding selection rule for microwave spectroscopy, $\Delta J = \pm 1$. (That in Raman work the rotational quantum number changes by two units rather than one is related to the fact that the molecular polarizability, in contrast to the permanent dipole moment, is not a vector quantity, and so in every complete rotation, it returns twice to its original value. Thus the polarizability changes with a frequency which is twice the rotational frequency of the molecule.)

The expression for rotational energy levels of linear molecules has already been stated [cf. Eq. (10.10)].

$$\left.\begin{array}{l} \varepsilon_J = hBJ(J+1) \\ \quad\quad J = 0, 1, 2, \ldots \end{array}\right\} \tag{10.61}$$

It is the usual practice to define ΔJ as J in the upper state minus J in the lower state. Now, since for a pure rotational change the upper state J must necessarily be greater than the lower state J, by adopting the above definition we can ignore $\Delta J = -2$ in the present case, and restrict ourselves only to $\Delta J = +2$.

Combining with $\Delta J = +2$, the energy changes for the allowed transitions are obtained as

$$\left.\begin{array}{l} \Delta \varepsilon_s = hB(4J+6) \text{ ergs} \\ J = 0, 1, 2, \ldots \end{array}\right\} \qquad (10.62)$$

where J is the rotational quantum number in the *lower* state. Since $\Delta J = +2$, we may refer to the lines arising from these energy changes as S branch lines; this is indicated by putting subscript s.

If the molecule gains an amount of rotational energy, as given by Eq. (10.62), from a photon during collision, we get an S branch line on the low-wavenumber side of the exciting line. This is therefore a Stokes line. The frequencies (in cm^{-1}) of Stokes lines are consequently given by

$$\bar{v}_s = \bar{v}_{ex} - hB\,(4J+6)/hc = \bar{v}_{ex} - \bar{B}\,(4J+6) \text{ cm}^{-1} \qquad (10.63)$$

where $\bar{v}_{ex}$ is the frequency (in cm^{-1}) of the exciting radiation. The corresponding equation for anti-Stokes lines of the S branch is, evidently,

$$\bar{v}_s = \bar{v}_{ex} + \bar{B}\,(4J+6) \text{ cm}^{-1} \qquad (10.64)$$

where, as before, J is the rotational quantum number in the lower state.

Figure 10.38 shows schematically the allowed transitions between the rotational energy levels and the predicted pattern for the rotational Raman spectrum. The relative intensities depend on the relative populations of the rotational levels, as given by Eq. (10.20). Since many rotational levels are populated, downward transitions are quite as likely as upward ones, and consequently Stokes and anti-Stokes lines are comparable in intensity.

It is seen from Eqs. (10.63) and (10.64) that the frequency separation of the first Stokes or anti-Stokes line (which coresponds to $J = 0$) from the exciting line is $6\bar{B}$ cm^{-1}, while the separation between successive lines on either side of the exciting line is $4\bar{B}$ cm^{-1}. From measurements of the rotational Raman spectrum we can thus immediately obtain a value of $\bar{B}$ (i.e. B/c) and from it the moment of inertia and bond length. Homonuclear diatomic molecules (e.g. O_2, H_2), as we have already seen, give neither infrared nor microwave spectra since they possess no dipole moment, but such molecules *do* give a rotational Raman spectra. So now for the first time we have seen a method for obtaining molecular parameters of homonuclear diatomic molecules.

It has already been stated (p. 269) that the alternate rotational levels of linear molecules like O_2, CO_2, which are composed of nuclei with zero spin and have a centre of symmetry, are completely unoccupied. This is revealed in the Raman spectrum by the absence of alternate spectral
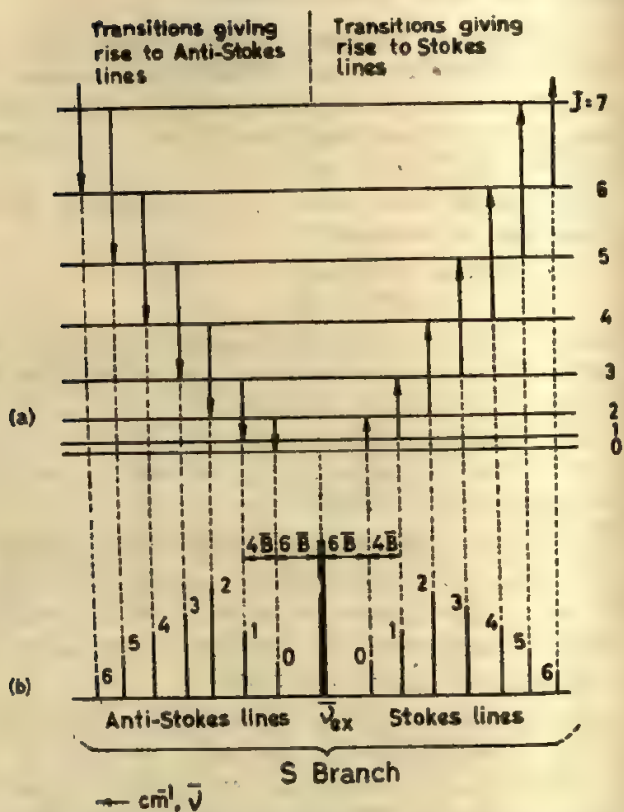
Fig. 10.38 (a) The allowed transitions between the rotational energy levels of a diatomic molecule. (b) The predicted pattern for the rotational Raman spectrum arising from the transitions. The spectral lines are numbered according to their lower J values.

lines; for example, in the case of O_2, every level with an *even* value of J is empty, and so the transitions which are labelled $J = 0, 2, 4, \ldots$ in Fig. 10.38 will be missing from the spectrum of O_2. This leads to a line spacing of $8\bar{B}$ instead of the usual $4\bar{B}$ discussed above. On the other hand, in the case of molecules containing nuclei with non-zero spin and having a centre of symmetry (e.g. H_2, $H - C \equiv C - H$), the spectral lines show a strong, weak, strong, weak,......alternation in intensity.

In the case of symmetric top molecules, rotation about the top axis produces no change in the polarizability, but end-over-end rotations do produce such a change. The rotational energy levels have already been stated [cf. Eq. (10.23)].

$$\varepsilon_{J,K} = hBJ\,(J+1) + hK^2\,(A - B) \text{ ergs}$$
$$J = 0, 1, 2, \ldots .$$
$$K = 0, \pm 1, \pm 2, \ldots \pm J \tag{10.65}$$

where K, it will be recalled, is the rotational quantum number for axial rotation.

The selection rules for Raman spectra may be shown to be $\Delta K = 0$ and $\Delta J = 0, \pm 1, \pm 2$, except for $K = 0$ states when ΔJ can be only ± 2. The selection rule $\Delta K = 0$ implies that rotations about the top axis are Raman inactive.

As before, we restrict ourselves to positive ΔJ. We then have the following two expressions for rotational energy transitions:

(i) $\Delta J = +1$ (R branch lines)

$$\Delta \varepsilon_R = \varepsilon_{J+1,K} - \varepsilon_{J,K}$$
$$= 2hB \ (J+1) \text{ ergs} \tag{10.66}$$

where $J = 1, 2, 3, \ldots\ldots$, but not zero. [$J$ cannot be zero, since, according to Eq. (10.65), when $J = 0$, K can be only zero and, as stated above, when $K = 0$, ΔJ can be only ± 2.]

(ii) $\Delta J = +2$ (S branch lines)

$$\Delta \varepsilon_s = \varepsilon_{J+2,K} - \varepsilon_{J,K}$$
$$= hB \ (4J+6) \text{ ergs} \tag{10.67}$$
$$J = 0, 1, 2, \ldots\ldots$$

Thus in the Raman spectrum of a symmetric top molecule, we shall have two series of lines of frequencies:

$$\bar{\nu}_R = \bar{\nu}_{ex} \pm 2hB \ (J+1)/hc = \bar{\nu}_{ex} \pm 2\bar{B} \ (J+1) \text{ cm}^{-1}$$
$$J = 1, 2, \ldots\ldots$$
$$\bar{\nu}_s = \bar{\nu}_{ex} \pm hB \ (4J+6)/hc = \bar{\nu}_{ex} \pm \bar{B} \ (4J+6) \text{ cm}^{-1}$$
$$J = 0, 1, 2, \ldots\ldots$$

It follows then that the lines in the R branch will be $4\bar{B}, 6\bar{B}, 8\bar{B}, 10\bar{B}$, $\ldots\ldots$ cm^{-1} from the exciting line, while the S branch lines will occur at $6\bar{B}, 10\bar{B}, 14\bar{B}, \ldots$ cm^{-1}. Clearly, every alternate R line will be overlapped by an S line, and the complete spectrum will thus be expected to show a marked alteration in intensity.

In the case of spherical top molecules (e.g. CH_4, SiH_4), the polarizability does not alter with rotation. So pure rotations of spherical top molecules are Raman inactive. Bond lengths in such molecules must therefore be obtained from the fine structure of vibration-rotation spectra.

All rotations of asymmetric top molecules, on the other hand, are normally Raman active and, in consequence of this, their Raman spectra are quite complicated.

10.9.4 Vibrational Raman Spectra

The transition energies of the vibrational Raman spectra are easily derived. For every vibrational mode we can write an expression of the form of Eq. (10.42):

$$\varepsilon = h\nu_e \left(v + \tfrac{1}{2}\right) - h\nu_e\, a \left(v + \tfrac{1}{2}\right)^2 \text{ ergs} \Big\}$$
$$v = 0,\ 1,\ 2,\ldots\ldots \qquad \Big\} \tag{10.68}$$

where, as before, ν_e is the equilibrium oscillation frequency and a is the anharmonicity constant.

The selection rule for energy transitions is, as for the infrared spectroscopy, $\Delta v = \pm 1, \pm 2, \pm 3, \ldots$, with the probability of $\Delta v = \pm 2$, $\pm 3, \ldots$, decreasing rapidly. Considering only the $v = 0 \rightarrow v = 1$ transition, we have in general

$$\Delta\varepsilon_{\text{fundamental}} = (\varepsilon)_{v=1} - (\varepsilon)_{v=0}$$
$$= h\nu_e\,(1 - 2a)\ \text{ergs}$$

Corresponding to each active fundamental vibration we can then write for the Raman lines:

$$\bar{\nu}_{\text{fundamental}} = \bar{\nu}_{ex} \pm h\nu_e\,(1 - 2a)/hc$$
$$= \bar{\nu}_{ex} \pm \bar{\nu}_e(1 - 2a) \tag{10.69}$$

where, as before, the plus sign refers to the anti-Stokes lines, the minus sign refers to the Stokes lines, and $\bar{\nu}_{ex}$ is the frequency (in cm^{-1}) of the exciting radiation.

Since, as we saw earlier, very few of the molecules exist in the $v = 1$ state at ordinary temperatures, the anti-Stokes lines will be normally expected to be much weaker than the Stokes lines.

When the chemical formula of a given molecule is known, we can predict for each symmetry group, to which the molecule might belong, the number of normal vibrational modes that will be Raman active and infrared active. A comparison of the Raman spectra and infrared spectra with the predicted patterns then reveals whether the assumed symmetry group is the correct one. Consider, for example, the AB_3 type molecules. In general, we would expect for them $(3 \times 4 - 6) = 6$ normal modes of vibration. The two simplest possible shapes for this type of molecules are symmetric plannar (symmetry group D_{3h}) or regular pyramidal (symmetry group C_{3v}). For both the planar and pyramidal shapes, one stretching mode and one bending mode are each doubly degenerate and so only four different fundamental frequencies should be observed. Now, if the AB_3 molecule is planar, it can be predicted that of the four observable frequencies one should appear only in the Raman spectrum, one only in the infrared spectrum, and two in both Raman and infrared spectra. For a pyramidal AB_3 molecule, however, it can be predicted that all normal modes are both Raman and infrared active, and so all four different fundamental frequencies should appear in both Raman and infrared spectra. Let us take the nitrate ion (NO_3^-) and the chlorate ion (ClO_3^-) as examples. That the observed spectra are consistent with a planar structure for NO_3^- and a pyramidal one for ClO_3^- is shown by the data given in Table 10.10.

Table 10.10   Fundamental Frequencies (in cm⁻¹) Observed in Raman and Infrared Spectra for Nitrate and Chlorate Ions

Vibration	NO_3^-		ClO_3^-	
	Raman	Infrared	Raman	Infrared
Sym. stretch, v_1	1049	—	982	994
Sym. deformation, v_2	—	830	610	624
Asym. stretch, v_3	1355	1350	940	950
Asym. deformation, v_4	690	680	450	434

10.9.5 Summary

It is evident from the above discussion that the uses of Raman spectroscopy are similar to those of infrared and microwave spectroscopy. If the rotational Raman lines are resolved, molecular parameters may be determined as in microwave spectroscopy, while if only vibrational Raman lines are observed, information may be obtained about the symmetry of the molecule and interatomic forces. A major disadvantage of Raman spectroscopy is the weakness of its spectra which generally leads to poor resolution compared to microwave and infrared spectra. On the merit side, however, it may be said to have brought microwave and infrared studies to the visible region where photographic methods can be conveniently used to record the spectrum. Thus, allowing sufficiently long exposure times, even the weakest of lines can be detected on a photographic plate. In recent years, moreover, the use of LASER devices (which are a source of extremely sharp and intense monochromatic light beams) has opened up possibilities for very high resolution and high sensitivity work in Raman spectroscopy.

Rotations and vibrations of heteronuclear molecules can be studied in both infrared and Raman spectroscopy. Homonuclear molecules, however, are inactive in infrared (and also in microwave), but they are Raman active and so can be studied by Raman spectroscopy. In the study of polyatomic molecules, Raman and infrared spectra generally supplement each other. Both types of spectra are usually needed to establish the symmetry group of a molecule of unknown symmetry.

10.10   Electronic Spectra

At ordinary or room temperature, molecules have the arrangement of electrons that gives them the lowest energy. This electronic arrangement is therefore referred to as the *normal*, or *ground*, *electronic state*. Other electronic arrangements are also possible, but being of much higher energy than the ground electronic state these are not ordinarily encountered and are referred to as *high-energy*, or *excited*, *electronic states*. We can, however, raise the molecules to the excited electronic states by

heating them to thousands of degrees in an arc or electric discharge. Then when the molecules return from the excited electronic state to the ground electronic state they generally emit ultraviolet or visible radiation. By studying the emission of radiation, one can often deduce something about the excited state of the molecule. However, an alternative method of knowing about the excited state is to pass ultraviolet or visible radiation into the sample at room temperature and to measure the radiation that is absorbed for transition to a high-energy electronic state.

We see from the above that in spectral transitions of a molecule in the visible and ultraviolet regions the electrons of the molecule acquire energy, or lose energy. For studies in the visible and ultraviolet regions one therefore uses the term *electronic spectroscopy*. The subject can be divided into two broad areas — one dealing with the electronic spectra of small and simple molecules and the other dealing with those of larger polyatomic molecules.

Experiments usually done for spectroscopic studies in these two areas, as also the types of information derived from them, are generally different. For small molecules, for example, experiments are generally done on samples in gas phase; the absorption or emission of quanta can therefore lead to vibrational and rotational energy changes, in addition to the change in electronic energy. The vibrational changes produce a 'coarse structure' and rotational changes a 'fine structure' on the electronic spectra. So by analysing the detailed structure of the electronic spectra we can obtain information on the rotational and vibrational energies, and hence size, shape and flexibility of the molecule in both the ground and excited electronic states. In contrast to this, spectroscopy in the microwave and infrared regions, it will be recalled, usually tells us about molecules as they exist in the ground state.

Larger polyatomic molecules, on the other hand, have been studied mostly in solution at room temperature; consequently, no rotational fine stucture or emission of radiation is observed, and one obtains an electronic spectrum containing rather broad absorption bands with little or no detail. From the observed frequency of such an absorption band we can derive information on the relative energies of the ground and excited electronic arrangements, but the actual structure of the excited electronic state cannot be deduced.

10.10.1 *Electronic Spectra of Diatomic Molecules*

We saw earlier that pure rotation spectra can be obtained only for molecules possessing a permanent electric dipole moment, and vibrational spectra for those showing change of dipole moment with motion. Homonuclear diatomic molecules (e.g. H_2, N_2) thus do not give rotation and vibration-rotation spectra. Electronic spectra, however, are given by all molecules, including homonuclear diatomic molecules, since changes

in electronic arrangement in a molecule are always accompanied by a change of dipole moment.

Measurements of electronic spectra provide information on the relative energies of the various possible electronic arrangements that a molecule can have. It has been found that the allowed electronic energies of a molecule form a pattern that is characteristic of the molecule itself and is devoid of the uniformity and order that have characterized the vibrational and rotational energy patterns.

With an excited electronic arrangement the molecule can vibrate just as it can with the ground-state arrangement. Figure 10.9, for example, shows the allowed vibrational energies for two different electronic arrangements — one in the ground state and the other in an excited state — for a typical diatomic molecule. It should be mentioned that the molecule can adopt many other excited electronic arrangements, each of which would lead to a set of vibrational energy levels. For our present purpose, however, it is sufficient just to consider one of these excited states. Again, each vibrational level of the molecule in each of its electronic states will have its own set of rotational levels, as indicated by the short horizontal lines in Fig. 10.9.

10.10.2 *Vibrational Coarse Structure of Electronic Spectra*

Let us first discuss the vibrational structure of electronic spectra ignoring the rotational fine structure. For this we drop the rotational energy term from Eq. (10.1) to write

$$E_t = E_e + E_v$$

or, considering energy per molecule,

$$\varepsilon_t = \varepsilon_e + \varepsilon_v$$

Using the expression for ε_v from Eq. (10.42) we can write

$$\left. \begin{array}{l} \varepsilon_t = \varepsilon_e + h\nu_e \, (v + \tfrac{1}{2}) - h\nu_e \, a(v + \tfrac{1}{2})^2 \text{ ergs} \\ \qquad v = 0, \, 1, \, 2, \, \cdots \end{array} \right\} \qquad (10.70)$$

The energy levels corresponding to this equation are shown in Fig. 10.39 for two electronic states. Following the previous practice the lower states are indicated by a double prime (″) and the upper states by a single prime(′). Since an excited electronic state normally corresponds to a weaker bond, and hence a smaller ν_e, the vibrational levels in the excited state would be more closely spaced than those in the ground state. This is shown in Fig. 10.39.

In electronic transitions, the accompanying change in the vibrational quantum number is *not* limited by the selection rule mentioned earlier in connection with vibrational transitions (Section 10.7.2). Thus, any transition $v'' \longrightarrow v'$ has some probability and the spectrum would be expected to show a multitude of lines. The situation, however, is considerably simple for electronic absorption from the electronic ground
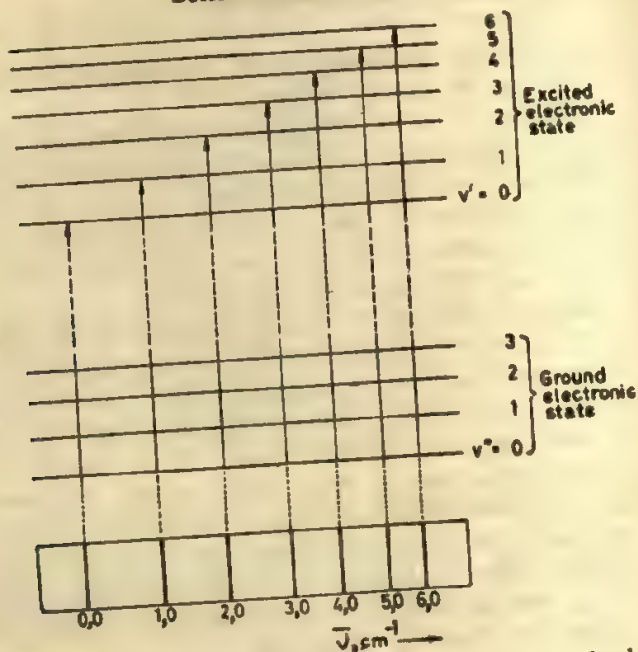
Fig. 10.39 Transitions between vibrational energy levels associated with the ground electronic state and a higer electronic state. The vibrational 'coarse' structure of the electronic absorption band that these transitions would produce is shown in the lower portion of the illustration. (The spacing between the electronic states is not in correct proportion to the other spacings.)

state to an excited state, because in the ground state almost all the molecules exist in the lowest vibrational level, and so only transitions from $v'' = 0$ to various v' are to be considered, as shown in Fig. 10.39. The resulting spectral pattern is shown at the bottom of the figure. Following the usual practice, these transitions are labelled according to their (v', v'') numbers, as for example, $(0,0)$, $(1,0)$, $(2,0)$, $(3,0)$, etc. The set of lines, corresponding to these transitions, is called a v' *progression*, since the value of v' increases by unity from line to line in the set.

An expression for the spectral line frequencies is easily derived from Eq. (10.70):

$$\Delta \varepsilon_t = (\varepsilon'_e - \varepsilon''_e) + (\varepsilon_{v'} - \varepsilon_{v''}) \text{ ergs} \tag{10.71}$$

$$\therefore \quad \overline{v}_{spect.} = \frac{\Delta \varepsilon_t}{hc} = \frac{(\varepsilon'_e - \varepsilon''_e)}{hc} + \{\overline{v}'_e (v' + \tfrac{1}{2}) - \overline{v}'_e a' (v' + \tfrac{1}{2})^2\}$$

$$- \{\overline{v}''_e (v'' + \tfrac{1}{2}) - \overline{v}''_e a'' (v'' + \tfrac{1}{2})^2\} \text{ cm}^{-1} \tag{10.72}$$

where $\overline{v}'_e = v'_e/c$, and $\overline{v}''_e = v''_e/c$.

If some half a dozen lines in a v' progression can be measured, we can calculate from Eq. (10.72) the energy difference of the electronic states

$(\varepsilon'_e - \varepsilon''_e)$, as also the values for the vibrational frequency (ν_e) and anharmonicity constant (a), in both the ground and the excited electronic states.

Most vibrational-electronic spectra are more complicated than the one represented in Fig. 10.39, where we have considered only transitions from the ground state to one excited electronic state. There are, however, many more excited electronic states (ε'_e) for a molecule, just as there are for atoms, and transitions may occur between several of them. Each of these electronic transitions will give rise to a band having a vibrational structure of the type shown above. So the electronic spectrum of a molecule will consist of many such bands, some of which will overlap also.

The situation is rather more complex for emission spectra. In emission electronic transitions, the molecule which may have been previously excited to any (ε'_e, v') state can return to any (ε''_e, v'') state below it. The spectrum will therefore show a great many v' progressions.

Let us now use the potential energy view to describe the diatomic-molecular energies for the ground and excited electronic states. We have already had examples of the potential energy versus internuclear distance curves while dealing with the molecule as a vibrating system in Section 10.7.5. By potential energy we then meant the energy of the molecule exclusive of kinetic energy of vibration, and the molecule was also considered to be at ordinary or room temperature, i.e. in the ground electronic state. The potential energy curve and the vibrational energy level pattern of Fig. 10.27 thus actually correspond to the ground-state electronic arrangement of the diatomic molecule. A similar diagram can also be drawn for any excited electronic state, in which the molecule is stable in respect of dissociation into its atoms. Of course, there will probably (though not necessarily) be differences between the two states in the value of such parameters as equilibrium oscillation frequency (ν_e), equilibrium internuclear distance (r_e), or dissociation energy (D_e), which will result in a different (though not dissimilar) potential energy curve [see Morse function, Eq. (10.41)] for the excited state.

We recall that the potential energy curve, also referred to as the Morse curve, represents the energy of the molecule as the internuclear distance changes between the limits (of compression and extension) shown in the curve. In other words, corresponding to any vibrational energy (see Fig. 10.27) the two points on the curve represent the limiting internuclear distances in compression and extension, i.e. at the turning points in the vibrational motion. Since it is at the turning points that the oscillating atoms move most slowly, we would ordinarily expect that the vibrating molecule would spend most of its time at these points, or we may say, the molecule would most probably be found *on* the curve. Let us now look at the quantum-mechanical picture. Figure 10.40 shows the variation of ψ^2 (where ψ is the vibrational wave function) with internuclear distance for various vibrational states. The significance of such
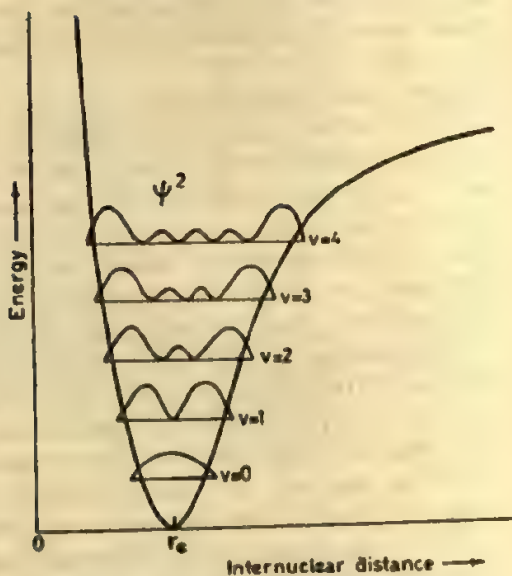
Fig. 10.40 The probability distribution for a diatomic molecule in various vibrational states

plots is that the nuclei are most likely to be found at distances apart that correspond to the maxima of the curve for a given vibrational state. The quantum theory thus says that in the $v = 0$ state, the most probable internuclear distance is the equilibrium one, r_e, in sharp variance with the classical picture given above. However, it is seen that, as v increases, the most probable internuclear distances steadily approach the limiting distances given by the points on the Morse curve, and the quantum-mechanical picture converges on the classical one.

Out of a large number of possible electronic states with different potential energy curves, the three pairs of curves shown in Fig. 10.41 have been selected as illustrative. In Fig. 10.41(a) we show the upper electronic state having a slightly larger equilibrium internuclear distance than the lower one. We have earlier discussed the origin of a v' progression. We may now mention that the vibrational lines in a progression, e.g. $(0,0)$, $(1,0)$, $(2,0)$, etc., are not all observed to be of the same intensity. For example, in some spectra, the intensity increases to a maximum at a certain value of v' and then decreases, while in some others there may be only a few lines followed by a continuous band. Such intensity variations are readily explained in terms of the *Franck-Condon principle*. In essence, this principle states that the *time required for an electronic transition to occur is so short compared to the time required for one cycle of vibration that the internuclear distance of the vibrating molecule does not undergo appreciable change during the transition*. This principle suggests that a transition occurs vertically on a potential energy diagram, since the values of r are the same in both
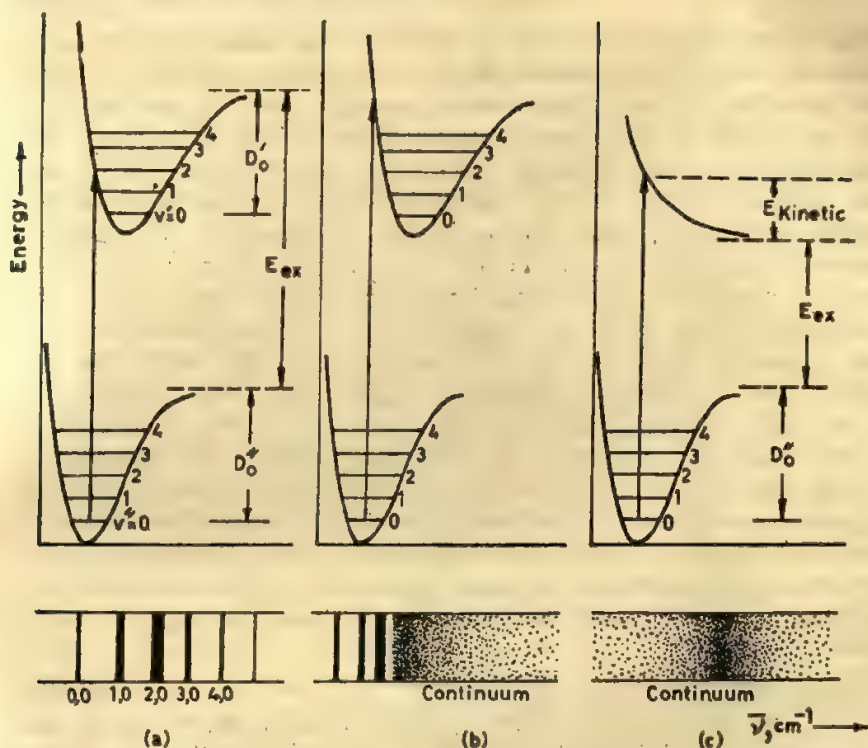
Fig. 10.41 Electronic transitions illustrating the Franck-Condon principle. (a) Indicated transition results in a band of maximum intensity. (b) Indicated transition produces continuous absorption. (c) All transitions lead to continuous absorption and dissociation in the higher state.

the initial and final states. Let us consider that the molecule is initially in the ground electronic state (ε''_e) and that vibrationally it is in the $v'' = 0$ state. As mentioned above, the most probable internuclear distance in the lowest vibrational state is the equilibrium distance (r_e), which corresponds to the minimum of the potential energy curve. In the illustration of Fig. 10.41(a), the most probable transition is that indicated by the vertical line from the point corresponding to $r = r_e$ on the $v'' = 0$ level to the upper vibrational level $v' = 2$, where it meets the potential energy curve. Thus the strongest spectral line in this case is the (2,0) line. However, it is seen from Fig. 10.40 that there is some, although small, probability of the molecule being found with an internuclear separation greater or smaller than the equilibrium value. So, there is some chance of the transition starting from near the ends of the $v'' = 0$ level and ending in the $v' = 0, 1, 3, \ldots$, levels. In view of the shape of the distribution curve for the $v = 0$ level (Fig. 10.40) we would expect an intensity variation among these lines as shown at the foot of Fig. 10.41(a).

In the situation represented in Fig. 10.41(b), the bond in upper electronic state is considerably weaker than in the ground state as evidenced by the considerably larger equilibrium separation and the smaller curvature and depth of the potential energy curve in the upper state. We now find that the most probable transition occurs to a state where the excited molecule has an energy higher than that corresponding to the asymptote. From such states the molecule will dissociate without any vibrations into a normal atom and an excited atom, with an energy excess above that needed for dissociation appearing as the kinetic energy of the separated atoms. Since the atoms formed by dissociation can take up any value of kinetic energy, the transitions to such states are not quantized and a continuous absorption band results. The spectrum in the case of Fig. 10.41(b) will, therefore, consist of a series of lines (produced by quantized transitions) of increasing intensity in the direction of shorter wavelength (or higher frequency) suddenly terminating in a continuum (non-quantized transitions), which represents dissociation.

The lower frequency limit of the continuum clearly represents absorption of energy just sufficient to cause dissociation and no more, so that dissociation products depart with virtually zero kinetic energy. We may therefore write.

$$hc\bar{\nu}_{(continuum\ limit)} = D''_0 + E_{ex} \text{ ergs} \tag{10.73}$$

where D''_0, as shown in Fig. 10.40(b), is the dissociation energy of the normal molecule and E_{ex} is the *excitation energy* of one of the atoms produced by dissociation; D'_0 in Fig. 10.41(b) represents the dissociation energy of the excited molecule. It should be noted that both D''_0 and D'_0 are reckoned from the $v = 0$ state. Knowing either of the two quantities D''_0 and E_{ex} we can deduce the other from Eq. (10.73).

Fig. 10.41(c) illustrates a case in which the excited state has no stability with respect to dissociation products, as shown by the upper curve having no minimum. In this case every transition leads to dissociation and so only continuous absorption can be observed.

10.10.3 *Rotational Fine Structure of Electronic Spectra*

We have so far described the vibrational coarse structure of the electronic spectrum as consisting of one or more series, or progressions, of convergent "lines". Normally, under low resolution, each of these vibrational "lines" appears broad and diffuse. If, however, the resolution is sufficiently good, each such "line" can be observed as a set of closely spaced lines. This is the rotational fine structure and is caused by rotational transitions accompanying electronic-vibrational transitions.

Taking into account the rotational changes, we write for the total energy (excluding kinetic energy of translation) of the molecule, [cf. Eq. (10.1)]:

$$\varepsilon_t = \varepsilon_e + \varepsilon_v + \varepsilon_r$$

From Eq. (10.10) we can write immediately

$$\varepsilon_t = \varepsilon_e + \varepsilon_v + BhJ\,(J+1) \text{ ergs}$$

Changes in the total energy of a molecule may then be written as

$$\varepsilon_t = (\varepsilon'_e - \varepsilon''_e) + (\varepsilon_{v'} - \varepsilon_{v''}) + \{hB'J'\,(J'+1) - hB''\,J''\,(J''+1)\} \text{ ergs} \qquad (10.74)$$

where B', J' refer to the upper electronic state ε'_e and B'', J'' to the lower state ε''_e.

We have already seen that equilibrium internuclear distances (and hence moments of inertia) in the lower and upper electronic states may differ considerably [see, for example, Fig. 10.41(b)]. Since the value of B depends on the equilibrium moment of inertia [Eq. (10.11)], it is clear that B' and B'' will differ. If, as is often the case, the bond in the upper state is longer, then B' is smaller than B''.

If we ignore the rotational changes, Eq. (10.74) reduces to Eq. (10.71), representing electronic-vibrational transitions, e.g. (0,0), (1,0) etc., considered previously under vibrational coarse structure. Representing the frequency of any such transition by $\nu_{(v',v'')}$, Eq. (10.74) can be written:

$$\Delta\varepsilon_t = h\nu_{(v',v'')} + hB'J'\,(J'+1) - hB''J''\,(J''+1) \qquad (10.75)$$

The selection rule for J depends on the type of electronic transition. Thus for transitions where *both* the upper and lower states have no electronic angular momentum about the internuclear axis, the selection rule is $\Delta J = \pm 1$ only; so for these transitions P and R branches only will occur. For all other transitions, the selection rule is $\Delta J = 0$ or ± 1, so Q branches will appear in addition to P and R branches. There is, however, an added restriction that there cannot be a transition from one $J = 0$ state to another $J = 0$ state.

We now have three cases:

(i) $\Delta J = +1$, i.e. $J' = J'' + 1$ (R branch lines)
Combining with Eq. (10.75) we obtain

$$\Delta\varepsilon_t = h\nu_{(v',v'')} + h(B' + B'')\,(J''+1) + h\,(B' - B'')\,(J''+1)^2 \text{ ergs} \qquad (10.76)$$

where $J'' = 0,\ 1,\ 2,\ \ldots\ldots$

(ii) $\Delta J = -1$, i.e. $J' = J'' - 1$ (P branch lines),

$$\Delta\varepsilon_t = h\nu_{(v',v'')} - h\,(B' + B'')\,J'' + h\,(B' - B'')\,(J'')^2 \text{ ergs} \qquad (10.77)$$

where $J'' = 1,\ 2,\ 3,\ \ldots\ldots$

These two equations can be combined into the expression

$$\Delta\varepsilon_t = h\nu_{(v',v'')} + h\,(B' + B'')\,m + h\,(B' - B'')\,m^2 \text{ ergs} \qquad (10.78)$$

$$m = \pm 1,\ \pm 2,\ \ldots\ldots$$

where m, replacing $J'' + 1$ in Eq. (10.76) and J'' in Eq. (10.77) has positive values for R branch lines ($\Delta J = +1$) and negative values for P branch lines ($\Delta J = -1$). Clearly m cannot be zero, since this would require J' and J'' to be -1, which is impossible.

Expressing Eq. (10.78) in spectroscopic units, cm^{-1}, we obtain the frequencies of the P and R branch lines as:

$$\bar{v}_{P,R} = \frac{\Delta \varepsilon_t}{hc} = \bar{v}_{(v',v'')} + \left(\frac{B' + B''}{c}\right) m + \left(\frac{B' - B''}{c}\right) m^2 \text{ cm}^{-1} \quad (10.79)$$

$$m = \pm 1, \pm 2, \ldots \ldots$$

Since m cannot be zero there will be no spectral line at $\bar{v}_{(v',v'')}$. This frequency is referred to as the *band origin*.

(iii) $\Delta J = 0$, i.e. $J' = J''$ (Q branch lines)

From Eq. (10.75) we then obtain

$$\Delta \varepsilon_t = h v_{(v',v'')} + h (B' - B'') J'' + h (B' - B'') (J'')^2 \text{ ergs} \quad (10.80)$$

$$J'' = 1, 2, 3, \ldots.$$

Note that here J'' cannot be zero, because this would imply a transition from one $J = 0$ state to another $J = 0$ state, which, as stated before, is not allowed.

The frequencies of the Q branch lines, from Eq. (10.80), are

$$\bar{v}_Q = \frac{\Delta \varepsilon_t}{hc} = \bar{v}_{(v',v'')} + \left(\frac{B' - B''}{c}\right) J' + \left(\frac{B' - B''}{c}\right) (J'')^2 \text{ cm}^{-1} \quad (10.81)$$

where $J'' = 1, 2, 3, \ldots.$

Since J'' cannot be zero, there will, again be no line at the band origin.

It is clear from Eqs. (10.79) and (10.81) that the spacing of the branch lines is not constant and that the variation of spacings in any branch depends on the magnitudes of B' and B''. Thus, if $B' < B''$, as is usually the case, we note that (i) the R branch appears on the *high*-wavenumber side of the band origin $\bar{v}_{(v',v'')}$ and the line spacing decreases with increasing m, with the result that the branch converges to a line, called the *band head*, and then doubles back on itself, (ii) the P branch lines occur on the *low*-wavenumber side of the origin and the line spacing increases with increasing m, and (iii) the Q branch lines also lie on the *low*-wavenumber side of the origin and their spacing increases with increasing J'. The three branches are shown separately in Fig. 10.42, while the complete spectrum (band) will be a superposition of the three. We thus see that for $B' < B''$, the band head appears at the high frequency (violet) end of the spectrum and the band dies away (said to be *degraded* or *shaded*) towards the low frequency (red) end of the spectrum. Conversely, if $B' > B''$, i.e. when the internuclear distance in the upper electronic state is smaller than that in the lower state, the above situation will be reversed. Thus, (i) the R branch, still occurring on the *high*-wavenumber side, will now diverge with increasing m, (ii) the P branch will converge to a band head on the *low*-wavenumber side of the origin, and (iii) the Q branch lines will be on the *high*-wavenumber side of the origin and their spacing will increase with J''. The complete spectrum will thus show a band head at the low frequency (red) end of the spectrum and
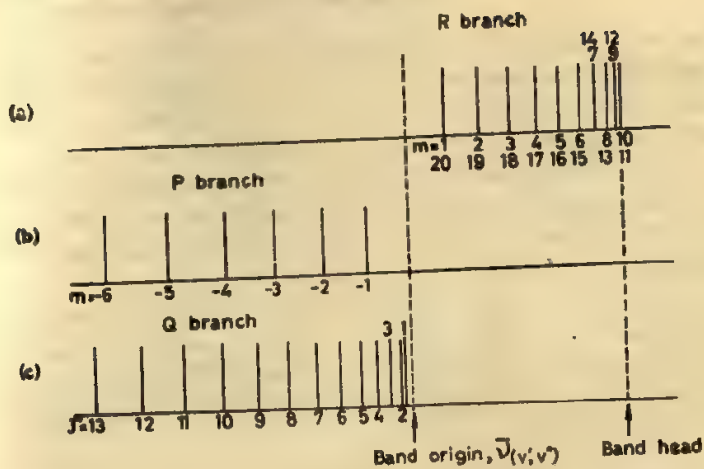
Fig. 10.42 Rotational fine structure of an electronic-vibrational transition of wavenumber $\bar{v}\,(v',\,v'')$ for a diatomic molecule, for which B' is less than B''. The R, P and Q branches are shown separately in (a), (b) and (c), respectively. The superposition of (a), (b) and (c) gives the complete spectrum. (After C. N. BANWELL *Fundamentals of Molecular Spectroscopy*, McGraw-Hill Book Co. Inc., New York, 1966)

the band will be degraded towards the high frequency (violet) end of the spectrum. If, however, the upper and lower electronic states have the same internuclear distance, B' and B'' will be equal; consequently, the spectrum will resemble a pure vibration-rotation spectrum (Section 10.8) and no band heads will be observed. Therefore, simply by looking at the rotational fine structure of an electronic spectrum one can say whether the internuclear distance increases or decreases as a result of the electronic transition. A close analysis of the band often yields accurate values for the internuclear distances in both the upper and lower electronic states.

10.10.4 *Electronic Spectra of Polyatomic Molecules*
An important feature of the chemical bond is that it is fairly localized in nature, (see Section 6.9). We have thus seen in vibrational spectroscopy that the vibrational frequencies of particular atomic groupings such as $C - H$, $C = O$, $C = C$, etc., are fairly independent of the nature of the molecule. Therefore, we may, at least as an approximation, consider the electronic structure (and hence the spectrum) of each bond in isolation. The complete electronic spectrum of a molecule is then the sum of the spectra of its constituent bonds. The result is naturally very complex. The rotational fine structure is very difficult to resolve even in the spectra of relatively simple molecules in gas phase, although some vibrational structure may be observed. In pure liquids, or in solution,

molecular rotation is hindered and all rotational structure is lost. Frequently, the vibrational structure is also lost due to blurring of the rotational structure. The electronic absorption band of a liquid is thus rather broad, with little or no fine structure. We are unable in such a case to deduce the actual structure of the excited electronic state and we can only hope to understand something about the electronic change that takes place in the molecule. However, as we shall discuss shortly, this understanding itself is of considerable interest to us.

The electronic absorption band, devoid of fine structure, is characterized by the wavelength at which the absorption is maximum (λ_{max}, quoted either in Angstrom units or in millimicrons) and by the molar extinction coefficient at this wavelength (ε_{max}). The latter is defined in terms of the Beer-Lambert law:

$$\varepsilon_{max} = \frac{1}{cl} \log_{10} \frac{I_0}{I} \tag{10.82}$$

where I_0 and I are the intensities of light of wavelength λ_{max}, before and after passing through l cm of a solution containing c moles per litre of the solute. Both λ_{max} and ε_{max} for a given solute vary somewhat with the solvent, so that it is necessary to specify the solvent in which these values are obtained.

In organic molecules, three types of electrons may be distinguished: σ electrons (i.e. electrons in σ-bonding molecular orbitals), π electrons (i.e. electrons in π bonding MO), and non-bonding electrons (called n electrons). The first two types were discussed in Section 6.4. Many molecules contain electrons that play no part in bonding and are mainly located in atomic orbitals, such as those of oxygen, sulphur, nitrogen and halogens; these electrons are called *non-bonding electrons*. The absorption of radiation by organic molecules in visible and ultraviolet region involves the promotion of σ-, π- or n-electrons from the ground state (i.e. from bonding molecular orbitals or atomic orbitals) to higher-energy states, called *antibonding orbitals* (Section 6.4). The antibonding orbital corresponding to σ MO is called the σ^* (sigma star) orbital and that corresponding to π MO is called the π^* (pi star) orbital. As the n electrons do not occupy MOs there are no antibonding orbitals associated with them. The relative energies of the bonding, non-bonding and antibonding orbitals in a simple molecule are indicated schematically in Fig. 10.43, which also shows the types of transitions observed and the spectral regions of the corresponding absorption bands. The energy required for the $\sigma \to \sigma^*$ transition is very high and so the absorption band occurs at shorter wavelength, in the 125–135 mμ region. (The range below 200 mμ is often called the *vacuum ultraviolet* region, because the atmospheric oxygen absorbs so strongly in this region that the use of an evacuated spectrograph is a necessity.) The $\pi \to \pi^*$ and $n \to \sigma^*$ transitions, however, appear at longer wavelengths, near the borderline
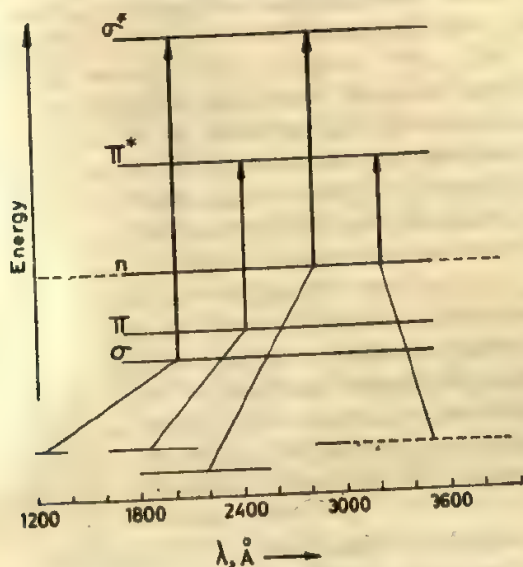
Fig. 10.43 Schematic energy levels and transitions in simple organic molecules. The regions of the electronic spectrum corresponding to the transitions are shown at the bottom of the diagram.

of the near and far ultraviolet, while $n \rightarrow \pi^*$ transitions occur at still longer wavelengths, coming well into the near ultraviolet and visible regions. Compounds in which all valence-shell electrons are involved in single σ-bond formations, such as saturated hydrocarbons, can only undergo $\sigma \rightarrow \sigma^*$ transitions, and so do not absorb in the near ultraviolet region. (An exception, however, is cyclopropane, which shows λ_{max} at about 190 mμ.) Hexanes, heptanes and octanes are thus useful as solvents in UV spectroscopic work.

The insertion of groups containing n electrons, e.g. $-$OH, $-$Cl and $-$NH$_2$ groups, allows the possibility of $n \rightarrow \sigma^*$ transitions, in addition to $\sigma \rightarrow \sigma^*$ transitions. The $n \rightarrow \sigma^*$ transitions are of lower energy than $\sigma \rightarrow \sigma^*$ transitions and usually give bands in the ordinary ultraviolet region. Some examples of $n \rightarrow \sigma^*$ transitions are: CH_3OH, $\lambda_{max}^{vapour} = 183$ mμ; CH_3Cl, $\lambda_{max}^{vapour} = 173$ mμ; CH_3I, $\lambda_{max}^{hexane} = 258$ mμ; $(CH_3)_3N$, $\lambda_{max}^{vapour} = 227$ mμ.

Unsaturated hydrocarbons, i.e. hydrocarbons containing multiple bonds, exhibit both $\sigma \rightarrow \sigma^*$ and $\pi \rightarrow \pi^*$ bands. The $\pi \rightarrow \pi^*$ bands occur at 180–190 mμ in the case of aliphatic compounds and at 200–210 mμ in the case of simple aromatic compounds. Compounds containing unsaturated groups (A = B), e.g. C = O, C = N also absorb in the region of 190 mμ due to the $\pi \rightarrow \pi^*$ transition, and, in addition, since the groups contain non-bonding electrons (e.g. on oxygen and nitrogen), the molecules also show absorptions at long wavelengths owing to $n \rightarrow \sigma^*$ and

$n \rightarrow \pi^*$ transitions. Examples of $n \rightarrow \pi^*$ transitions are shown by acetone ($> C = O$), $\lambda_{max}^{hexane} = 279$ mμ; azomethane ($-N = N-$), $\lambda_{max}^{ethanol}$ = 338 mμ; nitrosobutane ($-NO$), $\lambda_{max}^{ether} = 665$ mμ. We thus see that, in contrast to the $\pi \rightarrow \pi^*$ transitions, the $n \rightarrow \pi^*$ transitions are quite sensitive to the nature of the atoms which are multiply-bonded. This is, of course, reasonable since the n electrons are not involved in the bonding and they are controlled by the atom (O or N) to which they belong in the ground state. Different substituents on the A = B group also produce variations in the wavelength of the $n \rightarrow \pi^*$ transition. Thus, considering the $> C = O$ group alone, λ_{max} varies from 279 mμ for acetone to 290 mμ for cyclohexanone. Placement of a halogen, amino, hydroxyl, or alkoxyl group on the $> C = O$ group produces a significant shift of the wavelength of the $n \rightarrow \pi^*$ transition to shorter wavelengths. As a result, the absorption of simple carboxylic acids and their derivatives are often difficult to determine. For example, λ_{max} for $n \rightarrow \pi^*$ bands occur at 220 mμ in acetyl chloride and acetamide, at 208 mμ in acetic acid, and at 211 mμ in ethyl acetate.

An isolated functional group that shows absorption of a characteristic nature in the ultraviolet or visible region, is called a *chromophore*. Some simple chromophoric groups and their absorption characteristics are listed in Table 10.11.

Table 10.11 Absorption Characteristics of some Simple Chromophoric Groups

Chromophore	Example	λ_{max} (mμ)	ε_{max}	Solvent*
$> C = C <$	Ethylene	171	15,530	Vapour
$> C = O$	Acetone	189	900	Hexane
		279	15	Hexane
$-CO_2H$	Acetic Acid	208	32	Ethanol
$-CO_2R$	Ethyl acetate	211	57	Ethanol
$-COCl$	Acetyl chloride	220	100	Hexane
$-CONH_2$	Acetamide	178	9,500	Hexane
		220	63	Water
$-NO$	Nitrosobutane	300	100	Ether
		665	20	Ether
$-NO_2$	Nitromethane	201	5,000	Methanol
		274	17	Methanol
$-N = N-$	Azomethane	338	4	Ethanol
$= N_2$	Diazoacetic ester	249	10,050	Ethanol
		378	16	Ethanol

*Saturated hydrocarbons and compounds containing alcohol groups and ether groups are transparent, i.e. they show no absorption in the accessible region of the spectrum ($\lambda > 200$ mμ).

The magnitude of ε_{max} for a particular absorption is directly proportional to the probability of the corresponding electronic transition. Thus

a large extinction coefficient indicates that the transition is more probable.

Groups that do not in themselves show characteristic absorption in the accessible region of the spectrum ($\lambda > 200$ mμ) but which, when attached to a chromophore, increase the intensity of its absorption and usually causes λ_{max} to increase, are called *auxochromes*. Common examples of such groups are —OH, —SH, —NH$_2$ and —Br. All of them contain non-bonding electrons; transitions involving these electrons produce the auxochromic effects.

When a molecule contains several functional groups, separated by two or more single bonds, so that their electronic distributions are not affected by each other, the absorption spectrum is very largely the sum of the absorption bands of the individual functional groups. When, however, two or more functional groups are conjugated (that is, separated by only one single bond) in the molecule, λ_{max} shifts to longer wavelength and ε_{max} increases. The effect of conjugation of carbon–carbon double bonds is clearly revealed by the approximate data for $\pi \rightarrow \pi^*$ transitions given in Table 10.12.

Table 10.12 Ultraviolet Absorptions of some Conjugated Polyenes

	λ_{max} (mμ)	ε_{max}
—C=C—C=C—	217	21,000
—C=C—C=C—C=C—	258	35,000
—C=C—C=C—C=C—C=C—	310	77,000

As the number of alternating single and double bonds increases, the high intensity $\pi \rightarrow \pi^*$ absorption band generally moves to longer and longer wavelength, and by the time there are about ten double bonds, with alternating single bonds, the absorption moves into the visible region, so that the compounds appear coloured. (The observed colour is, of course, complementary to the absorbed colour.) Thus lutein, which gives egg yolk its yellow colour, is a compound with nine alternating single and double bonds, and the compound carotene which is responsible for the characteristic colour of carrots, has eleven double bonds in conjugation.

When chromophoric groups containing non-bonding electrons are conjugated, both the $\pi \rightarrow \pi^*$ and $n \rightarrow \pi^*$ bands increase in wavelength and intensity. As a simple example, approximate data for some oxygen-containing molecules are collected in Table 10.13. Since p-benzoquinone absorbs at about 435 mμ (that is, in the blue region), in ordinary reflected light it appears yellow to the eye.

Many metal ions form coloured coordinated ions. The colours, which evidently arise from absorptions of radiation in the visible spectral region, are often attributed to electronic changes in the metal ions. The absorp-

Table 10.13 Ultraviolet Absorptions of some Oxygen-containing Molecules

	λ_{max} (mμ)	
	$\pi \to \pi^*$ (strong)	$n \to \pi^*$ (weak)
—C=O	180	280
—C=C—C=O	220	320
—C=C—C=C—C=O	270	350
O=⟨⟩=O	245	435
(*p*-benzoquinone)		

tion of visible radiation by complex ions depends on two conditions, namely that the metal ion must have one or more *d* electrons but not the full complement of ten, and that the metal ion must be surrounded by ligands or electron-repelling groups, located at certain positions so as to change the energies of some *d* orbitals relative to other *d* orbitals (*crystal field splitting*, see Section 6.11). Thus a *d* electron in the lower energy level can absorb a quantum of radiation of such frequency that it is raised to a higher-energy level (see Fig. 6.34). The two requirements are fulfilled in transition metal complex ions, which we also know to have a pronounced tendency to be coloured. By contrast, metal ions which have no *d* electrons at all or have a complete complement of ten *d* electrons (as for example, Mg^{+2} and Zn^{+2} ions), do not tend to give coloured solutions.

Ultraviolet absorption spectra do not yield as much detailed information as infrared spectra. Moreover, many saturated compounds absorb very little in the accessible region of the ultraviolet spectrum, whereas all molecules with the exception of homonuclear diatomic molecules absorb in the infrared region. Ultraviolet spectroscopy is, however, very useful in deriving structural information when used in conjunction with other evidence.

10.11 Nuclear Magnetic Resonance Spectroscopy

Earlier we had occasions to refer to the magnetic effects connected with the properties of electrons (Section 3.3). In this section we consider the important consequences of the fact that many atomic nuclei possess a mechanical spin, or angular momentum.

The spin angular momentum of a nucleus (p_n) depends on the nuclear spin, or spin quantum number, I, in the same way that the orbital angular momentum of an electron depends on the quantum number l (Section 5.4) and the rotational angular momentum of a molecule depends on the rotational quantum number J [Eq. (10.9)]. Thus the quantum mechanical expression for p_n is

$$p_n = \frac{h}{2\pi} \sqrt{I(I+1)} \qquad (10.83)$$

The simplest nucleus is the proton. Its mass $(1 \cdot 66 \times 10^{-24}$ g) is the unit of atomic mass (AMU) and its charge $(+ 4 \cdot 80 \times 10^{-10}$ esu), which is the unit of atomic charge, is equal in magnitude but opposite in sign to the electronic charge. The spin of the proton is also 1/2.

Besides the proton, another particle which is a constituent of all nuclei (except, of course, the hydrogen nucleus) is the neutron. It is a neutral particle having a mass equal to that of the proton (i.e. unit atomic mass) and also a spin of 1/2.

A nucleus which is composed of Z number of protons and n number of neutrons has a total mass of $(Z + n)$ AMU (ignoring a small mass defect associated with nuclear binding energy) and a total charge of $+ Z$. The total spin value of this nucleus will be a vector combination of $(Z + n)$ spins, each of magnitude 1/2. Unfortunately, the theory of nuclear structure has not advanced to such a point that the spin of a particular nucleus can be predicted from values of nuclear charge and mass. However, from rationalization of observed spins some empirical rules have been formulated. Thus, (*i*) nuclei with even numbers for the values of both nuclear charge (i.e. Z) and mass $(Z + n)$ have zero spin, i.e. $I = 0$; (*ii*) nuclei with odd charge and even mass (hence both Z and n odd) have integral spin, i.e. I is an integer; and (*iii*) nuclei with odd mass have half-integral spins, i.e. I is an integer times 1/2. For example, the spin quantum numbers of a few common nuclei are as follows:

Nucleus	^{1}H	^{2}D	^{10}B	^{12}C	^{14}N	^{16}O	^{19}F	^{31}P	^{32}S	^{35}Cl
I	1/2	1	3	0	1	0	1/2	1/2	0	3/2

(The prefix to the nuclear symbol specifies the nuclear mass, e.g. ^{12}C indicates the nucleus of carbon with mass 12.)

A charged particle spinning about an axis is equivalent to a circular electric current, which, in turn, gives rise to a magnetic field. A spinning nucleus thus behaves as a tiny bar magnet whose axis is coincident with the axis of spin. If we take for the simplest nucleus, the proton, a classical model of a rotating spherical shell of charge q and mass m_p with angular momentum p_n, the value of the magnetic moment (i.e. the strength of the nuclear dipole) can be shown to be

$$\mu = \frac{q}{2m_p.c} p_n \qquad (10.84)$$

where c is the velocity of light.

However, the simple rotating shell model for a proton is not adequate and it becomes necessary to modify Eq. (10.84) by inclusion of a numerical factor. This factor, which is represented by g, and called the *nuclear splitting factor*, or simply the *nuclear g value*, may not be calculated

theoretically and must be determined from experimental data for each type of nucleus. Introducing this factor and replacing p_n in Eq. (10.84) by its value from Eq. (10.83), the expression for the nuclear magnetic moment becomes

$$\mu = g \frac{qh}{4\pi m_p c} \sqrt{I(I+1)} \qquad (10.85)$$

$$= g\beta_n \sqrt{I(I+1)} \qquad (10.86)$$

where $\beta_n = qh/4\pi m_p c = 5\cdot05 \times 10^{-24}$ erg. gauss^{-1} is the unit of nuclear magnetic moment, called the *nuclear magneton*.

Since nuclei with even values of nuclear charge and mass, e.g. ^{12}C and ^{16}O, have $I = 0$, their magnetic moment (μ), from Eq. (10.85), is also zero. There are however many other useful nuclei having $I \neq 0$ and hence $\mu \neq 0$. Among them the proton with $I = 1/2$ is outstanding. Since neither ^{12}C nor ^{16}O is magnetic, it is necessary to consider only the protons in many organic compounds.

10.11.1 Interaction Between Nuclear Spin and Magnetic Field

The potential energy of a nuclear dipole in a magnetic field is given by an equation which is completely analogous to the equation for the potential energy of an electrical dipole in an electric field. Thus the potential energy of a nucleus of magnetic moment μ in a magnetic field of strength H is

$$U_n = - H\mu \cos \theta \qquad (10.87)$$

where θ is the angle between the magnetic moment vector and the direction of the magnetic field.

According to quantum mechanics, the angle θ is not a continuous variable but can have only certain discrete values; in other words, in an applied magnetic field, the spin angular momentum vector for a nucleus cannot point in any arbitrary direction, but can have only a discrete set of orientations. This is the result of a phenomenon, known as *space quantization*, (c.f. Section 3.3). The angular momentum vector can point only such that its components along the direction of the magnetic field are given by $m_I(h/2\pi)$, where the quantum number m_I can have any of the values $I, I-1, \ldots, -(I-1), -I$. The situation for a nucleus with $I = 1$ is shown in Fig. 10.44(a). The angular momentum of the nucleus [Eq. (10.83)] is

$$p_n = \sqrt{1 \times 2} \, (h/2\pi) = \sqrt{2} \, (h/2\pi)$$

Since $I = 1$, the possible values of m_I are 1, 0 and -1. Thus, if we consider a semicircle with the above p_n as the radius, it is plain that the vector arrow corresponding to p_n can point so as to have components ($p_n \cos \theta$) of magnitude $h/2\pi$, 0, or $-h/2\pi$ in the direction of the magnetic field. The orientations of the angular momentum vector for $I = 1/2$ are
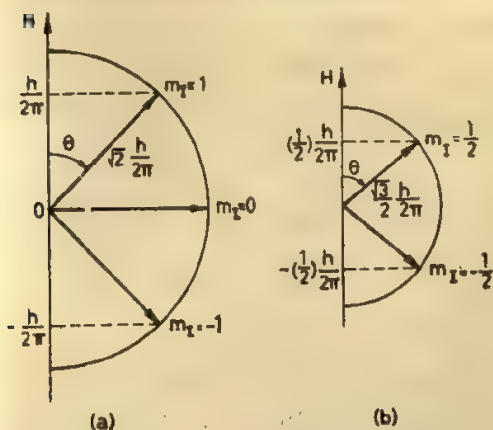
Fig. 10.44   (a) The three spin orientations allow-
ed to a nucleus with $I = 1$ in a magnetic field
H. The possible values of the component of the
spin angular momentum in the direction of the
magnetic field are $h/2\pi$, 0 and $-h/2\pi$. (b) Spin
orientations for a nucleus with $I = \frac{1}{2}$.

shown in Fig. 10.44(b). For a given value of I there are thus $(2I + 1)$
different values of m_I and hence $(2I + 1)$ different values of θ. Corres-
ponding to each value of θ there is a component of the nuclear magnetic
moment, $\mu \cos \theta$, in the direction of the applied field. From Eq. (10.86)
we have

$$\mu \cos \theta = g\beta_n \sqrt{I(I + 1)} \cos \theta$$

Since $\sqrt{I(I + 1)} \cos \theta$ equals m_I, we can represent the $(2I + 1)$
values of $\mu \cos \theta$ by

$$\mu_{m_I} = g\,\beta_n\,m_I$$

and the $(2I + 1)$ different energy levels by

$$U_n = -Hg\beta_n m_I \tag{10.88}$$

The selection rule for transitions between these energy levels is
$\Delta m_I = \pm 1$.

Thus the separation between neighbouring energy levels (where m_I
differs by unity) is

$$\Delta U_n = |Hg\beta_n| \tag{10.89}$$

where the modulus sign, $|\ldots|$, indicates that positive energy differences
only should be considered.

In Eq. (10.89) we have the basis for a spectroscopic technique. Thus,
if a transition as given by Eq. (10.89) can be carried out, the frequency
of the radiation absorbed or emitted in the process will be given by

$$\nu = \frac{\Delta U_n}{h} = \left|\frac{g\beta_n}{h} H\right| \text{ cycles/sec} \tag{10.90}$$

We thus see that unlike rotational, vibrational and electronic transitions, discussed earlier, which occur in the absence of external fields, transitions between nuclear magnetic energy levels can occur only in the presence of an applied magnetic field. The ferquency associated with such a transition, it is seen from Eq. (10.90), depends on the strength of the applied field. Moreover, such a transition, in contrast to rotational, vibrational and electronic transitions, cannot be observed by simply sending through the sample electromagnetic radiation of frequency given by Eq. (10.90). The question of how to effect transitions between the nuclear magnetic energy levels is discussed later.

The study of transitions between nuclear magnetic energy levels forms the subject of nuclear magnetic resonance (NMR) spectroscopy. Since the transition frequency, as shown above, depends on the strength of the field, we can, in principle, arrange to obtain spin spectra in any region of the electromagnetic spectrum of our choice, simply by using an appropriate field. For practical reasons, however, the fields normally used are of the order of 15,000 gauss. In our subsequent discussion of NMR spectroscopy, for simplicity we shall confine our attention to the proton as the representative nucleus.

Let us now calculate the approximate frequency for nuclear magnetic transitions for protons. The value of the g factor derived from careful measurements is 5·585. We have already $\beta_n = 5\cdot05 \times 10^{-24}$ erg/gauss. Since I for proton is 1/2, m_1 can be only $+1/2$ and $-1/2$. The frequency associated with the transition from the level with $m_1 = +1/2$ to $m_1 = -1/2$ is then given by [Eq. (10.90)]:

$$\nu = \frac{5\cdot05 \times 10^{-24} \times 5\cdot585}{6\cdot62 \times 10^{-27}} H = 4\cdot26 \times 10^3 \, H \text{ cycles/sec}$$

If we choose $H = 15,000$ gauss, ν for protons is 64 megacycles per second (Mc/s) which falls in the short-wave radio frequency range of the electromagnetic spectrum. Compared to protons, all other nuclei (except tritium) have smaller g values, so their spectra occur in lower frequencies falling between 10 and 60 Mc/s for the same field strength.

10.11.2 Population of Energy Levels

In a magnetic field, spin magnetic moments do not all occupy the lowest available energy state — a simple consequence of thermal motion and the Boltzmann distribution. If n_1 and n_2 are the numbers of particles in the upper and lower magnetic energy levels, respectively, their ratio from the Boltzmann distribution law is

$$\frac{n_1}{n_2} = e^{-\Delta U_n/kT} \tag{10.91}$$

where ΔU_n is the energy difference between the two levels and k is the Boltzmann constant. Evidently, at all temperatures above absolute zero, the upper level will be populated to some extent, although this

population will be insignificant when ΔU is large. In the case of nuclear spins, however, ΔU is extremely small, and so the upper level will be appreciably populated. Let us calculate this for protons. In a field of 15,000 gauss, the energy difference between the two energy levels of the proton, calculated from Eq. (10.89), is

$\Delta U_n = 4.23 \times 10^{-19}$ erg.

At room temperature ($T = 300°$K), $kT = 4.14 \times 10^{-14}$. Since $\Delta U_n/kT$ is very small compared to 1, we may approximate its exponential by $1 - \Delta U_n/kT$. Thus, for the case under consideration, Eq. (10.91) gives

$$\frac{n_1}{n_2} = 1 - \frac{4.23 \times 10^{-19}}{4.14 \times 10^{-14}} = 1 - 1.02 \times 10^{-5} = 0.9999898$$

Since the transition from the lower to the upper level is associated with absorption of radiation and that from the upper to the lower level is associated with emission of radiation, net absorption will be recorded only if there is an excess of protons in the lower energy level. In the above example, we find that the excess of protons in the lower energy level is only about one in 10^5. It is this very small, but nevertheless finite, excess of protons in the lower energy state that gives rise to *net* absorption. Without this small excess there would be no nuclear magnetic resonance.

The smaller the value of n_1/n_2, the higher the net absorption and hence sensitivity. Since $\Delta U_n \propto H$, high field strengths are used to increase the sensitivity. However, the necessity that the field be homogeneous places an upper limit of 25,000 gauss on the fields that can be applied. The sensitivity can also be increased by making the measurements at low temperatures [see Eq. (10.91)].

10.11.3 *Nuclear Resonance*

We have seen that the spin angular momentum vector for a nucleus can be oriented only so that its components are integral or half-integral in the direction of the applied field. Since the vector quantity is given by Eq. (10.83), it is clear that, if I is integral or half-integral, the vector arrow can never be exactly in the direction of the filed. An example of this for an integral spin case and another for a half-integral spin case are shown in Figs. 10.44(*a*) and (*b*), respectively. Thus, since the magnetic moment vector always lies more or less across the field, it follows that it will be under the influence of a force tending to align i' in the field direction.

Now, from a classical point of view, the behaviour of a spinning proton, which may be pictured as a tiny bar magnet rotating about its axis, is analogous to that of a gyroscope spinning in frictionless bearings. It is a known fact that when a force (torque) is applied to a spinning gyroscope, its axis does not tilt but merely *precesses* about the direction of the force. Similarly, a spinning proton, behaving as a magnetic gyroscope, will precess about the direction of the applied field (Fig. 10.45), keeping the
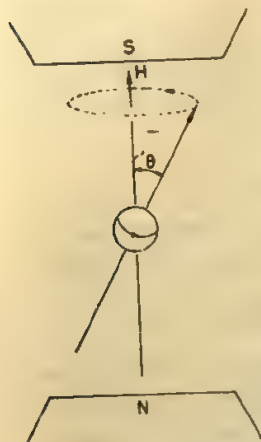
Fig. 10.45 A spinning proton, behaving a sa magnetic gyroscope, precesses about the direction of the applied megnetic field *H*, with a constant angle θ

angle θ between its spinning axis and the field direction, constant. So long as this angle is constant, the potential energy of the proton in the field, given by Eq. (10.87), is also constant and no energy is absorbed from the field.

In order to cause a change of the angle θ, a second magnetic field is to be applied *perpendicular* to the main field. The secondary magnetic field must not be a stationary one, however, as otherwise its effect in one half-cycle of the precessional motion will be cancelled by the effect in the other half-cycle. To produce a net effect the secondary field must also rotate about the direction of the main field *with a frequency equal to that of the precessing proton*. The secondary magnetic field can then interact with the precessing proton and energy can be exchanged; if the frequencies differ there will be no interaction. Thus, when the frequency of the rotating secondary field and the frequency of the precessing nucleus become equal, they are said to be in *resonance*, since in this condition transition from one nuclear spin state to another can readily occur, giving rise to absorption or emission of energy.

The British physicist Larmor calculated the frequency of the precessional motion for an orbiting electron in a magnetic field. The expression for the precessional frequency (or Larmor frequency) of a spinning particle has the same form:

$$\omega = \frac{\text{magnetic moment}}{\text{angular moment}} \times H \text{ radians/sec}$$

$$= \frac{\mu H}{2\pi p_n} \text{ cycles/sec}$$

Substituting for μ and p_n their expressions from Eqs. (10.86) and (10.83) respectively, we obtain

$$\omega = \frac{g\beta_n H}{h} \text{ cycles/sec} \tag{10.92}$$

This equation is identical with Eq. (10.90). We thus see that the Larmor frequency is just the frequency separation between the nuclear magnetic energy levels. This shows that particle spins can interact with electromagnetic radiation.

To sum up, what emerges from the above discussion is that, *in order to produce nuclear magnetic resonance (absorption or emission of energy), it is necessary to apply a secondary magnetic field rotating in a plane perpendicular to the direction of the main field with a frequency equal to the frequency of the precessional motion of the nucleus due to the main field* [Eq. (10.92)].

A rotating magnetic field can be produced in a simple way by sending the output current of a radio-frequency crystal oscillator through a helical coil (solenoid) of wire. In NMR spectrometers, the sample under investigation is taken in a small glass tube placed between the pole faces of a d-c electromagnet (Fig. 10.46). The coil that transmits the radio-
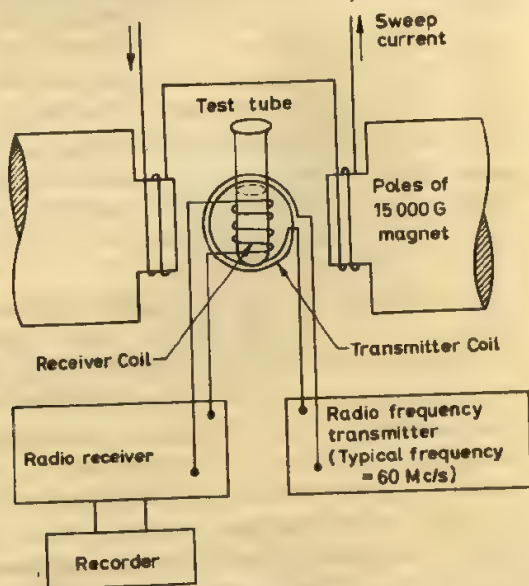
Fig. 10.46 Schematic representation of an NMR spectrometer.

frequency field is placed with its axis perpendicular to the direction of the main field produced by the electromagnet. The coil is made in two halves to allow the insertion of the sample holder. The electric current passing through the coil produces in it a magnetic field directed along its axis, and this field reverses its direction with the same frequency as the current. It is a general property of vectors that the resultant of two identical vectors rotating with the same frequency in opposite directions is equivalent to a vector having constant direction and periodic change of magnitude, which, in fact, represents an alternating motion. Thus the alternating magnetic field along the axis of the coil is equivalent to two

magnetic fields rotating with the same frequency but in opposite directions. Of these two rotating magnetic fields, the one whose direction of rotation is the same as the direction of the precessional motion of the nuclei will act as the secondary magnetic field. The other field rotating in the opposite direction can be ignored, since its average effect is zero. So to obtain a condition of resonance, the magnetic field at the proton and the frequency of the alternating current supplied to the coil from the oscillator must be such that Eq. (10.92) is satisfied. The nuclei can then absorb energy from the secondary field, if the system is not saturated. Coils located within the pole gap or wound about the poles of the magnet, allow a sweep to be made through the applied magnetic field to bring about the condition for resonance.

When resonance absorption of energy takes place, it can be thought of as producing nuclei in the excited state, which will then tend to return to the lower level in order to approach the Boltzmann distribution ratio. The radiation emitted in this process is picked up by the receiver coil, which is a separate radio-frequency coil consisting of a few turns of wire wound tightly around the sample tube. The receiver coil is perpendicular to both the main magnetic field and the radio-frequency transmitter coil in order to minimize pickup from these fields. It is the sample that provides this coupling between the receiver and the transmitter. The signal from the receiver coil can be displayed on an oscilloscope or a recorder chart.

Experimentally, the resonance condition may be obtained in two alternative ways. We might vary either the field strength of the electromagnet or the frequency of the oscillator, keeping the other fixed. Suppose we apply a fixed magnetic field and the Larmor frequency produced by it is, say, 60 Mc/sec; if the frequency of the oscillator is then varied over a range including 60 Mc/sec, resonance absorption will occur exactly at that frequency. On the other hand, we can fix the oscillator frequency at 60 Mc/sec and vary the applied field over a range until absorption occurs. The latter arrangement is simple and widely used in practice. Most NMR spectrometers in use today employ a fixed oscillator frequency of either 60 Mc/sec, 100 Mc/sec or 220 Mc/sec.

As we saw before, under ordinary conditions there is a small but finite excess of nuclei in a lower energy state. If, during resonance, upward transitions take place at a rate which is greater than the rate of reverse transitions, the excess of nuclei originally in a lower state will diminish, and accordingly, the intensity of the absorption signal will diminish. When the populations in the two states become equal, no further absorption can take place and the system is said to be *saturated*. The initial excess of nuclei in the lower state can be re-established if the system loses its absorbed energy. The processes by which the excess energy is shared either with the surroundings or with the nuclei are called *relaxation processes;* the time required for a fraction $1/e = 0.37$ of the

excess energy to be dissipated is the *relaxation time.* There are two kinds of relaxation processes: *spin-lattice relaxation* and *spin-spin relaxation.*

The term lattice refers to the surroundings, i.e. the framework of atoms or molecules containing the precessing nuclei. Atoms vibrating in a solid and molecules moving in liquids and gases have a variety of small magnetic fields associated with them. Energy transitions can occur by the interaction of such fields with the precessing nuclei. Thus, a field may be so oriented in the lattice that it induces a transition in a particular precessing nucleus from a higher to a lower energy state, the energy lost by the nucleus being transferred to the lattice as added translational, vibrational or rotational energy. The relaxation time (T_1) for spin-lattice relaxation (also referred to as *longitudinal relaxation*) varies greatly, being in general much shorter for non-viscous liquids; this difference is due to the fact that in nonviscous liquids there is greater freedom of molecular movement, and hence larger fluctuation of local magnetic fields, so that properly oriented magnetic fields, which may affect spin-lattice relaxation, are present relatively more frequently.

Spin-spin relaxation (also referred to as *transverse relaxation*) occurs by the mutual exchange of spins between two nuclei precessing in close proximity. Using the symbol T_2 for spin-spin relaxation time, for liquids usually $T_2 \approx T_1$, while for solids $T_2 \ll T_1$.

The magnitude of relaxation times profoundly influences the width of NMR spectral lines. The width of a spectral line is inversely proportional to the lifetime (Δt) of the excited state, i.e. the average time the system spends in the excited state. Thus sharp resonance lines are observed for relatively large Δt, and broad lines are observed for small Δt. This is best discussed in terms of the Heisenberg uncertainty principle, as given by Eq. (4.6). Dividing this equation by $h \Delta t$, we have

$$\frac{\Delta E}{h} = \Delta v = \frac{1}{2\pi\Delta t} \text{ c/sec} \qquad (10.93)$$

where ΔE is the uncertainty in the measurement of energy, or energy spread, of the excited state and Δv is the corresponding frequency spread. If both T_1 and T_2 are large, the excited state has a large lifetime and Δv is small. If, on the other hand, either T_1 or T_2 is small, the lifetime is short and Δv is large. Relaxation times for most nonviscous liquids and solids in solution are of the order of one second: $T_1 = T_2 = 1$ sec, so from Eq. (10.93) we find a frequency spread $\Delta v \approx 0.1$ c/sec. For solids and highly viscous liquids T_2 is shorter than T_1 and of the order of 10^{-4} sec. With this value, Eq. (10.93) gives $\Delta v \approx 10^3$ c/sec. So solids and very viscous liquids usually give spectra containing broad resonance lines, while for nonviscous liquids and gases sharp spectral lines can be obtained. Some liquids may, however, display broad resonance lines. In such cases, other factors which reduce spin-lattice relaxation times, such as the presence of paramagnetic molecules or ions in the sample, may play an important role.

10.11.4 Chemical Shift

A very important characteristic of the NMR technique is that it can distinguish protons in different molecular environments. If the resonance frequencies for all protons in a molecule were the same, as given by Eq. (10.92), then NMR spectra would show only one peak for the compound, and as such would be of little use to the organic chemist. However, we must now consider the fact that the field strength represented in Eq. (10.92) is the field strength experienced by the protons in the sample, and is *not* the same as the strength of the applied magnetic field. Protons whether in hydrogen atoms or molecules, are surrounded by an electronic charge cloud, having approximately spherical symmetry. A magnetic field induces electronic circulations in the charge cloud in a plane perpendicular to the applied field and in such a direction as to produce a field opposing the applied field, as shown in Fig. 10.47. The induced field
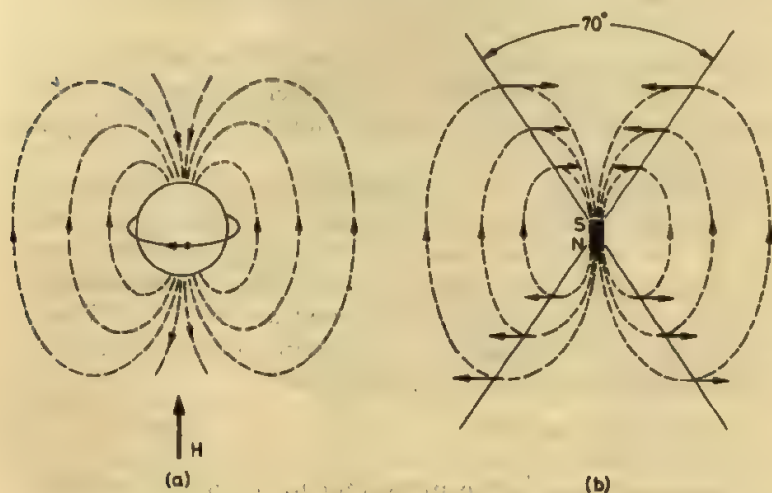
Fig. 10.47 (a) Diamagnetic circulation of an electron about a nucleus produces a field opposing the applied field H. (b) Field of point magnetic dipole.

is directly proportional to the applied field H and so can be represented by σH, where σ is a constant. The effective magnetic field experienced by the proton is therefore,

$$H_{eff} = (H - \sigma H) = H(1 - \sigma) \tag{10.94}$$

We can thus say that the proton is *shielded* from the external field by diamagnetic electron circulation and σ represents the shielding constant. The extent of shielding of a proton depends on the electron density around it in a molecule. A molecule may contain protons in different chemical environments. The average electron concentrations in these environments are different and so are the shielding effects on the protons. Consider, for example, the C–H and O–H bonds. Since oxygen is more

electronegative than carbon, the electron density around the CH proton (i.e. the proton in C–H bonds) should be considerably higher than that around the OH proton. We would thus expect that the shielding constant of the CH proton is greater than that of the OH proton. It then follows from Eq. (10.94) that, for a given applied field, the effective field at the OH proton is greater than that at the CH proton. Consequently, as the applied magnetic field is increased, the OH proton will come into resonance before the CH proton. The separation between the resonances (absorption peaks) for the same nucleus in different chemical environments is known as the *chemical shift*. It is easy to see that the magnitude of the chemical shift will be proportional to the strength of the applied field.

From chemical shifts we can know how many different types of protons there are in a molecule. Moreover, since the intensity of absorption at a given field strength will be proportional to the number of protons in a given environment in the molecule, the NMR spectrum can also tell us how many of each types of protons are present. These are the two important facets of NMR spectroscopy that make it a qualitative and quantitative analytical technique. As an illustration, we consider the NMR spectrum of ethanol obtained under low resolution [Fig. 10.48 (a)].
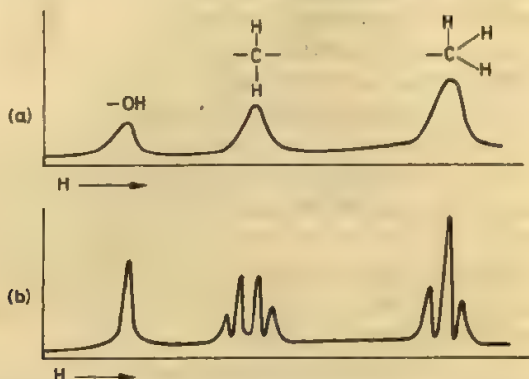
Fig. 10.48 Representation of NMR spectrum of ethanol (a) under low resolution and (b) under high resolution.

The spectrum shows three absorption peaks of intensity (area) ratio 1:2:3. The smallest peak is assigned to the single proton in the OH group, the next peak to the two protons in the CH_2 group and the largest peak to the three protons in the CH_3 group. That the absorption peak for the OH proton occurs at the lowest value of the applied field accords with the fact the OH bond is polar with the bonding electrons being on the average closer to the oxygen atom, and as a result the OH proton is relatively bare and unshielded from the applied field. The C–H bond being almost nonpolar, the bonding electrons in the CH_3 group are

nearly equally distributed between the carbon atom and the three protons. The CH_3 protons are thus well shielded and a larger applied field is required to bring them into resonance. The CH_2 peak occurs in between OH and CH_3 peaks, because the electron withdrawal by the oxygen of the OH group also has some effect on the electron distribution in the adjacent CH_2 group that reduces the degree of shielding for the CH_2 protons. It is interesting to note that dimethyl ether, $CH_3 OCH_3$, which is an isomer of ethanol, has six equivalent protons and accordingly the spectrum shows a single absorption peak.

Chemical shifts are very small compared to the strength of the applied field; their magnitude is a few milligauss at a field strength of about 10,000 gauss. Moreover, since electronic shielding (σH) is directly proportional to the strength of the applied field, the chemical shift value also varies with the field strength. Therefore in NMR analysis, chemical shifts are usually expressed on a relative basis, in a form independent of field strength. For a proton in a given environment, the chemical shift is defined by

$$\delta = \frac{H_r - H_s}{H_r} \times 10^6 \text{ ppm} \tag{10.95}$$

where H_s and H_r are the applied field strengths at which resonance occurs in a given substance and a reference substance, respectively. The reference substance is dissolved in the same solution as the sample (internal reference) so that both experience the same magnetic field. The chemical shift parameter δ is dimensionless; the factor 10^6 is included to express it as parts per million(ppm).

Chemical shifts of protons can also be expressed in terms of the number of cycles per second (cps) that they are displaced downfield from the reference substance.* This quantity will however depend on the oscillator frequency used by the spectrometer. In order to obtain the chemical shift as the dimensionless parameter, δ, the shift observed from the reference substance, in frequency units, is divided by the oscillator frequency used:

$$\delta = \frac{\text{Shift observed (cps)}}{\text{Oscillator frequency (cps)}} \times 10^6 \text{ ppm} \tag{10.96}$$

We might note at this point that most NMR spectrometers can, distinguish lines 0.1 milligauss or 0.4c/sec apart, which at an applied field of 15,000 gauss or oscillator frequency of 60Mc/sec represents a resolving power of about 1 in 10^8; such precision is not achieved by any other spectroscopic technique.

---

* If the spectrum is determined by variation of the field while the oscillator frequency is held constant, the differences actually measured are field differences in gauss; these are converted into frequency differences using the conversion:

milligauss $\cong$ 4.26 cps [calculated from Eq. (10.90)].

The substance now almost universally selected as reference for proton resonances is tetramethyl silane, $Si(CH_3)_4$, or TMS in short. Its chief advantages are:(i) it gives a single sharp peak (since all twelve protons in it are equivalent); (ii) its resonance peak occurs at an exceptionally high field, which is on the higher side of almost all other proton resonances in organic molecules, and (iii) it is chemically inert, magnetically isotropic and low boiling(b.p. 27°C), so that it can be readily recovered from most samples after use.

Resonance positions are indicated on δ-scale, or τ scale. On the δ-scale [Eq. (10.95)], δ is zero at the TMS and it increases downfield. On the τ-scale, τ is 10 at the resonance peak of TMS and decreases downfield, being related to δ by $\tau = 10 - \delta$. The δ-scale has the disadvantage that a large numerical value of δ implies a low-field resonance and hence a small shielding of the nucleus from the applied field. In this respect, the τ-scale is more convenient, a larger value of τ implying a greater shielding of the nucleus.

We know from the above discussion that the degree of electronic shielding of a proton is dependent on the electron density around it; the higher the electron density, the higher the shielding and hence the higher the field and the τ value at which the proton absorbs. As shown in the above illustration of ethyl alcohol, the electron concentration in the vicinity of the proton may differ as a result of differences in electronegativity of the attached atom. Thus if we consider the absorptions of protons of $CH_4 (\tau = 9.77)$, $CH_3I (\tau = 7.84)$, $CH_3Br (\tau = 7.32)$, $CH_3Cl (\tau = 6.95)$ and $CH_3F (\tau = 5.74)$, we find the results are in line with the electronegativity differences among the halogens. Similarly, we can interpret the absorptions of methyl proton attached to saturated carbon ($\tau = 9.1$), nitrogen ($\tau = 7.8$), and oxygen ($\tau = 6.5$) in terms of the relative electronegativities of the attached atoms

It should be noted that the local diamagnetic effect discussed above is not the only shielding mechanism operating on the proton. Thus if local diamagnetic currents only were responsible for shielding, the proton τ value would decrease with increasing electronegativity of the group to which the proton is attached, and one would therefore expect that the τ values for ethane, ethylene, and acetylene would decrease in that order. Experimentally, however, one finds that $\tau (CH_3.CH_3) > \tau (CH \equiv CH) > \tau (CH_2 = CH_2)$.* In order to explain this observed sequence, we must consider, in addition to local diamagnetic effects, another sort of effect coming from the neighbouring atom or from the rest of the molecule. This latter effect may be either *diamagnetic* (i.e. opposing the outer field H) or paramagnetic (i.e. supporting the outer field H). Though the field produced by the diamagnetic circulation of an electron about a nucleus (Fig. 10.47) opposes the applied field at that nucleus, it may however act paramagnetically, i.e. support

* The τ values are 9.04, 7.12 and 4.16 respectively.

the applied field at an adjacent or neighbouring proton. Similarly, the paramagnetic circulation of electrons, which supports the external field locally (Fig. 10.49), may however act diamagnetically

H
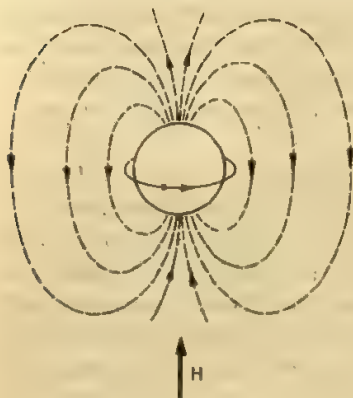
Fig. 10.49 Paramagnetic circulation of an electron about a nucleus produces a field supporting the applied field *H*.

at a neighbouring proton location. The diamagnetic effect on a proton reduces the effective magnetic field on the proton, and consequently, increases the shielding. The paramagnetic effect, on the other hand, causes deshielding, i.e. reduces the shielding. *If the symmetry axis of the charge distribution around a nucleus coincides with the direction of the external field* (which is, however, not possible all the time because of thermal motion) *only diamagnetic currents occur.* In all other cases, both diamagnetic and paramagnetic currents contribute. It should be noted that the charge distribution surrounding protons has approximately spherical symmetry irrespective of the presence of magnetic field or chemical bonding; so, even if a molecule, of which the proton is a part, changes its orientation with respect to the applied field direction due to incessant rotation and vibration, *mainly diamagnetic currents will flow around the proton* because of the almost axial symmetry of the charge cloud with respect to the field direction.

The electron circulations around the carbon atoms and protons in ethane, ethylene and acetylene when the molecule is oriented with the C—C axis either parallel or perpendicular to the field direction are shown in Fig. 10.50.

When ethane is oriented with its C—C axis parallel to the field direction [Fig. 10.50 (a)], mainly diamagnetic currents flow around carbon. However, these diamagnetic currents exert a weak paramagnetic effect on the protons since the C—H bonds are nearly perpendicular to the field direction. For the orientation.as shown in Fig. 10.50 (b), in which the C—C bond is perpendicular to the field direction, paramagnetic currents flow around carbon, producing a weakly paramagnetic effect on the protons. These paramagnetic effects from the adjacent carbon reduce the shielding of the protons by their own diamagnetic currents.

Proceeding to the unsaturated molecule ethylene, we see that para-
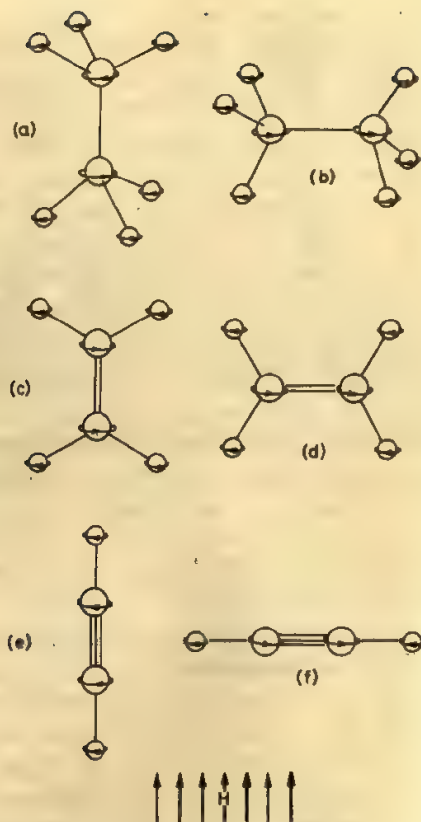
Fig. 10.50 The electron circulations around carbon atoms and protons in ethane, ethylene and acetylene in homogeneous magnetic field *H* directed from bottom to top of page.

magnetic currents around its carbon exert a diamagnetic effect on the protons for certain orientations of the molecule [Fig. 10.50 (c)] and a paramagnetic effect for other positions [Fig. 10.50 (d)]. Thus ethylenic protons are, on the whole, better shielded by magnetic effects from carbon than the protons of ethane. But since they are probably shielded less by their own diamagnetic currents than are the protons of ethane, because of the greater polarity of the C—H bond in ethylene, the final result becomes $\tau(CH_3-CH_3) > \tau(CH_2=CH_2)$.

For the linear molecule, acetylene, the diamagnetic currents flowing around carbon, when the C≡C bond is parallel to the field direction [Fig. 10.50 (e)] exert a diamagnetic effect on the adjoining proton. When the C ≡ C direction is perpendicular to the field direction [Fig. 10.50 (f)] paramagnetic currents flow around carbon, but they act diamagnetically at the proton location. As a result, the protons of acetylene are better shielded by the adjoining carbon atom than the protons of ethane and ethylene. However, because of the greater polarity of the C—H bond in acetylene (as shown by its acidic property), acetylenic protons are probably shielded less by their own diamagnetic currents than are the protons of ethane and ethylene, so that the final

result becomes $\tau(CH_3-CH_3) > \tau(CH\equiv CH) > \tau(CH_2=CH_2)$.

Diamagnetic electronic circulations exert a diamagnetic effect on a proton which is on, or close to (Fig.10.47), the axis of circulating electrons (e.g. in the group $-C\equiv C-H$), but exert a paramagnetic effect on the proton at right angles, or nearly at right angles, to the axis (e.g. in ethane). Thus both shielding and deshielding may arise from diamagnetic circulation. In acetylene, the diamagnetic electron circulation within the cylindrical π electron cloud (see Fig. 6.23) induces shielding at the axial proton, whereas in benzene, the π electron circulation, which is in the plane of the ring, causes deshielding at the protons lying in the plane (see Fig. 6.28); hence the relatively low value of τ for aromatic protons, as shown in Table 10.14. It is seen that substitution of benzene shifts the τ

Table 10.14   Typical Chemical Shifts for Various Types of Protons

Type of proton	Shift		Type of proton	Shift
	δ	τ		δ
Protons on saturated carbons			*Other protons*	
RCH_3	0.9	9.1	RNH_2	1.5
$RCH_2 R$	1.3	8.7	$C_6 H_5 NH_2$	3.4
$R_3 CH$	1.5	8.5		
$CH_3 CN$	1.97	8.03	$RCHO$	9.7
$CH_3 COCH_3$	2.09	7.91	$RCOOH$	11.0–12.0
$CH_3 CHO$	2.15	7.85	ROH	highly variable
$C_6 H_5 CH_3$	2.34	7.66		
$CH_3 OR$	3.4	6.6		
$RCH_2 OR$	3.7	6.3		
$RCH_2 Cl$	3.7	6.3		
$RCH_2 OOCR$	4.1	5.9		
$CH_3 NO_2$	4.28	5.72		
Protons on unsaturated carbons				
$RC \equiv CH$	2.4	7.6		
$R_2 C = CH_2$	4.5–5.0	5.0–5.5		
$R_2 C = CHR$	5.0–5.5	4.5–5.0		
Protons on aromatic rings				
$C_6 H_6$	7.27	2.73		
* $C_6 H_5 NO_2$	8.22, 7.48	7.60, 1.78,	2.52, 2.40	
* $C_6 H_5 NH_2$	6.52, 7.07	6.65, 3.49,	2.93, 3.35	

* The three values given refer to *ortho—*, *meta—*, and *para—*protons, respectively.

value for the absorption of the aromatic protons. Electron-withdrawing groups (e.g.—NO_2, —CO_2H) lower the τ value, while electron-donating groups (e.g.—OH, —NH_2) raise the τ value relative to benzene (2.73 τ), because of the local diamagnetic shielding effect.

10.11.5 *Spin-spin Interaction*

In addition to the chemical shift in molecules containing nonequivalent nuclei, NMR spectra have another valuable feature, that is, the splitting of many of the lines in the spectrum into two or more components. This phenomenon, known as *spin-spin splitting*, can be observed only with spectrometers of high resolution. As an illustration, we consider the high-resolution spectrum of a common sample of ethanol, represented in Fig.10.48(b). By comparing it with Fig. 10.48(a) we see that methyl absorption is now split into a triplet with areas of the three components in the approximate ratios 1:2:1 and methylene absorption is split into a quartet, having relative areas, approximately, 1:3:3:1. The spacing of component lines in spin-spin splitting (called the *spin-spin coupling constant* and denoted by the symbol J), in contrast to the chemical shift discussed above, is found to be independent of the applied field strength, which strongly suggests that the effect is intramolecular. The splitting of a resonance absorption is attributed to the effect on the nuclei (responsible for this absorption) of other magnetic nuclei in the same molecule. For example, we can explain the splitting patterns of Fig. 10.48(b) by assuming that the magnetic field at the protons in a group is influenced by the spin arrangements of the protons in the adjacent group. The methyl group in the ethanol molecule is adjacent to a methylene group with its two equivalent protons. For the two protons, there are three possible combinations of spin orientations, as
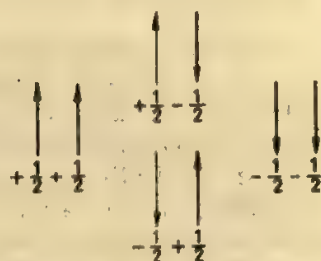
Fig. 10.51 Possible spin orientations of the protons of a methylene group.

shown in Fig. 10.51. The designations '+' and '—' shown here are, of course, purely arbitrary, but the important point that emerges from this representation is that there are three different values of the total spin of the methylene protons and that one of these values can be obtained in

two ways. If the effect of the instantaneous spin arrangements of the methylene protons can be transmitted to the protons of the methyl group, the magnetic field at the protons in the methyl group will have, on the average, three different values, and one of them will occur twice as often as either of the other two. The resonance absorption of the methyl protons would therefore be split into three peaks (a triplet) having relative areas of $1:2:1$.

For the three equivalent protons of the methyl group, there are four different values of total spin (Fig.10.52), which may affect the resonance of the protons of the methylene group, and moreover, two of the four values can be obtained in three different ways. The methylene proton resonance will therefore be split into four peaks having relative areas of $1:3:3:1$.
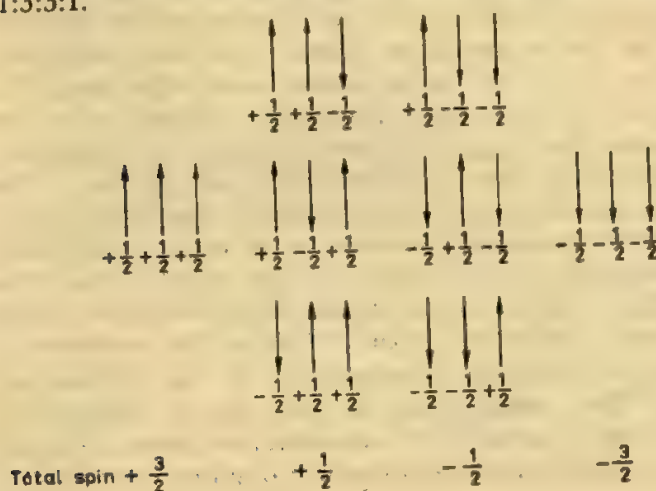
Fig. 10.52 Possible spin orientations of the protons of a methyl group.

It should be noted that a hydroxyl proton is not immutably locked in any particular ethyl alcohol molecule; it is, in fact, exchanged among different ethyl alcohol molecules over a period of time. The rate of this *chemical exchange* (proton transfer) is relatively slow in pure ethyl alcohol, but is markedly increased by acidic or basic impurities that are ordinarily present. If the rate of chemical exchange is rapid, the hydroxyl proton experiences an averaged effect of the spin orientations of the methylene protons and its absorption peak therefore shows only a singlet [see Fig. 10.48 (b)]. Similarly, the hydroxyl proton also does not cause splitting of the methylene proton absorption, if there is rapid chemical exchange; the methylene proton absorption thus occurs as a quartet due to the effect of the methyl group alone. In a highly purified sample of ethanol, on the other hand, the rate of chemical exchange is very slow, so the hydroxyl proton will experience the spin orientations of the methylene group; this will result in a triplet for the hydroxyl proton

absorption. For the same reason, the absorption of the methylene protons will be influenced by the spin of the hydroxyl proton, in addition to the spins of the methyl protons, with the result that the absorption peak will be split into more than four components.

The multiplicity of a given group of equivalent protons is clearly related to the number of protons on adjacent atoms. As a simple rule, the multiplicity of a given group is $(n + 1)$, where n is the number of protons on adjacent atoms. In simple cases of interacting nuclei, the component peaks of a multiplet are symmetric about a midpoint and their relative areas are numerically proportional to the coefficients of the terms in the expansion $(1 + r)^n$. To illustrate, the following multiplicities will be predicted for the following compounds: $n-$propyl iodide $(CH_3CH_2CH_2I)$: a 3-proton triplet (relative areas 1:2:1), a 2-proton sextet (1:5:10:10:5:1) and a 2-proton triplet (1:2:1); isopropyl iodide $[(CH_3)_2 . CHI]$: a 6-proton doublet (1:1) and a 1-proton septet (1:6:15:20:15:6:1); methyl ethyl ether $(CH_3OCH_2CH_3)$: a 3-proton singlet, a 2-proton quartet (1:3:3:1) and a 3-proton triplet (1:2:1).

It should be noted that the aforesaid rule for determining the multiplicities of resonance absorptions hold only for simple cases in which the coupling constants of the interacting adjacent groups have nearly the same value and in which the separation of resonances of interacting groups is much larger than the coupling constant of the groups. In the case of pure ethyl alcohol, for example, the coupling constants differ considerably and one does not find a quintet (that would be predicted by the simple multiplicity rule) for the CH_2 group in the high resolution spectrum. While the absorption for the CH_2 protons is split into a quartet by the methyl protons, each component of the quartet is again split into a doublet by the hydroxyl proton, so that (assuming the symmetry of the multiplets) in this case a CH_2 multiplet of eight peaks would be expected; this, in fact, agrees quite well with the experimental result.

The most important application of NMR spectroscopy in organic chemistry is the analysis and identification of compounds containing hydrogen. The observation of proton chemical shifts in a spectrum indicates the types of hydrogen containing groups present in the molecule, while the relative areas of the absorptions give directly the proportions in which these groups occur. The multiplet structure of each group further reveals the number of protons coupled to that group and thus provides information about the way in which the different groups are linked together in the molecule.

10.11.6 *Nuclei Other Than Proton*

In the previous sections we have discussed NMR spectra of protons with spin . There are however other nuclei with spin $\frac{1}{2}$ and these also will give

rise to NMR signals if an appropriate magnetic field and radio-frequency are applied. Nuclei, other than proton, with spin $\frac{1}{2}$ include ^{13}C, ^{19}F, ^{31}P, ^{29}Si, and various metals such as ^{117}Sn, ^{119}Sn, ^{195}Pt, and ^{207}Pb. Of these the ^{13}C nucleus, probably the most important for the general chemist, gives rise, however, to only extremely weak signals and satisfactory NMR spectra are not easy to obtain. All other nuclei exhibit the phenomena of chemical shift and spin-spin coupling which are generally considerably larger than their proton counterparts. This can be attributed to the greater number and mobility of extranuclear electrons producing greater diamagnetic shielding.

Let us now consider nuclei with spin greater than $\frac{1}{2}$. We have seen in Section 10.11.1 that in an applied magnetic field any nucleus with spin I can have $2I + 1$ possible orientations (see Fig. 10.44), each associated with a slightly different energy level. The spacings between the energy levels, in a given field, being all identical, any spinning nucleus will, in principle, give rise to a single resonance line when the condition of resonance is satisfied. In practice, however, nuclei with spin greater than $\frac{1}{2}$ are not much used in themselves, since their resonance absorptions are intrinsically very weak and not easy to observe. We should, however, consider the effect of such nuclei on the NMR spectra of neighbouring protons, arising from spin-spin coupling. Of wide occurrence are ^{14}N (spin $I = 1$), $^{35}Cl (I = 3/2)$. $^{81}Br (I = 3/2)$ and $^{127}I(I = 5/2)$.

Consider, as an example, the group $N-H$. Since the spin of the nitrogen nucleus (^{14}N), with $I = 1$, can have three orientations in an applied field (Fig. 10.44a), the direct coupling of nitrogen and proton spins will split the proton resonance into a *triplet*, and moreover, since the three spin orientations of nitrogen are equally likely, each line of the triplet will have the same intensity. In general, a nucleus with spin I and hence $1I + 1$ spin orientations of equal probability, in an applied field will be expected to split the resonance of a neighbour into a multiplet of $2I + 1$ lines with equal intensity. Thus a single chlorine nucleus ($I = 3/2$) would tend to produce quartet structures for its neighbours while a single iodine nucleus ($I = 5/2$) would produce sextets. In practice, however, these splittings are not observed due to rapid transitions between spin states caused by *quadrupole relaxation* (see below).

Quadrupole effects   All nuclei with spin $I > 1/2$ possess, in addition to the magnetic moment, an electric quadrupole moment which arises because of non-sphericity of the nuclei. Such nuclei are shaped either like a symmetrical egg (elongated poles) or a tangerine (flattened poles) and thus have a charge distribution which is non-spherical. The *electric quadrupole moment*, which is a measure of this departure from sphericity is positive for egg-shaped and negative for tangerine-shaped, and is zero for spherical (i.e. with spin 1/2 or 0) nuclei.

The electric quadrupole moment interacts with a surrounding electric field and, if such a field has a pronounced gradient at the nucleus, the

quadrupole electric moment of the nucleus will tend to lie in the field direction. (An electric field gradient may arise from electron charge distribution in a molecule or from ions and dipoles, as in a solid.) The coupling between the quadrupole moment and the field gradient may be so strong as to prevent the coherent alignment of the spin magnetic moment of the nucleus in an applied magnetic field. The quadrupole moment thus provides a mechanism by which the nuclear spin orientation may be relaxed. This mechanism is called *quadrupole relaxation*.

The efficiency of quadrupole relaxation depends on the symmetry of the surroundings. Thus, since univalent atoms, such as halogens, will always be situated in a field gradient of a single bond, they will experience efficient relaxation. On the other hand, the relaxation of polyvalent atoms will vary from molecule to molecule. For example, the quadrupole relaxation of nitrogen is very efficient in ammonia, a pyramidal molecule, in which the three positively charged hydrogen nuclei on one side of the nitrogen produce a strong electric field gradient at the nitrogen nucleus; the relaxation is however very weak in the ammonium ion NH_4^+, which consists of a nitrogen nucleus at the centre of a regular tetrahedron of nuclei and thus has no field gradient at the nitrogen nucleus.

Quadrupole relaxation has two effects in NMR spectroscopy: (a) broadening of the NMR signal from a nucleus possessing a quadrupole moment; (b) destroying, partially or completely, coherent coupling between nuclei with corresponding effects on sharpness and multiplicity of resonances. As we have seen earlier (Section 10.11.3), the width of a spectral line is inversely proportional to the lifetime (Δt) of the excited state. When there is quadrupole relaxation, Δt of a spin state may be very short, of the order of 10^{-4} sec or less, and accordingly from Eq. (10.93) we have a frequency spread $\Delta \nu \approx 10^3$ cycles/sec. The resonance line of a nucleus with quadrupole relaxation may thus be extremely broad and even be difficult to detect. Quadrupole relaxation, as we have seen above, tends to destroy coherent coupling between nuclei. If the relaxation is highly efficient, for example, in halogen nuclei, the coupling is completely destroyed and the resonances of neighbouring nuclei therefore remain sharp. If, on the other hand, the relaxation is less efficient, as in many nitrogen containing molecules, the coupling is only partially destroyed, thus permitting multiplets but broad resonances from neighbouring nuclei. The most commonly occurring quadrupolar nucleus in routine NMR spectroscopy is ^{14}N and its effect is usually to broaden the resonance lines of neighbouring nuclei.

Since any quadrupolar nucleus contained in a well-ordered single crystal of a solid substance experiences exactly identical surroundings as similar nuclei in other regions of the lattice, all the quadrupole moments will tend to lie in the same direction. Thus even in the absence of an external magnetic field these nuclei can absorb energy from a suitable

radio-frequency field to undergo transition between energy levels. This resonance phenomenon, which occurs in the frequency range 1–1000 Mc/sec, is known as the *nuclear quadrupole resonance* (NQR) or *pure quadrupole resonance* to emphasize the fact that an external magnetic field is not applied. NQR spectroscopy essentially employs the quadrupolar nucleus as a probe to measure electric field gradients in the crystal. Such data are invaluable in applications of crystal field theory. Quadrupolar nuclei that have been tried include ^{14}N ($I=1$), ^{35}Cl, ^{37}Cl ($I=3/2$), ^{79}Br, ^{81}Br ($I=3/2$), and ^{127}I ($I=5/2$). NQR frequencies of Cl in covalent bonds are around 30 Mc/sec, whereas Br and I have higher frequencies. Only solids can be studied for NQR spectroscopy, and samples may be in the form of single crystals or crystalline powder.

10.12   Electron Spin Resonance Spectroscopy

Electron spin resonance (ESR) spectroscopy, also called *electron paramagnetic resonance* (EPR) spectroscopy, provides a powerful tool for the study of chemical species with unpaired electrons. These chemical species may be atoms, ions, molecules, or molecular fragments having an odd number of electrons. An electron possesses a spin and, associated with the spin, there is a magnetic moment. The presence of an unpaired electron in a chemical species thus allows energy levels (Zeeman levels) to be produced from the interaction of its spin magnetic moment with an applied magnetic field. Transitions can be induced between these levels in a manner similar to that in NMR spectroscopy.

10.12.1 Splitting of Electron Energy Levels by a Magnetic Field

The electron, like the proton, has a spin quantum number of 1/2 associated with its spin, and in the presence of an applied magnetic field the spin angular momentum is quantized such that its component along the direction of the field can be either $+1/2$ ($h/2\pi$) or $-1/2$ ($h/2\pi$) [cf. Fig. 10.44(b)]. In a magnetic field H, the electron dipole is thus subjected to a torque acting to make it either parallel or antiparallel to the direction of the magnetic field and precess about the magnetic field directions with a frequency which is proportional to both the magnetic field and the electron magnetic moment, resembling the situation for protons in NMR spectroscopy (Section 10.11.3).

Because an electron bound to an atom possesses, in addition to spin about its own axis, an orbital motion about the nucleus, the electron magnetic moment is better expressed in terms of the product $g\beta$, where β is the Bohr magneton given by $eh/4\pi m_e c$ and equals 9.2732×10^{-21} erg/gauss, and g is the spectroscopic splitting factor. (For a completely free electron, the value of g is 2.0023 but it differs significantly when

strong coupling occurs.) Thus for an electron the separation between neighbouring energy levels is (cf. Eq. 10.89):

$$\Delta E = g \beta H \qquad (10.97)$$

For a free electron ($g = 2.0023$) the frequency of radiation absorbed, from Eq.(10.97), is

$$= (2.0023)(9.2732 \times 10^{-21}) H / 6.626 \times 10^{-27}$$
$$= (2.802 \times 10^6) H \, c/sec.$$

Thus when a magnetic field of 3000 gauss is used, the absorption frequency is 8.4×10^9 c/sec which falls in the microwave region of the electromagnetic spectrum (Fig.10.10).

In a magnetic field, the electron spin magnetic moments do not all occupy the lowest energy level. By the Boltzmann distribution law the ratio of the numbers n_1 and n_2 of the electrons in the upper and lower energy states, respectively, is given by

$$\imath n_1 / n_2 = e^{-\Delta E / 2kT} \qquad (10.98)$$

where ΔE is the energy difference between the two levels and k is the Boltzmann constant. Since ΔE is given by Eq. (10.97),

$$n_1 / n_2 = e^{-g \beta H / 2kT} \qquad (10.99)$$

The smaller the value of n_1 / n_2, the higher the absorption probability and, hence, the sensitivity of the measurements. The sensitivity therefore increases steeply with field strength.

Transitions between the electron energy levels in a magnetic field can be produced and spectroscopic measurements can be made in a manner similar to that in NMR spectroscopy. Thus for obtaining an ESR spectrum, the sample containing an unpaired electron is placed in a constant magnetic field and simultaneously irradiated by a radio-frequency field(in the microwave region) that produces a rotating field perpendicular to the fixed magnetic field direction. As in NMR, the resonance frequency satisfies the relation:

$$\omega = g \beta H / h \, c/sec. \qquad (10.100)$$

Energy absorbed from the rotating field at resonance causes the electron spins to flip from the lower energy level to the higher energy level [Fig. 10.53 (a)]. The absorption of energy is measured electrically and recorded on a chart.

10.12.2 Instrumentation

A Klystron oscillator operated at frequencies around 10^{10} c/sec and 3.5×10^{10} c/sec is commonly used to generate a microwave field in an ESR spectrometer. The field is applied to a rectangular microwave cavity which contains the sample and is connected to one arm of a microwave impedance bridge system. The sensing element of the spectrometer is the microwave cavity which is constructed in such a way as to maximize the applied magnetic field at the sample held in the cavity. The cavity is
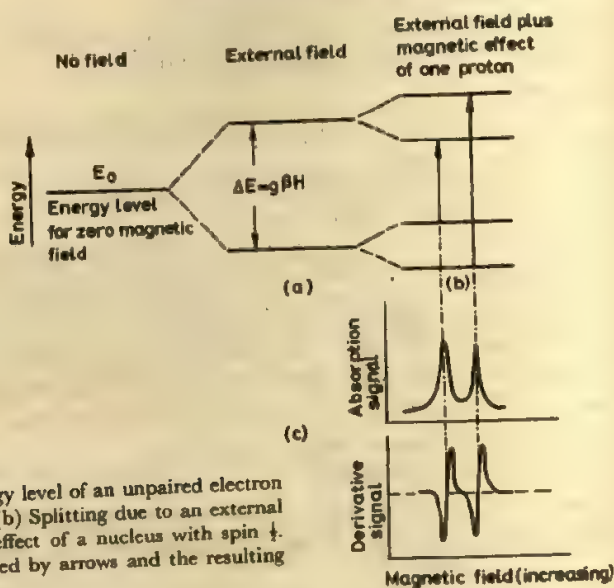
Fig. 10.53 (a) Splitting of energy level of an unpaired electron by an external magnetic field. (b) Splitting due to an external magnetic field plus magnetic effect of a nucleus with spin $\frac{1}{2}$. Allowed transitions are indicated by arrows and the resulting ESR spectrum is shown in (c).

placed between the poles of an electromagnet, which provides a homogeneous magnetic field and which can be varied from near zero to 5000 gauss.

The bridge method is normally employed in the detection scheme with a crystal detector. The detector is usually a silicon-tungsten crystal rectifier which converts microwave power to a direct-current signal. Magnetic field modulation is usually employed to produce resonance. The magnetic field is swept over a small range through the resonant condition by varying the current in a pair of sweep coils mounted on the cavity walls. Phase-sensitive detection results in the recorder presentation as the derivative of the microwave absorption spectrum against magnetic field.

10.12.3 ESR Spectra

For obtaining ESR spectra the sample may be used in the form of a single crystal, solid powder, liquid or solution. The total area under the absorption peak is proportional to the number of unpaired electrons in the sample. Comparison can be made with a standard having the same line shape as the unknown. The usual standard is diphenylpicrylhydrazyl which is completely in the free-radical state and contains 1.53×10^{21} unpaired electrons per gram.

Since an unpaired electron for spin resonance is usually near or at the periphery of the free-radical species with which it is associated, its g

Determination of Molecular Structure

value is always close to 2.0023, and consequently no counterpart of chemical shifts in NMR is observed in ESR. Interactions however occur between the magnetic moment of the unpaired spinning electron and the magnetic moments of those nuclei in the free radical which have intrinsic spins (Section 10.11). Such interactions are possible as the unpaired electron in many free radicals is not rigidly attached to a particular atom but occupies an orbital embracing several atoms. The interactions cause further splitting of the electron energy levels and give rise to *hyperfine splittings*. Whereas the multiplet *fine structure*, which occurs only in ionic crystals, arises when the paramagnetic material has more than one unpaired electron, the smaller *hyperfine structure*, which occurs both in crystals and free radicals, arises through coupling of the unpaired electron with neighbouring nuclear spins, in much the same way as coupling occurs between nuclear spins (Section 10.11.5).

Considering, for example, the simplest case of an unpaired electron interacting with one proton (nucleus with spin $\frac{1}{2}$), the magnetic field actually felt by the electron is $H_0 + \Delta H$ or $H_0 - \Delta H$, where H_0 is the applied field and ΔH is the effect originating from the magnetic dipole moment of the proton. The probabilities will be equal for the electron experiencing the higher field $(H_0 + \Delta H)$ due to parallel alignment with the proton or the lower field $(H_0 - \Delta H)$ due to antiparallel alignment. Therefore, instead of a single absorption line, two lines of equal intensity will occur in the ESR spectrum. Figure 10.53(b) shows schematically the splitting of the electron energy level due to an external magnetic field plus the magnetic effect of a nucleus with spin 1/2.

In general, each electronic energy level will be split into $2I + 1$ levels due to a nucleus with spin I, thus giving rise to $2I + 1$ resonance absorption lines. Phase-sensitive detection used in ESR results in the recorder presentation of the first derivative of the absorption spectrum against the magnetic field [Fig. 10.53 (c)]. A superheterodyne arrangement is also used especially for very narrow absorption lines.

If a radical species contains several nuclei with intrinsic spins, the unpaired electron then experiences interaction with each nucleus resulting in a more complicated splitting pattern. The splittings can be treated in much the same way as were the nuclear magnetic interactions in NMR spectroscopy. Quite generally, $2nI + 1$ spectral lines result from interaction with n equivalent nuclei of spin I and the intensity distribution of the lines equals the coefficients of the binomial expansion $(1 + r)^n$ similar to that in NMR spectroscopy.

To illustrate, the interaction of an unpaired electron with four equivalent protons $(I = \frac{1}{2})$ in 1, 4—benzosemiquinone will be expected to produce a multiplet of five peaks (Fig. 10.54) with an intensity ratio of 1:4:6:4:1. The lines in the primary multiplet may also be split further due to weaker coupling of the electron with other nuclei in the same free radical species. Analysis of hyperfine splittings and the number and
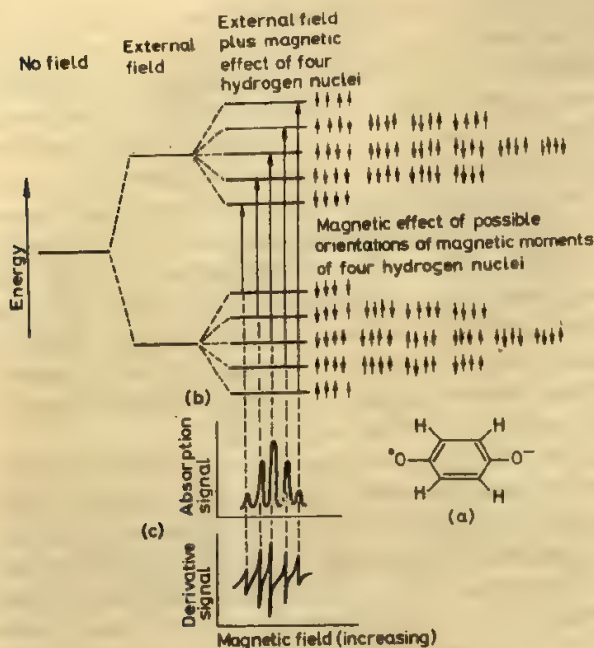
Fig. 10.54 (a) Free-radical ion 1,4–benzosemiquinone., (b) Expected splittings and transitions and (c) ESR spectrum of the radical ion.

relative intensities of multiplet structures give information on the distribution of the unpaired electron and the degree of its interaction with the nuclei in the molecule.

Example 10.2 What would be the ESR hyperfine patterns for the semiquinones (Fig. 10.55) which are formed as intermediates in the oxidation of (a) 2,6–dimethyl-4-t-butyl phenol, (b) 2,6-di-t-butyl- 4-methyl phenol and (c) 2,4,6-tri-t-butyl phenol with lead oxide in cyclohexane?
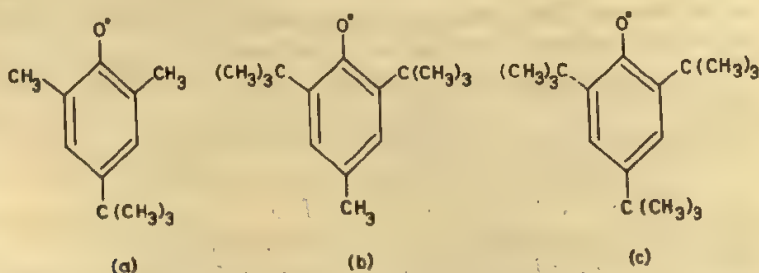
Fig. 10.55 Semiquinone intermediates formed by the oxidation of respective phenols.

Solution

(a) The unpaired electron interacts with the six equivalent protons of the two methyl groups [Fig. 10.55(a)] to produce a large septet with an intensity ratio of 1:6:15:20:15:6:1. Each of these lines is split again into a triplet by weaker coupling of the electron with the two ring protons. The ESR spectrum would therefore exhibit a *septet* of closely spaced triplets.

(b) A *quartet* of closely spaced *triplets*, the primary quartet arising from the three protons of the 4-methyl group [Fig. 10.55(b)].

(c) A three line spectrum (1:2:1 ratios of intensities) from interaction of the odd electron with two ring protons [Fig. 10.55 (c)].

Since ESR, by its very nature, cannot respond unless unpaired electrons are present, it provides a definite means of ascertaining beyond any doubt the presence of free radicals in chemical species. Moreover, ESR gives information not only on the presence and number of unpaired electrons, as measurements of paramagnetism can often do, but also on the distribution of such electrons and the extent of its interactions with atoms in the free-radical type molecule.

When the sample is used in the form of liquid or solution, the interactions are usually isotropic (that is independent of the orientation of the free-radical). However, anisotropic interactions play an important role for free radicals trapped in a solid or highly viscous medium, and the ESR hyperfine splitting then depends, if the radical is not spherically symmetric, on the orientation of the free radical with respect to the magnetic field direction. Anisotropy of interactions results in broadening and distortion of the ESR lines, and the interpretation of spectra becomes more difficult.

10.13 Mössbauer Spectroscopy

Mössbauer spectroscopy, named after Rudolf Mössbauer (1958), relates to transitions between energy levels of nuclei of atoms. When an element is formed by the radioactive decay of an isotope of the same element or of a different element, it is often produced initially in an excited nuclear state and after a short period, of the order of microseconds, it reverts to the ground state emitting energy in the form of γ-rays. It is the study of this γ-ray emission from excited nuclei and its subsequent reabsorption by other nuclei that constitutes Mössbauer or γ-ray spectroscopy.

10.13.1 Principles of Mössbauer Spectroscopy

We explain in this section the essential principles of Mössbauer spectroscopy taking the iron nucleus ^{57}Fe as our example. Radioactive

isotope ^{57}Co, which is a relatively long-lived species having a half-life of some 270 days is a convenient source of ^{57}Fe. A simplified energy level scheme showing the decay of radioactive ^{57}Co producing ^{57}Fe is shown in Fig. 10.56. The Cobalt nucleus, following an electron capture,
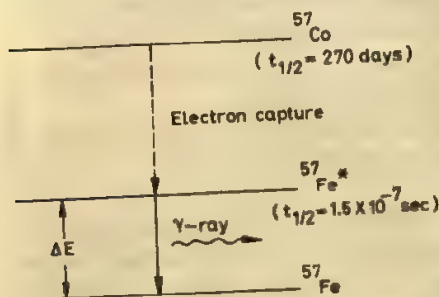
Fig. 10.56 A simplified energy level diagram showing the decay of radioactive ^{57}Co to the excited state ^{57}Fe* and then to the ground state ^{57}Fe.

produces a ^{57}Fe nucleus in an excited energy state, designated ^{57}Fe*. The latter very rapidly drops to the ground state ^{57}Fe, the energy change involved being $\Delta E = 2.30 \times 10^{-8}$ ergs (per nucleus), which is thus emitted as a radiation of frequency $v = \Delta E/h = 3.5 \times 10^{18}$ c/sec (γ-ray). If now a second ^{57}Fe nucleus in the ground state were placed in this emitted radiation beam it would be expected to be excited into the ^{57}Fe* state by absorbing energy from the beam. A γ-ray detector—a scintillator of a Geiger counter—placed in the path of the beam behind the absorber would detect this happening. However, two factors prevent this γ-ray resonance absorption.

Example 10.3 Calculate the line width of the γ-ray emission from ^{57}Fe* nucleus having a half-life of about 10^{-7} sec.

Solution

Mean lifetime $\Delta t = t_{1/2}/\ln 2$
From Eq. (10.93):
$$\Delta v = 1/(2\pi \Delta t) = 0.110/t_{1/2} - \gamma$$
Natural line width $= \Delta = 0.110/10^{-7}$
$$\simeq 10^6 \text{ sec.}^{-1}$$
Relative line width $= \Delta v/v = 10^6/3.5 \times 10^{18}$
$$\simeq 3 \times 10^{-13}$$

The γ-ray emission frequency, as shown in Example 10.3, is very sharp having very low line-width. Consequently, any effect which produces a change in the energy levels of the nuclei or in the radiation frequency itself will prevent resonant absorption of the γ-ray. One very important factor which gives rise to such an effect is the *nuclear recoil*. It is easily seen by applying the de Broglie relationship [Eq.(4.1)] that a γ-ray photon of frequency 10^{18} c/sec has a relatively large momentum. Consequently, when such a photon is emitted by a nucleus, the nucleus recoils considerably so as to conserve the total momentum. It is however well known that when a moving body emits radiation a stationary observer

sees a shifted frequency. This is called the *Doppler effect* and the frequency shift $\triangle v$ is given by

$$\triangle v = v\,v/c \quad \text{c/sec.} \tag{10.101}$$

where v is the relative velocity of source and observer and c is the velocity of the emitted radiation. For our $^{57}Fe^*$ nucleus, the frequency shift due to recoil is of the order of 10^{12} c/sec (see Example 10.4) which, though small compared with the emission frequency of 3.5×10^{18} c/sec, is indeed very large when compared with the line width of 10^6 c/sec. Nuclear recoil thus shifts the emitted frequency some millions of line-widths away from the position of the absorption frequency thereby preventing resonance absorption. In fact, it is possible to observe γ-ray absorption if the source material is moved relative to the sample to compensate for the recoil energy loss. Mössbauer's main contributions, which are indeed very simple when viewed against this background, were to use solid crystal lattices as the γ-ray source and further to cool both source and sample (absorber) to low temperatures. The emitting nucleus, firmly fixed in a solid lattice, has a very large apparent mass and hence negligible recoil velocity, while by cooling to low temperatures the thermal motions of the lattice atoms, and hence the resulting Doppler effect, are also reduced to a minimum.

Example 10.4 Calculate the recoil velocity of a free Mössbauer nucleus $^{57}Fe^*$ when emitting a γ-ray of frequency 3.5×10^{18} c/sec. What is the Doppler shift of the γ-ray frequency to an outside observer?

Solution

Eq. (4.2): Momentum of γ ray photon $= h/\lambda = hv/c$

Recoil velocity = Momentum/Nuclear mass $= (hv/c)/m$

$$= \frac{(6.62 \times 10^{-27})(3.5 \times 10^{18})/(3 \times 10^{10})}{(57/6.02 \times 10^{23})}$$

$$= 8.2 \times 10^{3}\ \text{cm/sec}$$

Eq. (10.101): $\triangle v = (3.5 \times 10^{18})(8.2 \times 10^{3})/(3 \times 10^{10})$
$$= 9.6 \times 10^{11} \quad \text{c/sec.}$$

We have seen three components of a Mössbauer spectroscopic arrangement—source, sample, and detector. We now need some scanning device so that the absorption of a particular sample can be precisely located. The Doppler effect here becomes a convenient tool. For example, a relative velocity v of 1 cm/sec between source and sample produces, according to Eq. (10.101), a Doppler frequency shift of about 10^8 c/sec; this is about 100 line-widths and thus represents a reasonably wide scan of the spectrum. Since for any relative velocity the Doppler shift is constant, to scan a complete spectrum point by point there should be provision for setting up a large number of different relative velocities of source and sample, say, a hundred velocities ranging from $+1$ cm/sec through 0 to -1 cm/sec.

Two experimental arrangements for setting up variable velocities are shown in Fig. 10.57. In the simpler arrangement in Fig. 10.57(a), a ^{57}Co
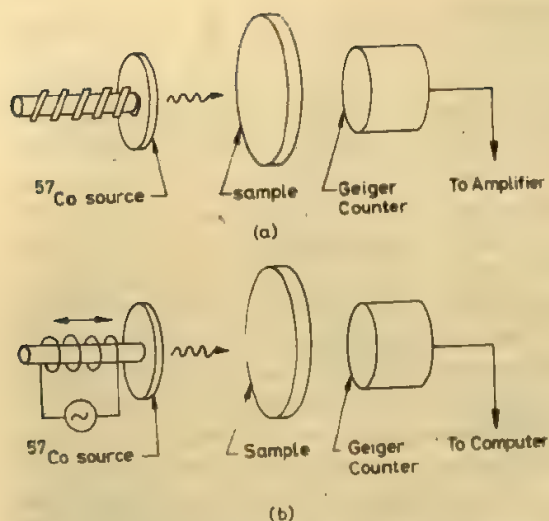
Fig. 10.57 Two arrangements of Mössbauer spectroscopy:
(a) shows source mounted on a screw thread drive and (b)
that on an oscillatory drive.

source mounted on a screw thread drive constitutes a Doppler shifting device. Rotation of the screw gives a steady velocity to the source. Different velocities can be set up by varying the screw speed. A Geiger counter placed behind the sample shows a sudden drop in the count rate, when at a certain velocity the sample starts to absorb γ-rays emitted by the source. A more convenient arrangement is the one shown in Fig. 10.57(b). Here the source piece of ^{57}Co is mounted on an oscillating drive, which is essentially a loudspeaker coil and an alternating current of a few cycles per second is applied to make it oscillate back and forth. This oscillatory motion gives the source a varying velocity relative to the sample, the velocity being zero at the turning points of the motion and maximum at the centre. The Geiger counter output is in this case fed to a multichannel computer which collects and sums the results from each point of the movement of the source. A period of several minutes to a few hours is usually sufficient to obtain a good spectrum. The final spectrum is displayed as a plot of counts/sec versus cm/sec, a fall in counts/sec signifying absorption of γ-ray by the sample.

The apparatus for Mössbauer spectroscopy thus essentially consists of a Doppler shifting device, a Geiger counter, and a small computer. The source and sample should ideally be maintained at the temperature of liquid helium. The source should be fairly stable, with a half-life of at least several weeks, so that frequent replacement does not become necessary and the intensity of γ-ray emission stays essentially constant during the experiment of several hours. To obtain a good spectrum, the

velocity of the source must be very precisely controlled, since an error of even 0.01 cm/sec in the velocity shifts the frequency by more than one line-width and may thus render the absorption undetectable.

10.13.2 Applications of Mössbauer Spectroscopy

Chemical Shift. When the absorber nucleus is in chemical surroundings different from those of the source nucleus, it does not absorb at the same frequency; this effect is referred to as the *chemical shift* (or the *isomer shift*) and is usually reported in cm/sec. The Mössbauer spectrum of the ferrocyanide ion, $[Fe(CN)_6]^{-4}$, in Fig. 10.58 (a), which shows a sharp absorption peak at a re-
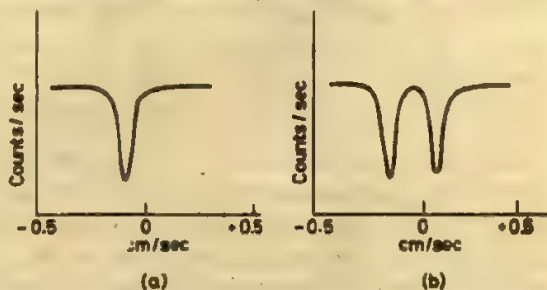
Fig. 10.58 The Mössbauer spectra of (a) the $[Fe(CN)_6]^{-4}$ ion and (b) the $[Fe(CN)_5NO]^{-2}$ ion. The spectrum in (b) shows quadrupole splitting.

lative velocity of about -0.05 cm/sec, illustrates such a shift. The magnitude of chemical shifts is influenced by the electron density at the concerned nucleus. We have seen in Chapter 5 that p, d, etc, orbitals have zero electron density at their nuclei; consequently it is the s electron density which is important. From measurement of chemical shifts one may thus obtain relative s electron density and from it an estimate of the bond character of atoms chemically attached to the Mössbauer nucleus. For example, the Mössbauer nucleus ^{119}Sn exhibits chemical shifts of 0, 0.21 and 0.37 cm/sec, respectively, in compounds containing tin in Sn^{+4}, 4— covalent (tetrahedral) and Sn^{+2} valence states; the values are seen to match almost linearly with the number of s electrons in the respective electron configurations (for outer shell): s^0p^0, sp^3 and s^2p^0. Mössbauer spectroscopy thus affords a relatively simple means of ascertaining the valence state of an unknown tin compound.

Nuclear size is another important factor affecting the chemical shift. Theoretically it may be shown that the relationship is of the form:

$$\text{Chemical shift} = K(\varrho_e^2 - \varrho_g^2)(\frac{R_e - R_g}{R_g}) \qquad (10.102)$$

Where ϱ_e^2 and ϱ_g^2 represent s electron density at the excited and ground state nuclei; R_e and R_g are the radii of the nucleus in excited and ground

states; K is a universal proportionality factor. R_e and R_g are usually different and the *sign* of the chemical shift depends on whether R_e is larger or smaller than R_g. For any given nucleus, obviously, $(R_e - R_g)$ $/R_g$ is constant and the chemical shifts can thus be used to determine relative densities of s electrons. Measurements of the excitational change of nuclear size from Mössbauer spectroscopy has great importance for theories of nuclear structure.

Quadrupole effects The majority of Mössbauer nuclei are found to have non-zero spins and also most of them have half-integral rather than integral spins. Further, according to a selection rule, the spin of the excited state must be different from that in the ground state. It thus follows that either or both of the nuclear states will have a spin greater than $\frac{1}{2}$; in other words, one or both will have electric quadrupole moment (see Section 10.11.6) and this will interact with electric field gradients at the nucleus produced by its surroundings.

For a number of Mössbauer nuclei, the spin (I) is $\frac{1}{2}$ in the ground state and 3/2 in the excited state; both ^{57}Fe and ^{119}Sn are in this category. With $I = 3/2$, there are $2I + 1$ or 4 possible orientations for the excited nucleus in an electric field, as shown in Fig. 10.59(a); the orientations are specified by the quantum number m_I being 3/2, $\frac{1}{2}$, $-\frac{1}{2}$ and $-3/2$ (cf Section 10.11.1). Since the angle which the nucleus makes with the field
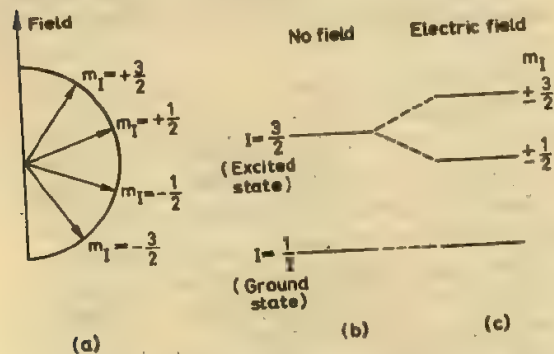
Fig. 10.59 (a) The four spin orientations allowed to a nucleus with $I = 3/2$ in an electric field. (b) The ground and excited state energy levels of the nucleus in the absence of an electric field. (c) The corresponding energy levels in the presence of a field.

gardient is the same in the $m_I = +\frac{1}{2}$ and $m_I = -\frac{1}{2}$ states, these two states have the same energy in the electric field. Similarly, the two states $m_I = \pm 3/2$ have the same energy, though different from that of the $m_I = \pm \frac{1}{2}$ states. Interaction with the electric field gradient thus results in splitting of the excited nuclear energy into *two* levels. If the quadrupole moment is positive (cigar-shaped nucleus), the $\pm$ 3/2 states are raised in

energy and the $+\frac{1}{2}$ states are lowered [Fig. 10.59(b)], while a reverse situation exists where the quadrupole moment is negative (tangerine-shaped nucleus). The Mössbauer spectrum of the nitroprusside ion, $[Fe(CN)_5NO]^{-2}$, is now easily examined. While the $[Fe(CN)_6]^{-4}$ is sufficiently symmetrical to have no net field gradient at the iron nucleus, replacement of one CN group by NO in $[Fe(CN)_5NO]^{-2}$ produces a sufficient field to cause observable quadrupole splitting [Fig. 10.58(b)]. It should be noted that the electric field causing the splitting here is internal, being inherent in the structure of the ion. Useful data on crystal fields can thus be obtained in many cases from such spectra with multiplet structure. Arguments as above can further be extended to the cases where both ground and excited state nuclei have a quadrupole moment.

Magnetic field effects Since, as we have noted above, most of the Mössbauer nuclei have non-zero spin, both in the ground and excited states, we shall expect them to interact with a magnetic field in the manner already described in Section 10.11.1. Thus each energy state with nuclear spin I will be split into $2I+1$ energy levels, the spacing between them being $\Delta E = g\beta_n H$, where H is the magnetic field at the nucleus. Now, since the nuclear splitting factor g usually has different values in the ground and excited states, the extent of splitting in each state will be different. We should note, in addition, that the g-values may have opposite signs for the two states (for instance, in the case of ^{57}Fe, the ground state g is positive and the excited state g is negative). The splitting of the energy levels of ^{57}Fe in the ground state ($I=\frac{1}{2}$, g positive) and in the excited state ($I=3/2$, g negative) will, therefore, be as shown in Fig. 10.60(b). The transitions shown in the energy level diagram correspond-
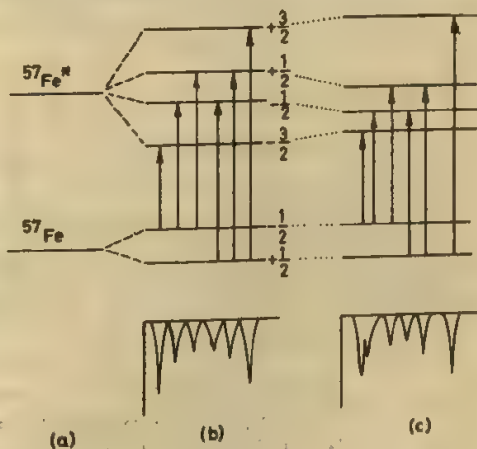
Fig. 10.60 (a) The ground and excited state energy levels of ^{57}Fe. (b) The splittings produced by magnetic field. (c) The splittings produced by simultaneous magnetic and electric fields. The overall spectra produced by transitions, indicated by arrows, are shown at the foot of (b) and (c).

ing to the selection rules $\Delta m_I = 0$ or ± 1 give rise to a six-line spectrum. The relative peak heights correspond to the relative transition probabilities which can be obtained by detailed calculations. It should be mentioned that the magnetic field to cause energy level splitting may be applied externally, but it may often be present internally due to the interaction of the nucleus with its surrounding electrons in sufficient magnitude to cause observable effect. In the latter case, it is quite possible to estimate the magnitude of the internal fields by 'calibrating' the spectrum using the external field.

When there exists an electric field within the sample in addition to internal or an externally applied magnetic field, the quadrupolar shifts due to the former are superimposed on the magnetic splitting described above. The effect can be easily described in qualitative terms. Thus in Fig. 10.59 we have seen that for a positive quadrupole moment the $\pm 3/2$ states are raised in energy while the $\pm\frac{1}{2}$ states are lowered. This effect when superimposed on the energy level pattern, shown in part (b) of Fig. 10.60, gives rise to the pattern shown in part (c). The selection rules and transition probabilities being unchanged, a six-line spectrum is again produced, but now the lines are not equally spaced. Iron difluoride, FeF_2, has been found to give a Mössbauer spectrum of this type.

10.14   Mass Spectrometry

Quite a different type of spectral process is represented by mass spectrometry. The mass spectrometer produces charged ions, most commonly by electron bombardment of the sample vapour, and sorts out these ions into a spectrum according to their mass/charge ratio. The ions consist of the molecular or *parent ion*, that is, the ion produced from the original molecule by loss of one electron, and ionic fragments of the original molecule. A *mass spectrum* is a record of these different kinds of ions, and the relative number of these ions are characteristic for the compound.

Analysis of the mass spectrum can produce a wealth of information concerning the ionization and fragmentation patterns of organic molecules, from which valuable information on the structure of these molecules can be derived.

Mass spectrometry is also used extensively for the determination of molecular weights, for ascertaining isotopic ratios of some elements present in different compounds, and as an essential adjunct to the use of stable isotopes in tracer work and reaction mechanism studies. It is also possible to determine the ionization potential of a molecule and the bond dissociation energies using mass spectrometry.

10.14.1 Instrumentation and Procedure

Several types of mass spectrometers are available. A simple, Dempster type mass spectrometer consists of four units: (a) inlet system; (b) ion source; (c) accelerating system; and (d) ion collector, amplifier and readout system.

A high vacuum is maintained throughout the spectrometer. Different inlet sample systems are used for handling different types of material-gases, liquids and solids. Several methods may be used for ionization of the sample, such as the electron bombardment of the sample vapour, thermal vaporization of the sample from a metallic surface, and irradiation of the sample vapour with high energy UV radiation. In mass spectrometers designed for application to organic compounds, the method most commonly employed for producing ions is electron bombardment of the sample vapour. Even relatively nonvolatile organic compounds can be vaporized at a reasonably low temperature in a high vacuum.

The sample vapour is introduced into the *ion source* (Fig. 10.61), an
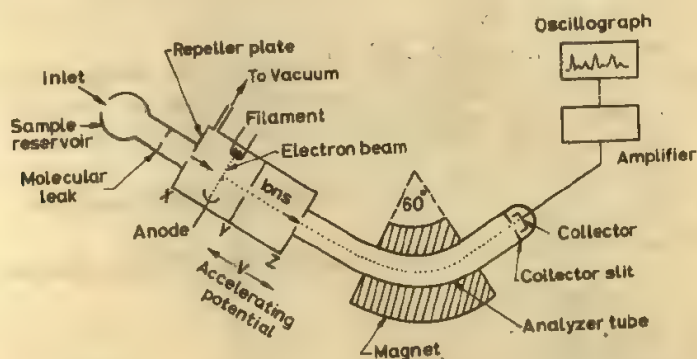
Fig. 10.61 Schematic diagram of a Nier 60° sector mass spectrometer.

ionization chamber, maintained at a pressure between 10^{-5} and 10^{-7} mmHg, where the vapour stream is bombarded by an electron beam with energy between 8 and 100 eV. A range from 8 to 15 eV is employed in molecular weight determinations as the range of energy corresponds to the ionization potential range for many organic molecules, and its use thus results in the formation of positive ions by molecules losing one electron. The mass of such an ion, called *parent ion*, corresponds to the molecular weight of the molecule.

When the energy of the electron beam is increased beyond 15 eV, the initially formed parent ions undergo decomposition producing fragment ions, which are characteristic of the molecular structure. An energy of about 70 eV has been found to produce good fragmentation of reproduci-

ble intensity, whereas energies above 70 eV lead to the formation of an increasing number of doubly charged ions due to the removal of two electrons from the molecule.

The positively charged ions formed in the ion source are drawn out by a small electrostatic field between the large repeller plate X (charged positively) and the first accelerating plate Y. After emerging through the slit in Y, the ions are subjected to a strong electrostatic field potential V of $400-4000$ volts between the first accelerator plate and the second accelerator plate Z. The ions thus accelerated enter the analyzer unit through the slit in Z.

In the magnetic analyzer the fast moving ions are reflected, by the application of a magnetic field, through an angle of 180° over a semicircular path or at 60-90° as in sector instruments (see Fig. 10.61).

The separation of ions occurs as follows. An ion of mass m and charge e, on passage through an accelerating electrostatic field of voltage V attains a velocity v. The kinetic energy $(1/2) mv^2$ of the ion equals its potential energy eV before acceleration. Thus,

$$(1/2)mv^2 = eV \qquad (10.103)$$
$$\text{or } v = (2eV/m)^{1/2} \qquad (10.104)$$

When the fast moving ion next enters the magnetic field H, it diverts the ion into a semicircular trajectory of radius r producing a centripetal force Hev, which is balanced by a centrifugal force mv^2/r. Therefore,

$$mv^2/r = H He \qquad (10.105)$$

The radius of curvature r of the trajectory is given by

$$mv^2/r = Hev \qquad (10.106)$$

Substituting for v from Eq. (10.104), Eq. (10.106) becomes

$$r = (2V/H^2)^{1/2} (m/e)^{1/2} \qquad (10.107)$$

Rearranging,

$$m/e = H^2 r^2 / 2V \qquad (10.108)$$

Only those ions whose trajectory in the magnetic field, as described by Eq. (10.107), coincides with the arc of the analyzer tube, will be brought to a focus on the collector slit. Other ions will strike the analyzer tube (which is grounded) at some point, be neutralized and pumped out of the system along with other neutral species. Thus the ion species which will be collected under a given magnetic field H and accelerating potential V are those having mass/charge ratio (m/e) satisfying Eq. (10.108). Ions are thus sorted according to their m/e ratio, not their mass alone. For example, two ions m^+ and $(2m)^{+2}$ will describe the same path and be collected together.

To obtain a mass spectrum, either the accelerating voltage V or the magnetic field strength H is varied continuously at a constant rate, resulting in ions of differing m/e attaining one after another the fixed trajectory of radius of curvature r. Usually the magnetic field is held

constant and the accelerating potential is varied. This produces a *voltage scan* of the spectrum. On the other hand, *a magnetic scan* of the spectrum is produced when the magnetic field is varied, while maintaining a constant accelerating potential. A voltage scan allows a spectrum to be obtained in a very short period (less than 2 seconds); a magnetic scan would not, however, be so rapid due to the inductance of the magnet.

The current carried by the ion beam reaching the collector slit is small (10^{-8} to 10^{-10} amp) and must be amplified before recording. The electrical signal is amplified by an electron multiplier or vibrating multiplier and fed to a recording device, preferably an oscillograph. In an oscillograph, a series of mirror galvanometers of different sensitivities are deflected by the amplified current and the mirrors reflect an ultraviolet radiation beam onto a moving strip of photographic paper to produce a mass spectrum. The response time of such a system is extremely rapid, as compared to conventional pen and paper recorders.

The mass spectral data are commonly presented in the form of bar graphs (see Fig. 10.62) in which the relative abundance (intensity) of ions
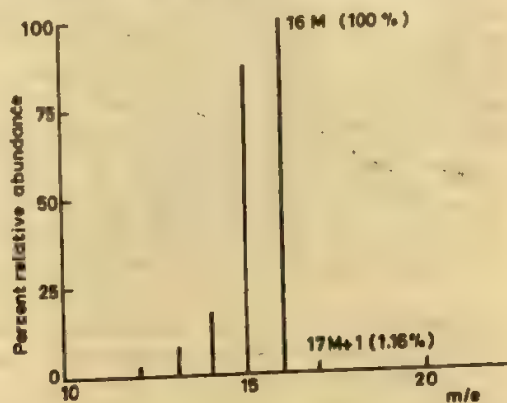
Fig. 10.62 Mass spectrum of methane.

is plotted against their m/e ratio. The relative abundance of any ion is given as the percentage of the corresponding peak relative to the most intense peak (most abundant ion). Thus the most intense peak (the so-called *base peak*) is assigned a value 100 and other peaks are reported as percentages of the base peak.

The resolving power of a mass spectrometer is affected by many factors, including (a) radius of the ion trajectory, (b) the width of the accelerator and collector slits, and (c) the uniformity of kinetic energy of ions of same m/e ratio, as they enter the magnetic analyser unit. The factor (c) is a limiting factor in single-focussing type spectrometers described above, with which a resolving power in the order of 1 part in 7500 is the best that can be achieved. In a double-focussing spectrometer, a radial electrostatic field placed between the ion source and the magnetic field causes 'velocity focussing' so that ions of the same kinetic

energy only will pass through the subsequent magnetic field. This results in a very high resolution of the spectrum, and resolving power better than 1 in 60,000 can be reached.

10.14.2 Interpretation and Applications

Fragmentation processes When a molecule A is bombarded by electrons of medium energy (8 to 15 electron volts), the most important and common process that occurs initially is the formation of the molecular ion by the ionization of the molecule, through the loss of one electron:

$$A + e^- \longrightarrow A^+ + 2e^- \qquad (10.109)$$
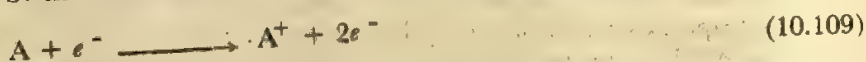
The molecular ion A^+ is formed when the energy of the bombarding electrons is equal to the ionization energy of the molecule. It is therefore possible to determine the ionization potential of the molecule from mass spectrometry.

The intensity of the molecular ion peak goes on increasing as the energy of the bombarding electron beam is increased, till the excess energy is high enough to break the bond in the molecular ion, resulting in fragments. The accelerating potential of the bombarding electrons which initiate this fragmentation is referred to as the *appearance potential* of the fragment ion. It is thus possible to determine the bond dissociation energies from a knowledge of the appearance potentials of fragement ions. When the energy of the bombarding electrons is increased further, more than one bond in the molecular ion may be cleaved, and the process may finally lead to a complete fragmentation of the molecule.

Example 10.5 It is found that the appearance potential of CH_3^+ from CH_4 is 14.4 eV and that from $^\circ CH_3$ radicals is 9.8 eV. Calculate the bond dissociation energy of one of the CH_4 bonds.

Solution

$$CH_4 \xrightarrow{14.4 eV} CH_3^+ + H^\circ + e^-$$

$$^\circ CH_3 \xrightarrow{9.8 eV} CH_3^+ + e^-$$

Therefore

$$CH_4 \xrightarrow{(4.6\ V)} H^\circ + CH_3$$
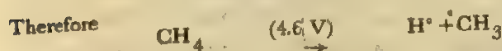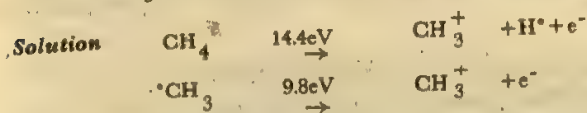
Bond energy $= (4.6 eV) (3.83 \times 10^{-20}\ cal/eV) (6.02 \times 10^{23}\ mole^{-1})$
$= 106\ kcal/mole$

Identification and analysis of mixtures The fragmentation process of the molecular ion is not random, because the excess energy is best relieved via breakdown pathways which lead to well-stabilised fragments, the analogy being closest to the high-energy processes such as pyrolysis. And since sufficient molecules are present for the probability law to hold in the dissociation process, the resulting fragments will always occur in the same relative abundance for the particular compound. Because of the

uniqueness of the molecular fragmentation, as no two molecules are fragmented and ionized in exactly the same manner on electron bombardment, the mass spectrum becomes a sort of 'fingerprint' for each compound. Sufficient differences in these molecular fingerprints permit identification of different compounds even in complex mixtures.

A remarkable feature of mass spectrometric analysis is that mixtures with a large number of components can be handled without preliminary fractionation. Hydrocarbon mixtures containing up to as many as 30 components can be analyzed and quantities as low as 0.001 mole per cent can be detected. Calculations are usually performed on high-speed computers. Moreover, if spectra are recorded separately for each compound in a fairly pure state, the spectral data for mixtures then permit calculation of their mole per cent compositions.

Determination of moleculer formulae In determination of a molecular formula the most important single item of information is the molecular weight. With the molecular weight known, an elemental analysis will then permit the assignment of the molecular formula. A mass spectrometer may be used to measure the molecular weight of most organic compounds to the nearest whole number. Even a moderately accurate elemental analysis of a compound will then permit the assignment of its molecular formula. With modern high resolution mass spectrometers, however, a molecular weight can be determined with high accuracy. This in many cases will restrict the number of possible molecular formulae to two or three alternatives and the appropriate formula may then be selected using the tabulations of Beynon and Williams (1963), the computational method of Lederberg (1964), or computer analysis.

Example 10. 6 What resolving power is needed to differentiate between the molecular ions of compunds A and B of formulae $C_{11}H_{20}N_6O_4$ and $C_{12}H_{20}N_4O_5$, both having the same integral mass 300?

Solution
The atomic weights of ^1H, ^{14}N, and ^{16}O when related to $^{12}C = 12.000$ are:

$$^1H = 1.0078$$
$$^{14}N = 14.0031$$
$$^{16}O = 15.9949$$

Molecules A and B, though having the same integral mass 300, have different non-integral masses:

A $C_{11}H_{20}N_4O_6$	—	300.1542
B $C_{12}H_{20}N_4O_5$	=	300.1429
Difference	=	0.0113

Resolving power of spectrometer = 0.0113/300 or 1 part in 27000

Molecular ion The mass spectrum of a compound, as we have already seen, consists of the mass-to-charge ratios of the ion fragments and the relative abundance of these ions plus the molecular (parent) ion. Since the molecular ion is formed by the loss of one electron from the molecule

[Eq. (10.109)], the m/e ratio of the molecular ion peak gives the molecular weight M of the compound to the nearest whole number. However, using a high-resolution mass spectrometer, the m/e ratio of the molecular ion, and hence molecular weight of the compound, could be measured with an accuracy of the order of one part in a million by comparison with an ion of exactly known m/e value. Though the peak with the highest m/e ratio in the mass spectrum would normally be expected to be the molecular ion peak, this however is found to be so only for 80-90 per cent of organic compounds. For the remainder, either the molecular ion peak is too weak for a definite identification or the presence of a higher molecular weight impurity complicates the spectral analysis.

The intensity of molecular ion peak is related to the stability of the molecular ion which, in turn, is related to molecular structure. For example, a conjugated π-electron system tends to stabilize a molecular ion and so also a cyclic structure. Such compounds usually give rise to relatively strong molecular ion peak. On the other hand, compounds whose structural features make the molecular ion unstable relative to its fragmentation products, give rise to weaker molecular ion peaks. An approximate order for decreasing intensity of molecular ion peaks of compounds is given below:

Aromatic compounds $>$ cycloalkanes, conjugated alkenes $>$ aldehydes, ketones, alkenes, carboxylic acids, amides, ethers, amines, n-alkanes $>$ branched alkanes, halides, nitriles, alcohols.

The validity of an apparent molecular-ion peak may therefore be tested by considering the peak intensity. Thus an apparent molecular-ion peak of relatively low intensity, produced from a compound known to be aromatic, is a suspect, and so also one of relatively high intensity, produced from a compound known to be an alcohol. The former may actually be due to an impurity and the latter due to an ion fragment derived by the loss of water molecule.

An apparent molecular-ion peak should also be tested by applying the rule which holds for all organic compounds composed of the common elements, carbon, hydrogen, oxygen, nitrogen, phosphorus, sulphur, selenium, and the halogens, that true molecular-ion peaks are always of *even* m/e ratio, unless the molecule contains an *odd* number of nitrogen atoms, in which case the molecular ion will have an *odd* m/e value. Consequently, no peak of odd m/e ratio can be molecular-ion peak of a nitrogen-free organic compound, but must be due to a fragment ion, an ion resulting from ion-molecule collision, or a nitrogenous impurity.

Natural isotope abundance While an accurate determination of molecular weight restricts the number of possible molecular formulae to a few, a further restriction on the number can be achieved by study on the natural abundance of stable isotopes for elements.

Table 10.15 gives the natural abundances of the principal stable isotopes of the main elements in most organic molecules. Inspection of the table shows that, apart from bromine, the natural isotope of major

Table 10.15 Natural Abundance of Principal Stable Isotopes

Element	Mass	%	Mass	%	Mass	%
H	1	99.985	2	0.015		
C	12	98.892	13	1.108		
N	14	99.635	15	0.365		
O	16	99.759	17	0.037	18	0.204
F	19	100.00				
P	31	100.00				
S	32	95.03	33	0.75	34	4.22
Cl	35	75.77			37	24.23
Br	79	50.537			81	49.463
I	127	100.00				

abundance has the lowest mass number. The molecular (parent) ion (and associated mass M) is considered to be that derived from a molecule composed solely of the most abundant isotopes of the elements present. However, since the mass spectrometer will also record the presence of ions arising from less abundant molecules containing heavy isotopes of one or more of the constituent atoms, peaks at masses 1 and 2 or more units larger than the parent ion will also appear, thus giving a cluster of peaks (sometimes called the *molecular ion cluster*) with m/e of M, $M+1$, $M+2$, etc. (Fig. 10.62). In general, the relative abundance (intensity) of the parent ion peak (P_M) is considerably greater than the relative abundance of higher peaks (P_{M+1}, P_{M+2} etc.). However because of relatively large natural abundances of heavier isotopes of chlorine, bromine and sulphur, compounds containing these elements usually show prominent peaks for P_{M+2}, P_{M+4}, etc. besides P_M.

Example 10.7 Calculate the peak-intensity ratios for the molecular ion cluster of (a) methane and (b) acetyl acetone ($C_5H_8O_2$).

Solution (a) The molecular ion cluster (Fig. 10.62) consists of two peaks at $m/e = 16$ and 17 (M and $M+1$). The M peak is due to $(^{12}C^1H_4)^{\cdot+}$ and the $M+1$ peak is due mainly to $(^{13}C^1H_4)^{\cdot+}$. [The peak at $m/e = 18$, i.e. $M+2$ owing to $(^{12}C^1H_2\,^2H_2)^{\cdot+}$ is insignificant because of the very low natural abundance of ^2H(0.015 per cent) making it unlikely to occur in combina   with another ^2H.]

Assuming that the ionization potentials of $^{12}C^1H_4$ and $^{13}C^1H_4$ are similar, the expected ratio of peak intensities on the basis of the natural abundance of ^{13}C is

$$(P_{M+1}/P_M) 100 = (1.108/98.892) 100$$
$$= 1.12 \text{ (cf. Fig. 10.62)}$$

(b) The (M + 1) peak may be due to molecular ion species containing either ^{13}C, ^2H or ^{17}O. Based on the natural abundance of ^{13}C (Table 10.15):

$$(P_{M+1}/P_M) 100 \simeq \text{(Number of C's) } (1.108/98.892)100$$
$$\simeq 5 \times 1.12 = 5.60$$

Again on the basis of the natural abundance of ^2H:

$$(P_{M+1}/P_M)100 \simeq \text{(Number of H's) } (0.015/99.985)100$$
$$\simeq 8 \times 0.015 = 0.12$$

On the basis of the natural abundance of ^{17}O:

$$(P_{M+1}/P_M)100 \simeq \text{(Number of O's) } (0.037/99.759)100$$
$$\simeq 2 \times 0.037 = 0.074$$

The (M + 2) peak may arise due to contributions from (1) $(^{12}C_5 \, ^1H_8 \, ^{18}O \, ^{16}O)^{\cdot +}$, (2) $(^{13}C_2 \, ^{12}C_3 \, ^1H_8 \, ^{16}O_2)^{\cdot +}$, (3) $(^{13}C \, ^{12}C_4 \, ^2H^1H_7 \, ^{16}O_2)^{\cdot +}$, (4) $(^{13}C \, ^{12}C_4 \, ^1H_8 \, ^{17}O^{16}O)^{\cdot +}$, and (5) $(^{12}C \, ^2H_5 \, ^1H_7 \, ^{17}O^{16}O)^{\cdot +}$. Considering only (1), since it makes the largest contribution, the expected ratio is

$$(P_{M+2}/P_M) 100 \simeq \text{(Number of O's) } (0.204/99.759)100$$
$$\simeq 2 \times 0.204 \simeq 0.41$$

***Example* 10.8** What is the probable formula of the compound of mass $M = 196$ whose $M+1$ peak is 13.4% and $M+2$ peak 0.4% of the parent peak? The compound consists of only C, H and O.

Solution Let the compound be $C_xH_yO_z$. Since the $M+1$ peak arises mainly from the contribution of ^{13}C and the $M+2$ from that of ^{18}O;

$x(1.108/98.892)100 = 13.4$ or $x = 12$
and $z(0.204/99.759)100 = 0.4$ or $z = 2$
$y = 196 - 12 \times 12 - 2 \times 16 = 20$
The formula would be $C_{12}H_{20}O_2$

The above calculations of the peak intensity ratios are only approximate. However, Beynon and Williams (1963) have calculated the P_{M+1}/P_M and the P_{M+2}/P_M ratios for all possible combinations of C,H,O and N up to a molecular weight of 500. The use of such tabulations may help in the assignment of a molecular formula to a compound. However, the molecular ion cluster must be of sufficient intensity so that these ratios can be measured with reasonable accuracy to permit computation.

In the absence of these tabulations, approximate formulae can be used

to calculate the peak-intensity ratios. Thus, for a compound $C_wH_xN_yO_z$:

$$(P_{M+1}/P_M)100 = 1.12w + 0.015x + 0.366y + 0.037z \tag{10.110}$$

$$(P_{M+2}/P_M)100 \cong 0.204z + 0.006w(w-1) + 0.004\,wy + 0.0002\,wx. \tag{10.111}$$

The P_{M+2}/P_M ratio is usually small for compounds consisting of C, H, N and O. However, since ^{34}S has a relatively large natural abundance (4.22 per cent), its presence in a molecule contributes to an unusually large $(M+2)/M$ peak-intensity ratio making it readily detectable with a mass spectrometer.

Once the molecular formula has been decided, the number of double-bond equivalents (R) for the compound $C_wH_xN_yO_z$ can be calculated from the equation $\tag{10.112}$

$$R = \tfrac{1}{2}(2w - x + y + 2)$$

R represents the sum total of the number of rings and double bonds. For example, for benzaldehyde (C_7H_6O), the value of R is 5, accounting for 4 double bonds and 1 ring. A triple bond, as in acetylene or a nitrite, is counted as two double-bond equivalents.

Structural analysis When working from a mass spectrum for structural analysis, it is advisable to tabulate the m/e ratios and the relative abundances of all the prominent peaks, starting with the highest mass, and also to record the groups lost to give these peaks. Possible molecular structures can then be postulated, employing a file of common fragment ions encountered in mass spectra. The postulated structures are tested against all known data. Final confirmation usually requires a comparison of the mass spectrum with that of an authentic sample.

Study of isotopic exchange Another important application of mass spectrometry is in the study of exchange reactions involving non-radioactive stable isotopes. By determining the change in the mass spectrum of a compound on isotopic exchange one can ascertain, without laborious chemical degradation techniques, the position of the isotope in the molecule and also the extent to which exchange has taken place. These isotopes can also serve as tracers, when studied by mass spectrometry, to determine the ultimate fate of the compound in chemical or biological reactions.

Metastable peak Fragmentation of an ion of mass m_1 into a new ion of mass m_2 and a neutral molecule or a radical, $m_1^+ \rightarrow m_2^{+} +$ uncharged particle, normally gives peaks corresponding to the parent m_1^+ and the daughter m_2^+ ions in the mass spectrum. However, if m_1 is accelerated completely before decomposition, the peak is recorded only at m_1, while if it decomposes to give m_2^+ in the ion source before entering the accelerating region, then only m_2^+ peak will be recorded.

There may also be an intermediate situation where m_1^+ decomposes to give m_2^+ - while being accelerated. The resulting peak is recorded at neither m_1^+ nor m_2 but as a rather broad, poorly focussed peak, called a *metastable peak*, at a position m^*, given by the equation

$$m^* = (m_2)^2 \, m_1$$

The metastable peak at m^* is smaller than both peaks at m_1 and m_2. The study of metastable ions is helpful in determining the mode of fragmentation of a molecule.

10.15   *Electron Diffraction by Gases and Vapours*

This method depends on the wave-like nature of electrons. L. de Broglie's suggestion that matter has wave properties was first verified by Davisson and Germer in 1927 for electrons (see Section 4.2). The wavelength associated with electrons was found to agree with the de Broglie relationship $\lambda = h/mv$, where m and v are the mass and velocity of the electron respectively. The velocity v of an electron depends on the potential drop through which it passes. An electron of charge e moving through a potential drop V will have energy of motion Ve; equating this to the kinetic energy, $\frac{1}{2}mv^2$, we get.

$$v = \sqrt{2Ve/m}$$

From the de Broglie relationship we then have

$$\lambda = h/\sqrt{2meV}$$

The value of $h/\sqrt{me}$, calculated from known values, is found to be nearly 10^{-8} in cgs units, so that $\lambda = 10^{-8} \ \sqrt{2V}$ cm.

Here the potential V is in esu (1 esu of potential $= 300V$). We can express the potential in volts, for which the above equation takes the form

$$\lambda = \sqrt{\frac{150}{V}} \times 10^{-8} \text{ cm} \tag{10.113}$$

Thus the wavelength associated with an electron is inversely proportional to the square root of the accelerating potential. A beam of electrons accelerated through a potential drop of 10,000 V will have, according to Eq. (10.113), a wavelength of 0.12 A, which is of the same order of magnitude as the interatomic distances in metals. Thus, if such a beam is sent through a thin metallic foil, the electrons are scattered by the atoms of the metal, giving rise to diffraction which can be observed as a set of concentric rings on a photographic plate. Each ring in the diffraction pattern corresponds to an angle of diffraction which again depends on the wavelength of the electrons and the interatomic spacing.

Diffraction also occurs when an electron beam is passed through gases or vapours, even though the molecules have random orientations with respect to the incident beam. Here also the diffraction photograph shows a set of concentric rings, but they are much more diffuse than the rings in the diffraction pattern of a metal foil. Since the molecules in a gas or

vapour are sufficiently far apart for them not to interfere with each other, the corresponding diffraction pattern is characteristic of the structure of individual molecules.

Any stable substance that has a vapour pressure of at least a few millimetres of mercury at a moderate temperature can be studied by the electron diffraction method. In a typical experiment, a beam of electrons
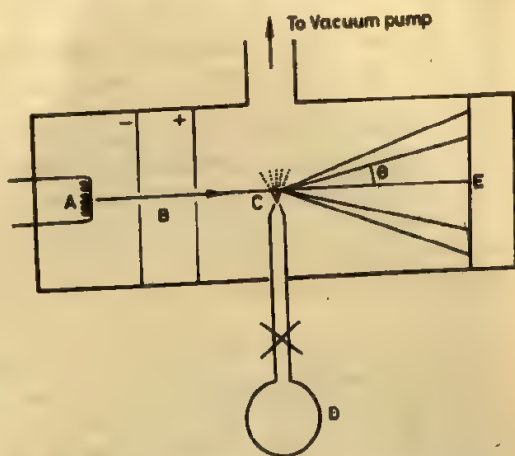
Fig. 10.63 Schematic diagram of electron-diffraction apparatus. (A) filament; (B) accelerating voltage and slits; (C) nozzle for forming a jet of gas; (D) gas sample; (E) photographic plate.

collimated by a magnetic system and then passed through a stream of the sample gas before falling on a photographic plate for a few seconds. The gas is introduced into the system through a nozzle by momentarily opening a stopcock. The whole scattering chamber is kept highly evacuated (pressure in the region of 10^{-5} mmHg), otherwise the residual molecules would produce undesired scattering, leading to a blurred diffraction pattern. The photographic plate after development shows a dark central region due to undiffracted beam, surrounded by diffuse, concentric circles of alternating intensity. The blackness of any area in the plate is related to the number of electrons that struck that area. By an appropriate method, the degree of blackness can be measured along a line from the centre of the pattern to the periphery (that is, at various values of the angle θ between incident and scattered beam) and converted to relative intensity of the scattered electrons (defined below). From the diffraction pattern we can thus construct an experimental scattering-curve, representing the relative intensity of scattered electrons as a function of the scattering angle θ (Fig. 10.64).

The collisions between a beam of accelerated electrons and a stream of gas molecules are either elastic or inelastic. Inelastic collisions give rise to *incoherent atomic scattering*, while elastic collisions produce coherent scattering, which again is made up of two components, known as *coherent atomic scattering* and *coherent molecular scattering*. All these three types of scattering occur in the electron diffraction by gases, and so the total diffraction

pattern, from which the total or experimental scattering curve [Fig. 10.64(d)] is constructed, consists of three types of scattering, whose contributions to the experimental scattering curve are as shown in parts (a), (b) and (c) of Fig. 10.64.
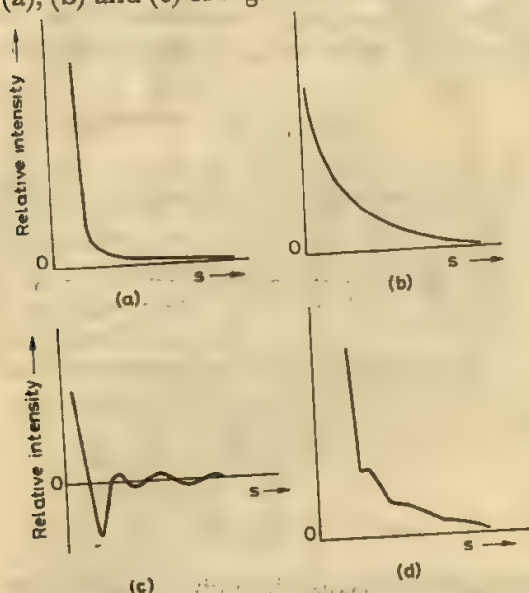
Fig. 10.64 (a) Incoherent atomic scattering; (b) Coherent atomic scattering; (c) Coherent molecular scattering. (d) Total resultant scattering. [Since the de Broglie wavelength is a constant for a fixed value of the accelerating potential difference, the parameter s, which is defined by Eq. (10.115), is a constant times $\sin\frac{\theta}{2}$.]

Incoherent atomic scattering occurs due to the fact that an electron may excite an atom to any of a number of higher energy levels and thus lose a corresponding amount of energy. The electrons that suffer incoherent scattering will therefore have a whole range of wavelengths. The incoherent scattering is thus monotonic, falling off rapidly with the scattering angle θ (Fig. 10.64), and shows no maxima or minima. A monotonic variation of intensity also occurs due to coherent atomic scattering, so that the resultant effect of these two types of scattering is to produce a steeply falling, monotonic background in the total diffraction pattern. It is the molecular coherent scattering, which depends on the structure of the molecule, that gives rise to the concentric rings of the total diffraction pattern and hence to the maxima and minima of the experimental scattering curve.

The theory for the scattering of electrons by gas molecules was developed by Wierl. He considered the scattering of electrons by a molecule, fixed in space, and then averaged the result over all possible

orientations of the molecule. The following equation is a simplified form of the Wierl equation representing the relative intensity of the molecular coherent scattering alone:

$$\frac{I_m(\theta)}{I_0} = K\left[\sum_{\substack{i=1 \\ (i \neq j)}}^{N} \sum_{j=1}^{N} Z_i \, Z_j \, \frac{\sin(s\,r_{ij})}{s\,r_{ij}}\right] \tag{10.114}$$

where $s = 4\dfrac{\pi}{\lambda}\sin\dfrac{\theta}{2}$ $\tag{10.115}$

In Eq. (10.114), the ratio of the molecular scattering intensity to the incident beam intensity, $I_m(\theta)$ is equal to the fraction of incident

electrons scattered at an angle θ; K is a constant which depends on the geometry of the apparatus; Z_i and Z_j are the atomic numbers of the ith and jth atoms (which may or may not be joined by a chemical bond) a distance r_{ij} apart in a molecule of N atoms. The sums are taken over all pairs of atoms in the molecule. The wavelength of the electrons is λ (which is constant for a fixed value of the accelerating potential) and θ is the scattering angle (Fig. 10.63).

The desired structural information for a molecule cannot be obtained directly from the experimental scattering curve and indirect methods must be used. In the simplest of these, known as the *correlation method*, the first step is to assume a model for the sample molecule and to select trial values for the various distances (r) between all the atoms. Using these values a calculated scattering curve is then obtained from Eq. (10.114) and compared with the experimental scattering curve. The two curves will usually be different at first, but the values of r_{ij} can be varied systematically and the process repeated. The set of values for the interatomic distances that is found to give the best fit of the calculated curve with the experimental curve is considered to be the correct one. The method is evidently laborious and subject to error, especially where more than a few independent distances are to be determined. If, however, the molecule possesses symmetry elements so that some of the distances become necessarily equal to one another, the problem becomes simpler and the results more reliable. As an example, we may consider carbon tetrachloride CCl_4. If we assume that CCl_4 belongs to the point symmertry group of a regular tetrahedron (see Section 10.2), then the molecule has four equal C–Cl distances, six equal Cl Cl distances, and further, C–Cl distances are equal to $\sqrt{8/3}$ times the C-Cl distance. There is thus only one independent distance to be determined. Assuming this independent parameter to be r_{C-Cl} and since $Z_C = 6$ and $Z_{Cl} = 17$, Eq. (10.114) becomes

$$\frac{I_m(\theta)}{I_0} = K\left[4 \times 6 \times 17\,\frac{\sin(s\,r_{C-Cl})}{s\,r_{C-Cl}} + 6 \times 17 \times 17\,\frac{\sin(\sqrt{8/3}\,s\,r_{C-Cl})}{\sqrt{8/3}\,s\,r_{C-Cl}}\right] \tag{10.116}$$

A series of values of sr_{CCl} are assumed and the corresponding values of $I_m(\theta)/I_0$ are calculated from Eq. (10.116). The plot of $I_m(\theta)/I_0$ against sr_{C-Cl} gives a curve having maxima and minima at various values of sr_{C-Cl}. This calculated curve is then compared with the experimental curve [Fig. 10.64 (d)], constructed from the electron diffraction photograph of the sample, and the corresponding maxima and minima of the two curves are identified. At maximum or minimum we thus have a value of sr_{C-Cl} (from the calculated curve) and a value of s (from the experimental curve), so that division of sr_{C-Cl} by s gives a value of r_{C-Cl}. A set of r_{C-Cl} values can be obtained in this way from the positions of maxima and minima. If the assumption of regular tetrahedral symmetry, for the molecule is correct, this set of values will be found to cluster around a mean value, which is then the desired interatomic distance.

The above method is useful for small symmetric molecules requiring only a limited number of molecular parameters, but the method becomes more difficult and prone to error as the number of parameters increases. Two sources of error are worth mentioning. In the first place, because of low atomic number, the scattering due to light atoms, particularly hydrogen, is small; consequently, bond lengths involving hydrogen atoms are difficult or impossible to determine by electron diffraction. Secondly, a fairly good agreement with the experimental curve does not ensure that the assumed structure is correct, because a somewhat better agreement may possibly be obtained using a quite different structure. This difficulty, however, does not arise when the symmetry of the molecule can be assumed with certainty and the correlation method could then be used to derive values for a limited number of molecular parameters.

By the *radial distribution method*, first introduced by Pauling and Brockway in 1935, interatomic distances can be obtained directly from experimental diffraction data without having to assume a trial structure. The molecule is considered to be continuous in space having regions of varying scattering power. From the diffraction data it is possible to derive a function, known as the radial distribution function, which gives the probability of finding two atoms at a distance r apart. Maxima in this function should occur at values of r that correspond to interatomic distances in the molecule. Difficulties arise in applying the method to bigger molecules where there may be pairs of atoms at approximately the same distance apart resulting in overlapping radial distribution peaks; and, moreover, spurious peaks may also occur. These difficulties notwithstanding, the radial distribution method was widely used in the early work on electron diffraction to obtain a trial structure which could then be refined by the correlation method.

As mentioned previously, atomic scattering gives rise to background blackening of the diffraction pattern. One of the most important

advances in the electron diffraction work in recent years is the use of a specially designed, rapidly rotating sector placed in front of the photographic plate. By a careful choice of the shape of the sector most of the steeply falling background blackening particularly near the centre of the pattern, can be eliminated. This permits the desired diffraction pattern to be obtained in a more quantitative manner, and the positions of the true maxima (due to molecular scattering) in the experimental scattering curve to be located very accurately (with a densitometer) up to much higher values of s than was previously possible. With the improvement in technique and interpretation, the results obtained from electron diffraction study of small molecules can now be compared with those obtained from spectroscopic sources; and, moreover, for molecules which are too big to be studied by spectroscopic methods at present, the electron diffraction technique can provide reasonably accurate data.

10.16 Electric Dipole Moments

In terms of the wave-mechanical picture, as we saw in Chapter 6, a molecule may be looked upon as an assembly of positively charged nuclei surrounded by a negatively charged 'cloud', which is made up of contributions from electrons in various orbitals. The nuclei and the electron cloud are, to some extent, mobile and so when the molecule, whether it is polar or nonpolar, is subjected to a constant electric field, the electron cloud will be attracted by the positive plate and the nuclei will be attracted by the negative plate with the result that there will occur a small displacement of the 'centre of gravity' of negative charge relative to that of positive charge (Fig. 10.65). This separation of the
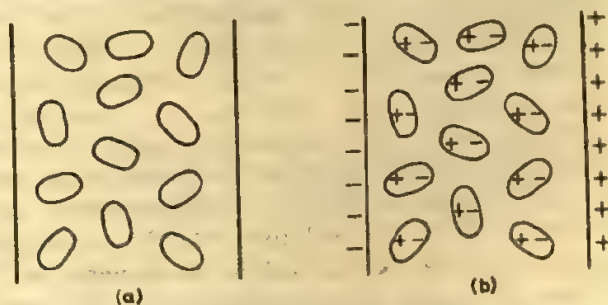
Fig. 10.65 The effect of an applied electric field on molecules having no permanent dipole moment: (a) field off; (b) field on.

centres of positive and negative charges in the molecule in the presence of an electric field is described by the statement that the field has induced an *electric dipole* in the molecule; and the molecule is said to have suffered a *distortion polarization*. The electric dipole moment of two equal but

opposite charges, $+q$, and $-q$, at a distance r apart is defined as qr. Since q is of the order of one electron and the charge on an electron is 4.80×10^{-10} e.s.u., and since r is of the order of 1 Å or 10^{-8} cm, dipole moments are of the order of 10^{-18} e.s.u. cm. A new unit, the debye, D, is therefore defined such that 1 debye or $1 D = 1 \times 10^{18}$ e.s.u. cm. It should be noted that the electric dipole moment is a vector quantity and its direction is conventionally taken to be the direction from the positive charge to the negative charge.

The average dipole moment, m_i, induced in a molecule is directly proportional to the *local intensity* F of the electric field acting on the molecule; thus, $m_i = \alpha_d F$

$$(10.117)$$

The constant of proportionality α_d is a molecular property and is called the distortion polarizability; it is the induced dipole moment per unit field strength and is a measure of the ease with which the molecule can be polarized, that is, the ease with which positive and negative charges can be displaced with respect to each other in an electric field. Since the dipole moment has the dimensions of charge times length and the electric field strength has the dimensions of charge divided by length square, it is evident that polarizability has the dimensions of a volume. It has the same order of magnitude as the volume of a molecule, i.e. 10^{-24} cm^3. The distortion polarizability may vary in different directions if the molecule is not symmetrical; α_d in that case represents a mean value. The induced dipole moment is independent of temperature; this is because whenever the position of a molecule changes due to collision, a new dipole is again induced in it in the direction of the field (Fig. 10.65).

There are, however, a vast majority of molecules in which the centres of positive and negative charge do not coincide, even in the absence of an applied electric field. These molecules therefore have a permanent dipole moment. For these polar molecules an applied electric field produces, in addition to distortion polarization, another effect known as *orientation polarization*, since the field tends to align the permanent dipoles along its own direction. This alignment is, however, disturbed by thermal collisions which tend to produce random orientation of the permanent dipoles. It follows then that the orientation polarization, which depends on the average component of the permanent dipole moment (μ) in the direction of the applied field, should be temperature dependent and should decrease with an increase in temperature. The average component of the permanent dipole moment, i.e. the average value of $\mu \cos \theta$, θ being the angle at which μ is oriented with respect to the field direction, represents the contribution (m_o) of the orientation polarization effect to the total average dipole moment of the molecule. It was shown by Debye that $\bar{m}_o = F\mu^2 / 3kT$.

Comparing with Eq. (10.117), we define the orientation polarizability, α_0, as $\alpha_0 = \mu^2 / 3kT$.

Hence for polar molecules the total polarizability, α_t, is given by

$$\alpha_t = \alpha_d + \alpha_o = \alpha_d + \mu^2/3kT$$

and the total average dipole moment per molecule in the electric field is then (10.118)

$$m_t = \alpha_t F = F\left(\alpha_d + \frac{\mu^2}{3kT}\right)$$

As before, F is the intensity of the electric field actually acting on the molecule. For nonpolar molecules, $\mu = 0$ and thus distortion polarizability is the only kind of polarizability.

Suppose the strength of a uniform electric field in the evacuated space between two charged plates is E_o. Let us now imagine that many molecules of a substance are introduced into the evacuated space. This substance, assumed to be an insulator, is called the dielectric; it may be a gas, liquid or solid. Since the dipoles induced in the molecules of the dielectric act in opposition to the applied field (Fig. 10.65) and thus partially candel the charges on the plates, the field strength (E) in the dielectric is less than the value (E_o) in vacuum. It can be shown from the principles of electrostatics that (10.119)

$$E = E_0 - 4\pi I$$

in which I, the *dielectric polarization*, is the dipole moment per unit volume of the dielectric.

The ratio E_o/E is a property of the dielectric known as the dielectric constant, D. (It can be distinguished from the symbol D of the debye unit, since the latter always follows a number). Dividing both sides of Eq. (10.119) by E, replacing E_o/E by D and rearranging we obtain (10.120)

$$E = 4\pi I/(D-1)$$

The electric field F actually acting on a molecule within the dielectric substance, as required by Eq. (10.118), is a little greater than E, because of the effect of the surrounding molecules. It can be shown that $F = E + 4/3\pi I$. Substitution of E from Eq. (10.120) then gives (10.121)

$$F = \frac{4\pi I}{3}\left(\frac{(D+2)}{(D-1)}\right)$$

The polarization I, which is the dipole moment per unit volume, will be given by the total average dipole moment per molecule, $\overline{m}_t$, multiplied by the number, n, of molecules per unit volume of the dielectric. Thus, from Eqs. (10.118) and (10.121), we have

$$I = n\overline{m}_t = nF\left(\alpha_d + \frac{\mu^2}{3kT}\right) = \frac{4\pi nI}{3}\left(\frac{D+2}{D-1}\right)\left(\alpha_d + \frac{\mu^2}{3kT}\right)$$

Rearranging this equation

$$\frac{4}{3}\pi n\left(\alpha_d + \frac{\mu^2}{3kT}\right) = \frac{D-1}{D+2} \qquad (10.122)$$

Since n is given by $n = N_\varrho/M$ where N is the Avogadro number, and ϱ and M are, respectively, the density and molecular weight of the dielectric substance, Eq. (10.122) can be written as

$$\frac{D-1}{D+2}\frac{M}{\varrho} = \frac{4}{3}\pi N\left(\sigma_d + \frac{\mu^2}{3kT}\right)$$

(10.123)

The left-hand side of this equation is represented by the symbol P_m and is called the total molar polarization of the substance; thus

$$P_m = \frac{D-1}{D+2}\frac{M}{\varrho}$$

(10.124)

(10.125)

and $\quad P_m = P_d + P_o = \frac{4}{3}\pi N\left(\alpha_d + \frac{\mu^2}{3kT}\right)$

where $P_d = \frac{4}{3}\pi N\alpha_d$ and $P_o = \frac{4}{3}\pi N(\frac{\mu^2}{3kT})$

are the *molar distortion polarization* and the *molar orientation polarization*, respectively. Equation (10.125) is known as the *Debye equation.*

If the dielectric substance is composed of molecules which do not have a permanent dipole moment, the above equations reduce to

$$P_m = \frac{D-1}{D+2}\frac{M}{\varrho} = \frac{4}{3}\pi N\alpha_d$$

(10.126)

which is known as the *Clausius-Mosotti equation.*

10.16.1 Determination of Dipole Moments

The Debye equation (10.125) provides the necessary relationship for the determination of polarizability (α_d) and the permanent dipole moment*(μ) from the measurable quantities: dielectric constant (D) and density (ρ). The determination of dielectric constant involves the measurement of the capacitance of a condenser filled with the given substance and then that for a vacuum between the plates. It can be seen from Eq. (10.125) that the molar polarization is a linear function of the reciprocal of the absolute temperature. We can, therefore, measure D and ρ over a range of temperature and plot P_m, calculated from Eq. (10.124), against $1/T$. The slope of the straight line graph will be equal to $4\pi N\mu^2/9k$, from which μ can be calculated, while the intercept at $1/T = 0$ will give the molar distortion polarization P_d and hence α_d.

The Debye equation is based on the assumption that the molecules do not interact with each other. It is therefore not applicable to polar

*In the remainder of this Section we refer to permanent dipole moments simply as dipole moments for brevity.

liquids, since there is strong interaction between the dipoles of closely packed polar molecules. However, in dilute solutions in nonpolar solvents such as benzene and carbon tetrachloride, the polar molecules will be on the average relatively far apart and the Debye equation can then be applied. The application of the Debye equation becomes most reliable when the substance under investigation is in the form of gas or vapour. Not all substances, however, can be studied in the gas phase over a range of temperature wide enough to give good values of the dipole moment.

(i) Vapour-temperature method The method involves the determination of the dielectric constant and density of the vapour at a series of temperatures. The density is usually calculated from the gas laws. Possible error due to departure from ideal behaviour may be eliminated by measuring the dielectric constant over a range of pressures at each temperature and extrapolating P_m, calculated from Eq. (10.124), to zero pressure. The total polarization P_m is then plotted against $1/T$ and the slope of the straight line is measured. Denoting the slope by b, it is seen from Eq. (10.125) that $b = 4\pi N\mu^2/9k$. Hence $\mu = \sqrt{9bk/4\pi N}$.

Since $k = 1.38 \times 10^{-16}$ erg per degree, and $N = 6.02 \times 10^{23}$, it can be readily shown that $\mu = 0.0128 \sqrt{b} \times 10^{-18}$ e.s.u cm $= 0.0128 \sqrt{bD}$.

The intercept of the above plot on the P_m axis, moreover, gives the value of the distortion polarization P_d.

(ii) Dilute solution method When a polar solute is dissolved in a nonpolar solvent, the total molar polarization is the sum of the polarization contributions of the two components, namely, solvent and solute. If x_1 and x_2 are the mole fractions and P_1 and P_2 are the molar polarizations of the nonpolar solvent and polar solute, respectively, the total molar polarization $P_{1,2}$ of the solution, if dilute, is given by

$$P_{1,2} = x_1 P_1 + x_2 P_2 \tag{10.127}$$

At each temperature, the molar polarization of the solvent is calculated from Eq.(10.124), using the measured values of the dielectric constant and density of the solvent. The molar polarization $P_{1,2}$ of the solution, at each temperature is given by

$$P_{1,2} = \frac{D_{1,2} - 1}{D_{1,2} + 2} \frac{x_1 M_1 + x_2 m_2}{\ell_{1,2}} \tag{10.128}$$

in which $D_{1,2}$ is the measured dielectric constant and $\ell_{1,2}$ the density of the solution; M_1 and M_2 are the molecular weights of the solvent and solute respectively.

Both P_1 and $P_{1,2}$ being evaluated from experimental measurements, P_2 of the solute can be calculated from its composition from Eq. (10.127).

The values of P_2 obtained in this way are found to vary to some extent with the concentration of the solution at constant temperature. The effect, which is attributed to the presence of interactions between polar

molecules, can be minimized by extrapolating the $P_{i,2}$ values, either graphically or by means of a suitable equation, to infinite dilution. Values of $P_{2,\infty}$, that is, P_2 at infinite dilution, can be obtained in this way for a series of temperatures and the value of μ can then be calculated from the Debye equation. (It should be noted that besides mutual interactions of the solute molecules there are also interactions between the solute and the solvent molecules. The latter effect, referred to as the solvent effect, is attributed to the polarization induced in the nonpolar solvent molecules by the electric fields of the dipoles of the polar solute. The solvent effect is not eliminated by the extrapolation to infinite dilution, and other semi-empirical methods have been proposed.)

The dilute-solution method is limited by the range of temperatures over which solutions can be studied. The limitation can be removed, however, by making use of refractivity method.

(iii) Refractivity method . This method, even though it involves some approximations, is simpler and more useful than the temperature method, because it requires measurements at only one temperature. The method depends on the behaviour of polar molecules in oscillating electric fields of high frequency.

We have so far considered two types of polarizations, namely, distortion polarization P_d and orientation polarization P_o [Eq. (10.125)]. The distortion polarization, as we have mentioned above, depends on the displacement of both electrons and nuclei in the molecule. It is thus made up of two effects: (a) displacement of the electrons (relative to the nuclei) towards the positive pole of the applied electric field, and (b) slight displacement of nuclei with respect to one another. The first effect is known as the *electron polarization* P_e and the second effect as the *atom polarization* P_a (a term, which is somewhat misleading). Thus, $P_d = P_e + P_a$, and correspondingly, the distortion polarizability α_d is the sum of α_e and α_a, respectively, called the electron and atom polarizabilities. The total polarization P_m is then the sum of P_e, P_a and P_o. The speed of response of these three types of polarization to an alternating electric field differs greatly. Thus the atom polarization responds more slowly than the electron polarization, while the reorientation process of a polar molecule is even slower. Now imagine that an alternating electric field of increasing frequency is applied. As long as the frequency is not too high, such as in the radio-frequency range of the electromagnetic spectrum, all the three types of polarization can follow the alternating field and so all of them contribute to the total polarization P_m . As the frequency of the field continues to rise through the range corresponding to the infrared region of the electromagnetic spectrum, the orientations of the molecules can no longer alter rapidly enough to follow the alternating field, so that there is no orientation contribution to the total polarization. At still higher frequency, in the visible region ($\sim 10^{15}$ c/s), the nuclei also

are no longer able to follow the alternating field because of their relatively large mass, with the result that the polarization drops again and only the contribution from electron polarization remains. The plot of the polarization against the frequency of the applied field gives rise to a curve as shown in Fig. 10.66.
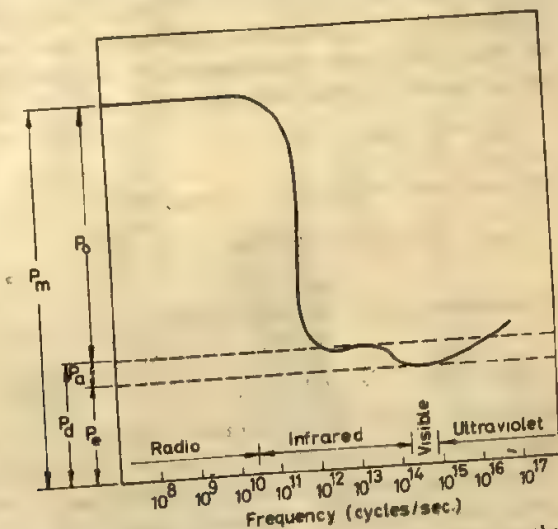
Fig. 10.66 Dependence of the molar polarization on the frequency of the applied field.

An important consequence of Maxwell's electromagnetic theory of light is the relationship between the dielectric constant D and the refractive index n_R of a substance:

$$D = n_R^2 \tag{10.129}$$

This relationship requires that both the dielectric constant and the refractive index be measured at the same frequency. The dielectric constant is normally measured by electrical methods at relatively low frequencies ($<10^6$ c/s). It can be seen from Fig. 10.66 that at these frequencies, all the three types of polarization (electron, atom, and orientation) contribute to the total polarization for a polar substance. The refractive index, however, is measured by optical techniques at much higher frequencies ($>10^{14}$ c/s); at these frequencies there is only the contribution due to electron polarization. That for polar molecules there is a large difference between D and n^2R (for instance, the value of D for water is 80 and the value of n_R is 1.33) is a consequence of this fact. As would be expected, the difference is much smaller for nonpolar molecules; for benzene, for instance, $D = 2.27$ and $n = 1.50$.

When the Maxwell relationship (10.129) is introduced into the Clausius-Mosotti equation (10.126) and correspondingly α_d (which is the

sum of $\alpha_{\vec{c}}$ and $\alpha_{\vec{a}}$) is replaced by $\alpha_{\vec{c}}$, for the reason mentioned above, we obtain the Lorentz-Lorenz equation:

$$\frac{n_R^2 - 1}{n_R^2 + 2} \frac{M}{\rho} = \frac{4}{3} \pi N \alpha_e$$

The quantity on the right-hand side of this equation is called the *electron polarization*, represented by P_e and that on the left-hand side is called *molar refraction*, represented by R_m. Thus,

$$R_m = \frac{4}{3} \pi N \alpha_e = P_e \qquad\qquad (10.130)$$

We can rewrite the Debye equation (10.125) in the following form

$$P_m = \frac{49}{9} \frac{\pi N}{kT} \mu^2 + \frac{4}{3} \pi N \alpha_e + \frac{4}{3} \pi N \alpha_a \qquad\qquad (10.131)$$

Subtracting Eq. (10.130) from Eq.(10.131) we obtain

$$P_m - R_m = \frac{4}{9} \frac{\pi N}{kT} \mu^2 + \frac{4}{3} \pi N \alpha_a = 4 \frac{\pi N}{kT} \mu^2 + P_a \qquad\qquad (10.132)$$

where the quantity P_a is called the *atom polarization*. The value of R_m is calculated from the refractive index of the pure substance for visible light (for most purposes, the D-line of sodium is used), while P_m is calculated from the dielectric constant measured at radio frequencies. When measurements of the dielectric constant have been made on a series of solutions of different dilutions, as in the dilute-solution method described above, the value of $P_2 \infty$ may be used in Eq. (10.132) in place of P_m. The value of μ can then be calculated from this equation, if the atom polarization P_a is known. The latter quantity is, however, difficult to determine experimentally. Fortunately, for most substances they are relatively small (Fig. 10.66), not more than 2 or 3 cm³, and as a rough approximation, P_a may be taken as 5–10 per cent of P_e and hence of R_m. Thus, knowing the values of P_m and R_m from measurements at just one temperature, we can calculate the dipole moment from Eq. (10.132). Most dipole moment values have been determined in this way. The data, however, are not so reliable as the temperature method data because of the approximation for atom polarization.

A few typical values of dipole moments are collected in Table 10.16. The trend in the values for the hydrogen halides is in line with the electronegativity difference between the halogens. The value of zero for the dipole moments of polyatomic molecules like CO_2, CCl_4, BCl_3 is due to their structural symmetry.

(iv) Other methods The most accurate values of dipole moments are obtained from microwave spectroscopy. As we saw in Section 10.6.3, a molecule exhibiting pure rotational spectrum must have a permanent electric dipole moment. The application of an external electric field causes perturbation of its rotational energy levels due to interaction, and as a consequence, the absorption lines of the pure rotational spectrum are

shifted (*Stark effect*). The Stark shift, Δv, will therefore be a function of both the electric field strength E and the dipole moment μ. For a linear molecule Δv is found to be proportional to $(\mu E)^2$ while for a symmetric top it is proportional to μE. We can thus determine dipole moments simply by observing the Stark shift. Since the measurement is made on samples in the vapour state and at a low pressure, the results are uncomplicated by molecular interactions and solvent effects.

Table 10.16 Dipole Moments of Molecules (in debyes)

Cl_2	0	H_2O	1.84	C_6H_5Cl	1.7
CO_2	0	H_2O_2	2.1	C_6H_5Br	1.7
CS_2	0	H_2S	0.93	C_6H_5I	1.2
CCl_4	0	HCN	2.93	C_6H_5OH	1.7
C_6H_6	0	SO_2	1.63	$C_6H_5NO_2$	4.23
C_6Cl_6	0	NH_3	1.44	$C_6H_5NH_2$	1.56
BCl_3	0	PCl_3	0.80	C_6H_5CN	4.37
				$C_6H_5CH_3$	0.4
RCl	2.05	HI	0.44	$(C_6H_5)_2O$	1.15
RBr	2.05	HBr	0.82	$(C_6H_5)_2CO$	2.95
RI	1.9	HCl	1.08		
ROH	1.7	HF	1.82		
RNH_2	1.3				
RNO_2	3.4				
R_2O	1.15	*cis* = dichloroethylene 1.9			
R_2CO	2.7	*trans* = dichloroethylene 0			

10.16.2 Structural Information from Dipole Moment

Since the dipole moment arises from the separation of charges due to the difference in electronegativity of the two atoms connected by a chemical bond, it should be possible to associate a dipole moment with every bond in the molecule. The dipole moment of a polyatomic molecule is then the vector sum of the individual bond dipole moments. For the resultant of two bond moments μ_1 and μ_2 which make an angle θ with each other, the following equation for the vector addition can be used:

$$\mu = (\mu_1^2 + \mu_2^2 + 2\mu_1\mu_2 \cos\theta)^{\frac{1}{2}} \tag{10.133}$$

Consider the example of H_2O. Since oxygen is much more electronegative than hydrogen, a dipole moment can be associated with each O-H bond, the oxygen atom forming the negative end of the dipole in each case. Since H-O-H in H_2O is known to be 104.5°, the vector addition of two O-H bond moments of about 1.5D each will account for the observed dipole moment 1.84D for water.

On the basis of addivity of bond moments we can derive information

about the symmetry of polyatomic molecules from their dipole moment data. Thus, it is evident that a molecule with a centre of symmetry will have a zero dipole moment since each bond moment is cancelled by an equal and oppositely directed bond moment. Again, for a molecule which has more than one rotation axis or a rotation-reflection axis, bond moments will cancel out giving a zero dipole moment. Thus among the common point symmetry group listed in Table 10.2, only the C_{nv} groups remain, and a molecule belonging to any of these groups will have a finite dipole moment. The dipole moment data of Table 10.16 can be interpreted in the light of this analysis.

As an illustration of the application of Eq. (10.133), let us consider the dipole moments of disubstituted benzene derivatives. Since the benzene ring is planar and hexagonal, the angle between the dipole vectors of two *ortho*-groups is 60°, while for two groups in the *meta*-position the angle is 120° and for two groups in the *para*-position it is 180°. For chlorobenzene $\mu = 1.7D$, and since benzene itself has a zero dipole moment, $\mu C - Cl = 1.7D$. From the vector addition rule we would therefore expect the moment of *ortho*-dichlorobenzene to be $\sqrt{3}\ \mu C - Cl$ (i.e. 2.94D), that of *meta*-dichlorobenzene to be $\mu C - Cl$ (i.e. 1.7D) and that of *para*-dichlorobenzene to be zero (see Fig. 10.67). These may be
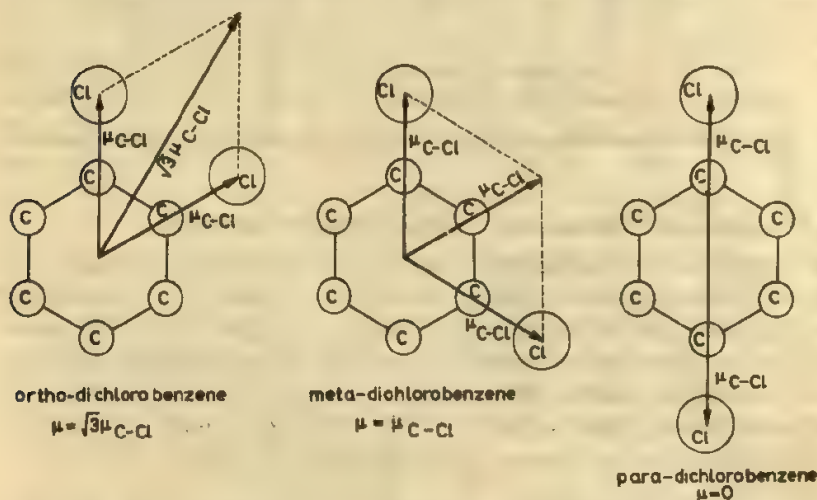
Fig. 10.67 Vector addition of bond dipole moments in dichlorobenzenes.

compared with the observed values for the respective isomers: 2.53D, 1.67D and 0. It can be seen that the calculated values for the *meta*- and *para*-isomers are in excellent agreement with the observed values, but there is considerable discrepancy for the *ortho*-derivative. In fact, this is found to be a general rule for disubstituted benzene derivatives. This discrepancy, or the so-called *ortho*-effect, may be due to either or both of the following reasons:. (i) the angle between the dipole vectors (in this

case, C—Cl bond vectors) may be increased due to mutual repulsion of the adjacent groups (Cl atoms), or (ii) the magnitudes of the bond moments may be altered by mutual interaction due to their proximity.

Dipole moment measurements for aromatic compounds have given a number of interesting results. Nitrobenzene has a dipole moment of 3.95D and there is no doubt that the $-NO_2$ group is negatively charged with respect to the benzene ring. However, the dipole moment of para-nitrotoluene is 4.4D, which indicates that the $-CH_3$ group is positively charged with respect to the ring. Conversely, a dipole moment less than 3.95D for a *para*-substituted nitrobenzene would indicate that the substituent is negatively charged with respect to the benzene ring. The dipole moment of *para*-dinitrobenzene is evidently zero.

It should be noted that the dipole moment of a *para*-disubstituted benzene molecule with identical groups at the *para*-positions can be zero only if the dipole vectors of the two groups lie along the bonds by which the groups are linked to the ring. Thus the zero dipole moment for para-dichlorobenzene is a good evidence for the coplanarity of the $C-Cl$ bonds and the benzene ring; the same argument applies to *para*-dinitrobenzene. On the other hand, the fact that the dipole moment of *para*-dihydroxybenzene is not zero (the observed value is 1.64D) clearly indicates that the O—H bonds lie out of the plane of the ring. In conclusion, we may note that when a decision about the molecular symmetry depends on whether the molecule in question has or has not a net dipole moment, a reliable conclusion can be drawn from the dipole moment consideration. The same cannot be said, however, when the conclusion depends on the consideration of the magnitude of the dipole moment.

Suggested Reading

BARROW, G. M., *The Structure of Molecules,* Benjamin, New York, 1963.

BRAND, J. C. D. and J. C. SPEAKMAN, *Molecular Structure,* Edward Arnold, London, 1962.

WHEATLEY, P.J., *Molecular Structure,* Oxford University Press, London, 1968.

BANWELL, C.N., *Fundamentals of Molecular Spectroscopy,* McGraw-Hill Book Co. Inc., New York, 1972.

INGRAM, D.J.E., *Spectroscopy at Radio and Microwave Frequencies,* Plenum Press, New York, 1967.

RAO, C.N.R., *Chemical Applications of Infrared Spectroscopy,* Academic Press, New York, 1963.

CROSS, A.D. and R.A. JONES, *Introduction to Practical Infrared Spectroscopy,* Butterworths, London, 1969.

COLTHUP, N.B., L.H. DALY and S.E. WIBERLEY, *Introduction to Infrared and Raman Spectroscopy,* Academic Press, New York, 1964.

GILSON, T.R.G. and P.J. HENDRA, *Laser Raman Spectroscopy,* John Wiley, London, 1970.

KING, G.W., *Spectroscopy and Molecular Structure,* Holt, Rinehart and Winston Inc., New York, 1964.

RAO, C.N.R., *Ultraviolet and Visible Spectroscopy—Chemical Applications,* 3rd edn., Butterworths, London, 1975.

JACKMAN, L.M. and S. STERNBELL, *Nuclear Magnetic Resonance in Organic Chemistry,* Pergamon Press, London, 1969.

BERSHON, M. and J.L. BAIRD, *An Introduction to Electron Paramagnetic Resonance,* Benjamin, New York, 1966.

GOLDANSKII, V.I. and R.H. HERBER, *Chemical Applications of Mössbauer Spectroscopy,* Academic Press, New York, 1968.

GREENWOOD, N.N. and T.C. GIBB, *Mössbauer Spectroscopy,* Chapman and Hall, London, 1971.

GONSER, U. (Ed.), *Mössbauer Spectroscopy,* Springer Verlag, Berlin, 1975.
BEYNON, J.H., *Mass Spectrometry and Its Application to Organic Chemistry,* Elsevier, Amsterdam, 1960.
JOHNSTON, R.A.W., *Mass Spectrometry for Organic Chemists,* Cambridge University Press, London, 1972
BEYNON, J.H. and A.W. WILLIAMS, *Mass and Abundance Tables for use in Mass Spectrometry,* Elsevier,
Amsterdam, 1963.
LEDERBERG, J., *Computation of Molecular Formula for Mass Spectrometry,* Holden-Day, San Francisco, 1964.

Problems

10.1 List the symmetry elements and give the point groups for the following molecules: (a) dichloromethane, (b) carbon tetrachloride, (c) *cis*-dichloroethylene, (d) *trans*-dichloroethylene, (e) naphthalene, (f) *ortho-meta* -and *para*-dichlorobenzene, and (g) 1,3,5-trichlorobenzene.

10.2 How many revolutions per second does a CO molecule make when $J = 1$ and $J = 10$? The CO bond length is 1.128 A.

10.3 What is the change in the rotational constant B when deuterium is substituted for hydrogen in the hydrogen molecule?

10.4 The separation of lines in the rotational spectrum of the HCl molecule was found to be 20.6 cm^{-1}. Calculate the internuclear distance.

10.5 Draw rotational energy level diagram for HBr. Which rotational level of HBr has the highest population?

10.6 The first rotational absorption of $^{12}C^{16}O$ has been observed at $\overline{v} = 3.84235$ cm^{-1} and that of $^{13}C^{16}O$ at $\overline{v} = 3.67337$ cm^{-1}. Taking the mass of ^{16}O to be 15.9949 and that of ^{12}C to be 12.00, calculate the atomic weight of ^{13}C. Assume that the bond length is unchanged by isotopic substitution.

10.7 The species $^{16}O^{12}C^{32}S$ and $^{16}O^{12}C^{34}S$ have been investigated in the microwave region. The measured frequencies of the line $J = 1$ $J = 2$ for the two species are 24325.92 Mc/s and 23732.33 Mc/s, respectively. Calculate the bond lengths C–O and C–S.

10.8 Two adjacent lines in the microwave spectrum of HCN have frequencies of 17.73×10 and 26.59×10^{10} c/s. Calculate the moment of inertia.

10.9 Assuming that the H_2 molecule is a harmonic oscillator with $\overline{v}_e = 4395$ cm^{-1} and $r_e = 0.742$ A, calculate the maximum displacement $(r - r_e)$ as a percentage of r_e when $v = 0$ and $v = 10$.

10.10 The infrared spectrum of HCl exhibits a fundamental absorption band at $\overline{v} = 2886$ cm^{-1}. (a) Calculate the force that would be required to stretch the H–Cl bond by 1 Å, assuming Hooke's law behaviour. (b) Calculate also the vibrational amplitude in $v = 0$ state. (c) Calculate the shift in the absorption frequency caused by replacement of H by D. (Note: The simple harmonic force constant for a molecule is virtually independent of any factor other than electrostatic interactions. The force constant for DCl may therefore be assumed to be the same as that for HCl.)

10.11 One of the fundamental vibrational modes of H_2O occurs at 3652 cm^{-1}. What would be the frequency of the corresponding mode in $H_2^{18}O$ and D_2O?

10.12 Using the data of Table 10.4 and 10.8, plot the potential energy versus internuclear distance curve near the equilibrium distance for HF and HI. Add to this diagram the allowed vibrational energies as horizontal lines. Note the difference in vibrational spacing for HF and HI.

10.13 The fundamental band for CO is centred at 2143.3 cm^{-1} and the first overtone at 4259.7 cm^{-1}. Calculate the equilibrium oscillation frequency $\overline{v}_e$ and the anharmonicity constant g. Also calculate the zero-point energy of CO.

10.14 The vibrational spectrum of HCN shows two strong absorptions at 727 cm^{-1} and 3270 cm^{-1}, two absorptions of medium intensity at 1433 cm^{-1} and 2085 cm^{-1} and two weak absorptions at 1370 cm^{-1} and 2800 cm^{-1}. Suggest assignments to these bands.

10.15 The fundamental band for HCl is centred at 2886 cm^{-1}. Assuming that the internuclear distance is constant at 1.273 Å-, calculate the wavenumber of the first two lines of each of the P- and R- branches of HCl.

10.16 Given that $\overline{v}_e = 215.0$ cm^{-1} and $a = 0.0028$ for I_2, (a) compute the relative populations at 300°K of the first four vibrational levels on the basis of Boltzmann distribution [see Eq. (10.2)], ($g = 1$ for all vibrational levels); (b) calculate the average vibrational energy of I_2 at room temperature. (The population of levels greater than $v = 3$ can be neglected.)

10.17 The values of $\overline{v}_e$ and g for upper and lower states of CO are 1515.61 cm^{-1}, 0.0114 and 2170.21 cm^{-1}, 0.0062 respectively. The (0.0) transition is observed at 64,746.55 cm^{-1}. Calculate the energy difference of the two electronic states.

10.18 The values of U_e and a are 1580.36 cm^{-1} and 0.0076, respectively, for the ground state of molecular oxygen. The dissociation energy of the oxygen molecule in the ground state is 8.294 x 10^{12} erg. From these data plot the Morse curve for oxygen. Add the allowed vibrational energies as horizontal lines to this diagram. [The constant β in the Morse function, Eq. (10.41), is equal to $(8\pi^2 \mu a D_e c/h)^{\frac{1}{2}}$, where μ, a, $\overline{U}_e$, c and h are as previously defined.]

10.19 The onset of absorption continum in the spectrum of I_2 vapour occurs at 4995 Å. I_2 molecule in the vapour state is known to dissociate into one ground state atom and one excited atom. The energy of excitation of the atom is 21.70 kcal/mole.
Calculate the dissociation energy of I_2 in its ground electronic state.

10.20 The absorption spectrum of oxygen consists of a series of bands which terminate in continuous absorption at 1761 Å. An oxygen molecule in the upper state dissociates into one ground state atom and one excited atom. The excitation energy of the latter is 1.967 eV. Calculate the dissociation energy of O_2 in its ground electronic state in kcal/mole.

10.21 The zero-point energy of O_2 in the ground state corresponds to 793 cm^{-1}, and the difference in potential energy minima for the two electronic states corresponds to 49,800 cm^{-1}. Determine the dissociation energy of O_2 in its upper electronic state in kcal/mole. Use the data of Problem 10.20.

10.22 In the Raman spectrum of CCl_4 obtained by using the mercury arc line at 4385.3 Å for excitation, lines are observed at 4400.0, 4418.8 and 4447.0 Å. Calculate the Raman shift for each of these lines.

10.23 The Raman line associated with a vibrational mode, which is both Raman and infrared active, is found at 4600 Å when excited by incident light of wavelength 4358 Å. Calculate the wavelength of the centre of the corresponding infrared absorption band.

10.24 In a magnetic field of 15,000 gauss, a phosphorus isotope absorbs at 25.8 Mc/s. Calculate the nuclear g factor for this isotope.

10.25 Calculate the strength of the magnetic field in which protons will have a Larmor frequency of 60 Mc/s.

10.26 Predict the pattern of high resolution NMR spectrum of isopropyl alcohol which is not free from water. (Note. The fine structure of the –OH resonance is destroyed due to rapid exchange with protons of water.)

10.27 Which valency states of copper and silver will show a strong ESR signal?

10.28 What would be the ESR spectrum for vanadium (IV) in vanadyl acetylacetonate? Spin $I = 7/2$ for ^{51}V nucleus. (*Ans.* An eight-line pattern).

10.29 Sketch the energy level diagram and predict the ESR spectrum resulting from the radical ion $(SO_3)_2 NO^-$. The nitrogen nucleus has one unit of spin. (*Ans.* A three-line pattern)

10.30 Predict the ESR spectrum resulting from coupling of an unpaired electron with (a) two equivalent protons, (b) two nonequivalent protons. Sketch the corresponding energy level diagrams.

10.31 Predict the pattern of the γ-ray spectrum of a Mössbauer nucleus that has spins of 3/2 and 5/2 in its ground and excited states. Consider the following cases: (a) No internal electric field gradient is present at the nucleus and no magnetic field is applied; (b) electric field gradient present but no magentic field; (c) no electric field gradient but magnetic field present; (d) both electric field gradient and magnetic field present. [*Ans.* (a) 1 line; (b) 5 lines; (c) 12 lines; (d) 12 lines.]

10.32 The bond energy of H_2 is 104.16 kcal/mole and the ionization energy of a hydrogen atom is 13.60 eV. What appearance potential might be calculated for H^+ in a mass-spectrometric analysis of H_2? (*Ans.* 18 V)

10.33 What resolving power of a mass-spectrometer would differentiate between the molecular ions of compounds, nonane and napthalene, both having the same integral mass 128? (*Ans.* 1360)

10.34 The molecular-ion cluster in a mass spectrum of an organic compound consists of only the parent ion peak at M = 142 and a M + 1 peak which is 1.1 per cent of the parent peak. Suggest the composition of the compound. (*Ans.* CH_3I. Note that I is a non-isotopic element.)

10.35 Calculate the $(M+1)/M$ and $(M+2)/M$ peak intensity ratios for (a) $C_5 H_5 NO_2$ and (b) $C_5H_5 NS$.

10.36 Explain how the intensity of the molecular-ion peak in relation to the rest of the spectrum may give clue as to the class of the compound.

10.37 Calculate the dipole moment and the distortion polarizability of bromine pentafluoride from the following data for the dielectric constant of the vapour:

$T(^\circ K)$	345.6	374.9	402.4	430.8
D	1.00632	1.00552	1.00491	1.00438

10.38 The molar polarization of n-butylamine determined by extrapolation to infinite dilution in benzene at 25°C is 64.0 cm^3. Given that the refractive index of pure n-butylamine is 1.399 and density is 0.737 g/cm^3, calculate its dipole moment.

10.39 Calculate the dipole moment of diethyl ether from the following data for its solution in cyclohexane at 20°C:

X_2	0.12325	0.08854	0.0472	0.0000
D	2.246	2.178	2.109	2.033
ϱ	0.7691	0.7720	0.7751	0.7784

The refractive index and density of pure diethyl ether are 1.352 and 0.710 respectively.

10.40 The dipole moments of chlorobenzene and nitrobenzene are 1.70 D and 4.23 D, respectively. Calculate the dipole moment of (a) 1,3-chloronitrobenzene; (b) 1,4-chloronitrobenzene; (c) 1-nitro-3,5 -dichlorobenzene; and (d) 1,3,5-trichlorobenzene.

Appendix 1

Reduced Mass of Two Particles

Considering any pair of particles with an interacting force whose magnitude depends only on the separation of the particles and which acts along the line joining the particles, we shall see in the following that despite free movement of both the particles we may consider one particle to be fixed, provided we replace the mass of the other particle by the reduced mass of the two particles.

As shown in Fig. A1.1, the vectors r and R are the position vectors of the particles m and M with respect to the origin O and they describe the respective positions of the two particles relative to the fixed Cartesian axes X, Y and Z. Then the position vector of the particle m with respect to the particle M is given by

$$r' = r - R \qquad (A1.1)$$

Since we have assumed that the force of interaction between the two
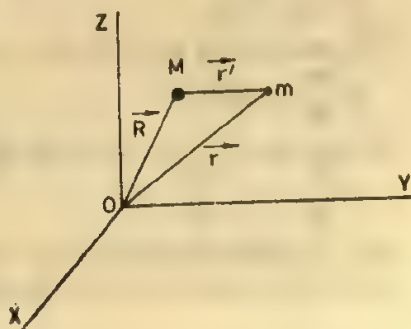
Fig. A1.1 Motion of particles m and M relative to fixed axes XYZ

particles is along the line joining them and depends only on the distance
of their separation, the vector force F_m acting on the particle m is given by

$$F_m = f(r') \, r' \qquad \text{(A1.2)}$$

where $f(r')$ represents an arbitrary scalar function of r'.

The acceleration of the particle m produced by the force F_m is d^2r/dt^2,
when expressed in relation to the fixed axes X, Y, Z. Hence from Newton's
second law of motion

$$m \, \frac{d^2r}{dt^2} = F_m \qquad \text{(A1.3)}$$

where m is the mass of the particle m.

From Eqs. (A1.2) and (A1.3)

$$m \, \frac{d^2r}{dt^2} = f(r') \, r' \qquad \text{(A1.4)}$$

According to Newton's third law of motion, the force on the particle M
is equal to that on the particle m but opposite in direction, so that

$$M \, \frac{d^2R}{dt^2} = -f(r') \, r' \qquad \text{(A1.5)}$$

We have from Eqs. (A1.4) and (A1.5)

$$\frac{d^2r}{dt^2} = \frac{1}{m} f(r') \, r' \qquad \text{(A1.6)}$$

$$\frac{d^2R}{dt^2} = -\frac{1}{M} f(r') \, r' \qquad \text{(A1.7)}$$

Subtracting Eq. (A1.7) from Eq. (A1.6), we get

$$\frac{d^2r}{dt^2} - \frac{d^2R}{dt^2} = \left(\frac{1}{m} + \frac{1}{M} \right) f(r') \, r' \qquad \text{(A1.8)}$$

Again, differentiating Eq. (A1.1) twice with respect to time t, we have

$$\frac{d^2r'}{dt^2} = \frac{d^2r}{dt^2} - \frac{d^2R}{dt^2} \qquad \text{(A1.9)}$$

Consequently, from Eqs. (A1.8) and (A1.9)

$$\frac{d^2r'}{dt^2} = \left(\frac{1}{m} + \frac{1}{M} \right) f(r') \, r' = \frac{1}{\mu} f(r') \, r' \qquad \text{(A1.10)}$$

where μ, the reduced mass of the two particles m and M, is defined by
the equation

$$\frac{1}{\mu} = \frac{1}{m} + \frac{1}{M} \qquad \text{(A1.11)}$$

We can rewrite Eq. (A1.10) in the form

$$\mu \, \frac{d^2r'}{dt^2} = f(r') \, r' \qquad \text{(A1.12)}$$

Comparing Eq. (A1.12) with Eq. (A1.4)

$$m \, \frac{d^2r}{dt^2} = \mu \, \frac{d^2r'}{dt^2} \qquad \text{(A1.13)}$$

Eq. (A1.13) implies that if we replace the mass m by the reduced mass
μ we may consider M to be the fixed origin for describing the motion of m.

Appendix 2

The Electronic Configurations of the Ground States of the Elements

Period	Element	Atomic No.	K 1s	L 2s 2p	M 3s 3p 3d	N 4s 4p 4d 4f	O 5s 5p 5d 5f	P 6s 6p 6d	Q 7s
1	H	1	1						
	He	2	2						
	Li	3	2	1					
	Be	4	2	2					
	B	5	2	2 1					
2	C	6	2	2 2					
	N	7	2	2 3					
	O	8	2	2 4					
	F	9	2	2 5					
	Ne	10	2	2 6					
	Na	11	2	2 6	1				
	Mg	12	2	2 6	2				
	Al	13	2	2 6	2 1				
3	Si	14	2	2 6	2 2				
	P	15	2	2 6	2 3				
	S	16	2	2 6	2 4				
	Cl	17	2	2 6	2 5				
	Ar	18	2	2 6	2 6				
	K	19	2	2 6	2 6	1			
	Ca	20	2	2 6	2 6	2			
4	Sc	21*	2	2 6	2 6 1	2			
	Ti	22*	2	2 6	2 6 2	2			
	V	23*	2	2 6	2 6 3	2			

Period	Element	Atomic No.	K	L		M			N				O				P			Q
			1s	2s	2p	3s	3p	3d	4s	4p	4d	4f	5s	5p	5d	5f	6s	6p	6d	7s
	Cr	24*	2	2	6	2	6	5	1											
	Mn	25*	2	2	6	2	6	5	2											
	Fe	26*	2	2	6	2	6	6	2											
	Co	27*	2	2	6	2	6	7	2											
	Ni	28*	2	2	6	2	6	8	2											
4	Cu	29*	2	2	6	2	6	10	1											
	Zn	30*	2	2	6	2	6	10	2											
	Ga	31	2	2	6	2	6	10	2	1										
	Ge	32	2	2	6	2	6	10	2	2										
	As	33	2	2	6	2	6	10	2	3										
	Se	34	2	2	6	2	6	10	2	4										
	Br	35	2	2	6	2	6	10	2	5										
	Kr	36	2	2	6	2	6	10	2	6										
	Rb	37	2	2	6	2	6	10	2	6			1							
	Sr	38	2	2	6	2	6	10	2	6			2							
	Y	39*	2	2	6	2	6	10	2	6	1		2							
	Zr	40*	2	2	6	2	6	10	2	6	2		2							
	Nb	41*	2	2	6	2	6	10	2	6	4		1							
	Mo	42*	2	2	6	2	6	10	2	6	5		1							
	Tc	43*	2	2	6	2	6	10	2	6	5		2							
	Ru	44*	2	2	6	2	6	10	2	6	7		1							
	Rh	45*	2	2	6	2	6	10	2	6	8		1							
5	Pd	46*	2	2	6	2	6	10	2	6	10									
	Ag	47*	2	2	6	2	6	10	2	6	10		1							
	Cd	48*	2	2	6	2	6	10	2	6	10		2							
	In	49	2	2	6	2	6	10	2	6	10		2	1						
	Sn	50	2	2	6	2	6	10	2	6	10		2	2						
	Sb	51	2	2	6	2	6	10	2	6	10		2	3						
	Te	52	2	2	6	2	6	10	2	6	10		2	4						
	I	53	2	2	6	2	6	10	2	6	10		2	5						
	Xe	54	2	2	6	2	6	10	2	6	10		2	6						
	Cs	55	2	2	6	2	6	10	2	6	10		2	6			1			
	Ba	56	2	2	6	2	6	10	2	6	10		2	6			2			
	La	57	2	2	6	2	6	10	2	6	10		2	6	1		2			
	Ce	58†	2	2	6	2	6	10	2	6	10	1	2	6	1		2			
	Pr	59†	2	2	6	2	6	10	2	6	10	3	2	6			2			
	Nd	60†	2	2	6	2	6	10	2	6	10	4	2	6			2			
	Pm	61†	2	2	6	2	6	10	2	6	10	5	2	6			2			
	Sm	62†	2	2	6	2	6	10	2	6	10	6	2	6			2			
6	Eu	63†	2	2	6	2	6	10	2	6	10	7	2	6			2			
	Gd	64†	2	2	6	2	6	10	2	6	10	7	2	6	1		2			
	Tb	65†	2	2	6	2	6	10	2	6	10	9	2	6			2			
	Dy	66†	2	2	6	2	6	10	2	6	10	10	2	6			2			
	Ho	67†	2	2	6	2	6	10	2	6	10	11	2	6			2			
	Er	68†	2	2	6	2	6	10	2	6	10	12	2	6			2			
	Tm	69†	2	2	6	2	6	10	2	6	10	13	2	6			2			
	Yb	70†	2	2	6	2	6	10	2	6	10	14	2	6			2			
	Lu	71†	2	2	6	2	6	10	2	6	10	14	2	6	1		2			
	Hf	72*	2	2	6	2	6	10	2	6	10	14	2	6	2		2			

Period	Element	Atomic No.	K	L		M			N				O				P			Q
			1s	2s	2p	3s	3p	3d	4s	4p	4d	4f	5s	5p	5d	5f	6s	6p	6d	7s
	Ta	73*	2	2	6	2	6	10	2	6	10	14	2	6	3		2			
	W	74*	2	2	6	2	6	10	2	6	10	14	2	6	4		2			
	Re	75*	2	2	6	2	6	10	2	6	10	14	2	6	5		2			
	Os	76*	2	2	6	2	6	10	2	6	10	14	2	6	6		2			
	Ir	77*	2	2	6	2	6	10	2	6	10	14	2	6	9					
	Pt	78*	2	2	6	2	6	10	2	6	10	14	2	6	9		1			
6	Au	79*	2	2	6	2	6	10	2	6	10	14	2	6	10		1			
	Hg	80*	2	2	6	2	6	10	2	6	10	14	2	6	10		2			
	Tl	81	2	2	6	2	6	10	2	6	10	14	2	6	10		2	1		
	Pb	82	2	2	6	2	6	10	2	6	10	14	2	6	10		2	2		
	Bi	83	2	2	6	2	6	10	2	6	10	14	2	6	10		2	3		
	Po	84	2	2	6	2	6	10	2	6	10	14	2	6	10		2	4		
	At	85	2	2	6	2	6	10	2	6	10	14	2	6	10		2	5		
	Rn	86	2	2	6	2	6	10	2	6	10	14	2	6	10		2	6		
	Fr	87	2	2	6	2	6	10	2	6	10	14	2	6	10		2	6		1
	Ra	88	2	2	6	2	6	10	2	6	10	14	2	6	10		2	6		2
	Ac	89*	2	2	6	2	6	10	2	6	10	14	2	6	10		2	6	1	2
	Th	90†	2	2	6	2	6	10	2	6	10	14	2	6	10	1	2	6	1	2
	Pa	91†	2	2	6	2	6	10	2	6	10	14	2	6	10	2	2	6	1	2
	U	92†	2	2	6	2	6	10	2	6	10	14	2	6	10	3	2	6	1	2
	Np	93†	2	2	6	2	6	10	2	6	10	14	2	6	10	4	2	6	1	2
	Pu	94†	2	2	6	2	6	10	2	6	10	14	2	6	10	5	2	6	1	2
7	Am	95†	2	2	6	2	6	10	2	6	10	14	2	6	10	7	2	6		2
	Cm	96†	2	2	6	2	6	10	2	6	10	14	2	6	10	7	2	6	1	2
	Bk	97†	2	2	6	2	6	10	2	6	10	14	2	6	10	8	2	6	1	2
	Cf	98†	2	2	6	2	6	10	2	6	10	14	2	6	10	10	2	6		2
	E	99†	2	2	6	2	6	10	2	6	10	14	2	6	10	11	2	6		2
	Fm	100†	2	2	6	2	6	10	2	6	10	14	2	6	10	12	2	6		2
	Mv	101†	2	2	6	2	6	10	2	6	10	14	2	6	10	13	2	6		2
	No	102†	2	2	6	2	6	10	2	6	10	14	2	6	10	14	2	6		2

* Transition elements
† Lanthanide and actinide elements

Tetrahedral sp³ Hybrids

The electronic configuration of tetravalent carbon is considered to be $1s^2\, 2s^1\, 2p^1_x\, 2p^1_y\, 2p^1_z$. Accordingly, we can write the four valence orbitals of carbon as $\psi(2s)$, $\psi(2p_x)$, $\psi(2p_y)$, $\psi(2p_z)$. Expressions for these wave functions can be written as products of respective angular functions and radial functions from Tables 5.2 and 5.3. The radial functions $R_{2,0}(r)$ and $R_{2,1}(r)$ do not, however, differ greatly from each other. We may therefore neglect the radial functions and focus our attention only on the angular part of the wave functions (Table 5.2). [Accordingly, following Pauling (see Section 6.7), the bond forming strength of each of the functions $\psi(2p_x)$, $\psi(2p_y)$ and $\psi(2p_z)$ is calculated to be $\sqrt{3}$ times that of $\psi(2s)$.]

We now write for the sp^3 hybrids

$$\psi_i = a_i \psi(2s) + b_i \psi(2p_x) + c_i \psi(2p_y) + d_i \psi(2p_z) \quad i = 1, 2, 3, 4 \qquad (A3.1)$$

where the possible values of the coefficients are restricted by the normalization condition:

$$a_i^2 + b_i^2 + c_i^2 + d_i^2 = 1 \qquad (A3.2)$$

The tetrahedral orientation of sp^3 orbitals may be visualized as the carbon atom at the centre of a cube with x-, y-, z-axes parallel to the edges of the cube and the four orbitals being directed from the centre towards alternate corners of the cube (Fig. A3.1).

Let us choose the direction in which the first orbital ψ_1 has its maximum to be along the $(1, 1, 1)$ diagonal of the cube. (Note, however, that this choice of direction is arbitrary.) Therefore the coefficients b_1, c_1 and d_1 must be equal, and ψ_1 can then be written as
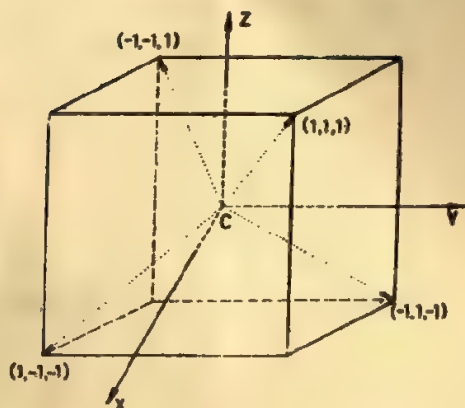
Fig. A3.1 Coordinate system for tetra-
hedral carbon orbitals

$$\psi_1 = a_1 \, \psi(2s) + b_1 \, [\psi(2p_x) + \psi(2p_y) + \psi(2p_z)] \tag{A3.3}$$

The normalization condition (A3.2) becomes

$$a^2_1 + 3b^2_1 = 1 \tag{A3.4}$$

Since along the $(1, 1, 1)$ diagonal

$$\sin\theta = \sqrt{2/3}$$
$$\cos\theta = 1/\sqrt{3}$$
$$\sin\varphi = \cos\varphi = 1/\sqrt{2}$$

the values of $\psi(2p_x)$, $\psi(2p_y)$ and $\psi(2p_z)$ in these directions are (see **Table 5.2**):

$$\psi(2p_x) = \psi(2p_y) = \psi(2p_z) = 1/2\sqrt{\pi}$$

Since $\psi(2s) = 1/2\sqrt{\pi}$, the bond forming strength of ψ_1 relative to that of $\psi(2s)$ as unity is $a_1 + 3b_1$. Using the normalization condition [Eq. (A3.4),] this bond strength becomes $a_1 + \sqrt{3(1 - a^2_1)}$. To find the value of a_1 for which the bonding strength is maximum, we equate the first derivative with respect to a_1 to zero. Thus,

$$\frac{d}{da_1} \, [a_1 + \sqrt{3(1 - a^2_1)}] = 0$$

This gives $a_1 = 1/2$, and Eq. (A3.4) gives $b_1 = 1/2$. The first hybrid orbital ψ_1 is thus

$$\psi_1(1,1,1) = \tfrac{1}{2} \, [\psi(2s) + \psi(2p_x) + \psi(2p_y) + \psi(2p_z)]$$

Similarly, the remaining three hybrids can be shown to be

$$\psi(1, -1, -1) = \tfrac{1}{2} \, [\psi(2s) + \psi(2p_x) - \psi(2p_y) - \psi(2p_z)]$$
$$\psi(-1, 1, -1) = \tfrac{1}{2} \, [\psi(2s) - \psi(2p_x) + \psi(2p_y) - \psi(2p_z)]$$
$$\psi(-1, -1, 1) = \tfrac{1}{2} \, [\psi(2s) - \psi(2p_x) - \psi(2p_y) + \psi(2p_z)]$$

Ionization Potentials

Ionization Potentials of the Elements at 0°K*

Element	Ionization potentials eV						
	1st	2nd	3rd	4th	5th	6th	7th
H	13.6						
He	24.6	54.4					
Li	5.4	75.6	122.4				
Be	9.3	18.2	153.9	217.7			
B	8.3	25.1	37.9	259.3	340.1		
C	11.3	24.4	47.9	64.5	392.0	489.8	
N	14.5	29.6	47.4	77.4	97.9	551.9	666.8
O	13.6	35.1	54.9	77.4	113.9	138.1	739.1
F	17.4	35.0	62.6	87.2	114.2	157.1	185.1
Ne	21.6	41.1	64.0	97.2	126.4	157.9	
Na	5.1	47.3	71.6	98.9	138.6	172.4	208.4
Mg	7.6	15.0	80.1	109.3	141.2	186.9	225.3
Al	6.0	18.8	28.4	120.0	153.8	190.4	241.9
Si	8.1	16.3	33.5	45.1	166.7	205.1	246.4
P	11.0	19.7	30.2	51.4	65.0	220.4	263.3
S	10.4	23.4	35.0	47.2	72.5	88.0	281.0
Cl	13.0	23.8	39.9	53.5	67.8	96.7	114.3
Ar	15.8	27.6	40.9	59.8	75.0	91.3	124.0
K	4.3	31.8	46.0	60.9		99.7	118.0
Ca	6.1	11.9	51.2	67.0	84.4		128.0
Sc	6.6	12.9	24.8	73.9	92.0	111.1	
Ti	6.8	13.6	28.1	43.2	99.8	120.0	140.8
V	6.7	14.2	29.7	48.7	65.2	128.9	151.0
Cr	6.8	16.6	32.3	51.2	73.2	90.3	168.4
Mn	7.4	15.7	34.1	53.6	76.3	101.1	119.2

Element	Ionization potentials eV						
	1st	2nd	3rd	4th	5th	6th	7th
Fe	7.9	16.3	30.7				
Co	7.9	17.5					
Ni	7.6	18.2					
Cu	7.7	20.3	29.5				
Zn	9.4	17.9	40.0				
Ga	6.0	20.4	30.6	63.8			
Ge	8.1	15.9	34.1	45.5	93.0		
As	10.5	20.3	28.0	49.9	62.5	127.0	
Se	9.8	21.3	33.9	42.7	72.8	81.4	
Br	11.8	19.1	25.7	50.3			
Kr	14.0	26.4	36.8				
Rb	4.2	27.4					
Sr	5.7	11.0					
Y	6.6	12.3	20.4				
Zr	7.0	14.0	24.0	33.8			
Nb	6.8	14.1	24.4	37.9	50.2		
Mo	7.2						
Ru	7.5	28.7					
Rh	7.7	18.2	31.2				
Pd	8.3	20.0	33.5	49.0			
Ag	7.6	22.0	36.2				
Cd	9.0	16.8	38.3				
In	5.8	18.8	27.9	57.8			
Sn	7.3	14.5	30.5	39.4	80.7		
Sb	8.6	18.6	24.7	44.0	55.5		
Te	9.0	21.6	30.7	38.0	60.5		
I	10.4	19.1	31.5	41.8			
Xe	12.1	21.1	32.0				
Cs	3.9	23.4					
Ba	5.2	10.0					
La	5.6	11.4	19.2				
Sm	5.6	11.4					
Eu	5.7	11.4					
Gd	6.2						
Yb	6.2						
Lu	5.0						
W	8.0						
Re	7.9						
Os	8.7						
Ir	9.2						
Pt	9.0	19.4					
Au	9.2	20.0					
Hg	10.4	18.7	34.3				
Tl	6.1	20.3	29.7	50.5			
Pb	7.4	15.0	32.2	42.1	69.4		
Bi	8.5	16.8	25.7	45.5	56.2		
Rn	10.7						
Ra	5.3						

* To obtain values in kcal/mole multiply the listed values by 23.06. The values at 298°K may then be obtained, to a good approximation, by adding 1.5 kcal/electron removed to these values.

Properties of Elements

Properties of Atoms in Bulk The values in parentheses in the column of atomic weights are the mass numbers of the most stable or best known isotopes. Melting points and boiling points in parentheses are uncertain. The data for gases are applicable only when these are in their usual molecular state, such as H_2, N_2, O_2, He, Ne, Ar, etc.

Element	Symbol	At. No.	At. wt. ($C^{12} = 12.000$)	Density g/cm³ at 20°C	Melting point °C	Boiling point °C	Crystal structure of solid
Actinium	Ac	89	(227)	...	(1600)	...	....
Aluminium	Al	13	26.98	2.699	660.2	2060	Fcc
Americium	Am	95	(243)	11.7	(850)	:..	....
Antimony	Sb	51	121.75	6.62	630.5	1440	Rhombic
Argon	Ar	18	39.95	1.66 × 10⁻³	−189.4	−185.8	Fcc
Arsenic	As	33	74.92	5.73	814 (36 atm)	610	Rhombic
Astatine	At	85	(210)	...	...	...	...
Barium	Ba	56	137.34	3.5	704	1640	Bcc
Berkelium	Bk	97	(247)	...	...	...	...
Beryllium	Be	4	9.01	1.82	1350	1530	Hcp
Bismuth	Bi	83	208.98	9.80	271.3	1420	Rhombic
Boron	B	5	10.81	2.3	2300	2550	...
Bromine	Br	35	79.91	3.12 (liquid)	−7.2	58	Orthorhombic
Cadmium	Cd	48	112.40	8.65	320.9	765	Hcp
Calcium	Ca	20	40.08	1.55	850	1440	Fcc
Californium	Cf	98	(249)	...	...	...	...
Carbon	C	6	12.01	2.22	>3700	4830	Amorphous Hexagonal Cubic

Properties of Elements

Element	Symbol	At. No.	At. wt. (C^{12} = 12.000)	Density g/cm^3 at at 20°C	Melting point °C	Boiling point °C	Crystal structure of solid
Cerium	Ce	58	140.12	6.9	600	1400	...
Cesium	Cs	55	132.90	1.9	28	690	Bcc
Chlorine	Cl	17	35.45	1.51 (liquid)	—101	—34.7	Tetragonal
Chromium	Cr	24	52.00	7.19	1890	2500	Bcc
Cobalt	Co	27	58.93	8.9	1495	2900	Hcp
Copper	Cu	29	63.54	8.96	1083	2600	Fcc
Curium	Cm	96	(247)	...	...	...	...
Dysprosium	Dy	66	162.50	8.56	...	...	...
Einsteinium	Es	99	(254)	...	...	...	...
Erbium	Er	68	167.26	9.16	...	...	...
Europium	Eu	63	151.96	5.24	...	...	...
Fermium	Fm	100	(253)	...	...	...	...
Flourine	F	9	19.00	1.14 (liquid)	—223	—188	...
Francium	Fr	87	(223)	...	...	...	...
Gadolinium	Gd	64	157.25	7.95	...	...	...
Gallium	Ga	31	69.72	5.91	29.78	2070	Fc ortho
Germanium	Ge	32	72.59	5.36	958	2700	Diamond cubic
Gold	Au	79	196.97	19.32	1063	2970	Fcc
Hafnium	Hf	72	178.49	11.4	1700	(3700)	Hcp
Helium	He	2	4.003	0.166 × 10^{-3}	—272.2 (26 atm)	—268.9	...
Holmium	Ho	67	164.93	10.12	...	...	...
Hydrogen	H	1	1.008	0.0837 × 10^{-3}	—259.2	—252.8	Hexagonal
Indium	In	49	114.82	7.31	156.4	1450	Fc tetra
Iodine	I	53	126.9	4.93	114	183	Orthorhombic
Iridium	Ir	77	192.2	22.5	2454	(5300)	Fcc
Iron	Fe	26	55.85	7.87	1539	2740	Bcc
Krypton	Kr	36	83.80	3.488 × 10^{-3}	—157	—152	...
Lanthanum	La	57	138.91	6.15	826	1800	...
Lawrencium	Lw	103	(257)	...	...	...	...
Lead	Pb	82	207.19	11.34	327.4	1740	Fcc
Lithium	Li	3	6.94	0.53	186	1609	Bcc
Lutetium	Lu	71	174.97	9.74	...	...	...
Magnesium	Mg	12	24.31	1.74	650	1110	Hexagonal
Manganese	Mn	25	54.94	7.43	1245	2150	Cubic complex
Mendelevium	Md	101	(256)	...	...	...	...
Mercury	Hg	80	200.59	13.55	—38.87	357	Rhombic
Molybdenum	Mo	42	95.94	10.2	2625	4800	Bcc
Neodymium	Nd	60	144.24	7.05	840	...	...
Neon	Ne	10	20.18	0.839 × 10^{-3}	—248.7	—245.9	Fcc
Neptunium	Np	93	(237)	...	...	...	...
Nickel	Ni	28	58.71	8.90	1455	2730	Fcc
Niobium	Nb	41	92.91	8.57	2415	3300	Bcc
Nitrogen	N	7	14.007	1.165 × 10^{-3}	—209.9	—195.8	Hexagonal

Element	Symbol	At. No.	At. wt. ($C^{12} =$ 12.000)	Density g/cm³ at 20°C	Melting point °C	Boiling point °C	Crystal structure of solid
Nobelium	No	102	(253)	...	...	...	...
Osmium	Os	76	190.2	22.5	2700	(5500)	Hcp
Oxygen	O	8	15.9994	1.332 × 10⁻³	−218.4	−183.0	...
Palladium	Pd	46	106.4	12.0	1554	4000	Fcc
Phosphorus	P	15	30.97	1.82	44.1	280	Cubic
Platinum	Pt	78	195.1	21.45	1773	4410	Fcc
Plutonium	Pu	94	(242)	...	...	...	...
Polonium	Po	84	(210)	9.24	600	...	Monoclinic
Potassium	K	19	39.1	0.86	63	770	Bcc
Praseodymium	Pr	59	140.91	6.63	940	...	...
Promethium	Pm	61	(147)	...	...	...	...
Protactinium	Pa	91	(231)	...	(3000)	...	...
Radium	Ra	88	(226)	5.0	700	1140	...
Radon	Rn	86	(222)	...	−71	−61.8	...
Rhenium	Re	75	186.2	20.5	3170	(5900)	Hcp
Rhodium	Rh	45	102.91	12.44	1966	(4500)	Fcc
Rubidium	Rb	37	85.47	1.53	39	680	Bcc
Ruthenium	Ru	44	101.07	12.2	2500	(4900)	Hcp
Samarium	Sm	62	150.35	7.7	(1300)	...	...
Scandium	Sc	21	44.96	2.5	1200	2400	Fcc
Selenium	Se	34	78.96	4.81	220	680	Hexagonal
Silicon	Si	14	28.09	2.33	1430	2300	Diamond cubic
Silver	Ag	47	107.87	10.49	960.5	2210	Fcc
Sodium	Na	11	22.99	0.97	97.5	880	Bcc
Strontium	Sr	38	87.62	2.6	770	1380	Fcc
Sulphur	S	16	32.06	2.07	119.0	444.6	Orthorhombic
Tantalum	Ta	73	180.95	16.6	2996	(6100)	Bcc
Technetium	Tc	43	(99)	11.46	2140	...	...
Tellurium	Te	52	127.6	6.24	450	1390	Hexagonal
Terbium	Tb	65	158.92	8.33	327	...	...
Thallium	Tl	81	204.37	11.85	300	1460	Hcp
Thorium	Th	90	232.04	11.5	1800	(5200)	Fcc
Thulium	Tm	69	168.93	9.35	...	...	...
Tin	Sn	50	118.69	7.298	231.9	2270	Bc tetra
Titanium	Ti	22	47.9	4.54	1820	(5100)	Hcp
Tungsten	W	74	183.85	19.3	3410	5930	Bcc
Uranium	U	92	238.03	18.7	1133	(4300)	Orthorhombic
Vanadium	V	23	50.94	6.0	1735	3400	Bcc
Xenon	Xe	54	131.3	5.495 × 10⁻³	−112	−108	Fcc
Ytterbium	Yb	70	173.04	7.01	...	...	...
Yttrium	Y	39	88.91	5.51	1490	(4600)	Hcp
Zinc	Zn	30	65.37	7.133	419.46	906	Hcp
Zirconium	Zr	40	91.22	6.5	1750	(5050)	Hcp

Index

Index

ATOMIC STRUCTURE AND CHEMICAL BOND
Including Molecular Spectroscopy
Second Edition

This book is an introduction to modern concepts of atomic and molecular structure, the nature of the chemical bond, and molecular spectroscopy. In addition, the book gives a complete description of the spectroscopic methods, including the more recent ones and several other techniques of molecular structure determination such as mass spectrometry, electron diffraction and dipole moment. This second edition, besides broadening some of the existing topics, incorporates a few new ones like electron spin resonance spectroscopy, Mossbauer spectroscopy, and mass spectrometry.

An important feature of the book is that it presents introductory quantum chemistry and molecular spectroscopy in a single volume, specially adapts it to self-study. The discussion on molecular spectroscopy also lays emphasis on the physical principles and on the elucidation of relationships between experimental results and molecular parameters rather than on bare experimental facts. In Chapter 7 in this edition, the treatment of bonding in coordination compounds has been expanded to include topic related to ionic and covalent bonding. The bibliography has been expanded, and new problems added at the end of each chapter.

The book will be of value to both undergraduate and graduate students of chemistry, and also of physics insofar as the quantum theory and it applications especially to atomic structure and bonding, and to spectroscopy are concerned.

Manas Chanda is Professor at the Indian Institute of Science, Bangalore, where he has been teaching and conducting research in Materials Science for several years. He had his university education in pure and applied chemistry at Calcutta and received his Ph D from the Indian Institute of Science, Bangalore. An active member of the Materials Science Group at the Institute, he has written many papers and three monographs on different aspects of the science of materials.